



# Pavement Surface Characteristics Concrete New Construction (MnROAD Study)

Minnesota  
Department of  
Transportation

**RESEARCH  
SERVICES  
&  
LIBRARY**

**Office of  
Transportation  
System  
Management**

Bernard Igbafen Izevbekhai, Principal Investigator  
Office of Materials & Road Research  
Minnesota Department of Transportation

**February 2016**

Research Project  
Final Report 2015-48

**MnROAD**  
Office of Materials and Road Research



To request this document in an alternative format call [651-366-4718](tel:651-366-4718) or [1-800-657-3774](tel:1-800-657-3774) (Greater Minnesota) or email your request to [ADArequest.dot@state.mn.us](mailto:ADArequest.dot@state.mn.us). Please request at least one week in advance.

## Technical Report Documentation Page

1. Report No. <b>MN/RC 2015-48</b>	2.	3. Recipients Accession No.	
4. Title and Subtitle <b>Pavement Surface Characteristics Concrete New Construction (MnROAD Study)</b>		5. Report Date <b>February 2016</b>	
7. Author(s) <b>Bernard Igbafen Izevbekhai</b>		6.	
9. Performing Organization Name and Address <b>Office of Materials &amp; Roads Research Minnesota Department of Transportation 1400 Gervais Avenue Maplewood, MN 55109</b>		8. Performing Organization Report No.	
12. Sponsoring Organization Name and Address <b>Minnesota Department of Transportation Research Services &amp; Library 395 John Ireland Boulevard, MS 330 St. Paul, Minnesota 55155-1899</b>		10. Project/Task/Work Unit No.	
		11. Contract (C) or Grant (G) No. <b>(c) MPR-6(021)</b>	
15. Supplementary Notes <b><a href="http://www.lrrb.org/pdf/201548.pdf">http://www.lrrb.org/pdf/201548.pdf</a></b>		13. Type of Report and Period Covered <b>Final Report</b>	
		14. Sponsoring Agency Code	
16. Abstract (Limit: 250 words)  <p>In pavement infrastructure, functional characteristics are mainly preponderant over structural characteristics as the former typically govern pavement rehabilitation, maintenance and reconstruction decisions. Evidently, agencies invest in provision or restoration of friction (skid resistance) and make policies to minimize traffic noise. Most agencies accept (or reject) construction projects based mainly on initial ride quality. Consequently, this study examined various concrete textures imparted on new pavements in the 2007, 2010 and 2011 MnROAD test cell construction and monitored their ride quality, friction, tire pavement noise, visual conditions and acoustic impedance over time. The study successfully developed an in-situ impedance tube evaluation method for pervious concrete for a proxy to material and hydraulic conductivity condition. It also created tenable time-series equations for the progression of the various texture characteristics and developed a friction degradation model based on traffic and texture type. Advanced data analysis showed that longitudinal texturing and negative textures were strongly associated with pavement quietness. Investment analysis revealed that certain surfaces produced noise reduction of 6 decibels over the transverse time. Those textures including pervious concrete and diamond grinding were found to be cost-beneficial for noise abatement consideration. This research also associated rectangular texturing with anomalous laser-induced ride-quality measurements. Further analysis also accentuated a correlation of pavement condition to surface acoustics thus recommending the development of impedance tube for pavement joint condition monitoring. Additionally, This research recommended drag pre-textured longitudinal-tining as the optimal texture for durability, quietness and skid resistance based on the overall research results.</p>			
17. Key Words <b>time series, ride quality, friction, hysteresis, Mann—Whitney Wilcoxon, tire/pavement noise, texture</b>		18. Availability Statement <b>No restrictions. Document available from: National Technical Information Services, Alexandria, Virginia 22312</b>	
19. Security Class (this report) <b>Unclassified</b>	20. Security Class (this page) <b>Unclassified</b>	21. No. of Pages <b>339</b>	22. Price

# **Pavement Surface Characteristics Concrete New Construction (MnROAD Study)**

## **Final Report**

*Prepared by:*

Bernard Igbafen Izevbekhai  
Office of Materials & Road Research  
Minnesota Department of Transportation

**February 2016**

*Published by:*

Minnesota Department of Transportation  
Research Services & Library  
395 John Ireland Boulevard, MS 330  
St. Paul, Minnesota 55155-1899

This report represents the results of research conducted by the authors and does not necessarily represent the views or policies of the Minnesota Department of Transportation. This report does not contain a standard or specified technique.

The author and the Minnesota Department of Transportation do not endorse products or manufacturers. Trade or manufacturers' names appear herein solely because they are considered essential to this report.

## **Acknowledgements**

Author appreciates Minnesota Department of Transportation, Office of Materials and Road Research for active support of this project. Maureen Jensen who was the Research Manager from project conception through data collection and analysis phase and Glenn Engstrom, Director of the Office of Materials and Road Research are acknowledged. Author is also indebted to the Technical Liaison of this study Benjamin Worel (MnROAD Operations Engineer) for the diligent review and constructive criticism he provided in the course of this study and report. Reviews conducted by Eddie Johnson and Dave Van Deusen of the MnDOT Office of Materials & Road Research were very instrumental to bringing this project to a final completion. Appreciations are due to Bruce Holdhusen who was Administrative Liaison for this elaborate project.

Author is particularly indebted to Robert Orthmeyer of Federal Highway Administration for his immeasurable assistance to facilitate furtherance of vital areas of this study including funding of the longitudinal tme initiatives and equipping of our Lightweight Profiler with a ROLINE laser. He also provided the GRIP tester through the FHWA Loans program to enable friction measurements.

## TABLE OF CONTENTS

<b>CHAPTER 1: INTRODUCTION &amp; STATE OF THE PRACTICE</b> .....	<b>1</b>
<b>1.1 Fundamentals of the Pavement Surface</b> -----	<b>1</b>
1.1.1 Surface Texture .....	1
<b>1.2 Pavement Smoothness (International Roughness Index, IRI)</b> -----	<b>2</b>
1.2.1 Geometric Surface Features Joints, Curl &Warp, and Faulting Features .....	7
1.2.2 Quantification of IRI as a Proxy for Larger Scale Texture Effects.....	8
<b>1.3 Fragmentation &amp; Survival of Friction</b> -----	<b>11</b>
1.3.1 Hysteresis and Adhesion .....	11
<b>1.4 Tire Pavement Noise</b> -----	<b>14</b>
1.4.1 Tire Pavement Acoustic Durability .....	16
1.4.2 Active and Reactive Fields .....	18
<b>1.5 Noise Generation Mechanisms</b> -----	<b>19</b>
1.5.1 The Stick Snap and Stick Slip Phenomena .....	20
1.5.2 The Clap Phenomenon.....	20
1.5.3 The Horn (Amplification) Effect .....	20
1.5.4 Pipe Resonance (Organ Pipe Effect) .....	20
1.5.5 Cavity Resonance (Balloon Simulation) [1.27], [1.29] [1.30].....	20
<b>1.6 Acoustic Impedance Theory</b> -----	<b>21</b>
<b>1.7 Pavement Geometrical Variables</b> -----	<b>24</b>
1.7.1 Texture Direction.....	24
1.7.2 Numerical Example:.....	24
1.7.3 Pavement Surface Variables: Mean Profile Depth .....	25
1.7.4 Pavement Surface Characteristics Asperity Interval and Groove Width .....	28
1.7.5 Texture Orientation .....	28
<b>1.8 Tire Texture and Contact Phenomena</b> -----	<b>30</b>
1.8.1 Fujikawa Bendstein Models .....	32
1.8.2 Wu and Nagi Model .....	33
1.8.3 Clapp et al Model .....	35
1.8.4 Hamet [1.38] Model & Hamet and Klein Model [1.39] .....	37
1.8.5 Donovan’s Equation for Sound Generation .....	38
1.8.6 Hanson’s Model [1.26].....	39
1.8.7 Byrum’s Analysis [1.43] Effect of Tine Spacing on Tire Carcass Vibration .....	39
1.8.8 Dynamic Friction Models for Longitudinal Tire .....	40
1.8.9 Fragmentation of Surface Profiles .....	41
1.8.10 Summary of the Contact Theories .....	43
<b>1.9 Environmental Considerations</b> -----	<b>44</b>
1.9.1 Atmospheric Variables: Temperature .....	47
1.9.2 Atmospheric Variables: Relative Humidity.....	48
1.9.3 Atmospheric Pressure .....	51
1.9.4 Section Summary.....	51
<b>1.10 Resonance Phenomena</b> -----	<b>51</b>
1.10.1 Helmholtz Resonance in Tire Pavement Interaction.....	52
1.10.2 Resonance “Pipe” Phenomenon in Pavement Surfaces .....	53
<b>CHAPTER 2: TEXTURE CONSTRUCTION AND MEASUREMENTS</b> .....	<b>56</b>
<b>2.1 Textures Constructed At Mnroad and Initial Data Collection In 2008</b> -----	<b>56</b>
<b>2.2 Experimental Sections &amp; Texturing Process (2008)</b> -----	<b>59</b>
2.2.1 Pervious Pavements.....	60
2.2.2 Cell 39 Pervious Overlay.....	63
2.2.3 Diamond Grinding Experiment (Cells 37, 7, 8, 9 &71).....	67
2.2.4 Turf Drag Finish .....	68

2.2.5	Broom Drag Texturing .....	70
2.2.6	Longitudinal Tining Cell 5 .....	71
<b>2.3</b>	<b>Initial Surface Characteristics Testing -----</b>	<b>72</b>
2.3.1	Friction Testing .....	76
2.3.2	Sound Absorption Measurements on Pavement Test Cells .....	80
2.3.3	On Board Sound Interaction (OBSI) Collection Process.....	81
2.3.4	Initial Ride Measurement .....	81
2.3.5	Hydraulic Conductivity Measurements in Pervious Concrete.....	81
<b>2.4</b>	<b>Texturing In 2010 Construction At The Mnroad Research Facility -----</b>	<b>86</b>
2.4.1	Background.....	86
2.4.2	Construction Texturing.....	86
2.4.3	Early Performance Evaluation .....	87
2.4.4	On Board Sound Intensity .....	89
2.4.5	Sound Absorption .....	89
2.4.6	Friction .....	90
2.4.7	Section Summary.....	91
<b>2.5</b>	<b>2011 Construction Texturing -----</b>	<b>92</b>
2.5.1	Background.....	92
2.5.2	Performance Evaluation .....	92
<b>2.6</b>	<b>Cell 63 Drag Surface Rehabilitation -----</b>	<b>99</b>

<b>CHAPTER 3: DEVELOPMENT OF A PROCESS FOR ACOUSTIC IMPEDANCE (SOUND ABSORPTION) MEASUREMENT AND APPLICATION .....</b>	<b>101</b>
<b>3.1 Development of a Process for Acoustic Impedance (Sound Absorption) -----</b>	<b>101</b>
3.1.1 Background.....	101
3.1.2 Description of Equipment.....	101
3.1.3 Collection Frequency & Process .....	102
3.1.4 Data Processing .....	103
<b>3.2 Application of Test Results OBSI-Sound Absorption Correlation in the Frequency Domain -----</b>	<b>104</b>
3.2.1 Background.....	104
3.2.2 Data Collection and Measurement.....	105
3.2.3 Lemma for Component Sound Absorption Analysis.....	110
3.2.4 The Pervious Concrete Model .....	112
3.2.5 Interim Model Validation .....	113
3.2.6 Concluding Remarks .....	114

<b>CHAPTER 4: ANNUAL REPORTS.....</b>	<b>115</b>
<b>4.1 Second Year Performance Report-----</b>	<b>115</b>
4.1.1 Preface .....	115
4.1.2 OBSI-MPD for Non-Pervious Pavements .....	119
4.1.3 Examination of the Hansen Model .....	122
4.1.4 Examination of the Bendstein et al Model.....	123
4.1.5 Texture Performance .....	125
4.1.6 IRI trends in New Textures .....	131
4.1.7 Concluding Remarks .....	140
<b>4.2 Third Year And Fourth Year Annual Report-----</b>	<b>141</b>
4.2.1 Surface Characteristics Versus Time Trends.....	141
4.2.2 Mean Profile Depth .....	141
<b>4.3 Autoregressive Integrated Moving Average Arima and Probability Density Function for MNRoad Surface Characteristics Data-----</b>	<b>178</b>
4.3.1 Autoregressive Time Series Models.....	179
4.3.2 Texture Characteristics and Acoustics Over Time .....	194
<b>4.4 Representation of Surface Characteristics by Probability Density Function -----</b>	<b>195</b>
4.4.1 A probability density function .....	196
4.4.2 Observed IRI OBSI Trends in Various Texture Types after 3 Years .....	203

<b>CHAPTER 5: ADVANCED DATA ANALYSIS AND MODEL DEVELOPMENT.....</b>	<b>222</b>
<b>5.1 Statistical Examination of the Effect of Texture Direction and Texture Orientation on Noise &amp; Friction</b>	<b>222</b>
5.1.1 Effect on Noise .....	222
5.1.2 5.1.2 Effect on Friction.....	229
5.1.3 Section Conclusion .....	231
<b>5.2 Pavement Texture Induced Roughness Anomolies -----</b>	<b>231</b>
5.2.1 Introduction .....	231
5.2.2 Experimental Design .....	232
5.2.3 Spatial Domain Analysis of Lateral Wander in a Light Weight Inertial Device .....	233
5.2.4 Results .....	236
5.2.5 Section Summary.....	242
<b>5.3 Return on Investment in Quiet Pavements in Comparison to Standard Sound Abatement Walls -----</b>	<b>243</b>
5.3.1 Background.....	243
5.3.2 Introduction .....	243
5.3.3 Implication of OBSI Difference .....	244
5.3.4 Near Field – Far Field Compatibility.....	245
5.3.5 Benefit Cost Analysis of Pavement Surfacing / Overlay .....	249
5.3.6 Sensitivity & Limitation .....	254
5.3.7 Section Conclusion .....	254
<b>5.4 Development of Friction Degradation Models -----</b>	<b>254</b>
5.4.1 Background.....	254
5.4.2 Introduction .....	255
5.4.3 Data Analysis.....	255
5.4.4 Model Improvement and Validation.....	263
5.4.5 Section Summary.....	264
<b>5.5 Effects of Pavement Condition on Concrete Pavement Smooptness and Acoustics -----</b>	<b>264</b>
5.5.1 Introduction .....	265
5.5.2 Pipe Resonance and Helmholtz Resonance in Deteriorated Concrete Joints.....	265
5.5.3 Effect of Faulting Induced International Roughness Index on Board Sound Intensity Levels .....	272
5.5.4 Effect of Built In Warp or Curl.....	276
5.5.5 Association of faulting with international roughness index.....	279
 <b>CHAPTER 6: CONCLUSIONS AND RECOMMENDATION .....</b>	 <b>308</b>
 <b>REFERENCES .....</b>	 <b>313</b>



## LIST OF TABLES

Table 1.1: Noise Generation and Amplification Mechanisms and Associated Variables.....	21
Table 1.2: Temperature Effects .....	45
Table 1.3: European Union (EU) Temperature Correction Factors for Sound intensity Level .....	46
Table 1.4: SI* For A Range of Relative Humidity and Temperature .....	51
Table 2.1: Equipment and Testing Scheme for Test Sections .....	56
Table 2.2a: Location Allocation for Pre-2008 Textures and 2008 Texturing.....	57
Table 2.2b: Summary of Concrete Pavement Textures Constructed at MnROAD (2008).....	58
Table 2.2C: New Textures in 2008 and 2009 .....	59
Table 2.3: GRIP Test Results .....	77
Table 2.4a: Initial Friction Test Results.....	78
Table 2.4b: Initial friction Test.....	79
Table 2.5: Summary Data for Sound Absorption on MnRoad Pavements .....	80
Table 2.6: IRI of Some Test Cells Measured With the LWP Fall 2008 .....	82
Table 2.7: Hydraulic Conductivity Measurements on Porous Test Cells .....	85
Table 2.8: Performance Data .....	89
Table 3.1: Sound Absorption Database Table .....	104
Table 3.2: Typical OBSI and SA at Coincident Frequencies (Cell 85 Outside Lane September 2009).....	108
Table 3.3: Component Absorption Coefficients $\alpha(F)$ Obtained From All MnRoad.....	111
Table 3.4: OBSI SA Model Parameters.....	112
Table 4.1: MPD IRI OBSI of Pervious Pavements Test Cells.....	116
Table 4.2: Summary Output SA-MPD Relationship .....	118
Table 4.3: Regression results for Pervious Pavement OBSI vs. IRI & MPD .....	118
Table 4.4: Summary OBSI CTM MPD Relationship for all Concrete Cells .....	120
Table 4.5: OBSI Time Series of Inner Lane of a 1993 Transverse Tined Cell (Cell 36).....	180
Table 4.6: Texture and Noise Performance over Time.....	194
Table 5.1: Configuration of Textures Data Set 1.....	223
Table 5.2: Configuration of Texture Data.....	223
Table 5.3: Acoustic Response (OBSI-100 dBA) of Transverse Turf & Longitudinal Turf.....	226
Table 5.4: Summary of Full Width Grind (2007) and Grind Improvement (Cell 9 2009 OBSI, Drag Textures).....	237
Table 5.5: Mann Whitney Wilcoxon Test for Data Similarity Roline vs. Triple Laser .....	241
Table 5.6: Interactive Prediction of Far Field Response from Near Field Response.....	249
Table 5.7: Effect of Near field Detected Difference on Projected Far Field Difference.....	249
Table 5.8: Cost Benefit Analysis Results; Case 1 Rehab of Drag Texture.....	252
Table 5.9: Cost Benefit Analysis Results; Case 1 Rehab of a Transverse Tined Pavement Texture.....	253
Table 5.10: Summary Network Ribbed-Data for MnDOT Current Texturing .....	257
Table 5.11: Summary Network Ribbed – Data for MnDOT Current Texturing.....	258
Table 5.12: MnROAD Friction Survival Model.....	263
Table 5.13: Legend of Texture Descriptors .....	263

## LIST OF FIGURES

Figure 1.1: PIARC Classification of Texture in Wavelength Form and Usage [1.6] .....	2
Figure 1.2: Light weight Profiler .....	4
Figure 1.3: Profilogram of a Surface .....	4
Figure 1.4: PSD - Inertial Profiler IRI Response and PSD Response.....	5
Figure 1.5: Wavelengths Where Body Bounce and Axle Hop are Prominent.....	6
Figure 1.6: Body Bounce and Axle Hop Response .....	6
Figure 1.7: ProVAL Output for IRI of a 1-inch Faulted Pavement .....	8
Figure 1.8: IRI Multiplier Algorithm.....	9
Figure 1.9: PROVAL Output for IRI of a 1-inch Faulted Pavement.....	11
Figure 1.10: Hysteresis and Adhesion Forces in TPIN.....	12
Figure 1.11: OBSI Assembly showing SRTT, Mounting Rig, Microphones and Cables.....	15
Figure 1.12: Output of an OBSI Measurement.....	16
Figure 1.13: Implication of OBSI Difference.....	19
Figure 1.14: Sound Absorption Measurement with Impedance Tube.....	22

Figure 1.15: Sine Wave of Sound Intensity Function in the Spatial/ Time Domain.....	24
Figure 1.16: Frequencies due to transverse tines are coincident with typical tire resonant frequencies.....	25
Figure 1.17a: Texture Configuration and Relevant Dimensions .....	26
Figure 1.17b: Mean Profile Depth.....	27
Figure 1.18: (a) and (b) Schematics of Similar MTD but Different Surface Performance and (c) Positive and negative Texture .....	29
Figure 1.19: Texture Configuration and Relevant Dimensions .....	31
Figure 1.20: Texture-Planing Configuration and Relevant Dimensions.....	33
Figure 1.21: Hysteresis Effects at Tire Asperity Interface.....	34
Figure 1.22: Schematics of Indentor and Deformed Tire (Clapp et al) [1.22].....	36
Figure 1.23: CLAPP's Prediction of Acoustic Pressure from Indentor Pressure Distribution .....	36
Figure 1.24: Clapp 1988 Model of a PSD of Input forces .....	40
Figure 1.25: Hysteresis in Friction .....	42
Figure 1.26: Relationship between Normalized SI and Temperature .....	48
Figure 1.27: Water Vapor in Air at Various RH and Temp Ranges .....	49
Figure 1.28: Effect of Relative Humidity on SI*.....	50
Figure 1.29: Texture or Groove in Helmholtz Resonance Phenomena.....	52
Figure 1.30: Pipe Resonance Phenomena in Grooves and Joints .....	54
Figure 2.1: Cells 85 to 89 Pervious Pavements Full Depth Factorial .....	60
Figure 2.2: Layout of Pervious Concrete Cell .....	61
Figure 2.3: Cross Section Through Pervious cells 85, 86, 88, and 89 .....	62
Figure 2.4: Cross Section Through Impervious cells 87.....	63
Figure 2.5: Pervious Concrete Placement and Vibration.....	64
Figure 2.6: Pervious Overlay Multi-Drum Screed Compactor .....	64
Figure 2.7: Pervious Overlay Surface.....	65
Figure 2.8: Cell 89 Pervious Concrete on Clay and Cell 88 Pervious Asphalt on Cla .....	65
Figure 2.9: Establishing 10 ft. Joints in Cells 85 and 89 .....	66
Figure 2.10: Cell 85 and Proximate Cross Drain Prior to Concreting (Rail Road ballast Base is exposed.).....	66
Figure 2.11: Configuration of Cell 9: Ultimate Grind .....	67
Figure 2.12: Grinding Process for Configuration of Cell 9: Ultimate Grind .....	67
Figure 2.13: Cell 9 Innovative Grind.....	68
Figure 2.14: Cell 6 Mainline Interim Turf Texturing .....	69
Figure 2.15: Finished Surface with Alpha Methyl Styrene (AMS) Curing Compound.....	69
Figure 2.16: Broom Drag Used for Texturing of Cell 13 and Cell 53 .....	70
Figure 2.17: Broom Drag Texturing of Cell 13 .....	71
Figure 2.18: Turf Finish of Concrete Pavement .....	72
Figure 2.19: Cell 5 Pre-ground Longitudinal Grind Sand Volumetric Technique ASTM E-965.....	73
Figure 2.20: Sand Volumetric Technique ASTM E-965 Test Result on Innovative Grind Cell 7 .....	73
Figure 2.21: Sand Volumetric Technique ASTM E-965 Test Result on Conventional Grind Cell 8 .....	74
Figure 2.22: Sand Volumetric Technique ASTM E-965 Test Result on Broom Drag Cell 14.....	75
Figure 2.23: Sand Volumetric Technique ASTM E-965 Test Result on Cell 53 with Aggressive Texturing Exhibiting Higher MPD .....	75
Figure 2.24: Turf Drag in Cell 14.....	76
Figure 2.25: Third Octave Frequency Response of 2 Sets of Microphones .....	81
Figure 2.26: In-situ Hydraulic Conductivity Measurement Device. (Crude Perveammeter).....	84
Figure 2.27a: MnROAD Mainline Cell 72 Construction.....	87
Figure 2.27b: Composite Cells .....	88
Figure 2.28: SA Coefficient Spectrum (a) 6/7/10 and (b) 10/17/10 .....	90
Figure 2.29: a) CTM Cell 72 (b) MPD Driving (c) MPD Passing.....	91
Figure 2.30: International Roughness Index Results .....	93
Figure 2.31: OBSI Results .....	94
Figure 2.32: Friction Number Results .....	95
Figure 2.33: CTM Results .....	95
Figure 2.34: FN and MPD Surface Comparison of Longitudinal Tine to Innovative grind and Tranverse Broom.....	96
Figure 2.35: OBSI Surface Comparison.....	97
Figure 2.36: Cell 6 (Longitudinal Tine) and Cell 71(Ultimate Grinding Configuration OBSI Spectra Compared.....	98

Figure 2.37: Cell 6 and Cell 71 (For Comparison) A-wtd OBSI.....	98
Figure 2.38: Cell 63 OBSI.....	99
Figure 2.39: Cell 63 Rehabilitated Drag IRI.....	100
Figure 2.40: Cell 63 Rehabilitated Drag Friction .....	100
Figure 3.1: Impedance Tube Adapted to In-Situ Testing.....	102
Figure 3.2: Schematics of Construction / Circuitry .....	103
Figure 3.3: Cross Sections through the Pervious Concrete Overlay.....	106
Figure 3.4: Max Effects of Pervious Pavement Observed at Resonant Frequency of 1000 Hz.....	107
Figure 3.5: Typical OBSI and SA at Coincident Frequencies .....	109
Figure 3.6: Pervious and Non-Pervious Concrete Sound Absorption Factor and Sound intensity at Coincident Frequencies.....	113
Figure 4.1: Circular Track Meter ASTM E-2157 .....	116
Figure 4.2: TriOD Versus ROLINE IRI of pervious surface filtered with 250-mm filter using FHWA ProVAL Software.....	117
Figure 4.3: Distribution of OBSI, IRI and MPD of Pervious Cells .....	119
Figure 4.4: OBSI versus MPD for All Non-Pervious Textures .....	120
Figure 4.5: OBSI versus MPD for All Non-Pervious Longitudinal Textures.....	121
Figure 4.6: OBSI versus MPD for All Non-Pervious Longitudinal Textures.....	121
Figure 4.7: Hansen et al Models Fitted with 433 Data Set .....	122
Figure 4.8: Hanson Model Examined with Data .....	123
Figure 4.9: Testing of Bendsten (Fujikawa) Model Validation .....	124
Figure 4.10: Bendstein Model Improved by Normalizing the Deriving Model Constants .....	125
Figure 4.11: Texture Performance of Longitudinal Tine Later Ground .....	126
Figure 4.12: Texture Performance of a Heavy Turf Drag Cell .....	126
Figure 4.13: Texture Performance of a 2008 Longitudinal Broom Drag.....	127
Figure 4.14: Performance of a Year 2000 Turf Dragged Surface.....	127
Figure 4.15: Performance of a Year 2000 Turf Dragged Surface.....	128
Figure 4.16: Performance of a Year 2008 Pervious Concrete Overlay.....	128
Figure 4.17: Performance of a Year 2008 Transverse Turf Dragged Surface .....	129
Figure 4.18: Performance of a Year 2004 Turf Dragged Surface. There is Evidence of Texture Degradation.....	129
Figure 4.19: Performance of a Year 2010 Exposed Aggregate .....	130
Figure 4.20: Performance of a Year 2008 Full Depth Pervious Concrete Surface. ....	130
Figure 4.21: Performance of a Year 2008 Pervious Concrete on Clay Subgrade Turf Dragged Surface .....	131
Figure 4.22: IRI of a PASSRC Unbonded Overlay textured with Longitudinal Tine and corrected with Traditional Grinding.....	132
Figure 4.23: IRI of a 1993 Transverse Tined Pavement Built on PASB .....	132
Figure 4.24: IRI of a 1993 Transverse Tined Pavement Built on PASB .....	133
Figure 4.25: IRI of a 1993 Transverse Tined Pavement.....	133
Figure 4.26: IRI of a 2008 Drag Pavement.....	134
Figure 4.27: IRI of a 2008 Turf Dragged Thin Concrete Cell .....	134
Figure 4.28: IRI of a 2006 Broom Dragged Whitetopping Cell .....	135
Figure 4.29: IRI of a 2008 Turf Dragged Thin Concrete Cell .....	135
Figure 4.30: IRI of a 2008 Pervious Overlay Cell .....	136
Figure 4.31: IRI of a 2000 Turf Dragged 7.5 inch Concrete Cell with Various Dowels .....	136
Figure 4.32: IRI of a 2006 60 Year Design 10 Sensor Installation Textured Transversely with Broom. ....	137
Figure 4.33: IRI of a 2004 Turf Dragged Taconite aggregate Concrete Cell 8 inches thick. Base Varying from 6 inches to 4 ft. ....	137
Figure 4.34: IRI of a 2004 Turf Dragged Whitetopping Cell .....	138
Figure 4.35: IRI of a 2004 Turf Dragged Thin Concrete Cell with Rocking Panels. ....	138
Figure 4.36: IRI of a 2010 Composite Concrete Cell Textured with Exposed Aggregates .....	139
Figure 4.37: IRI of a 2008 Full Depth Pervious Concrete Built on Pervious Base and Sand Subgrade .....	139
Figure 4.38: IRI of a 2008 Full Depth Pervious Concrete Built on Pervious Base and cohesive Subgrade .....	140
Figure 4.39: Longitudinal Tine.....	142
Figure 4.40: Traditional Grind.....	142
Figure 4.41: Traditional Grind.....	143
Figure 4.42: Innovative Grind .....	143

Figure 4.43: 2008 Innovative Grind .....	144
Figure 4.44: Drag texture.....	144
Figure 4.45: Drag Texture .....	145
Figure 4.46: Drag Texture .....	145
Figure 4.47: Drag Texture .....	146
Figure 4.48: Exposed Aggregate .....	146
Figure 4.49: Pervious Concrete Surface .....	147
Figure 4.50: Pervious Concrete Surface .....	147
Figure 4.51: Pervious Concrete Surface .....	148
Figure 4.52: Transverse Tine.....	148
Figure 4.53: Innovatively Ground DL and Conventionally Ground PL.....	149
Figure 4.54: Grinding Comparisons .....	150
Figure 4.55: Improved Innovative Grind.....	151
Figure 4.56: Conventionally Ground Longitudinal Tined Texture .....	151
Figure 4.57: Asphalt-Surface. Later Longitudinal Tine.....	152
Figure 4.58: Drag texture Friction Numbers.....	152
Figure 4.59: Drag Texture Friction.....	153
Figure 4.60: Drag Texture Friction.....	153
Figure 4.61: Drag Texture .....	154
Figure 4.62: Drag Texture .....	154
Figure 4.63: Drag Texture .....	155
Figure 4.64: Drag Texture .....	155
Figure 4.65: Drag Texture .....	156
Figure 4.66: Drag Texture .....	156
Figure 4.67: Drag Texture .....	157
Figure 4.68: Drag Texture .....	157
Figure 4.69: Friction of Exposed Aggregates.....	158
Figure 4.70: Friction in Pervious Concrete.....	158
Figure 4.71: Friction in Pervious Concrete Surface.....	159
Figure 4.72: IRI of a Transverse Tined Textured Cell (1993 Cell 12 Transverse Tine - Mainline) .....	160
Figure 4.73: IRI of a Transverse tined Textured Cell (Cell 37 - LVR).....	160
Figure 4.74: IRI of a Transverse tined Textured Cell (Cell 38-LVR).....	161
Figure 4.75: IRI of a Transverse Tined Textured Cell (Cell 40 – LVR).....	161
Figure 4.76: IRI of a Transverse Tined Textured Cell (Cell 96 – Mainline) .....	162
Figure 4.77: IRI of a Transverse Tined Cell that was Diamond Ground (Cell 96 – mainline).....	162
Figure 4.78: IRI of a Transverse Tine Textured Cell (Cell 97 – mainline).....	163
Figure 4.79: Longitudinal drag Test cell (Cell 14 – Mainline).....	163
Figure 4.80: IRI of a Drag Textured Cell (Cell 52 – LVR) .....	164
Figure 4.81: IRI of a Drag Textured Cell (1993 Cell 32 Turf Drag – LVR) .....	164
Figure 4.82: IRI of Pervious Concrete Overlay Cell (Cell 39 – LVR) .....	165
Figure 4.83: IRI of a Pervious Concrete Cell on Sand Subgrade (Cell 85 – LVR) .....	165
Figure 4.84: IRI of a Pervious Concrete Cell Built on Clay Subgrade (Cell 89 – LVR) .....	166
Figure 4.85: IRI of an Exposed Aggregate Textured Two Lift Concrete Cell (Cell 72 – mainline).....	166
Figure 4.86: IRI of a 60 Year Design – Transverse Broom Drag Cell (Cell 53 (2008 Transverse Tine) – LVR) .....	167
Figure 4.87: IRI of A taconite aggregate Drag Textured Cell (Cell 54 turf drag – LVR) .....	167
Figure 4.88: IRI of a Turf dragged Whitetopping Cell (2004 Cell 60 Whitetopping turf drag – mainline) .....	168
Figure 4.89: IRI of a Turf dragged Whitetopping Cell (2004 Cell 61 Whitetopping Turf Drag – Mainline).....	168
Figure 4.90: IRI of a Turf dragged Whitetopping Cell (2004 Cell 62 Whitetopping turf drag – mainline) .....	169
Figure 4.91: Sound Absorption of a Non-Pervious Concrete Cell (1993 Cell 32 turf drag – LVR).....	170
Figure 4.92: Sound Absorption of a Non-Pervious Concrete Cell (Cell 38 – LVR) .....	170
Figure 4.93: Sound Absorption of a Non-Pervious Concrete Cell (Cell 40 – LVR) .....	171
Figure 4.94: Sound Absorption of a Non-Pervious Concrete Cell (Cell 7 – mainline.....	171
Figure 4.95: Sound Absorption of a Non-Pervious Concrete Cell (Cell 5 (DG 2008-2011 Tran Tine Later – mainline).....	172
Figure 4.96: Sound Absorption of a Non-Pervious Concrete Cell (Cell 6 – mainline) .....	172
Figure 4.97: Sound Absorption of a Non-Pervious Concrete Cell (Cell 7 – mainline) .....	173

Figure 4.98: Sound Absorption of a Non-Pervious Concrete Cell (Cell 8 – mainline) .....	173
Figure 4.99: Sound Absorption of a Non-Pervious Concrete Cell (Cell 9 – mainline) .....	174
Figure 4.100: Sound Absorption of a Non-Pervious Concrete Cell (Cell 14 – mainline).....	174
Figure 4.101: Sound Absorption of a Pervious Concrete overlay Cell (Cell 39 – LVR).....	175
Figure 4.102: Sound Absorption of a Pervious Concrete overlay Cell (Cell 85– LVR).....	176
Figure 4.103: Sound Absorption of a Pervious Concrete Overlay Cell (Cell 89 – LVR).....	177
Figure 4.104: Sound Absorption of a Pervious Concrete overlay Cell (Cell 64 – Parking Lot).....	177
Figure 4.105: Driving Lane of Cell 12 (1993 Transverse Tine) .....	181
Figure 4.106: Pervious Concrete Overlay OBSI (Cell 39 Outside Lane – LVR) .....	181
Figure 4.107: Pervious Cell 39 Inside Lane OBSI .....	182
Figure 4.108: Pervious Cell 85 Inside Lane OBSI .....	182
Figure 4.109: Pervious Cell 85 Outside Lane OBSI.....	183
Figure 4.110: Pervious Cell 89 Inside Lane OBSI .....	183
Figure 4.111: Pervious Cell 89 Outside Lane OBSI.....	184
Figure 4.112: Cell 13 Driving Lane OBSI.....	184
Figure 4.113: Cell 13 Passing Lane OBSI.....	185
Figure 4.114: Cell 14 Driving Lane OBSI.....	185
Figure 4.115: Cell 14 Passing Lane OBSI.....	186
Figure 4.116: Cell 36 Inside Lane OBSI .....	186
Figure 4.117: Cell 36 Transverse Tine Outside Lane OBSI.....	187
Figure 4.118: Cell 71 Driving Lane OBSI.....	187
Figure 4.119: Cell 71 Passing Lane OBSI.....	188
Figure 4.120: Cell 32 2000 Thin Concrete Pavement with Turf Dragged Surface OBSI.....	188
Figure 4.121: Cell 36 Inside Lane Ribbed Friction .....	189
Figure 4.122: Cell 36 Inside Lane Smooth Friction .....	189
Figure 4.123: 1993 Transverse Tine Cell 36 Outside Lane Ribbed Friction.....	190
Figure 4.124: Cell 36 Outside Lane Smooth Friction.....	190
Figure 4.125: Cell 36 Inside Lane Ribbed IRI.....	191
Figure 4.126: Cell 36 Inside Lane Smooth IRI.....	191
Figure 4.127: Cell 36 Outside Lane Ribbed IRI.....	192
Figure 4.128: Cell 36 Outside Lane Smooth IRI.....	192
Figure 4.129: 1993 Transverse Tine Cell 12 DL IRI.....	193
Figure 4.130: 1993 Transverse tine Cell 12 DL IRI.....	193
Figure 4.131: Cell 36 Inside Lane IRI .....	193
Figure 4.132: Cell 40 Inside Lane IRI .....	194
Figure 4.133: 1/3rd Octave Sound Intensity Spectrum (a) Cell 72 Compare Dates and (b) 11/17/2010 Compare Cells.....	195
Figure 4.134: Traffic ESALs versus time in the 4 MnROAD Lanes.....	198
Figure 4.135: Probability Density Function of Various Test Cells Driving Lane Subject to 5 years of Interstate traffic .....	199
Figure 4.136: Probability Density Function of various Test Cells Subject to 5 years of Passing Lane Interstate traffic .....	200
Figure 4.137: Probability Density Function of various Concrete Test Cells Subject to 5 years of Environmental factors (No traffic).....	201
Figure 4.138: Probability Density Function of various Test Cells Traffic Lane Subject to 5 years of Low Volume Traffic.....	201
Figure 4.139: Probability Density Function of all MnROAD Concrete Cells Subject to 5 years (or more) of Interstate Traffic.....	202
Figure 4.140: OBSI IRI Codependence .....	203
Figure 4.141: IRI OBSI Correlation in a Conventionally Ground Texture on an Unbonded Concrete Overlay .....	204
Figure 4.142: IRI versus OBSI in a Transverse Tine Textured Pavement.....	205
Figure 4.143: IRI OBSI Correlation in an Exposed Aggregate Test Cell.....	206
Figure 4.144: Comparative Response of an Innovative Ground texture (Top) and a conventionally ground texture (Bottom) .....	207
Figure 4.145: IRI OBSI Relationship in a Conventionally Ground Textured Unbonded Overlay Test Cell.....	208
Figure 4.146: Comparative response of a Turf Drag texture in the MnROAD Low Volume Road .....	209

Figure 4.147: Comparative Response of a Turf Drag Texture in the MnROAD Low Volume Road .....	210
Figure 4.148: Drag, Conventional .....	211
Figure 4.149: Drag, Conventional Grind Transverse Tine .....	212
Figure 4.150: Longitudinal Tine Innovative Grind, Conventional Grind .....	213
Figure 4.151: Transverse Tine, Turf Drag, Broom Drag .....	214
Figure 4.152: Innovative Grind, Transverse Tine, Pervious Concrete .....	215
Figure 4.153: Pervious Concrete Transverse Tine .....	216
Figure 4.154: 2008 Innovative Grind, 2004 Drag, and 2004 Drag .....	217
Figure 4.155: 2004 Drag, 2011 Grind Of Drag Surface, 2011 Grind of Tined Surface .....	218
Figure 4.156: 2011 Innovative Grind, 2011 Exposed Aggregate .....	219
Figure 4.157: 2008 Pervious Concrete .....	219
Figure 4.158: 2000 Drag Surfaces .....	220
Figure 4.159: 2000 and 2004 Drag Surfaces .....	221
Figure 5.1: Transverse Broom versus Longitudinal Broom .....	225
Figure 5.2: Transverse Tine versus Longitudinal Grind Data .....	227
Figure 5.3: Transverse Tine and Longitudinal Tine .....	229
Figure 5.4 Differences in MPD for Longitudinal and Transverse Textures .....	229
Figure 5.5: Differences in Friction Numbers of Transverse and Longitudinal Grind .....	230
Figure 5.6: Differences in OBSI of Transverse versus Longitudinal Broom .....	230
Figure 5.7: Inertial Profiler Dually Equipped with Roline (Line) Laser and Triple Laser (Triple) laser. Note Line laser beam and triple laser beam on pavement. ....	233
Figure 5.8: Concrete Surface Configurations Examined .....	233
Figure 5.9a: Typical Boxcar Configuration .....	234
Figure 5.9b: Geometry of Lateral Wander Across an Ultimate Grind Configuration .....	234
Figure 5.9c: Single Point Laser Interaction with Boxcar Configuration in Lateral Wander .....	234
Figure 5.10a: Effective Profilogram of Ultimate Grind Configuration .....	235
Figure 5.10b: PSD of Ultimate Grind Configuration .....	235
Figure 5.11a: Triple Laser and Roline Laser Interaction with Boxcar Configuration .....	236
Figure 5.11b: Cell 9 Ultimate Grind Showing Vivid Dips in Triple Laser Profilogram. Second Line without Dips is Roline Profilogram .....	236
Figure 5.12: Triple Vs Roline on a Broom Drag Texture .....	238
Figure 5.13: IRI of Triple and Roline in Turf Drag Textures .....	238
Figure 5.14: Triple Vs Roline in 2 Ultimate Grind Cells .....	239
Figure 5.15: Triple Vs Roline in 2 Ultimate Grind Cells .....	239
Figure 5.16: Triple versus Roline IRI on an Ultimate Ground Texture .....	240
Figure 5.17: Triple versus Roline IRI on an Ultimate Ground Texture .....	240
Figure 5.18: IRI of Triple and Roline in Separate Lanes with Different Configurations .....	241
Figure 5.19: Implication of sound Intensity reduction in the “A” weighted scale .....	245
Figure 5.20: Cumulative Percentage OBSI Data (Izevbekhai [1.52]) .....	247
Figure 5.21: Near field far field (25-ft Offset) Geometry from source .....	248
Figure 5.22: Network Ribbed Tire Friction for Concrete. (Concrete textures are Turf & Broom Drag) .....	256
Figure 5.23: Friction Survival in I-94 Turf Drag Test Section in Sauk Rapids MN .....	259
Figure 5.24: MnROAD Texture Versus Time Patterns .....	260
Figure 5.25: Friction Survival in MN-21 Turf Drag Section in Jordan MN .....	261
Figure 5.26: Details of Dimensions of Spalled and Deteriorated Joints .....	266
Figure 5.27: Progression of Joint Deterioration Showing Dimensions of Acoustic Relevance .....	267
Figure 5.28: Evidence of Concrete Joint Deterioration in MnROAD Cells after 13 Years .....	268
Figure 5.29: Effect of Faulting on IRI, Which Affects OBSI .....	272
Figure 5.30: Sinc Wave of Sound Intensity Function in the Spatial/ Time Domain .....	274
Figure 5.31: Proval IRI Analysis - Power Spectral Density .....	274
Figure 5.32: Quarter Car Vibration Variables .....	276
Figure 5.33: An Exaggerated Warped Slab .....	277
Figure 5.34: Idealized Profile of Warped Slab .....	278
Figure 5.35: Analysis - Power Spectral Density for Uniformly Warped Panel .....	279
Figure 5.36: Faulting Vs IRI in Cell with 2008, 2011 Intervention after 1993 Construction .....	280
Figure 5.37: Faulting Vs IRI in Cell with 2008, 2011 Intervention after 1993 Construction .....	281

Figure 5.38: Faulting Vs IRI in Cell Ground in 2007 after 1993 Construction .....	282
Figure 5.39: Faulting Vs IRI in Cell Ground in 2007 after 1993 Construction .....	283
Figure 5.40: Faulting Vs IRI in Cell with 2008 Grinding after 1993 Construction .....	284
Figure 5.41: Faulting Vs IRI in Cell without Intervention Since 1993 Construction .....	285
Figure 5.42: Faulting Vs IRI in Cell with 2008 Intervention after 1993 Construction .....	286
Figure 5.43: Faulting Vs IRI in Cell with 2008 Intervention after 1993 Construction .....	287
Figure 5.44: Faulting Vs IRI in Cell with 2000 Intervention and 2013 Rehabilitation Including Grinding after 1993 Construction .....	288
Figure 5.45: Faulting Vs IRI in Cell without Intervention after 1993 Construction .....	289
Figure 5.46: Faulting Vs IRI in Cell with 2007 Grinding Strips on the outside Lane after 1993 Construction .....	290
Figure 5.47: Faulting Vs IRI in Cell without Intervention after 1993 Construction .....	291
Figure 5.48: Faulting Vs IRI in Cell with Pervious Overlay 2008, Grinding 2013 after 1993 Construction .....	292
Figure 5.49: Faulting Vs IRI in Cell with 2013 Intervention after 1993 Construction .....	293
Figure 5.50: Faulting Vs IRI in Cell with 2000 Intervention after 1993 Construction .....	294
Figure 5.51: Faulting Vs IRI in Cell with 2008 Intervention Following Culvert Study after 1993 Construction .....	295
Figure 5.52: Faulting Vs IRI in Cell with 2004 Intervention after 1993 Construction .....	296
Figure 5.53: Faulting Vs IRI in Cell with 2004 and 2013 Intervention after 1993 Construction .....	297
Figure 5.54: Faulting Vs IRI in Cell with 2004 and 2013 Intervention after 1993 Construction .....	298
Figure 5.55: Faulting Vs IRI in Cell with 2004 and 2013 Intervention after 1993 Construction .....	299
Figure 5.56: Faulting Vs IRI in Cell with 2004 and 2013 Intervention after 1993 Construction .....	300
Figure 5.57: Faulting Vs IRI in Cell with 2008 Pervious Intervention after 1993 Construction .....	301
Figure 5.58: Faulting Vs IRI in Cell with 2010 Composite Pavement Intervention after 1993 Construction .....	302
Figure 5.59: Faulting Vs IRI in Cell Original form Before Interventions .....	303
Figure 5.60: Faulting Vs IRI in Cell with Original Whitetopping cells Before 2011 Grinding .....	304
Figure 5.61: Faulting Vs IRI in Cell with 2008 Pervious Intervention after 1993 Construction .....	305
Figure 5.62: Validation of effect of Faulting on IRI .....	307

## Executive Summary

In pavement infrastructure, functional characteristics being generally preponderant over structural characteristics unequivocally govern pavement rehabilitation, maintenance and replacement decisions. Evidently, agencies invest in provision or restoration of friction (skid resistance) and make policies to minimize traffic noise. Most agencies accept (or reject) construction projects based mainly on initial ride quality. Other surface features such as faulting and cracking in addition to terminal ride quality are output parameters in all concrete design tools including PAVEMENT-ME and the Minnesota Department of Transportation's MnPAVE-RIGID software for concrete pavement design. Consequently, a study of these functional characteristics is indispensable to an overall investment in concrete pavement infrastructure. The objective of this study was to evaluate how new concrete surfaces performed over time with respect to friction, noise, texture, faulting and smoothness. This study began with construction of the various textures in the MnROAD facility to facilitate monitoring in a controlled environment. Subsequent monitoring was designed to produce initial data for analysis of the various surface characteristics and how they interact with one another. The study was also aimed at providing a time series or a simple performance model with respect to time and traffic for mean profile depth, smooth and ribbed tire friction, tire pavement interaction noise, acoustic impedance for various texture types. Additionally the study performed advanced analysis of pavement surface characteristics data garnered from the study.

In the original 1993 test cells at the MnROAD facility, the predominant texturing indicative of what was prevalent in the network at that time was the transversely tined texture. The original transversely tined cells that were still available through a major period of this study thus included low volume road cells 36-40, and Mainline cells 12, 96 and 97. In 2000, three cells (cells 6, 32 and 52) were drag-textured. Later in 2004 when some whitetopping cells 60-63 as well as the Taconite aggregate cell 54 were built, they were also textured with the turf drag. The need to study surface characteristics was identified as a major focus area for the phase 2 of MnROAD to improve pavements' ability to provide safe, quiet, smooth and durable surfaces.

New concrete surface textures built in 2008, 2010 and 2011 construction projects include:

- Pervious pavements. Two 7-inch pervious concrete pavements (cells 85 and 89 and a 4 – inch pervious overlay cell 39).
- Two longitudinal drag cells 13 and 14.
- Exposed aggregate texturing cell 72 in 2010.
- Longitudinal tined cell 6 pre-textured with longitudinal turf drag.
- Two transverse broom textured cell (Cells 5 and 53).
- Two longitudinal tine cell 6 + Cell 40 and cell 13 in 2013).
- Two transverse broom Cells 53 in 2008) and Cell 5 in 2011.
- Transverse tined cells were preponderant at MnROAD until 2008. Cells 36, 38 and 12 are still Transverse tined.

The study performed five major tasks:

Task 1: State of the Practice (in Concrete Pavement Surface Characteristics)



This task examined the current “state-of -the –art” based on completed research and publications in surface characteristics. It discussed various theories behind surface variables. It discussed research work done on mean profile depth, friction and tire pavement noise as well as ride accentuating contact geometry and how these affect the surface variables. This led to the development of the work plan for the remaining tasks.

#### Task 2: Test Sections Constructed in 2008, 2010 and 2011

This task elucidated specifications for the various textures constructed in 2008, 2010 and 2011 at the MnROAD research facility and created a construction / texturing report for the textures created in the test cells. The various texture patterns intended to facilitate the search towards optimum texturing for adequate skid resistance, pavement quietness and minimal ride quality impact. The study monitored the resulting textures

#### Task 3: Development and Validation of a Sound Absorption Measurement Process

Originally, this study, as many others, expected sound absorption to be the major mechanism of pavement quietness. Analysis in this study rejected the hypothesis. Testing revealed insignificant variation in sound absorption coefficient in non-pervious concrete and significant variation in pervious concrete pavements. It also showed poor correlation of sound absorption to On-Board-Sound-Intensity (OBSI) measurements. It validated the hypothesis that pavement quietness relates more to how the textures facilitate air compression relief and minimize tire-tread- block impact in pavement interaction.

#### Task 4: Annual Monitoring, Time Series Analysis and Statistical Representation

This task determined a time -series prediction model (without de-trending) for each texture type. Some of the surface characteristic data were arranged in a quasi-normal distribution that showed a reasonable statistical prediction of the degree of quietness of each texture type with respect to the other. Evidently, most surface characteristics especially OBSI and International Roughness Index (IRI) were in a time series. For example in a transverse tined cell (cell 36) the OBSI time series was of the form:

$$Y_{(t)} = \mu + Y_{t-1} + \phi_1 (Y_{t-1} - Y_{t-2}) + \phi_2 (Y_{t-2} - Y_{t-3})$$

Where  $\mu = 0.563$ ,  $\phi_1 = 0.180$   $\phi_2 = 0.413$

This time-series prediction-model successfully represented and validated the seasonality as well as the degradation trends. Transformation of the surface characteristics data into a probability density function accentuated the quietness of various surfaces textures statistically. A quasi probability density function shows that a drag texture has 7% probability of being quieter than 100 dBA while a transverse drag has only 1% of being quieter than 100 dBA. However, some engineered textures in the plot showed a 75% probability of being quieter than 100 dBA.

#### Task 5: Advanced Data Analysis:

This task performed major advanced analyses.

**Effect of Texture Direction and Texture Orientation:** The Mann Whitney Wilcoxon method showed to a 95% confidence level that, there was a clear difference between the OBSI data set for transversely textured pavements and longitudinally textured pavements. This lent credence to

the hypothesis that texture direction would affect tire pavement noise. Texture direction did not seem to affect IRI significantly. However, certain longitudinal textures exhibited anomalous IRI with non-continuous (single or triple) lasers.

**Laser Induced Anomalies in Ride Measurements:** This task compared IRI measured with a triple laser and line laser, most of the new textures did not show significant disparity of IRI in the two lasers except the longitudinal tine. The problem of laser induced anomalies is also prevalent in the ground textures which are outside the purview of this study.

**Analysis of Investment in Surface Characteristics:** Benefit-cost analysis of investment in quiet pavements was performed. The probability that each surface would be quieter than 100 dBA was applied to the benefit to give an adjusted benefit/cost ratio. Two ratios were computed from two scenarios: replacing a drag texture and replacing a transverse tined texture. It showed that investment in quiet surfaces may be cost saving if the standard initial 10 dBA reduction expected from noise wall construction is not required.

**Development of Friction Survival Model with MnROAD Concrete Surface Textures:** This study developed a friction-survival model for ribbed and smooth tire friction of the MnROAD textures. The model retained typical initial Friction Number values as initial values of the model and showed decays that were indicative of the durability of texture types in providing skid resistance. This model was successfully validated in the Minnesota network with their actual traffic volumes. It applies to both the smooth and ribbed tire as shown below where F is the friction, k is the growth rate, t is the age of the concrete in years, DE is the number of Estimated Standard Axle Loads (ESALs) calculated for design year and FE represents the twentieth year projected ESALs

Ribbed

$$F = 22.01 \sin(kt) + 29.21 \cos(kt)[1 + e^{-0.1t}]$$

Mainline Smooth

$$F = \left[ \left( \frac{801000}{DE} \right) \left( \frac{FE}{DE} \right) \right] [\sin(kt) + 18.36 \cos(kt) [1 + e^{-0.8t}]]$$

Low Volume Road (Smooth)

$$F = -4.56 \sin(kt) + 15.56 \cos(kt) [1 + e^{0.031t}]$$

**Analysis of Relationship between Pavement Condition and Pavement Acoustics:** This subsection developed a set of equations that showed that the acoustic signal from a deteriorated joint is different from that of a deteriorated joint. It also validated this lemma through the analysis of data and showed that there was a correlation between OBSI and IRI. This important observation forms the basis for the development of acoustic monitors for pavement condition.

This study shows that there is a correlation between near-field and far-field noise reduction. The concept furnished a strategy to evaluate the economic benefit of quiet pavements. From the methods used and the surfaces evaluated, the Ultimate Grind (A rehabilitated surface modification through diamond grinding) and pervious concrete appear to be the two surfaces that are cost effective based on either transverse tine or drag-pre-textured longitudinal tine textures.

When transverse tined surfaces are rehabilitated, then the innovative grind, the 4.75 mm asphalt aggregate surface, as well as new SuperPave asphalt surface appear to be relatively cost-effective based on the criteria used. The Friction degradation formula developed in this study was improved and validated in the network. This formula facilitates prediction of frictional adequacy during traffic-based texture selection.

Above all this study provided useful information on pavement functional requirements: ride, friction, texture, tire pavement noise, sound absorption, isotropy or direction and mathematical variables such as texture orientation. These useful tools facilitate pavement infrastructure planning particularly because most rehabilitation projects will likely occur not for want of structural sufficiency but for want of functional reliability. Most new concrete textures exhibited texture-degradation patterns that are very rapid within the first one to two years. The residual texture thereafter was a function of mix design and texture configuration. The degradation of exposed aggregate is so rapid that texture orientation changes even from positive to negative and vice versa in consecutive years.

Modification of an impedance tube for in-situ sound absorption measurements in this study showed that both pervious and non-pervious pavements mainly reduce noise by tread block impact relief and air compression relief instead of absorption. Most non-pervious absorption coefficients are within 0.02 to 0.04 while pervious coefficients range from 0.15 to 0.8 yet some non-pervious textures are 50% of the time quieter than pervious concrete. After the cell-construction, turf drag was occasionally as quiet as the conventional grind but the former seldom exhibited comparable skid resistance.

The surface types were scored according to the criteria of Noise (OBSI), Texture Durability, Skid Resistance, Hydroplaning Resistance, (Point Laser Effect), IRI Line Laser Induced Anomaly, Economics, Splash & Spray, Current Acceptance, with a score of 0 to 5 where 5 represents excellent performance on a criterion was summed to obtain a composite score. Ranking in the order of excellence (from best to worst) included Longitudinal Tine, Longitudinal Drag, Transverse Tine with Drag Pre-texture, Transverse Drag, Pervious Concrete, Exposed Aggregate, Roller Compacted concrete surface. Contrary to European experience, exposed aggregate surface was not quiet and within the first few months of service, it exhibited remarkable changes in texture orientation. Sufficient skid resistance is achievable with any of the texturing type by adjusting the actual configuration. In most of the surface properties, ensemble averages did not amount to the sum of the annual averages. This lack of ergodicity indicated that there might be other cycles such as daily or monthly cycles in the time series. Built-in-warp and curl as well as diurnal warp and curl swings introduced time series fluctuations to most functional characteristics.

This study concludes that most texture types can be optimized for performance. There is no frictional advantage of using the quicker-draining but noisier transverse drag. It was found tenable to describe surface characteristics data trends either by use of time series or a probabilistic approach as well as fragmentation of frequency related content. Frequency content fragmentation in OBSI, adhesion and hysteresis in friction and wavelength features in ride measurements are the proven examples. Most quiet pavements proved cost-effective with prorated decibel savings when 10 decibel reduction is not necessarily required. Above all this study

provided useful information on pavement functional requirements: ride, friction, texture, tire pavement noise, sound absorption, isotropy or direction and mathematical variables such as texture orientation. These useful tools facilitate pavement infrastructure planning particularly because most rehabilitation projects will likely occur not for want of structural sufficiency but for want of functional reliability.

This research provides a summary of performance of the various textures with scores for the various performance measures. Along with the use of the longitudinal turf drag, there may be occasional benefit in using the drag as pre-texture and longitudinal tine as texturing. Pre-textured longitudinal tine appears to provide more friction and texture durability than the currently specified drag textures. This study lends itself to spontaneous implementation. Apart from providing a logical strategy choosing texture types, it described and validated their intrinsic and obvious benefits. Due to built-in warp and curl as well as seasonal and diurnal swings, it may be beneficial to perform diamond grinding as a preventative maintenance in the tenth year of the sixty-year design and shift the first rehabilitation from the seventeenth year to the twenty second year. This will reduce built-in warp and curl, minimize pavement dynamics, improve pavement performance, reduce IRI and increase reliability. Analysis suggested that an acoustic monitoring device is feasible. Study recommends prototype design particularly of a concrete joint monitoring tool

# Chapter 1: Introduction & State of the Practice

## 1.1 Fundamentals of the Pavement Surface

The challenge to provide safe, smooth riding and quiet pavements necessitates knowledge of the variables that influence these qualities. In order to build pavements that meet these needs, we must deepen the understanding of what affects pavement surface characteristics, how they change over time,

### 1.1.1 Surface Texture

When concrete pavements are built, the surface is originally finished with an automated pan finisher that is part of the paving equipment. Although it is a sub-standard practice, areas of spot defects are usually manually finished and bull floated or struck off. A surface texture to provide the necessary friction for safety is added through one of many methods. The surfaces are described generally by the texturing methods, how comfortable it is to ride on them and how noisy they are. The basic construction texturing methods [1.2] include drag finishing, tining and exposed aggregate. In the drag techniques, a work bridge consisting of a uniformly loaded inverted burlap turf or broom is dragged behind the concrete paver. The surfaces formed are the burlap dragged, turf dragged or the broom dragged surface. They are generally referred to as the hessian drag finish in their similitude to the burlap or cloth (hessian  $\approx$  pertaining to a cloth) [1.2] [1.3]. While the bridge is dragged along and behind the paver, the uniformly loaded burlap broom or turf may alternately be manually swept across the pavement, thus creating a transverse broom or turf surface. Similarly, a rake may be dragged along with the paver to impart a longitudinal tining or while the bridge advances to each convenient spot, the rake is manually dragged across the plastic surface to impart the transverse tine configuration. Although most agencies specify an initial texture configuration comprising of one or a combination of any two described above, some states require that the surface should be diamond ground immediately after the pavement is cured. The standard and most common process of texturing a concrete surface when it is hardened is the diamond grinding process. Diamond grinding which is done as a rehab involves the removal of a small quantity of the surface pass by the impartation of a required configuration on the surface with a rotating drum fitted with diamond cutting tools and spacers. The various types of grinding configuration form part of what this study contributed in part. By adjusting the blade and spacers, specified configurations are imparted on the pavement surface. The pavement texture is usually described according to the finish type which refers mainly to the surface configuration within the macro and micro texture range that characterize the surface. ASTM E 965 [1.4] discussed the sand volumetric method of texture evaluation. In this method, a known volume of glass beads of particle size ranging from 150 micrometers to 250 micrometers is spread to a maximum area over a textured surface. The average depth of spread is the calculated estimated texture depth (ETD). Since this method is cumbersome, a laser equipped device the circular track meter (CTM) ASTM E-2157 [1.5] was used. This device is equipped with a radial arm that sweeps a line laser across the textured surface and returns a mean profile depth [MPD]. Rasmussen et al [1.6] examined what texture features may affect other surface characteristics. Rasmussen et al [1.6] showed how the categorization influences various surface characteristics [1.6]. FIGURE 1.1 also shows the general effect of various texture ranges on surface characteristics. The PIARC classification suggests that a texture wavelength range of 1-mm to 200-mm wavelength will affect tire pavement noise. However the wavelengths typically found in surface finish of concrete pavements typically range from 0.5-mm to 25-mm and thus

fall within the PIARC range. Above this range, surface features are general construction or distress induced waveforms that affect other surface characteristics especially pavement roughness (IRI).

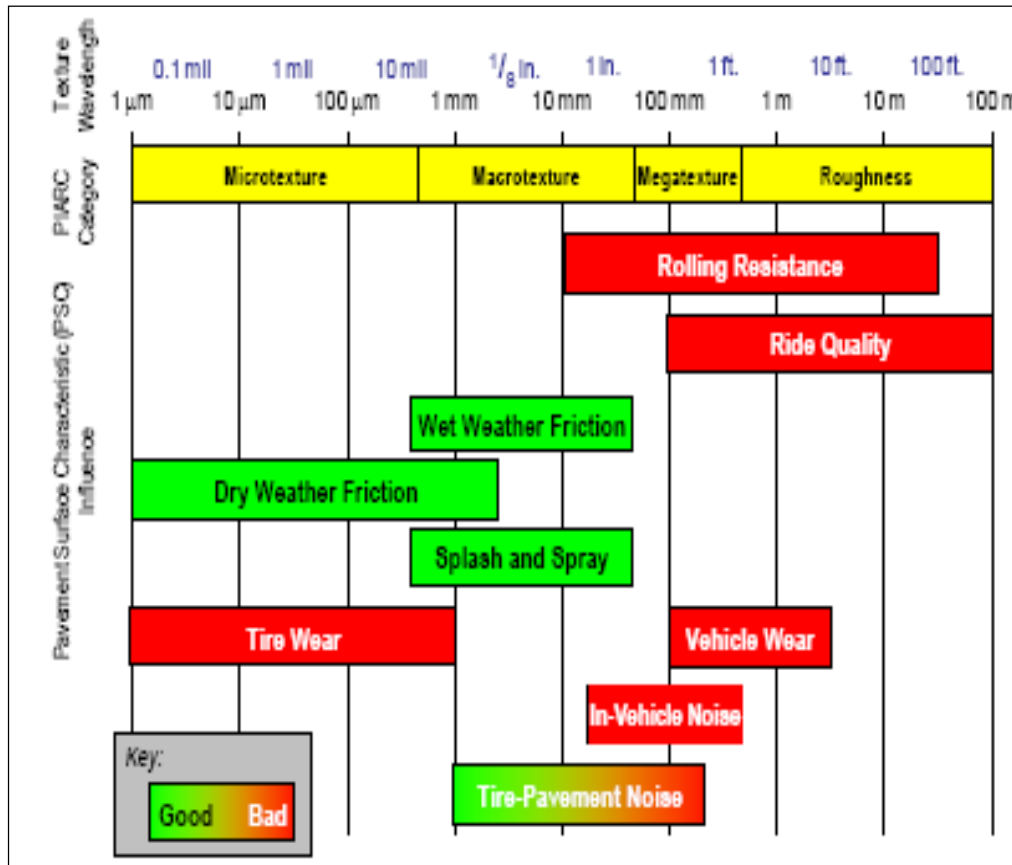


Figure 1.1: PIARC Classification of Texture in Wavelength Form and Usage [1.6]

Wayson [1.7] and The World Roads Congress (PIARC) categorized texture according to wavelength. In this categorization, texture wavelengths ranging from 1-μm to 0.5-mm is referred to as micro-texture. Wavelengths from 0.5-mm to 50-mm is referred to as macro-texture and 50-mm to 500 mm is regarded as mega-texture. Wavelength ranging from 500-mm to 100-m is classified as pavement roughness.

### 1.2 Pavement Smoothness (International Roughness Index, IRI)

A primary feature of a pavement surface is how comfortable it feels to ride on it. One of the greatest expectations of road users is that the pavement should provide ride comfort [1.1] [1.2]. There has also been some evidence not validated but indicative of the influence of ride quality on pavement noise [1.8]. When vehicles ride on pavements there are larger wavelengths that characterize how smoothly the pavement rides. Ride smoothness is affected by joints, warp or curl phenomena, faulting, pavement distress, rocking panels, load transfer devices or pavement surface distresses. Vehicular suspension systems also affect the degree to which different vehicles respond to the same pavement. In consequence, pavement smoothness was standardized

to two main indices known as the ride number (RN) and international roughness index (IRI) governed by standard suspensions of the standard car.

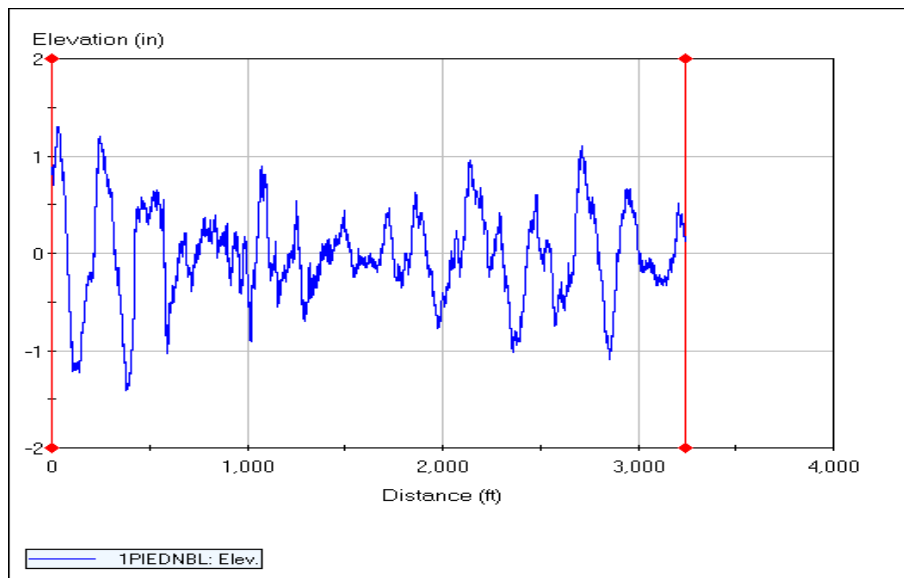
International roughness index is the internationally accepted measure for pavement smoothness or ride quality [1.9], [1.10] simply defined as the average deviation from an assumed plane of the response of the quarter car to a given pavement surface. It is a statistic that summarizes the roughness qualities impacting vehicle response based on the golden-car quarter car response at a standard simulation speed of 49.7 mph (80 km/h) [1.11]. The international roughness index is spectrally the average rectified value of the slope power spectrum density (PSD) of a pavement profilogram [1.12]. International roughness is measured by any of the various inertial devices including the light weight profiler (Figure 1.2) that was used in this experiment. In a single ride measurement, the output is a profilogram, a ride summary (Figure 1.3). A PSD plot is also available for the detection of causative wavelengths.

Certain features inherent in the pavement are construction related. These include design features such as joint interval, joint width and load-transfer devices as well as performance and response features such as built-in warp and curl, diurnal warp and curl, joint faulting and joint slap. Most of the features are related to either how the pavement was constructed or how it is performing. By distinction, construction and design related features include joint interval, joint thickness and load transfer devices. Even the pavement design thickness is included in the litany of design features. Performance features are joint faulting, warp curl or even rocking panels. Certain features inherent in the pavement are construction related. These include design features such as joint interval, joint width and load-transfer devices as well as performance and response features such as built-in warp and curl, diurnal warp and curl, joint faulting and joint slap. Most of the features are related to either how the pavement was constructed or how it is performing. By distinction, construction and design related features include joint interval, joint thickness and load transfer devices. Even the pavement design thickness is included in the litany of design features. Performance features are joint faulting, warp curl or even rocking panels.

Joint opening may also be a performance item if it has increased due to joint deterioration, spalling or panel movement. Design and construction features induce various degrees of disturbance to vehicles. These disturbances are translated mainly through body bounce and axle hop and joint slap to noise in various ways. Body bounce impact is of low frequency while the axle hop is at higher frequency (see Figure 1.5). However joint slap occurs with sealed and unsealed joints but the noise is higher when the joints are unsealed or the seals are broken. Existing Studies showed that larger joint opening [1.13] resulted in higher noise.

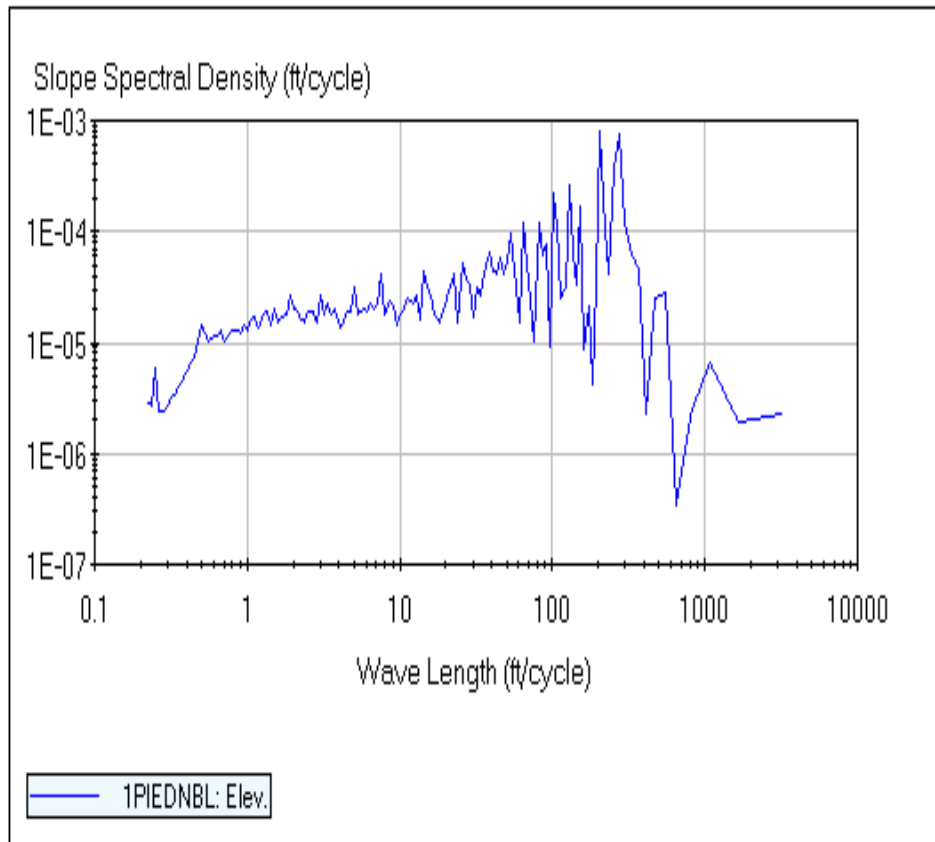


**Figure 1.2: Light weight Profiler**



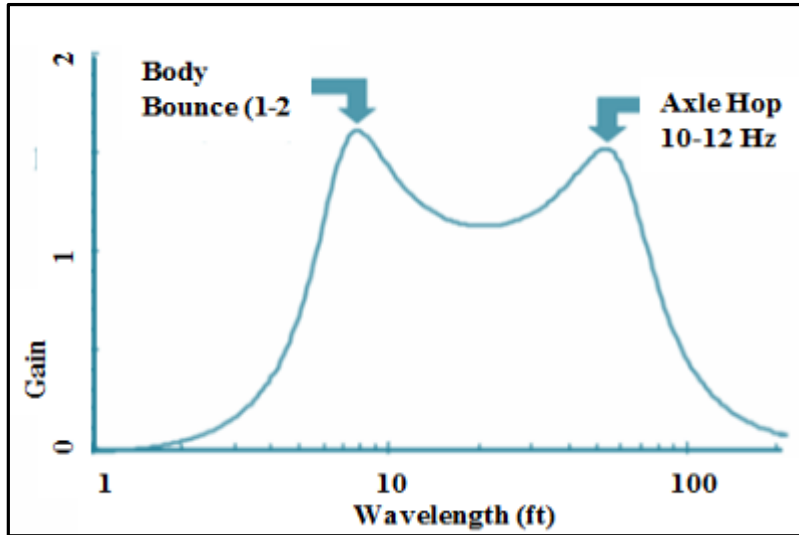
**Figure 1.3: Profiling of a Surface**





**Figure 1.4: PSD - Inertial Profiler IRI Response and PSD Response**

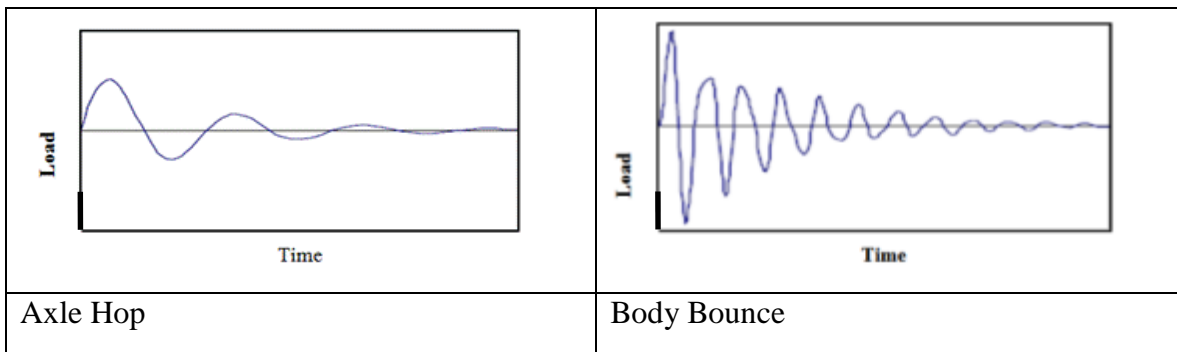
According to Sayer et al [1.10] the dynamic loads imposed by heavy vehicles on roads occur at two distinct frequencies. These are the body bounce and axle hop frequencies. The body bounce frequency is associated with the sprung mass of the vehicle (approximately 90 per cent of the total mass of a loaded vehicle) while the axle hop is associated with the un-sprung mass of the vehicle. The typical body bounce frequency is between 2 and 3 Hz, while the typical axle hop frequency is between 13 and 18 Hz. The body bounce frequency translates to peak loads at intervals of between 2.7 and 3.7 Hz for a vehicle running at 40 km/h (11.1 m/s). This would thus also coincide with the distress features observed on the road.



**Figure 1.5: Wavelengths Where Body Bounce and Axle Hop are Prominent.**

**Mechanism of Ride Effects**

The phenomena of vehicle dynamics due to surface unevenness have been discussed [1.9] and the effects analyzed [1.14] and [1.15]. It is convenient to discuss two major scenarios: body bounce and axle hop. Lower frequency responses (1.5 to 4 Hz) occur with body motions of a vehicle, where the vehicle’s body (sprung mass) bounces, or pitches and rolls, in relation to the vehicle’s tires (unsprung mass) and the pavement surface. Macro and micro texture effects have also been analyzed by others including Newland [1.14] and Donovan [1.15]



**Figure 1.6: Body Bounce and Axle Hop Response**

In the investigation of joint slap Donovan indicated that whether a joint is sealed or not will determine the joint slap and noise. This is a classic case of ride issues caused by joints being associated with noise sources. Joint slap is problematic when there is fast moving traffic in many adjacent lanes of traffic and the event of tire and joint encounter becomes frequent and somewhat continuous. The effect of a deteriorated joint on noise is discussed in Chapter 5. The impact in an acoustic media is impulsive and the result is transient but lasting longer than the time of impact.

### 1.2.1 Geometric Surface Features Joints, Curl & Warp, and Faulting Features

It has been asserted that IRI is a proxy for major distress features including warp, curl and joint faulting [1.16]. To illustrate this, an example of a faulted pavement is presented. Presently it will be proven that increase in severity and increase infrequency of faulting each causes increase in IRI by using FHWA PROVAL program [1.13].

Consider a continuum of faulted panels. We assume the panels to be rigid and faulting to be panel rotation that causes a vertical movement at the joint. Let the degree of that movement be unity. The profile can be described as a saw tooth model  $Y = R \text{ Frac } y/x$  where x is referenced at 0 at the leave slab joint and L (15 ft.) and max 1 inch at the approach slab joint. Y is referenced to the horizontal plane where a faulting of 1 inch implies that the 15 ft. panel lies at an angle of  $\tan^{-1} \frac{1}{180}$ . Figure 1.7a and 7b show the saw tooth surface feature and the PSD.

$$\text{IRI (Faulting Induced)} = \text{IRI(Max)} * \sum_{i=1}^N \frac{F_i}{F_{max}} \frac{n_i}{N} \quad (\text{Equation 1.1})$$

where

N is number of panels,

n represents the number of faulted panels in the range,

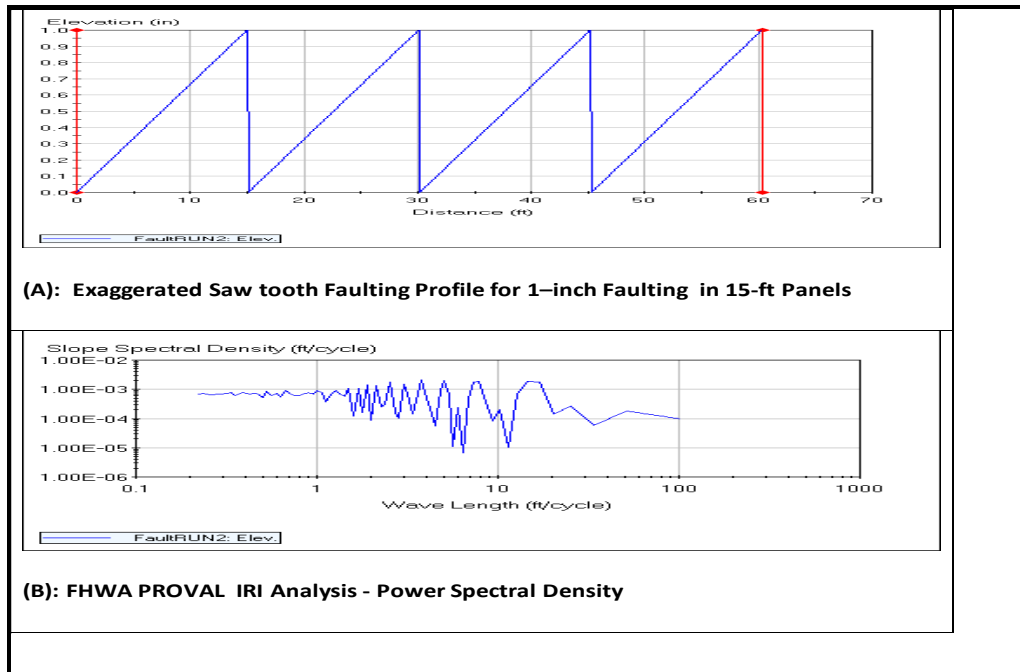
F is the warp in mm,

Fmax is the maximum faulting mm,

$\frac{F_i}{F_{max}}$  = ratio of the fault to 1 inch,

$\frac{n_i}{N}$  is the number of panels in the faulting range.

This is applicable to a situation where various degrees of faulting occurs throughout the test sections and a reasonable bar chart represents ranges of faulting whose mean is represented by IRI<sub>(Max)</sub> is the IRI obtained when all the 15 ft. panels are faulted to 1 inch. IRI<sub>(Faulting Induced)</sub> is the dependent variable. IRI<sub>(Max)</sub> may be obtained for other panel lengths if they are not 15-ft. PROVAL [1.13] showed the max IRI to be 440 in/mile. It computed IRI at 220 in/mile when 1/2 the panels were faulted to 1 inch. It was 110 inches /mile when half the panels were faulted to 1/2 inch. This example suggests proportionate increase in IRI due to increase in severity and frequency of occurrence since IRI is proportionately a proxy for distress frequency and severity. Therefore if IRI increases with degree of faulting and frequency of joint, the noise arising from the joints, due to faulting and slapping can be expected to increase. At the minimum, the concatenations when the tire interacts with joints are higher when the joints are more deteriorated and are more frequent when the joints are at smaller interval.



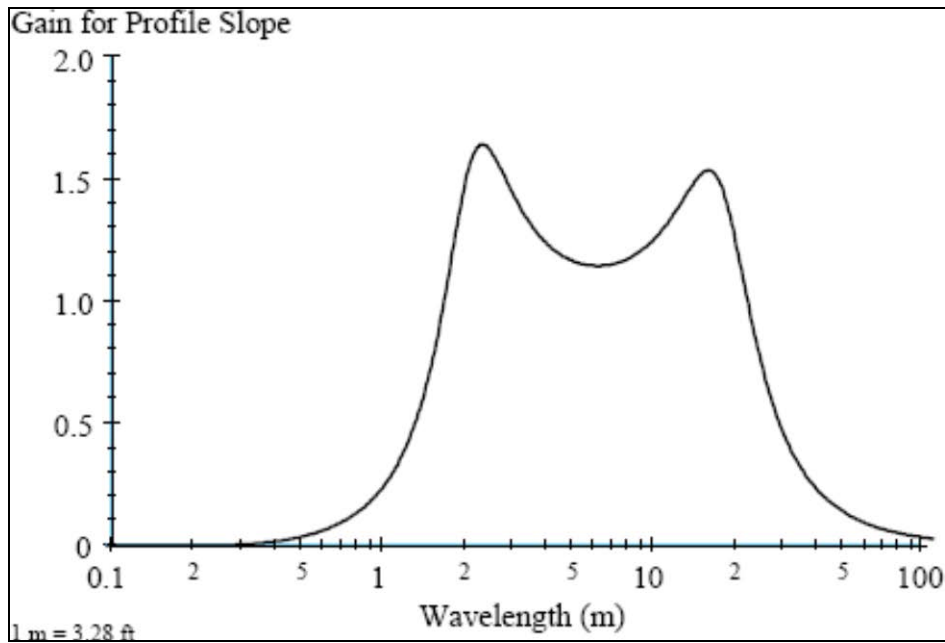
**Figure 1.7: ProVAL Output for IRI of a 1-inch Faulted Pavement**

### **1.2.2 Quantification of IRI as a Proxy for Larger Scale Texture Effects**

From the foregoing, it is logical to deduce that the larger scale (mega texture and gigatexture) pavement features can be seen as subsets of a quantity that evaluates pavement roughness. International roughness is a proxy for pavement roughness [1.15]. IRI is based on the vertical response of the suspension of the quarter car normalized to a speed of 50 miles per hour, riding over the pavement surface. The unit (m/Km) or inches per mile superficially indicates unevenness (mega texture and gigatexture) per unit length. IRI is summarily a measure of pavement smoothness or ride quality based on the response of the quarter car. This single number is also viewed as the accumulation of the vertical displacement of a standard car per unit horizontal distance travelled with reference to an assumed neutral plane [1.9], [1.10]

This subsection explains physically why internal roughness index may result in changes in sound intensity. This is explained in terms of degree of faulting of faulted joints and joint intervals providing frequency and severity of concatenations that occur when the tire rides over the joints.

International roughness index is a standard measurement of pavement smoothness. Various vehicles respond to various surface profiles according to their natural frequencies, their sprung masses, spring constants and dashpot constants. Preliminary research indicates that rougher pavements may be noisier than smoother pavements. The international roughness index is a standard measure of ride quality. This measurement is only as good as the degree to which the equipment or ride algorithm responds to the preponderant frequencies in the pavement surface. The response multiplier algorithm in Figure 1.8 is expected to mimic human response to the corresponding frequencies.



**Figure 1.8: IRI Multiplier Algorithm**

The International Roughness Index is designed to be more sensitive to certain frequencies than others in order to represent how the rider feels. In addition to amplified response of the quarter car to certain frequencies, errors resulting from any deviation from the smooth profile are only predictable to the degree of response of the quarter car algorithm to that profile. The international roughness index has been defined [1.10] as the average rectified value (ARV) [1.10] of the slope power spectrum density of the profilogram. The IRI was defined as a mathematical property of a two-dimensional road profile (a longitudinal slice of the road showing “elevation” as it varies with longitudinal distance along a travelled track on the road). The elevation which is shown on a profilogram is the interpreted elevation based on the quarter car suspension parameters at a 50 mile-per-hour simulated speed. As such, IRI can be calculated from profiles obtained with any valid measurement method, equipped with the smoothness measurement accelerometer.

The IRI algorithm is therefore subject to the resonant frequency of the quarter car and provides different multipliers for different frequencies to mimic the human comfort level. In consequence, certain dominant frequencies have much more effects than others in tactile and in sonic spectra. Wilde, Izevbehai and Krause [1.17] showed that for 15 foot joints, the IRI algorithm is more sensitive than the RN algorithm and conversely for the 25 foot string line spacing. IRI has been shown to correlate very well with the subjective rating of users (PSR) and is a function of the pavement distresses. Khazanovich et al [1.16] described the development of the distress model for IRI of the jointed plain concrete pavement as a function of the joint-faulting, spalling and transverse cracking is described. Yu et al showed IRI to be an agglomeration of numerous roughness sources such as faulting and joint interval. Each sub variable is considered its respective influence on IRI will be evident. Consider faulting of joints. When a tire rides over a faulted joint there is a tactile as well as a sonic effect. When faulting or any other distress type is more severe, there is a corresponding increase in the severity of the noise One of the causative and analyzable factors is joints which occur at known intervals. An example of a 15 ft joint interval with a faulting of 1inch on each panel is analyzed.

To investigate the impact of surface roughness on Sound pressure Whitehouse [1.18] defines surface roughness as follows;  
 According to Stoimenov et al, [1.19] the sound pressure level change  $\Delta\text{SPL}$  due to a change in surface roughness is

$$\left(\frac{R_{z2}}{R_{z1}}\right) = \left(\frac{IRI_2}{IRI_1}\right) \text{ generally}$$

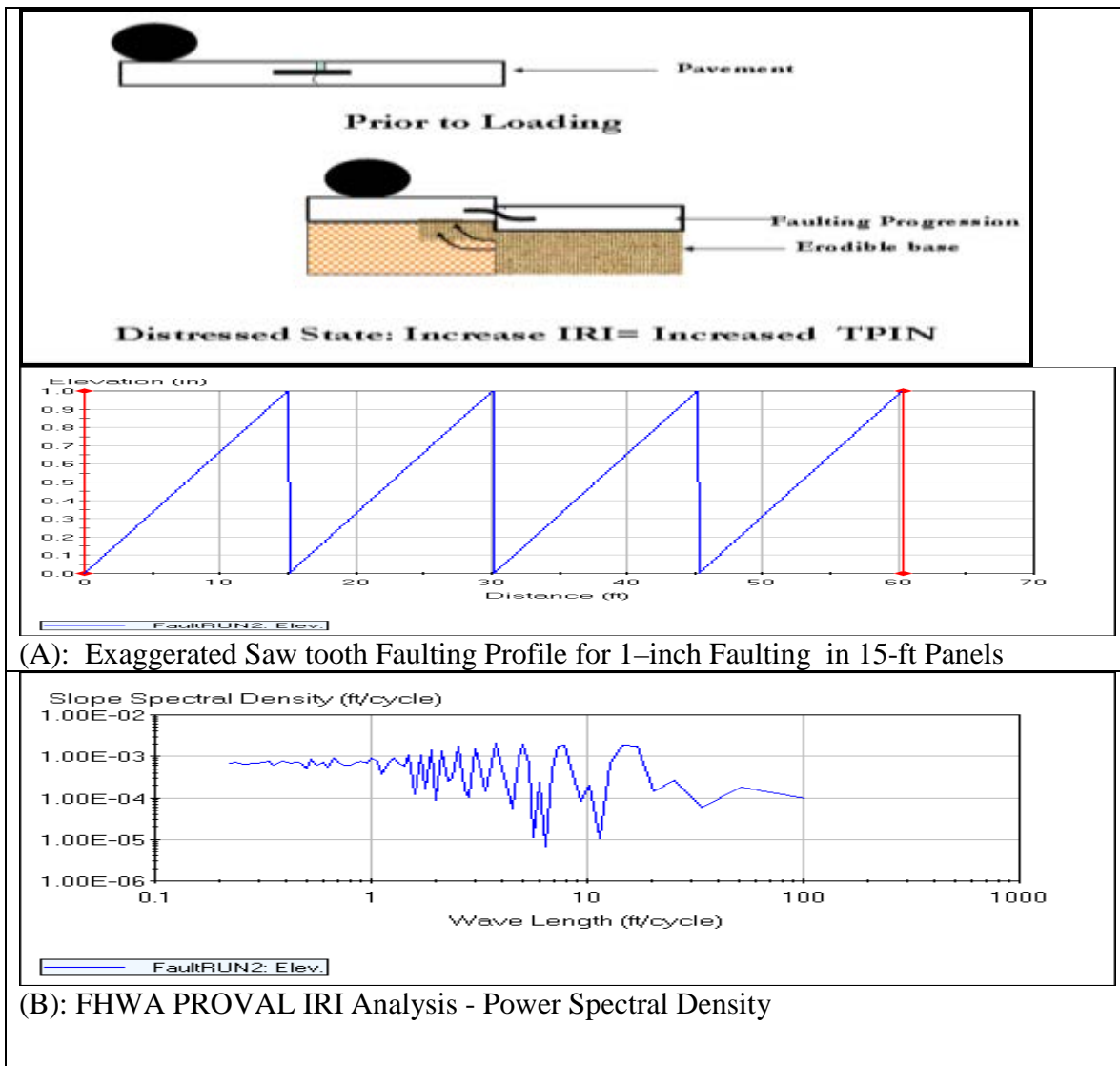
$$\Delta\text{SPL} = 20\log_{10} \left(\frac{R_{z2}}{R_{z1}}\right)^m = 20 \log_{10} \left(\frac{IRI_2}{IRI_1}\right)^m \text{ dB} \quad (\text{Equation 1.2})$$

This example is limited by the fact that actual noise calculated was not OBSI but was sound pressure. Sound pressure level is directly correlated to sound intensity level when correct pressure and sound intensity references are done. The difference may be due to environmental effects. It is sufficient then Substituting, Takahashi [1.20] assigns  $m = 0.8$  for a hemispherical shape on a flat surface. A change of IRI from 1 m /km to 2 m/km is typical after 15-20 years of good performing pavements moderately maintained and subjected to freeway traffic volume of 50000-AADT with truck traffic of 1800.

$$\Delta\text{SPL} \cong \Delta \text{SIL} = 20 \log_{10} \left(\frac{2}{1}\right)^{0.8} \text{ dB} = 4.81 \text{ dB} \quad (\text{Equation 1.3})$$

where

SPL and SIL are sound pressure levels and sound intensity levels respectively. The above equation shows that an increase in IRI results in an increase in OBSI. The above example shows that if the ride quality of pavement deteriorates from 62.5 inches per mile to 125 inches/mile, there may be a change of 4.8 dBA in the noise levels all things being equal. This is a simplified relationship however, based on the foreknowledge that the IRI multiplier algorithm is non-uniform in all frequencies. Nevertheless it shows that OBSI will increase with increase in IRI by derivation of simple equations and through the use of FHWA PROVAL program to analyze ideal profilograms, it is evident that higher IRI may result in higher sound intensity for each source type. The equations show that increase in the magnitude of factors causative to IRI predict increase in IRI and in consequence may predict OBSI increase. It is conceivable and probably tenable that poorly riding roads are not only bumpy in the tactile domain but also in the sonic domain. Starting variables for a stepwise statistical model will thus include IRI.

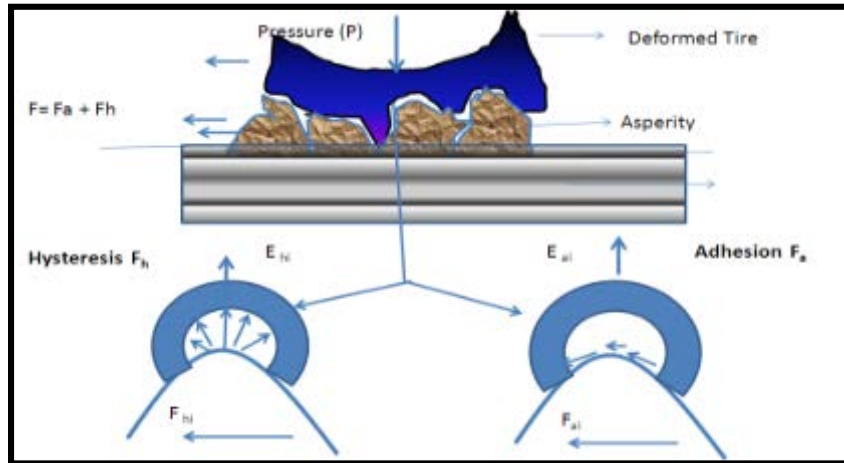


**Figure 1.9: PROVAL Output for IRI of a 1-inch Faulted Pavement**

### 1.3 Fragmentation & Survival of Friction

#### 1.3.1 Hysteresis and Adhesion

According to Wu and Nagi [1.21], tire pavement forces are categorized into hysteresis and adhesion. It was postulated that the development and relief mechanism of these forces are related to tire pavement noise. Wu and Nagi show the free body diagram of a continuum of asperities enveloped by a collapsed portion of a tire. The tire deforms over the asperities and follows the surface configuration in an ideal situation. Energy dissipation occurs from the tire collapse but restoration does not happen as quickly as the deformation. This phenomenon is hysteretic and results in the effect of negative pressures in the interaction. Breakage of the suction pressures due to negative pressures result in “stick and snap” noise due to a pressure distribution described by Clapp et al [1.23] results in noise generation. As the tire moves, tangential forces, bearing forces and suction forces are developed between the tire and the asperities.



**Figure 1.10: Hysteresis and Adhesion Forces in TPIN**

Given the free body diagram above, if  $A$  is actual contact area,  $Q$  is volume of finite deformed rubber element,  $A_n$  is nominal Area,  $S$  = Interface shear strength  
 $D$ = Energy dissipated per unit volume;  $P$  = pressure of the rubber block,  $b$  is rubber sliding distance and  $w$  is normal load, it can be shown [1.22] that

Adhesion coefficient

$$f_a = \frac{A}{A_n} \frac{s}{p} = \frac{F_a}{w} \quad (\text{Equation 1.4})$$

This relationship has been useful heretofore in the computation of frictional forces. By calculating acoustic source strength some of the sound energy due to pavement contact can be determined. The Wu and Nagi model [1.21] suggest that texture orientation is an important tire pavement noise predictor. By keeping the deformed tire volume and deformation energy constant the hysteresis component can be normalized into

$$Hn = \frac{Q}{A_n} \quad (\text{Equation 1.5})$$

where

$A_n$  is projected area. In most positive textures this quantity is much smaller than in negative textures. Hysteresis forces are therefore higher and in consequence, noise level should be higher with positive texture.

Clapp et al [1.22] developed a model that predicts contact pressure. This model idealizes the contact as an elastic half mass on a continuum of asperities and develops a contact pressure distribution. In the development of the model, an indenter in contact with the tire carcass is analyzed. The mathematical process is based on the theory of elasticity. Based on the Clapp model, higher indentation pressures lead to higher sound intensity level.

A process for categorizing texture orientation has been demonstrated. However, a mathematical relationship between texture orientation and sound intensity was not feasible at this time. It has been shown from references that the texture orientation may have influence on tire pavement interaction noise. From free body diagrams and envelopment theories, it is likely that upwardly



spiked textures (positive textures) will be noisier than negative textures. Texture orientation will be included in the starting variables of a stepwise regression analysis towards a statistical prediction model of sound intensity level. According to Wu and Nagi [1.21], tire pavement forces are categorized into hysteresis and adhesion. It was postulated that the development and relief mechanism of these forces are related to tire pavement noise. Hysteresis is that component of tire-pavement friction that does not significantly depend on aggregate asperities micro-texture or macro-texture but on the suction forces between the surfaces in contact. This condition is formed when energy is dissipated in the instantaneous deformation of the tire over a contact patch and the rarefaction of the deformed part over the same patch. The effective contact area is reduced when texture degradation occurs.

Suhbi and Reza [1.23] investigated the effects of temperature and surface texture on the friction force developed at the tire-pavement interface during skidding. Ten field sites representing a variety of asphalt pavements in the State of Ohio were selected for the study. Five laboratory briquettes made from the same materials used in the construction of the pavements were prepared for each of the sites. Skid resistance measurements were performed on the briquettes using a portable British pendulum tester. The friction force was considered to consist of two parts, namely, the wet adhesion and the hysteresis components. The adhesion and hysteresis components were measured separately using water and liquid hand soap as lubricants. To simulate the changes due to wear and aging of pavements, several cycles of mechanical polishing were conducted and the available contact area after polishing was determined using a digital image processing technique. Tests were conducted at five different temperatures. The hysteresis component of friction decreased with increasing temperature regardless of surface texture state. The adhesion component was more sensitive to surface texture effects. Hysteresis was found to account for the larger part of the total friction force. Combined friction decreased with increasing temperature on a polished surface; hence it is recommended that skid numbers obtained at any arbitrary temperature be normalized with respect to a value at a reference temperature, for example, 293 K (68°F).

An Australian study [1.24] of the effect of surface texture on stopping distance gave interesting results. The target initial speeds were adequately maintained throughout the experiment. Braking performance appeared to show little variability in relation to the main effects of speed, site and conditions being manipulated in the study, as shown by the results of the main ANOVA, and the subsequent ANOVAs carried out for each speed. Speed had a much greater impact on stopping distance than the other variables. Site and Condition both had a significant effect. Apart from the effect of speed, the only effect that was large enough to have practical significance was the interaction of site, speed and condition. In wet conditions, at higher speeds, stopping distances were noticeably greater at the site that had low skid resistance as measured by the British pendulum tester. There was less variation in the mean deceleration than in the stopping distance as it is limited by physical factors and applies for longer periods at higher speeds. However, lower deceleration was evident on trials with a longer stopping distance. Izevbekhai and Watson [1.25] evaluated wet weather accidents and crash rates in identified test sections where current texturing practices had replaced previous textures. Using descriptive statistics, Mann-Whitney-Wilcoxon and Chi-Square before and after comparison, the authors (2008) concluded that to a 95 percent confidence level, the current texturing practices did not cause increase in wet weather accidents and crash rates. A detailed study report by Izevbekhai, and Watson [1.25] accentuated

the individual test section data and statistical analysis in great detail. Hanson et al [1.26] and found correlation between asphalt texture depth and noise using the CPX noise measurement system. That correlation was not found in concrete drag texture.

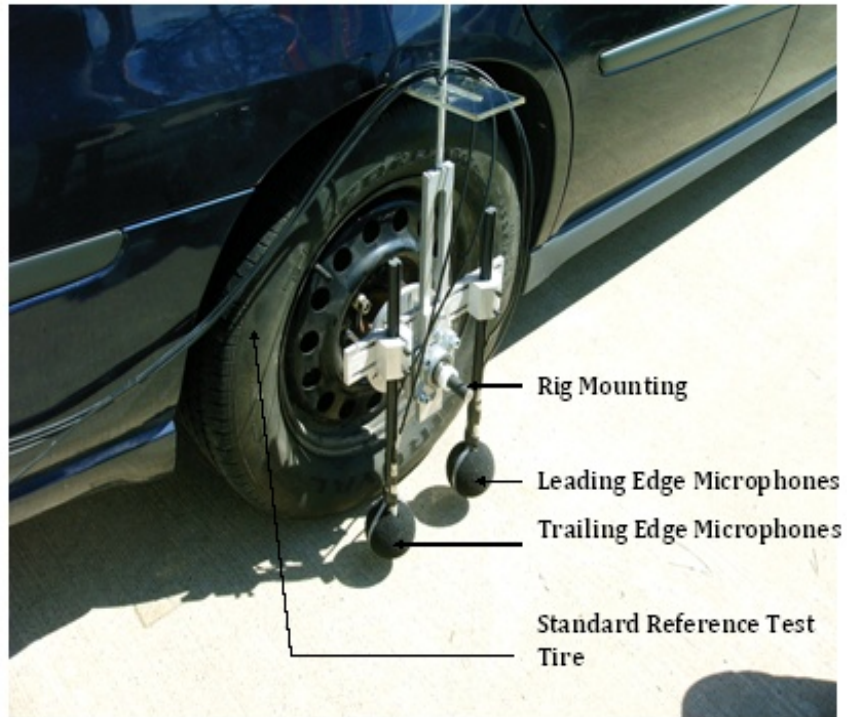
#### **1.4 Tire Pavement Noise**

The texture type and pavement condition are among the properties that govern tire pavement interaction including sound [1.27] [1.28]. Sound is the sensation produced by stimulation of the organs of hearing from vibrations transmitted through the air or other medium thus necessitating statement of OBSI in the A- weighted Scale (human hearing scale) [1.29]. It is also the mechanical vibrations transmitted through an elastic medium, traveling in air at a speed of approximately 1087 feet (331 meters) per second at sea level. Noise is undesired sound. All sound is characterized by sound pressure, sound intensity sound pressure level or sound intensity levels. When sound pressure  $N/m^2$  or sound intensity ( $Watts/m^2$ ) is referenced as a ratio to the pressure (or sound intensity) threshold of human hearing, it becomes Sound Pressure level (dBA) or sound intensity level (dBA). The Federal (United States) standard for traffic noise measurement is the statistical pass by (SPB) method. In this method, a set of microphones are stationed 25 ft. or 50 ft. from the roadway. The researchers make a record the various vehicle types crossing the line of microphones as well as the speed at which they cross and ensure that an acceptable range of each vehicle type and classification is included in a set of complete readings along with the measured noise [1.27]. Subsequently the statistical pass by number is determined from an averaging of the noise levels from a standard distribution of the vehicle types [1.27].

Although SPB mimics reception at homes in the vicinity of the roadway yet it is a reflection of a large range of sources some of which are not traffic related. For instance industrial noise is inadvertently recorded in addition to the vehicular noise. Although efforts are made to separate the traffic noise from other sources, those efforts are not sufficient to completely eliminate other sources. Consequently the Statistical pass-by is inadequate to characterize tire pavement noise. Considering the importance of tire pavement noise, efforts to measure this component led to the close proximity (CPX) method. This method encloses a test tire equipped with sound intensity meters housed to minimize influx of noise from other sources. The housing is pulled along as a trailer at about 40 miles per hour [1.27]. The test method is acceptable but not robust in spectral isolation of undesired noise sources as it relies on the housing. Housings are believed to act as local reverberation sources thus accentuating the inexactitude of CPX in TPIN characterization. Consequently the On board sound intensity method was adopted as an interim AASHTO standard for measuring tire pavement noise [1.28]. This method ensures that microphones are arranged very close to the contact patch and that by a Hamming window, [1.29] only emissions from the tire pavement patch are recorded.

As already defined, noise is understood as “unwanted sound according to differing perception and interest of the recipient [1.27] [1.31]. Noise, like all other sounds, is the auditory effect of transmission of acoustic energy. This research evaluates tire pavement noise which is a near field noise and recognizes the merits and demerits of every noise field. Moreover, while little or nothing can be done to influence other sources of noise apart from convoluted and labyrinthine legislative processes, the pavement surface variables can be controlled in design and construction especially within the relevant frequency range. When pavements are quieter, the OBSI value is lower but OBSI difference is not a rectilinear relationship. It is significant that the near field

measurement using OBSI typically ranges from 96-dBA to 120-dBA. Other metrics such as statistical pass-by have other ranges. Consequently the sound intensity metric used must be mentioned along with the noise data as comparisons across metrics need further correlation functions.



**Figure 1.11: OBSI Assembly showing SRTT, Mounting Rig, Microphones and Cables**

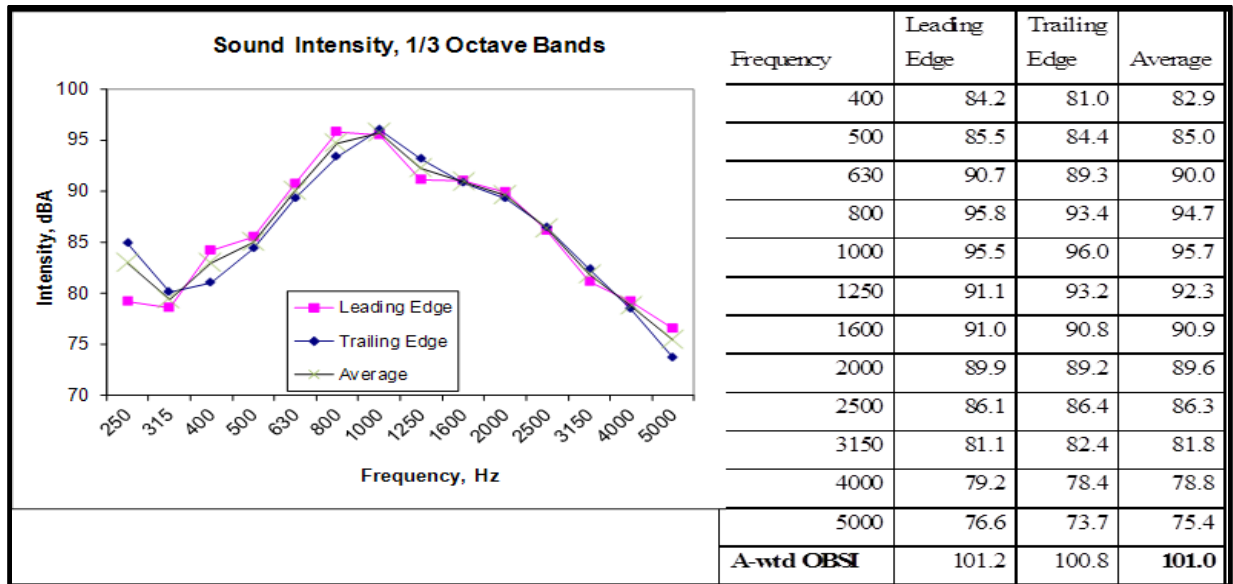


Figure 1.12: Output of an OBSI Measurement

The OBSI is referenced to the human hearing spectrum by the “A” weighting. In this weighting, the sound intensity relative to intensity level of the threshold of hearing is measured by on board sound intensity (OBSI) test. This test is conducted at 60 miles per hour and records the noise from the contact patch alone. It is facilitated by a set of sophisticated microphones installed near the contact patch so that the leading microphone captures the leading edge while the trailing microphone captures the trailing edge.

The OBSI analysis is based on the interim protocol adopted by AASHTO in 2008 [1.28]. The OBSI parameter is the logarithmic sum of sound intensity at each of the designated 3<sup>rd</sup> octave frequencies of 400, 500, 630, 800, 1000, 1250, 1600, 2000, 2500, 3150, 4000 and 5000 Hz.

$$OBSI = 10 * \log \sum_{i=1}^{12} 10^{\left(\frac{SI_i}{10}\right)} \dots\dots \quad (\text{Equation 1.7})$$

where

SI<sub>i</sub> (i=1, 2, 3, 12) are sound intensities in decibel based on the "A" - weighted scale [dB (A)] that is characterized by a reference pressure of 10<sup>-12</sup> Watts/m<sup>2</sup>. This is the sound intensity at the threshold of human hearing.

#### 1.4.1 Tire Pavement Acoustic Durability

Sandberg and Ejsmont [1.28] pages 266 to 273 discussed the Parameters that enhance pavement quietness ascribing the highest influence to pavement porosity. They defined pervious pavements as those containing interconnected voids that are >= 15% while categorizing any pavement with < 10% voids as dense, 10-15% as semi-dense and >15% as pervious. They identified the tire-pavement-noise-reduction parameters as:

- **Pavement thickness d** that interacts with durability against clogging, tortuosity and void content to provide a sustained noise level
- **Residual air void content** also referred to as porosity  $\Omega$  a dimensionless quantity
- **Airflow resistance per unit length R<sub>s</sub>** in KN-s/m<sup>4</sup> or lb.-s/ft<sup>4</sup>

- **Tortuosity  $q$**  a dimensionless quantity that is a microcosm of the air flow resistance. It describes the shape function of the air void that may be idealized in a model from the basic angularity, flatness or aspect ratio of the aggregate if known. This parameter is difficult to measure directly but its value is deduced from other measurements.

Sandberg et al does not come up with a model correlating this parameter to **sound absorption  $\alpha$**  but admits that modeling of noise reduction is a complicated process. Pervious pavements exhibit 4 properties that render pavement quiet. These include:

- Reduction of the noise generated by compression and rarefaction of air trapped between contact patch and pavement
- Reduction of the effective horn amplification mechanism
- Acoustical absorption that absorbs noise from all sources
- Reduction of the texture impact mechanism. The optimum size that will not compromise void content is 3/8 to 1/2 inch aggregate size. But ordinarily, the smaller aggregates encountered in pervious pavements versus exposed aggregate reduces noise.

Noise reduction strategies fulfill the following requirements:

- Maximize sound absorption at most important frequencies
- Minimize airflow resistance in order to affect air displacement mechanisms maximize flatness of surface in contact with pavement to minimize texture impact mechanism. Ordinarily, the critical frequency at high speed is 1000 Hz and at low speed 600 Hz.

Sandberg et al showed that air flow resistance ranges from 20-50 KN-s/m<sup>4</sup> for high speed roads to 10-30 KN-s/m<sup>4</sup> for low speed roads. The effect of voids, thickness and porosity considered together is to move the peak absorption frequency. The secondary and tertiary peaks of the absorption frequency curve are moved down into the most sensitive range. Sandberg et al also gave the following clues for noise / sound absorption characteristics versus time:

**Laterally Grooved or Tined PCC** will experience continuous reduction in noise over time and may never be come as quiet as the ground surface before terminal serviceability

**Smooth Dense Asphalt:** Noise level increases in 1-2 years remains stable and until end of service life where poor surface rating dictates noise level...

**Rough Textured Surface Dressing:** loss of larger asperities results in reduced noise levels the first year reduced friction may also be associated with this.

Smooth Textured Concrete Surface; are stable over time.

**Exposed Aggregates Concrete** is initially quiet but increase parabolically over time.

**Grooved or Tined Surfaces:** Grooves may become shallow over time; asperities may degenerate non-uniformly leading to increased noise. This implies that if the grooves are durable there will be stability over time

**Pervious Pavements:** As they get clogged freeze thaw action may lead to deterioration of pavement resulting in further loss of quiet pavement properties. Clogging reduces the effect of pavement thickness, porosity and tortuosity.

#### 1.4.2 Active and Reactive Fields

The current state of the art indicates advancement in close proximity measurements [1.28] and [1.29] when sound is generated and transmitted, the actual sound energy can be viewed as comprising two components. These are the active component and the reactive component whose corresponding fields are called active and reactive fields. The active field is a real sound transmission field but the reactive field is indicative of energy conversion into other forms. Fahy [1.30] explained reactive field as by the component of the solution to the general wave equation that mathematically represents the wave form that appears to be travelling into a source. The active components of the product of U and P (SI (r, t)) are expressed as:

$$SI \text{ active } (r, t) = \frac{A^2}{\rho_0 c w 2 r^2} \left(k - \frac{i}{r}\right) [1 + \cos 2 (wt - kr)] \quad (\text{Equation 1.8})$$

$$SI \text{ reactive } (r, t) = \frac{A^2}{\rho_0 w 2 r^3} \left(k - \frac{i}{r}\right) [\sin 2 (wt - kr)] \quad (\text{Equation 1.9})$$

where

- k is a wave number,
- W is angular speed,
- r is radial distance from source,
- t is time,
- A is a complex amplitude parameter.

Tire pavement interaction noise is a near field measurement while statistical pass by is a far field measurement. In a far field  $r \gg \lambda$  while the converse obtains in a near field. It is evident that in near field, radiation is purely radial but the reactive component is quite influential.

$$\text{Since } \frac{|SI_a|}{|SI_r|} = Kr \quad (\text{Equation 1.10})$$

The influence of the reactive field in near-field measurements affects the repeatability of tests. However the far field tests are fraught with errors that are accentuated with distance from the source. These include the different rates at which higher and lower frequency components are diminished over distance. That being a more serious source of error renders the near field measurements more reliable. This research evaluates tire pavement noise which is a near field noise and recognizes the merits and demerits of every noise field. Moreover, while little or nothing can be done to influence other sources of noise apart from convoluted and labyrinthine legislative processes, the pavement surface variables can be controlled in design and construction especially as the definition of OBSI includes the frequency over which noise is logarithmically summed. The On-board sound intensity method based on AASHTO TP 76-09 performs this summation of sound intensity level over 12 third octave frequencies. The OBSI parameter is the logarithmic sum of sound intensity of each of the designated frequencies of 400, 500, 630, 800, 1000, 1250, 1600, 2000, 2500, 3150, 4000 and 5000 Hz.

$$10 * \log_{10} [10^{\{SI_1/10\}} + 10^{\{SI_2/10\}} + .. + 10^{\{SI_{12}/10\}}] \quad (\text{Equation 1.11})$$

Where

$SI_1, SI_2 \dots, SI_{12}$  are sound intensities in dB at each of the 12 third octave frequencies denoted by subscripts 1 to 12.

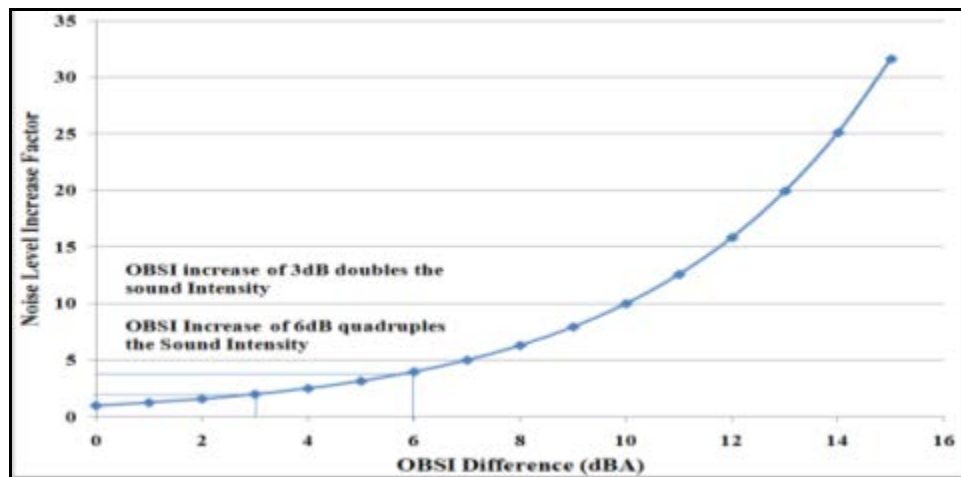
When pavements are quieter, the OBSI value is lower but OBSI difference is not a rectilinear relationship. The implication of an OBSI difference in terms of actual percentage reduction in sound level deserves explanation. A 3-dBA reduction in a noiseforce due to enhancement of that source is tantamount to approximately 50 percent loss of sound intensity from a uniform source. If  $OBSI_{(1)} - OBSI_{(2)} = n$  where  $OBSI_{(1)}$  and  $OBSI_{(2)}$  respectively measured sound intensity before and after a pavement surface treatment and “n” is the difference in Watts /m<sup>2</sup> then

$$10 \log \left( \frac{SI_2}{SI_0} \right) - 10 \log \left( \frac{SI_1}{SI_0} \right) = n \quad (\text{Equation 1.12})$$

$SI_0$  is the sound intensity at the threshold of human hearing, then

$$\left( \frac{SI_2}{SI_1} \right) = 10^{\frac{n}{10}} . \quad (\text{Equation 1.13})$$

For instance where  $n= 3$  dB, then actual sound intensity ratio is 2. The ratio is 4 when  $n$  is 6 dB (Figure 1.13). It is significant that the near field measurement using OBSI typically ranges from 96-dBA to 110-dBA. Other metrics such as statistical pass-by have other ranges. Consequently the sound intensity metric used must be mentioned along with the noise data as comparisons across metrics need further correlation functions. However since maximum difference anticipated is in the vicinity of 15 dBA, the above curve is sufficient for most tire pavement noise reductions or increases anticipated in practice of tire pavement noise.



**Figure 1.13: Implication of OBSI Difference.**

### 1.5 Noise Generation Mechanisms

Noise is generated through various active processes in the tire pavement interaction process. It is expedient to ascertain the association between causative or associated surface variables and these mechanisms. Tire pavement interaction noise generation and amplification mechanism proposed

by Sandberg et al [1.27] and Rasmussen et al [1.29] Bernhard & McDaniel [1.31], are summarized in a Table 1. The major noise generation and amplification mechanisms are now discussed in the light of possible associative or causative variables as well as measures that may minimize the generation or amplification mechanism.

### **1.5.1 The Stick Snap and Stick Slip Phenomena**

This “stick-snap” [1.30] [1.31] phenomenon also causes vibration in the tire tread and carcass and produces sound energy. This is similar to the sound produced when a suction cup is pulled off a surface. Inside the contact patch, the tread blocks stick momentarily and then slip against the roadway surface in a tangential direction [1.32]. This “stick-slip” phenomenon causes squeaks and squeals, like a sneaker on a basketball court. This mechanism generally produces high-frequency sounds. These mechanisms are not likely to be significant when textures are mainly negative. Negative textures provide minimum tire asperity indentations and would likely minimize this generation mechanism.

### **1.5.2 The Clap Phenomenon**

Air movement around the tire also contributes to the generation of noise. Air is pumped in and out of the tread passages as these passages are compressed in the contact patch. The compression of the air, and thus the amplitude of the sound, depends on the tread pattern, the rapidity of the distortion of the passages, and the pavement porosity. The sound produced is similar to that produced by clapping hands (Table 1.1) [1.28] [1.32]

### **1.5.3 The Horn (Amplification) Effect**

The geometry of the tire and the pavement can also enhance noise generation in the same manner as the geometric features of a musical instrument. The tire and the pavement surface at the entrance and exit of the contact patch act like a horn to amplify noise generated by air pumping and tread vibrations. The horn shape directs sound outward from the tire–pavement interface. [1.27] [1.29] [1.30]. Horn effect is minimized by negative texture orientation longitudinal texture direction and pervious pavements.

### **1.5.4 Pipe Resonance (Organ Pipe Effect)**

Grooves or channels in the tread pattern act like organ pipes, creating channel or pipe resonance. Just as resonant vibration of air in organ pipes amplifies the musical notes, vibration of air in the channels of the tread pattern also amplifies and radiates sound. Longitudinal texture direction and negative texture orientation in pavement reduce the effective channelization in the tires.

### **1.5.5 Cavity Resonance (Balloon Simulation) [1.27], [1.29] [1.30]**

The enclosed space inside the tire has a cavity resonance that is perceptible internal and external to the vehicle. Vibration of the air within the tire carcass can be minimized by low IRI, negative texture orientation and longitudinal direction.

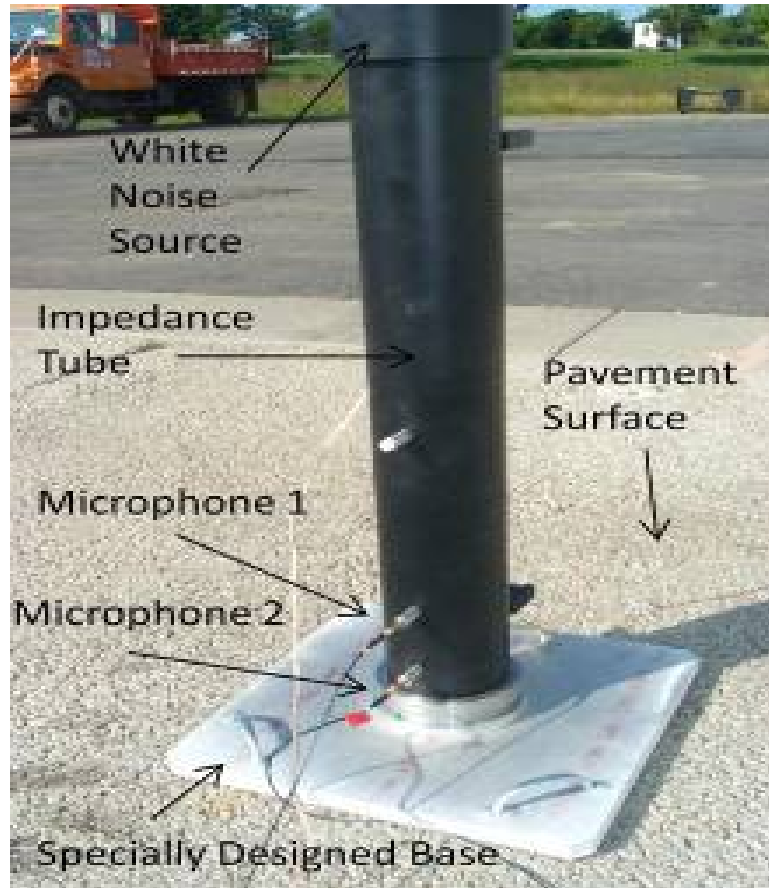


**Table 1.1: Noise Generation and Amplification Mechanisms and Associated Variables**

Generation Phenomenon	Description	Explanatory or Analogous Sound Source	Associated Variable
Tread block impact	Tread blocks impact pavement as tire rolls	Hammer	Texture Direction →more impact
Air compression	Rarefaction in trailing Edge	Whistle	Texture direction→uninterrupted pressure relief. Pervious pavement→more relief
	Helmholtz Resonator	Narrow necked bottle	Asperity interval~Helmholtz resonance
	Horn Effect due to tire geometry	Bullhorn	Texture direction
Tire Resonance	Sound similar to tapping a balloon	Balloon effect( in vehicle noise)	+ve Orientation→more taps →more noise
Acceleration	Acceleration records a force due to circular motion at constant speed	Particle acceleration	Longitudinal direction forestalls “perfect storm”
Stick Slip, snap	Rhythmic making and breaking of contact with suction. Hysteresis in tire contact	Basketball shoes squeaking; Plunger effect	-ve orientation→less suction
Pipe Resonance	Air is compressed in a transverse tine which acts as a pipe across an unsealed joint	Organ Pipe	Longitudinal grinding →less pipe resonance
Clap Phenomena	Air is compressed and not relieved quick enough	Clapping of hands	Pervious pavements, longitudinal texture relieve air compression

### 1.6 Acoustic Impedance Theory

Sound Absorption Coefficient ( $\alpha$ ) is the ratio of the absorbed sound energy to the transmitted sound energy when a white noise of frequency ranging from 315 to 1800 Hz is projected into the pavement within an impedance tube placed normal to the pavement surface.



**Figure 1.14: Sound Absorption Measurement with Impedance Tube.**

The sound absorption test is a process that measures the sound absorptiveness of a pavement surface. During the test, the sound analyzed is not generated by the interaction of the rolling tire with pavement surface but by noise source above the impedance tube. On the BSWA 425 device, a white noise source is used. White noise is a random audio signal with a flat power spectral density that contains noise at the same power at all frequencies. During the test, the impedance tube is placed on the pavement surface and a set of sensitive microphones are attached to the pre-installed housing at the lower end of the tube. These microphones are also connected to an analyzer. The noise source sends the incident sound energy (white noise) to the surface and the incident and reflected waves are captured by the two microphones. Software windows the reflected waves and converts the data to the 3rd octave sound absorption coefficient at 315, 400, 500, 750, 1000, 1250 and 1650 Hertz. Thus, the coefficients need to be between one and zero where a value of one would mean that all of the sound is being absorbed.

Sound absorption output is generated as a function of frequency as shown in Equation 1.14. Ordinarily, the result is generated in a narrow band but 3rd octave band results are reported. The system is designed to capture frequencies within the multi-coincidence range [1.36]. Berengier et al[1.33] discussed that the sound absorption coefficient ( $R_p$ ) is expressed as a function of frequency:

$$|R_p(f)|^2 = 1 - \frac{1}{k_r^2} \left| \frac{P_r(f)}{P_d(f)} \right|^2 \quad (\text{Equation 1.14})$$

where

$k_r$  is the spreading factor,  
 $P_r$  is the reflected sound energy and  
 $P_d$  is the incident sound energy .

The output of a sound absorption factor is typically in the form of the sound absorption at the seven frequencies defined earlier. Hence, factor is therefore expressed as a function of frequency.

The noise source sends the incident sound energy to the surface and the incident and reflected waves are captured by the two microphones. Software windows the reflected waves and converts the data to the 3<sup>rd</sup> octave sound absorption coefficient at 315, 400 500, 750, 1000, 1250 and 1650 hertz [1.32]. The Octave is the preferred way of reporting frequency based data. For a range of frequencies the n-th octave is given by the following

$$\frac{F_{n+1}}{F_n} = 2^{\frac{1}{n}} \quad (\text{Equation 1.15})$$

For instance the 3<sup>rd</sup> octave with the lowest frequency at 400-Hz has the second at  $400 * \sqrt[3]{2} \cong 500\text{hz}$ . When the tire rides over a pervious pavement, there is initial compression of the air at the orifice of the cavities, this causes a displacement in the volume and the resonant frequency at which absorption is maximized is given by the following Equation [1.34].

$$f_0 = \frac{c}{2\pi} \sqrt{\frac{S}{V} \left( l + \frac{\pi b}{2} \right)} \quad (\text{Equation 1.16})$$

where

$c$  = speed of light  
 $f_0$  = Resonant frequency of the pervious system  
 $S$  = Surface area of cavity  
 $V$  = volume of Void  
 $l$  = diameter of asperity  
 $b$  = Average surface void radius

The peaks of acoustic absorption occur at frequencies that can be calculated according to the relationship

$$f_{\text{peak}} = nc/4l \quad (\text{Equation 1.17})$$

where

$f_{\text{peak}}$  is the frequency at peak absorption,  
 $n$  is an odd integer number corresponding to the peak (1 for 1st peak, 3 for 2nd peak and so on),  
 $c$  is the effective speed of wave in the medium (343 m/s for air at 20 °C),  
 $l$  is the thickness of the sample.

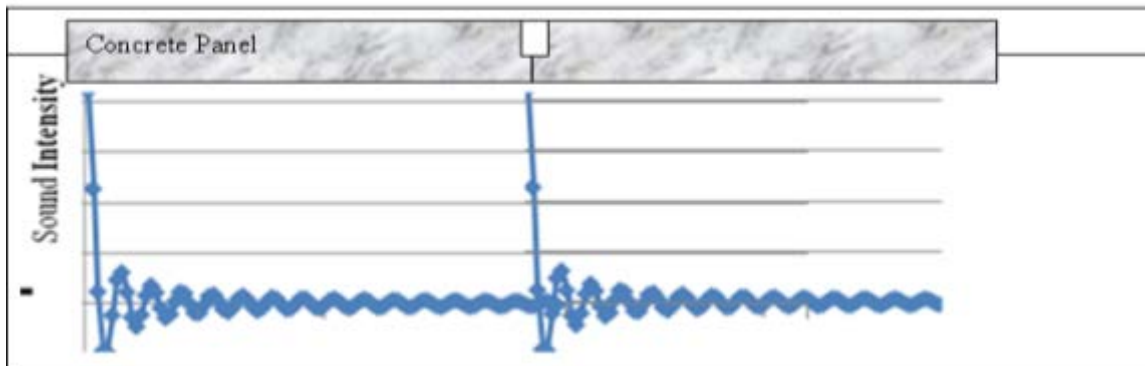
While Allard et al [1.25] studied the effect of corrugation on cavity resonance, multiple attempts have been made to tie Horoshenkov's equation to the envelopment theory of Hamet [1.37] and Hamet and Klein [1.38] but the work of Clapp et al [1.22] appears to validate that lemma.

## 1.7 Pavement Geometrical Variables

### 1.7.1 Texture Direction

Texture direction refers to the dominant direction of texturing. Textures are either mainly longitudinally textured or transversely textured. Conceptually, there is additional tread block impact due to the transverse tining. This phenomenon is not as severe in the longitudinal tining that enhances additional air pressure relief in the direction of motion of the tire. Transversely textured pavements are believed to be generally noisier than longitudinally textured pavements all other variables equal.

The time domain transform of the Boxcar configuration is the symmetric sinc function. In principle the rectangular distribution in the spatial domain results in a pattern of frequencies in the time domain where it rises from 0 to an infinite value in a discrete pattern of increasing frequency subsequently decaying rapidly from infinity to zero. Repeats of this phenomenon in time domain as well as proximity to the resonant frequency results in the “whine” that is characteristic of transverse textures. The relatively less frequent occurrence of this phenomenon in longitudinal textures accounts for the difference in noise levels (Figure 1.15). The transverse texture is a boxcar profile that provides an interesting acoustic feature in time domain. The time domain transform of the “BOXCAR” configuration is the asymmetric sinc function.



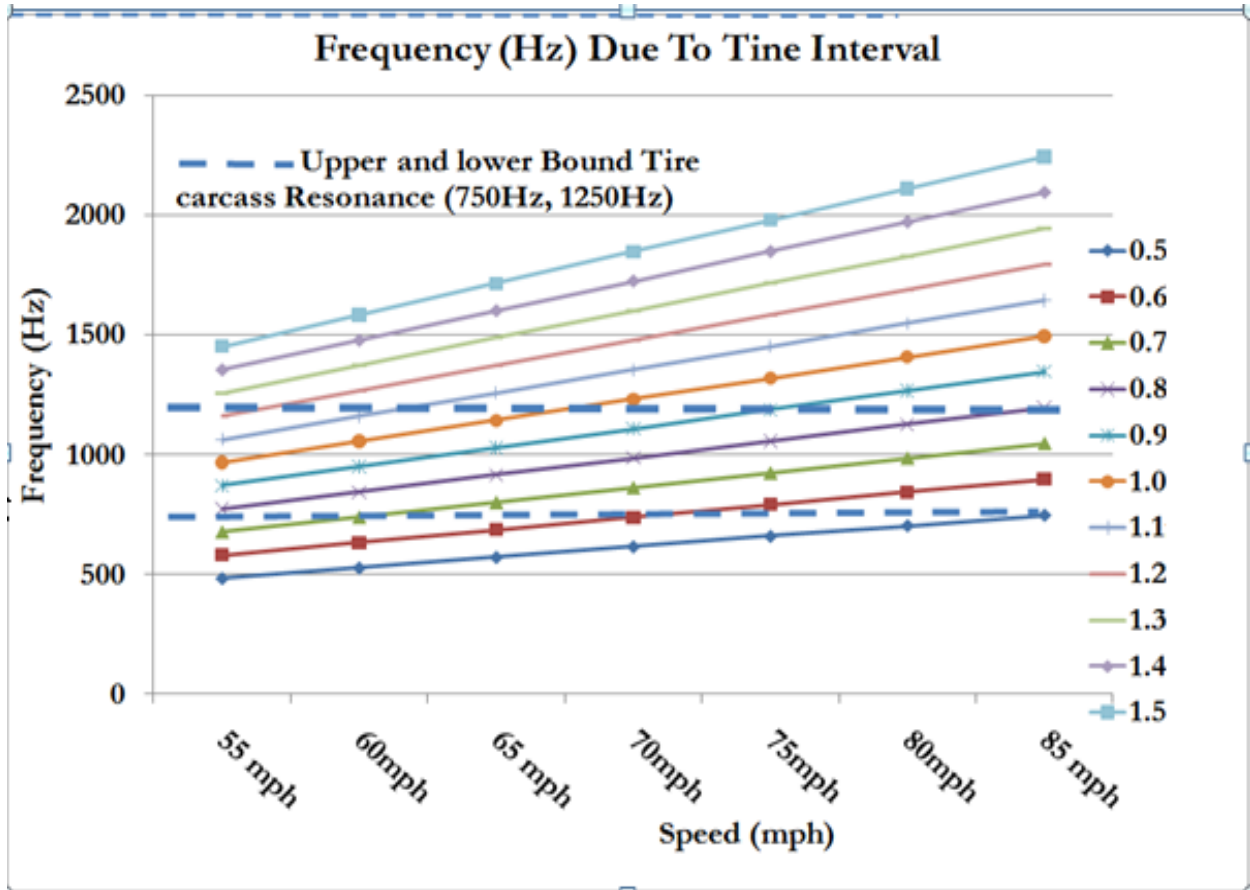
**Figure 1.15: Sine Wave of Sound Intensity Function in the Spatial/ Time Domain**

Whine is introduced by transverse textures due to resonance of the tire carcass. Additionally the time domain pattern of successive sine acoustic profiles due to tread block impact contributes to the noise levels of transverse textures. Transverse textures may therefore be louder than longitudinal textures. Texture direction is therefore worth considering as an explanatory variable.

### 1.7.2 Numerical Example:

Consider a longitudinal tine or ground pavement, there is no influence of intervening asperities as the riding surface is above the grooves at all times. In that case the sound intensity is due to tread block impact and air compression relief.

Consider a transverse tined pavement and particularly the transverse grooves encountered by the moving tire. A repeating pattern of grooves of 1 inch intervals at 60 miles per hour results in a frequency of 1050 hertz. Typical range of tine spacing is 0.5 to 1.5 inch. Expected frequencies due to various speeds are calculated and the resulting chart is shown in Figure 1.16.



**Figure 1.16: Frequencies due to transverse tines are coincident with typical tire resonant frequencies**

This pavement surface whine is the main noise source because the tire carcass is at resonance at a frequency of approximately 1000 Hz. Sandberg [1.36] shows that in a range of frequencies from 750 to 1250 Hz, resonance is likely. The tire resonance accounts for the higher noise due to transverse textures at common freeway speeds.

It is conclusive that transverse textures introduce thread block impact to the noise spectrum and are thus noisier than longitudinal textures of the same pavement. Texture direction will therefore be a starting variable in the development of a prediction model for sound intensity level.

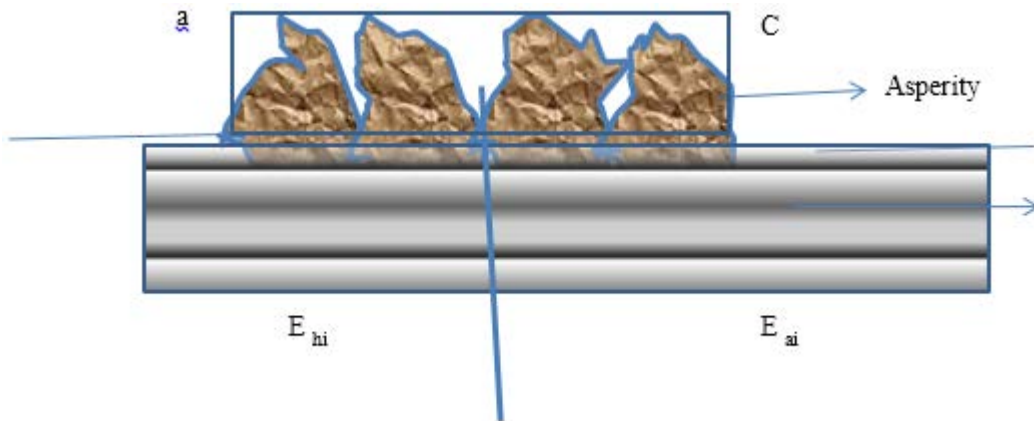
### **1.7.3 Pavement Surface Variables: Mean Profile Depth**

The previous subsection discussed texture orientation as a potential prediction variable for OBSI. The current section examines mean profile depth in tire pavement interaction. In this section, the tire pavement asperity indentation and bridging section are relevant to this section.

Mean profile depth is an average height of the complement of the texture asperities. It is therefore not a physical characteristic of the surface but describes the implied space above the texture. It is also not a primary surface feature. Models particularly of and Clapp et al [1.22] and Hamet [1.37] as well as Hamet and Klein [1.38] do accentuate the importance of tire envelopment and the preference of this variable to actual OBSI in tire pavement interaction. There is insufficient analytic procedure to conclusively adopt or reject MPD as a variable however, since it is a variable that is the same irrespective of texture direction, asperity interval it may be analyzed further in a stepwise regression analysis. An intrinsic relevance to the model will result in its retention as part of the model while a rejection will mean that it has no significant influence on OBSI

This section discusses tire pavement contact and deduces that the actual tire envelopment, the air trapped between tire and pavement and tire asperity envelopment appear to govern the acoustic properties. These are elucidated in various contact theories in the preceding chapter. The models discuss the interfacial processes and mechanisms that cause noise. Different references and models discuss actual tire texture integration mechanism. In the interim, mean profile depth is defined in ASTM E-950 as the average depth of asperities in the surface. This is a misnomer when the measurements processes are considered.

Consider a surface with asperities as in the Figure 1.17. If a textured surface is enclosed in a rectangular space that cordons the asperity, the volume of the space between asperities and the top of body divided by the base area of box is the mean texture depth. Thus if the maximum height of asperities is H, the average height of the rectangular space is H (average).



**Figure 1.17a: Texture Configuration and Relevant Dimensions**

$$H \text{ average} = \frac{H \sum_{i=1}^N a_i - \sum_{i=1}^N a_i h_i}{\sum a_i} \quad (\text{Equation 1.18})$$

where

- a is area of area of asperity
- N is number of asperities;
- H is height of hypothetical box and
- h is the height of asperity.

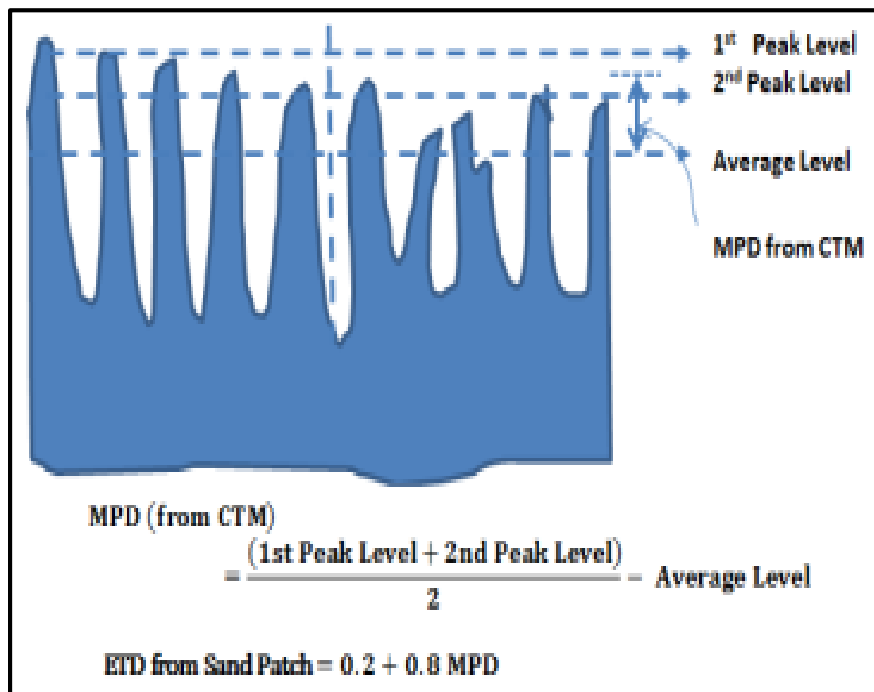
In the ASTM E-950 test, the schematic volume is filled with glass beads. The numerator of the equation above becomes the volume of glass beads and the denominator is the area of spread. In ASTM E-2157, the mean profile depth derived from laser depth to the asperity or groove. This is similar to Estimated Texture Depth (ETD)

$$ETD = \frac{V}{A} \quad \text{(Equation 1.19a)}$$

where

V is the volume of glass beads,  
A is the area of maximum spread of the beads.

Schematics in the computation of mean profile depth ASTM E-2157 are shown in Figure 1.17b.



**Figure 1.17b: Mean Profile Depth**

$$\begin{aligned} \text{MPD from CTM} &= \frac{1\text{st Peak Level} + \text{Second Peak Level}}{2} \\ &\quad - \text{Average Level} \quad \text{(Equation 1.19b)} \end{aligned}$$

$$\text{ETD from Sand Patch Test} = 0.2 + 0.8 \text{ MPD} \quad \text{(Equation 1.19C)}$$

By the definition of estimated texture depth it is a secondary parameter that characterizes the complement of the volume occupied by asperities within as assumed rectangular box. The configuration of the top of the box is dependent on the skill of the sand patch tester as well as the relative height of the asperities. The more uniform they are the more uniform is the assumed surface but in a texture of high variability the surface is less likely arithmetically uniform. This is

the foundation of the uncertainty of ETD or MPD to characterize surface properties and influence pavement surface characteristics predictions. A more realistic surface variable will characterize the actual asperity, intervals as well as the tire bridging features enunciated by Hamet and Klein [1.38] who idealized the actual tire pavement contact into contact models to facilitate prediction of pavement surface characteristics. Moreover, envelopment theories produced by Wu and Nagi, Clapp et al and Donavan, separately provide explanation for texture and tire interaction but there is no tenable explanation for sound intensity through MPD. As it stands envelopment profiles are different from MPD since such profiles bridge between asperities and thus do not replicate the entire area measured by MPD. Mean Profile Depth has not been successfully used as a qualitative predictor of friction where tire asperity envelopment has been studied by Wu and Nagi [1.22]. It is therefore doubtful if it can be used to predict noise. The Klein contact model [1.38] is an envelopment theory indicating that sound can be predicted from the actual envelopment configuration through the use of source strength. However, the actual envelopment phenomena are very complex and are outside the scope of this analysis. Donavan [1.15] showed that the  $dV/V$  ratio when a tire bridges over asperities is fundamental to noise generation. There is no direct correlation between  $V$ , or  $dV$  and MPD. It is therefore inconclusive that MPD would be an explanatory variable for OBSI. However the actual envelopment and bridging volume are predictors but these are transient and very difficult to measure.

#### **1.7.4 Pavement Surface Characteristics Asperity Interval and Groove Width**

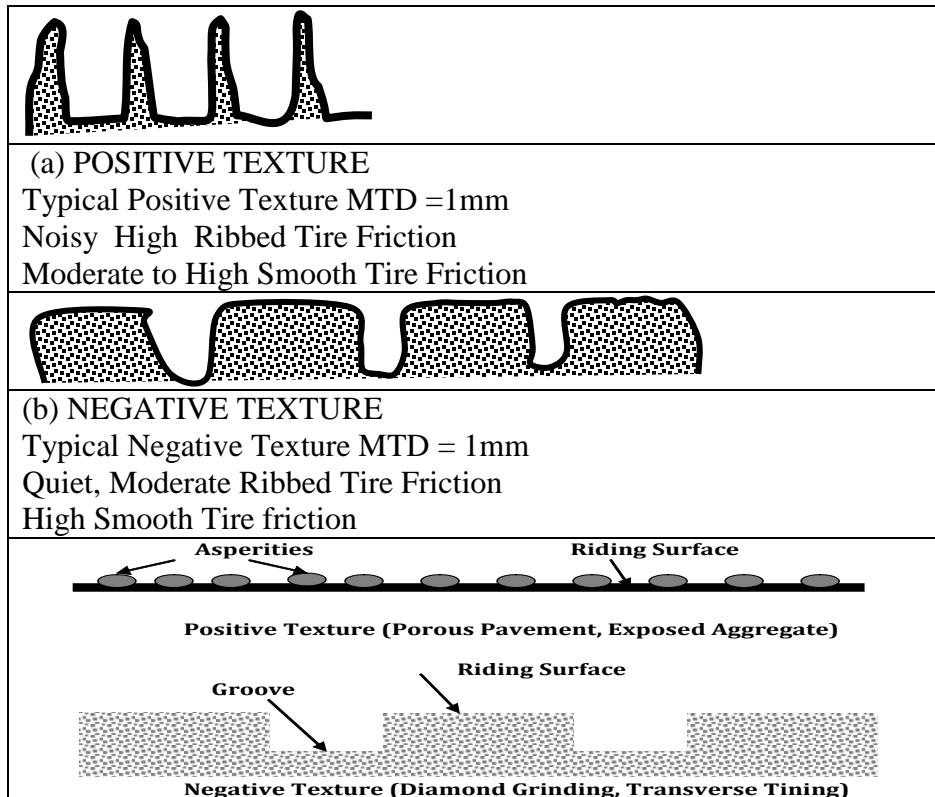
A primary texture dimensional parameter that may influence groove bridging is the asperity interval. It is reasonable to expect that a characteristic dimension representing groove interval should be a starting variable in the development of a prediction model for sound intensity. Instead of MPD it can be shown [1.15] that  $dV/V$  governs the frequency of the noise generated noise generated and  $V$  determines the sound pressure. It can be shown that sound pressure varies with groove dimensions. Data obtained by Donavan in an experiment in which dimensions of groove and land was varied. Results showed that the sound pressure level varies with groove dimensions. Donavan [1.15] had varied dimensions of groove and depth in a lab and made the observation.

#### **1.7.5 Texture Orientation**

Texture orientation is conventionally defined qualitatively as the indicator of spikiness or otherwise of a texture configuration [1.39]. The spiky textures are defined as positive and the converse is true for negative texture. Texture orientation is a categorical variable that describes how the asperities are more spiked than the grooves. In a negative texture, the asperities are more flattened and the grooves are more spiked while the converse obtains for positive textures. It is generally known among practitioners that positive textures are noisier than negative textures. However, there is no current mathematical categorization of texture orientation. A mathematical process is proposed in this section.

Examples of real-world pavement that provide extremes of positive texture include chip seal and epoxy bound aggregate surface course. Conversely, the grooved PCC provides its macro texture through a “negative” texture feature.





**Figure 1.18: (a) and (b) Schematics of Similar MTD but Different Surface Performance and (c) Positive and negative Texture**

Upwardly pointed asperities (positive textures) are likely to be noisier than downwardly rounded asperities all things being equal. It is not clear if air compression is minimized but thread block impact may be increased with positive texture.

Hamet et al [1.38] showed that there is an envelopment phenomenon of tires over textures that influence the actual acoustic behavior. While Hamet et al do not negate the prediction of texture asperity influences; they indicate that the actual stresses during contact require an in-depth application of the elastic behavior of the tires. This was corroborated by Clapp et al. [1.23], Although Flintsch et al [1.38] did not directly relate texture orientation to noise, their method of comparing the RMS MPD to the MPD is a quantitative measure that of that property later found useful in noise prediction. Moreover, Bendstein et al [1.39] who stated that actual stresses are determined by the influences of positive versus negative texture on sound. Moreover, the Clapp model implicitly accentuates the likelihood of higher pressures when textures are positively oriented. The Clapp model predicts higher pressures for more pointed asperities. These models are all accentuated in Donovan's [1.15] conclusion that sound pressure pulse depends on the relative change in volume (of enveloped opening) ( $dV/V$ ) but the actual pressure depends on the area of the groove. More pointed asperities (positive texture result in higher envelopment and higher  $dV/V$ . Therefore based on the analysis of Wu and Nagi, Clapp et al and Donovan, it is indicative from physical concepts that the positive textures may be noisier than negative textures. At the minimum, texture orientation is worth considering as an explanatory variable.

Many researchers including Flintsch et al [1.39] attempted to derive a mathematical process for positive and negative texture using the circular track meter RMS-MPD and MPD ratio to categorize pavements as positive and negative texture. They did not validate the process and it was never used or referenced for want of consistency and reliability. While kurtosis is indicative of the flatness or spikiness of texture configurations, textures typically encountered in practice will always be spiky if their kurtosis is computed. It does not provide the positive versus negative dichotomy unless an arbitrary value is set as a pivot. However when a continuum of asperities and grooves are observed, the skewness of the amplitude distribution function (not the skewness of the surface) determines positive and negative texture. The concept of amplitude distribution function thus facilitates the quantification of texture orientation.

The Amplitude Distribution Function (ADF) of a profile [1.18] describes a probability function that a profile of the surface has a certain height  $Y_i$  at any position  $x$ . By convention  $Y$  is referenced at zero for the deepest part of the groove. According to Standards: ISO 4287-1997 [1.19] skewness of a profile is a parameter that describes the shape of the ADF and not the shape of the configuration. Skewness is a simple measure of the asymmetry of the ADF, or, equivalently, it measures the symmetry of the ADF of a profile about its mean line.

$$Skewness = \frac{\sum_{i=1}^N (Y_i - \bar{Y})^3}{(N-1)S^3} \quad \text{(Equation 1.20)}$$

where

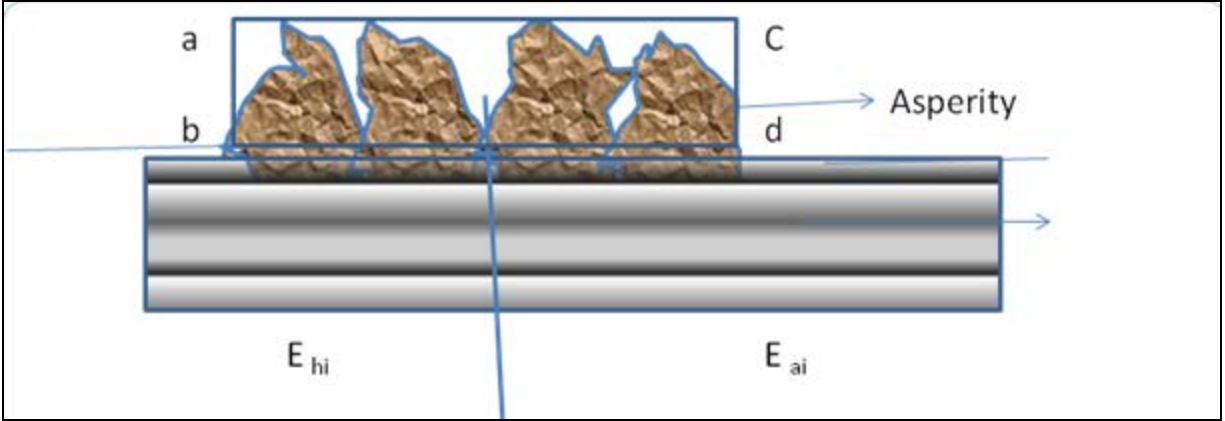
- $Y$  is zero at the bottom of groove,
- $\bar{Y}$  is the mean,
- $S$  is the standard deviation,
- $N$  is the number of data points.

It must be noted that in Equation 1.20 the skewness of the probability density function is indicated and not the skewness of the profile asperity ordinates. A worked example of some texture configurations is now performed to validate this proposed use of skewness as a texture orientation metric. Four texture configurations innovative grind, conventional grind, transverse tine and turf/broom drag are analyzed. It is evident that conventional grinds are mildly positively oriented, innovative grinds are negatively oriented and transverse tined are negatively oriented. Ideally, drag textures are sometimes neutral textures because of their proximity to the sine wave the accuracy of the worked example (method of slices) may not result in zero skewness. In consequence of the above expression and the result of the worked example, it is now tenable to propose a reliable method of texture orientation quantification as follows:

$$\text{Texture Orientation } (\mathcal{K}) = \text{Sgn Skewness of ADF} \quad \text{(Equation 1.21)}$$

### 1.8 Tire Texture and Contact Phenomena

Consider a surface with asperities in the Figure 1.19 below



**Figure 1.19: Texture Configuration and Relevant Dimensions**

The following analysis will show that mean profile depth is not a property of the texture amplitude distribution but of the complement of the distribution. If a textured surface is enclosed in a rectangular space abcd that encloses the asperity, the volume of the space between asperities and the top of body divided by the base area of box is arithmetically equivalent to the mean texture depth. Thus if the maximum height of asperities is H the mean texture depth can be conceived as

$$\text{It has been shown that ETD} = \frac{H \sum_{i=1}^N a_i - \sum_{i=1}^N a_i h_i}{\sum a_i} \quad (\text{Equation 1.22})$$

where

- a is area of asperity,
- h<sub>i</sub> is the height of individual asperity,
- N is number of asperity,
- H is height of hypothetical box,
- h is the height of asperity.

In the ASTM E-965 [1.4] test, the schematic volume is filled with glass beads. Where the numerator of the equation above becomes the volume of glass beads and the denominator is the area of spread. The mean profile depth is still the average height of space between asperities and not an average height of asperities. This is significant in predicting the influence of MPD as this variable better describes the complement of an agglomeration or continuum of asperities rather than the asperities.

$$\text{The MPD} = \frac{V}{A} \quad (\text{Equation 1.23})$$

where

- V is the volume of glass beads,
- A is the area of maximum spread of the beads.

By the definition of mean profile depth it is a secondary parameter that characterizes the volume not occupied by texture asperities within as assumed rectangular box. The configuration of the top of the box is dependent on the skill of the sand patch tester as well as the relative height of the asperities. The more uniform they are the more uniform is the assumed surface but in a

texture of high variability the surface is less mathematically uniform. It is therefore futile to base a noise model on a variable that does not really explain the texture asperity distribution.

Many authors [1.14] [1.21] [1.23] [1.41 to 1.43] have idealized the actual tire pavement contact into contact models to facilitate prediction of pavement surface characteristics. These models include but are by no means limited to

- Bendstein-Fujikawa [1.40], [1.41]: A Texture Unevenness Approach
- Clapp Eberhardt and Kelly Model [1.22]: Two Dimensional Contact Pressure Theory
- Wu and Nagi [1.21]: Tire Pavement Adhesion and Hysteresis Phenomena
- Hamet and Klein [1.38]: Tire-Texture Envelopment Phenomena
- Donovan [1.15]: Prediction of Acoustic Pressure
- Byrum [1.42]: A Unique Frequency Band Approach.

Each of these models is reviewed in relation to what surface configuration may be relevant.

### **1.8.1 Fujikawa Bendstein Models**

Bendstein H, Andersen B Thomsen S [1.40], and Fujikawa [1.41] investigated tire road noise and the mean Profile depth (MPD) and demonstrated that road roughness may play an important role in the generation of tire vibration and radiated noise. One of these studies theoretically predicted the relationship between road roughness parameters and tire vibration and radiated noise. By roughness they referred to unevenness of texture configuration as would be shown shortly. Their measure of noise was not OBSI but the close proximity noise level, (L in dB) used in Europe and is linearly correlated to OBSI. They proposed a method of noise prediction from two sets of measurements on actual road surfaces. First, the tire tread vibration was measured on three types of road surface. Second, tire/road noise was measured on 13 samples of road surface. The results indicated that the spacing and height unevenness of pavement asperities should be small to abate tire vibration and radiated noise. They introduced a special measure for unevenness (Y) to describe the difference in height between the highest points on a road surface profile measured by a laser over a length of 1 meter. Another measure (X) was also introduced to describe the average distance between the asperities in the road surface. Both parameters X and Y were indicators for the pavement surface texture configuration. The Mean Profile Depth (MPD) was also included in the description. They ascribed tire pavement sound levels to configuration, wavelength as well as to inter kerf height differentials. The experiment developed a relationship between road surface texture configuration and tire/road noise. Noise was measured by the CPX method using a passenger car equipped with microphones and two special tires:

- A tire with a rubber block tread pattern creating a high level of air pumping
- A tire with a rib tread pattern creating little air pumping.

The following formulas for the tire road noise L in dB were established [1.42]:

Tire rubber block tread pattern:

$$L = 1.8*Y + 0.34*X - 1.15*MPD + 93.2 \quad (\text{Equation 1.24})$$

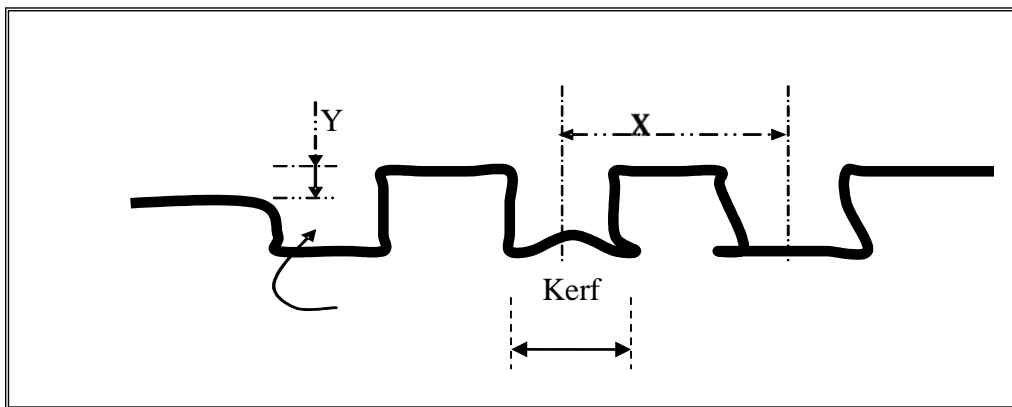
Tire with a rib tread pattern:

$$L = 1.07*Y + 0.33*X - 0.22*MPD + 91.1... \quad (\text{Equation 1.25})$$

Where

L is the Close Proximity (CPX) noise level.

An improvement to the Bendstein-Fujikawa approach requires determination of effective model parameters for various texture types after determination of the actual surface parameters that significantly influence tire pavement interaction noise. Effect of tie cannot be ignored in tire pavement studies. In this study the tire variable is eliminated by keeping the tire constant, using the ASTM standard SRTT. Subsequent experiments after this research may study the effect of tires with the used of various commercial tires on the pavement tested.



**Figure 1.20: Texture-Planing Configuration and Relevant Dimensions**

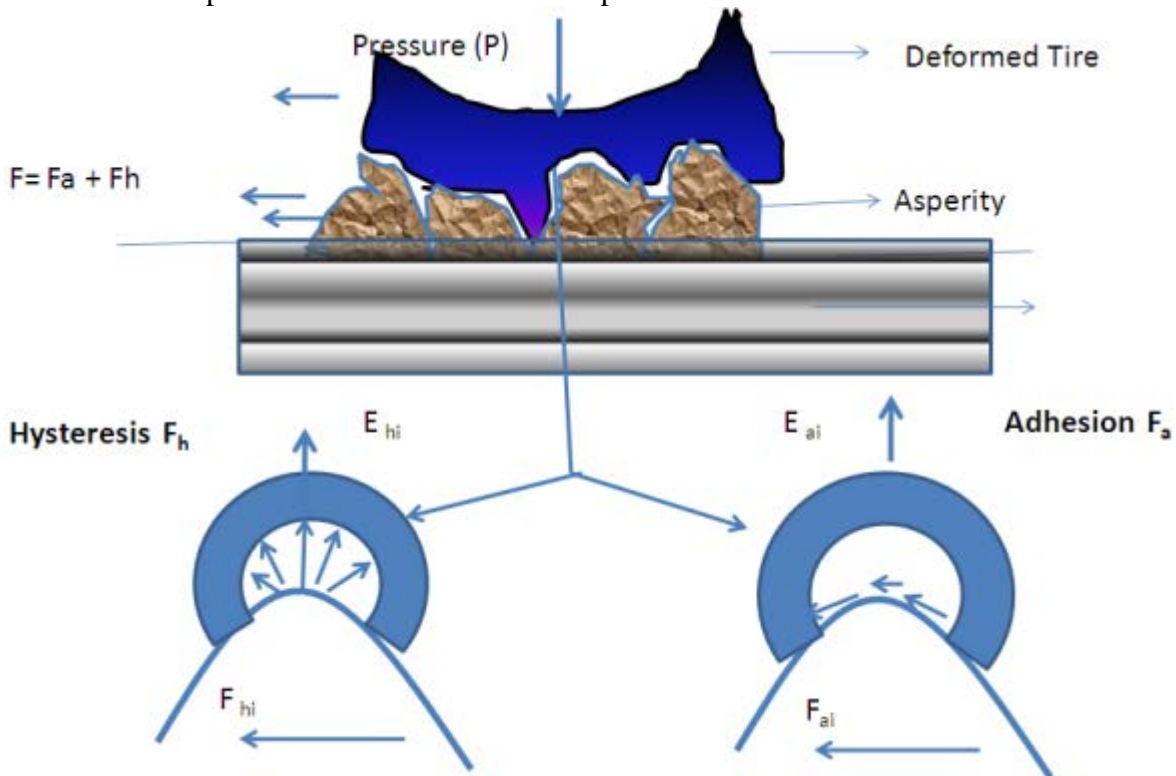
The Bendstein, Fujikawa model recognizes only texture wavelength, while keeping the analysis in the spatial domain. The process however does not specifically distinguish between a transverse texture and a longitudinal texture whereas these are diametrically opposite in acoustic performance response to the same tire contact.

Therefore the Fujikawa approach implies that MPD is relevant but not sufficient. They used MPD in their calculation but used a quantity similar to asperity interval and another which is the unevenness of pavement surface Y. The Fujikawa model indicates that the asperity interval and the IRI may be important variables in Sound intensity prediction.

### **1.8.2 Wu and Nagi Model**

According to Wu and Nagi [1.21], tire pavement forces are categorized into hysteresis and adhesion. It was postulated that the development and relief mechanism of these forces are related to tire pavement noise. Wu and Nagi show the free body diagram of an asperity. Consider a tire resting on a contact patch. The contact patch is made up of a set of asperities. Consider a single asperity. The tire deforms over the asperities and follows the surface configuration in an ideal situation. Energy dissipation occurs from the tire collapse but restoration does not happen as quickly as the deformation. This phenomenon is hysteretic and

results in the effect of negative pressures that contribute to the interaction. Breakage of this contact results in noise levels. As the tire moves, tangential forces, bearing forces and suction forces are developed between the tire and the asperities.



**Figure 1.21: Hysteresis Effects at Tire Asperity Interface**

Consider the free body diagram above.

If A is actual contact area,

Q is volume of finite deformed rubber element

An is nominal Area

S = Interface shear strength

D= Energy dissipated per unit volume.

P = pressure of the rubber block, b is rubber sliding distance and w is normal load

It can be shown that.

For Adhesion coefficient

$$f_a = \frac{A}{A_n} \frac{s}{p} = \frac{F_a}{w} \quad \text{(Equation 1.26)}$$

For Hysteresis coefficient,

$$f_h = \frac{Q}{A_n} \frac{D}{bp} = \frac{F_h}{w} \quad \text{(Equation 1.27)}$$

This relationship has been useful in the computation of frictional forces but has not until now been exploited for acoustics. By calculation of acoustic source strength the sound energy due to pavement contact can be determined. Clapp et al idealized the process for computing pressure distribution and showed that the pressure distribution is positively correlated to sound generated.

The Wu and Nagi model suggests that texture orientation is an important tire pavement noise predictor. By keeping the deformed tire volume and deformation energy constant the hysteresis component can be normalized into

$$Hn = \frac{Q}{A_n} \quad (\text{Equation 1.28})$$

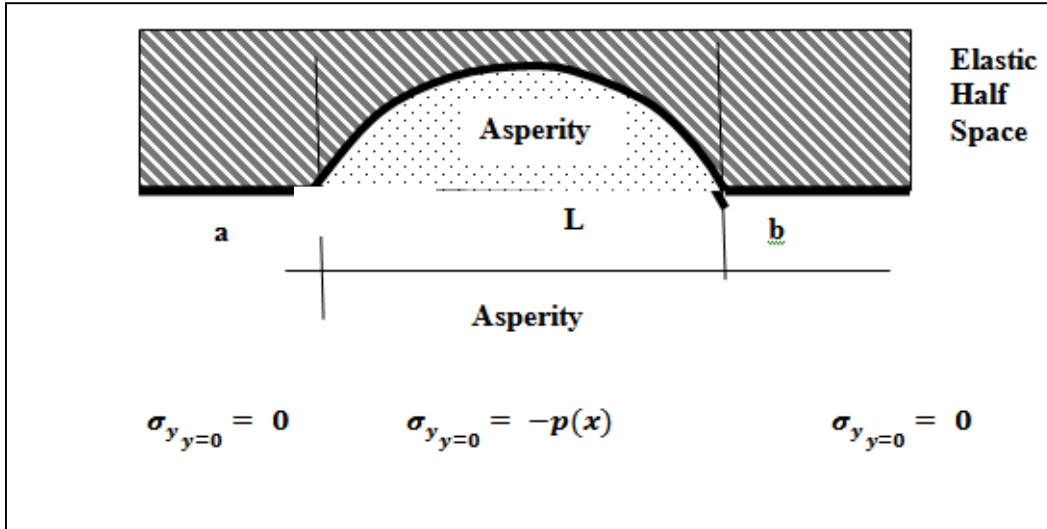
where

$A_n$  is projected area.

In most positive textures this quantity is much smaller than in negative textures. Hysteresis forces are therefore higher and then noise level should be higher with positive texture. The actual determination of noise level from hysteretic forces was not performed here as it involves a complex determination of source strength of a changing configuration in a dynamic system. Clapp et al [1.23] showed a tire pavement pressure distribution that is related to noise. This distribution is a function of the shape of the asperity. They approached the solution from a static analysis but did not extend the pressure distribution function to source strength determination.

### **1.8.3 Clapp et al Model**

Clapp et al [1.23] developed the algorithm for the factors causative to tire excitation mechanism. Factors were categorized as global forces and fluctuating forces that combine to produce the type and degree of tire excitation. They identified tire construction, inflation pressure and external loading as global forces. Astrom et al [1.43] also identified tread pattern, road surface texture and large road irregularities as the fluctuating forces. In a regular noise monitoring, the variables are the fluctuating forces. The tread patterns pertain to tire type which is standardized in this experiment. The road surface texture pertains to the texture type while the large irregularities refer to those waveforms as that generates pavement roughness (IRI) although environmental factors were not mentioned. Clapp et al then developed a model that predicts contact pressure that in turn predicts sound pressure. This model idealizes the contact as an elastic half mass on a continuum of asperities and develops a contact pressure distribution. In the development of the model, an indenter in contact with the tire carcass is analyzed. The mathematical process is based on the theory of elasticity

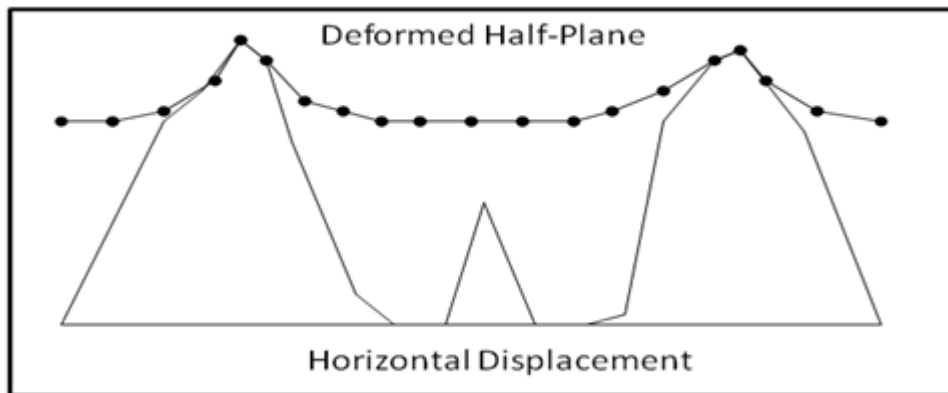


**Figure 1.22: Schematics of Indentor and Deformed Tire (Clapp et al) [1.22]**

$$p(x) = -(\sigma_y)_{y=0} = \frac{-E}{2(1-\nu^2)\sqrt{(x-a)(b-x)}} \int_a^b \frac{f'(t)\sqrt{(t-a)(b-t)}dt}{(t-x)} + \frac{c}{\sqrt{(x-a)(b-x)}} \quad (\text{Equation 1.29})$$

where

- p(x) = contact pressure distribution
- E = 1/2 plane modulus of elasticity
- ν = 1/2 plane Poisson's ratio
- x = horizontal contact position
- a, b = contact end points
- f' (t) = derivative of contact displacement function
- t = dummy variable of integration
- (σ<sub>y</sub>)<sub>y=0</sub> = vertical contact stress



**Figure 1.23: CLAPP's Prediction of Acoustic Pressure from Indentor Pressure Distribution**

The deduction from the Clapp et al [1.23] model is shown in Figure 1.22 and 23 above. It consists of an envelopment that is characterized by the asperity and bridging of the asperities. They suggest that the pressure distribution of the indentor envelopment is the scaled distribution of sound pressure and possibly of adhesion. Additionally the change or rate of change in volume



(of the inter asperity bridging feature [1.43] is the fundamental variable for sound generation. The model thus suggests the preponderance of a variable (envelopment) over the actual mean profile depth as an explanation of noise generation noting that the pressure distribution is positively correlated related to noise generated. Envelopment is determined by texture asperity interval and texture orientation. The dynamics of envelopment theory were expatiated further by Hamet and Klein [1.38].

#### **1.8.4 Hamet [1.38] Model & Hamet and Klein Model [1.39]**

The difference in acoustic properties of 2 texture configurations of the same mean texture depth was ascribed to different envelopment phenomena by Hamet et al [1.39] and also by Hamet [1.40]. Envelopment phenomena describe the spatial interaction of the transient tire deformation phenomena around the asperities to produce noise. Hamet idealized texture asperities envelopment phenomena in two strategies, static and dynamic envelopment.

Static Envelopment: In the static envelopment, cognizance is taken of the extreme case of texture-asperities as observed in pervious pavements. There exists a progressive improvement of acoustic properties with increase in cavity depth until a point is reached where any increase does not significantly affect acoustic properties. This situation calls for some rounding of the asperities to reflect only the effective asperities that affect tire pavement interaction. Experiments conducted at different elastic moduli found the same effect that the envelopment at constant inflation pressure depended on the elastic moduli of the surface. For various pavements, greater envelopment occurred at lesser inflation pressure and the acoustic properties of the rigid pavement section was less sensitive to changes in elastic properties than the flexible pavements

Dynamic Envelopment: This strategy is actually enunciated in 2 parts namely the (dynamic) rolling process and the dynamic envelopment process. The dynamic rolling process provides a finite element approach to the tire rolling on the pavement while the dynamic envelopment is simulated as a high pass filter of contact patch dimensions traveling on the road surface and facilitating noise prediction from (perceived) texture.

The dynamic rolling process uses a PSD analysis of texture and elastic properties to predict noise. As a corollary, it provides a correlation between measured road texture spectra and calculated acoustic spectra. In this part of the second strategy, a bare tire model was used. This eliminated envelopment phenomena but, tire pattern-induced air-pumping-phenomena. It appeared that the medium and low frequency tire noise were from tire vibration related mainly to texture. This corroborated the initial findings of Hamet [1.38] and Hamet et al, [1.39] who proposed 3 sub-models of the tire pavement phenomena in this sub-strategy to include:

- The Tire (Vibration behavior)
- The tire road mechanical interaction and the acoustic radiation of the tire.
- The horn effect.

The tire is represented by a linear 3-dimensional Greens function of position and time.

Hamet et al [1.39] introduced a local stiffness  $s_e$  and contact pressure

$$\mathbf{F}''(\mathbf{x},t) = s_e \Delta \mathbf{h}(\mathbf{x},t) H(\Delta h, 0) \quad (\text{Equation 1.30})$$

where

$\Delta h(x,t) = \mathbf{H}_{(\text{thread})}(x,t) - \mathbf{h}_{\text{road}}(x,t)$  which is the relative position of tire and road surface.

**In the dynamic envelopment process**, unlike the static process, the tire and road surface are not stretched out in superposition. The length and width are finite in the dynamic process and it simulates more closely the travel of a contact patch. The force of interaction is minimum at entrance and exit and maximum at the kern of the contact zone. In consequence of the finite zone of contact a high pass filter is inadvertently created as would in practice. The envelopment function is given by

$$z(\text{env})(x) = \mathbf{F}''(\mathbf{x}_c, \mathbf{x}/v) / S_e \quad (\text{Equation 1.31})$$

where

- z is envelopment function,
- $X_c$  is the center of an envelopment in the x –axis
- V is velocity
- $S_e$  is area of envelopment
- v is the rolling speed

This model originally indicated non-dependence on speed but that is still being verified

The static contact model described By Hamet et al was developed to extend the texture-noise relationships to pervious pavements in the critical frequency range where tire belt vibration noise predominates due to air-pumping phenomenon [1.21] and [1.17]. The Klein model is an envelopment theory indicating that sound can be predicted from the actual envelopment configuration. It was Donovan [1.15] who went ahead and developed actual envelopment noise generation equations. This is discussed in the next section.

### **1.8.5 Donovan's Equation for Sound Generation**

Hamet and Klein showed the effect of envelopment but the use of source strength to generate actual sound intensity was attempted by Donovan [1.15]. He showed that the source strength of a tire interacting with a groove depended on the volume change due to the interaction. He showed that an acoustic function  $q(t)$  can be expressed as

$$q(t) = \log \frac{\Delta V}{V} (1 - \cos(2\pi \frac{t}{T})) \text{ for } T > t > 0$$

$$q(t) = 0 \text{ for all other } t. \quad (\text{Equation 1.32})$$

where

- v is volume of texture configuration,
- q (t) is a noise amplitude function,
- t is time,
- T is period.

In Equation 1.32, T is the duration of volume change and t is any time within the period. Donovan [1.15] also proved that the source strength of a groove is proportional to logarithm of the cross section of the groove which suggests that effective groove area reduction is a quiet pavement strategy. With the work of Clapp, Hamet et al and Donovan, it is difficult to accept models that are based on mean texture depth.

### 1.8.6 Hanson's Model [1.26]

#### **Non-Pervious Concrete pavements:**

$$\text{Noise level (dBA)} = 95 + 13 (\text{Texture Depth}) \text{ with } R^2 = 0.67 \quad (\text{Equation 1.33})$$

#### **Pervious pavements:**

$$\text{Noise level (dBA)} = - 0.42 \text{ Porosity (\%)} + 103.7 \text{ with } R^2 = 0.67 \quad (\text{Equation 1.34})$$

Hanson's correlation [1.26] for non-pervious pavements did not consider properties that influence the envelopment features proposed by Klein, and Hamet et al. These correlations suggest that texture depth in concrete pavements governs noise when those pavements are non-pervious. The relationship is however inadequate to characterize concrete surface because it ignores texture orientation, pavement age and texture type. To establish a better relationship is one of the prime challenges of this current study. While most current research [1.38] and [1.39] show that MPD is not a significant variable in sound intensity, Hanson et al indicate otherwise. There is no consensus that mean profile depth is a significant variable in the prediction of sound intensity. Other models by Bendstein [1.41] and Fujikawa[1.42] will be discussed later in detail

### 1.8.7 Byrum's Analysis [1.43] Effect of Tine Spacing on Tire Carcass Vibration

Byrum et al [1.43], performed noise testing at the Ontario test site with various texture intervals at approximately 96 km/h (60 mph). According to Byrum et al [1.43] certain ripple effect inherent in the texture resulted in reduced tire excitation in the fundamental tire carcass modes of vibrations up to less than 1,000 Hz. At this velocity, a spacing of 16 mm (630-mil) would strike, or tap, the front of the contact patch at a frequency of approximately 1,675 Hz. A significant rise in noise level was visible in the noise testing results for the 16-mm (630-mil) tining near 1,600 Hz. A feature spacing of 8-mm (315-mil) was impacting the front of the contact patch at a frequency of approximately 3,250 Hz. The acoustic spectral plot revealed there was not much reduction in noise level in this frequency range for the experimental 8-mm (315-mil) spacing grooves, compared with the 16-mm (630-mil) grooves. The 8-mm feature impact-frequency lines up with another key structural response frequency for typical car tires around 2,500 to 3,500 Hz, thought to be related to tread block excitation. Therefore Byrum's experiment corroborated the knowledge that various frequency features in the texture configuration can result in tire resonance.

**Stress Distribution Modeling:** According to Canudas –De-Wit et al [1.44] Clapp developed a model to approximate tire pavement interaction using a two dimensional contact theory. In this model (Figure 1.24). A rigid material is used to represent the pavement while a semi-infinite elastic half plane is used to represent the tire. Relating interfacial stress and noise, A uniformly distributed load is applied to the rubber to force contact with the pavement. The pressure distributions associated with the individual contact areas produce forces that excite the tire structure. The mathematical model can predict the contact stress distribution between a hard pavement surface and the tire. The contact pressure fields can be transformed into a time-varying pressure by dividing the contact patch length by the vehicle speed to obtain a sampling frequency. At each point in the contact patch, there is pressure acting on the tire; a Fourier transformation is applied using a previously determined sampling frequency to generate a power

spectral density. This variation in input force was explained alternatively by the dynamic friction model without the ramification of input forces in a Fourier series.

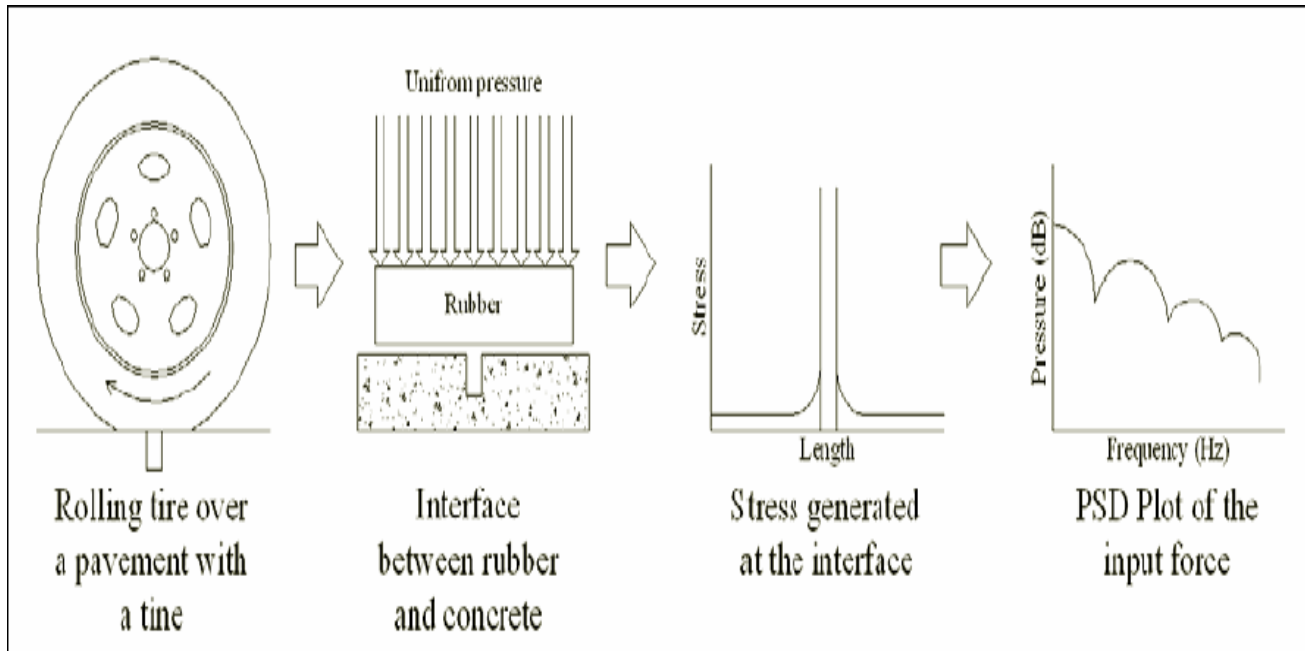


Figure 1.24: Clapp 1988 Model of a PSD of Input forces

### 1.8.8 Dynamic Friction Models for Longitudinal Tire

Astrom et al discussed the Luge model that gives a mathematical (Differential Equation 1. for the transient interactions in a tire pavement friction contact. The Model accommodates the hysteretic deformation of the contact patch tire element and analyzes a steady state slip analysis. The equations are:

$$\frac{\partial z}{\partial \zeta}(\zeta, t) + \sigma_0 \frac{\partial z}{\partial t}(\zeta, t) = v_r - \sigma_0 |v_r| / g(v_r)(\zeta, t) \quad \text{(Equation 1.35)}$$

$$g(v_r) = \mu_c + (\mu_s - \mu_c) e^{-\mu |v_r| / v_s} \alpha^0$$

where

- $\sigma_0$  rubber longitudinal lumped stiffness
- $\sigma_1$  is the rubber longitudinal lumped damping
- $\sigma_2$  is the viscous relative damping
- $\mu_c$  &  $\mu_s$  respectively are the normalized Coulomb friction and the normalized static friction in which  $\mu_c < \mu_s$
- $v_s$  is the Styrene relative velocity,
- $v_r = (r\omega - v)$  is the relative velocity
- $z(\zeta, t)$  is the distribution independent variable that describes the deflection of an elementary rubber element at time  $t$  situated at location  $\zeta$  along the contact patch
- the constant  $\alpha$  captures the steady state friction slip characteristics

$$F(t) = \int (\sigma_0) z(\zeta, t) + \sigma_1 \frac{\partial z}{\partial t}(\zeta, t) + \sigma_2 (v_r) \frac{\partial z}{\partial t}(\zeta, t) f_n(\zeta) d\zeta \quad \text{(Equation 1.36)}$$

The steady state equation places  $\frac{\partial z}{\partial \zeta}(\zeta, t) = 0$

$F_n(\zeta)$ , is the normal force-density-function along the contact patch.

This is a complex model that does not necessarily explain hysteresis. The model of Wu and Nagi [1.21] shown in Figure 1.25 is simple but explains the components of friction by developing equations from a free body diagram.

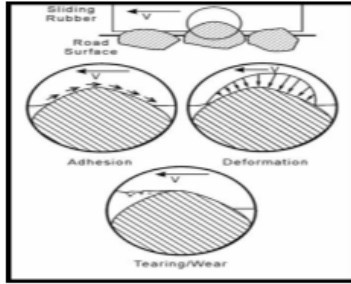
Other texture degradation or correlations presented by Bazlamit and Reza [1.23], Izevbekhai & Khazanovich [1.8] are not discussed here but will be elucidated in the research.

### **1.8.9 Fragmentation of Surface Profiles**

A global correlation of pavement surface characteristics does not yet exist. Sandberg et al discussed the correlation between sound absorption, porosity and tortuosity and also discussed the time decay functions for various pavement textures. Sandberg et al [1.30], Izevbekhai & Khazanovich [1.8] provided sufficient indication that there is a time degradation model for texture type, traffic volume, and international roughness index but do not exhaust the spectral content that are indicative or causative to these correlations.

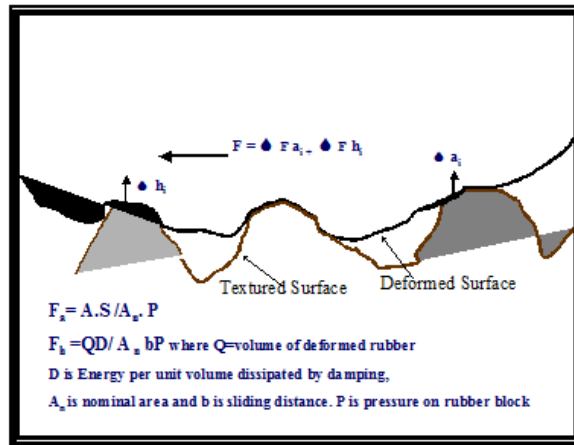
The following process converts a profile from the spatial to the spectral domain:

$$F(x) = a_n \sum \sin w \omega x + \sum b_n \sum \cos \omega x \quad (\text{Equation 1.37})$$



$F_a = A S / p A_n$   
 $F_{we} =$  Wearing force  
 $F_h = QD / A_s b p$   
 $f_a =$  Adhesion Coefficient  $= F_a / W$   
 $f_h =$  Hysteresis Coefficient  $= F_h / W$   
 $f_{we} =$  Wear Coefficient  $= F_{we} / W$   
 $B =$  Rubber Sliding Distance  
 $W =$  normal reaction  
 $A =$  actual Contact Area  
 $Q =$  Volume of Rubber participating in the deformation  
 $A_n =$  Nominal Area  
 $S =$  Interface Shear Strength  
 $D =$  Energy dissipated per unit volume of rubber damping  
 $P =$  Pressure on rubber Block

$$F = F_a + F_h + F_{we}$$



**Figure 1.25: Hysteresis in Friction**

For all aperiodic signals where  $f(x)$  is the profile and  $a_n$  and  $b_n$  must be determined

$$\begin{aligned}
 f(x) &= a_0/2 + \sum_{n=1}^{\infty} a_n \cos n\pi x/L + \sum_{n=1}^{\infty} b_n \sin n\pi x/L \\
 &= a_0/2 + a_1 \cos \pi x/L + a_2 \cos 2\pi x/L + a_3 \cos 3\pi x/L + \dots \\
 &\quad + b_1 \sin \pi x/L + b_2 \sin 2\pi x/L + b_3 \sin 3\pi x/L + \dots
 \end{aligned}
 \tag{Equation 1.38}$$

$$\begin{aligned}
 f(x) &= a_0/2 + \sum_{n=1}^{\infty} a_n \cos n\pi x/L + \sum_{n=1}^{\infty} b_n \sin n\pi x/L \\
 &= a_0/2 + a_1 \cos \pi x/L + a_2 \cos 2\pi x/L + a_3 \cos 3\pi x/L + \dots \\
 &\quad + b_1 \sin \pi x/L + b_2 \sin 2\pi x/L + b_3 \sin 3\pi x/L + \dots
 \end{aligned}
 \tag{Equation 1.39}$$

$$\text{Xi} = \sum_{n=0}^{N-1} a_n \cos (\nu 2\pi i/N) + b_n \sin (\nu 2\pi i/N)$$

where

$a_n$  and  $b_n$  are Fourier coefficients  $0, \leq \nu \leq N/2$   
 $x_i$  is the profile elevation

Consequently

$$a_n = \frac{1}{N} \sum_{i=0}^{N-1} x_i \cos(\nu 2\pi i/N)$$
$$b_n = \frac{1}{N} \sum_{i=0}^{N-1} x_i \sin(\nu 2\pi i/N)$$
$$w(\nu) = \nu / (N\Delta t)$$

where

$w(\nu)$  is the frequency corresponding to  $\nu$  and  $\Delta t$  is the sampling interval

It can therefore be proven that removal of highly amplified wavelengths will improve pavement smoothness. Otherwise, dominant waveforms can be detected and curve fitted to explore further the effect of those waveforms on the measured IRI. This further accentuation of the intent of the authors is covered in the following section with a real life example of a project that was drastically affected by stringline effects. These effects are visible in a Power Spectral density analysis of a ride quality profilograms well as the Spectral plot of the Noise frequency domain. Preliminary analysis conducted by this proposal indicates that correlations of pavement surface characteristics and prediction models

#### **1.8.10 Summary of the Contact Theories**

The 6 models converge to a common denominator: there are texture configuration dimensions and resonant phenomena that possibly influence OBSI. The next chapter will attempt physical derivations and further examination of some texture configuration variables. The next chapter will attempt to establish if identified significant variables are negatively or positively correlated to OBSI. However most detailed acoustic research indicated that sound intensity may be affected by environmental factors and in reality the European Union provided a directive for noise correlation due to temperature. Details of this correction are discussed in the next sub section. Tire pavement contact theories have been simplified and presented in the foregoing. All the references exhibit some commonalties

- Certain pavement surface ratios and variables may be very influential to surface properties. These include the asperity area ratio (ratio of indenter gross area to projected area, the ratio of the groove bridging volume to the total groove volume and the general envelopment function or configuration. These ratios will be properly defined and assigned more relevant measurable and determinate forms.
- By implication the indentors and gross contact areas are facilitated by tire carcass instantaneous collapse. The actual mechanical collapse and restoration phenomena of tires are outside the scope of this study. However, tire type and stiffness would have been relevant but that potential variability is eliminated by using a standard reference test tire (SRTT) in this research.

Based on the literature references from 5 authors, there is no consensus on MPD correlation to OBSI. Other authors do not mention MPD as variable that may be used for the prediction of OBSI. Based on the analysis and reviews of tire pavement envelopment, MPD is not likely to be a significant variable in terms of tire pavement noise but this will be investigated in subsequent

chapters. Based on the work of Bendstein et al and Fujikawa et al, definitive texture wavelength variable as well as an indicator of texture unevenness is suggested variables that influence noise. Izevbekhai [1.2] showed that texture unevenness may be correlated to IRI. Since Wu and Nagi showed that texture unevenness in concrete pavement texture directly affects IRI and it was established analytically that general surface unevenness and waveforms affect IRI, then asperity interval and IRI fit the requirements for OBSI explanatory variables.

A set of previous research reviewed indicated but did not validate that acoustic properties may be different even when certain texture parameters such as mean profile depth are similar. The next chapter attempts to physically examine how these variables may affect tire pavement noise.

### 1.9 Environmental Considerations

This subsection examines publications relating to possible effects of environmental variables on OBSI. It was shown that sound intensity depends on some environmental factors such as density and speed of sound as well speed of sound. Additionally, acoustic conditions are basically adiabatic and not isothermal. [1.45]

According to authorities [1.45], [1.46], [1.47], [1.48], [1.49], [1.50] & [1.51] in environmental concepts for sound intensity density and speed of sound are the environmental components of sound. Since these are affected by temperature, a temperature effect can be derived from first principles. According to Sandberg and Ejsmont [1.27], there was a realization in the 1980s that external tire-pavement noise was influenced by temperature. The need for reproducibility and repeatability necessitated measurement in a narrow temperature band. Currently in Europe auto tires are influenced by -1 dB per 10 degrees in a cold climate. To address this observation, the ISO working group delivered a first draft recommendation in 2003 (ISO/TC43/SCI/WG/27) [1.45]. Furthermore, the society of automotive engineers has addressed the problem [1.27] with sound-intensity normalized-measurement at 20°C (293 °k).The problem was compounded by the fact that the mechanism of noise generation was poorly understood. However, it was shown [1.27] that

$$L = a + bT \quad \text{(Equation 1.40)}$$

where

L = Sound Level [dB]

T = Temperature [°C]

(a,b) = Constant (b is temperature gradient)

Sandberg and Ejsmont obtained a temperature gradient of -0.042. Landsberger [1.47] obtained similar gradient in four out of five tires. In 2001, Landsberger also obtained varied air and road temperature gradients as shown in Table 1.2. There is a correction to the European Union directive on tire noise (2001/43/EC).The final result of an A-weighted sound level is normalized to a list surface reference temperature (T<sub>ref</sub>) by applying a temperature correction according to the following Equation [1.46] :

$$L_R (T_{ref}) = L_R (T) + K (T_{ref} - T) \quad \text{(Equation 1.41)}$$

where

L<sub>R</sub> = Corrected Sound Level [dB]

T<sub>ref</sub> = Reference Temperature 20°C



T = Measured Surface Temperature  
 K = Temperature Coefficient

For passenger tires:

K = -0.03 dBA/°c where T > Tref  
 K = -0.06 dBA/°c where T < Tref

For Light Trucks and Vans:

K = -0.02 dBA/°c

For class C<sub>3</sub> tires (heavy truck tires):

K = 0 No correction!

**Table 1.2: Temperature Effects**

TIRE	SPL TO TEMPERATURE GRADIENT DB/°C			
	53 Km/hr		80 Km/hr	
	Air Temp. Gradient	Road Temp. Gradient	Air Temp. Gradient	Road Temp. Gradient
1	-0.049	-0.035	-0.040	-0.036
2	-0.025	-0.020	-0.035	-0.031
3	-0.001	-0.001	+0.014	+0.015
4	-0.008	-0.006	-0.054	-0.0044
5	-0.068	-0.053	-0.070	-0.055
6	-0.010	-0.005	-0.042	-0.032

From this subsection, it was suggested by 3 three references that temperature increase may result in reduced sound intensity [1.48]; [1.49]; [1.50]. Since the EU sound intensity metric is the CPX method and not OBSI the correlation of OBSI with temperature, whether positive or negative is yet unknown. As an indication of variables that have been very influential temperature-based corrections are traditionally made to sound intensity measurements in Europe. The European Union issued a directive [1.31] with guidelines for temperature correction. Research conducted [1.50] had formed the basis for this directive.

$$L_R (T_{ref}) = L_R (T) + K (T_{ref} - T) \quad \text{(Equation 1.42)}$$

**Table 1.3: European Union (EU) Temperature Correction Factors for Sound intensity Level**

	K dBA/°c	
	T>Tref	T< Tref
Passenger Car tires	-0.03	-0.06
Light Truck and Van Tires	-0.02	
Heavy Truck Tires	None	

Tire-pavement interaction noise is a combination of longitudinal waves of various frequencies. It is affected by many factors such as pavement surface characteristics, pavement conditions, tire characteristics, and vehicle speed. Empirical observations led to the conclusion that ambient conditions affect noise as well. Several researchers and practitioners intensity [1.48]; [1.49]; [1.50] have proposed to correct pavement noise measurement results for the ambient air temperature, but no theoretical justification of this correction has been found in the literature. This limitation is addressed in this section by obtaining an analytical relationship between the gas media properties and theoretical sound intensity by considering a one-dimensional illustrative example. Although interim standard for On Board Sound intensity (OBSI) measurements [1.31] does not currently correct for temperature it requires that temperature is documented along with the acoustic measurements. In one of the equations, Fahy [1.30] showed that temperature increase may cause a decrease in OBSI according the square root of absolute temperature. However, neither Fahy [1.33] nor others derived or validated that lemma. A simple noise source in contact with an acoustic medium is analyzed. A noise response equation is derived by a one dimensional solution to a pulsating sound source coterminous with an acoustic medium. Specifically, a cylindrical mass of an acoustic medium in direct contact with and subject to the effect of a pulsating source is being analyzed. The pulsating source induces its amplitude and angular speed unto the medium whose density and acoustic speed contribute to the response of the medium. Consider the particular problem of a one-dimensional sound wave propagation through a gas cylinder. One end of the cylinder is subjected to displacement,  $Y_0$ , in the longitudinal direction with an amplitude  $A$  and circular frequency  $w$ . A method discussed in detail by Izevbekhai [1.8] shows that

$$SI = 0.5 (\rho c) w^2 A^2 \quad \text{(Equation 1.43)}$$

This equation shows that SI comprises two major components:

- The environmental component  $\rho c$ : How this quantity actually affects sound intensity may not be limited to those 2 quantities alone. For instance density is affected by temperature and volume as well as thermodynamic conditions as for instance in adiabatic versus isothermal condition. The variables that will be examined thus include atmospheric temperature, atmospheric pressure and relative humidity.
- The input and pavement feature component  $w^2 A^2$ . The angular frequency is a function of the texture spacing and tire speed. The amplitude is a function of the pressure wave generated by the tire pavement interaction. This may be related but not limited to

enveloped volume or to the ratio of bridged groove volume to total groove volume. In this experiment, the tire type has been kept constant and restricted to the SRTT (ASTM F2493 - 08) [1.29]. Moreover in the operation of the OBSI test, a constant speed of 60 miles per hour is used. This leaves the input variables with the pavement surface type, based on the standard tire at 60 miles per hour. These two conditions are required in OBSI measurements. The pavement surface variables likely to affect sound intensity would be texture orientation, texture asperity, texture direction, international roughness index will be examined.

In consequence, if speed and texture are kept constant, in the absence of any unexpected variable, environmental effects can be monitored.

- A third part that must not be ignored is the resonant frequency component. It is expected that certain wavelengths will resonate with the tire carcass or with the quarter car algorithm to bring about unusually high sound response. All resonant frequency tires are not identified but the tire carcass resonance in transversely tined pavements, Helmholtz resonance, the pipe resonance and IRI are discussed.

From the preceding derivation, temperature, relative humidity and atmospheric pressure are discussed in this section. Amplitude A and angular frequency w, are characteristics of the source, and thus do not depend on the acoustic medium sound intensity dependent on the density and speed of sound of the acoustic medium was derived. Evidently in a sound intensity testing or monitoring, if the surface, test equipment and measuring speed are constant, amplitude and angular speed components will be constant. Variability will then be attributed to environmental factors that have been identified as temperature, pressure and relative humidity.

### **1.9.1 Atmospheric Variables: Temperature**

By developing the relevant set of equations, normalized sound intensity was found to decrease with increase in absolute temperature. Additionally, it was conclusive that temperature affects normalized sound intensity to the degree that would necessitate temperature correction in the analysis of pavement response. The effect of atmospheric pressure and relative humidity were also examined. These variables influence normalized sound intensity. However the degree to which they affect normalized sound intensity was found to be negligible in comparison to temperature. Correction for temperature variation is thus recommended.

For subsequent analysis we will consider a normalized sound intensity, SI\*, defined as:

$$SI^* = \frac{SI}{0.5 w^2 A^2} \quad \text{(Equation 1.44)}$$

From Equation 1.44, it can be concluded that the normalized sound intensity is:

$$\frac{SI^*}{SI} = f(w, A) \quad \text{(Equation 1.45)}$$

where

w and A are input signals,

For air,  $\rho$  and  $c$  depend on atmospheric conditions (temperature, atmospheric pressure, relative humidity, etc.).

It is therefore likely that atmospheric conditions affect sound intensity. Specifically, the effects of temperature, atmospheric pressure and relative humidity are discussed in the next section. It can be shown from ideal gas laws [1.53] that

$$\rho = \frac{P}{RT} \quad \text{(Equation 1.46)}$$

where

$p$  ( $\text{kg/m}^2$ ) is pressure,

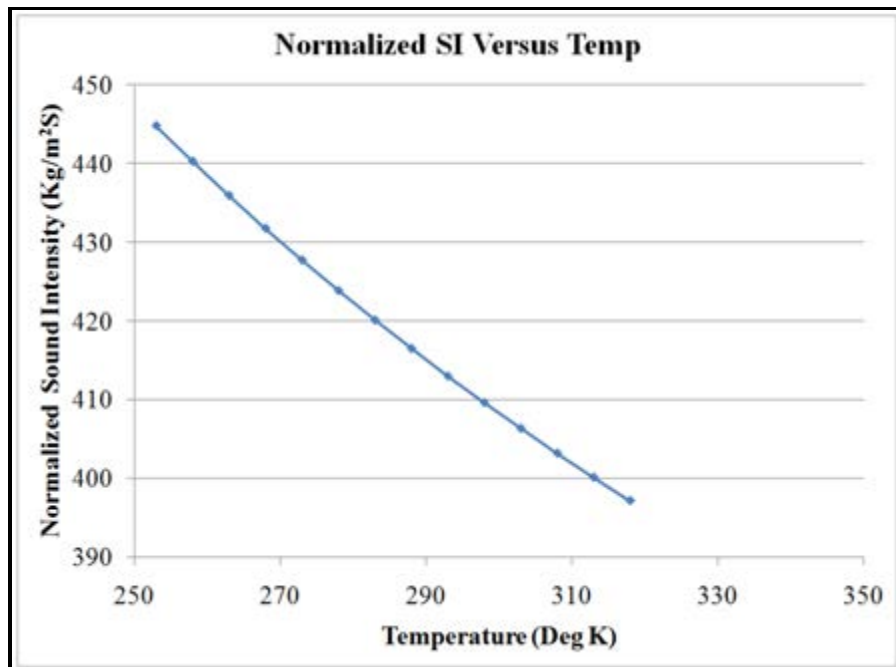
$R$  is the specific gas constant (= 287.058 (J/kg-K) for air),

$T$  is temperature given in Kelvin.

Speed of sound in air [1.54] approximates to  $C = 167 + 0.6 \cdot \text{SI}^*$  is introduced as a component of the sound intensity that is dependent solely on environmental factors. A combination yields

$$\text{SI}^* = \rho c = \frac{P}{RT} \left[ \frac{167}{T} + 0.6 \right] \quad \text{(Equation 1.47)}$$

From Figure 1.26, normalized SI versus temperature is a decreasing function. Since  $w$  and  $A$  are dependent on the input and do not depend on temperature particularly from 260 deg K to 308 deg K, then functionally,  $\text{SI} \sim \frac{1}{T}$  when  $P$  is constant (Equation 46)



**Figure 1.26: Relationship between Normalized SI and Temperature**

### 1.9.2 Atmospheric Variables: Relative Humidity

Relative humidity has little impact on the speed of sound and the density of air. This was established through analysis of physical concepts and numeric data from Bohn [1.56]. Water

vapor is lighter than air (molecular weight of H<sub>2</sub>O is 16 and air is 28 [1.57]). Water vapor thus decreases the density of air. The air and water vapor combine to form an atmospheric unit weight that depends on the moisture content that is related to the relative humidity. Relative Humidity [1.55 ]; [1.56] & [1.57] is defined as

$$RH \% = 100 \frac{P_{H_2O}}{P_{H_2O,SAT}(T)} \quad (\text{Equation 1.48})$$

where

RH is relative Humidity,

P H<sub>2</sub>O is the partial pressure of vapor,

PH<sub>2</sub>O Sat (T) is the pressure of saturated vapor at temperature (T).

According to the USEPA [1.55]

$$\rho = \rho_{da} (1 + x) / (1 + 1.609 x) \quad (\text{Equation 1.49})$$

where

x is the percentage of water vapor,

1.6 is the ratio of dry air density to vapor density,

$\rho_{da}$  is the density of dry air at a given temperature,

$\rho$  is the density due to humidity.

Some authors including [1.54] and [1.55] have created a chart that relates proportion of water vapor at certain temperatures to relative humidity. For convenience the chart is shown in figure 1.27.

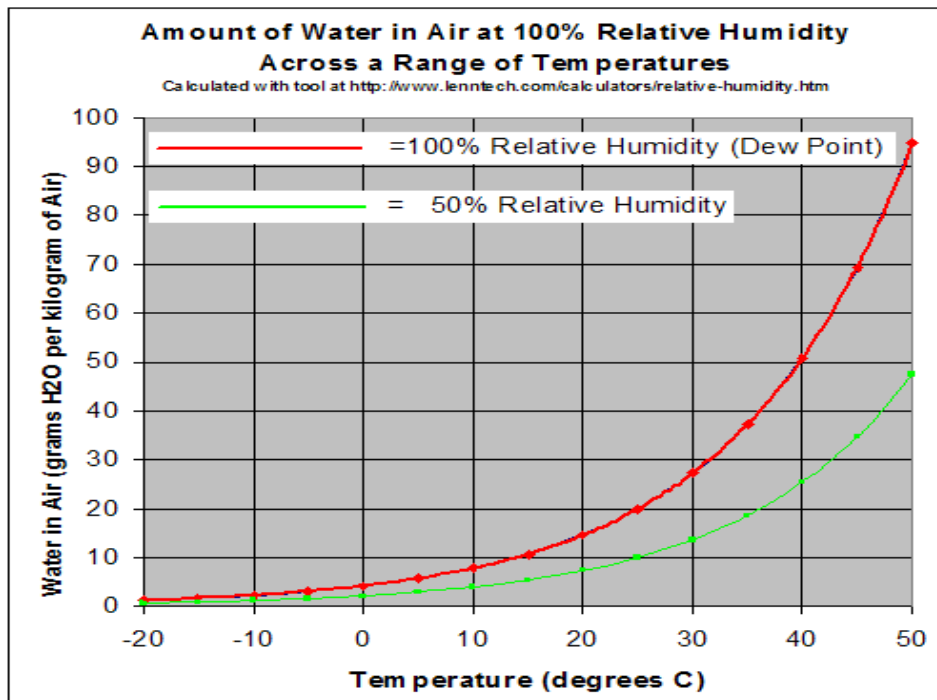


Figure 1.27: Water Vapor in Air at Various RH and Temp Ranges

Relative humidity also affects sound intensity slightly by increasing the speed of sound at a constant pressure [1.56]. Air density in Table 1.4 was calculated by starting from gravimetric values obtained from the above chart [1.58] to obtain the gravimetric ratio of water to air ( $x$ ). The dry air density ( $\rho_{da}$ ) values obtained from another reference [1.56] and  $x$  were used in Equation 1.48 to compute the air density ( $\rho$ ) corresponding to 50% and 100% relative humidity. The speed of sound in TABLE 1.4 were determined from the family of plots created by Bohn [1.55] that showed the changes in speed of sound due to relative humidity. From the percentage changes from Bohn [1.55] the actual speed of sound  $c$  at 50 % and 100% RH were computed by adjusting the  $c$  for dry air obtained from Sengpiel [1.45] with the percentage changes presented by Bohn [1.55]. The resulting “s” values at the various relative humidity are shown in Table 1.28.

SI\* in Table 1.4 at each relative humidity was computed as the product of the air density at that relative humidity and the speed of sound at that relative humidity. From the SI\* obtained, relative humidity does not appear to have any significant influence on normalized sound intensity. Table 1.4 shows that at a constant temperature, the variation in normalized SI through the full range (0 to 100 %) of relative humidity is relatively small. The dominance of temperature over humidity is accentuated by Figure 1.28 where the full-range of RH at 273 and 303 deg K are shown. The difference due to temperature far exceeds the effect of relative humidity change. The difference due to humidity may therefore not be significant enough to require correction in sound intensity.

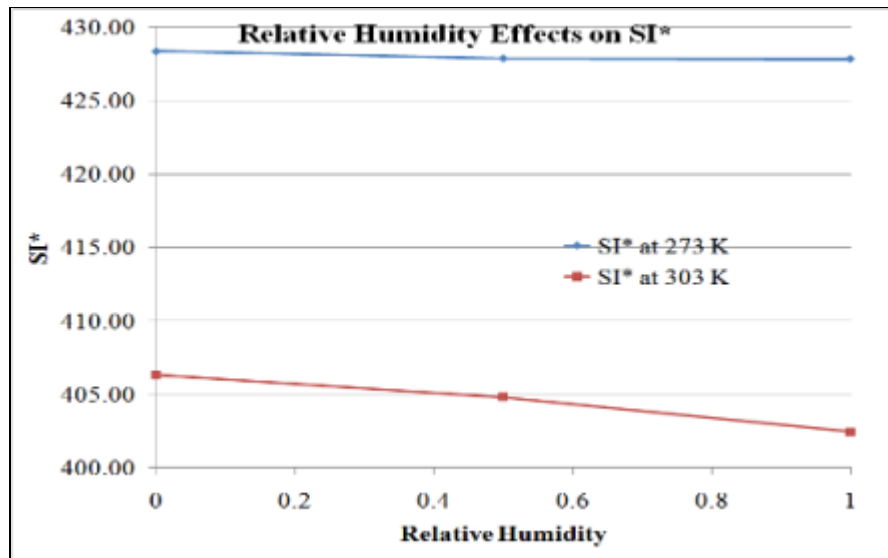


Figure 1.28: Effect of Relative Humidity on SI\*

**Table 1.4: SI\* For A Range of Relative Humidity and Temperature**

Temp K	Speed of Sound			Density kg/m <sup>3</sup>			SI*		
	Dry Air	50%	100%	Dry Air	50%	100%	Dry Air	50%	100%
273	331.3	331.4	331.6	1.293	1.291	1.290	428.3	427.8	427.8
293	349.1	350.3	351.5	1.164	1.156	1.145	406.3	404.8	403.4

### **1.9.3 Atmospheric Pressure**

Atmospheric pressure variation in a specific location does not influence OBSI significantly. Changes in altitude are likely to affect OBSI but such comparisons are likely to be confounded by temperature whose significance has been established beyond doubt. Atmospheric pressure data at the MnROAD test site varied from 991 to 1015 HectoPascal. The range included extreme storm event outliers where transient pressure drops were experienced.

### **1.9.4 Section Summary**

A temperature sound intensity equation was derived from a one dimensional solution to a sound source propagated through an acoustic medium. Temperature has a strong influence on OBSI to necessitate a correction to a standard temperature. The temperature is inversely proportional to temperature but not in a linear relationship. Temperature will be chosen as one of the explanatory variables in the statistical sound intensity level prediction model.

Other environmental variables such as relative humidity and atmospheric pressure were not statistically significant. The preceding derivation found input and pavement feature component to be  $w^2 A^2$ . The angular frequency is a function of the texture spacing and tire speed. The amplitude is a function of the pressure wave generated by the tire pavement interaction. This may be related but not limited to enveloped volume or to the ratio of bridged groove volume to total groove volume. In this experiment, the tire type is not a variable. Moreover in the operation of the OBSI test, a constant speed of 60 miles per hour is used. This leaves the input variables with the pavement surface type, based on the standard tire at 60 miles per hour. These two conditions are required in OBSI measurements. The pavement surface variables likely to affect sound intensity would be texture orientation, texture asperity, texture direction, international roughness index are now theoretically examined.

### **1.10 Resonance Phenomena**

From Equation 1.39 causative variable attributable to the pavement surface-tire characteristics is  $w^2 A^2$ . After examining the possible effects of asperity interval, texture direction, texture orientation and IRI, it is logical to examine resonant phenomena since in certain frequencies where resonance occurs, response may be higher than predicted from ordinary extrapolations. Certain resonant phenomena in pavements have been identified based on the use of equations developed by Pierce [1.56] and Kinsler et al [1.57]. The most common of these phenomena include Helmholtz resonance and Pipe resonance. Helmholtz resonance phenomenon arises from overcompensation in a cavity that is subjected to a pressure fluctuation transmitted through a necked orifice. This is typified by the simple harmonic movement of air in an orifice resulting in sound generation in the cavity. Pipe resonance occurs when a tire drives over a groove or joint

and the compression forces are transmitted in the direction of the joint. Instantaneous tire texture interaction favor the formation of these two prominent resonant phenomena. Another resonant frequency such as transverse tire perfect storm has been discussed in the preceding section.

### 1.10.1 Helmholtz Resonance in Tire Pavement Interaction

Consider a tire bridged over a texture groove as shown in Figure 1.29. Resonant frequency of SI due to air compression in a groove or joint  $\approx \xi \log dV/V$  [1.14] where  $\xi$  is constant. It was also shown by Donovan [1.15] that  $SPL \sim V$ . Where SPL is sound pressure level  $dV$  is change in groove volume due to tire bridging and  $V$  is the original groove volume. This is likened to a Helmholtz phenomenon that is characterized by the compression and rarefaction of a cavity of air of volume  $v$  typically at the orifice of area  $S$ . The ideal Helmholtz phenomenon is shown in Figure 1.29 and is largely demonstrated by the response of a narrow necked jar when air is blown over and into it.

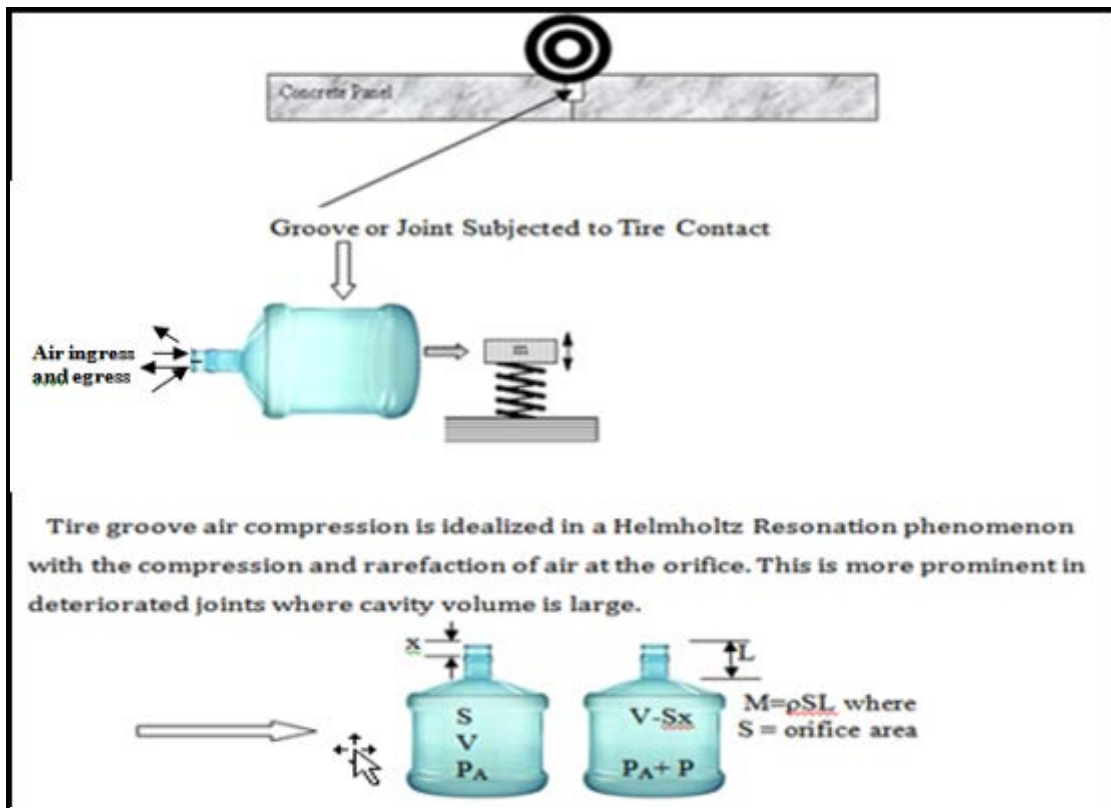


Figure 1.29: Texture or Groove in Helmholtz Resonance Phenomena.

The free body diagram in Figure 1.29 [1.59] shows the column of air in the orifice behaves as a spring in simple harmonic motion. To analyze a simple harmonic motion, a displacement and an acceleration function particularly of the form  $\frac{d^2x}{dt^2} = \frac{F}{m}$  is important. From Figure 1.29,

$$F = ma \text{ or } \frac{d^2x}{dt^2} = \frac{F}{m} \quad (\text{Equation 1.51})$$

$$\frac{P}{p_A} = -\gamma \frac{\nabla V}{V} = -\gamma \frac{\nabla Sx}{V}. \quad (\text{Equation 1.52})$$



$$\frac{d^2x}{dt^2} = \frac{pS}{\rho SL} = -\frac{\gamma SP_A}{\rho SL} x \quad (\text{Equation 1.53})$$

This is a simple harmonic motion. Substituting for  $c = \sqrt{\frac{\gamma P}{\rho}}$

$$\text{The resonant frequency is } f = \frac{c}{2\pi} \sqrt{\frac{S}{VL}} \quad (\text{Equation 1.54})$$

where

Actual definition of L is difficult. L according to Pierce [1.56] is affected by the spalled corners of the groove or joint,

assume

L to be 0.1 mm,

C = 330 m/s,

v = 2 mm<sup>2</sup>,

s = 10 mm<sup>2</sup>,

The frequency at resonance is 371 Hz

The value of S L and V can be manipulated to stay away from the resonant frequency of 750 to 1250 Hz. This is the regime of frequencies renowned for tire carcass resonance.

For a toroidal radius of 20 inches dV/V is small in a regular joint but if the groove width increases, the chord as shown in Figure 1.29 increases and therefore wider or deteriorated grooves will be noisier. Figure 1.30 shows the SPL levels for various groove width (b) and depth (d) combinations.

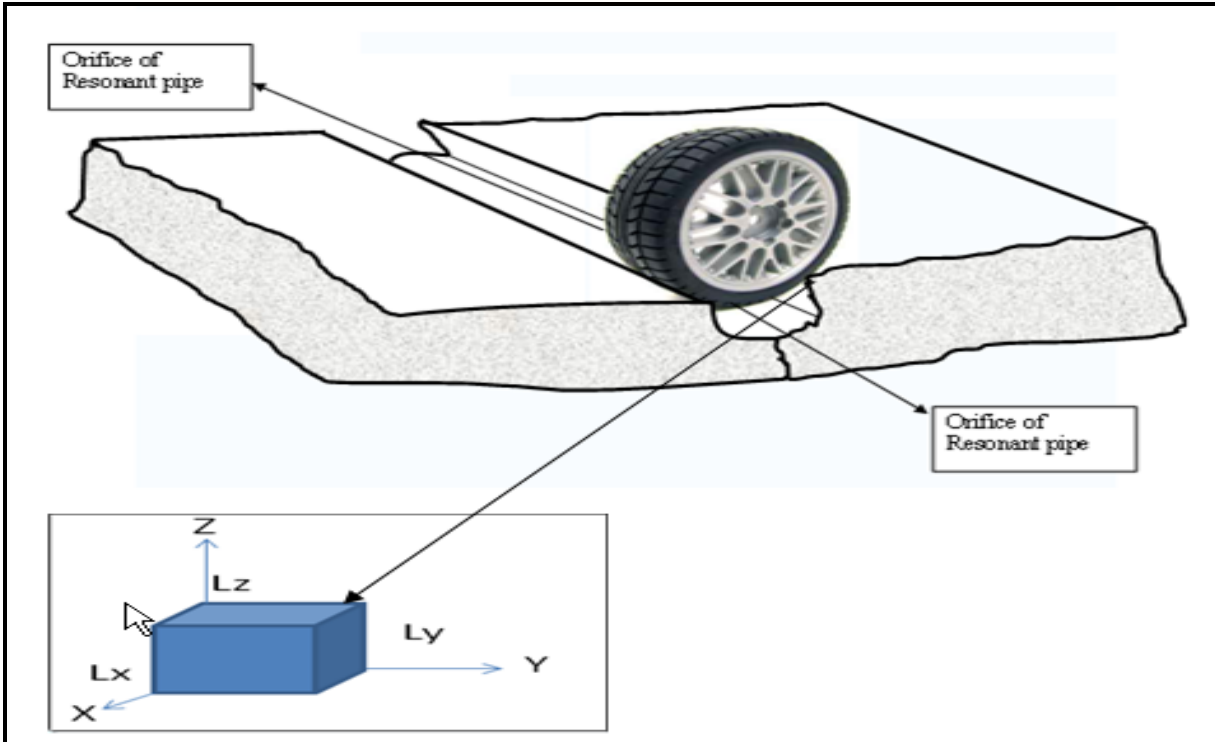
$$\text{SPL} \propto 20 \log \{P(R, T) \propto 20 \log [bd] \quad (\text{Equation 1.55})$$

Spacing asperities such that the pulse rates are reduced resulting in larger asperity intervals being quieter. When asperity intervals are held constant then the smaller the width and depth of groove, the quieter the pavement.

### **1.10.2 Resonance “Pipe” Phenomenon in Pavement Surfaces**

This section describes the type of resonance that occurs when a tire rides over a groove. Groove dimensions may lead to resonance depending on some numerical factors that are mentioned shortly. Consider an idealized joint in the pavement in the similitude of a rectangular box.

Assume that the action of tire though transient exerts pressure into the cavity as would a piston to a cylinder. There will be a corresponding pressure relief at the end of the pipe.



**Figure 1.30: Pipe Resonance Phenomena in Grooves and Joints**

According to Kinsler et al [1.59] the acoustic pressure is of the general form

$$P(lmn) = A_{(x)} \cos K_{xl} X \cos K_{ym} Y \cos K_{zn} Z e^{j\omega t} \quad (\text{Equation 1.56})$$

For a rectangular groove of dimensions  $L_x$ ,  $L_y$  and  $L_z$  it can be shown that the pipe resonant frequencies are expressed as;

$$\omega_0 = c \sqrt{\left(\frac{l\pi}{L_{jx}}\right)^2 + \left(\frac{m\pi}{L_{jy}}\right)^2 + \left(\frac{n\pi}{L_{jz}}\right)^2} \quad (\text{Equation 1.57})$$

where

A, B and C are model constants

$\omega_0$  is the resonant frequency

c is the acoustic speed

P is acoustic pressure,

l, m and n are non-zero non-negative whole numbers,

$L_x$ ,  $L_y$  and  $L_z$  are the geometric dimensions of the pipe or joint in this special case.

From the above equation, it can be deduced that there are many combinations of different geometric dimensions that will bring about resonance. This is valid for a continuous rectangular pipe system with uniform cross section and minimal deterioration. Also it is evident that the condition of the joint is an important factor in the acoustics of pavements. Where l, m and n are 1, m and n are respectively  $L_x$ ,  $L_y$  and  $L_z$ . Then  $\omega_0 = 1.7\pi c$ . This is higher than Sandberg's multi coincidence frequency range. However if the geometric dimensions are all reduced by 40% then resonance will occur because  $\omega_0 = \omega_0(\text{tire}) \approx 1000\text{hz}$ .

It appears therefore that when variables are causative or associative to sound intensity, certain resonance phenomena occur under certain conditions. The two main phenomena Helmholtz and pipe resonance are shown to affect the magnitude of sound intensity. Most importantly, resonant phenomena may synergistically impact tire carcass vibration and cause unusually high resonance that may translate to tire pavement noise

## Chapter 2: Texture Construction and Measurements

### 2.1 Textures Constructed At Mnroad and Initial Data Collection In 2008

This section describes the various texture configurations in the MnROAD Low Volume Road and the Mainline particularly how they were built and how they were textured in 2008. It also shows the initial testing and results.

**Table 2.1: Equipment and Testing Scheme for Test Sections**

<b>Equipment / Standard</b>	<b>OutPut</b>	<b># of Runs</b>	<b>Monitoring Frequency</b>
<b>Sand Volumetric Test (ASTM E 967)</b>	Mean Texture Depth (mm)	3/ Point 60 Points/cell	Seasonally
<b>Circular Track Meter (ASTM E-2157)</b>	Mean Profile Depth (mm)	3/ Point 60 Points/cell	Seasonally
<b>On Board Sound Intensity (AASHTO TP 76-09)</b>	OBSI (dBA) Tire Pavt Noise	3 Per Cell Lane	Seasonally
<b>Acoustic Impedance ASTM E 1050</b>	Sound Absorption Coefficient ( Ratio or %)	3/ Point 60 Points/cell	Seasonally
<b>Lock Wheel Skid trailer ASTM E-274</b>	Skid Resistance	3 Per Cell Lane	
<b>Grip Tester</b>	Grip Number	2 Runs/ Cell	
<b>Nuclear Density Gage</b>	Nuclear Density & Porosity	3/ Point 60 Points/ Pervious cell	Twice a year
<b>Light Weight Profiler</b>	International Roughness Index inches/mile (m/km)	3 Per Cell Lane	Seasonally
<b>MnDOT Pathways Van</b>	International Roughness Index inches/mile (m/km) Surface Rating, Faulting	3 Per Cell Lane	Seasonally

**Table 2.2a: Location Allocation for Pre-2008 Textures and 2008 Texturing**

FINISHING	Cell	Performance Specification
-Turf / Drag	13	Minimum of 1.2 mm Spot mean texture depth (MTD) behind the paver. Uniformity of 1.2 to 1.5 is the desired setting. The texturing will not proceed until the engineer certifies that texture lies within this range. This shall be maintained by the acceptable bristle density and uniform distributed load (UDL) achieved with a metal chain. Aggregate shall not be accepted, as UDL The surface should be void of scrapings unless the contractor guarantees that subsequent removal of the scrapings shall not result in tearing of the surface.
Broom Drag	14	Minimum of 1.2 mm (MTD) Spot tests behind the paver. Uniformity of 1.2 to 1.5 is the desired setting. The texturing will not proceed until the engineer certifies that texture lies within this range. This shall be maintained by the acceptable bristle density and uniform distributed load (UDL) achieved with a metal chain. Aggregate shall not be accepted as UDL The surface should be void of scrapings unless the contractor guarantees that subsequent removal of the scrapings shall not affect result in tearing of the surface.
Transverse Broom/Turf	53	Minimum of 1.2 mm Spot mean texture depth (MTD) behind the paver. Uniformity of 1.2 to 1.5 is the desired setting. The texturing will not proceed until the engineer certifies that texture and geometry lie within this range. This shall be maintained by the acceptable bristle density and uniform distributed load (UDL) achieved with a metal chain. Aggregate shall not be accepted, as UDL The surface should be void of scrapings unless the contractor guarantees that subsequent removal of the scrapings shall not result in tearing of the surface.
Longitudinal tining	5	To be achieved with a rake or other device that will imprint sufficient texture as would guarantee an MTD of 1.2 to 1.5mm behind the paver. The tining spacing shall be 1/2 inch from groove to groove and shall be parallel to the direction of travel. The tining depth and spacing shall be chosen to ensure sufficient friction but shall in no case be less than 1/4" in depth.
Pervious Concrete	85, 89	Porosity shall be 15 to 18 % and void ratio shall be 18 to 21%. The surface shall be void of laitance or slurry and should guarantee uniform porosity through the depth of the concrete. The matrix should be resistant to undesirable raveling and weathering. This shall be established during the trial mixing process. Unit weight may not exceed 135 pcf unless if by improved practice or otherwise, contractor achieves desired porosity while attaining 7-day flexural strength of 300psi.
Pervious Overlay	39	Specified by Others. Consists of 4 " pervious overlay on existing concrete primarily for a noise attenuation Study

**Table 2.2b: Summary of Concrete Pavement Textures Constructed at MnROAD (2008)**

Cell	Track	Mo/Year	Texture	Remarks
5	Mainline	Oct.2008	Longitudinal Timing 1 inch Centers	Later Conventionally Ground
6	Mainline	Oct.2008	Composite Pavement	2" Thermal Overlaid Concrete
13	Mainline	Oct.2008	Longitudinal Broom	
14	Mainline	2008	Longitudinal Time	
39	Low Volume	Sept./Oct.2008	Pervious Overlay	
53	Low Volume	Sept.2008	Transverse Broom Heavy Vs. Light	Inside Lane (Light Traffic Outside Lane (Heavy Traffic
85	Low Volume	Oct.2008	Pervious Concrete On Sand Sub Grade	6: Railroad Ballast (Sub Base) 6" CA15 (Base)
86	Low Volume	Oct.2008	Pervious Asphalt On Sand Subgrade	6" CA 15 (Base) 8" Railroad Ballast (Sub Base)
89	Low Volume	Oct.2008	Pervious Concrete On Clay Sub Grade	6: CA15 Base 6" Railroad Ballast Sub Base

**Table 2.2C: New Textures in 2008 and 2009**

Cell	Track	Mo/Year	Texture	Remarks
5	Mainline	Oct. 2008	Longitudinal Timing 1 inch Centers	Later Conventionally, correctively Ground
6	Mainline	Oct. 2008	Composite Pavement	2" Thermal Overlaid Concrete
7	Mainline	Oct. 2007	Conventional Grind	1/8" X 1/4" X 1/8"
8	Mainline	Oct. 2007	Innovative Grind	
9	Mainline	Oct. 2008	Ultimate Grind	Corrugated Landing
13	Mainline	Oct. 2008	Longitudinal Broom	
14	Mainline	Oct 2008	Longitudinal Time	
53	Low Volume	Sept. 2008	Light Transverse Broom Heavy Transverse Broom	Inside Lane Outside Lane
37	Low Volume	June 2007	Multiple Grind	Initial Pretest Cells, Retained
39	Low Volume	Sept./Oct. 2008	Pervious overlay	Matrix contains Sound absorbent fibers
53	Low Volume	Sept. 2008	Transverse Broom	Inside Lane (Light Texture) Outside Lane (Heavy Texture)
37	Low Volume	June 2010	Ultimate	TS 5 Strip
71	Mainline	June 2010	Ultimate Grind Conv. Grind	Driving lane Passing Lane
72	Mainline	June 2010	Exposed Aggregate	Driving lane Passing Lane

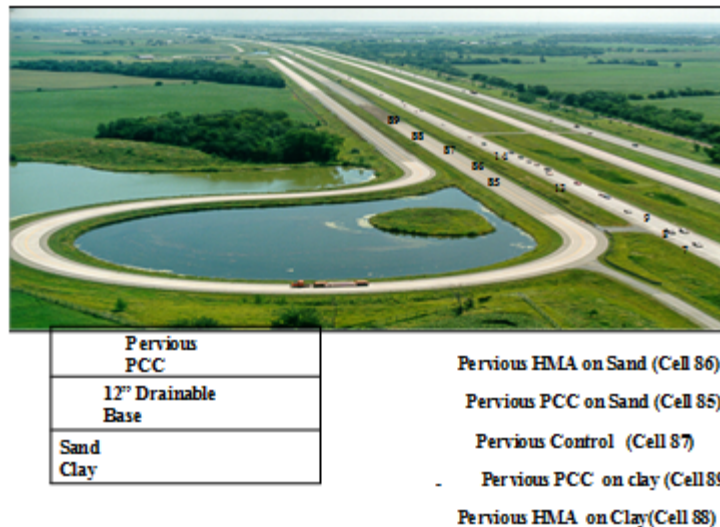
## 2.2 Experimental Sections & Texturing Process (2008)

The experimental textures are categorized as follows:

- a) Pervious Pavements
  - Pervious Overlay on Non Pervious Concrete substrate
  - Pervious Full depth Concrete on Clay Subgrade
  - Pervious Full depth on Sand Subgrade
- b) Turf Drag Cells
  - Transverse turf Drag
  - Longitudinal Turf drag
  - Longitudinal broom Drag
- c) Longitudinal Tining

### 2.2.1 Pervious Pavements

Two full depth pervious concrete pavements and one pervious overlay were constructed in 2008. The pervious overlay was placed over a skew-jointed 20 ft panel concrete pavement built in 1994. The Joints were in various degrees of disrepair but were averagely in fair condition prior to the overlay. The Overlay was performed on the 1<sup>st</sup> of October 2008. It was made of a unique self consolidating slip formable pervious mix developed by the CP tech center in Iowa State University. Remarkable Items in the mix included, fiber reinforcement and high workability but low water cement ratio of 0.3. MnDOT researchers instrumented the section with vibrating wire strain gauges, water blocks and thermocouples.

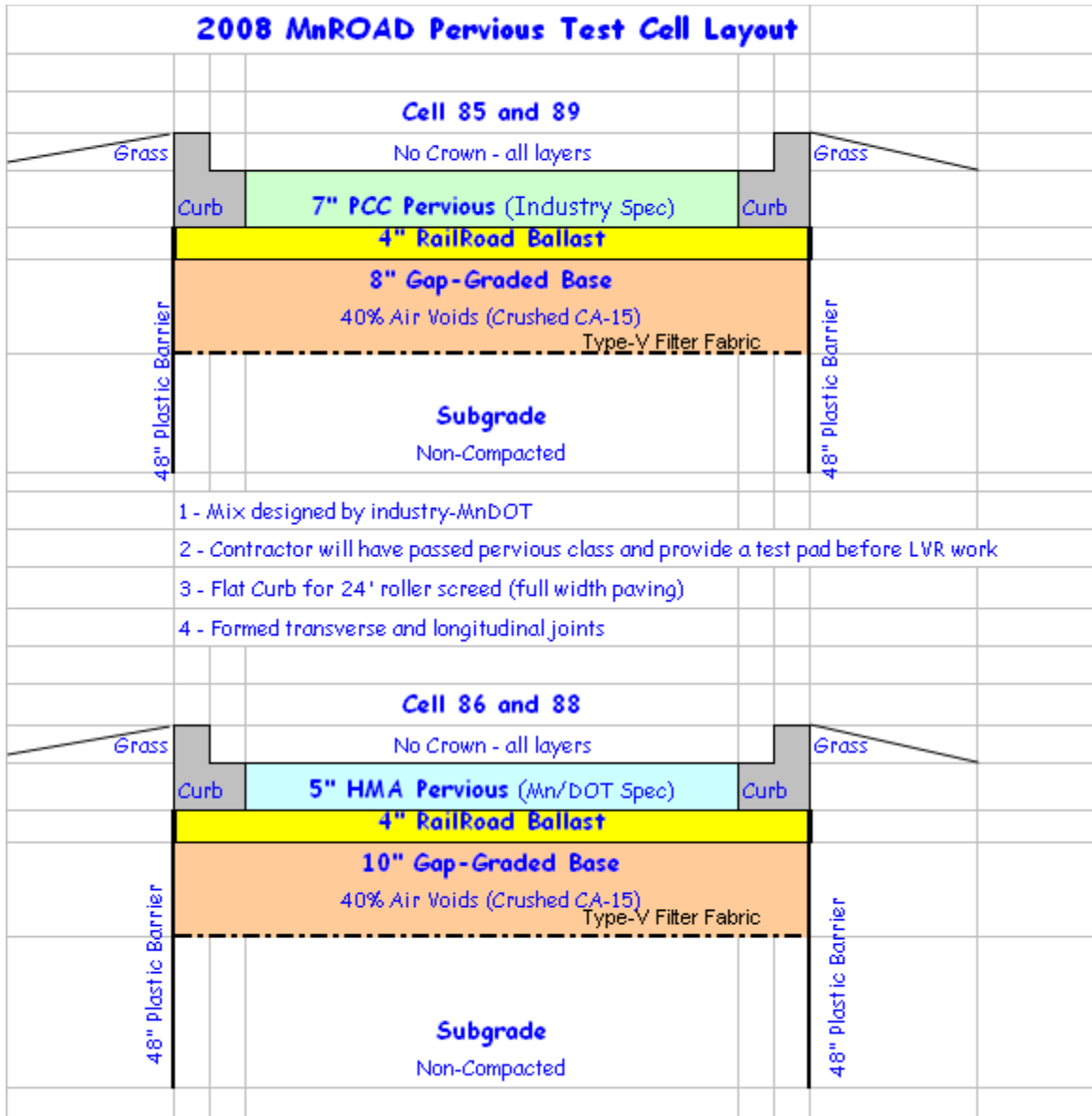


**Figure 2.1: Cells 85 to 89 Pervious Pavements Full Depth Factorial**

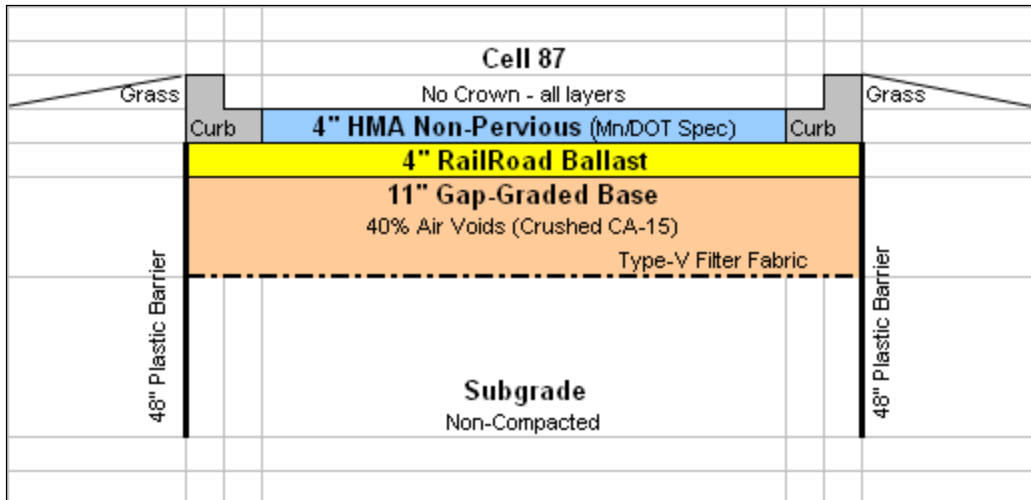
Cell 85 simulated an infiltration system and Cell 89 simulated a detention system due to respective clay and sand subgrades up to aquiclude. Each of these cells as well as Cells 86 and 88 (pervious Asphalt on Sand and Clay respectively) were built on a base made up of 8-inches of CA 15 aggregate. The 4-inch layer of railroad ballast consisted of 3-inch nominal sized aggregate. A porosity benefit was anticipated from the granular subgrade in Cells 85 and 89. Joints were cut to match joints in the existing curb. Cell 85 and 89 mix designs consisted of water / cement ratio of 0.3, 6% by volume sand. A comprehensive report is available at <http://www.lrrb.org/media/reports/201123.pdf>.







**Figure 2.3: Cross Section Through Pervious cells 85, 86, 88, and 89**



**Figure 2.4: Cross Section Through Impervious cells 87**

Pervious concrete improves surface drainage, minimizes peak flow and reduces noise through the minimization of slip-stick mechanism. Many authors including Sandberg [1.28] have associated pervious concrete with good wet weather friction and excellent hydroplaning reduction. Figures 2.2 to 2.4 show cross-sections of the pervious cells.

The Iowa State University report on pervious concrete for cold climates optimizes porosity with respect to performance at 20-25 % void content (13-18%) porosity. Center for Safe Quiet and Durable Highways in Purdue University recommends that for optimum noise attenuation performance, the aggregate should contain a blend retained on #4 and #8 sieves. Maintaining ½ inch “no fines)” gradation is optimal.

### **2.2.2 Cell 39 Pervious Overlay**

Cell 39 consisted of 4 inches of pervious concrete placed on 8 inches of an existing concrete pavement constructed in 1994. The concrete overlay met the requirement of 20 to 25 percent void content and single sized aggregate gradation. It maintained a water/ cementitious ratio of 0.3 and was designed to be self consolidating and slip formable. However, placement was achieved by direct discharge from the concrete truck. The concrete was screed roller compacted with a set of 3, 1-ft diameter by 13 ft. long vibratory drums rolling in the longitudinal axis. The drums were closely followed by the curing compound applicator that discharged enough BASF Confilm as curing compound to cover the surface. This was closely followed with the placement of 2 layers of polyethylene sheeting spread over the pavement and anchored from wind and other elements with a series of steel rods. The transverse joints were cut through the polyethylene sheeting to 1/3 of the overlay thickness. To facilitate drainage from the pervious pavement, a 10-ft wide French drain consisting of CA 15 aggregate was placed along the shoulder and against the pavement edge. The concrete surface was allowed to cure for 28 days before traffic was placed on it. Unique features of this pavement include the dispersion of polyolefin fibers and other non-fibrous polymers in the matrix and the addition of 6% sand (by volume) to enhance bonding with the substrate. Initial sound absorption test showed this pavement to be comparable to cell 85. The pervious overlay maximized the advantages of lesser tortuosity, more absorbent materials (fibers) and efficient placement. Figures 2.5 to 2.10 show construction pictures and the resulting surface.



**Figure 2.5: Pervious Concrete Placement and Vibration**



**Figure 2.6: Pervious Overlay Multi-Drum Screed Compactor**



**Figure 2.7: Pervious Overlay Surface**



**Figure 2.8: Cell 89 Pervious Concrete on Clay and Cell 88 Pervious Asphalt on Clay.**



**Figure 2.9: Establishing 10 ft. Joints in Cells 85 and 89**



**Figure 2.10: Cell 85 and Proximate Cross Drain Prior to Concreting (Rail Road ballast Base is exposed.)**

### **2.2.3 Diamond Grinding Experiment (Cells 37, 7, 8, 9 &71)**

Although this report studies texturing of new construction only it is expedient to mention a parallel Pooled fund study of diamond grinding textures, TPF 5-(134). MnROAD Cell 37 was the proving ground for the innovative diamond grinding. The initiative diamond ground thin strips of various configurations in one pass and diamond grinding in 2 passes. Cell 37 consists of 3 strips TS1, TS2, and TS3. Cells 7 and 8 were ground to the innovative and conventional configurations in summer of 2007. Cell 9 was ground to a friction improved innovative grind in fall 2007; Cell 71 passing and driving lanes were ground respectively to the conventional and ultimate innovative configuration in summer 2010.



**Figure 2.11: Configuration of Cell 9: Ultimate Grind**



**Figure 2.12: Grinding Process for Configuration of Cell 9: Ultimate Grind**



**Figure 2.13: Cell 9 Innovative Grind**

#### **2.2.4 Turf Drag Finish**

Cell 14 was turf dragged. Figures 2.14 to 2.18 show the inverted turf drag process and the turf drag finished surface respectively. This texture method involves dragging an inverted carpet over the finished surface to impart a longitudinal texture on the pavement surface. Cell 14 pavement subsections were 4 or 5 inches thick and placed over bituminous pavements in poor condition (whitening concrete overlay). The panels were cut into the 6 x 6 panels in some subsections and 12 x 12 in others. Mechanical load transfer devices were used.

The carpet was dragged along with a construction bridge behind the power. The bridge was followed by an Alpha methyl styrene (AMS) curing compound spray machine that coated the surface completely.





**Figure 2.14: Cell 6 Mainline Interim Turf Texturing**



**Figure 2.15: Finished Surface with Alpha Methyl Styrene (AMS) Curing Compound**

### **2.2.5 Broom Drag Texturing**

Cell 53 on the low volume road consists of aggressive transverse broom drag in the outside side lane and lighter transverse broom drag in the inside lane. Cell 53 is a test of the MnDOT 60 year concrete design. The pavement consists of 12 inches of high performance concrete dowelled with 1.25 inch Diameter Stainless steel clad dowels, underlain by 8 inches of Class 5 aggregate base, placed over 4 ft of Class 3 select granular material. This pavement was constructed by fixed form process, one lane at a time. Cell 13 was finished with a longitudinal broom drag. The broom device was constructed by the contractor and attached to a work bridge. Cell 13 was made up of various thicknesses ranging from 5 inch to 6 ½ inch thick. The contractor was required to provide 1.2 to 1.5 mm texture behind the paver and meet requirements of skid resistance. The pavement surface was cured with a coating of Alpha methylstyrene within 10 minutes of paving. (The work bridge was constantly 8-12 minutes behind the paver and 2-5 minutes behind the texturing machine. There was evidence of apparent texture loss in locations where the curing compound was over applied by the contractor on the surface.



**Figure 2.16: Broom Drag Used for Texturing of Cell 13 and Cell 53**



**Figure 2.17: Broom Drag Texturing of Cell 13**

### **2.2.6 Longitudinal Tining Cell 5**

Longitudinal tining is a standard method used by other states to produce surfaces that are quieter than transverse tining. The contractor was required to provide the tines 0.75 inch interval and groove depths meeting the requirements of skid resistance. The contractor adjusted the rake to 1 inch interval whereupon the pavement turned out to be low in skid resistance. As an intervention, the surface was ground on the 30<sup>th</sup> of October with the conventional grind.



**Figure 2.18: Turf Finish of Concrete Pavement**

### **2.3 Initial Surface Characteristics Testing**

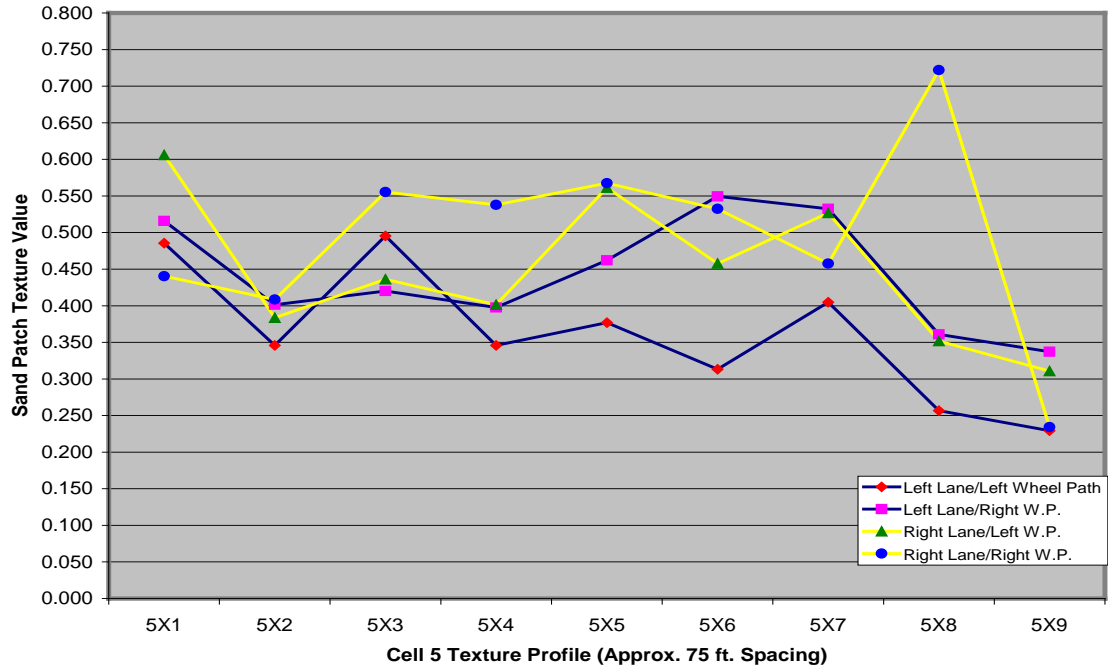
Basic surface characteristics testing performed on the new cells include the following;

- Texture measurements ASTM E-2157 using the circular track meter
- Texture measurement ASTM E-967 Using the sand volumetric method
- In-Situ Sound Absorption Measurement using the prescribed ISO Standard (NCAT Device)
- In-Situ (Dynamic) OBSI measurements using the provisional AASHTO standard
- Ride measurement using the MnDOT LISA Light weight profiler
- Friction Measurement using MnDOT Dynatest friction Lock wheel Skid trailer ASTM E-274
- Friction Measurement using FHWA Grip Tester from the FHWA Loans program

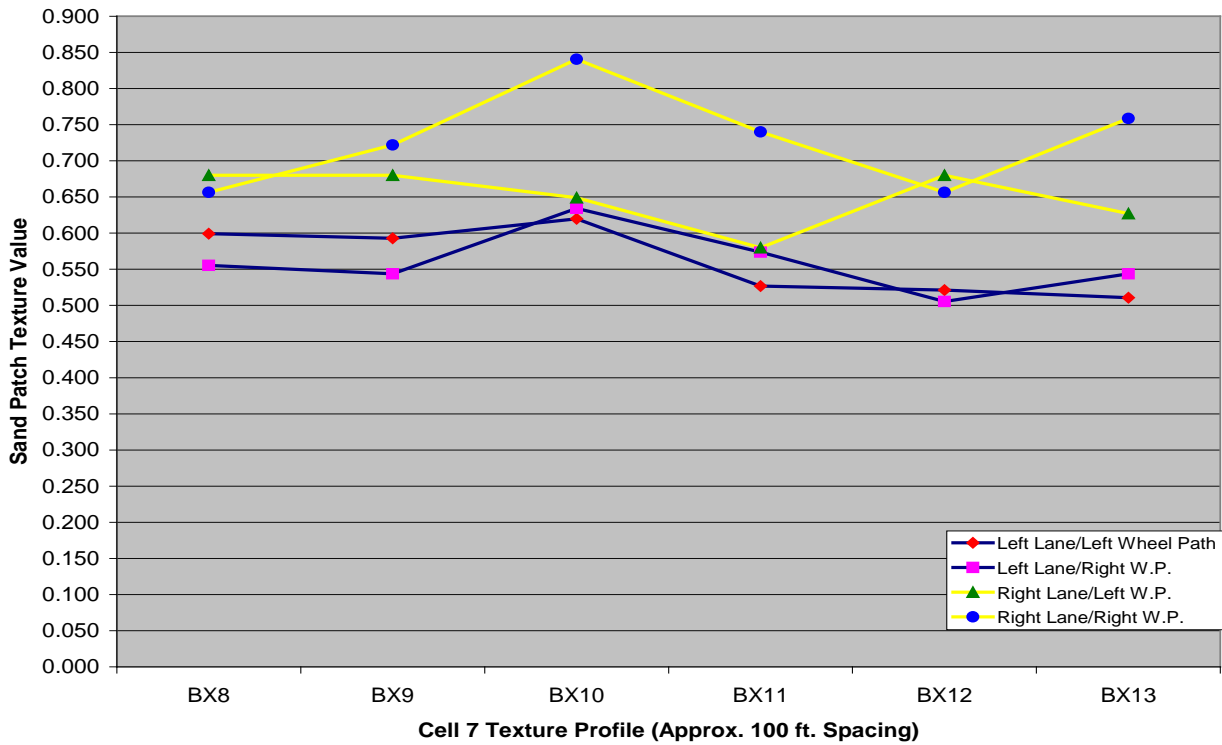
#### **Texture Measurements.**

For convenience texture is recorded in millimeters to enable a quick comparison to the 1mm standard specified.

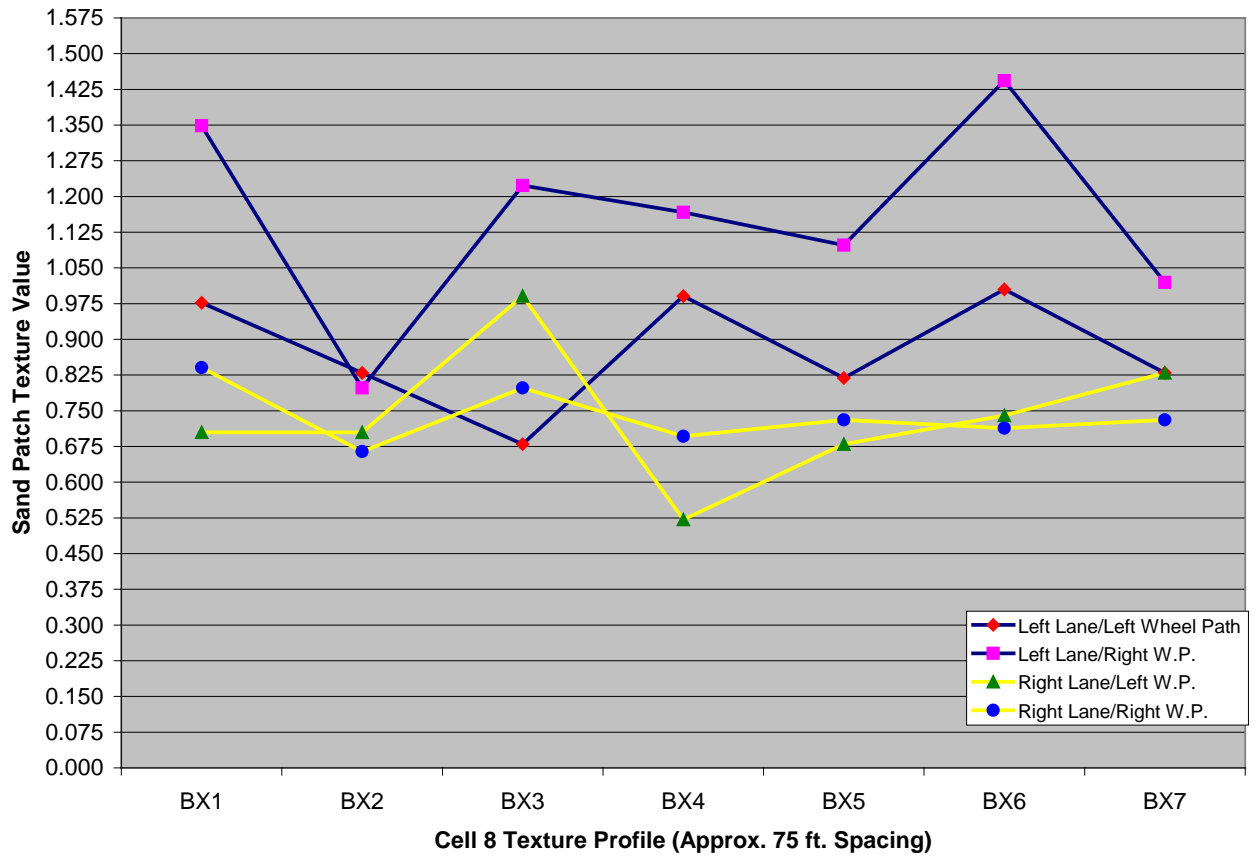
Texture Test of all cells were performed with the Sand Volumetric test protocol ASTM E 965-95 in which a known volume of glass beads was spread on the finished surface until the circle formed could not be further expanded. The average texture was measured by determining the height of the thin Cylinder formed on the finished surface. Figures 2.19 to 2.24 show the texture measurements on test spots that are marked and will be revisited in subsequent seasons [3 times a year (or 4 times a year when early winter measurements are feasible)].



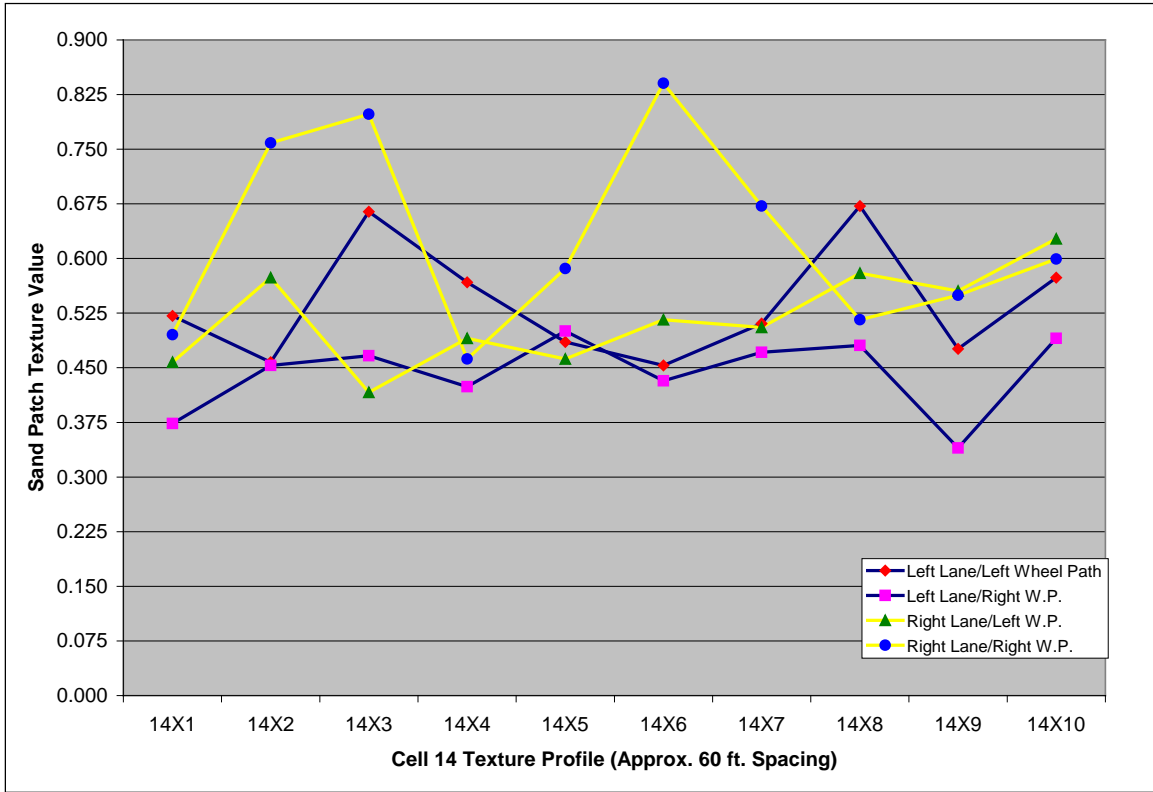
**Figure 2.19: Cell 5 Pre-ground Longitudinal Grind Sand Volumetric Technique ASTM E-965**



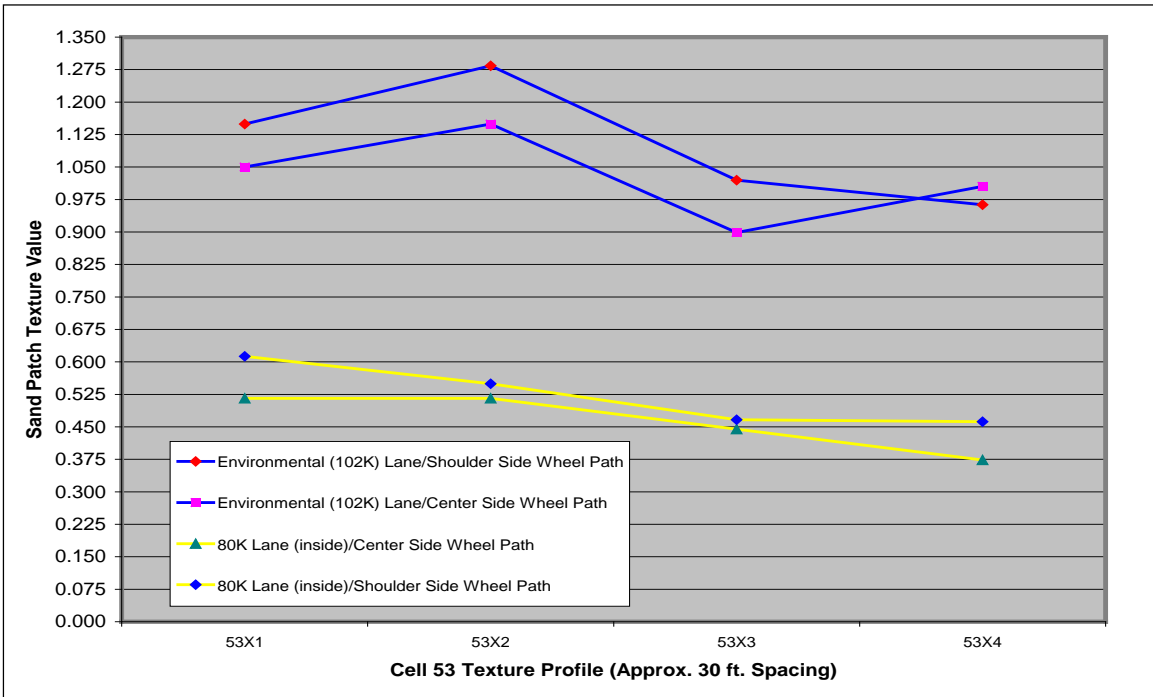
**Figure 2.20: Sand Volumetric Technique ASTM E-965 Test Result on Innovative Grind Cell 7**



**Figure 2.21: Sand Volumetric Technique ASTM E-965 Test Result on Conventional Grind Cell 8**



**Figure 2.22: Sand Volumetric Technique ASTM E-965 Test Result on Broom Drag Cell 14**



**Figure 2.23: Sand Volumetric Technique ASTM E-965 Test Result on Cell 53 with Aggressive Texturing Exhibiting Higher MPD**



**Figure 2.24: Turf Drag in Cell 14**

### **2.3.1 Friction Testing**

Friction measurements were performed with the MnDOT Dynatest Skid truck on the 17<sup>th</sup> of October 2008. Results of the test are shown in TABLE 2.6. Later in the month, the Federal highway loans program lent a grip tester to MnDOT. A more comprehensive friction measurement was performed on all the cells with the Grip tester. While the grip tester measures in International Friction index, it also provides a grip number that is easily correlated to the Skid number. Although thresholds were not established for the friction numbers, insufficient friction in cell 5 led to the grinding of that surface. The Grip tester results for cell 5 are for the ground surface. However at the request of FHWA, the 1 ft fog line of remaining longitudinally tined strip was also measured with the Grip tester. Through the Help of Federal Highway Administration three runs with the grip tester of various levels of wetting were performed on each cell. The initial run was performed with a low rate of flow resembling the semi-dry pavement condition lower than saturation level. Settings mimicked conditions to the wetness at incipient hydroplaning and where the degree of flooding exceeds the hydroplaning threshold of wetness.



**Table 2.3: GRIP Test Results**

ML Cell	Right WP				Left WP				Remarks
	Run 1		Run 2		Run 1		Run 2		
	Mean	SD	Mean	SD	Mean	SD	Mean	SD	
1	0.963	0.174	0.640	0.070	0.871	0.397	0.702	0.150	Bit
2	1.123	0.134	0.792	0.065	1.092	0.131	0.794	0.063	Bit
3	1.095	0.117	0.759	0.019	1.075	0.180	0.843	0.077	Bit
4	0.872	0.241	0.446	0.076	0.991	0.206	0.567	0.091	Chip Seal
5	1.149	0.074	0.951	0.093	1.184	0.101	0.956	0.138	CDG
6	0.837	0.212	0.443	0.110	0.864	0.266	0.448	0.083	Taconite
7	0.876	0.207	0.527	0.031	1.045	0.296	0.578	0.048	IDG
8	1.151	0.071	0.842	0.036	1.174	0.134	0.995	0.082	CDG
9	0.806	0.145	0.553	0.045	1.087	0.149	0.697	0.053	UDG
10	0.979	0.188	0.538	0.127	0.892	0.442	0.711	0.183	TT
11	0.895	0.212	0.455	0.060	0.942	0.264	0.631	0.137	TT
12	0.828	0.182	0.494	0.036	0.969	0.302	0.670	0.161	TT
13	0.928	0.133	0.536	0.057	1.113	0.251	0.770	0.076	Drag
14	0.703	0.192	0.547	0.051	0.792	0.510	0.724	0.091	Drag
15	0.720	0.145	0.514	0.064	0.999	0.381	0.694	0.160	Bit
16	0.705	0.152	0.512	0.049	0.784	0.510	0.797	0.168	Bit
17	0.710	0.180	0.531	0.055	0.782	0.519	0.804	0.179	Bit
18	0.723	0.157	0.541	0.058	0.587	0.548	0.757	0.160	Bit
19	0.784	0.152	0.592	0.041	0.426	0.510	0.799	0.172	Bit
20	0.526	0.155	0.343	0.095	0.448	0.524	0.560	0.147	Bit
21	0.440	0.090	0.319	0.081	0.215	0.370	0.550	0.116	Bit
22	0.445	0.091	0.342	0.064	0.211	0.370	0.592	0.117	Bit
23	0.732	0.192	0.468	0.042	0.612	0.544	0.738	0.199	Bit

**Table 2.4a: Initial Friction Test Results**

CELL	CONSTRUCTION_NUMBER	LANE	DAY	TIME	FN	PEAK	SPEED	AIR_TEMP	PVMT_TEMP	TIRE_TYPE
1	1	ML-Driving-RL	31-Oct-08	10:53	67.1	92.32	38.6	68	75	Ribbed
1	1	ML-Driving-RL	31-Oct-08	11:11	35.6	66.26	39.6	68	72.1	Smooth
2	3	ML-Driving-RL	31-Oct-08	10:53	58.1	91.29	38.8	68	79.3	Ribbed
2	3	ML-Driving-RL	31-Oct-08	11:10	58.8	99.88	39.5	68	81.3	Smooth
3	2	ML-Driving-RL	31-Oct-08	10:53	55.6	89.41	39.1	68	79.3	Ribbed
3	2	ML-Driving-RL	31-Oct-08	11:10	52.2	97.17	39.3	68	79.8	Smooth
4	3	ML-Driving-RL	31-Oct-08	10:53	53.1	81.77	42.5	68	78.6	Ribbed
4	3	ML-Driving-RL	31-Oct-08	11:10	39.7	54.46	39.6	68	78.8	Smooth
5	2	ML-Driving-RL	31-Oct-08	10:53	24.6	52.47	38.1	68	61.6	Ribbed
5	2	ML-Driving-RL	31-Oct-08	11:10	16.9	40.19	40.1	68	67.1	Smooth
6	2	ML-Driving-RL	31-Oct-08	10:53	41.8	66.88	40.8	68	80.3	Ribbed
6	2	ML-Driving-RL	31-Oct-08	11:10	35.9	53.55	40	68	83.3	Smooth
7	1	ML-Driving-RL	31-Oct-08	10:47	45.1	68.54	41.4	68	70.3	Ribbed
7	1	ML-Driving-RL	31-Oct-08	11:10	48.7	79.46	39.8	68	67.8	Smooth
8	1	ML-Driving-RL	31-Oct-08	10:46	54	82.2	41.3	68	69.8	Ribbed
8	1	ML-Driving-RL	31-Oct-08	11:09	55.3	94.17	40.2	68	68.6	Smooth
9	1	ML-Driving-RL	31-Oct-08	10:46	48.2	76.29	40.4	68	69.1	Ribbed
9	1	ML-Driving-RL	31-Oct-08	11:09	56.2	86.88	40.3	68	68.3	Smooth
10	1	ML-Driving-RL	31-Oct-08	10:46	51.1	77.75	39.1	68	69.5	Ribbed
10	1	ML-Driving-RL	31-Oct-08	11:09	35.5	47.05	40.1	68	69.1	Smooth
11	1	ML-Driving-RL	31-Oct-08	10:46	52	83.73	39.4	68	69.1	Ribbed
11	1	ML-Driving-RL	31-Oct-08	11:09	29.3	50.54	39.7	68	69.1	Smooth
12	1	ML-Driving-RL	31-Oct-08	10:45	51.9	76.08	40.2	68	69.8	Ribbed
12	1	ML-Driving-RL	31-Oct-08	11:08	31.1	52.4	40.1	68	68.6	Smooth
13	2	ML-Driving-RL	31-Oct-08	10:45	40.9	80.28	39.5	68	63.1	Ribbed
13	2	ML-Driving-RL	31-Oct-08	11:08	40	78.3	39.7	68	63.9	Smooth
14	3	ML-Driving-RL	31-Oct-08	10:45	36.2	73.32	40.4	68	63.4	Ribbed
14	3	ML-Driving-RL	31-Oct-08	11:08	29.6	50.06	39.9	68	62.8	Smooth
15	4	ML-Driving-RL	31-Oct-08	10:45	56.9	82.6	39.7	68	78.6	Ribbed
15	4	ML-Driving-RL	31-Oct-08	11:08	50.3	76.22	39.6	68	74.1	Smooth
15	4	ML-Passing-LL	30-Oct-08	13:44	57.6	84.8	39.8	68	92.8	Ribbed
15	4	ML-Passing-LL	30-Oct-08	13:55	48.5	74.65	40.3	68	90.1	Smooth
16	4	ML-Driving-RL	31-Oct-08	10:45	60.2	82.05	39.7	68	79.3	Ribbed
16	4	ML-Driving-RL	31-Oct-08	11:08	50.3	82.03	39.6	68	80.3	Smooth
16	4	ML-Passing-LL	30-Oct-08	13:44	58.2	86.02	39.7	68	91.3	Ribbed
16	4	ML-Passing-LL	30-Oct-08	13:55	54.1	82.05	39.8	68	91	Smooth
17	3	ML-Driving-RL	31-Oct-08	10:45	58.7	78.99	39.6	68	78.3	Ribbed
17	3	ML-Driving-RL	31-Oct-08	11:08	54.2	75.3	39.5	68	79.4	Smooth
17	3	ML-Passing-LL	30-Oct-08	13:44	60.7	84.76	39.7	68	91	Ribbed
17	3	ML-Passing-LL	30-Oct-08	13:55	56.7	80.91	39.9	68	89.5	Smooth
18	3	ML-Driving-RL	31-Oct-08	10:45	63.7	85.43	39.3	68	79	Ribbed
18	3	ML-Driving-RL	31-Oct-08	11:07	57.7	84.03	39.4	68	79	Smooth
18	3	ML-Passing-LL	30-Oct-08	13:44	59.5	81.26	39.7	68	90.7	Ribbed
18	3	ML-Passing-LL	30-Oct-08	13:54	55.9	76.03	40	68	90.7	Smooth
19	3	ML-Driving-RL	31-Oct-08	10:44	57	82.96	39.5	68	77.5	Ribbed
19	3	ML-Driving-RL	31-Oct-08	11:07	58	78.68	39.6	68	80.1	Smooth
19	3	ML-Passing-LL	30-Oct-08	13:43	58.7	83.55	39.9	68	91.3	Ribbed
19	3	ML-Passing-LL	30-Oct-08	13:54	57	82.36	40.2	68	83.1	Smooth
20	4	ML-Driving-RL	31-Oct-08	10:44	64.2	83.3	39.3	68	77.3	Ribbed
20	4	ML-Driving-RL	31-Oct-08	11:07	50.2	74.96	39.5	68	80.6	Smooth
20	4	ML-Passing-LL	30-Oct-08	13:43	60.4	77.68	39.7	68	90.8	Ribbed
20	4	ML-Passing-LL	30-Oct-08	13:54	46.3	71.99	39.8	68	89.8	Smooth
21	3	ML-Driving-RL	31-Oct-08	10:44	59	80.49	39.3	68	77.3	Ribbed
21	3	ML-Driving-RL	31-Oct-08	11:07	33	51.84	39.7	68	77.6	Smooth
21	3	ML-Passing-LL	30-Oct-08	13:43	53.9	77.9	39.9	68	89.5	Ribbed
21	3	ML-Passing-LL	30-Oct-08	13:54	32	54.66	41.3	68	89.5	Smooth
22	3	ML-Driving-RL	31-Oct-08	10:44	56	78.98	39.4	68	76.8	Ribbed
22	3	ML-Driving-RL	31-Oct-08	11:07	39.9	51.15	39.5	68	76.6	Smooth
22	3	ML-Passing-LL	30-Oct-08	13:43	54.7	77.62	40.4	68	91	Ribbed
22	3	ML-Passing-LL	30-Oct-08	13:54	24.4	43.37	41.1	68	90.3	Smooth
23	3	ML-Driving-RL	31-Oct-08	10:44	58.5	81.15	39.3	68	77.3	Ribbed
23	3	ML-Driving-RL	31-Oct-08	11:07	46.3	52.32	40.1	68	79	Smooth
23	3	ML-Passing-LL	30-Oct-08	13:43	51	84.19	39.8	68	89.8	Ribbed
23	3	ML-Passing-LL	30-Oct-08	13:54	46.4	61.43	40.1	68	90.5	Smooth
24	3	LVR-102K-OL	31-Oct-08	9:18	53.3	78.89	39.5	68	65.8	Ribbed
24	3	LVR-80K-IL	31-Oct-08	9:2	51.6	77.79	41.4	68	63.3	Ribbed
24	3	LVR-80K-IL	31-Oct-08	9:25	41.6	62.01	41.4	68	64.6	Smooth
27	4	LVR-102K-OL	31-Oct-08	9:14	63.2	85.72	41.9	68	62.6	Ribbed
27	4	LVR-80K-IL	31-Oct-08	9:5	62.5	87.31	40.2	68	61.1	Ribbed

Table 2.4b: Initial friction Test

CELL	CONSTRUCTION_NUMBER	LANE	DAY	TIME	FN	PEAK	SPEED	AIR_TEMP	PVMT
27		4 LVR-80K-IL	31-Oct-08	9:29	44	67.41	39.8	68	
28		3 LVR-102K-OL	31-Oct-08	9:14	63.1	85.71	38.3	68	
28		3 LVR-80K-IL	31-Oct-08	9: 5	59.6	89.13	40	68	
28		3 LVR-80K-IL	31-Oct-08	9:29	42.6	61.77	40	68	
31		2 LVR-102K-OL	31-Oct-08	9:15	57	81.96	39.8	68	
31		2 LVR-80K-IL	31-Oct-08	9: 5	56.1	82.72	39.9	68	
31		2 LVR-80K-IL	31-Oct-08	9:28	48.7	65.88	39.6	68	
32		4 LVR-102K-OL	31-Oct-08	9:15	62.9	84.95	39.4	68	
32		4 LVR-80K-IL	31-Oct-08	9: 5	58.3	91.18	40	68	
32		4 LVR-80K-IL	31-Oct-08	9:28	31.6	58.54	40.1	68	
33		4 LVR-102K-OL	31-Oct-08	9:17	60.2	81.57	39.5	68	
33		4 LVR-80K-IL	31-Oct-08	9: 3	59.9	85.14	40.7	68	
33		4 LVR-80K-IL	31-Oct-08	9:26	45.1	69.48	39.7	68	
34		4 LVR-102K-OL	31-Oct-08	9:17	60.7	83.81	39.7	68	
34		4 LVR-80K-IL	31-Oct-08	9: 3	65.1	83.93	40.2	68	
34		4 LVR-80K-IL	31-Oct-08	9:26	54.9	68.55	39.5	68	
35		3 LVR-102K-OL	31-Oct-08	9:16	60	80.95	39.3	68	
35		3 LVR-80K-IL	31-Oct-08	9: 3	61.8	85.22	39.7	68	
35		3 LVR-80K-IL	31-Oct-08	9:26	50.8	69.33	39.6	68	
36		1 LVR-102K-OL	31-Oct-08	9:16	59.7	89.66	39.6	68	
36		1 LVR-80K-IL	31-Oct-08	9: 3	64.7	88.22	39.5	68	
36		1 LVR-80K-IL	31-Oct-08	9:26	44.5	69.35	39.5	68	
37		1 LVR-102K-OL	31-Oct-08	9:16	55.8	80.48	39.4	68	
37		1 LVR-80K-IL	31-Oct-08	9: 3	64.6	88.52	39.9	68	
37		1 LVR-80K-IL	31-Oct-08	9:26	37.9	57.08	39.9	68	
38		1 LVR-102K-OL	31-Oct-08	9:16	64.6	85.45	39.1	68	
38		1 LVR-80K-IL	31-Oct-08	9: 3	62	88.33	39.6	68	
38		1 LVR-80K-IL	31-Oct-08	9:26	34.4	64.04	39.6	68	
39		2 LVR-102K-OL	31-Oct-08	9:16	55.4	88.78	39.5	68	
39		2 LVR-80K-IL	31-Oct-08	9: 4	56.8	90.95	39.7	68	
39		2 LVR-80K-IL	31-Oct-08	9:27	56.9	91.46	39.5	68	
40		1 LVR-102K-OL	31-Oct-08	9:16	62.8	92.29	39.5	68	
40		1 LVR-80K-IL	31-Oct-08	9: 4	58.2	85.85	40	68	
40		1 LVR-80K-IL	31-Oct-08	9:27	45	75.53	39.6	68	
52		2 LVR-102K-OL	31-Oct-08	9:15	61.7	93.85	39.9	68	
52		2 LVR-80K-IL	31-Oct-08	9:28	30.9	64.61	39.9	68	
53		2 LVR-102K-OL	31-Oct-08	9:15	54.8	82.1	39.6	68	
53		2 LVR-80K-IL	31-Oct-08	9: 4	51	68.64	40.3	68	
53		2 LVR-80K-IL	31-Oct-08	9:28	23.9	58.25	39.9	68	
54		3 LVR-102K-OL	31-Oct-08	9:15	55.7	89.05	39.6	68	
54		3 LVR-80K-IL	31-Oct-08	9: 4	51.2	83.4	39.8	68	
54		3 LVR-80K-IL	31-Oct-08	9:28	36.2	49.21	40.1	68	
60		3 ML-Driving-RL	31-Oct-08	10:46	47.7	72.21	40	68	
60		3 ML-Driving-RL	31-Oct-08	11:09	18.6	29.32	41.2	68	
61		3 ML-Driving-RL	31-Oct-08	10:46	51.4	78.73	39.6	68	
61		3 ML-Driving-RL	31-Oct-08	11:09	19.2	28.48	40.6	68	
62		3 ML-Driving-RL	31-Oct-08	10:46	51.9	77.75	40.3	68	
62		3 ML-Driving-RL	31-Oct-08	11:09	17.5	28.59	41.4	68	
63		3 ML-Driving-RL	31-Oct-08	11:09	19.6	33.52	40.6	68	
77		1 LVR-102K-OL	31-Oct-08	9:14	61.9	86.03	39.7	68	
77		1 LVR-80K-IL	31-Oct-08	9: 5	61.3	83.52	40.1	68	
77		1 LVR-80K-IL	31-Oct-08	9:29	58.6	79.28	39.8	68	
78		1 LVR-102K-OL	31-Oct-08	9:14	61.5	86.47	39.7	68	
78		1 LVR-80K-IL	31-Oct-08	9: 5	60.7	84.57	40.3	68	
78		1 LVR-80K-IL	31-Oct-08	9:29	54.5	75.64	39.9	68	
79		1 LVR-102K-OL	31-Oct-08	9:14	62.4	83.88	39.8	68	
79		1 LVR-80K-IL	31-Oct-08	9: 5	60.6	84.34	39.8	68	
79		1 LVR-80K-IL	31-Oct-08	9:29	56.3	76.23	39.5	68	
92		2 ML-Driving-RL	31-Oct-08	10:46	53.2	80.46	39.9	68	
92		2 ML-Driving-RL	31-Oct-08	11:09	40.4	61.8	39.7	68	
96		2 ML-Driving-RL	31-Oct-08	10:46	52.9	82.8	39.8	68	
96		2 ML-Driving-RL	31-Oct-08	11:09	41.1	66.93	40	68	
97		2 ML-Driving-RL	31-Oct-08	10:46	53.3	84.49	39.1	68	
97		2 ML-Driving-RL	31-Oct-08	11:09	35.9	48.53	39.4	68	

### 2.3.2 Sound Absorption Measurements on Pavement Test Cells

A sound absorption measurement was conducted in the new cells in MnROAD. The sound absorption test is a static test in the sense that the noise is not generated by the interaction of the rolling tire with pavement surface but by a white noise sound. White noise is similar to white light which contains all frequencies. The signal's spectral density has equal power in any band and at any frequency in a given bandwidth. The noise is transmitted to the pavement surface through a projection distance  $d_1$  and is reflected to a set of microphones at a distance  $d_2$  from the source. The reflected noise is received by a set of microphones that are connected to an analyzer that identifies and records the actual reflection or absorption of each frequency from zero to 2000 Hz. The absorption ratio for 315, 400, 500, 750, 1000, 1250, 1650 hertz were isolated for a broadband analysis. The absorption ratio for each frequency was plotted against the pavement surface. The results show evidence of higher absorption ratio in the pervious cells 87, 85, and 39. The mean porosity computed Cell 39 consists of a 4" pervious concrete pavement on an existing concrete substrate. Ordinarily, the reflectance of a concrete surface is higher than that of an aggregate base and it was expected that absorption ratios will be higher in Cell 85 than in Cell 39 but the converse happened.

**Table 2.5: Summary Data for Sound Absorption on MnRoad Pavements**

TEST CELL	Sound Absorption Coefficient							
	FREQUENCY							
	315	400	500	630	800	1000	1250	1600
Cell 87 Bituminous New	0.045	0.087	0.087	0.120	0.118	0.071	0.108	0.080
Cell 86 Pervious asphalt	0.352	0.363	0.363	0.379	0.433	0.467	0.531	0.569
Cell 85 Pervious Concrete	0.199	0.191	0.191	0.220	0.251	0.226	0.293	0.288
Cell 39 Pervious Overlay	0.317	0.246	0.246	0.236	0.208	0.211	0.296	0.221
Cell 62 White Topping	0.030	0.028	0.028	0.060	0.052	0.017	0.027	0.041
Cell 54 Taconite Concrete	0.002	0.031	0.031	0.068	0.056	0.012	0.033	0.040
Cell 53 HP Concrete	0.007	0.031	0.031	0.067	0.054	0.016	0.031	0.041
Cell 31 Taconite Asphalt	0.010	0.045	0.045	0.084	0.072	0.020	0.044	0.055
Cell 24 Asphalt New	0.037	0.070	0.070	0.109	0.107	0.051	0.091	0.077
Cell 19 Bituminous New	0.048	0.086	0.086	0.123	0.118	0.074	0.109	0.089
Cell 14 White Topping new	0.035	0.029	0.029	0.054	0.046	0.020	0.029	0.038
Cell 6 Composite	0.023	0.051	0.051	0.085	0.077	0.026	0.051	0.062
Cell 5 Thin UBOL	0.024	0.026	0.026	0.060	0.054	0.015	0.026	0.038
Cell 3 New Bit	0.126	0.119	0.119	0.139	0.129	0.076	0.128	0.156

### 2.3.3 On Board Sound Interaction (OBSI) Collection Process

The MnDOT OBSI equipment consists of a Chevrolet Impala, 8 intensity meters, connected via 4 communication cables to a Bruel and Kjaer Front-end Collector connected to a Laptop computer. The intensity meters are mounted on a rig system attached to a Standard Reference Test Tire that installed at the rear left side of the vehicle and After recording temperature, 4 intensity meters are plugged into the B &K Front End Unit, as well as 12v power supply and Ethernet (computer) cable. With this arrangement, the unit is capable of measuring repeatable tire pavement interaction noise at a speed of 60 miles an hour, thus measuring approximately 440 ft within 5 seconds. Mounting the rig, calibration of the microphones, and durometer evaluation of the tire are mandatory operational procedure prior to data collection

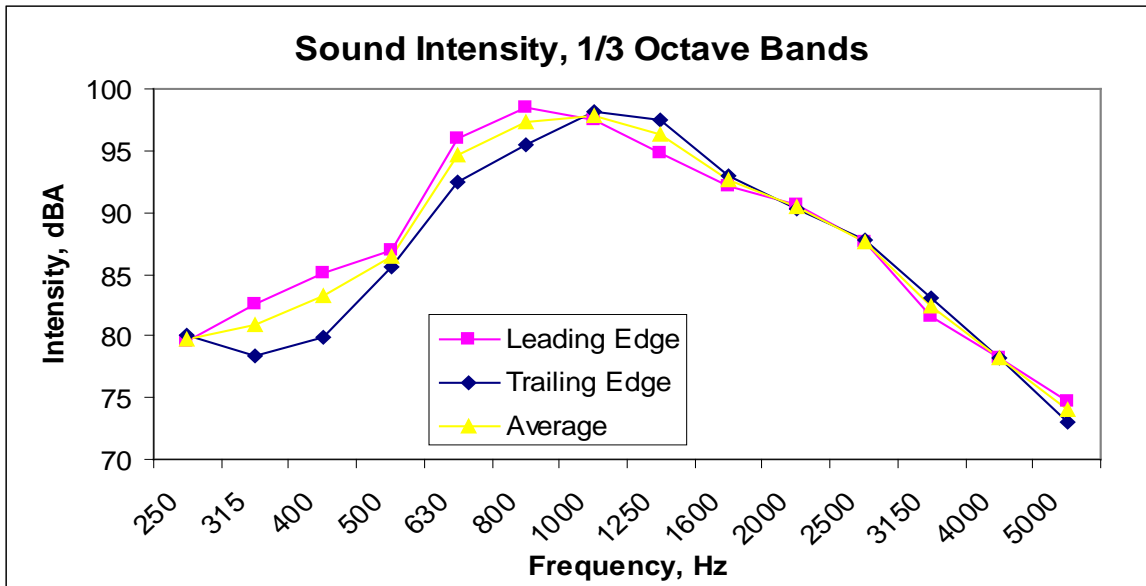


Figure 2.25: Third Octave Frequency Response of 2 Sets of Microphones

The new MnROAD Cells were measured except the transitional curves between the loops and the straight courses at the LVR cells. It was not practicable to safely attain 60mph measuring speed in these transitional curves and so it was not possible to measure cells 54 53 52 and 40 in the LVR during the fall of 2007. In the fall of 2008 the new cells were tested.

### 2.3.4 Initial Ride Measurement

Ride measurement was conducted on the new cells in the last week of November using the AMES light weight Profiler. A continuous run was made on the Right wheel path and the Left wheel path of the passing lane. The results were separated into cells by cropping the start and end stations of each cell of the cells.

### 2.3.5 Hydraulic Conductivity Measurements in Pervious Concrete

Hydraulic conductivity is measured with a device developed by MnDOT using an inverted Humboldt H-4245 sand cone as shown in Figure 2.36. Duct seal compound was used to create a seal between the pervious concrete and the bottom cone flanged opening.

The permeability was measured by recording the time it took for water to drop between two lines along the straight portion of the 1-gal plastic jar. Measurements were taken at several locations on the pervious test cell as shown in Figure 2.36 . Measurements are periodically repeated at these same locations in order to determine changes in permeability. An analytical process for the determination of flow time is explained below. The permeability was determined as follows. From continuity, the flow rate of the water in the plastic jar must equal the flow rate exiting the sand cone, Equation 1.

**Table 2.6: IRI of Some Test Cells Measured With the LWP Fall 2008**

Cell	Date	Lane	Wheel path	Reported IRI			Converted IRI		
				IRI Run1	IRI Run2	Avg. IRI	IRI Run1	IRI Run2	Avg. IRI
5	11/19/2008	Driving	LWP	50.7		50.7	0.80		0.80
6	11/19/2008	Driving	RWP	86.3	84.2	85.25	1.36	1.33	1.35
13	11/19/2008	Driving	RWP	78.9	78.5	78.7	1.25	1.24	1.24
14	11/19/2008	Driving	RWP	56.9	58.8	57.85	0.90	0.93	0.91
61	11/19/2008	Driving	RWP	60.3	60.7	60.5	0.95	0.96	0.95
62	11/19/2008	Driving	RWP	62.5	61.6	62.05	0.99	0.97	0.98
63	11/19/2008	Driving	RWP	86.3	83.5	84.9	1.36	1.32	1.34
92	11/19/2008	Driving	RWP	96.4	91.5	93.95	1.52	1.44	1.48
96	11/19/2008	Driving	RWP	184.9	187.4	186.15	2.92	2.96	2.94
97	11/19/2008	Driving	RWP	234.1	236.8	235.45	3.69	3.74	3.72
60	11/19/2008	Driving	LWP	82.7	81.3	82	1.31	1.28	1.29
61	11/19/2008	Driving	LWP	56.5	56.5	56.5	0.89	0.89	0.89
62	11/19/2008	Driving	LWP	51.6	50.4	51	0.81	0.80	0.80

$$\frac{\pi d^2}{4} dh = v_0 A_0 dt \quad (2.1)$$

Then Bernoulli gives Equation 2.

$$\frac{P_1}{\rho_1 g} + \frac{v_1^2}{2g} + z_1 + losses = \frac{P_2}{\rho_2 g} + \frac{v_2^2}{2g} + z_2 \quad (2.2a)$$

$$v_0 = \lambda \sqrt{2gh} \quad (2.2b)$$

Where  $\epsilon$  is a constant that accounts for piezometric head loss. Combining equations 1 and 2, reorganizing, and integrating both sides gives:

$$-\frac{\pi d^2 \sqrt{h}}{2\lambda \sqrt{2g} A_0} + C = T \quad (2.3)$$

The substituting the boundary conditions of  $h = H$  when  $T = 0$  gives:

$$-\frac{\pi d^2}{2\lambda \sqrt{2g} A_0} (\sqrt{h} - \sqrt{H}) = T \quad (2.4)$$

To compensate for the losses due to the reduction in cross-sectional area at the valve, the time it takes for the perveammeter to empty in air,  $T_{\text{air}} = 10$  s, is introduced. When  $T = 10$  s,  $H = 18.25$  in.,  $h = 12.0$  in., and  $\epsilon'$  is  $1/\epsilon$  substituting into Equation 4 gives:

$$\lambda' 10 = T \quad (2.5)$$

Equation 5 relates the hydraulic conductivity of the concrete as a function of the time it takes for the perveammeter to empty in air. Equation 5 is similar to:

$$Q = KiA \quad (2.6a)$$

$$V = KiAt \quad (2.6b)$$

Where  $Q$  is discharge,  $K$  is hydraulic conductivity,  $A$  is area,  $I$  is the hydraulic gradient,  $V$  is volume, and  $t$  is the time of discharge. Assuming a tortuous path around a rounded aggregate, the hydraulic gradient is equal to

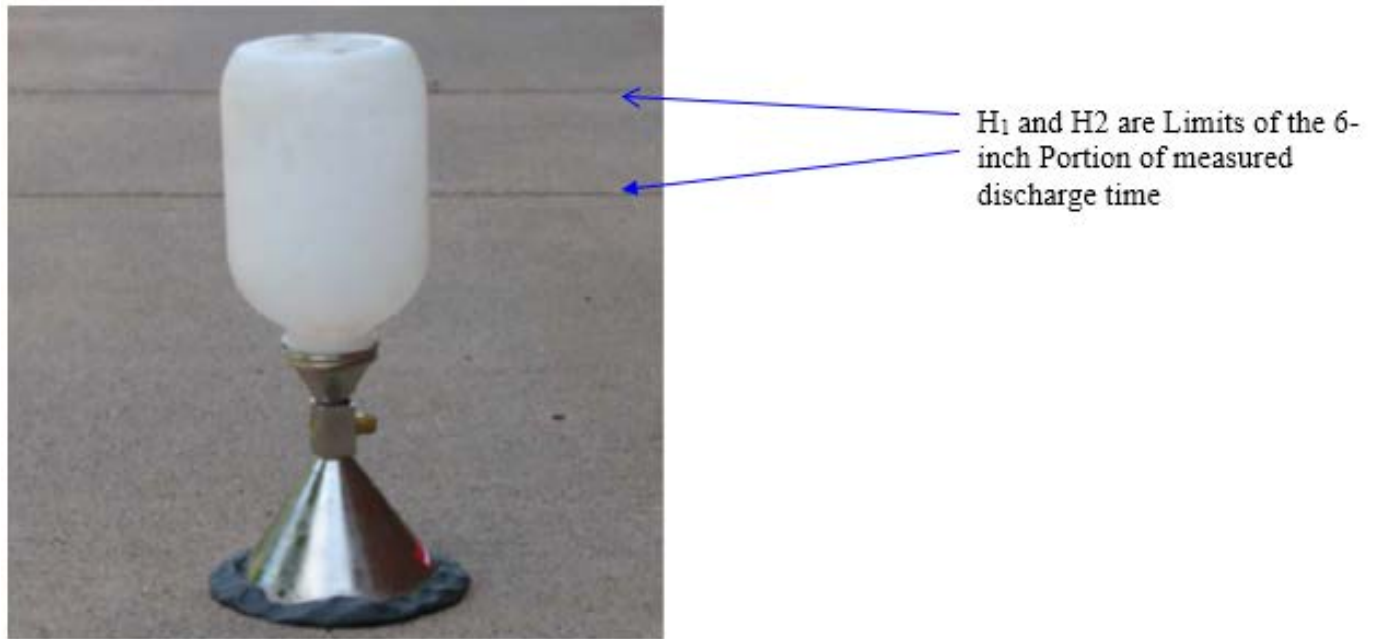
$$i = 2r/\pi r = 0.64. \quad (2.6c)$$

The effective porosity of the pavement system for a 7 in. thick pervious concrete with 20% porosity and 12 in. thick drainable base with 40% porosity is 33% therefore the effective volume available to store water is  $V = 0.33 \cdot 19 \cdot A$ .

Based on the apparatus used and the minimum time of discharge for good draining pavement, the discharge time for a 6 in. drop in head was 17 s which gives a hydraulic conductivity of  $K = 0.35$  in./s. The effective time to fill the storage is  $t_{\text{eff}} = 18$  s and is given by:

$$t_{\text{eff}} = \frac{V}{KA} \quad (2.7)$$

The effective hydraulic conductivity  $K_{\text{eff}} = 0.54 \text{ in./s}$  (1944 in./hr) is then found from Equation 6. The time for a 6 in/hr rainfall to fill the voids in the pavement is then given by  $t = V/(A \cdot 6 \text{ in/hr}) = 1.05 \text{ hrs}$  (3780 s). Since the water in our test is not restricted to vertical flow and can flow horizontally as well, a factor must be used to convert the effective hydraulic conductivity to one-dimensional flow. This conversion factor is obtained by dividing the effective time ( $t_{\text{eff}} = 18 \text{ s}$ ) it took to fill the storage by the actual rainfall simulated time:  $3780/18 = 210$ . Then the actual effective hydraulic conductivity is  $1944/210 = 9.26 \text{ in/hr}$  assuming laminar flow. The time of discharge for 6 in/hr flow is  $17\text{s} \cdot 9.26 \text{ in/s} = 157.42 \text{ s}$  (2.62 min). The threshold for 1.5 in/hr rainfall sustained is then 10.48 min. This procedure suggests  $\approx 10 \text{ min.}$  as the threshold for clogging.



**Figure 2.26: In-situ Hydraulic Conductivity Measurement Device. (Crude Perveammeter)**



**Table 2.7: Hydraulic Conductivity Measurements on Porous Test Cells**

Cell	Type	Base	Location		Lane	Head	Time
88	HMA	Clay	104.7' from East	30" from South	Environmental	8	3.5
88	HMA	Clay	104.7' from East	30" from South	Environmental	8	3.2
88	HMA	Clay	104.7' from East	7 ft. from South	Environmental	8	3.3
88	HMA	Clay	104.7' from East	7 ft. from South	Environmental	8	3.5
88	HMA	Clay	104.7' from East	30" from North	Traffic	8	3.8
88	HMA	Clay	104.7' from East	30" from North	Traffic	8	4.1
88	HMA	Clay	29.6' from West	30" from South	Environmental	8	3.5
88	HMA	Clay	29.6' from West	30" from South	Environmental	8	4.2
88	HMA	Clay	29.6' from West	7 ft. from South	Environmental	8	2.5
88	HMA	Clay	29.6' from West	7 ft. from South	Environmental	8	2.8
88	HMA	Clay	29.6' from West	30" from North	Traffic	8	3.6
88	HMA	Clay	29.6' from West	30" from North	Traffic	8	3.9
86	HMA	Sand	117.7' from West	30" from South	Environmental	8	2.1
86	HMA	Sand	117.7' from West	30" from South	Environmental	8	2.5
86	HMA	Sand	117.7' from West	7 ft. from South	Environmental	8	4.7
86	HMA	Sand	117.7' from West	7 ft. from South	Environmental	8	4.8
86	HMA	Sand	117.7' from West	30" from North	Traffic	8	1.9
89	Conc.	Clay	35.5' from East	30" from South	Environmental	8	8.6
89	Conc.	Clay	35.5' from East	30" from South	Environmental	8	8.4
89	Conc.	Clay	35.5' from East	6 ft. from North	Traffic	8	8.1
89	Conc.	Clay	35.5' from East	6 ft. from North	Traffic	8	8
89	Conc.	Clay	35.5' from East	30" from North	Traffic	8	5.2
89	Conc.	Clay	35.5' from East	30" from North	Traffic	8	5.9
89	Conc.	Clay	87.5' from East	30" from South	Environmental	8	11.1
89	Conc.	Clay	87.5' from East	30" from South	Environmental	8	10.9
89	Conc.	Clay	87.5' from East	6 ft. from North	Traffic	8	7
89	Conc.	Clay	87.5' from East	6 ft. from North	Traffic	8	7
89	Conc.	Clay	87.5' from East	30" from North	Traffic	8	5.2
89	Conc.	Clay	87.5' from East	30" from North	Traffic	8	5.5
85	Conc.	Sand	34' from East end	30" from South	Environmental	8	7.7
85	Conc.	Sand	34' from East end	30" from South	Environmental	8	7.6
85	Conc.	Sand	34' from East end	6 ft. from North	Traffic	8	3.6
85	Conc.	Sand	34' from East end	6 ft. from North	Traffic	8	3.6
85	Conc.	Sand	34' from East end	30" from North	Traffic	8	2.2
85	Conc.	Sand	34' from East end	30" from North	Traffic	8	2.5
85	Conc.	Sand	34' from East end	30" from North	Traffic	8	2.1
85	Conc.	Sand	94.2' from West	30" from South	Environmental	8	5
85	Conc.	Sand	94.2' from West	30" from South	Environmental	8	5.1
85	Conc.	Sand	94.2' from West	6 ft. from North	Traffic	8	3.9
85	Conc.	Sand	94.2' from West	6 ft. from North	Traffic	8	4.1
85	Conc.	Sand	94.2' from West	30" from North	Traffic	8	7.9
85	Conc.	Sand	94.2' from West	30" from North	Traffic	8	7.6

A sensitive stop watch was used each time the meniscus was at the designated mark. The degree of accuracy (1/100th) of a second was retained but rounded to the nearest one tenth of a second.

## **2.4 Texturing In 2010 Construction At The Mnroad Research Facility**

### **2.4.1 Background**

This section describes how an exposed aggregate surface was constructed at MnROAD. To achieve the requirements of an EAC finish, a high quality concrete mix was desired. To improve sustainability and minimize overall cost, the high quality mix layer was placed on a recycled aggregate concrete layer. Skid resistance, acoustic properties, and ride quality were measured before and after texturing, followed by seasonal monitoring for comparison with pre-existing transverse tined textures.

An exposed aggregate concrete (EAC) mix is used as the top layer of cells 71 and 72. The bottom layer of cell and 71 is concrete utilizing 50% recycled concrete aggregate (RAC). The bottom layer of cell 72 consists of an economical “Low Cost” mix (CHP) that utilizes a relaxed aggregate gradation. Figure 2.1 below shows a cross section of the two composite cells along with the aggregate base designations. All cells were constructed with 15- foot joint spacing. Cells 71 and 72 have 1- inch dowels throughout both lanes. Material properties and cost information are provided in detail in the MnDOT Construction Report [2.1]

The exposed aggregate concrete mix is an extremely rich mixture with more than 600 lbs of cement and 725 lbs of total cementitious material per cubic yard. Comparatively the low cost and recycled aggregate mixes only contain a total cementitious content of 600 lbs per cubic yard. This difference between the two mixes is the fly ash content. The low cost mix uses a high-class F fly ash content of 360 lbs per cubic yard, where the recycled mix only has 240 lbs per cubic yard. The sources for fine aggregate, cement and fly ash are the same for all three mixes. These facts are important for achieving the exposed aggregate texture. The third mix was a blend of recycled aggregate and virgin aggregate.

### **2.4.2 Construction Texturing**

Although both cells 71 and 72 were constructed using the high quality exposed aggregate mix in the top layer, three different surface treatments were used to evaluate a broader range of pavement types. Cell 71 was finished with diamond grinding, with an innovative diamond grind in the driving lane and the traditional diamond grind in the passing lane. Cell 72 was treated using common practices for exposed aggregate finishes, by applying a set retarder to the surface. The set retarder used was a water-based compound. This chemical provides etch retention and consistency in temperatures up to 130° F for up to sixteen hours [2.27]. The retardant is both odorless and non-flammable. It does not require the use of plastic covers, which minimizes the required application labor. This compound allows the unhardened surface mortar to be removed by brushing revealing the aggregate to the surface.



**Figure 2.27a: MnROAD Mainline Cell 72 Construction**

### **2.4.3 Early Performance Evaluation**

This section will provide the test methods and results from the early performance assessment of cell 70, cell 71 and cell 72. Strength, ride, noise and surface characteristics will be discussed in this section.

#### **Compressive, Flexural and Bond Strength**

Compressive and flexural strength specimens were made at the construction site at the time of paving using the three different concrete mixes used in cells 70, 71 and 72. Composite beams with 2 different mix layers were made using different combinations of the three mixes. The specimens were transported back to the MnDOT Office of Materials and Road Research after initial curing. They were tested by the concrete laboratory staff using ASTM C39, standard test method for compressive strength of cylindrical concrete specimens, and ASTM 257, standard test method for flexural strength of concrete using a simple beam with third-point loading.

As expected, the exposed aggregate concrete achieved higher flexural and compressive strength than the low cost mix and the recycled mix. This difference in strength illustrates the change in quality between the two layers of the composites. Interestingly, however, the two composites achieved slightly higher strength than the fully exposed aggregate concrete beams. When the composites were tested, they were placed in the third point bending machine such that the exposed aggregate concrete layer was in tension, and the lower quality (RAC or CHP) mix was in compression. Because of this load orientation, the measured flexural strength was essentially

the strength of the exposed aggregate concrete. This explains why exposed aggregate beam and the composite beams achieved comparable flexural strengths. In the future, composite beams should be tested in a multitude of different orientations, with the bond plain both vertically and horizontally, to avoid this phenomenon.

The bond strength between the two layers of the composite pavements is another very important property that may influence long-term performance. Instead, slant-shear cylindrical specimens were made to test bond strength in accordance with ASTM C882, standard test method for bond strength of epoxy-resin systems used with concrete by slant shear. The specimens were made at the paving site by bonding two layers of concrete, EAC over CHP or EAC over RAC, at an angled plane in a cylinder. Table 2.27B shows the measured bond strengths of EAC over RAC from cell 71 and EAC over CHP from cell 72. Specimens were also tested using the concrete from the demo slab.

Cell 70	Cell 71		Cell 73		Cell 72
	Innovative Diamond Grind	Traditional Diamond Grind	Traditional Diamond Grind	Traditional Diamond Grind	Exposed Aggregate
	3" EAC				3" EAC
6" RAC	6" RAC		6" LCST		6" LCST
8" Class 5	8" Class 6				8" Class 7
Clay	Clay				Clay

**Figure 2.27b: Composite Cells**

All of the specimens tested achieved bond strength well over 1000 psi, the minimum to be considered an adequate bond between concrete in pavement applications. It is interesting to note the reduced bond strength in the specimens made from the demo slab concrete. In addition, the bond between EAC and CHP seems to be stronger than the EAC and RAC in the demo slab concrete, however the opposite trend was observed in the specimens made from cells 71 and 72.

Performance Data Table 2.24 provides the performance data collected from the first two years of service for cells 70, 71 and 72. The resulting data for mean profile depth, friction number, international roughness index (IRI), sound absorption (SA) and on board sound intensity (OBSI) will be discussed in the subsequent sections.

**Table 2.8: Performance Data**

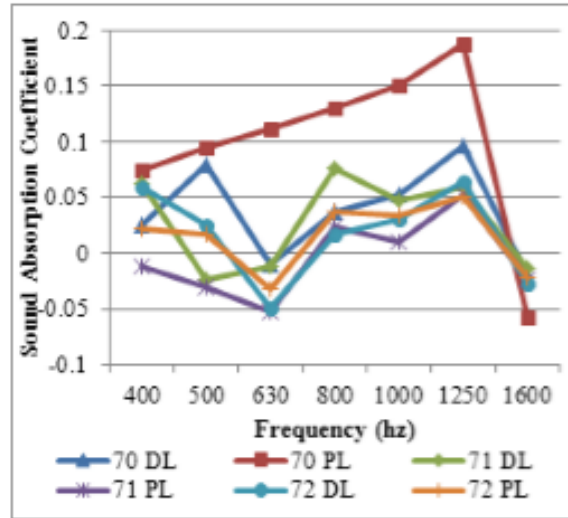
Property	Date	Cell 70 DL	Cell 70 PL	Cell 71 DL	Cell 71 PL	Cell 72 DL	Cell 72 PL
Surface Type		HMA	HMA	Innovative DG	Traditional DG	EAC	EAC
Mean Profile Depth (mm)	6/1/2010	0.20	0.40	1.11	0.88	0.72	0.83
	10/20/2010	0.25	0.44	0.99	0.83	0.78	0.85
Friction Number (Ribbed)	9/20/2010	52.5	53.8	44.9	49.2	44.2	48.8
Friction Number (Smooth)	9/20/2010	28.0	41.2	47.9	47.9	39.3	40.8
IRI (m/km)	6/7/2010	1.06	1.11	2.39	0.79	1.79	1.56
	9/21/2010	1.32	1.40	2.51	0.97	1.85	1.71
	11/16/2010	1.51	1.67	2.50	1.10	1.92	1.83
SA at 1000 Hz	6/7/2010	0.053	0.151	0.048	0.010	0.031	0.034
	10/18/2010	0.049	0.081	0.064	0.051	0.036	0.039
OBSI (dBA)	7/28/2010	100.4	100.7	96.9	100.2	101.6	101.6
	9/17/2010	101.1	101.6	98.8	101.5	103.0	103.0
	11/17/2010	103.0	103.3	100.9	103.4	104.5	104.4

#### **2.4.4 On Board Sound Intensity**

The On Board Sound Intensity (OBSI) test measures the noise generated from the tire – pavement interaction. One advantage of using the OBSI method to measure sound generation is that it allows the noise generated from the pavement-tire interaction to be isolated from other sources, such as engine noise and the surrounding landscape noise, making it favored to the traditional Statistical Pass By Method. OBSI testing is done according to the AASHTO TP 79-08 procedure. The process analyzes data recorded with microphones located close to the tire-pavement contact. The dominant noise generation source becomes the tire-pavement interaction when cars travel at freeway speeds. Therefore, the test is performed at 60 mph over a 440-foot stretch of pavement to adequately capture the desired noise source.

#### **2.4.5 Sound Absorption**

The Sound Absorption Coefficient is the ratio of the absorbed sound energy to the transmitted sound energy sent to the pavement surface was only measured to ascertain if exposed aggregate have increase or decrease absorption coefficient



(a) 6/7/10

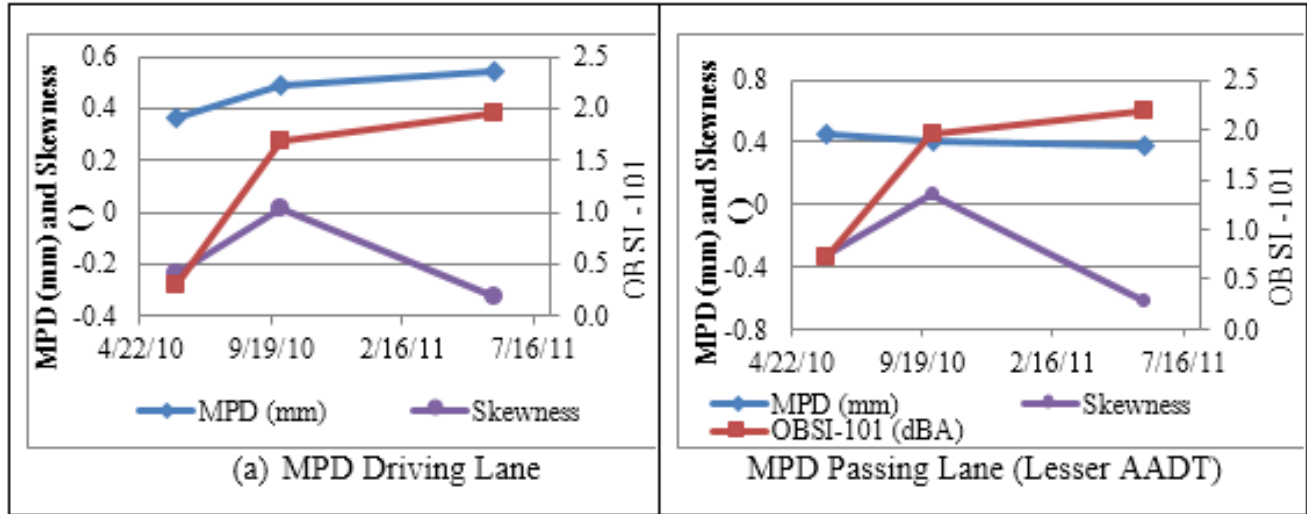
Figure 2.28: SA Coefficient Spectrum (a) 6/7/10 and (b) 10/17/10

#### 2.4.6 Friction

The standard method for testing friction at MnROAD utilizes the KJ Law Friction Trailer to perform skid testing of the pavement surface. Friction testing is done in accordance with the following three ASTM standards: ASTM E274 standard test method for skid resistance of paved surfaces, ASTM E501 skid testing using a standard ribbed tire, and ASTM E524 skid testing using a smooth tire. Both ribbed and smooth tires are used because they each measure adhesion and hysteresis differently. Since the ribbed tire removes the water from the surface more efficiently than the smooth tire, it generally examines the pavement friction on the micro-texture portion. The smooth tire, however, is more affected by the macro-texture. If the macro-texture does not adequately drain water on the pavement surface, the smooth tire will hydroplane and result in lower friction values. The locked-wheel skid trailer and truck setup is shown in Figure.

The test generates friction numbers ranging from 0 to 100, with higher numbers indicating higher friction. A pavement with a friction number of 25 from a smooth tire is considered a safe pavement with adequate skid resistance, while a pavement with a friction number less than 15 would require rehabilitation to achieve sufficient skid resistance.

The FHWA roughness categories place pavements with IRI values less than 1.5 as in “good” condition, with pavements with an IRI less than 2.6 considered “unacceptable”. All test cells did achieve acceptable IRI, but only the hot mix asphalt and traditional grind were categorized as “good” pavement. The exposed aggregate has higher IRI values than all surfaces except for the innovative diamond grind.



**Figure 2.29: a) CTM Cell 72 (b) MPD Driving (c) MPD Passing**

### 2.4.7 Section Summary

This section summarized the construction and early surface performance assessment of three composite test cells at the MnROAD (Cell 70, HMA over a recycled aggregate concrete; Cell 71, diamond grind concrete over recycled aggregate concrete; and Cell 72, exposed aggregate concrete over a low cost concrete) and emphasized the performance of the exposed aggregate finish. The construction of cells 70, 71 and 72 was part of a composite pavement project of Strategic Highway Research Program. The following conclusions were made on the different composites and surfaces tested and the exposed aggregate surface performance in relation to other contiguous test cells with familiar surface types.

- Early performance assessment of the three test cells suggest that the exposed aggregate concrete surface did not provide significant noise reduction, as it had higher OBSI than both the HMA and traditional diamond grind surfaces tested.
- Innovative diamond grinding of composite pavements may be beneficial for noise reduction. It showed lower OBSI than the HMA, EAC, traditional grind surfaces, and had greater sound absorption than EAC.
- Exposed aggregate surfacing provided more than adequate friction for driver safety, but does not show any advantage over typical HMA or diamond ground surfaces.
- Exposed aggregate surface tested has a similar texture (or mean profile depth) to traditional diamond ground surfaces, but may have reduced ride quality as laser induced IRI values due to isotropy.

The acoustic performance is highly dependent on aggregate content. Consequently, it is recommended to use crushed rock to reduce the texture orientation to a more likely negative value, blended with rounded aggregate to enhance quietness. However, the use of 100 %-rounded aggregates in a gap gradation is not encouraged as it may compromise friction.

## 2.5 2011 Construction Texturing

### 2.5.1 Background

Construction initiatives for 2011 summarily included:

- 1) Use of non-woven geotextiles in thin (5") unbonded concrete overlay.
- 2) Smaller panel sizes for unbonded overlays than currently found at MnROAD.
- 3) Longitudinally tined concrete pavement.
- 4) OGAB (open graded aggregate base) special.
- 5) Roller compacted concrete (RCC).
- 6) Repair of thin concrete overlays.

#### **Detailed construction report is published [2.2]**

These provided opportunities for some surface characteristics studies. In 2008, unbonded overlays (UBOL) had been constructed in cell 5. They consisted of a 4-inch and a 5-inch concrete overlay, 1 inch interlayer of permeable asphalt stabilized stress relief course (PASSRC), and existing concrete pavement. This cell degraded considerably, showing widespread cracking on the leave slab portion of each joint in the 4-inch UBOL. The cracks were much less pronounced, and occasionally nonexistent, in the 5-inch UBOL. To continue the UBOL study, a new initiative replaced the 4-inch concrete overlay and interlayer with 5-inch concrete overlay and a non-woven geo-fabric. The geo-fabric was instrumented with moisture and stress sensors to monitor the degree to which 1) the fabric provides stress relief and 2) the fabric provides lateral drainage.

Cell 6 was originally built in 2008 to study thermally insulated concrete pavements (i.e. composite pavements). Due to widespread distress, the cell was reconstructed. Reconstruction included a new drainable base made of a special gradation that balanced porosity and stability. This material was evaluated in lab and field elaborately, and results are discussed in this report. Furthermore, to expand the matrix of surface texture types at MnROAD, a longitudinally tined texture was performed on this cell. Repair work on Cell 63 was followed by traditional grinding to restore ride. This whitetopping cell was in various stages of surface deterioration prior to the rehab. Part of Cell 5 was finished with a transverse tined texture while cell 6 was textured with longitudinal tining after a drag pre-texturing. Some minor rehabilitation involving grinding of Cell 63 with the conventional grind was also performed.

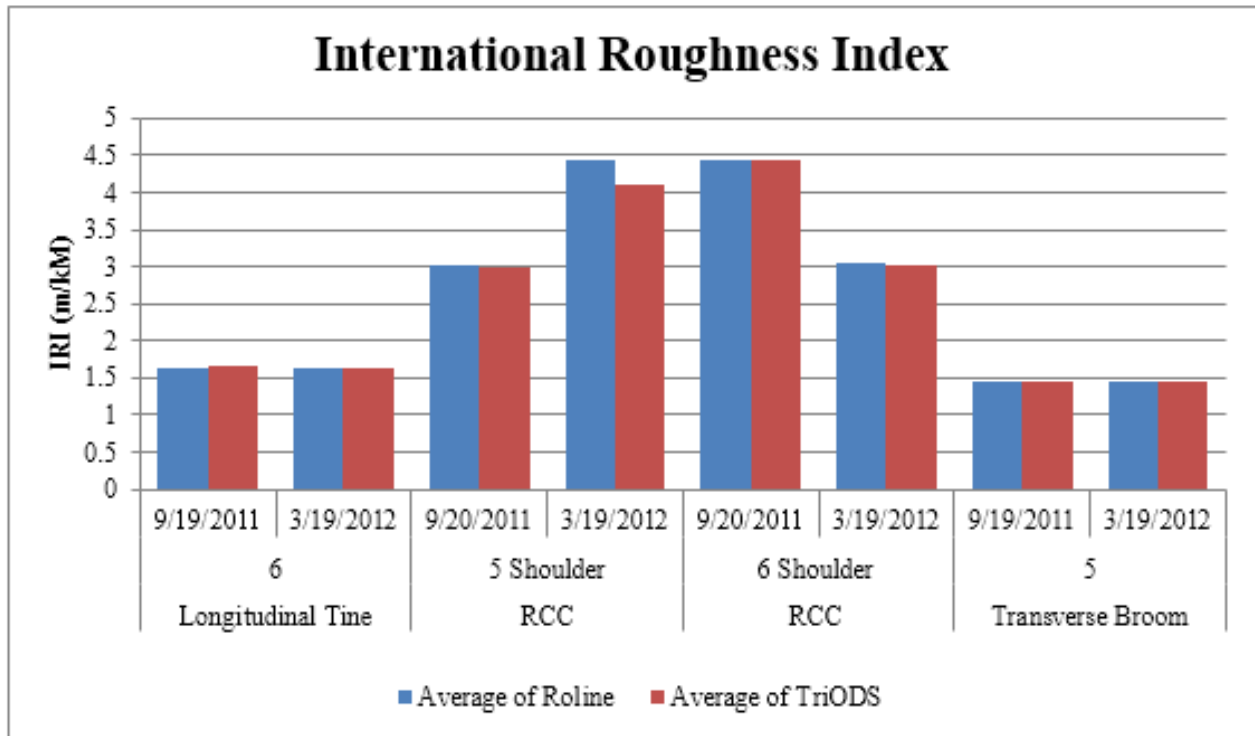
A roller compacted concrete shoulder built in cells 5 and 6 were not evaluated for surface characteristics.

### 2.5.2 Performance Evaluation

**Ride Quality:** The International Ride Index (IRI) is measured using two different pieces of equipment mounted on the Lightweight Inertial Surface Analyzer (LISA). The LISA shown in the figure below is a profile device used to measure the amount of vertical rise over a horizontal distance. This is done with two separate laser sources on the side of the vehicle: The ROLINE laser which takes continuous profile measurements over a four inch path, and the Triple Laser which measures three discrete profiles across the four inch path. The raw data collected from these lasers is then used to calculate two different IRI values. This is done with a mathematical

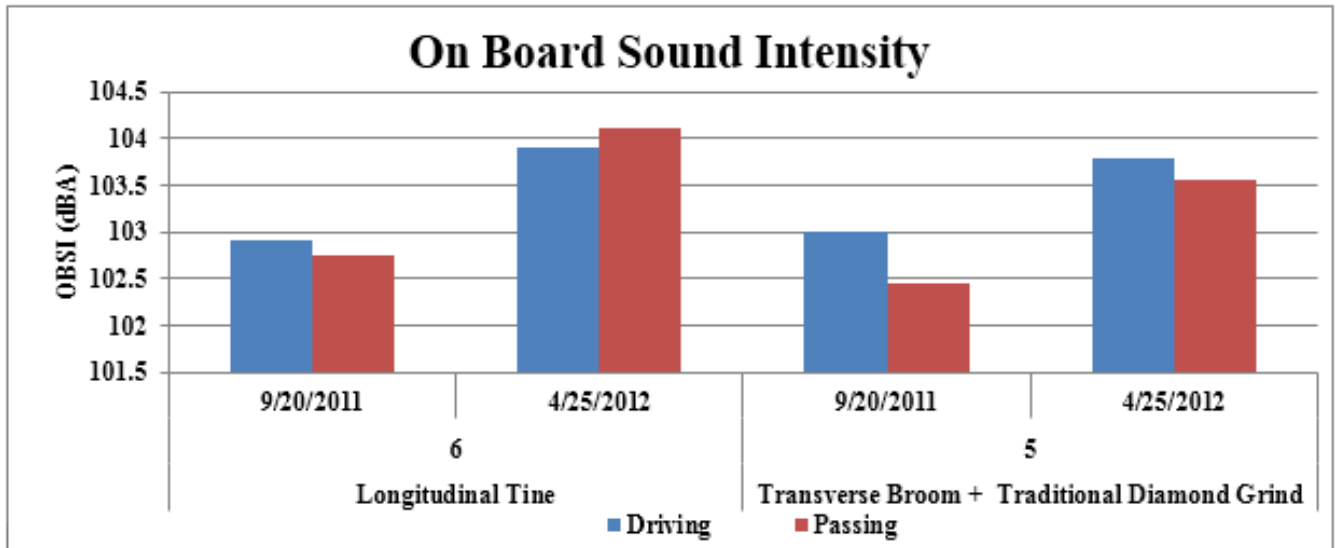


simulation that estimates the amount of vertical movement a vehicle would experience while driving. The simulation uses a higher IRI to correspond to a rougher pavement. It is important to note that the calculated IRI can be highly dependent on the section length; a single rough spot would have a larger negative influence on a shorter segment than it would on a longer one. Figures 2.30 to 2.34 show the initial test results



**Figure 2.30: International Roughness Index Results**

As you can see from this chart, IRI in cells 5 and 6 does not significantly change from right after construction to the following spring. The RCC shoulders have significantly higher IRI than the longitudinal tine and transverse broom. The longitudinal tine is only slightly higher in IRI than the transverse broom. **On Board Sound Intensity:** The On Board Sound Intensity (OBSI) test measures the noise generated from the tire interaction with the pavement surface (AASHTO TP 76-09).



**Figure 2.31: OBSI Results**

Because of the length required for this test, the new test sections in Cell 5 (505 and 605) were measured with the old diamond grind sections in Cell 5 (305 and 405), so the resulting OBSI is from a combination of both surface textures. It is evident from this chart that the OBSI was much higher in the spring than fall for both cells. Immediately after construction, the OBSI of the longitudinal tine in cell 6 was less than the transverse broom and diamond grind in Cell 5, however this trend was opposite in the spring.

**Friction Number:** Cell 5 and 6 were tested for friction with the standard method used at MnROAD. This method utilizes the KJ Law Friction Trailer shown in Figure 41 to perform skid testing of the pavement surface. This test is usually performed twice annually on all cells at MnROAD. Friction testing is done in accordance with the following three ASTM standards for skid resistance of paved surfaces: ASTM E274 using a full-scale tire, a pavement friction is typically compared to what is common in the network but though a threshold is typically not set institutionally in order to forestall data abuse and wanton frivolous law suits, due diligence is still maintained.

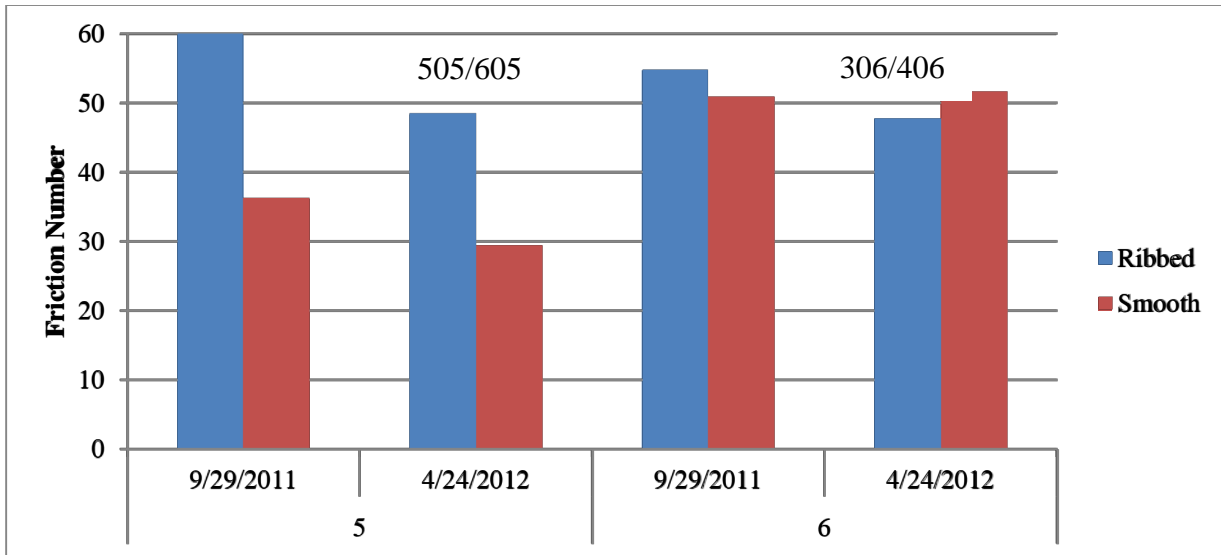


Figure 2.32: Friction Number Results

The friction number for both test cells was slightly lower in the spring than in the fall right after construction. The longitudinal tine in Cell 6 generally had a higher friction number than in cell 5.

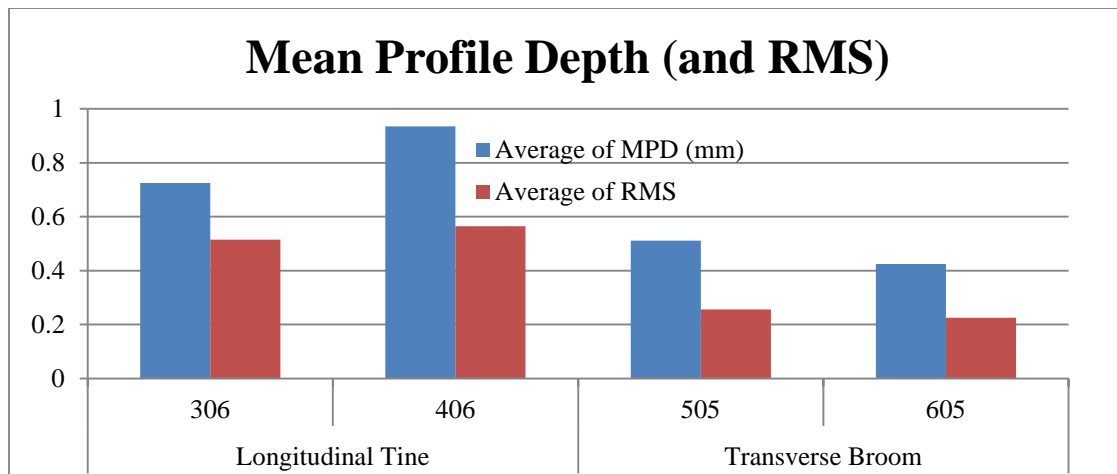
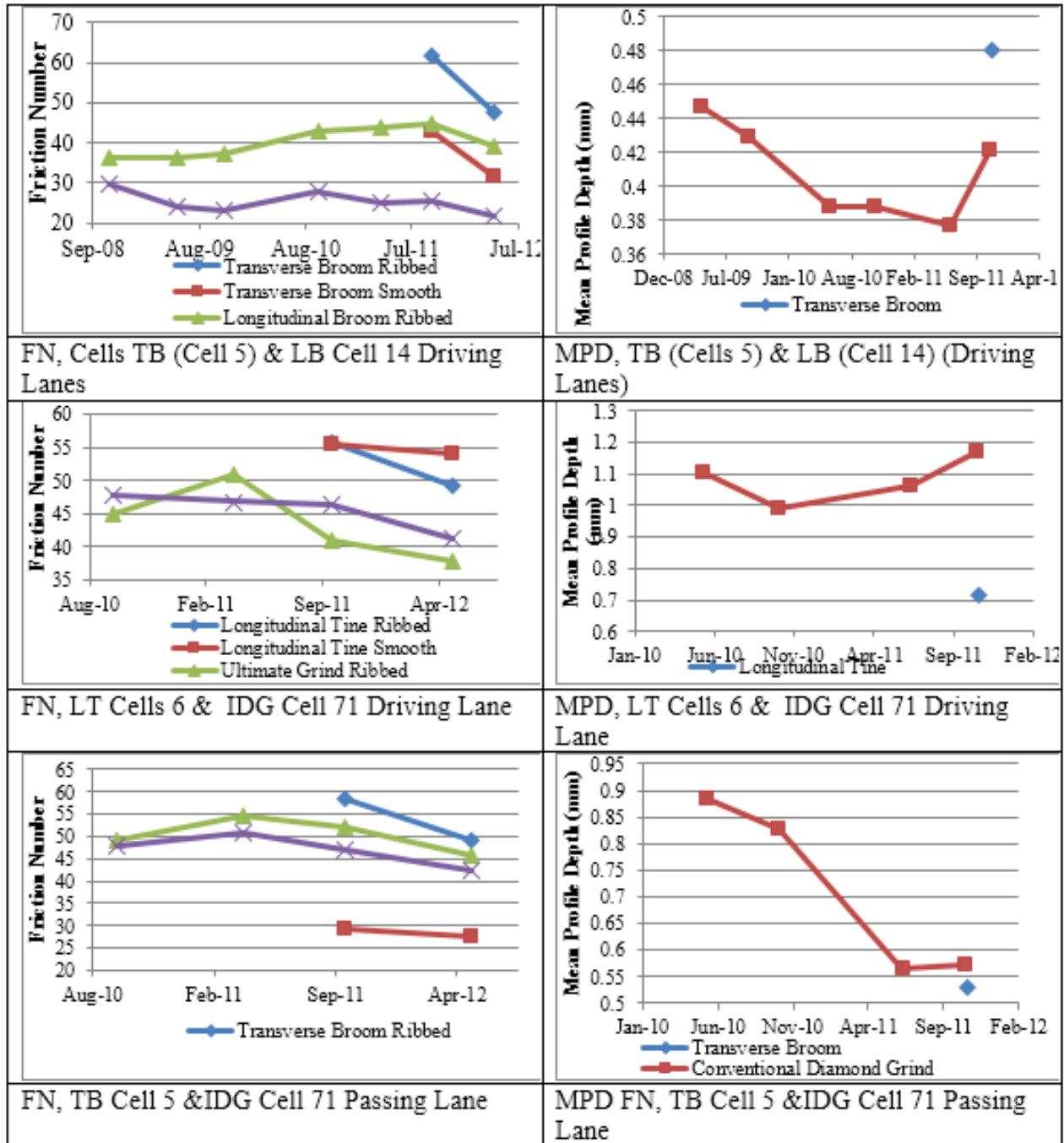


Figure 2.33: CTM Results

The transverse broom in Cell 5 has a lower MPD than the longitudinal tine in Cell 6. There is variation between the subsections of each cell, which suggests some inconsistency in paving.

**General Surface Comparison:** This purpose of this section is to do a qualitative/general comparison of the surface textures used in cells 5 and 6 to similar to textures on existing cells at MnROAD. The transverse broom in cell 5 will be compared to a longitudinal broom surface in cell 14 (constructed in October 2008). The longitudinal tine in cell 6 will be compared to the ultimate diamond grind in cell 71 (constructed in May 2010). Finally, the transverse boom/conventional grind in cell 5 (the second half of cell 5, 305 and 405, has an existing diamond grind texture) can be compared to the conventional grind in cell 71. Pavement Noise (OBSI), texture (MPD), and friction (FN) results will be used for this comparison.



**Figure 2.34: FN and MPD Surface Comparison of Longitudinal Tine to Innovative grind and Transverse Broom**

The transverse broom has higher friction and MPD than the longitudinal broom. The Longitudinal tine has higher friction than the ultimate diamond grind, however the MPD for the longitudinal tine is lower than the ultimate diamond grind. Friction number trends between the transverse broom and conventional diamond grind are dependent on the type of tire used, however MPD seems to be lower for the transverse broom than the conventional diamond grind.

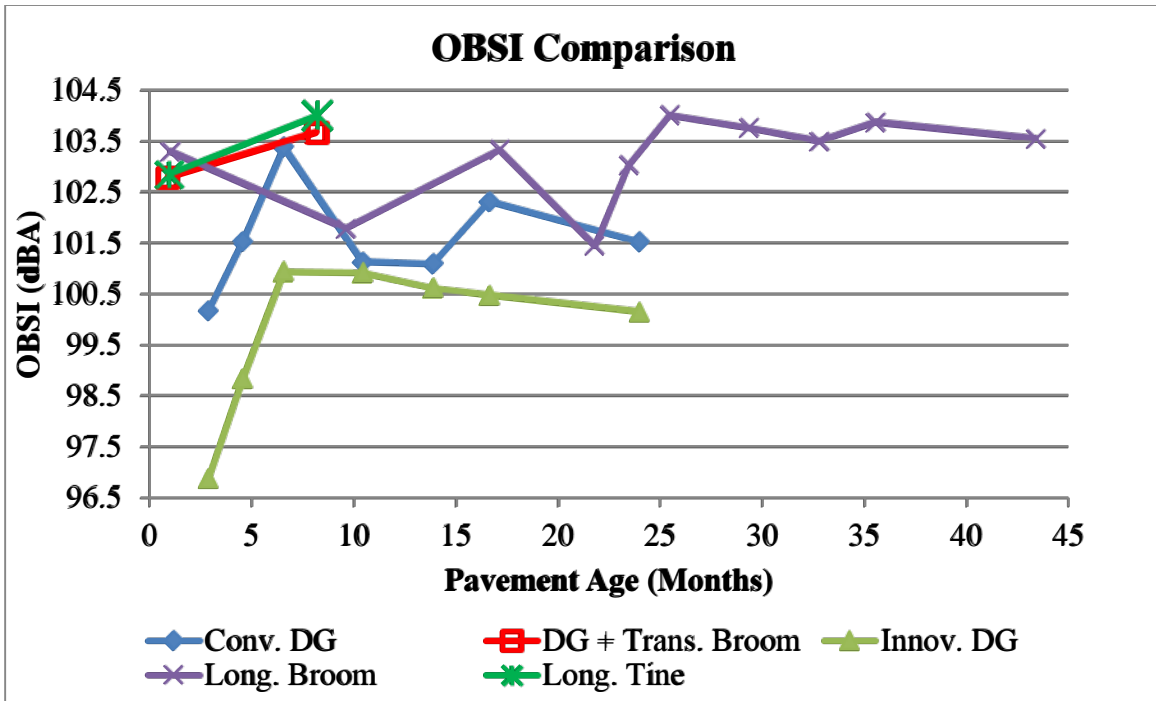


Figure 2.35: OBSI Surface Comparison

The plot above shows that the longitudinal tine in cell 6 and diamond grind plus transverse broom in in cell 5 is generally trending higher in OBSI than the other surface textures in the comparison with respect to pavement age. The following plots compare longitudinal tine and diamond grind. The driving lane in cell 71 is the ultimate diamond grind, whereas the passing lane in cell 71 is the traditional diamond grind. The data presented is from the first measurement taken after each cell was constructed.

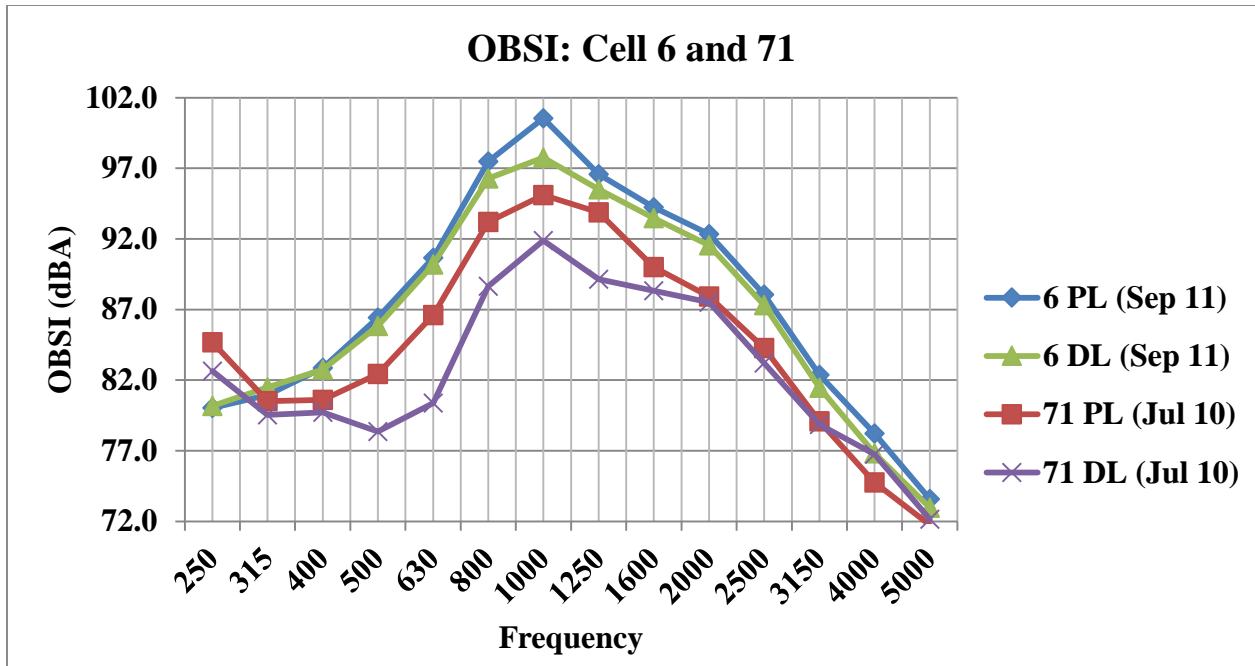


Figure 2.36: Cell 6 (Longitudinal Time) and Cell 71(Ultimate Grinding Configuration OBSI Spectra Compared

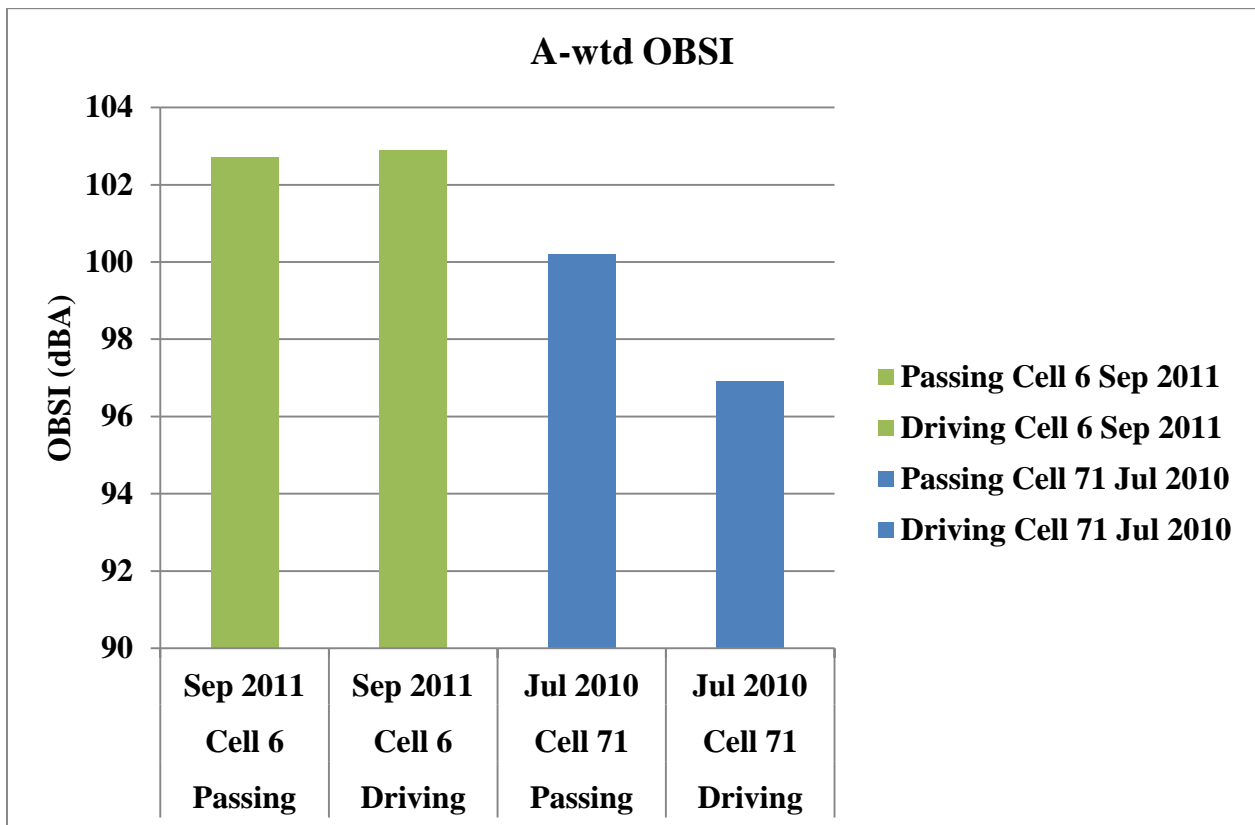
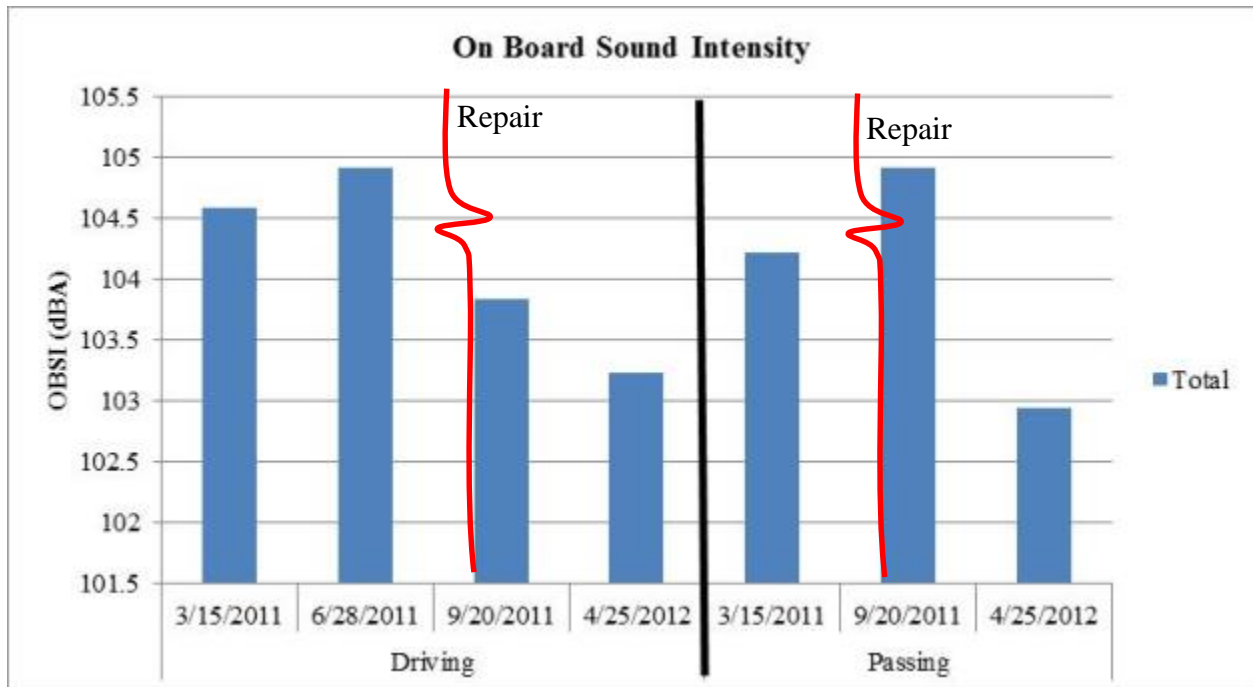


Figure 2.37: Cell 6 and Cell 71 (For Comparison) A-wtd OBSI

From the plots above, you can clearly see that the longitudinal tine has a higher OBSI than both the traditional diamond grind and the ultimate diamond grind.

## 2.6 Cell 63 Drag Surface Rehabilitation

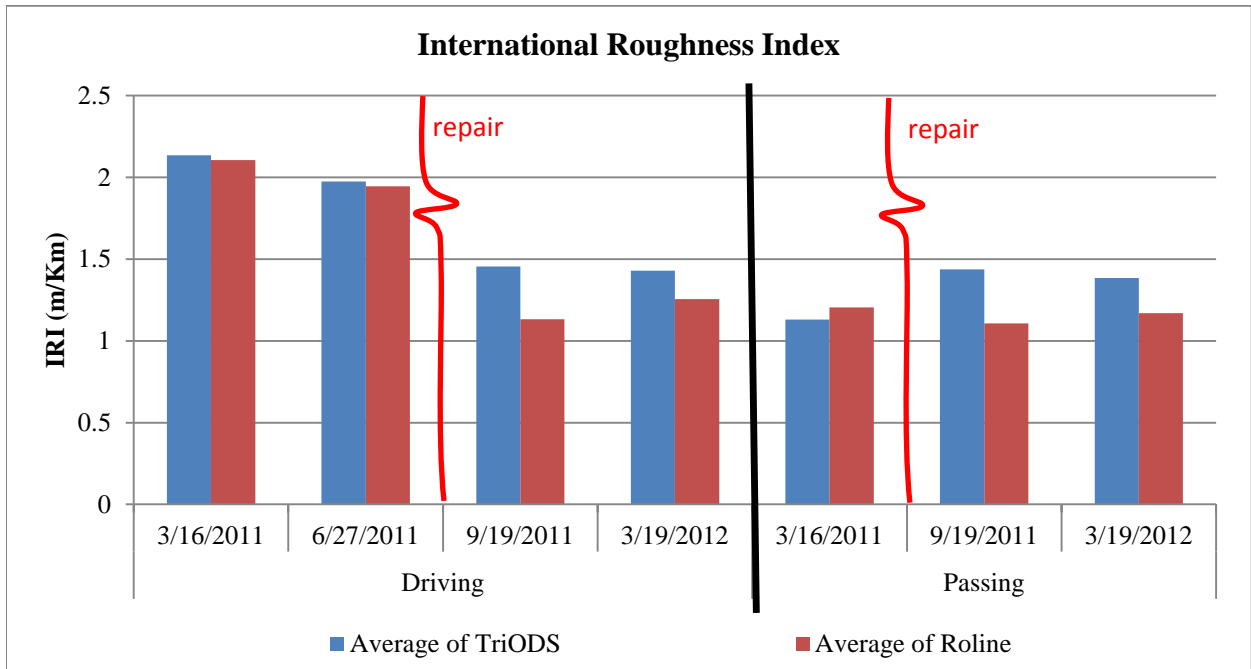
The following plots are provided to evaluate how the repairs done on the thin whitetopping in cell 63 improved performance. (Figures 2.38 to 2.311)



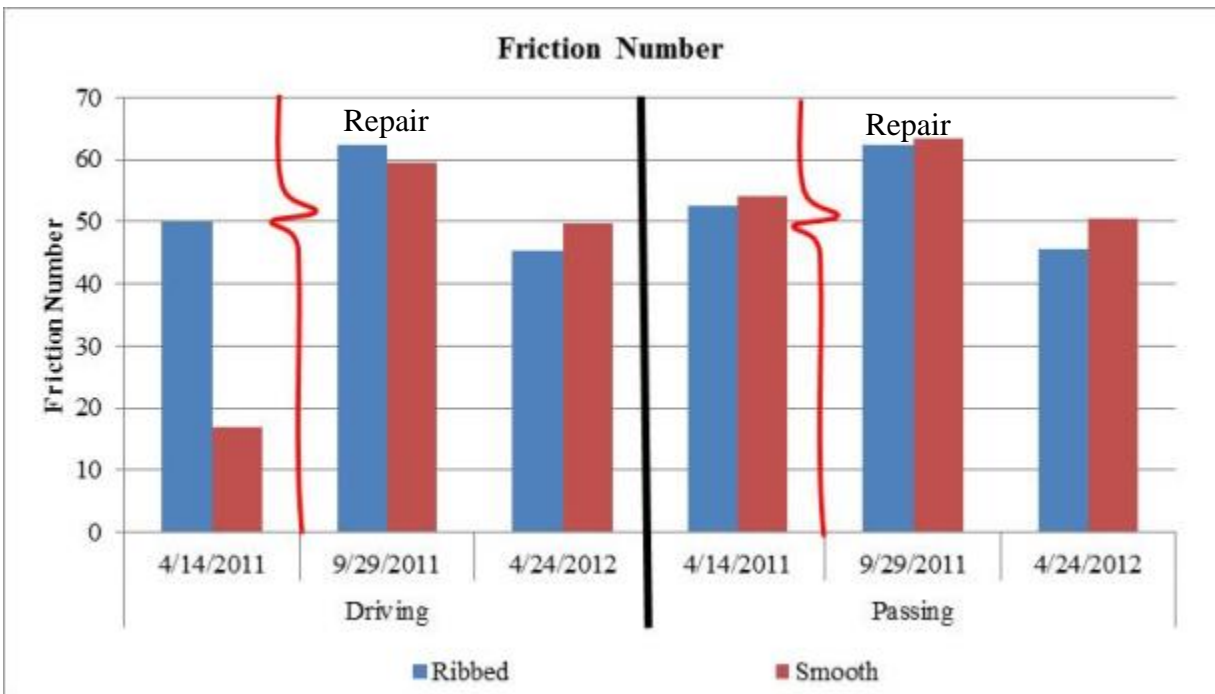
**Figure 2.38: Cell 63 OBSI**

From these plots, there are opposite trends in the change in OBSI due to the repairs between the driving lane and passing lane. In the driving lane, repairs showed to decrease the OBSI, whereas in the passing lane, repairs showed to increase OBSI. This trend is also true for ride, where in the driving lane ride is improved after repairs, and in the passing lane, IRI values are slightly increased. The results from friction testing are not as clear. It is possible that the broom finishing done on the repaired panels was flattened during the winter snow removal operations, causing lower friction in the spring. It seems that friction is greatly improved in the driving lane, but results are not as pronounced in the passing lane. Although friction in the passing lane was increase in the fall (for the passing lane), it dropped again in the spring. Detailed report in [2.2]

A comparative analysis shows that the goal of achieving the level of pavement quietness of the innovative diamond grind by performing longitudinal tine is still a work in progress. It can be projected that at low frequency, the longitudinal tine may be less noisy but a definite metric to evaluate this must include in its one third octave bands, frequencies that are less than 400 Hz.



**Figure 2.39: Cell 63 Rehabilitated Drag IRI**



**Figure 2.40: Cell 63 Rehabilitated Drag Friction**



## Chapter 3: Development of a Process for Acoustic Impedance (Sound Absorption) Measurement and Application

### 3.1 Development of a Process for Acoustic Impedance (Sound Absorption)

#### 3.1.1 Background

This Chapter develops the process for acoustic impedance measurement and validates it. Originally this task was called Effective Flow Resistivity which is a measure of the degree to which non-pavement surfaces absorb sound. It was considered more beneficial and cost effective to develop a process for measuring sound absorption in our pavements instead of evaluating non-pavement surfaces. Moreover, hiring a consultant for ROBOTEX analysis was already planned for a consultant contract that did not need to be duplicated. Consequently, this task describes how the equipment and data collection process for the modified ASTM E-1050 was set up. This test was timely and particularly important for pervious surfaces whose sound absorption properties are the first indicators of performance.

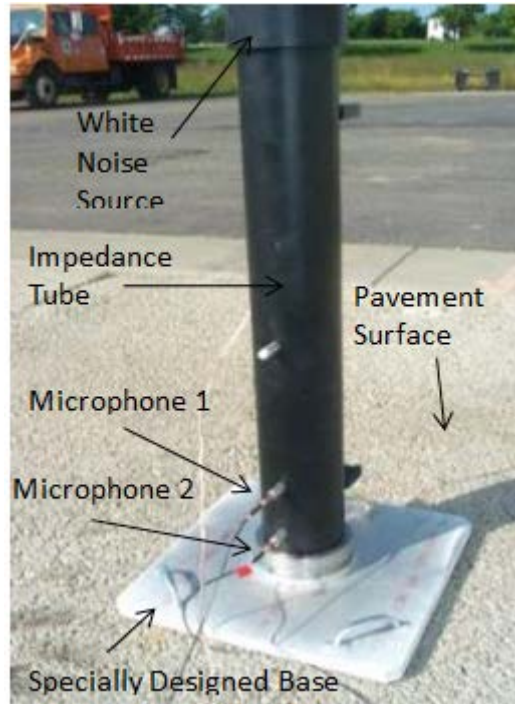
#### 3.1.2 Description of Equipment

MnDOT's BSWA 435 in-situ sound absorption measuring device consists mainly of a rigid impedance tube, capped by a white noise source, supported on a steady base and equipped with two microphones. The tube facilitates insulation from exterior sound source when the white noise source sends signals to the pavement surface. The 11 inch (100 mm) diameter tube accommodates two microphones that are connected to a frequency analyzer. These dimensions of the tube allow an analysis within a range of 20 and 800 Hertz. The separation of the incident noise from the reflected noise is accomplished by the transfer function method.

The sound absorption test is a process that measures the sound absorptiveness of a pavement surface. During the test, the sound analyzed is not generated by the interaction of the rolling tire with pavement surface but by noise source above the impedance tube. On the BSWA 425 device, a white noise source is used. White noise is a random audio signal with a flat power spectral density that contains noise at the same power at all frequencies. During the test, the impedance tube is placed on the pavement surface and a set of sensitive microphones are attached to the pre-installed housing at the lower end of the tube. These microphones are also connected to an analyzer. The noise source sends the incident sound energy (white noise) to the surface and the incident and reflected waves are captured by the two microphones. Software windows the reflected waves and converts the data to the 3<sup>rd</sup> octave sound absorption coefficient at 315, 400, 500, 750, 1000, 1250 and 1650 Hertz. Thus, the coefficients need to be between one and zero where a value of one would mean that all of the sound is being absorbed [3.1] & [3.2].

Output is generated as a function of frequency as shown in equation 3.1 (below). Ordinarily, the result is generated in a narrow band but 3<sup>rd</sup> octave band results are reported. Berengier et al [3.3] discussed that the sound absorption coefficient ( $R_p$ ) is expressed as a function of frequency:

$$|R_p(f)|^2 = 1 - \frac{1}{K_r^2} \left| \frac{P_r(f)}{P_d(f)} \right|^2 \quad (\text{Equation 3.1})$$



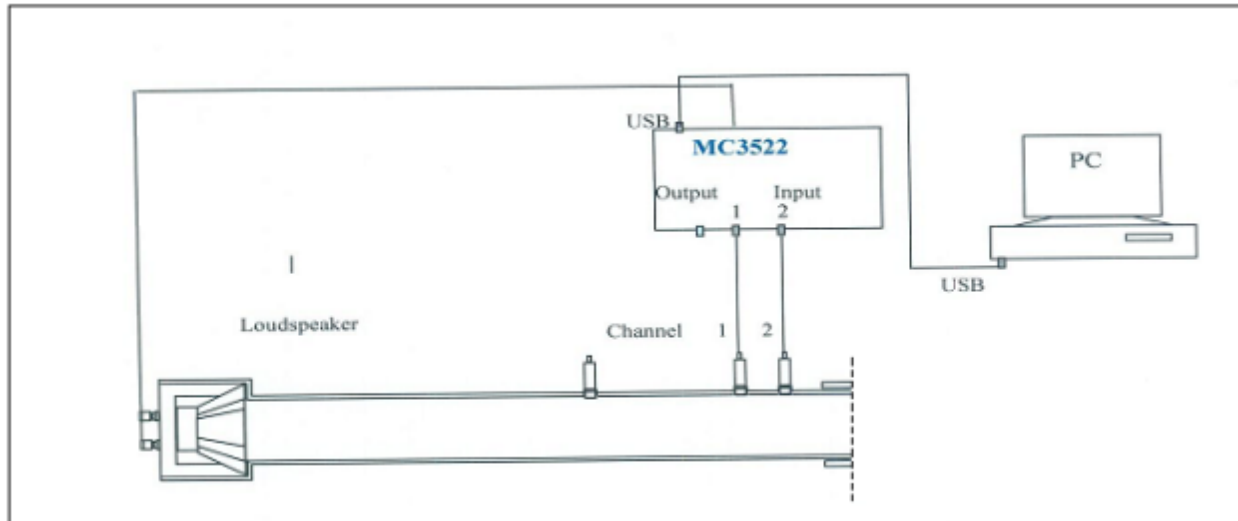
**Figure 3.1: Impedance Tube Adapted to In-Situ Testing**

Where:  $K_r$  is the spreading factor,  $P_r$  is the reflected sound energy and  $P_d$  is the incident sound energy [3.3] & [3.4]. The output of a sound absorption factor is typically in the form of the sound absorption at the seven frequencies defined earlier. An example of the application of this technology is shown in [3.4] hence; factor is therefore expressed as a function of frequency. With this information, the pervious surfaces can thoroughly be analyzed to evaluate acoustical properties. It is also used on other surfaces for an overall evaluation of surface parameters affecting tire – pavement noise. On-going studies are being conducted to find if/how these coefficients correspond to the On-Board Sound Intensity (OBSI) and surface porosities indicated by the Circular Track Texture Meter (CTM).

### **3.1.3 Collection Frequency & Process**

MnROAD plans on collecting information two times a year. Additional tests will be conducted on an as needed basis.

Start by unloading equipment and setting it up. Set-up consists of placing base plate on the end of the tube and connecting the wires and microphones as shown below. Once the set-up is complete and the equipment is running, the sound absorption program can be started (VA-Lab2). Enter general information about the date, the location, which device is being used (MC3522) and calibrate the microphones. Before any measurement can be taken, the atmospheric pressure (Pascal) and the temperature (degrees Celsius) need to be entered into the program. Then use the Transfer Function Method to capture the measurements.



**Figure 3.2: Schematics of Construction / Circuitry**

Each measurement consists of four steps:

1. Capture sound for 10 to 15 seconds.
2. Switch the microphone's positions.
3. Capture sound for another 10 to 15 seconds.
4. Save measurements as the test number being conducted (1, 2, 3, etc).

These steps are then repeated for each measurement. Each location needs to have at least two separate measurements to ensure that the results are accurately depicted.

The operator also needs to keep track of the locations of the various tests that are being conducted. Information consists of which cell, station number, lane, wheel-path and any general comments on the pavement condition. This information is collected on a Field Data Sheet and is later transferred to Excel. The cells that being tested get data from at least three different stations and different wheel-paths but the number of total measurements for a cell vary depending on the emphasis of sound absorption for that particular cell.

### **3.1.4 Data Processing**

The data files are saved as .txt files but contain a lot of information that isn't easily extracted from the file. In order to get the necessary information, a more user-friendly program (VA-Lab2) is used to create an Excel file for each test conducted. Then each Excel file has the sound absorption values for the various sound frequencies in an easily accessible manner. So, if 150 tests were completed then 150 Excel files would need to be created. Next, the Field Data Sheet is transferred to an identical Excel file. Finally, the measurements are broken apart by station, lanes, wheel-paths and cell numbers to get various averages for each tested cell and create graphs with this information. White noise has a flat PSD and is not a true reflection of tire – pavement noise but is sufficient to indicate differences brought about by the pavement surface.

### **Database Table**

Sound absorption data is stored in the table MNR.DISTRESS\_SOUND\_ABSORPTION. See the table below for a description of the data.

**Table 3.1: Sound Absorption Database Table**

Name	Type	Example	Description
CELL	NUMBER (3.0)	2	MnROAD cell number
STATION	NUMBER (7.1)	116405.5	Station number according to field markers
OFFSET	NUMBER (2.1)	13	Offset from centerline
LANE	VARCHAR(30)	Mainline Driving	Facility and lane being tested
WHEELPATH	VARCHAR (12)	LWP	Position of test
TRIAL	NUMBER (2.0)	1	Test number at certain location
OPERATOR	VARCHAR(30)	Tim Nelson	Name
DATE	DATE	10/11/2009	Date of test
TIME	TIME	11:15:22	Time of test
TEMPERATURE	NUMBER(2.0)	25	Temperature (degrees Celsius) at test
ATMOSPHERIC PRESSURE	NUMBER(6.0)	101400	Pascal – At time of test
CONDITION	VARCHAR (30)	Sunny	Weather at test
FREQUENCY	NUMBER(4.0)	1250	Sound frequency – Hertz
SOUND ABSORPTION	NUMBER(2.2)	0.24	Decimal percent of sound absorbed
COMMENTS	VARCHAR(30)	Near Core	Comments about test

SAMPLE RESULTS: <http://www.mrr.dot.state.mn.us/research/pdf/2011MRRDOC009.pdf>

### **3.2 Application of Test Results OBSI-Sound Absorption Correlation in the Frequency Domain**

#### **3.2.1 Background**

The foremost initiative in the use of the impedance tube early in this study was to identify if there is any correlation between sound absorption and OBSI. This investigation was designed primarily for a generic evaluation of OBSI and SA in the spatial domain correlation evaluation and subsequently for a more detailed correlation in the frequency domain.

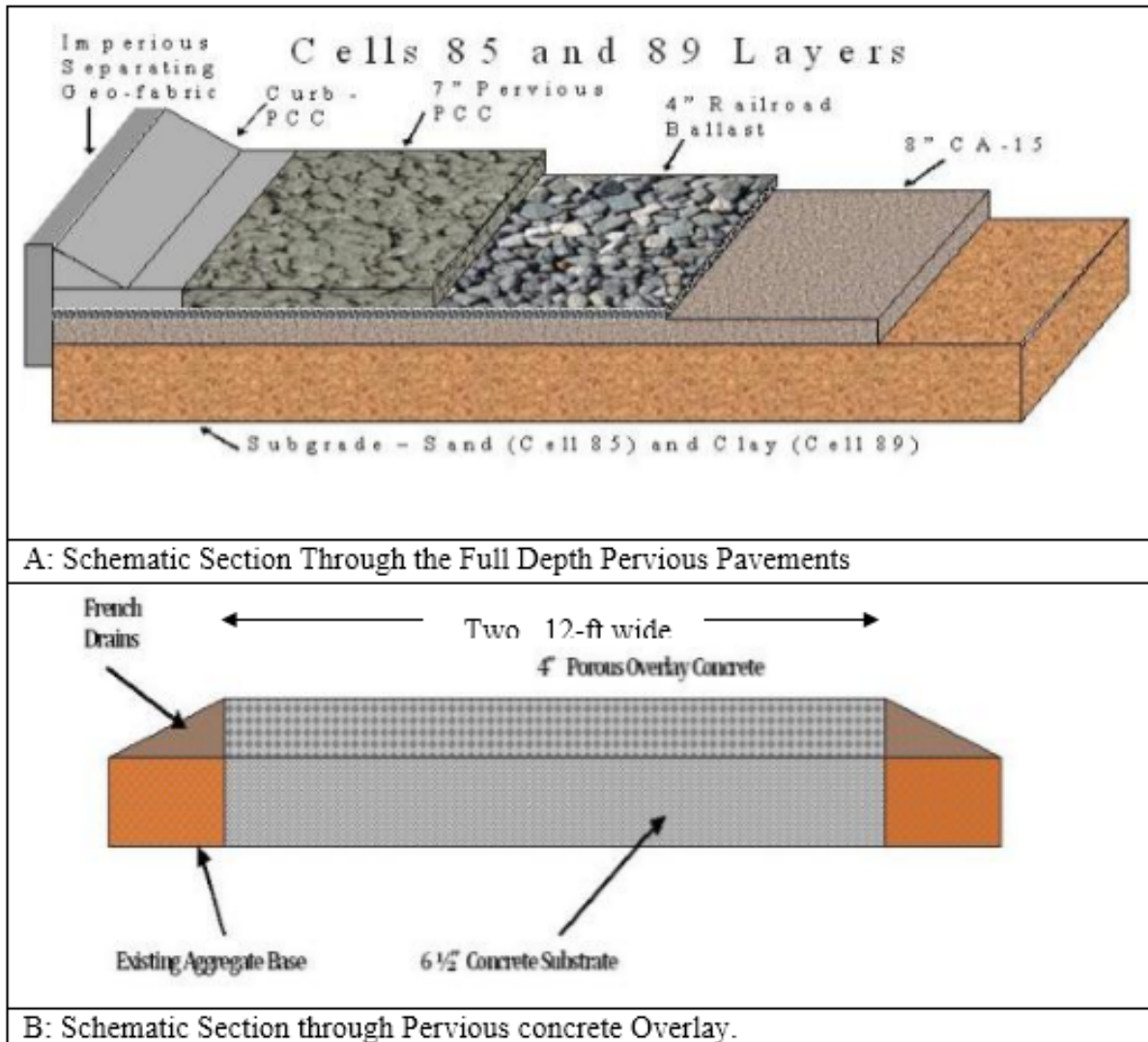
Pursuant to this, pervious and non-pervious OBSI and their SA are examined. Non-pervious pavements retain air entrainment in the paste. On the contrary, pervious pavements retain high porosity due to cavities distributed not necessarily (and very seldom) within the paste. Pervious pavements typically have unit weights that are less than 125-pcf compared to non-pervious pavements, whose infinitesimal void content results in higher unit weight of 146 to 150-pcf. Pervious pavements have a matrix that locks which does not absolutely encapsulate the aggregate system. Due to these characteristics of pervious pavements, they behave differently from non-pervious pavements particularly in porosity and sound absorption characteristics. This task investigates sound absorption of pervious and non-pervious pavements to ascertain if there is correlation of sound absorption and porosity to OBSI. Sound absorption coefficients of pervious pavement are generally higher than those of non-pervious pavements except for those non-pervious pavements that are enhanced for quietness. For instance, comparable sound levels are observed in innovative diamond ground surfaces and pervious pavements. Of the 304 sound absorption test conducted over a period of 12 months, and the corresponding OBSI measured, there was no clear correlation between sound absorption coefficient and OBSI. Ninety five percent of the OBSI for pervious pavements were less than 100-dBA that is classically the typical industrial pivot for quiet pavements. However, of the non-pervious pavements, 25 percent of the measured OBSI was less than 100-dBA. Comparable OBSI was obtained between pervious pavements and the innovative grinding where 90% of the measurements were less than 100-dBA as well. If sound intensity is correlated to OBSI, the pervious pavement data should exhibit that trend with the varying OBSI but that was not observed.

The process of ascertaining if relationship exists between OBSI and sound absorption in the spatial and spectral domain are elucidated. In the spatial domain, there is no significant correlation between OBSI and sound absorption in pervious pavements. However, in the frequency domain correlations between coincident third octave frequency SAs and sound intensities were noticeable but still not significant. Results suggest that sound absorption is not the mechanism by which pervious concrete pavements reduce noise. Since pervious pavements are generally relatively quiet, the mechanism of relief air compression is a tenable quietness mechanism for pervious concrete pavement. This is no different from the air compression relief provided by longitudinally ground, negatively-oriented textured non-pervious concrete pavements. From literature review, it was evident that sound absorption of pervious pavements is higher than normal concrete pavements. However, it is not known if this variable is correlated to sound intensity. Additionally, it is expedient to ascertain if the variable is significant enough to be included in the sound intensity prediction model. Sound Absorption Coefficient ( $\alpha$ ) is the ratio of the absorbed sound energy to the transmitted sound energy when a white noise of frequency ranging from 315 to 1800 Hz is projected into the pavement within an impedance tube placed normal to the pavement surface.

### **3.2.2 Data Collection and Measurement**

To facilitate this research, three pervious concrete cells were built. The Full depth sections as well as the pervious overlay sections are shown in TABLE 3.22, as well Figures 3.22 and 3.23. Sound absorption measurements were conducted as shown in Figure 3.21 and sound intensity measurements were conducted using the AASHTO interim standard TP76-09 explained in task 3. The experiment was limited by the fact that the pervious cells are of approximately the same

porosity and that 6 sections (3 sells 2 lanes wide) of pervious pavements were available for study. It was however possible to make many SA measurements repeatedly to 304 data set.



**Figure 3.3: Cross Sections through the Pervious Concrete Overlay**

The impedance tube with which the sound absorption test is conducted is based on ASTM E-1050 modified for in-situ measurements. By design of the tube practitioners are constrained to the limiting frequency for each diameter of tube. The tube used for this experiment is 6 inches in diameter. It is capable of reliably reporting SA up to 1600-Hz in the third octave. However, smaller diameter tubes are expected to provide reliability at higher frequencies but not beyond 2000-Hertz but the lower frequency effects are compromised. It follows that the available SA equipment does not provide information on SA at frequencies higher than 2000-Hz. This is a limitation of this experiment and consequently a topic for later research.

Porosity of the pervious cells was identified as the primary factor that enhanced the sound absorption characteristics of pervious pavements. Factors related to porosity included tortuosity and gravimetric properties of the pavement. The pavements were categorized broadly into

pervious concrete and non-pervious concrete. Two levels of analysis were performed. In the first level, a ratio of the pervious to non-pervious sound absorption at each frequency was calculated and plotted as shown in Figure 3.4.

It was evident that the maximum ratio in both pavement types occurred at. This underscores the advantage of pervious pavements in the multi-coincidence peaks encountered in tire pavement interaction. When pervious and non-pervious pavements were examined together and categorical variable of 1 was assigned to pervious pavement and 0 to non-pervious pavements, a reasonable correlation was observed with porosity. However, when the data was separated into individual pavement types, SA 1000-Hz was not well correlated to OBSI ( $R^2 = 0.0012$  and  $P = 0.12$ ). The P-value of 0.12 obtained (being  $\gg 0.05$ ) was not strong enough to provide sufficient evidence that SA is correlated to OBSI. It is evident therefore that SA (1000 Hz) is not reasonably correlated to OBSI. However it is still necessary to know if there is correlation at coincident frequencies in the 3<sup>rd</sup> octave band and the degree to which that occurs.

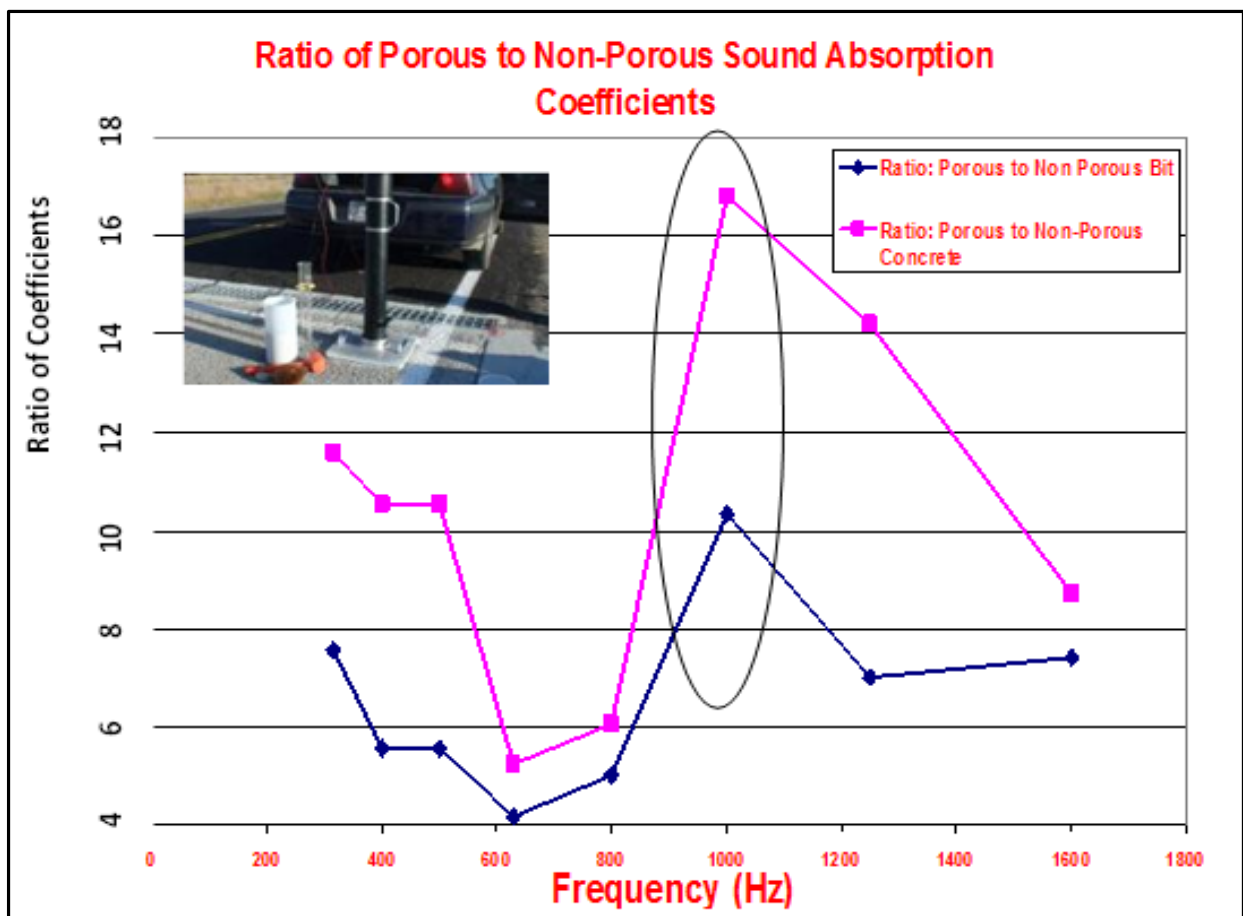


Figure 3.4: Max Effects of Pervious Pavement Observed at Resonant Frequency of 1000 Hz

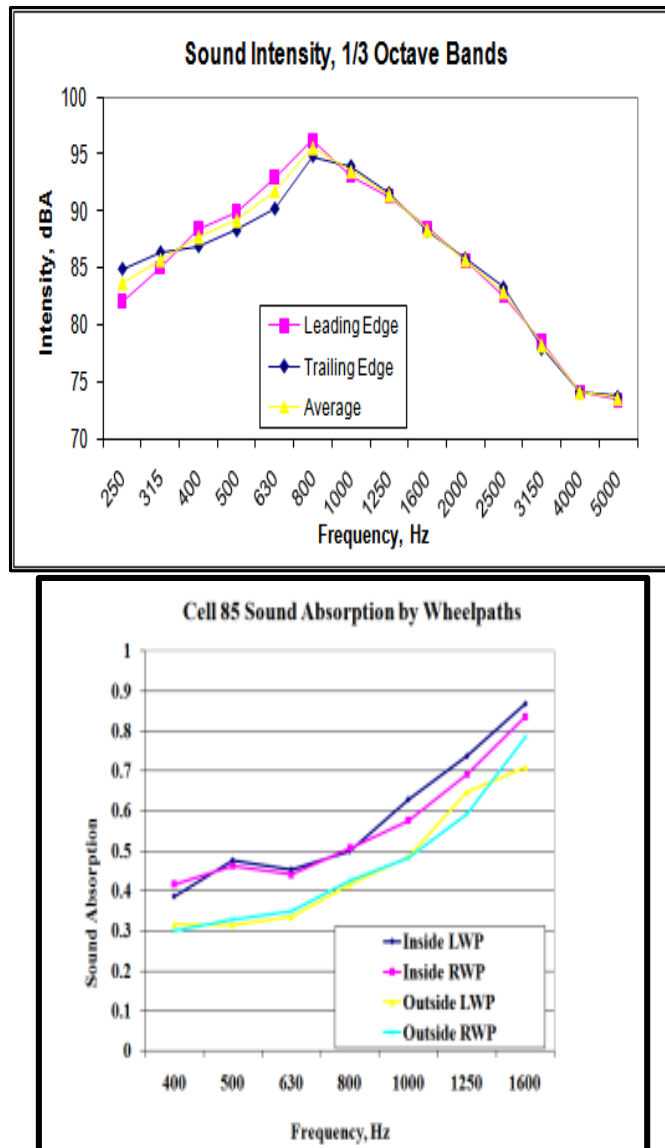
**Investigation of OBSI- SA Correlation in 3<sup>rd</sup> Octave Frequency Domain**

OBSI has been defined as the logarithmic sum of the sound intensity of 12 third octave frequencies. Similarly, in the sound absorption analysis, reference is made to only 7 frequencies in the third octave band. These frequencies are 400, 500, 630, 800 1000 1250 and 1600 Hertz. These seven frequencies are coincident with seven of the 12 OBSI frequencies. This implies that some of the relation if any may be concealed in the frequencies that are addressed by neither SA nor OBSI or may be concealed in the OBSI frequencies that are not considered for sound absorption. The latter possibility does not frustrate the initiative but it deserves an explanation.

**Table 3.2: Typical OBSI and SA at Coincident Frequencies (Cell 85 Outside Lane September 2009)**

Frequency	Leading Edge (dBA)	Trailing Edge dBA	Average	Sound Absorption
400	88.4	86.9	87.7	0.40
500	89.9	88.3	89.2	0.47
630	92.9	90.2	91.8	0.45
800	96.2	94.8	95	0.51
1000	93.0	93.9	93.5	0.61
1250	91.3	91.5	91.4	0.76
1600	88.5	88.2	88.4	0.86
2000	86	88	87	
2500	82.5	83.3	82.9	
3150	78.5	77.9	78.2	
4000	74.1	74.1	74.1	
5000	73.4	73.7	73.6	
A-wtd	100.7	100.0	100.4	





**Figure 3.5: Typical OBSI and SA at Coincident Frequencies**

(Cell 85 Outside Lane September 2009)

This section analyzes the Sound absorption results in a 2-step strategy.

- Step 1: Fragmentation of the Sound absorption coefficient into component factors: This entailed the separation of the sound absorption component into the aggregate and paste component and the porosity component.
- Step 2: Comparison of the sound absorption value to the corresponding OBSI at the same frequency and development of model parameters.

It was hypothesized that the sound absorption of the non-pervious concrete was made up of the sound absorption of the aggregate X<sub>agg</sub> as well as the sound absorption of the mortar phase X<sub>cem</sub>. Similarly, the sound absorption in the pervious pavements, the porosity phase was introduced

as the third component. It was extended from Sabine's [3.5] and [3.6] equations that the SA ratio was composed of the sound absorption ratios of the constituents of the surface type, whence the sound absorption ratio is ramified into components and idealized as aggregate component, cement constituent, flexible component, and the porosity component. Normal concrete provides only the aggregate and cement component. The model successfully identified developed and validated the above constituents of the sound absorption ratio (SA).

Thus  $\alpha_{\text{Concrete}} \approx \alpha_0 + K_1 \alpha_{\text{cem}} + K_2 \alpha_{\text{agg}} - \dots$  (Equation 3.5)

$\alpha_{\text{Pervious Concrete}} \approx \alpha_0 + K_3 X_{\text{cem}} + K_4 X_{\text{agg}} + K_5 X_{\text{por}}$  (Equation 3.6)

The analytical process to determine the correlation tabulated the sound intensity values corresponding to the sound absorption frequencies and sound absorption along different wavelengths for various cells using data from noise and sound absorption test results.

### 3.2.3 Lemma for Component Sound Absorption Analysis

A lemma facilitating the derivation of component absorption ratios is based on Sabine's [3] and (to some extent) Eyring's equations [3.5].

Sabine's equations calculate the attenuation time of an absorbent area

$$T_{60} = 0.161 V / (A + 4mV) S \dots \dots \dots \quad \text{(Equation 3.7)}$$

Where

$T_{60}$  is the time taken for the sound level to attenuate to  $10^{-6}$  of the original level.

This is equivalent to a 60dB loss of intensity.

$A = \alpha_{\text{tot}} S_{\text{tot}} \text{ m}^2$

$$\alpha_{\text{tot}} = (\alpha_T S_T + \alpha_R S_R + \sum \alpha_i S_i) / S_{\text{tot}} \dots \dots \dots \quad \text{(Equation 3.8)}$$

The  $\alpha$ s (alphas) are the sound absorption coefficient corresponding to the individual areas,  $\alpha_{\text{tot}}$  being total absorption coefficient.

$$\text{and } S_{\text{tot}} = S_T + S_R + \dots \dots \dots + \sum S_i \dots \dots \dots \quad \text{(Equation 3.9)}$$

Where

$S_R$  is the residual absorption area,

$S_T$  is the acoustical audience area,

$V$  is the control volume,

$S_{\text{tot}}$  is total area,

$S_T$  is the acoustic audience area.

The above lemma applies to acoustic design in which the proportioning of the absorbent faces and the occupants affect the overall attenuation. Izevbekhai [3.7] showed that with the use of lightweight concrete and enhanced fiber content for acoustic panels, sound absorption properties can be improved. The improvement was due to the substitution of coarse and fine aggregate with sawdust which is a relatively absorbent material. Moreover, the higher the sawdust substitution, the higher the sound absorption factor up to an optimum that was determined by strength requirements. It has already been shown in this experiment that sound absorption factor increases with porosity. It will be noted that components of the surface supply their component

area and sound absorption factors to make the total. It can be shown therefore that in a pervious concrete phase, the overall sound absorption or attenuation is related to the total air voids in the surface plus the area plus the non-pervious surface. Sound absorbing surfaces are therefore hypothesized to function as the product of total area fraction of each component and the component absorption factor. This is used in deriving component models of the pervious pavements. This understanding informed the development of the following equation:

$$SI(f) = \alpha_{0(f)} + K_1 \alpha_{solid(f)} + K_2 \alpha_{Cement(f)} + k_3 \alpha_{porosity(f)} \quad \text{(Equation 3.10)}$$

The three alphas ( $\alpha$ ) correspond to the coefficients that were found in the sound ABS component model and the model parameters to be obtained by minimizing summation of square residuals. An enhanced solver add-in to excel facilitated this process. To develop the model, sound absorption coefficients were measured at MnROAD cells 5, 14, 53, 54, 62 were noted for solid pavements and test results from cells 39, 85, 89 facilitated the models development for pervious concrete.

- The process determined the sum of squared residuals between the SI measured and the SI calculated from SA and minimized the value, using the enhanced solver component in Excel.
- Next the process plotted the calculated SI values versus the measured OBSI values and performed a least-squares regression line those points and found corresponding coefficient of determination ( $R^2$ )

Table 3.3 (below) shows the results for the different groups of surface characteristics and the corresponding  $R^2$  value.

**Table 3.3: Component Absorption Coefficients  $\alpha(F)$  Obtained From All MnRoad**

SA Factors	Coinciding OBSI and SA Frequency (Hz)						
	400 Hz	500 Hz	630 Hz	800 Hz	1000 Hz	1250 Hz	2000 Hz
$\alpha_{cementitious}$	-0.056	-0.058	-0.016	-0.002	0.125	-0.032	0.003
$\alpha_{aggregate}$	-0.064	-0.065	0.021	-0.052	0.068	-0.044	-0.012
$\alpha_{Porosity}$	0.400	0.395	0.362	0.396	0.459	0.480	0.489
$\alpha_{constant}$	0.100	0.100	-0.007	0.050	-0.210	0.113	0.104

**Table 3.4: OBSI SA Model Parameters**

		Pervious Concrete	Non-Pervious Concrete
Agg	k1	-37.32	-515
Cem	k2	99.53	165.90
Porosity	K3	75.02	87.14
Exponent	N	-0.186	0
Constant	Beta	19.94	55.60

### 3.2.4 The Pervious Concrete Model

Looking at the pervious concrete model

$$SI(f) = 99.5 X_{\text{cement}(f)} - 37.32 X_{\text{aggregate}(f)} + 73 X_{\text{porosity}(f)}^{-0.186} + 19.94 \quad (\text{Equation 3.11})$$

Where

$$R^2 = 0.5,$$

$$N=70$$

Non-pervious Concrete, regression yielded:

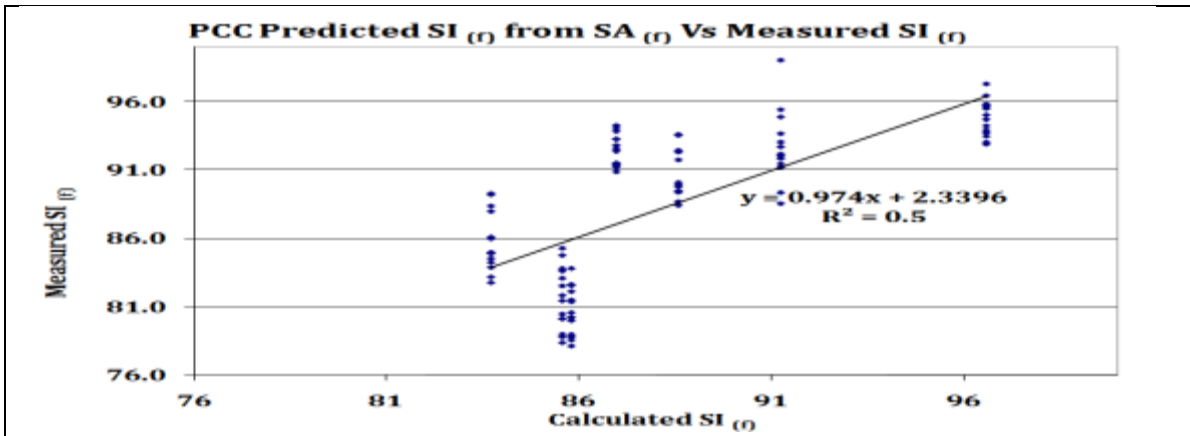
$$SI(f) = 165.9029 X_{\text{cement}(f)} - 5.516 X_{\text{aggregate}(f)} + 6.56 \quad (\text{Equation 3.12})$$

Where

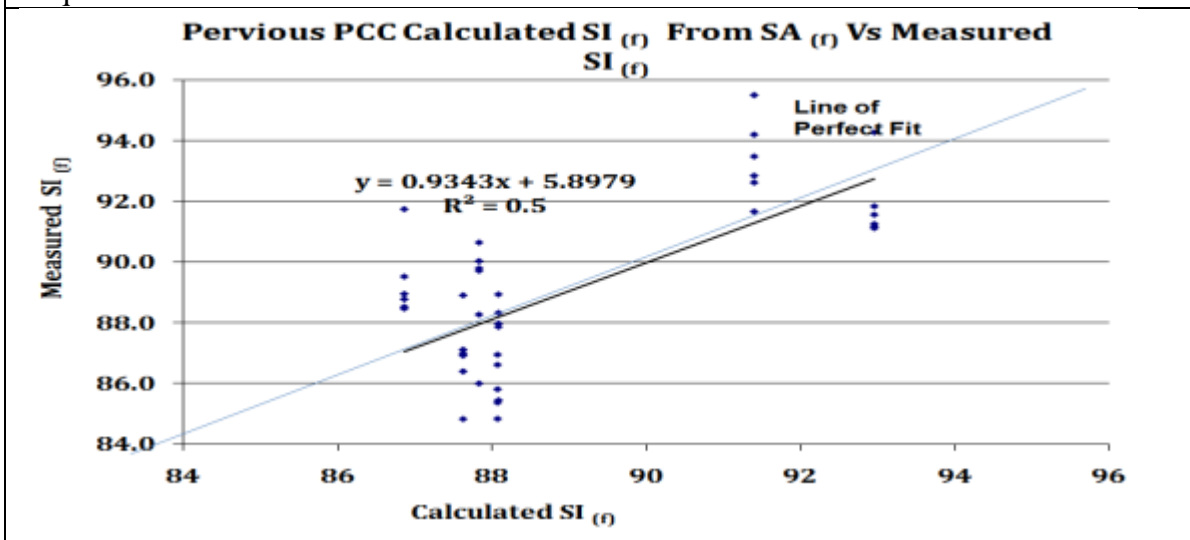
$$R^2 = 0.5$$

$$N=120$$

The coefficient of determination for each pavement group and corresponding model are shown in TABLE 3.22. It is also probable that with more data, the models will be validated. This model predicts the sound intensity at corresponding frequencies from the component sound absorption factors at that frequency. There is evidence that better correlation between sound intensity and OBSI is obtained in a frequency domain analysis but the coefficient of determination is not still high enough to suggest a strong correlation between OBSI and sound absorption. This is partly because there are 5 five octave OBSI frequency that are higher than the range of SA measurements. Furthermore, pervious pavements are not necessarily quieter than non-pervious pavements. This implies that the porosity benefit does not outweigh non-pervious surface features such as longitudinal grinding and smooth pavements. The initial conclusions that sound absorption may not be the major process by which pervious concrete reduces noise is thus validated in the frequency domain analysis.



(a) Normal Concrete Sound Absorption Factor and Sound Intensity at coincident frequencies



(b) Pervious Concrete Sound Absorption Factor and Sound Intensity at coincident frequencies

**Figure 3.6: Pervious and Non-Pervious Concrete Sound Absorption Factor and Sound intensity at Coincident Frequencies**

### 3.2.5 Interim Model Validation

The lemma developing the model for a phenomenological OBSI SA relationship is tenable based on time tested studies from Eyring et al Sabine [3.6] and Izevbekhai [3.7]. It is therefore necessary to continuously reexamine the developed model by applying it to SA and OBSI measurements in some test cells. The shortcoming of an early validation process is evident in the scarcity of data in each cell however aggregating the data for all cells violates the very essence of the model where corresponding fragmented SA and SI values are compared.

As would be expected the validation shows signs of tenability but lack sufficient data at this time. Consequently it is recommended that in the 7<sup>th</sup> year of the pervious pavement service life when the individual cell data sets are robust enough the process should be repeated. The pervious model appears to be less reliable at this time than the non-pervious model and the asphalt cells appear to validate the model more closely even when rheological factors were not applied.

This is an area for future research.

### **3.2.6 Concluding Remarks**

A successful modification of the ASTM E1050 for sound absorption measurement in-situ has been successfully improvised.

Sound absorption factors of non-pervious pavements ranges from 0.02 to 0.09 but the pervious pavement sound absorption ranged from 0.27 to 0.78. The OBSI of pervious pavements ranged from 97.6 dBA to 101 dBA while OBSI of non-pervious pavements ranged from 98.5-dBA to 107-dBA. Interestingly the innovative diamond grinding with OBSI ranging from 98.1 to 101 dBA is generally as quiet as the pervious pavements although its sound absorption factor is low.

It was then concluded that in the spatial domain SA had no direct correlation to OBSI ( $R^2=0.0018$ )

A spectral domain analysis showed improved correlation of SA to OBSI ( $R^2 = 0.5$ ). This was not sufficient however to conclude that SA is well correlated to OBSI. The number of coincident frequencies is only 7 out of 12 OBSI 3rd octave frequencies. If they were all coincident, a coefficient of determination of 0.5 would have been tenable.

With the exception of the innovative grinding, OBSI of pervious pavements were generally lower than OBSI of non-pervious concrete pavements that exhibited much less sound absorption than the pervious pavements. Consequently, the quietness property of pervious pavements is not necessarily driven by the mechanism of sound absorption. Possibly, the relief of air compression, which is the same mechanism employed in the innovative grinding noise reduction is the favored mechanism by which pervious concrete pavements reduce noise. This changes the direction of this experiment to evaluate characteristics of all texture types and minimize evaluation of sound absorption of non-pervious surfaces as that does not seem to be a variable.

Process of coincident frequency SI and SA analysis is limited by the degree to which Sabine's and Eyring's equations may be applied to pavements. The lemma is believed to be reasonably valid.

## Chapter 4: Annual Reports

### 4.1 Second Year Performance Report

#### 4.1.1 Preface

The aim of this second year performance report is to observe data from first and second year and deduce if there are trends that already emerge early in service. Author therefore adopts a summary, cursory and succinct approach. As the second year of study, these observations are early and may be affected by only a few seasons and years of data. They may not reflect the same observation and conclusion of the final report. This section is thus performed in brevity.

#### Mean Profile Depth, IRI & OBSI of Pervious and Non-pervious Pavements

This task investigates MPD to ascertain if it bears any significant relationship to OBSI IRI or any other surface property. This section work was an attempt to understand fundamental surface characteristics of various textures early in the study. The pervious surfaces appeared to be not only the most novel but the most non-descript thus drawing relatively more effort.

While monitoring porosity and sound absorption, it was necessary to investigate the effects of MPD of pervious and non-pervious pavements separately. Surface texture MPD of pervious pavements is difficult to define because of the communicating voids. However with the used of the circular track meter ASTM E- 2157, MPD values are obtained for pervious pavements. A plot of the response shows that the laser occasionally communicates deeply by mainly characterizes the pavement surface. Moreover, more aggressive texturing of pervious pavements results in higher MPD than less aggressive texturing of pervious pavements when measured with the Circular Track Meter (CTM) ASTM E-2157 However, this is a novel idea, the consequence of which is the dearth of previous research publications in this arena. This is attributed partly to the unreliability of measurement techniques available to most researchers to characterize mean texture depth of pervious pavements while the novelty of interest in pervious concrete has not afforded much research in this area. The pervious pavement MPDs measured by the CTM are generally higher than those of non-pervious concrete pavements. The extent to which these textures influence noise is not well understood. A proper understanding will entail variation of texture of pervious pavements but that will correspondingly vary the porosity and possibly confound the experiment.

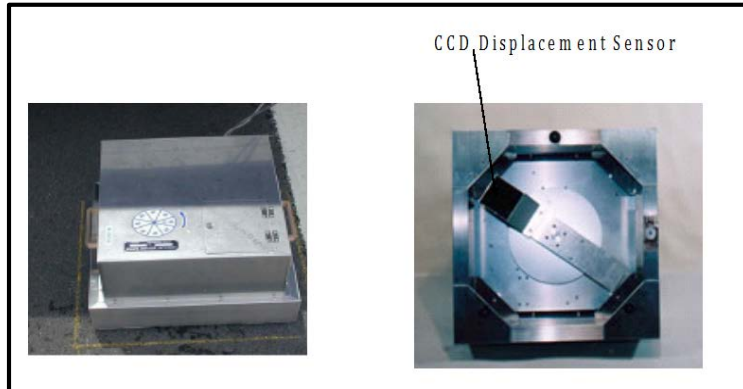
Sandberg et al [1.27] discussed optimization of pervious pavement texture. It is however doubtful if the mechanism of sound absorption contributes to the quietness of pervious pavements. However pervious pavements are comparable and slightly quieter than some well-designed innovative concrete diamond grinding configurations that are not pervious. It is also observed that an inter-mix of soft and hard aggregate will create an uneven surface in the pervious pavements later in service. For pervious pavements the lowest possible mega-texture and macrotexture at all wavelengths are desired. This implies that the chippings must be somewhat rounded. Optimal design of pervious pavement textures is predicated in the expectation of surface porosity, otherwise it is just as good as non-pervious pavements.

To facilitate this study, MPD of MnROAD pervious and non-pervious concrete pavements were measured in the spring and fall of 2009. The corresponding OBSI was also measured. In each lane the MPD was measured at 10 locations in each of the wheel tracks in cells 85 and 89. The

mean MPD was thus obtained from the mean of 20 measurements in each lane of cells 85 and 89 while an average of 40 measurements per lane was used in cell 39 which is 500 feet long. There was no shortage of non-pervious concrete cells in the research facility. However, the MTD (Sand Patch) is deduced from the MPD (CTM) according to the following established equation:

$$\text{MTD} = 0.947 \text{ MPD} + 0.069 \dots\dots\dots (\text{Equation.4.11})$$

MTD and MPD are expressed in millimeters. Based on this relationship in equation 1, it is sufficient to evaluate MPD instead of MTD.



**Figure 4.1: Circular Track Meter ASTM E-2157**

The results obtained are shown below indicating a minimum and maximum OBSI of 97.4 and 100.1 respectively and maximum and minimum MPD of 1.74 and 2.04 respectively. The Correlation coefficient of -0.3 was obtained indicating that there was a general reduction of OBSI with increase in MPD. Already this suggests an increase in surface porosity which is an indication of volumetric porosity. A coefficient of determination of 0.11 and a p-value of 0.32 indicated that there was no strong evidence of correlation between MPD and OBSI.

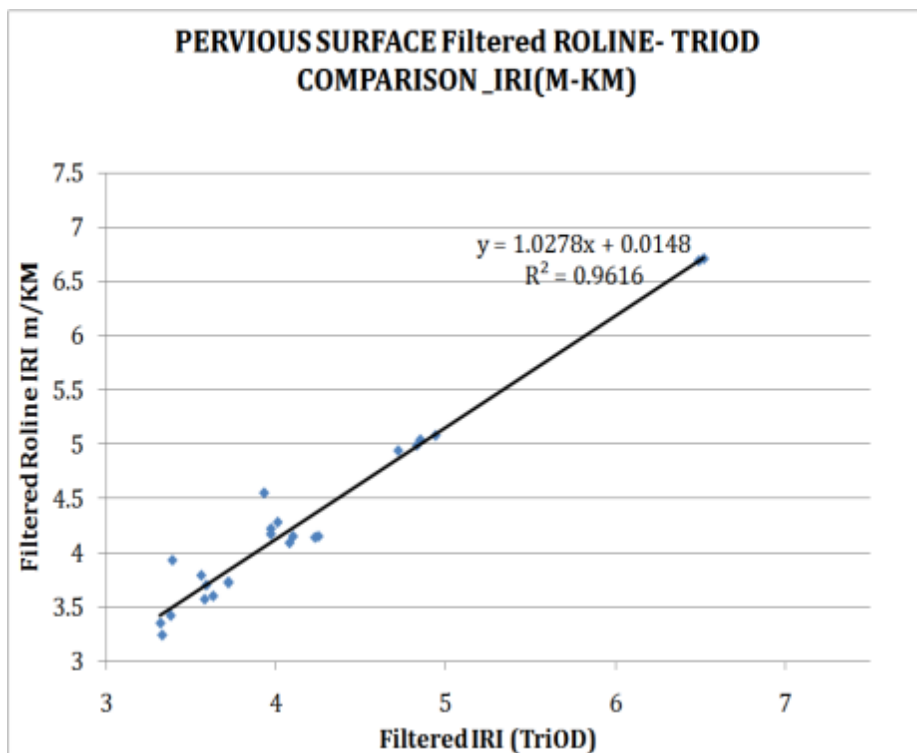
**Table 4.1: MPD IRI OBSI of Pervious Pavements Test Cells**

Cell	Tested	MTD	IRI (m/km)	OBSI
39I	April 2009	1.9	5.99	98.1
39I	Oct 2009	1.97	5.86	98.00
39O	April 2009	2.04	5.01	96.7
39O	Oct 2009	2.01	5.28	97.8
85I	April 2009	2.01	5.06	100
85I	Oct 2009	1.74	5.10	98.00
85O	April 2009	1.93	5.66	99.40
85O	Oct 2009	1.94	5.35	98.40
89I	April 2009	1.88	5.85	99.5
89I	Oct 2009	1.89	5.13	98.9
89O	April 2009	1.81	5.99	100.1
89O	Oct 2009	1.94	6.06	97.4



It was observed that the IRI obtained in the pervious concrete cells were much higher than those obtained in the normal pavements. To ascertain if this was due to the laser effect, two types of IRI measuring lasers were examined. Laser 1 consists of the Triple laser (TriOD) and laser 2 consists of a line laser approximately 6 inches wide. The TriOD laser consists of 3 laser points arranged 1.25 inches apart and the ROLINE consists of a line laser effectively 2.5 inches wide. The ROLINE mimics a tire footprint as it advances in the longitudinal direction. Based on results obtained for regular textures of solid pavements, the ROLINE IRI is always higher than the TriOD. The Pervious pavements exhibited quite the opposite phenomena with the ROLINE IRI being higher than the TriOD (Figures 6 b and c).

However, the difference between the two is not significant enough for the high IRI of pervious pavement cells to be ascribed to the surface texture although the higher ROLINE IRI is another interesting phenomenon.



**Figure 4.2: TriOD Versus ROLINE IRI of pervious surface filtered with 250-mm filter using FHWA ProVAL Software**

**Table 4.2: Summary Output SA-MPD Relationship**

Regression Statistics				
Multiple R	0.60	Adjusted R <sup>2</sup> Square	0.35	
R <sup>2</sup>	0.36	Standard Error	0.12	
		Observations	122	
ANOVA				
	Coefficients	Standard Error	t Stat	P-value
Intercept	1.34	0.26	5.24	0.0000
Density, pdf	-0.01	0.00	-5.70	0.0000
MPD	0.24	0.05	5.97	0.0000

Influence of MPD and Density on sound absorption of pervious pavements was also investigated. Results (Table 4.2) showed for 122 datasets that the two independent variables were very significant with P-values of  $10^{-6}$  for MPD and  $10^{-17}$  for density.

Pervious MPD influences SA but not OBSI. This analysis further accentuated the importance of porosity in sound absorption (or attenuation). It raises the question of the meaning of MPD in pervious pavement which suggests that MPD may be a measure of surface porosity of the pervious pavement. The extent to which it predicts envelopment and postulated by Hamet et al is not known. Unless the actual effective laser depth is known, the actual meaning of MPD in pervious pavements remains a matter of conjecture. It does not clearly show correlation to sound absorption coefficient. However when OBSI vs. IRI and CTM for pervious pavements were investigated, both dependent variables were insignificant. CTM MPD respectively exhibited p values of 0.33 and 0.72 respectively as shown in Table 4.8.

**Table 4.3: Regression results for Pervious Pavement OBSI vs. IRI & MPD**

Regression Statistics					
Multiple R	0.333		Adjusted R Square	-0.086	
R Square	0.113		Standard Error	1.105	
			Observations	12	
ANOVA					
	df	SS	MS	F	Significance F
Regression	2	1.374	0.687	0.562	0.588
Residual	9	11.007	1.223		
Total	11	12.382			
	Coefficients	Standard Error	t Stat	P-value	Lower 95%
Intercept	106.78	7.80	15.68	2.49E-07	89.13
MTD	-5.935	5.881	-1.013	0.337	-12.71
IRI (m/km)	-0.147	0.408	-0.360	0.726	-1.072

It must be noted that other parameters that were considered in pervious pavements are the same in all the non-pervious pavements. For instance the asperity interval is 12 mm in each case and the texture orientation is the same. It was therefore expedient to investigate the influence of IRI.

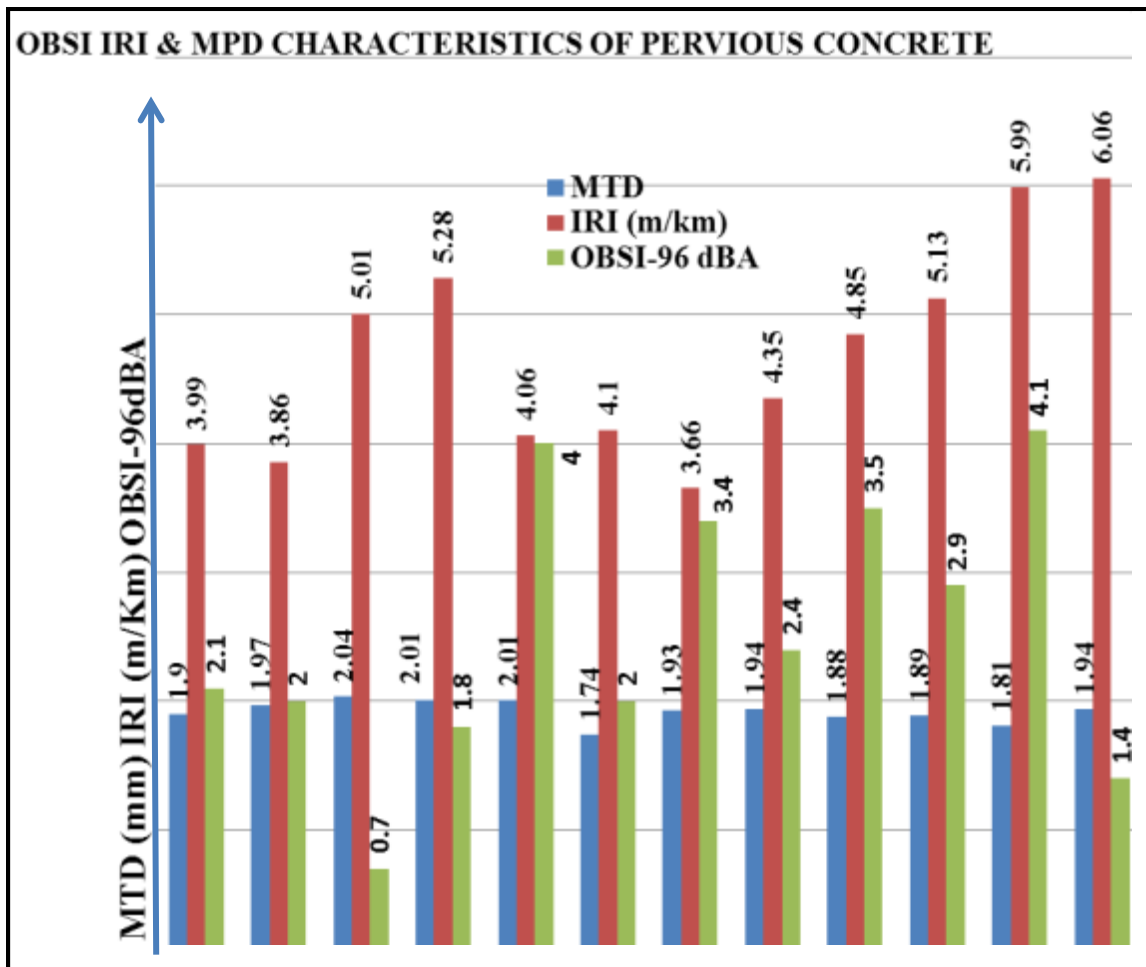


Figure 4.3: Distribution of OBSI, IRI and MPD of Pervious Cells

#### 4.1.2 OBSI-MPD for Non-Pervious Pavements

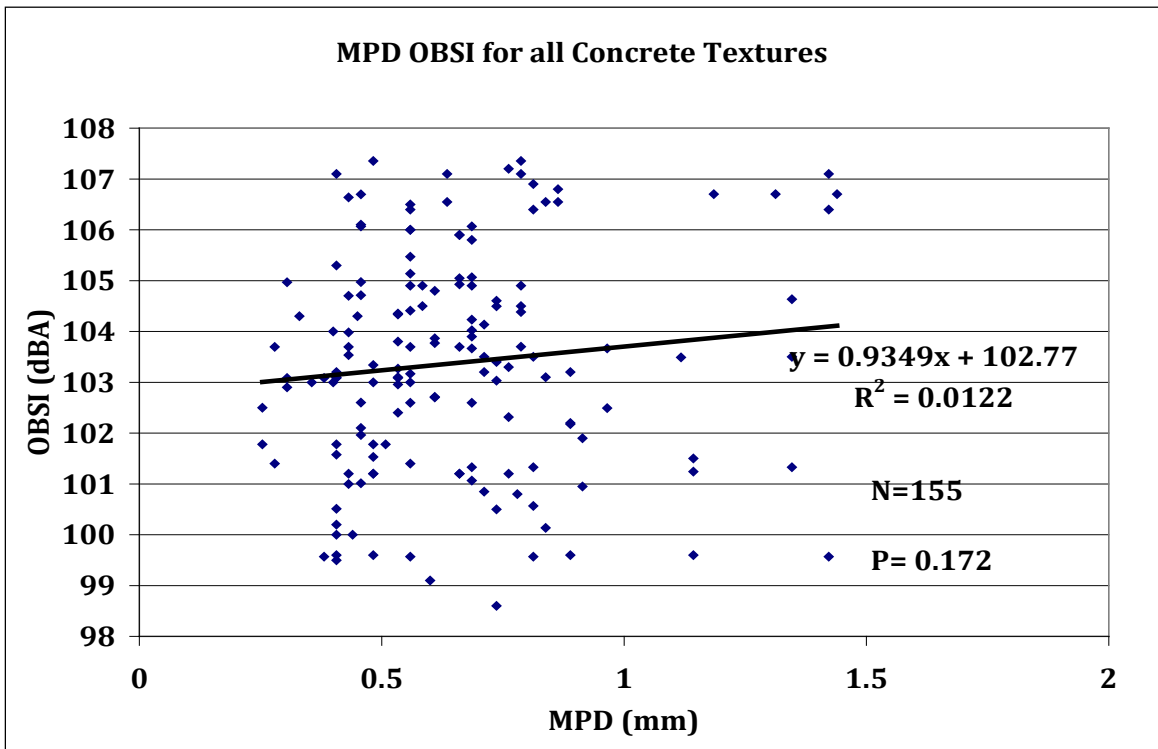
OBSI and corresponding MPD were simultaneously measured in all the MnROAD concrete test cells. Table 4.2 shows results of the MPD OBSI correlations. All non-pervious pavements together are poorly correlated to OBSI. A coefficient of determination of 0.006 and a P-value of 0.97 are clearly indicative of a low correlation. To ascertain if correlations may exist in texture types, separate correlations of MPD and OBSI were investigated in transverse and in longitudinal textures. In each case a coefficient of determination of 0.1 and 0.026 respectively was obtained.

MPD does not show any correlation to OBSI in the cells tested. The same observation was made by Bendstein (2005) who based on the findings of Fujikawa et al, introduced a correlation that was based some texture configuration parameters already described in chapter one. Figures 4. 4 and 4.5 show the application of Bendstein’s equation to the textures tested. Bendstein’s model resulted in a coefficient of determination of 0.24 which. This is an improvement over the direct OBSI MPD correlations obtained. Bendsten- Fujikawa approach and the data results obtained in

this experiment suggest that a consideration of texture configuration instead of MPD values may improve the OBSI prediction model.

**Table 4.4: Summary OBSI CTM MPD Relationship for all Concrete Cells**

SUMMARY OUTPUT				
Multiple R	0.110	Adjusted R Square	0.006	
R Square	0.012	Standard Error	2.161	
		N	155	
ANOVA				
	Coefficients	Standard Error	t Stat	P-value
Intercept	102.768	0.476	215.993	0.000
MPD	0.935	0.681	1.374	0.172



**Figure 4.4: OBSI versus MPD for All Non-Pervious Textures**

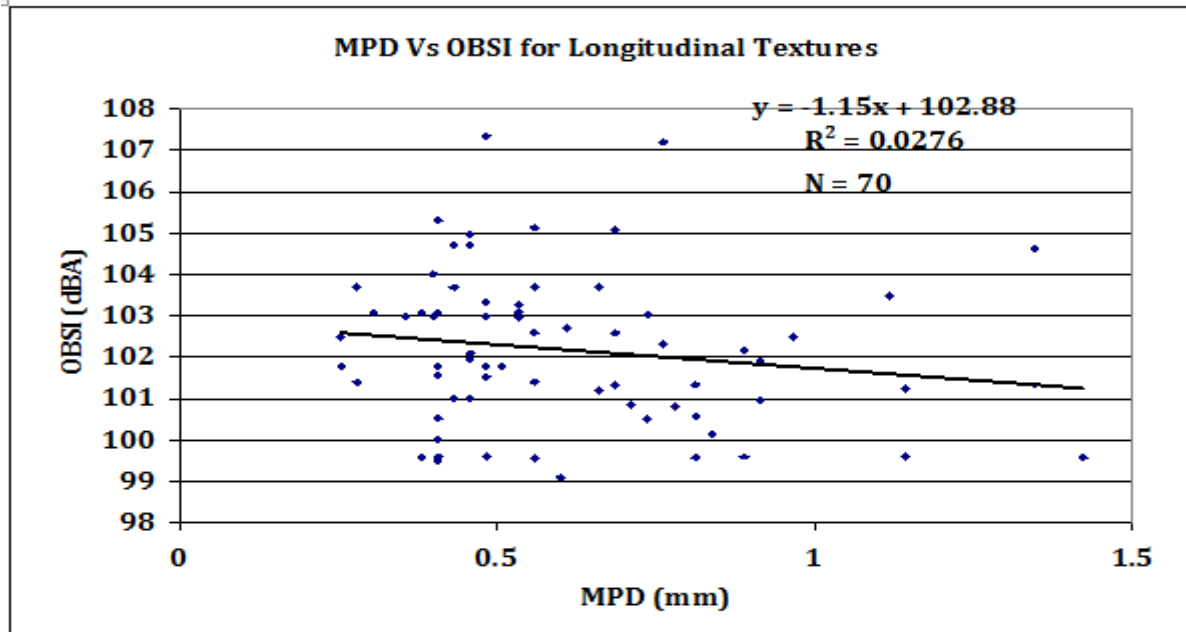


Figure 4.5: OBSI versus MPD for All Non-Pervious Longitudinal Textures

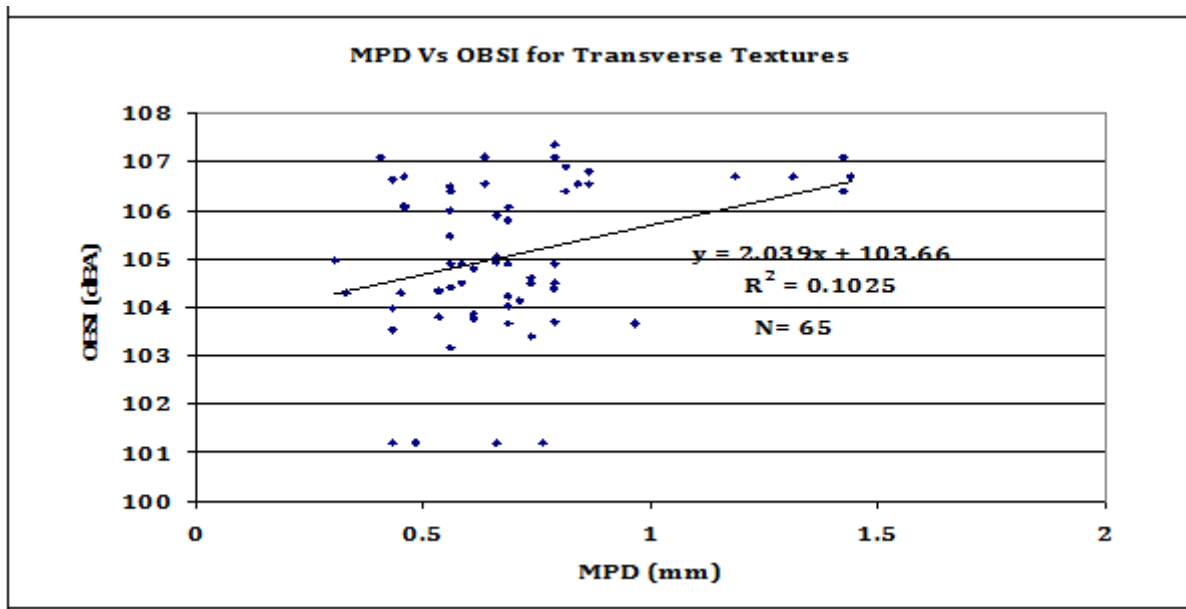


Figure 4.6: OBSI versus MPD for All Non-Pervious Longitudinal Textures

Separating OBSI into transverse and longitudinal textures seems to make a difference. Increased MPD in transverse textures resulted in increased OBSI while increased MPD in the longitudinal direction resulted in decreased OBSI. This indicated that texture direction has to be a significant variable.

Since MPD did not appear to be correlated to OBSI some existing models that considered MPD as a dependent variable were examined with the data obtained from measurements in the first and second year. Two models of prediction of tire pavement noise (CPX) from some surface variables are examined. These are the Hansen model and the Bendstein model [1.27], [1.40].

Since these models predicted CPX noise, it was logical to consider a tenable correlation between OBSI and CPX that was obtained from previous studies. That correlation facilitated a transcription of their models to predict OBSI.

#### 4.1.3 Examination of the Hansen Model

Hansen had a prediction model that was based on MPD alone. According to the model,  $L = 95 + 13$  (Texture Depth)

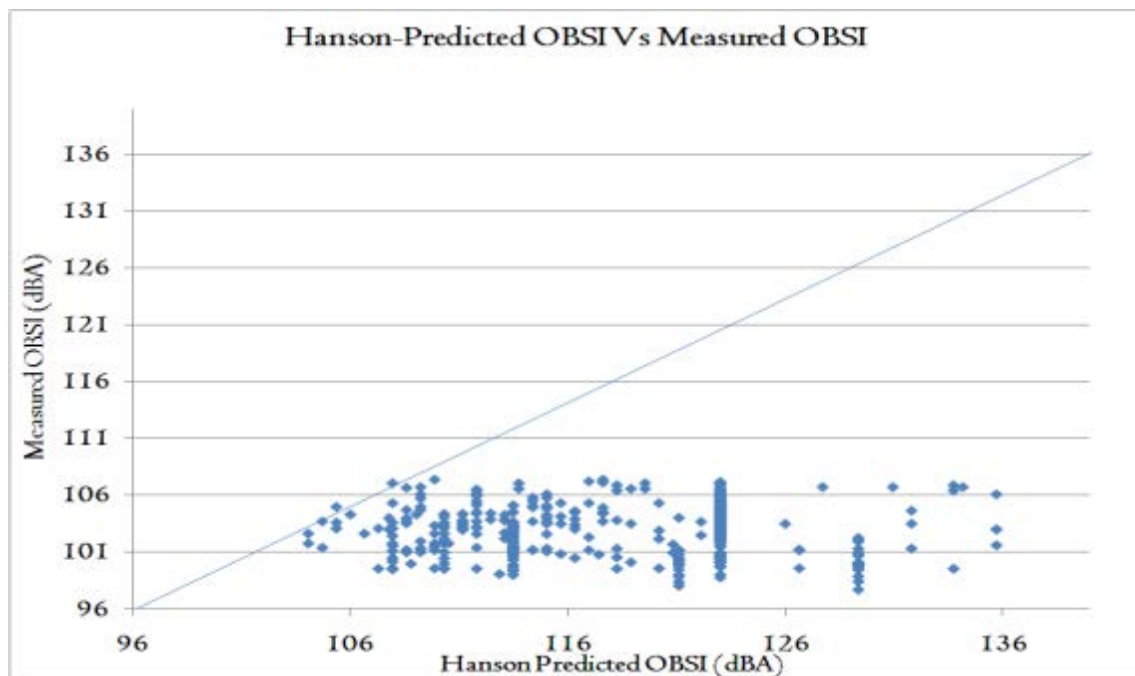
$$\text{CPX Noise level (dBA) } L = g + h * (\text{texture depth (mm)}) \quad (\text{Equation 4.11})$$

Where CPX noise level L is the close proximity noise level but Donovan and Lodico [4.1] established a correlation between OBSI and CPX, whence the model:

$$\text{OBSI} = (\text{CPX (L)} + 6.52) / 1.06 \quad (\text{Equation 4.12})$$

Therefore

$$\text{OBSI} = \{(g + h (\text{texture depth (mm)})) + 6.52\} / 1.06 \quad (\text{Equation 4.13})$$



**Figure 4.7: Hansen et al Models Fitted with 433 Data Set**

The predictions of OBSI from these models EQUATION 4.4 is shown in Figure 4.17. It is evident that there are missing components in the previous models that account insufficient prediction of OBSI. Those include temperature, IRI texture direction and texture spikiness as indicated in the product of this research. As a logical step, the dimensionless forms of the models are obtained by normalizing the variables. The form is fitted for an OBSI predictor as

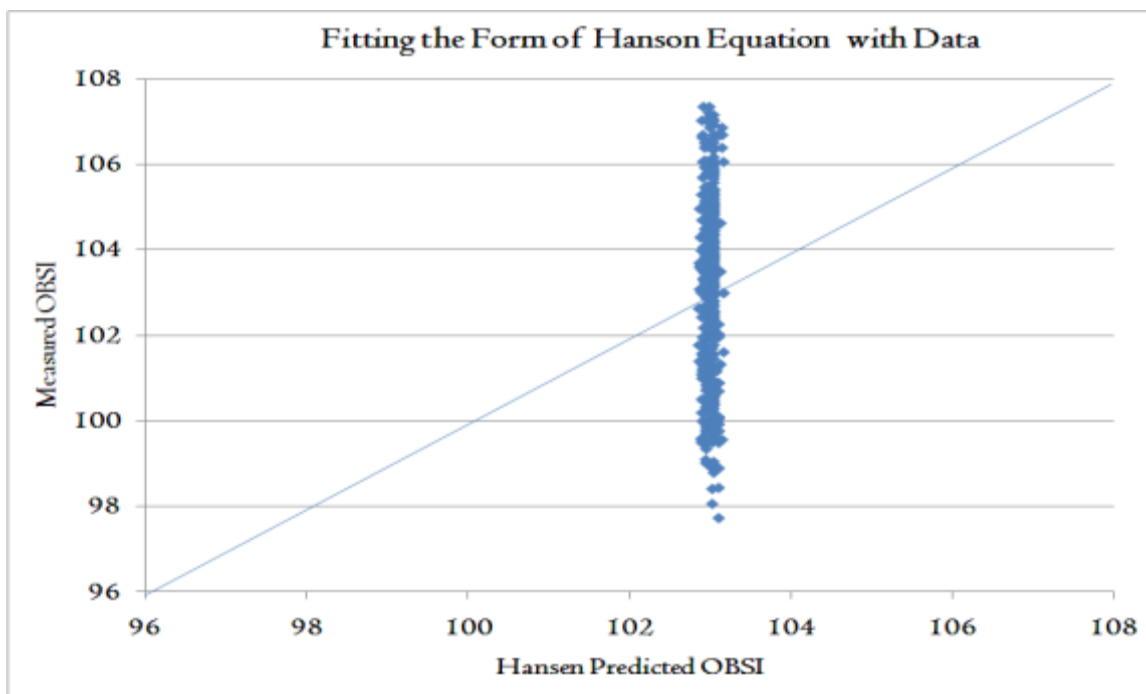
$$\text{OBSI (Hanson)} = G + H * (\text{TD/RD}) \quad (\text{Equation 4.14})$$

Where G and H are model constants and TD is texture depth and RD is Tire groove depth (9 mm)

Fitting the model with 501 data points resulted in

$$\text{OBSI (Hansen)} = 102.81 + 0.97 \text{ M/RD}. \quad (\text{Equation 4.15})$$

Where L is the CPX noise level equations above are combined to examine the 2 years of data set to ascertain the validity of this model. The result is shown in figure 4.8 where there is a skew in the data. This may imply that the model variables need improvement or that the model needs more variables. To improve this, the form of the model was adjusted by making the variables dimensionless using variables from the tire as denominator. Plotting the above resulted in Figure 4.18.



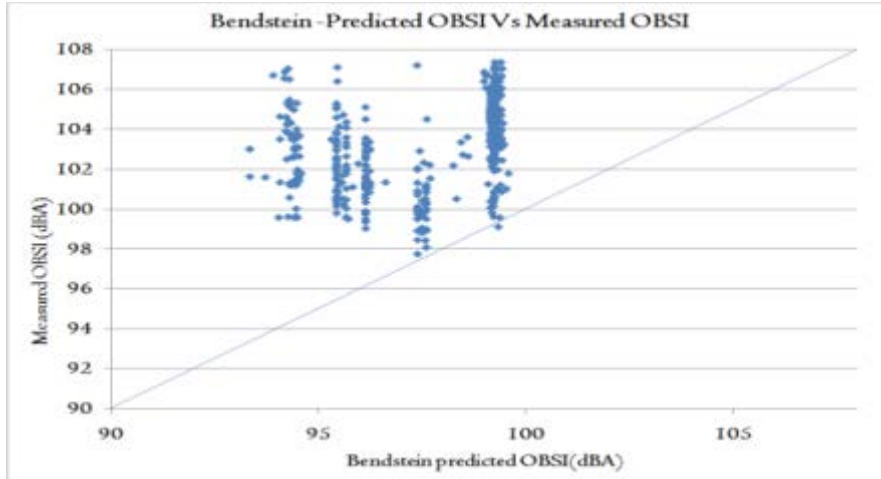
**Figure 4.8: Hanson Model Examined with Data**

Figure 4.8 shows that the Hansen predicted a single value of OBSI. This implies that MPD may be a weak predictor and surely that more variables are needed. The next logical step is to introduce a model that has more variables

#### **4.1.4 Examination of the Bendstein et al Model**

From Chapter 1, The Bendstein-Fujikawa et al model is

$$L = 1.07 * Y + 0.33 * X - 0.22 * \text{MPD} + 91.1 \quad (\text{Equation 4.16})$$



**Figure 4.9: Testing of Bendstein (Fujikawa) Model Validation**

where Y is the variation (Standard deviation) in texture depth and X (texture wavelength is similar to wavelength or asperity interval introduced in CHAPTER 3 and MPD is mean profile depth mentioned in CHAPTER 3. ASP is the asperity interval or texture wavelength, SD is standard deviation of texture depth and MPD is the mean profile depth. Fitting this model with 500 data set in this research resulted in Figure 4.9. Figure 4.9 shows the data to be skewed and with all predicted OBSI to be less than the measured OBSI. Once again this suggests the need for more data and possibly a modification of the model coefficients. To address this, a model form is considered.

Form of Bendstein Model is

$$\text{OBSI} = j + k (\text{SD}) + m (\text{ASP}) + n (\text{MPD}) \quad (\text{Equation 4.17})$$

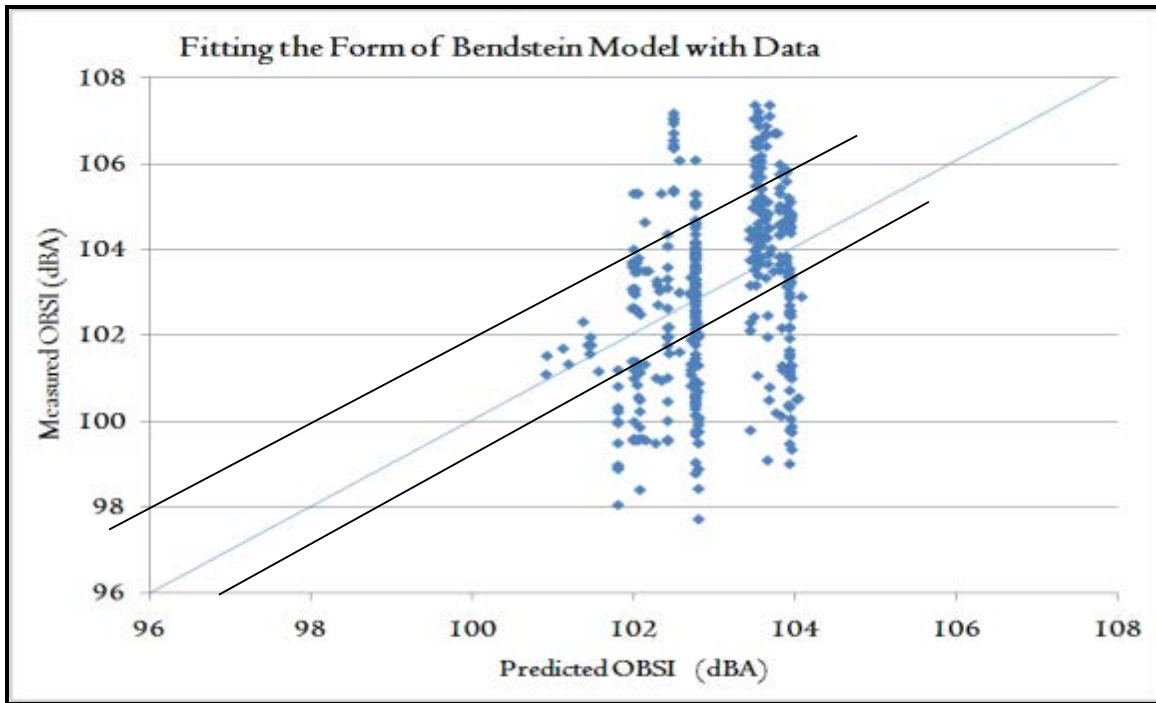
$$\text{OBSI (Bendstein)} = J + K * (\text{SD}) / \text{RD} + M * (\text{ASP} / \text{ASPT}) + N * (\text{MPD} / \text{RD}) \quad (\text{Equation 4.18})$$

where J, K, L, M & N are model constants. Fitting the model with 433 data points resulted in the equation 4.19 where RD is tire groove depth, ASPT is the tire tread block interval.

$$\text{OBSI (Bendstein)} = 102.33 - 36.14(\text{SD}) / \text{RD} + 4.11(\text{ASP} / \text{ASPT}) - 3.89(\text{MPD} / \text{RD}) \quad (\text{Equation 4.19})$$

The result of fitting this model form is shown in Figure 4.10





**Figure 4.10: Bendstein Model Improved by Normalizing the Deriving Model Constants**

The Bendstein et al model appears to be robust with the exception that extreme OBSI values ( $< 100$  dBA and  $> 104.5$  dBA) are not predicted. Though this was an improvement over the Hansen Model, more variables are needed. It is important for all the variables in a model to be significant. In fitting the Bendstein model, texture depth and texture variability are not significant based on an  $\alpha$  value of 0.05. The texture wavelength was significant. It is apparent from the Bendstein and Hansen models that more variables than those listed by Bendstein-Fujikawa and Hanson may be needed for a more realistic OBSI prediction. It is suspected at this stage that there may be environmental factors and texture variables extraneous to the Fujikawa model. These may include, temperature, texture wavelengths and texture kurtosis or skewness.

#### **4.1.5 Texture Performance**

This section shows the texture performance in each of the non-rehabilitated surfaces. Texture is measured with the Circular Track meter producing the mean Profile Depth in each case. The pervious pavements as well as the innovative grind exhibited higher MPD. Within 2 years there is interplay of paste erosion and actual texture degradation. Consequently the first 2 years of performance is occasionally fraught with anomalies that were explained in Chapter 2.

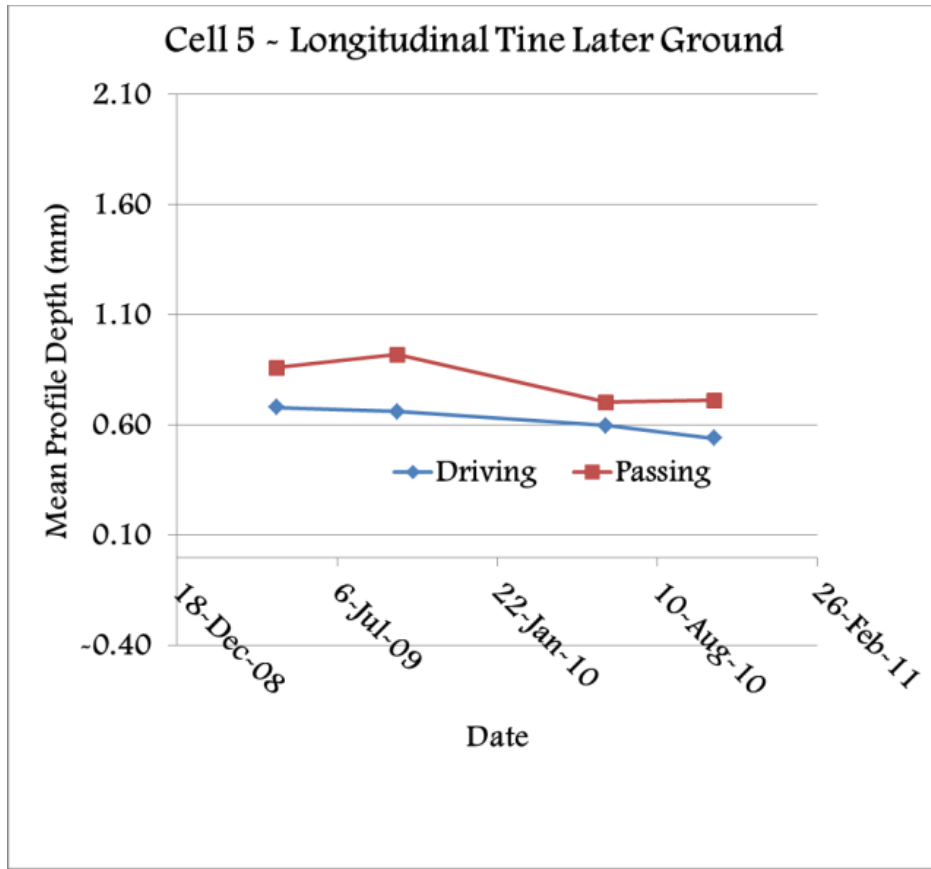


Figure 4.11: Texture Performance of Longitudinal Tine Later Ground

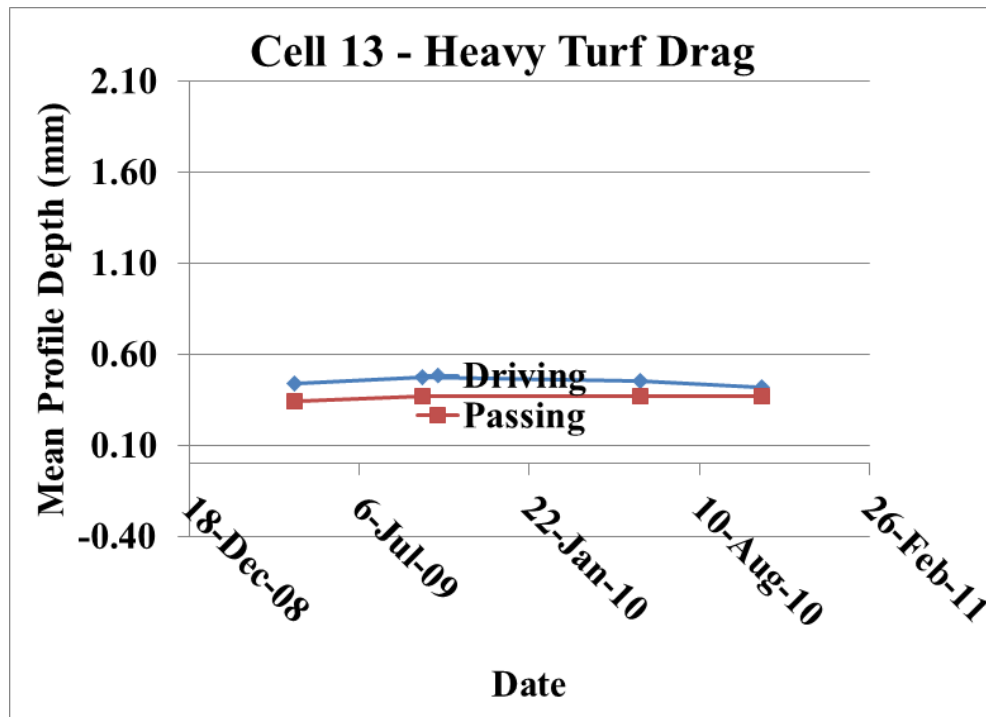


Figure 4.12: Texture Performance of a Heavy Turf Drag Cell

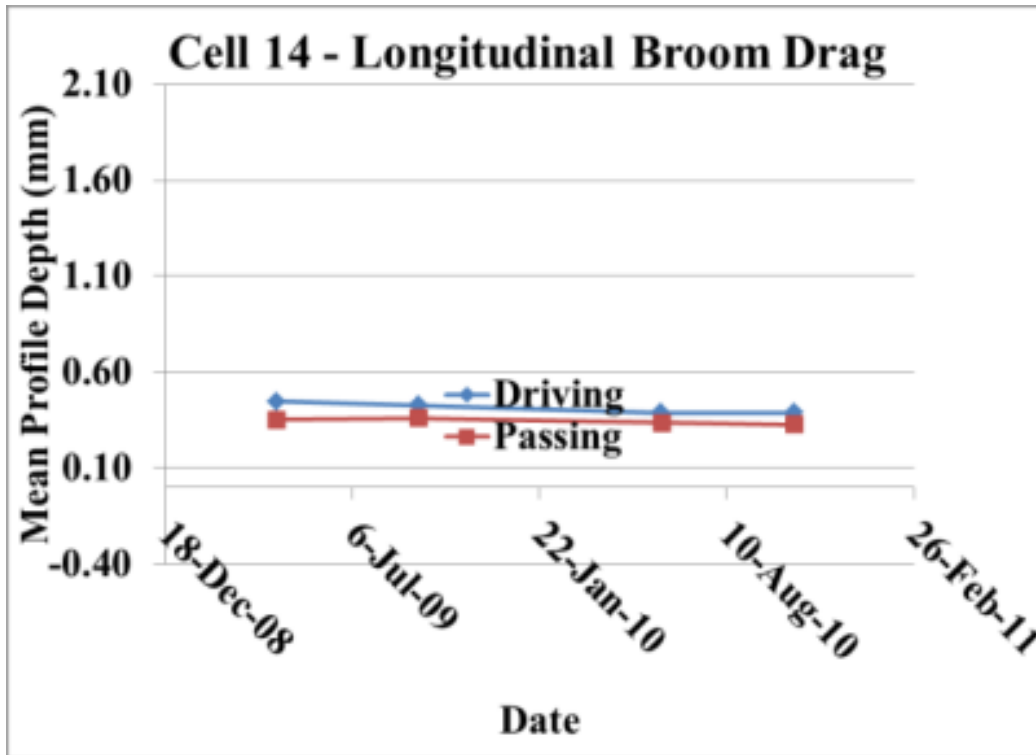


Figure 4.13: Texture Performance of a 2008 Longitudinal Broom Drag

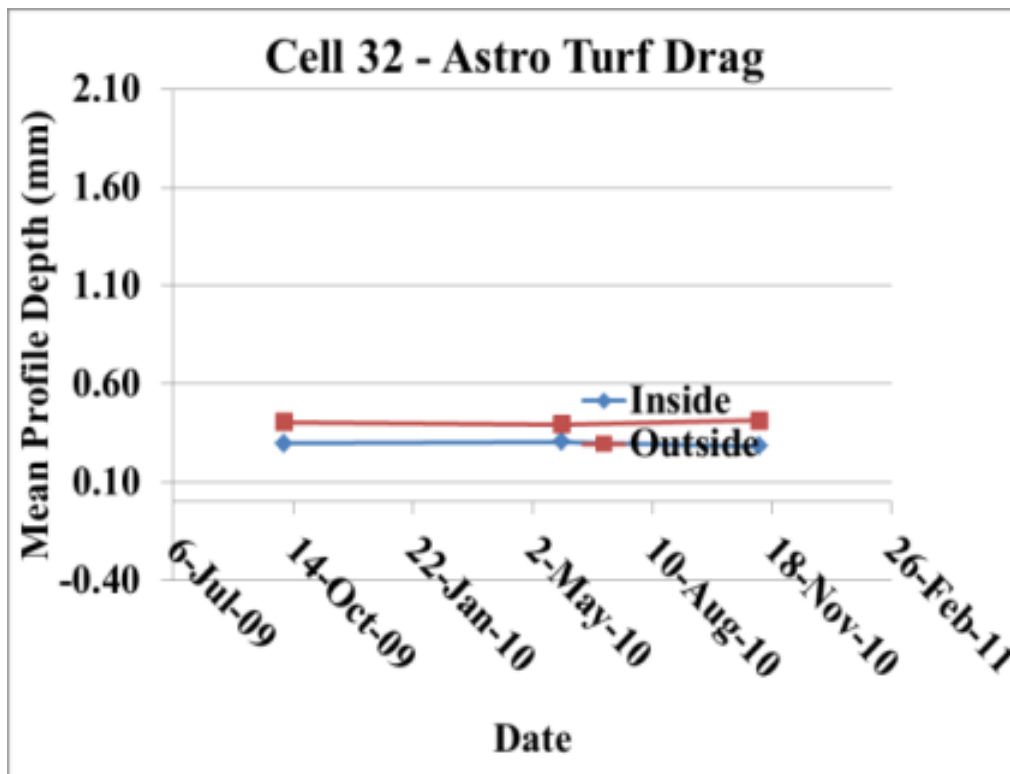


Figure 4.14: Performance of a Year 2000 Turf Dragged Surface

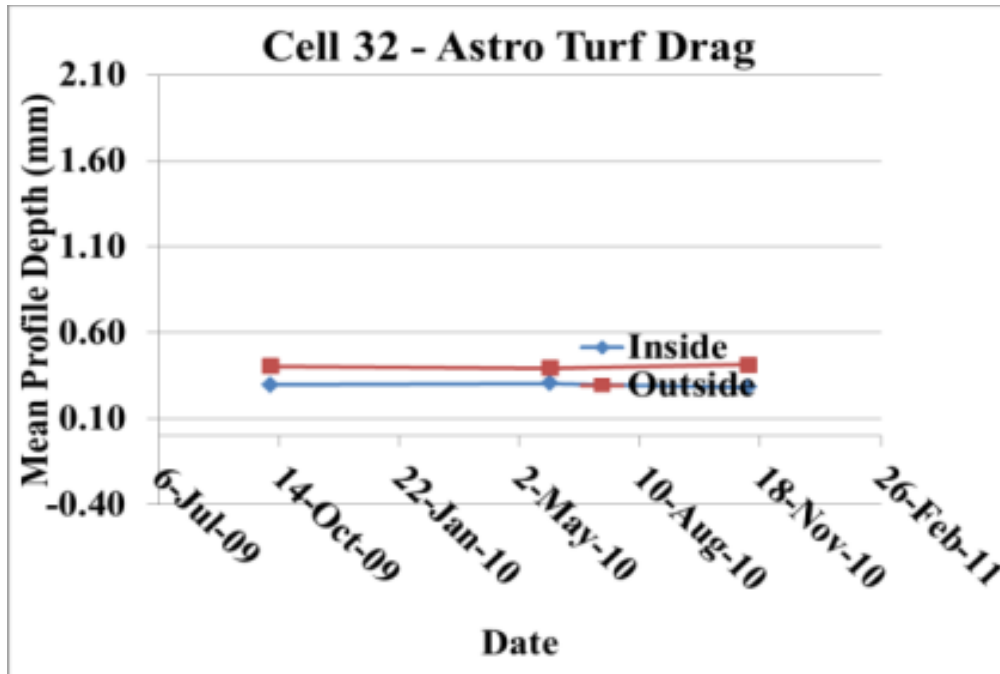


Figure 4.15: Performance of a Year 2000 Turf Dragged Surface

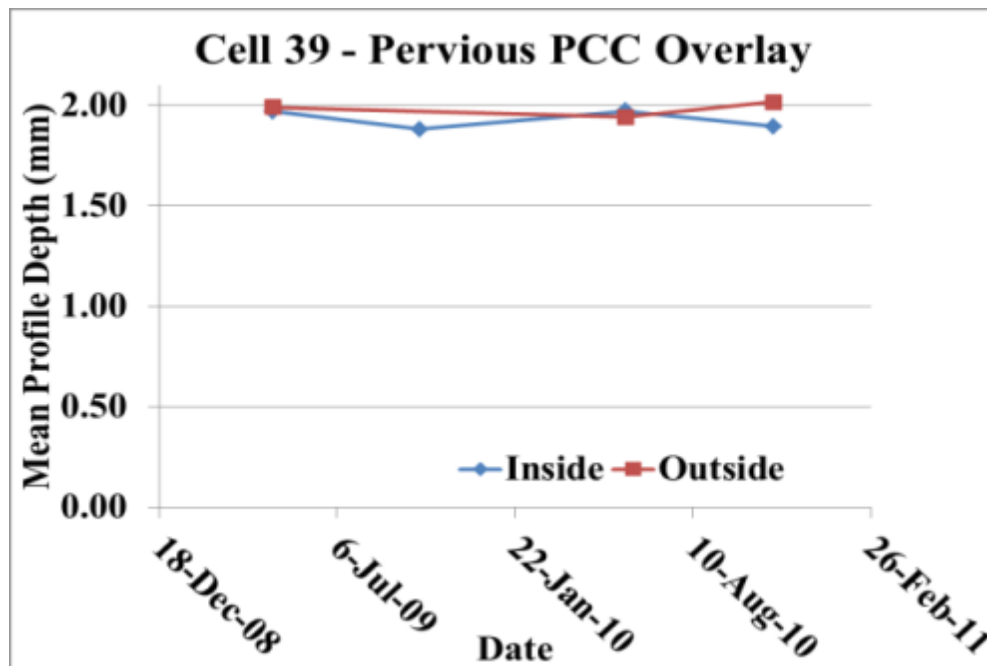


Figure 4.16: Performance of a Year 2008 Pervious Concrete Overlay

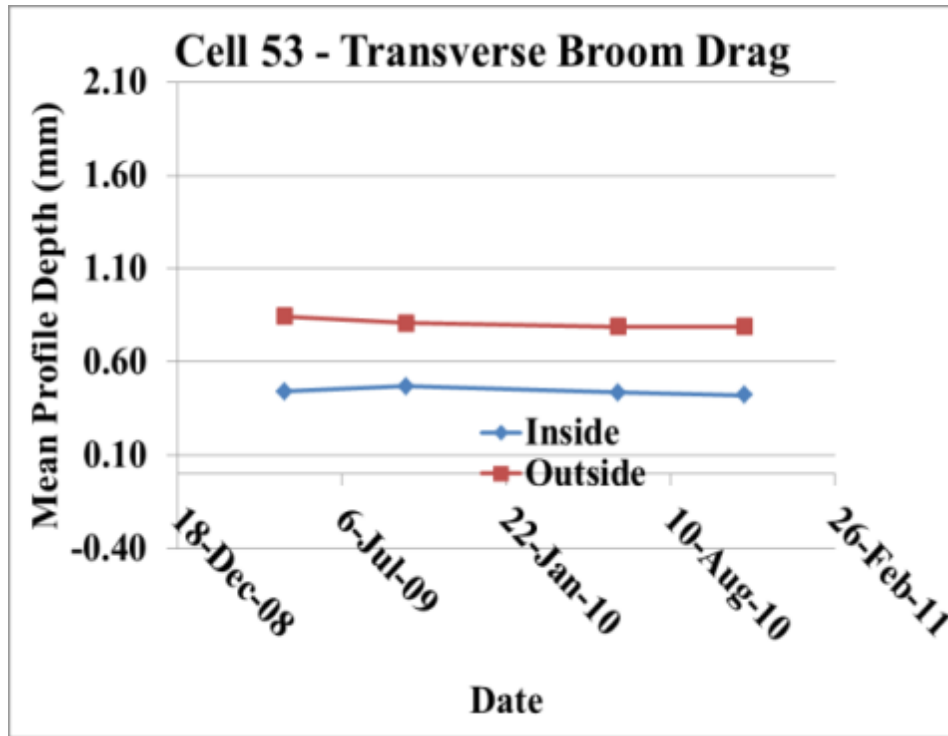


Figure 4.17: Performance of a Year 2008 Transverse Turf Dragged Surface (Aggressively dragged on the Outside and moderately dragged in the Inside Lane). Traffic impact appears inconsequential.

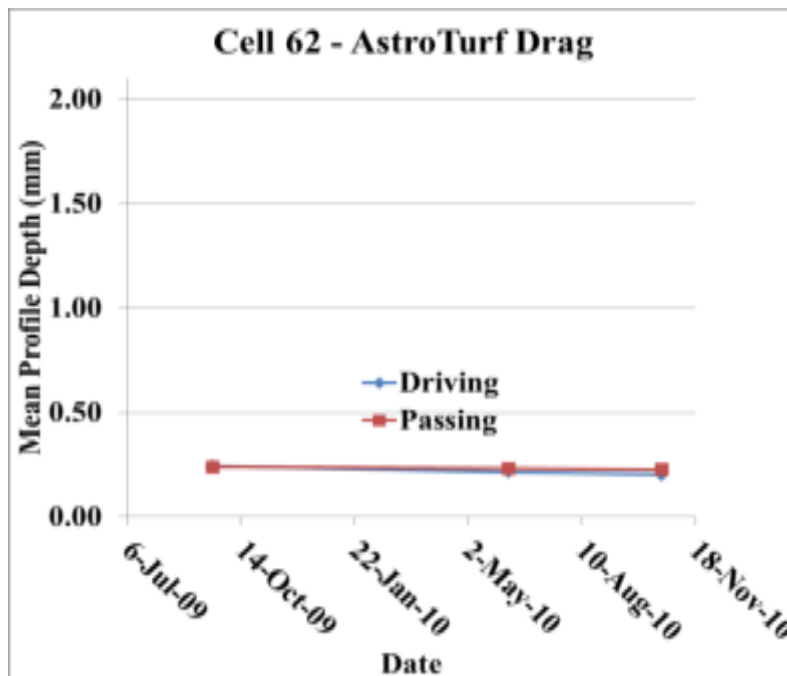
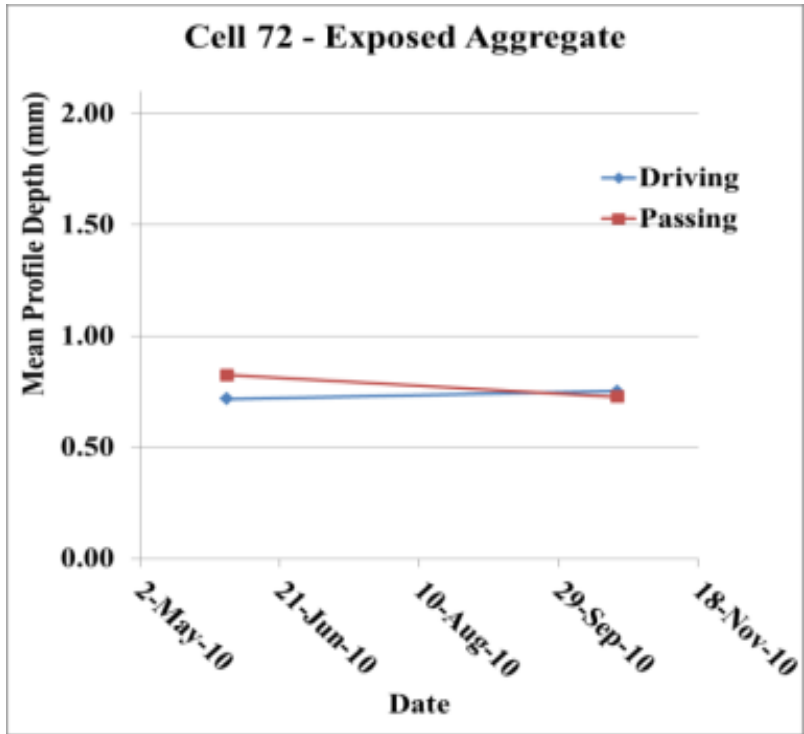
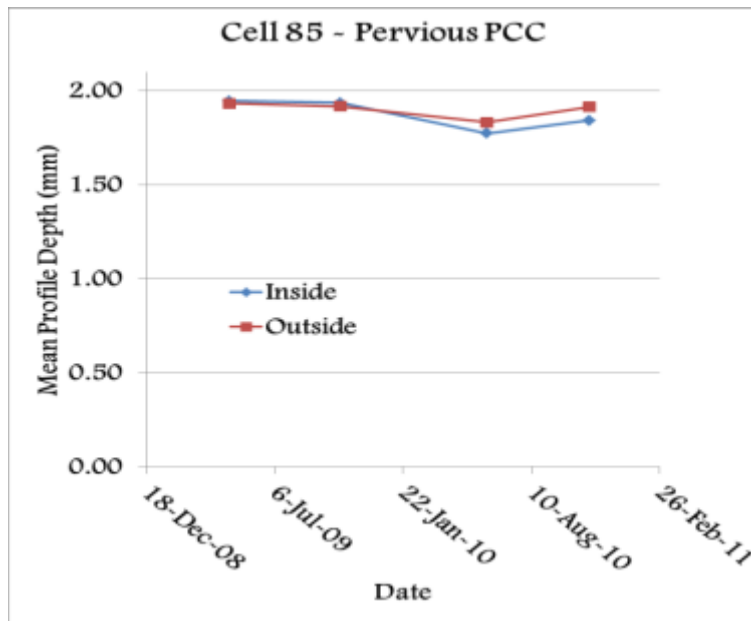


Figure 4.18: Performance of a Year 2004 Turf Dragged Surface. There is Evidence of Texture Degradation



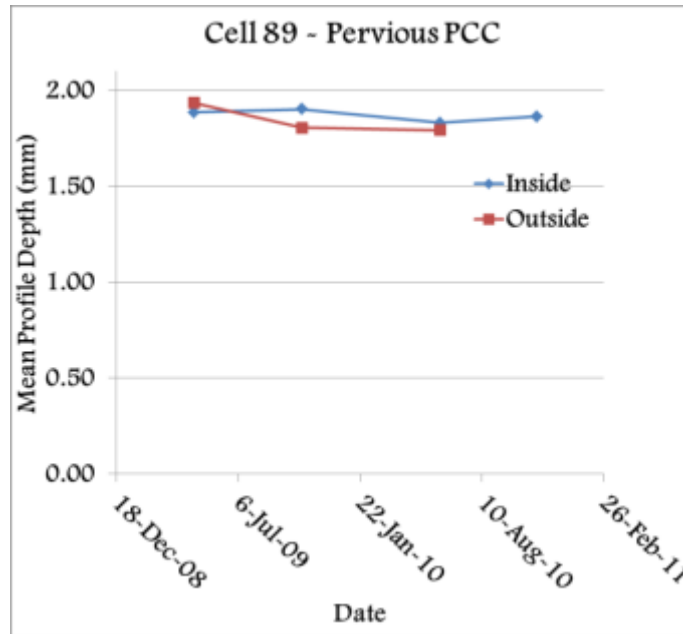
**Figure 4.19: Performance of a Year 2010 Exposed Aggregate**

In figure 4.19 surface, MPD appears to be relatively stable but with signs of increase in the Driving Lane. This is likely due to further removal of paste by Traffic.



**Figure 4.20: Performance of a Year 2008 Full Depth Pervious Concrete Surface.**

There is evidence of increasing MPD due to traffic in the inside lane



**Figure 4.21: Performance of a Year 2008 Pervious Concrete on Clay Subgrade Turf Dragged Surface**

MPD of inside and Outside lane are similar but there is no logical explanation as to how the inside lane would have higher MPD. Data is probably too early to reveal significant performance trend.

#### **4.1.6 IRI trends in New Textures**

Figure 4.122 to 4.138 show the IRI trends in each of the new concrete textures. It is noteworthy that the concept of IRI in new textures is not associated with the texture type but with the pavement design and construction. Other factors extraneous to the surface texture include climatic factors, base and subgrade type, degree of pavement degradation, pavement faulting, warp and curl. In recording the IRI performance, cognizance is taken of the possible associated factors though the plots are identified according to the texturing in each cell.

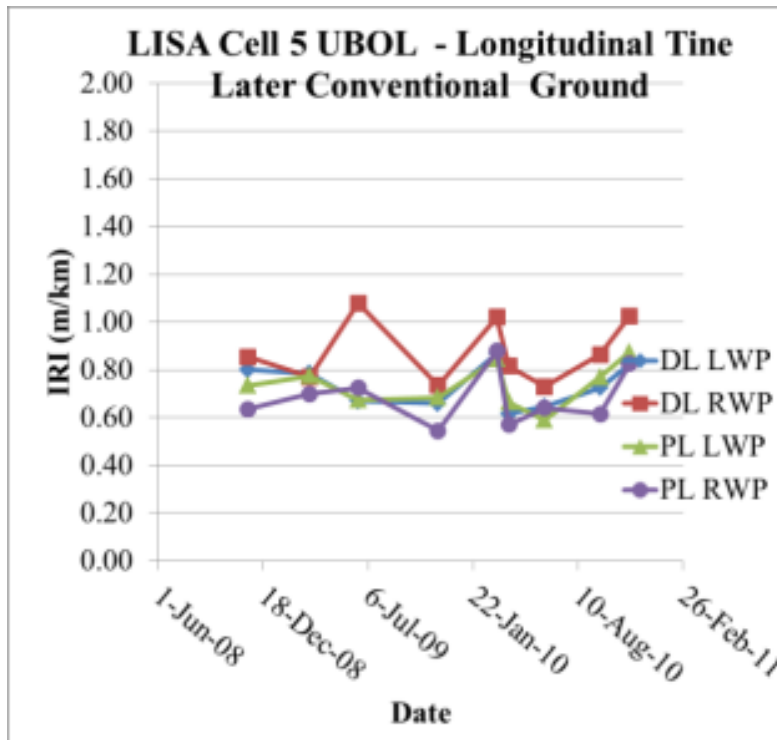


Figure 4.22: IRI of a PASSRC Unbonded Overlay textured with Longitudinal Tine and corrected with Traditional Grinding

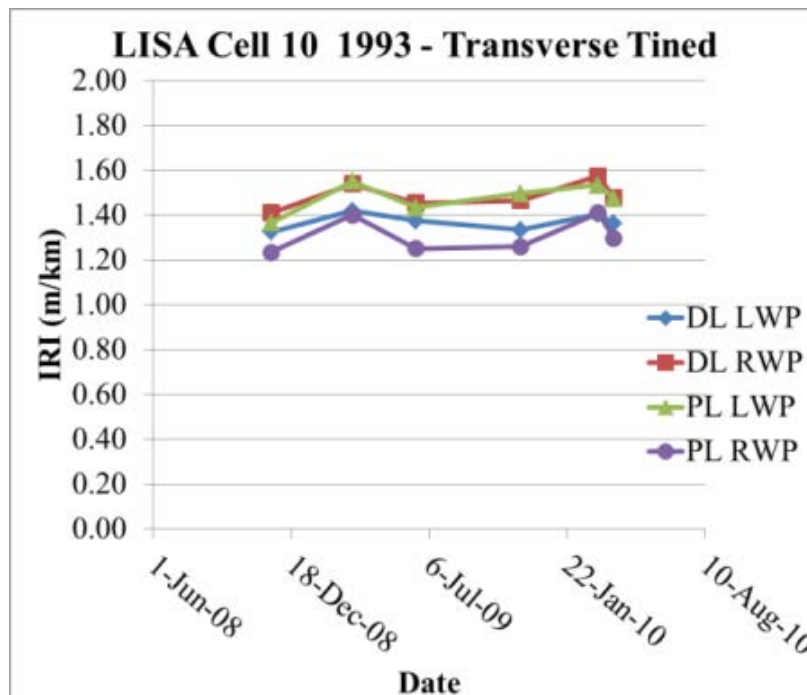


Figure 4.23: IRI of a 1993 Transverse Tined Pavement Built on PASB



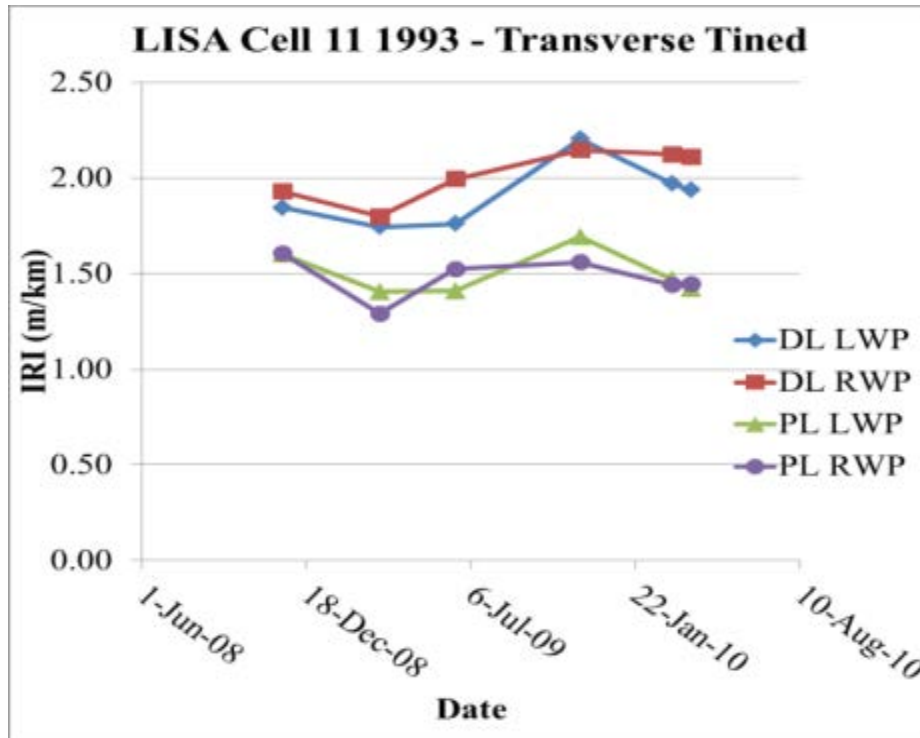


Figure 4.24: IRI of a 1993 Transverse Tined Pavement Built on PASB

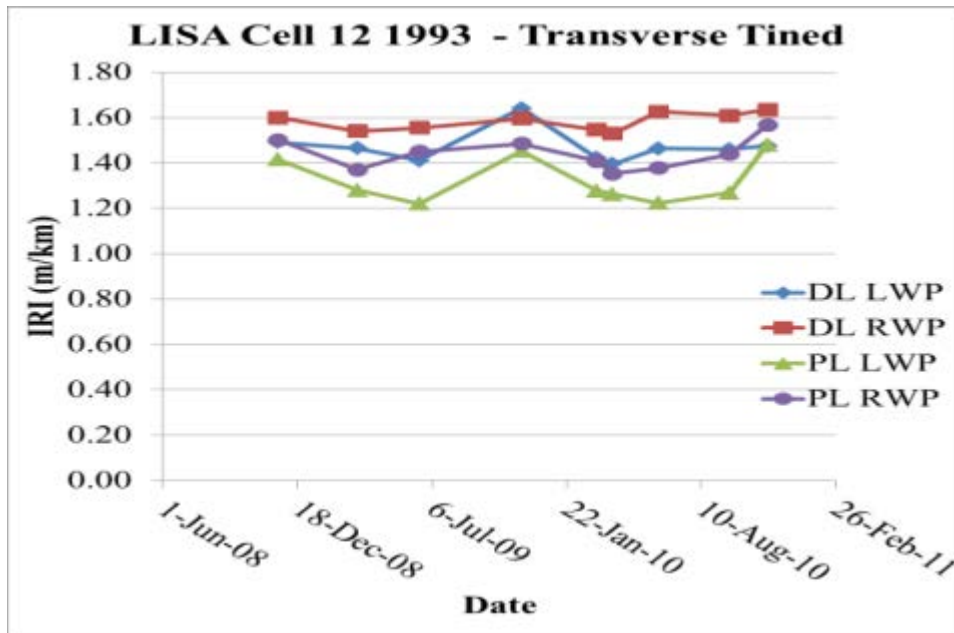


Figure 4.25: IRI of a 1993 Transverse Tined Pavement

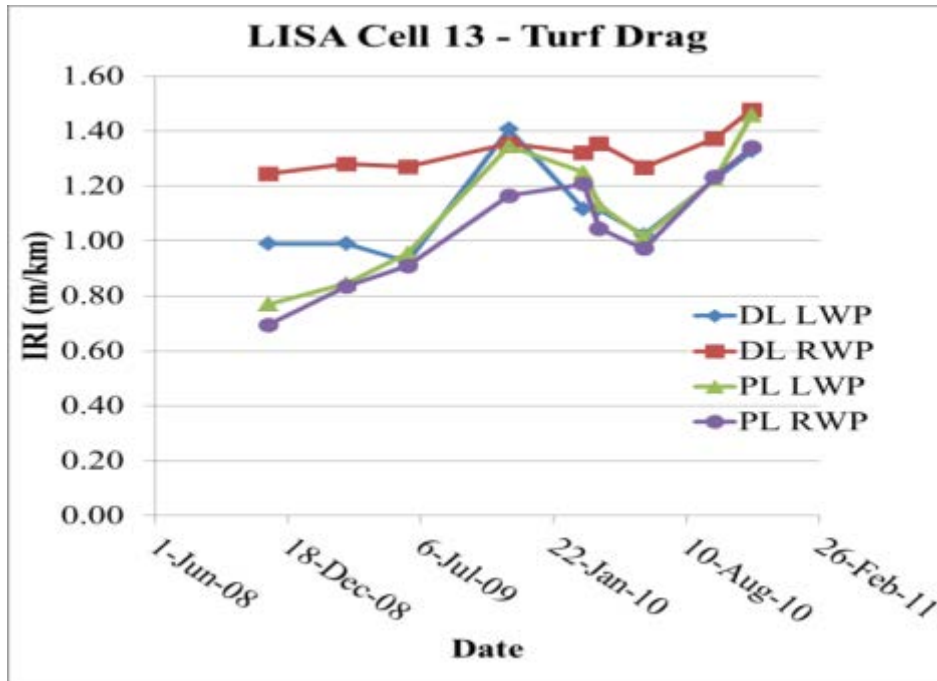


Figure 4.26: IRI of a 2008 Drag Pavement

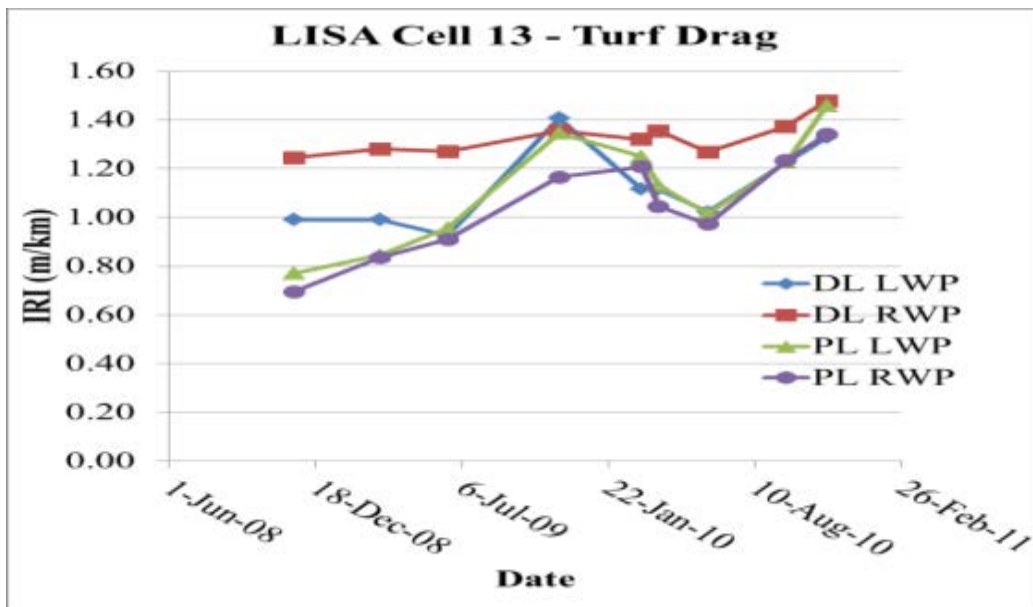


Figure 4.27: IRI of a 2008 Turf Dragged Thin Concrete Cell

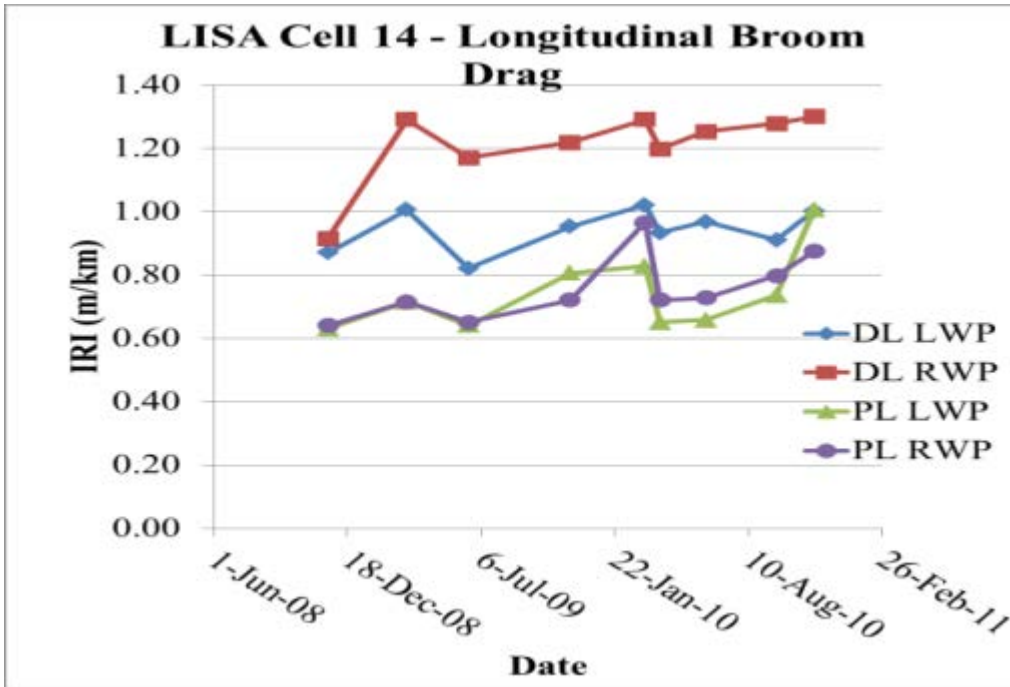


Figure 4.28: IRI of a 2006 Broom Dragged Whitetopping Cell

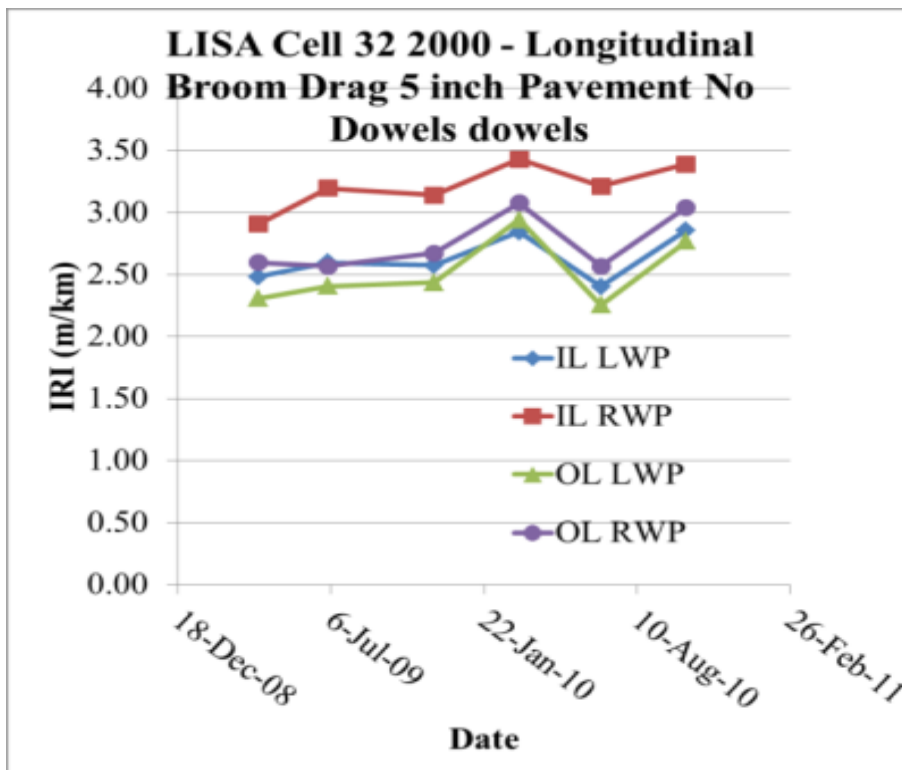


Figure 4.29: IRI of a 2008 Turf Dragged Thin Concrete Cell

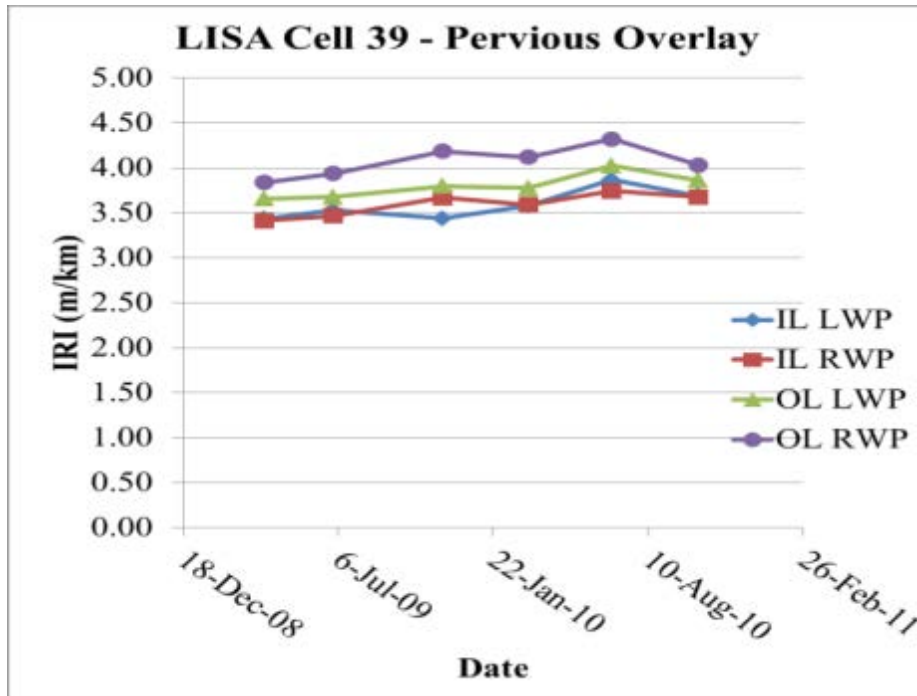


Figure 4.30: IRI of a 2008 Pervious Overlay Cell

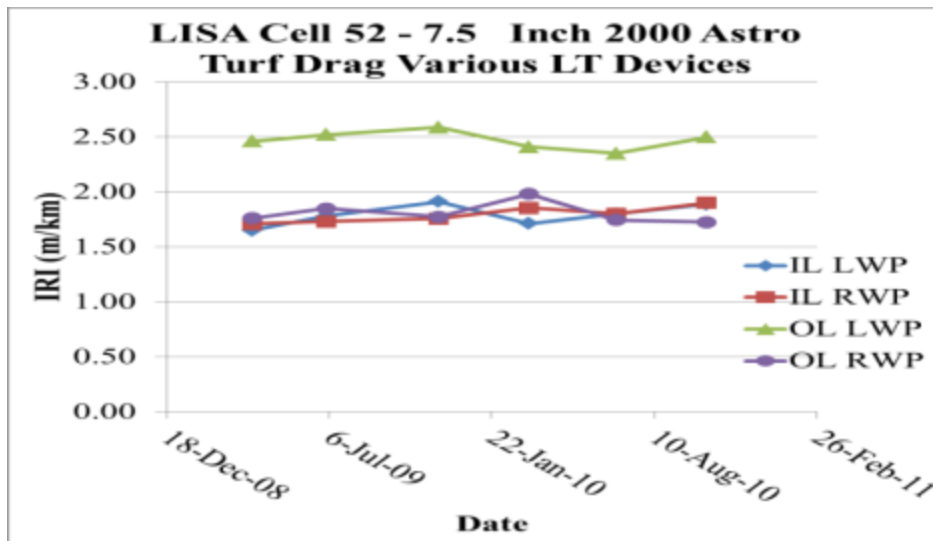


Figure 4.31: IRI of a 2000 Turf Dragged 7.5 inch Concrete Cell with Various Dowels

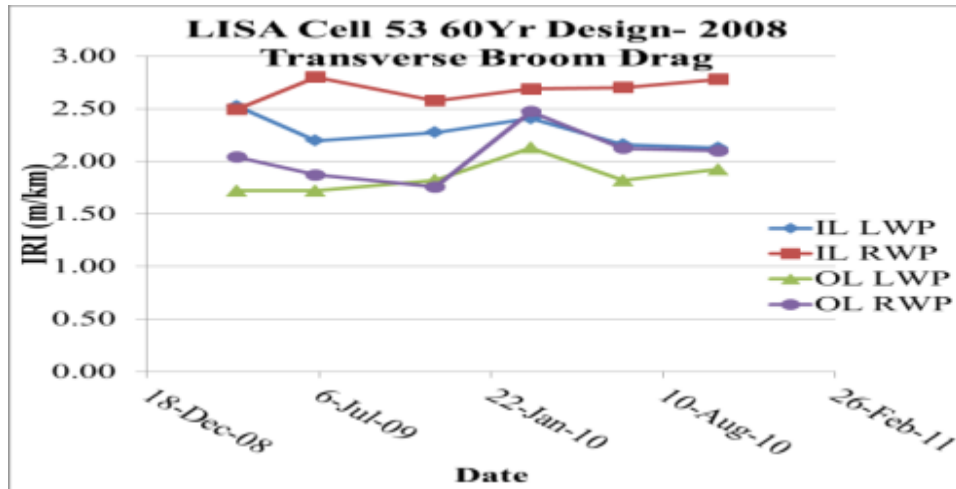


Figure 4.32: IRI of a 2006 60 Year Design 10 Sensor Installation Textured Transversely with Broom.

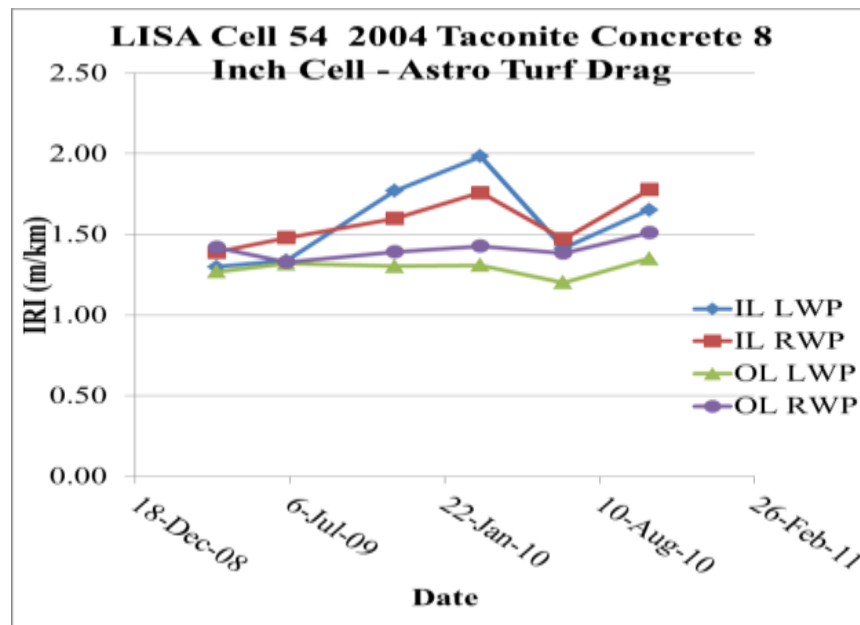


Figure 4.33: IRI of a 2004 Turf Dragged Taconite aggregate Concrete Cell 8 inches thick. Base Varying from 6 inches to 4 ft.

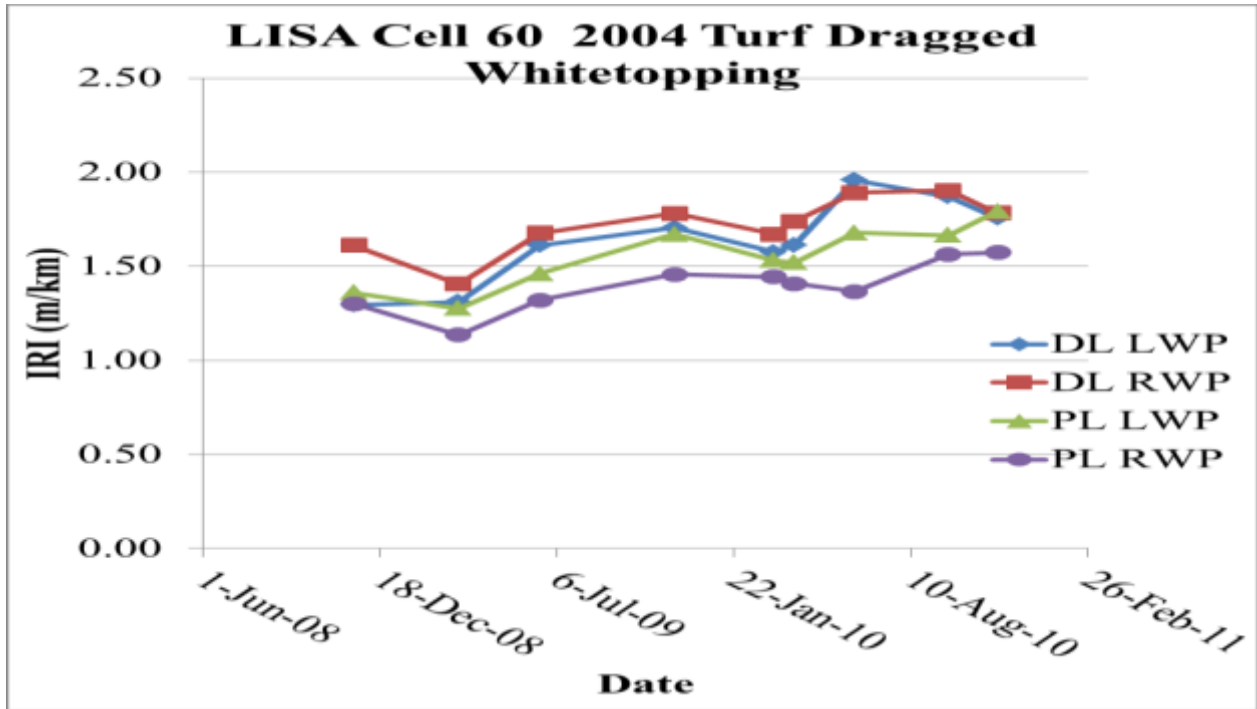


Figure 4.34: IRI of a 2004 Turf Dragged Whitetopping Cell

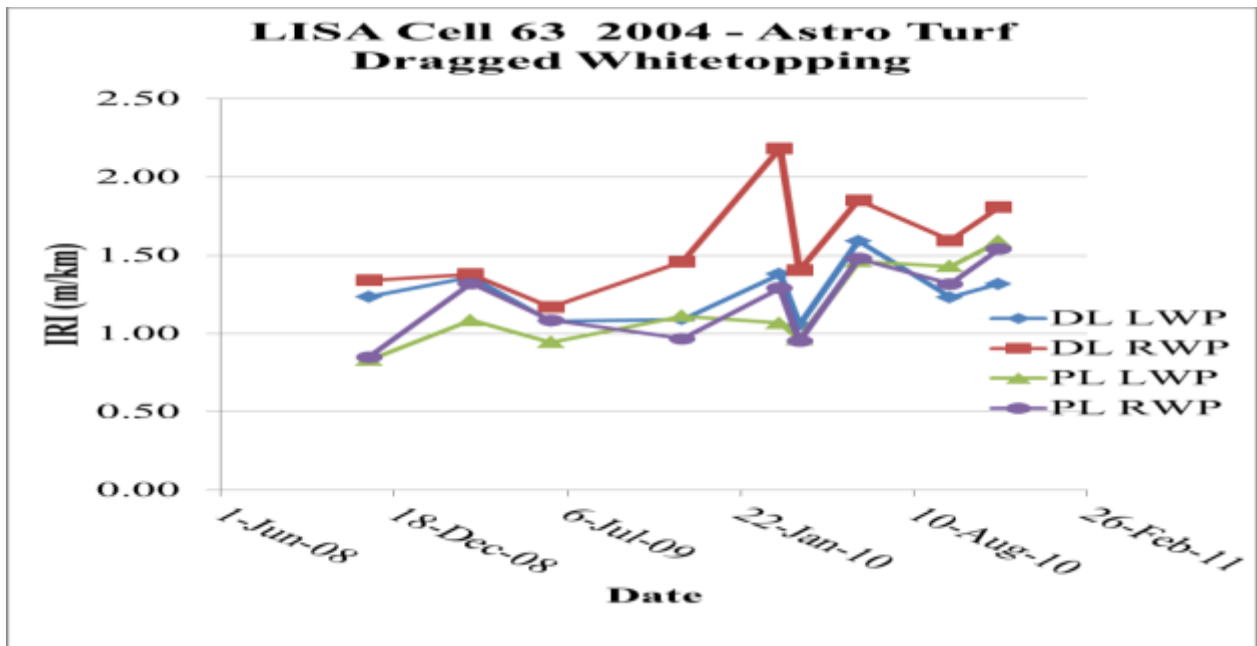


Figure 4.35: IRI of a 2004 Turf Dragged Thin Concrete Cell with Rocking Panels.

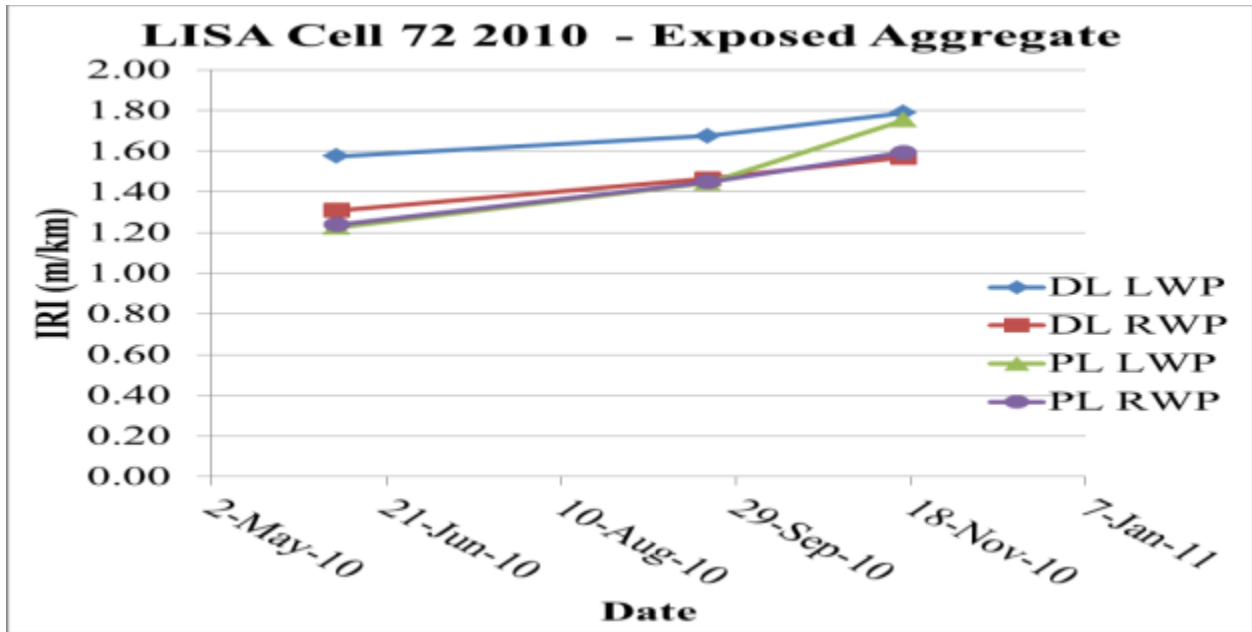


Figure 4.36: IRI of a 2010 Composite Concrete Cell Textured with Exposed Aggregates

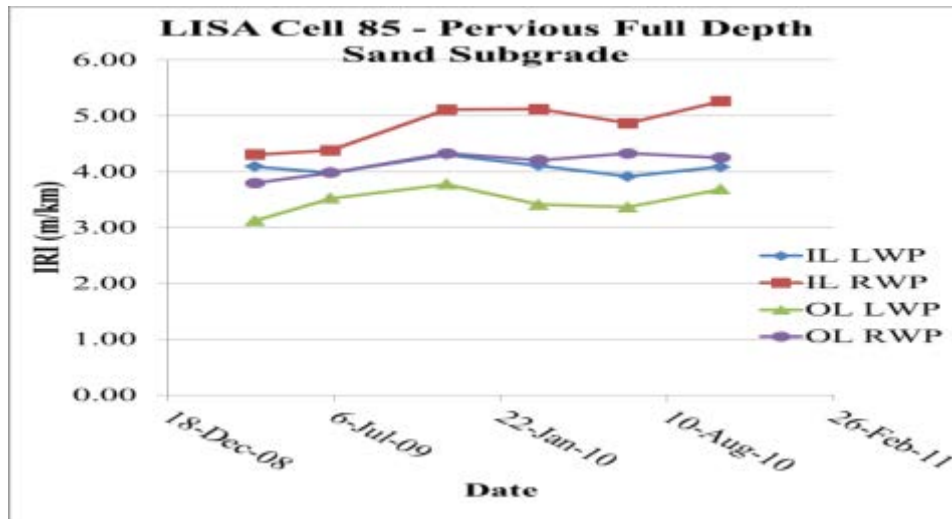
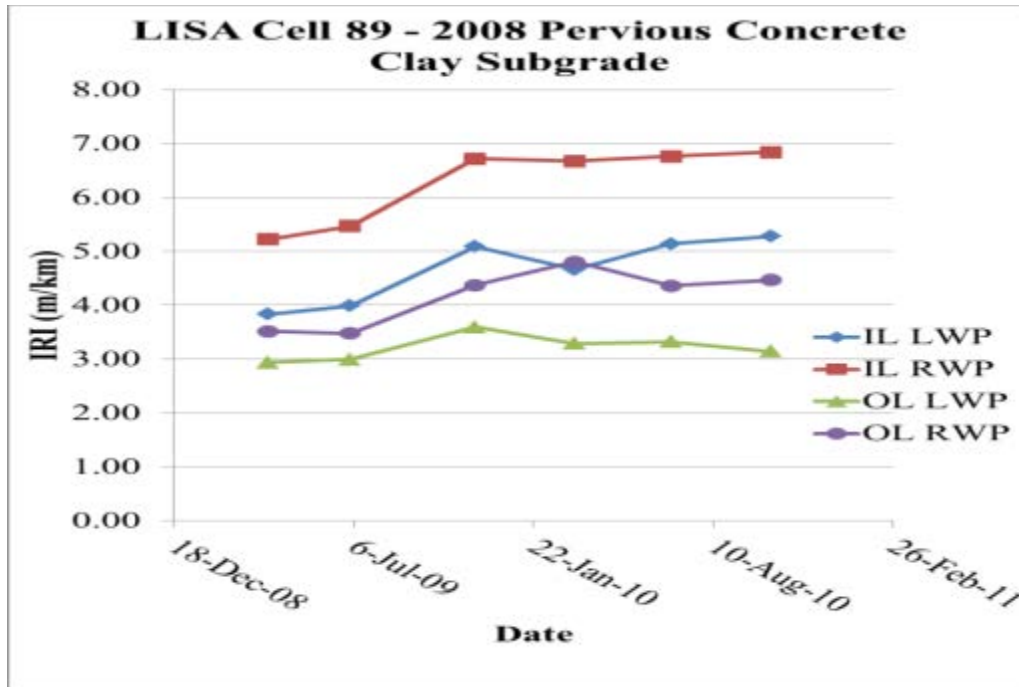


Figure 4.37: IRI of a 2008 Full Depth Pervious Concrete Built on Pervious Base and Sand Subgrade



**Figure 4.38: IRI of a 2008 Full Depth Pervious Concrete Built on Pervious Base and cohesive Subgrade**

#### 4.1.7 Concluding Remarks

From the data obtained above, it is important to reiterate that the objective behind development of an optimum texture is the provision of a safe quiet and durable surface with a comfortable ride quality. Observations show that the quiet pavements are not necessarily associated with low skid resistance or that the noisy pavements are not necessarily safe or that the quiet pavements are not necessarily unsafe or ride poorly. It appears that the ranges of each of these performance criteria are broad for each texture type and that one does not necessarily skew the other. This creates an environment for the possibility of ascertaining the intrinsic features that optimize surface characteristics. This provides some hope that optimum performance in all arenas can be derived from good texture designs.

There not enough data to correlate pervious pavement texture to OBSI however, there is a trend obtained from the current data set. The regression does show a trend in which the MPD and IRI have a negative coefficient. This implies that the more the MPD or IRI, the less the OBSI. There is not enough background information on pervious concrete yet to validate his unusual observation, but it appears faulty, otherwise it will be validated after more data is obtained. The coefficient of determination in this regression is 0.11 which is considered very weak. The weakness was characterized by relatively high p-values.

- However, there is no apparent correlation between SA and pervious pavement MPD. The p-value is 0.33 which is  $\gg 0.05$ .
- There is no apparent correlation between pervious pavements IRI and OBSI. The p-value obtained is 0.72 which is  $\gg\gg 0.05$ .
- There is correlation between MPD of pervious pavements and SA but no correlation between MPD and OBSI



- Due to the small sample size, the power of this regression is 50 percent.
- A nonlinear correlation may not be investigated until the sample space is large enough and the linear model suggests that additional step.
- In Non-Pervious Pavements, there is no significant correlation between OBSI and MPD.

As the second year of study, these observations are early and may be affected by only a few seasons and years of data. They may not reflect the same observation and conclusion of the final report. This report is therefore performed in brevity.

## **4.2 Third Year And Fourth Year Annual Report**

### **4.2.1 Surface Characteristics Versus Time Trends**

The 3<sup>rd</sup> and 4<sup>th</sup> year surface characteristics reports are combined in this report. This combination was done as a result of similarity in data interpretation in both years and trend that otherwise rendered separate annual reports merely repetitive. It is hypothesized that certain pavement surface characteristics would change according to environmental exposure, traffic and other extrinsic factors. It is therefore expected if that hypothesis is valid that surface characteristics will vary with time. This section documents the trends of texture, IRI and Friction over the 3<sup>rd</sup> and 4<sup>th</sup> years of some new cells. It also shows the current trend in certain cells that have been in service for a long time and examines how much changes are still occurring at their respective ages.

### **4.2.2 Mean Profile Depth**

Mean profile depth was measured with the circular track meter (ASTM E 2157). This section discusses the trend of MPD with time in the textures measured.

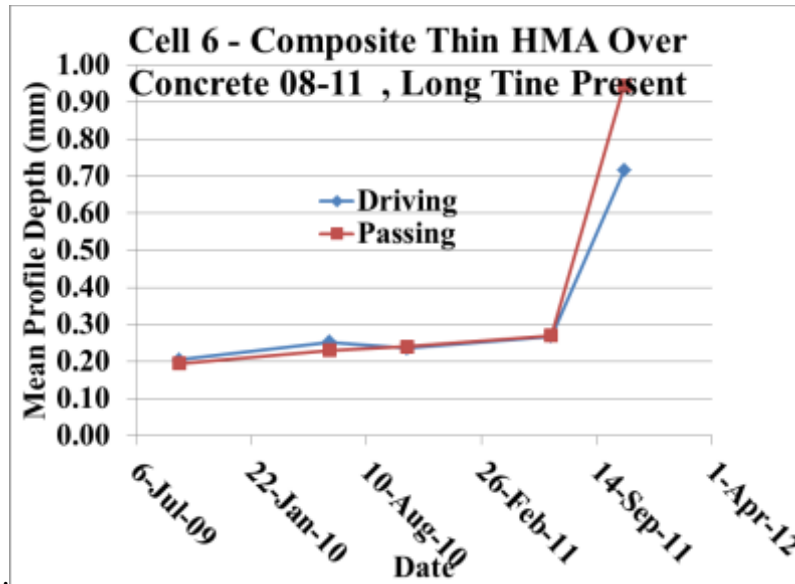


Figure 4.39: Longitudinal Tine

Cell 6 was initially a thin insulated concrete experiment from 2008 that suffered from early distress which led to a pavement constriction in September 2011. The 2011 initiative included longitudinal tining. See appendix.

The curve shows the low MPD on the asphalt surface and how the longitudinal tining resulted in an MPD ranging from 0.7 to 0.95

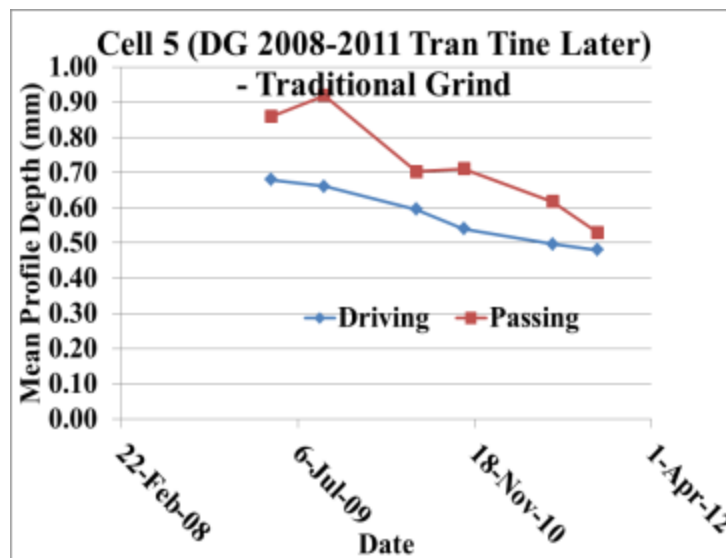


Figure 4.40: Traditional Grind

Figures 4.22 to 4.23 show that there is a rapid initial degradation in MPD in traditional grind. This feature was discussed by Izevbekhai and Khazanovich [1.8] in relation to some unusually high fins that occasional occur after diamond grinding. These fins are brittle and wear off very rapidly.

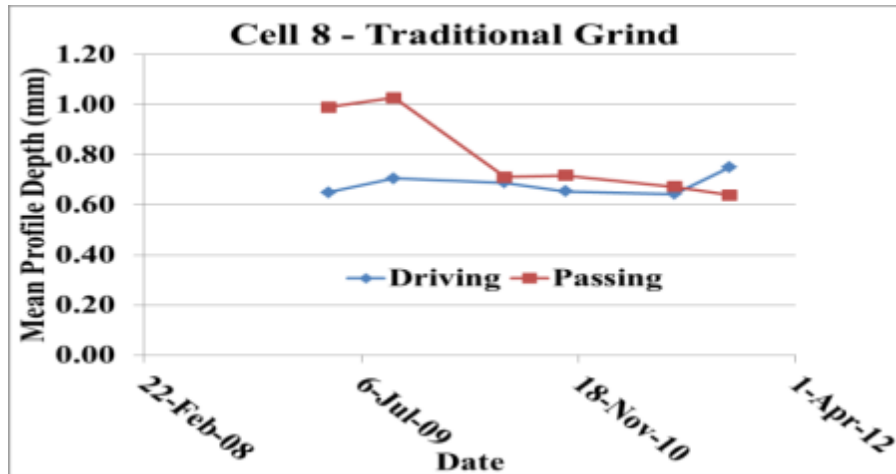


Figure 4.41: Traditional Grind

Figure 4.24 to 4.25 typify innovative grind that is more durable in MPD. The durability is attributed to the larger inter groove spacing (0.5 to 0.625 inches). These are not associated with brittle fins and are thus not subject to early degradation. The initial attempt at the innovative grind had no corrugations on the landing between grooves. This was therefore associated with lower MPD than the improvements in Improved innovative Grind (Cell 9) (2008) and 71 (2010). Figures 4.26 and 4.27 consist of drag textures established in the longitudinal direction.

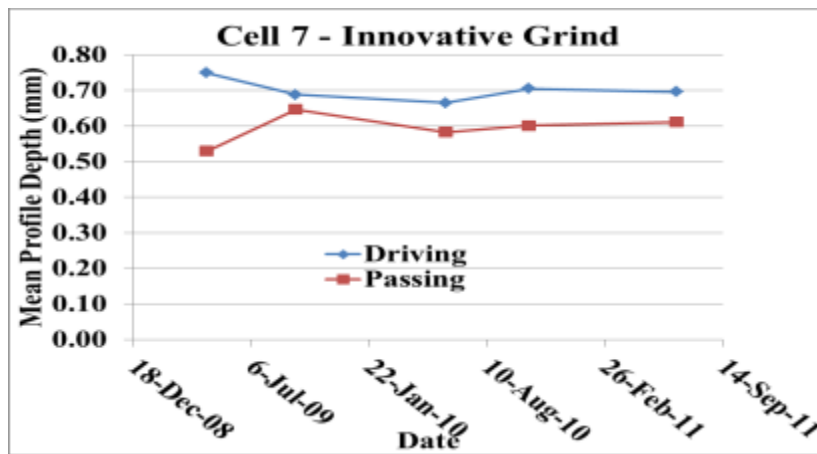


Figure 4.42: Innovative Grind

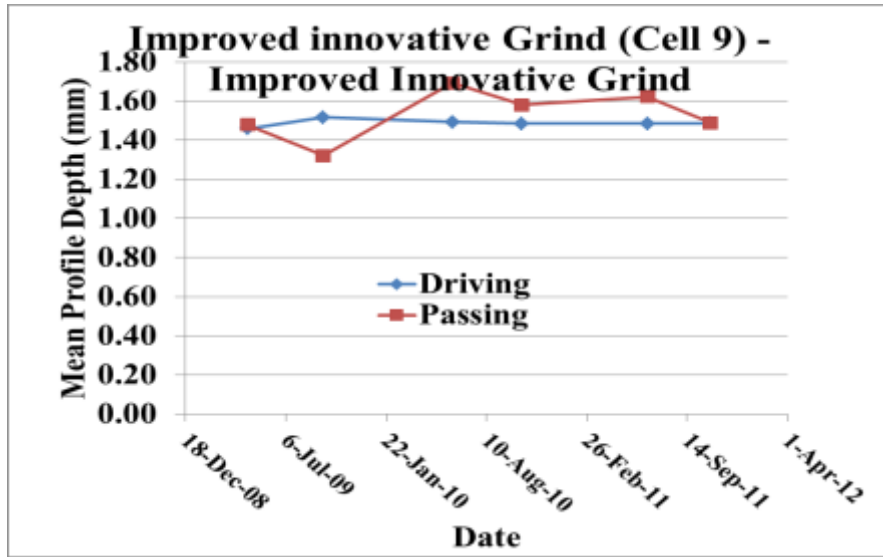


Figure 4.43: 2008 Innovative Grind

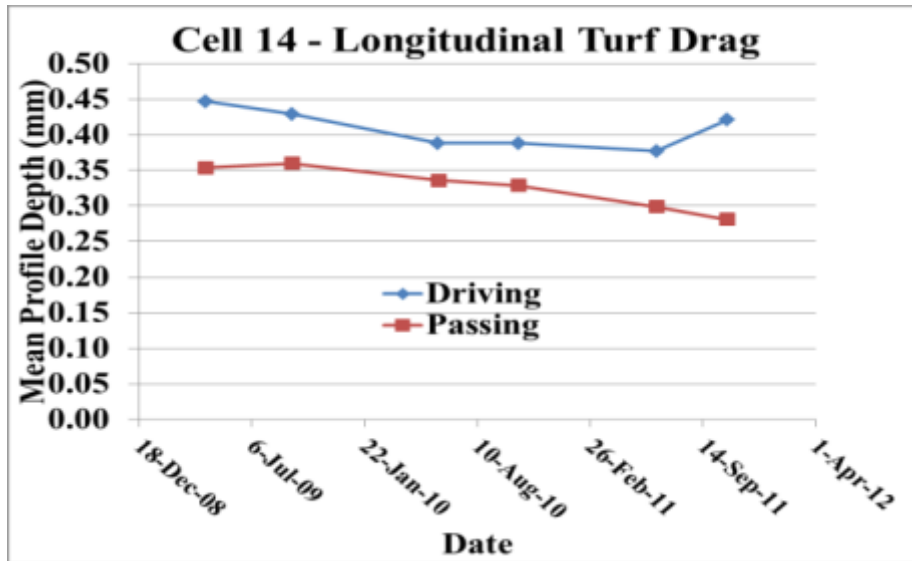


Figure 4.44: Drag texture

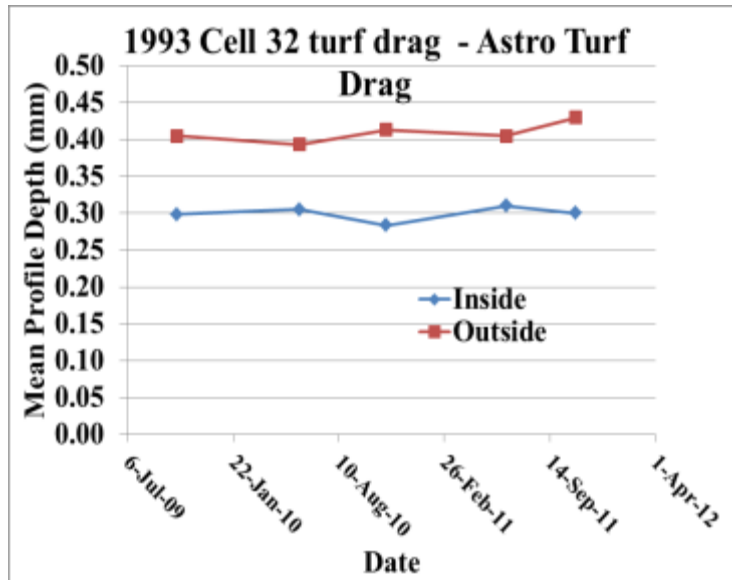


Figure 4.45: Drag Texture

Cells 32 and 52 in the LVR exhibit higher MPD in the untraveled lane. Partly this is attributed to the more aggressive texture on call 53 when they were constructed. Since 1993 Cell 32 turf drag was constructed and textured in 2000 and Cell 53 (2008 Transverse Tine) was constructed and textured in 2008, the observed texture depth values are not indicative of any interpretable survival trend. It is also known that prior to 2008 the outside lane receive a 102 kip 5 axle semi-trailer 80 times a day and one day per week.

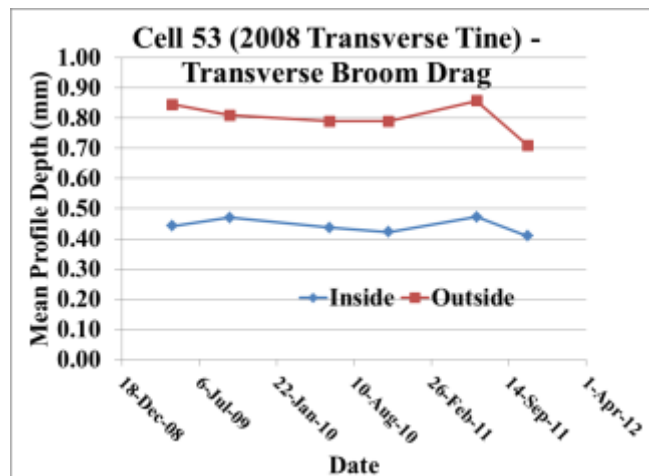


Figure 4.46: Drag Texture

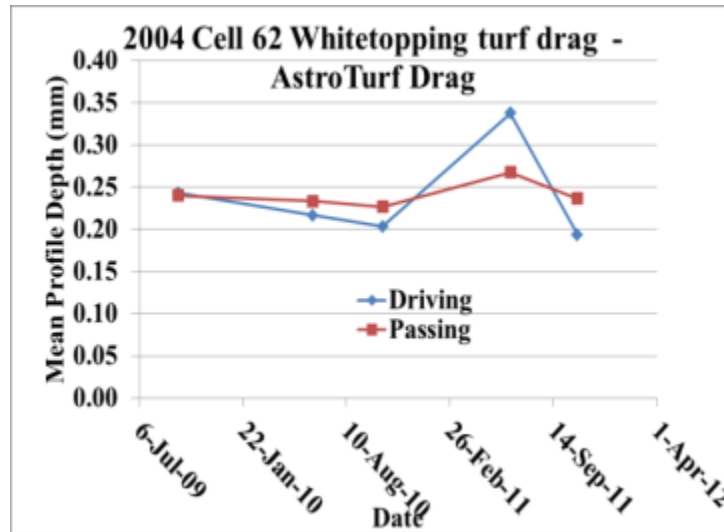


Figure 4.47: Drag Texture

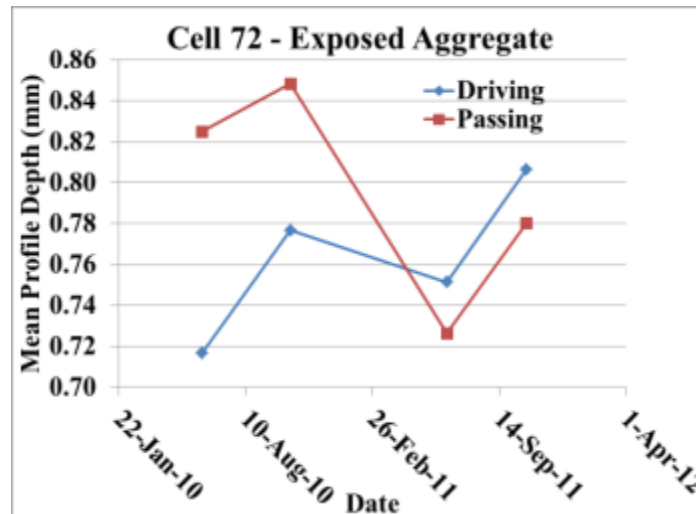
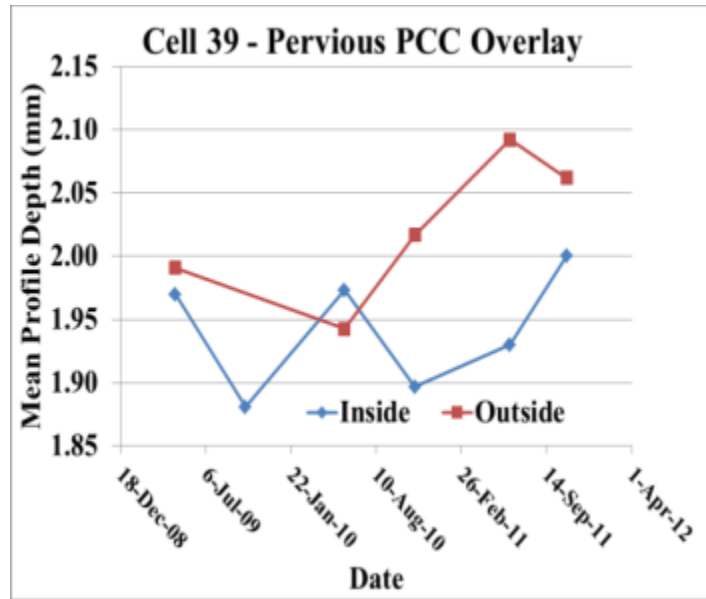


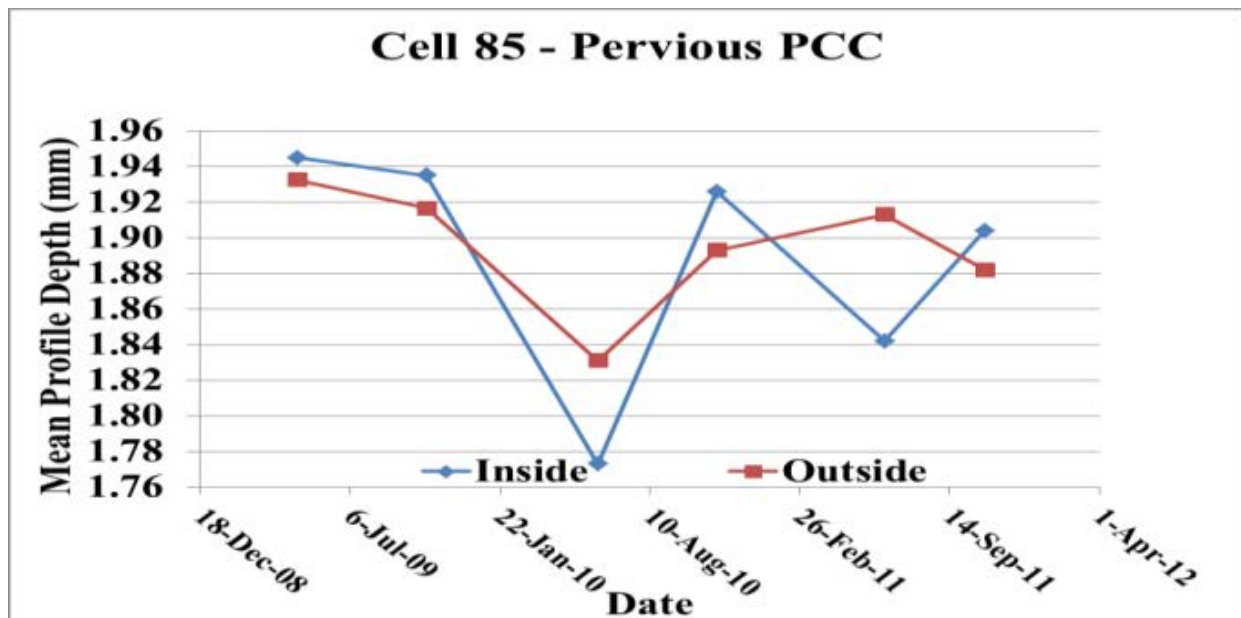
Figure 4.48: Exposed Aggregate

Exposed aggregate textures were discussed exhaustively by Izevbekhai and Akkari (2012). They showed that from the time of exposure, this surface type undergoes rapid changes in retexture orientation that results in rapid changes in other surface characteristics. The final performance would ultimately be based on the aggregate type and mix design and curing method which governs the time the texture (d) surface becomes relatively stable.



**Figure 4.49: Pervious Concrete Surface**

The MPD of pervious pavements cannot easily be defined particularly when the pervious structure consists of communicating voids. Communicating voids are the goals of most pervious design. They imply that the cavities are interconnected irrespective of the tortuosity of the drainage paths. The circular track meter determines the bottom of a cavity by an algorithm, consequently, the MPD of the pervious concrete cell are not as useful as the texture orientation that may be computed from the texture configurations. This was dealt with exhaustively by Izevbekhai and Akkari in 2011. However the MPD of pervious surfaces are generally very high as shown in Figures 4.211 to 4.214



**Figure 4.50: Pervious Concrete Surface**

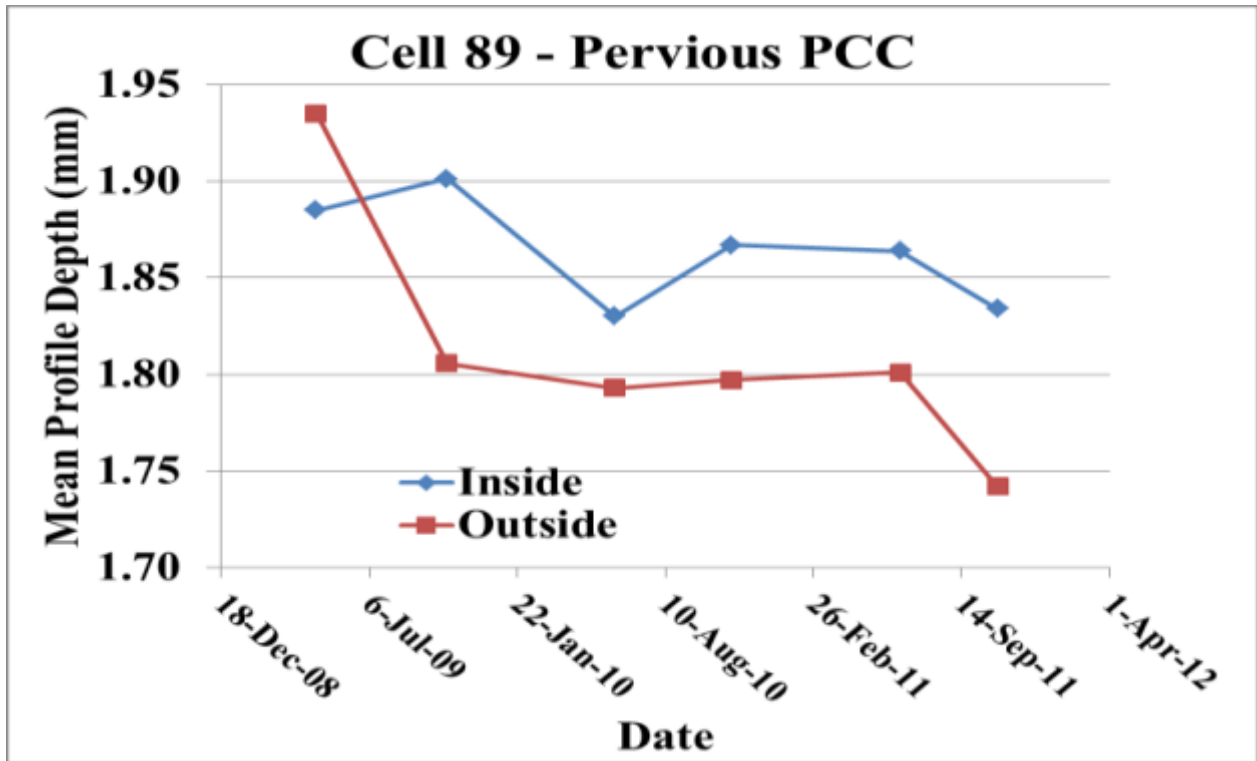


Figure 4.51: Pervious Concrete Surface

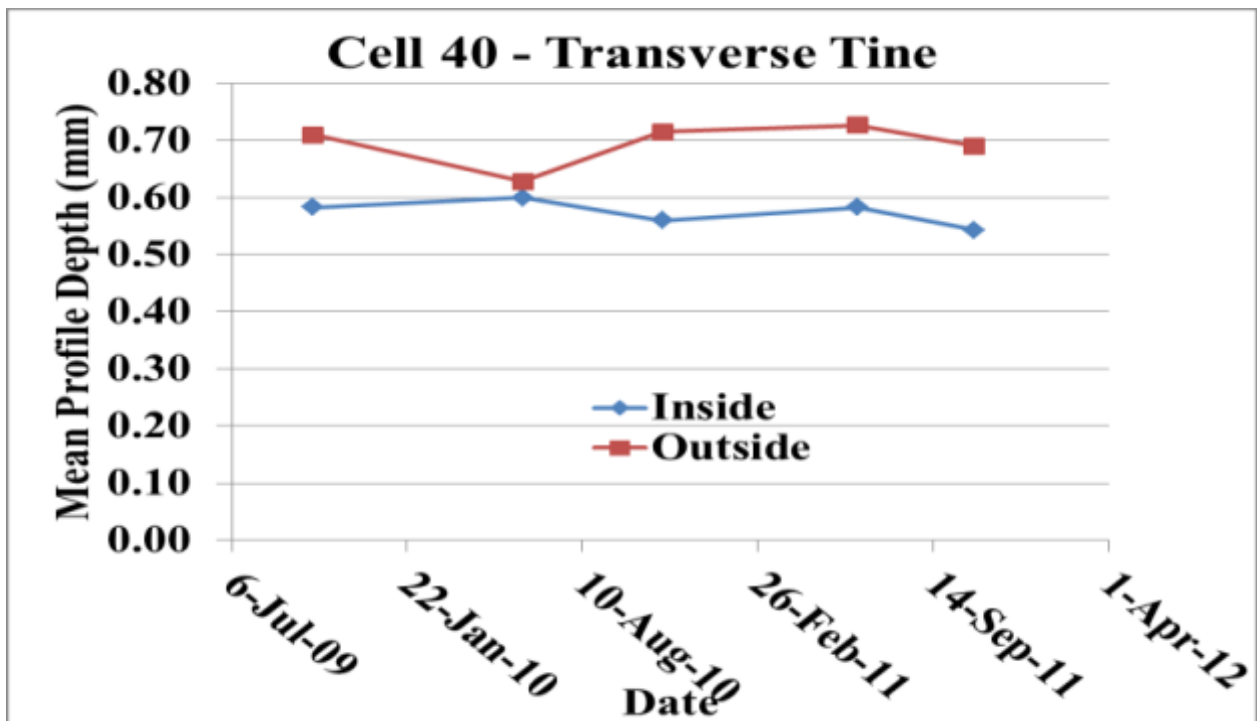


Figure 4.52: Transverse Tine

The transverse tine textures in MnROAD were built in 1993 and at this stage they seem to exhibit little or no texture degradation. They appear to be stable as they maintained uniform



MPD during the period of analysis spanning year 15 to year 19 The lower MPD in the inside (trafficked from 1993-2007) lane is explained by higher traffic volume in the inside lane resulting on a slight difference in texture degradation.

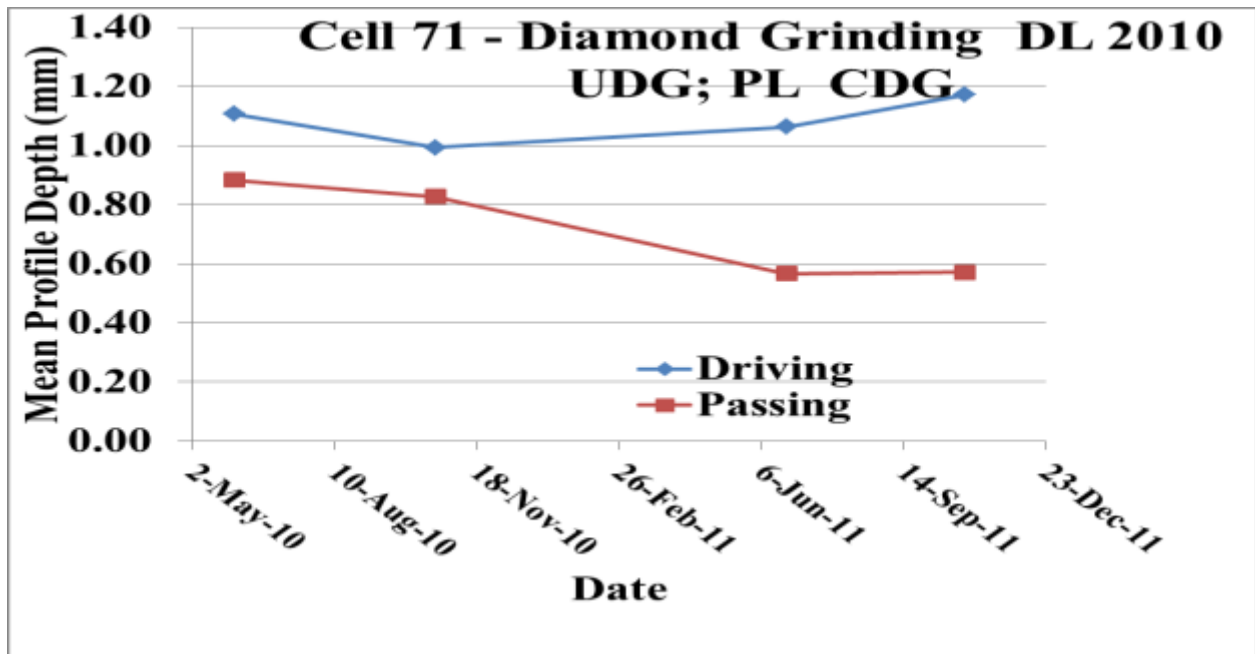
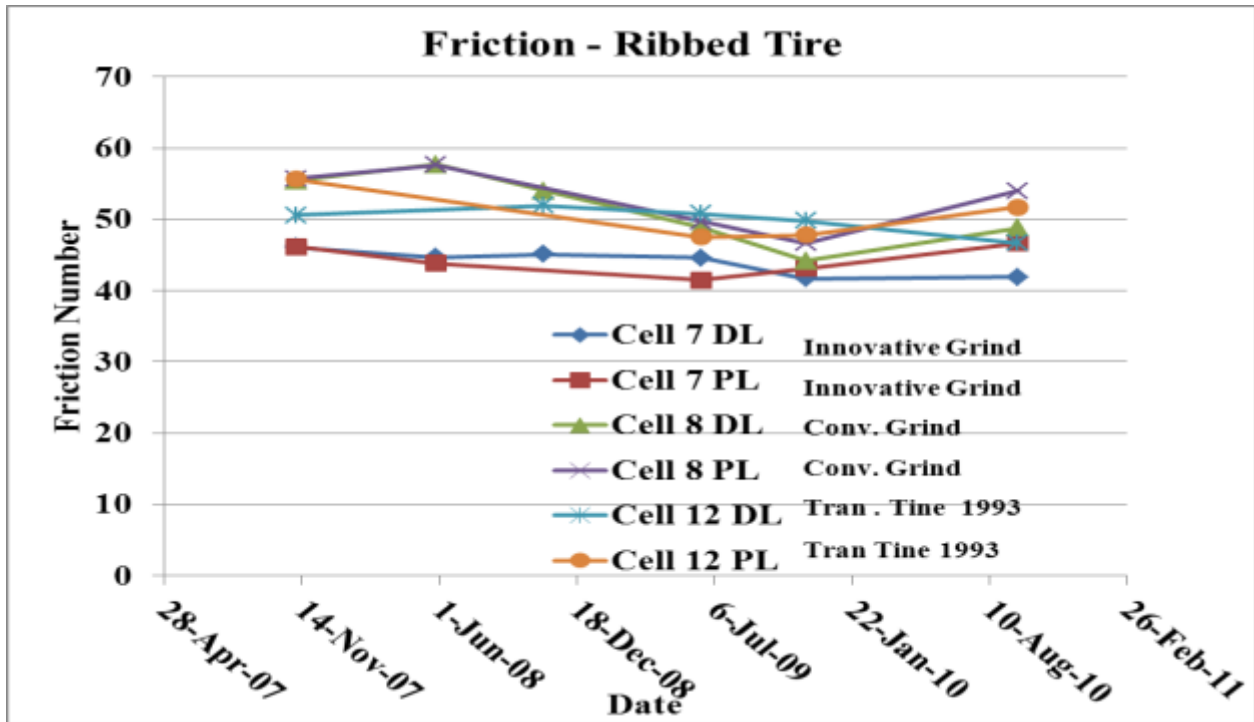


Figure 4.53: Innovatively Ground DL and Conventionally Ground PL

#### FRICITION

For a description of Friction measurements in MnROAD Data base guide (2009) may be referenced. In this research a choice was made to collect both ribbed and smooth tire ASTM E 274 procedure using the MnDOT Lock wheel skid trailer. A detailed report on Friction survival and the corresponding degradation models are performed in another task. In this task the data trend is discussed.



**Figure 4.54: Grinding Comparisons**

Figure 4.215 shows a comparison of ribbed tire friction of 3 texture types the innovative grind the conventional grind and the transverse tine. Cell 7 appears to have the friction numbers in the range of 40 to 43 but in a very tight range. A tight range is also exhibited by the transverse tined for reasons already explained for a previously observed similar pattern in texture depth. Cell 8 with the conventional grind shows a rapid initial degradation that is not as drastic as the MPD degradation already described. A strategy to improve friction resulted in the innovative grind was made in 2008. The improvement increased friction numbers closer to 50. Figure 4.218 shows a similar texture improvement arising from a rejection of the inadequate texture in Cell 5 (DG 2008-2011 Tran Tine Later) in 2006. The initial measurement of friction occurred when the surface still retained the initial longitudinal tine whose smooth tire friction was inadequate. As a corrective measure it was ground. Subsequent tests showed sufficient friction.

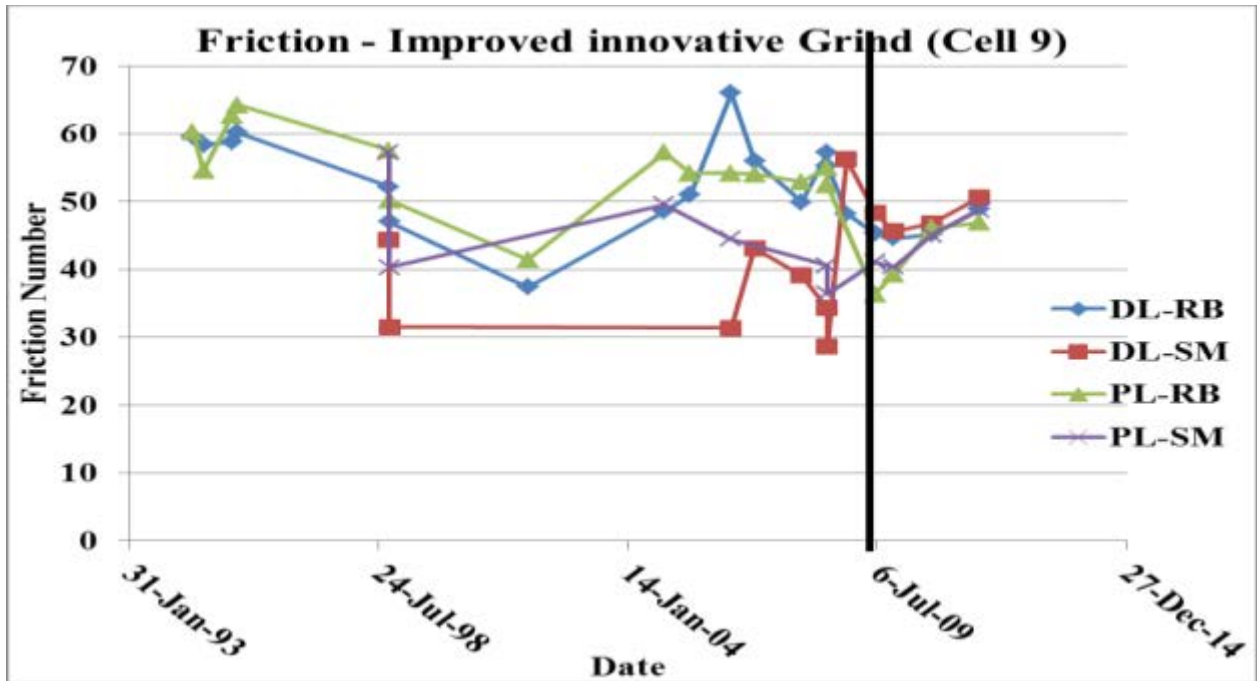


Figure 4.55: Improved Innovative Grind

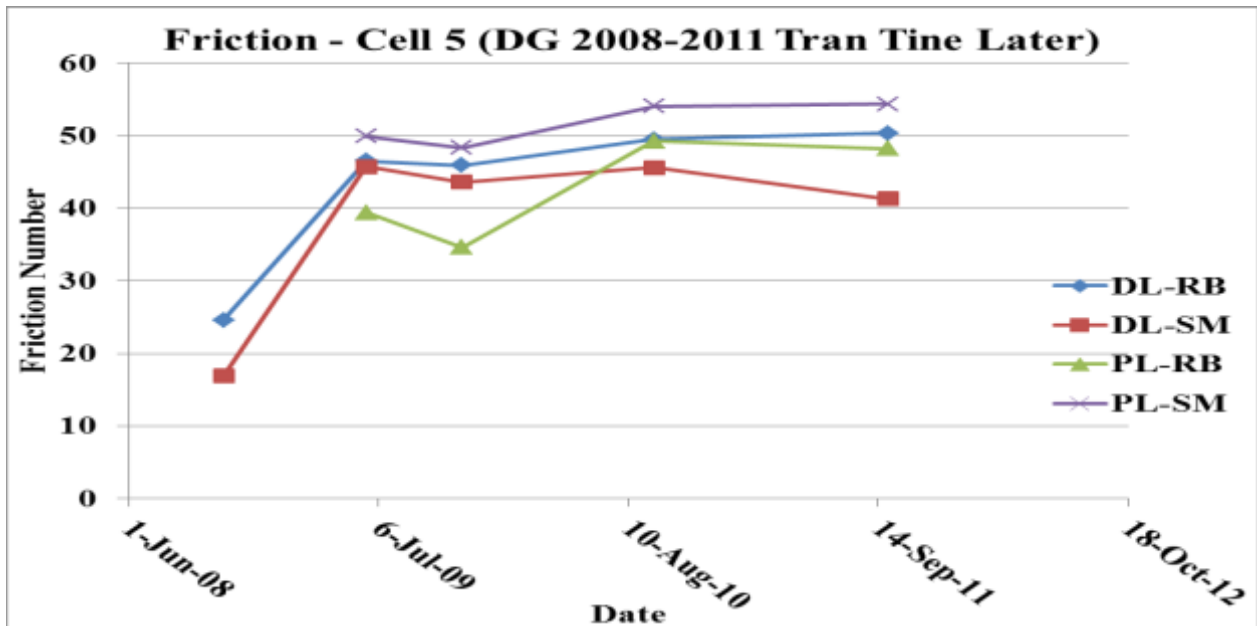


Figure 4.56: Conventionally Ground Longitudinal Tined Texture

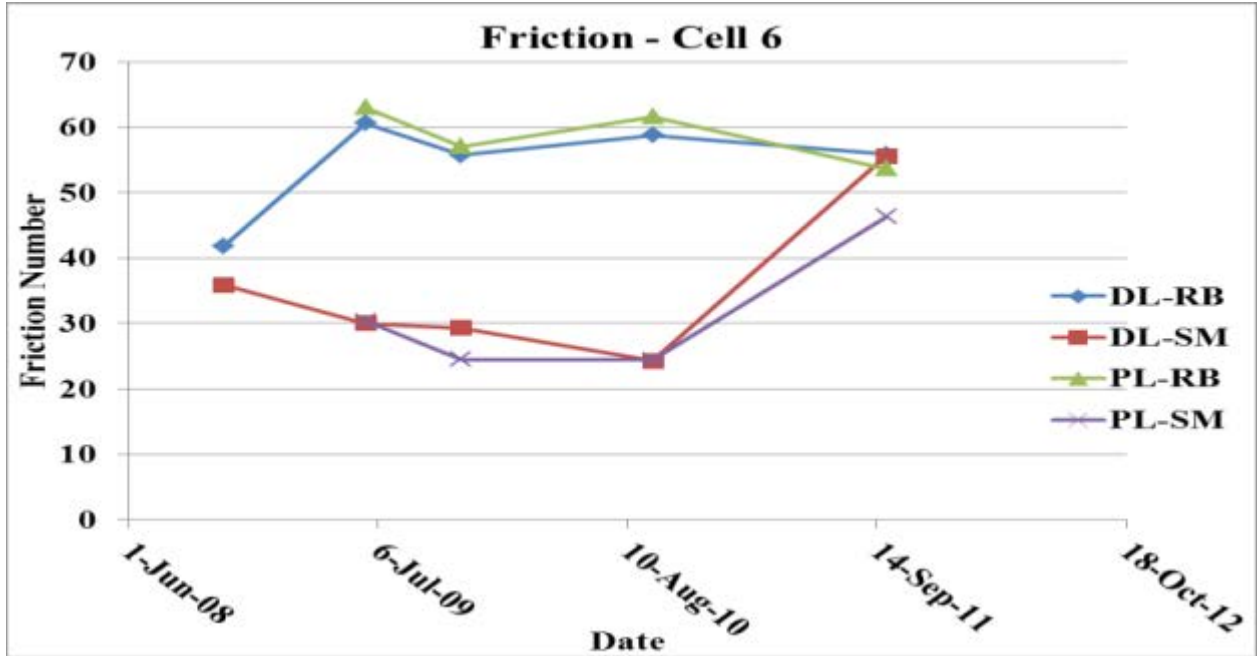


Figure 4.57: Asphalt-Surface. Later Longitudinal Tine

In Figure 4.219, smooth tire friction increased but ribbed tire friction slightly decreased when the asphalt surfacing was removed and a longitudinal textured concrete pavement was built in 2011.

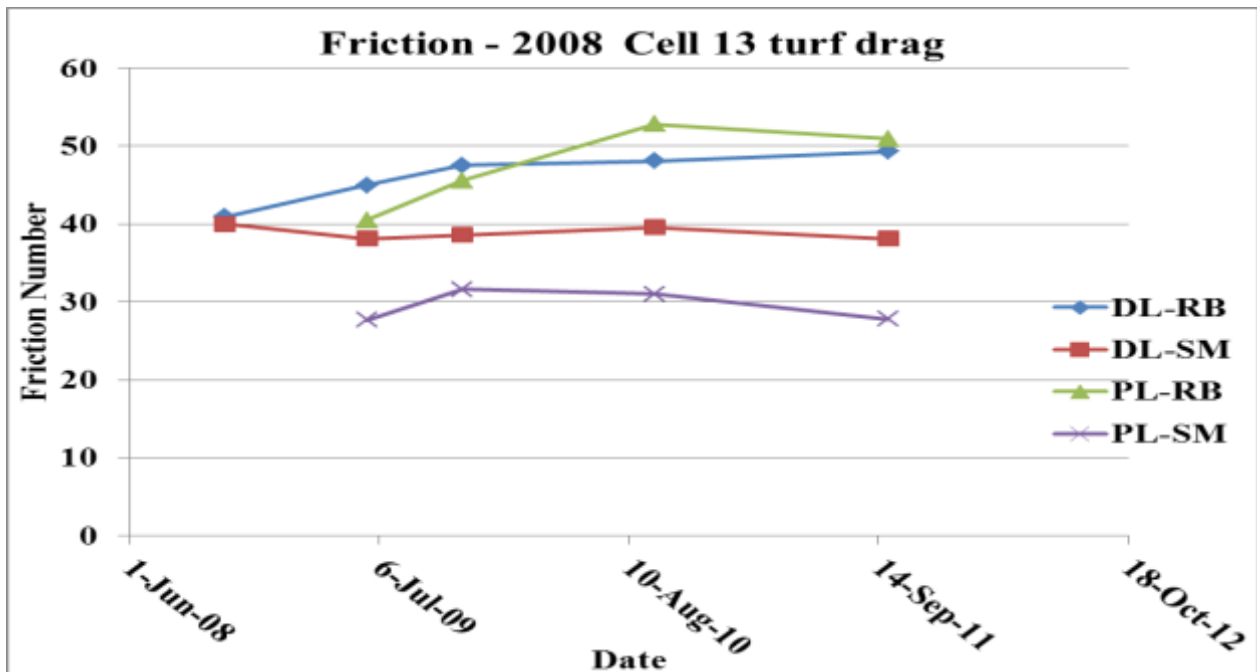


Figure 4.58: Drag texture Friction Numbers

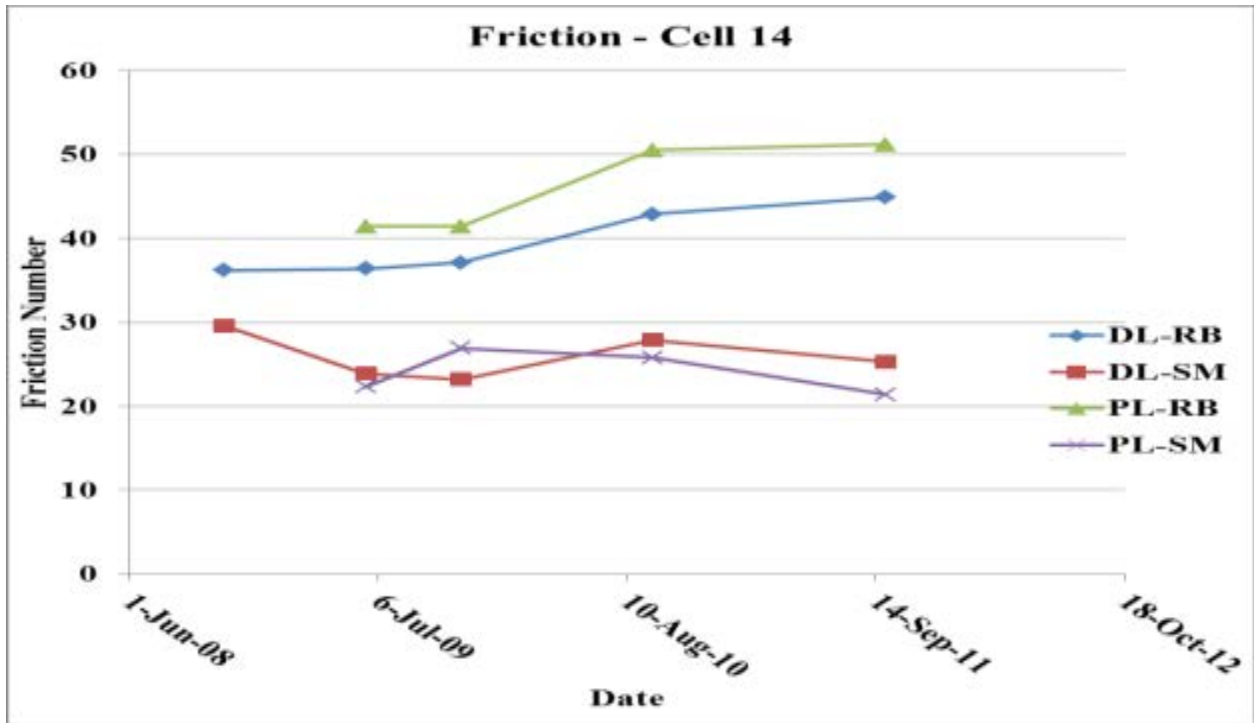


Figure 4.59: Drag Texture Friction

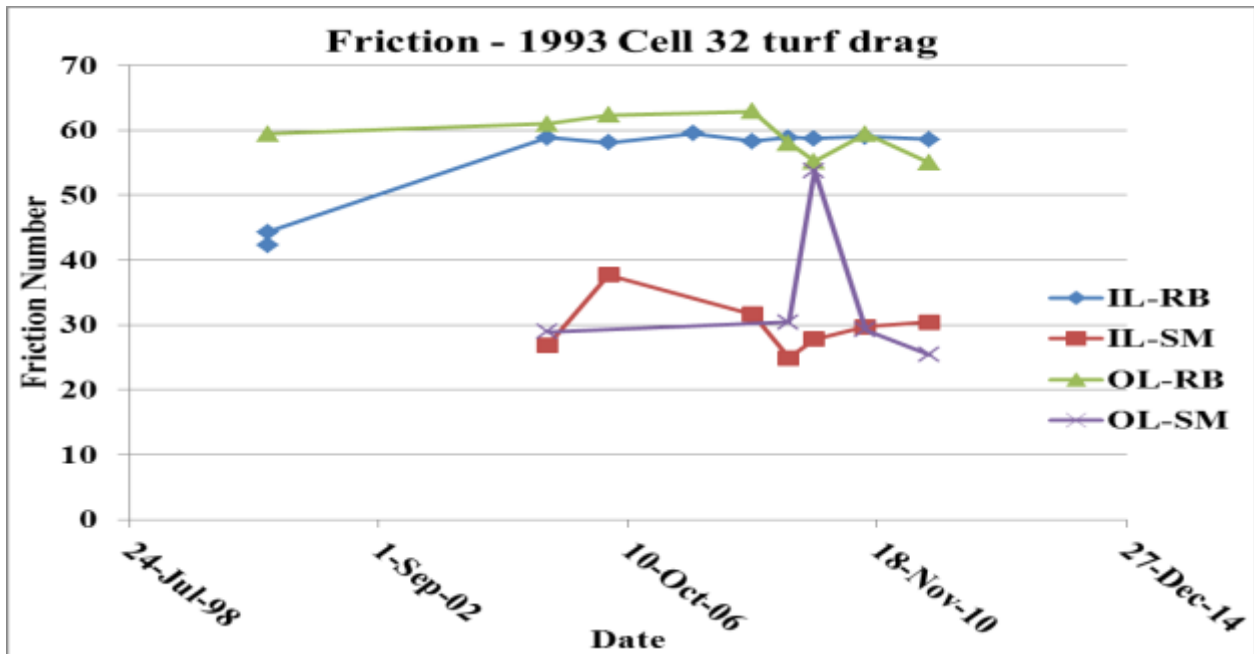


Figure 4.60: Drag Texture Friction

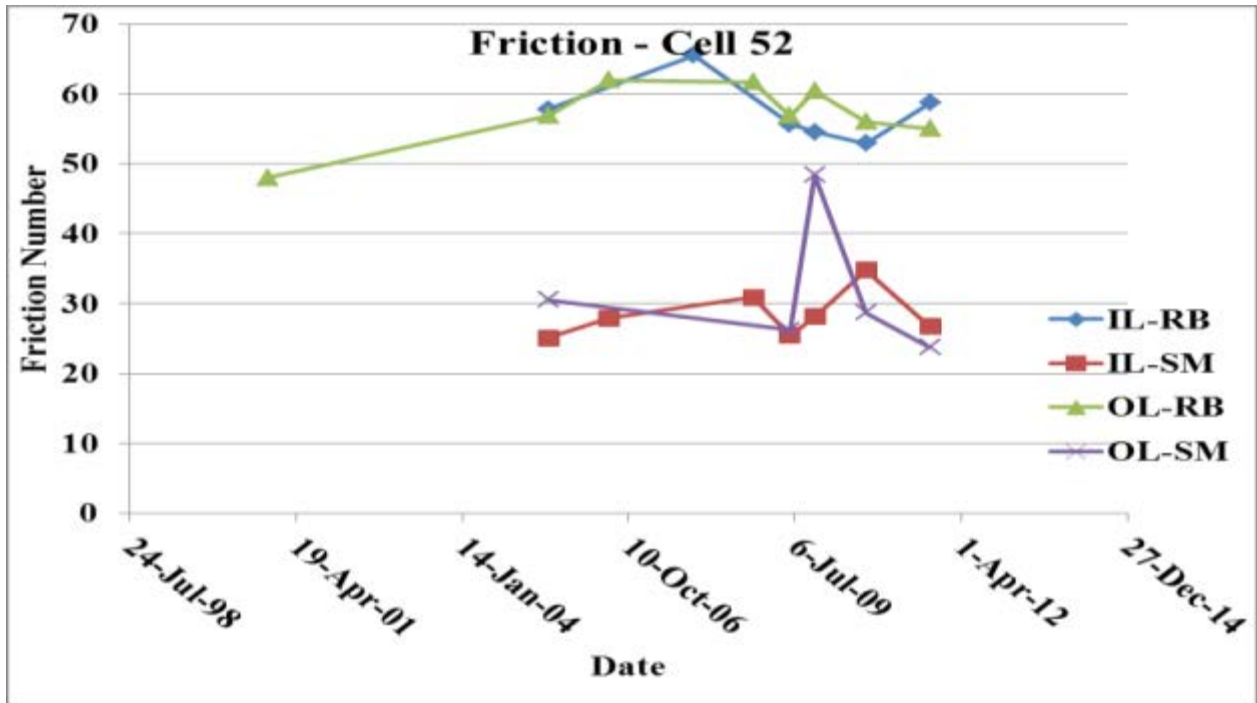


Figure 4.61: Drag Texture

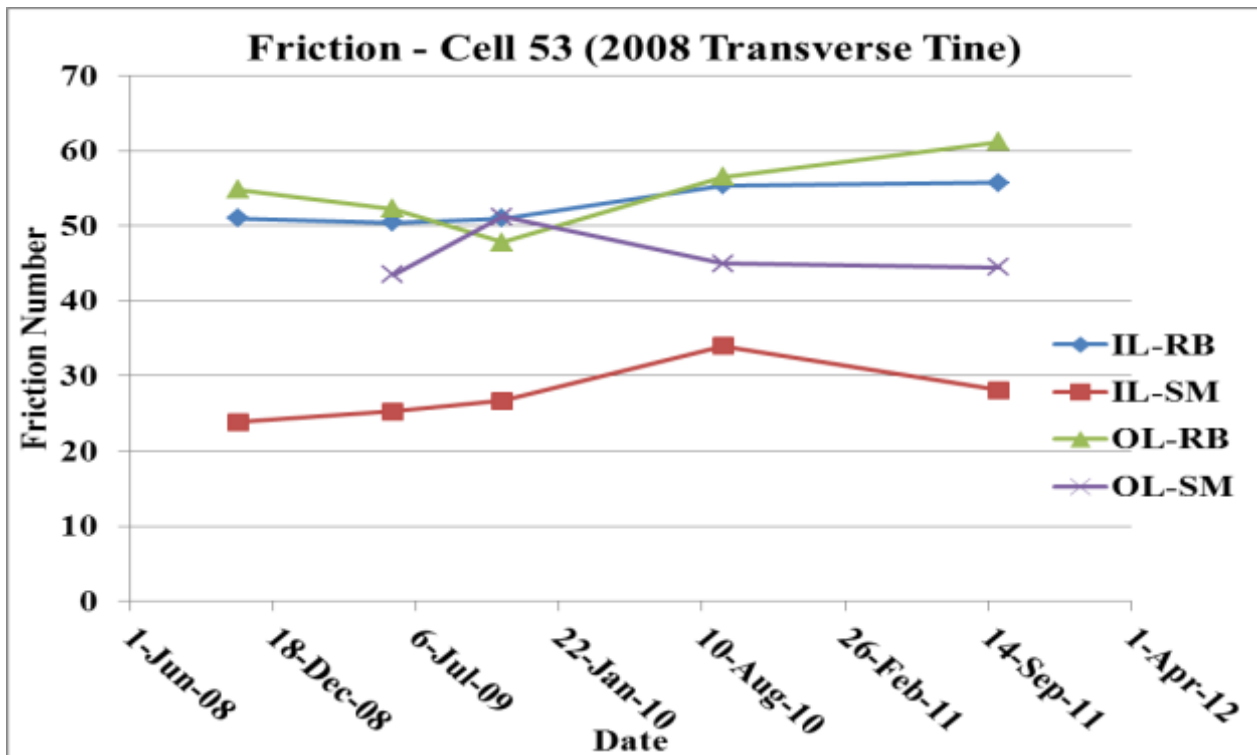


Figure 4.62: Drag Texture

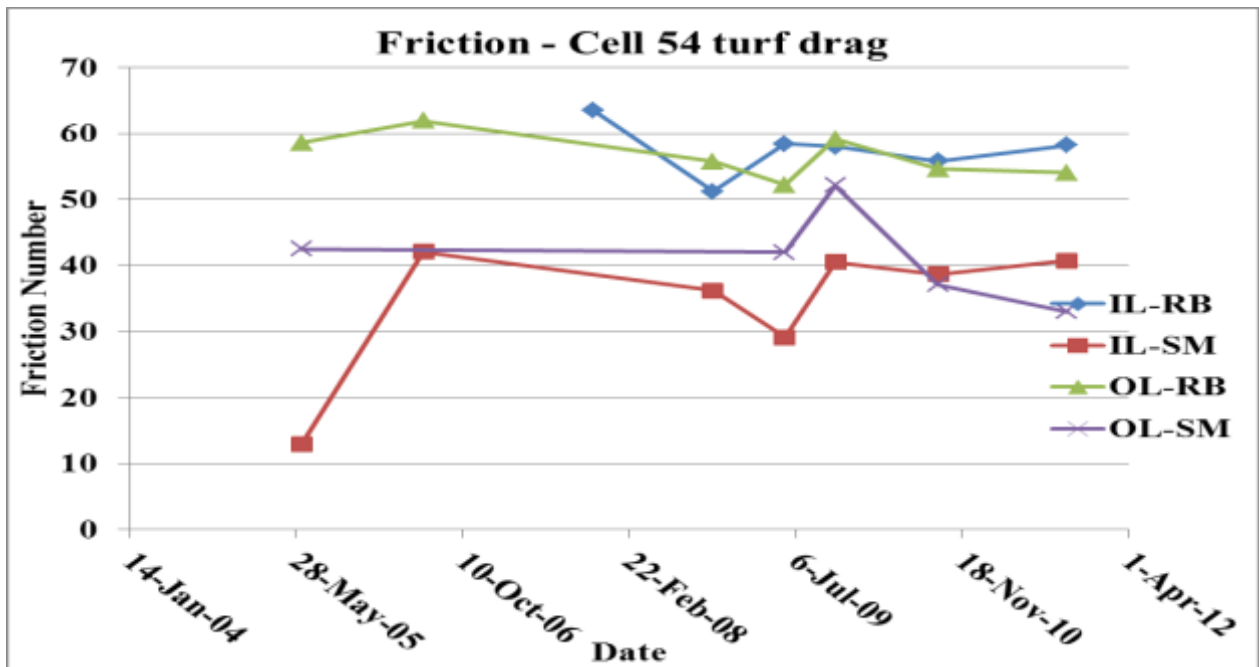


Figure 4.63: Drag Texture

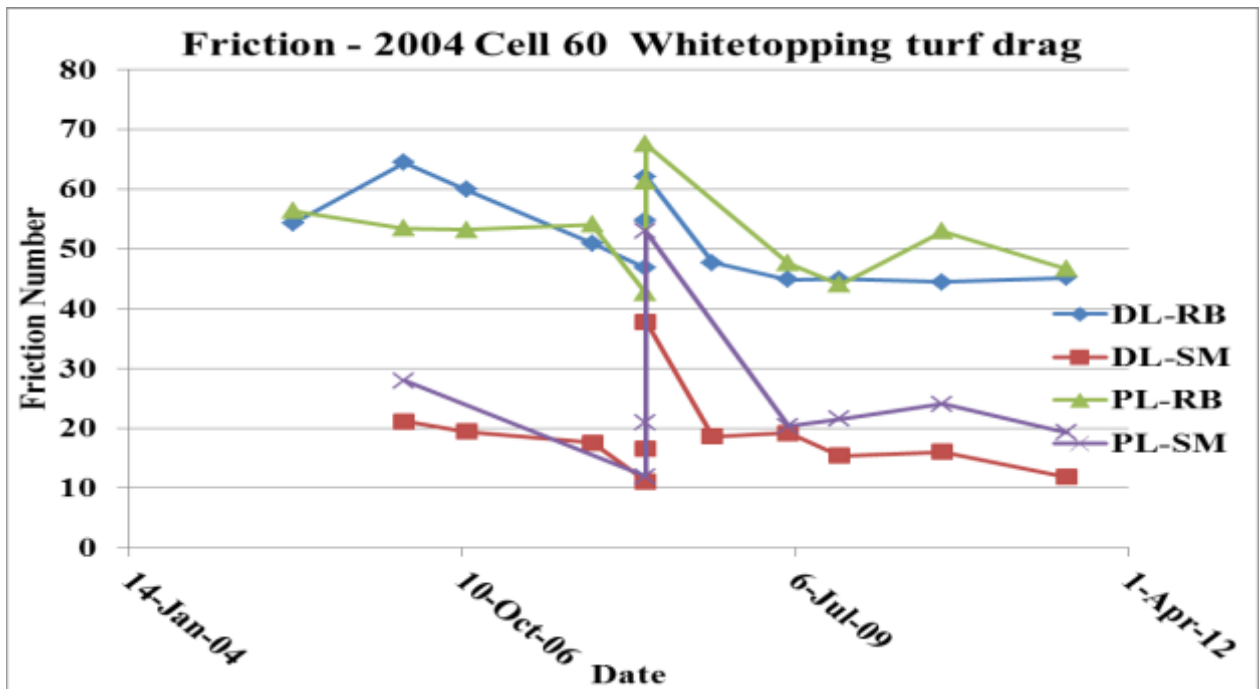


Figure 4.64: Drag Texture

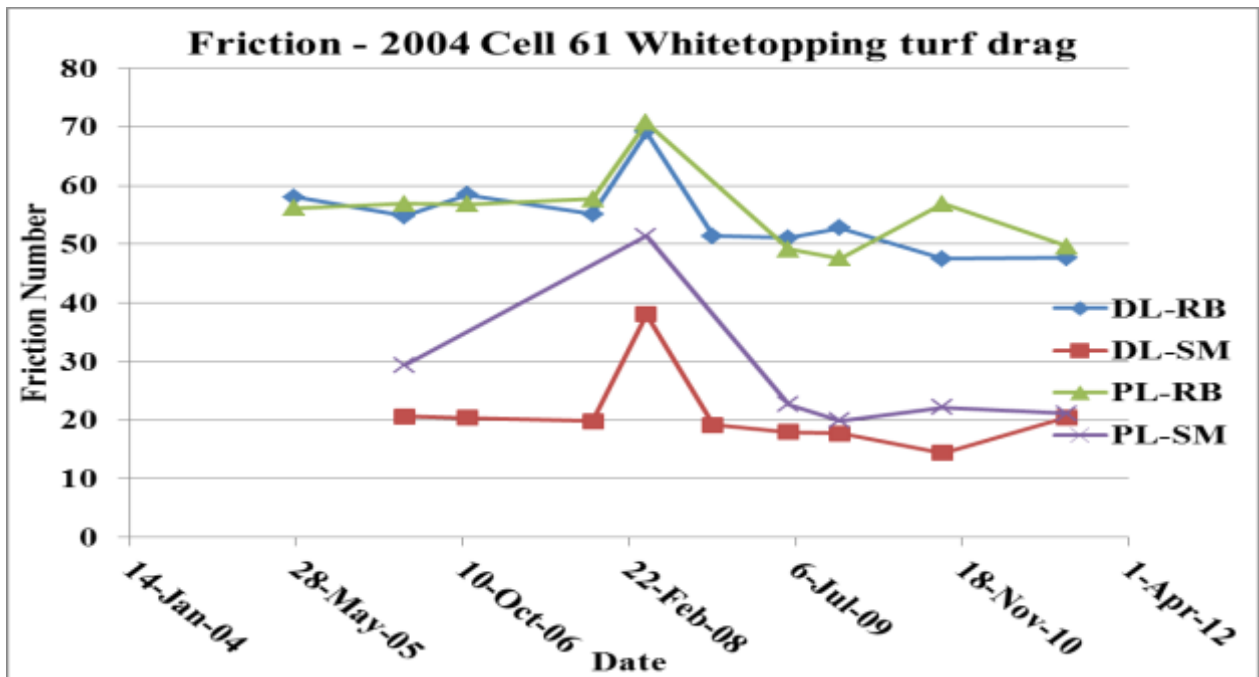


Figure 4.65: Drag Texture

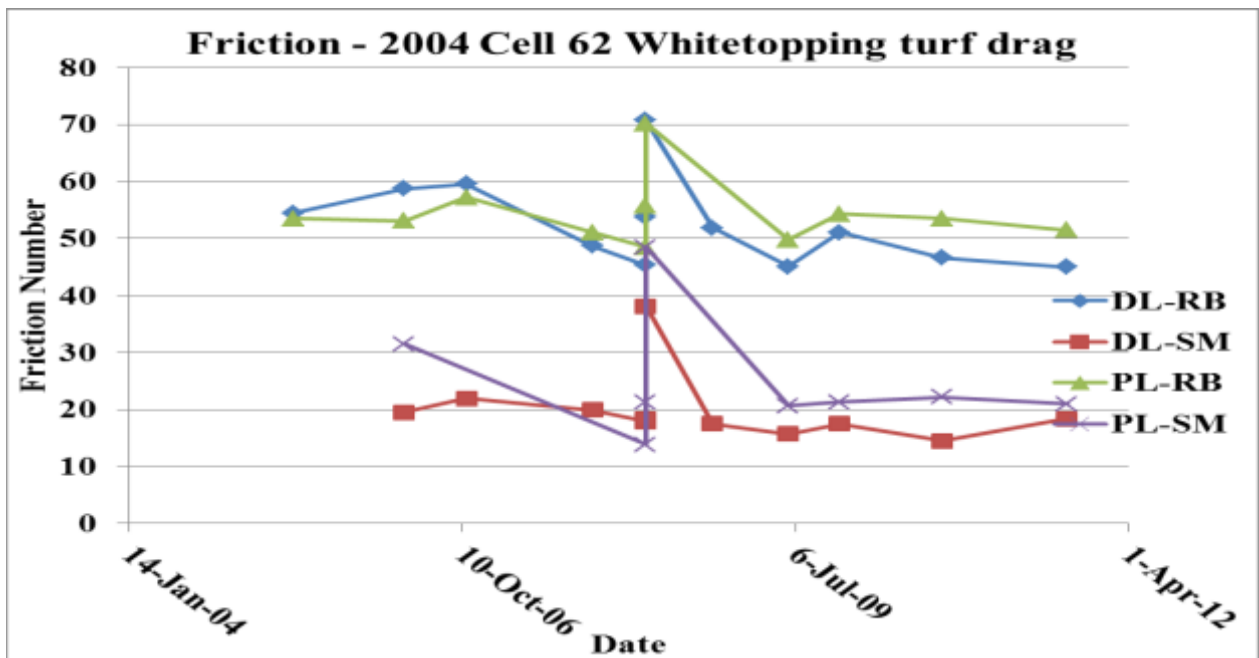


Figure 4.66: Drag Texture



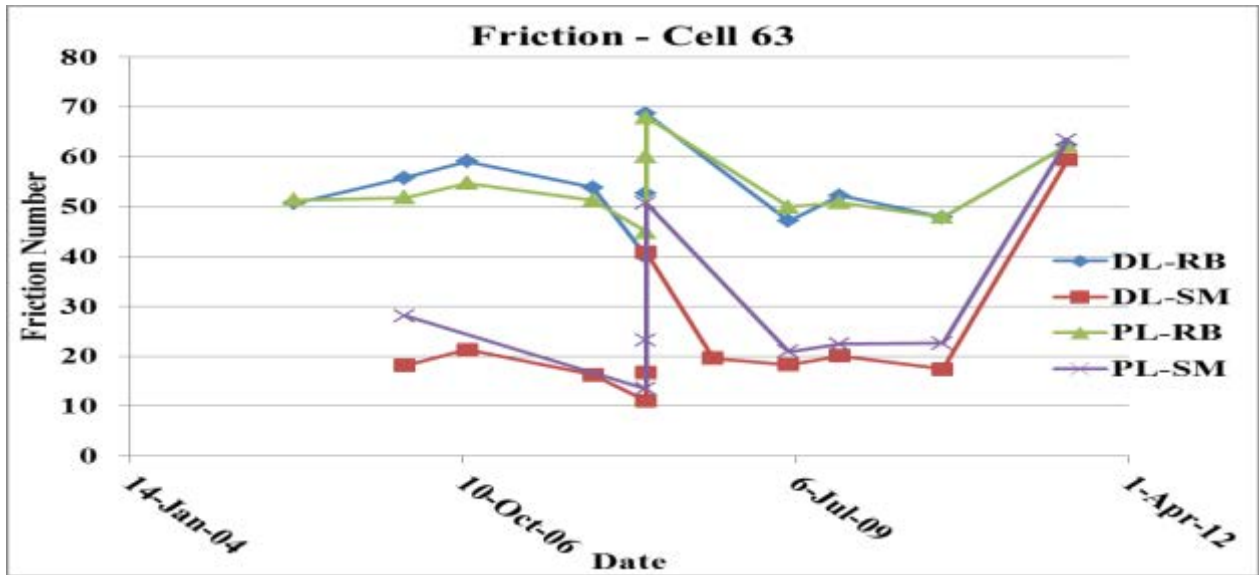


Figure 4.67: Drag Texture

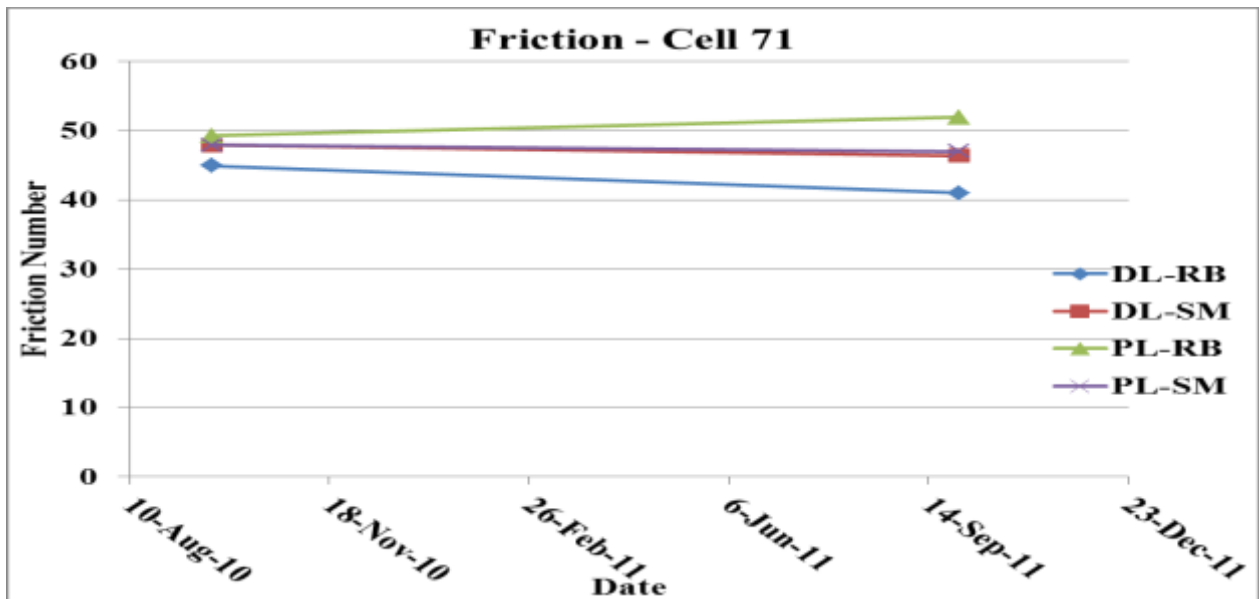


Figure 4.68: Drag Texture

The Innovative grind texture in Cell 71 Driving lane shows higher friction number in the smooth tire than in the ribbed tire. There is an enhancement of friction in bald tires when innovative grind textures are used. This phenomenon was observed in other innovative grind test cells.

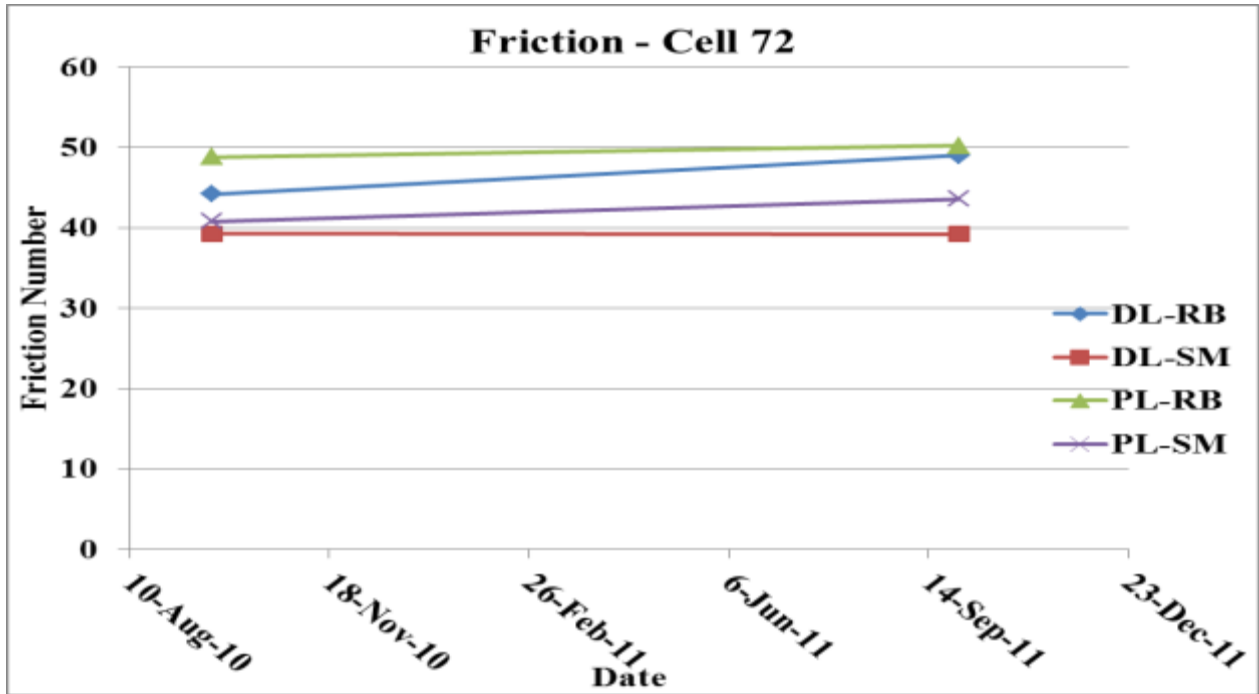


Figure 4.69: Friction of Exposed Aggregates

Exposed aggregate friction numbers were moderate and ranging between 40 and 50. Exposed aggregate seems to provide sufficient friction numbers. At this stage not many repeat tests had been conducted on this cell but the changes in texture orientation does not seem to reflect in friction numbers.

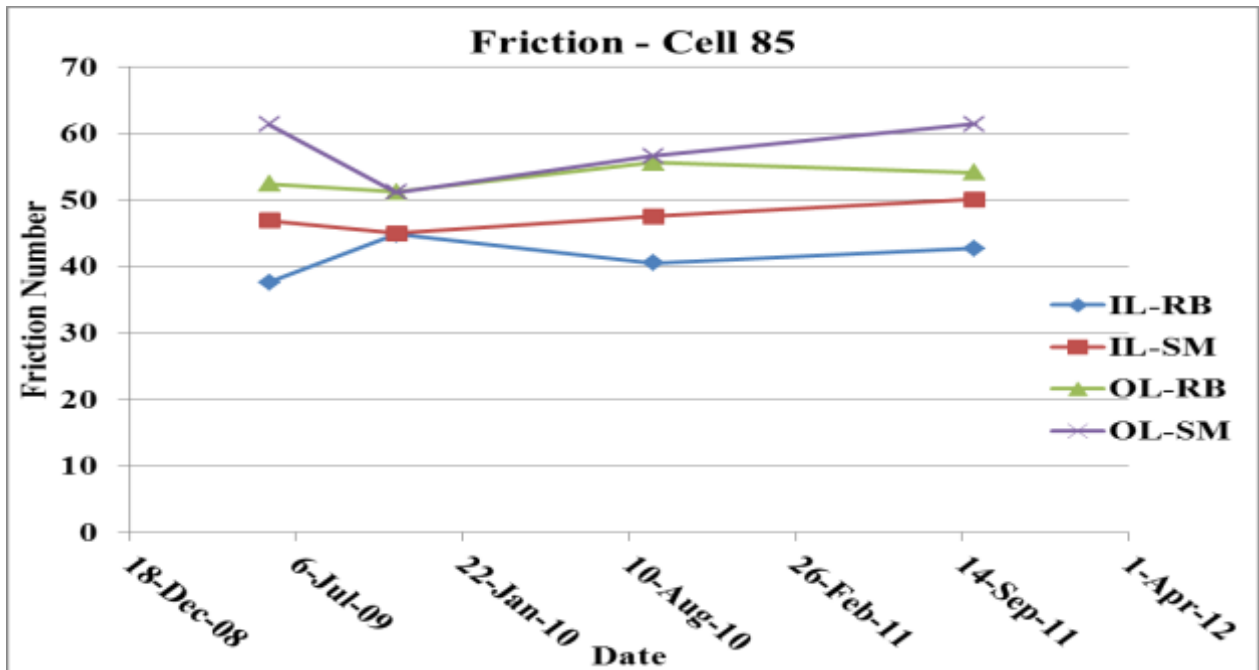
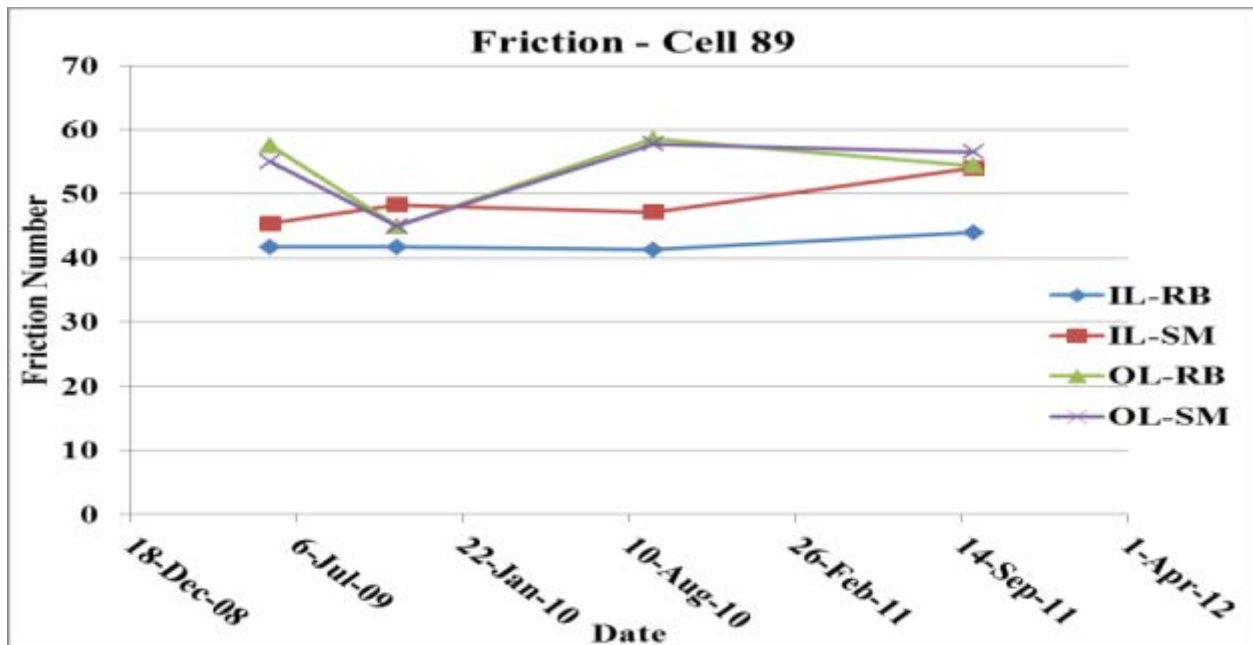


Figure 4.70: Friction in Pervious Concrete



**Figure 4.71: Friction in Pervious Concrete Surface**

Another unique case of higher smooth-tire friction than ribbed-tire friction was exhibited by the pervious concrete cells. This phenomenon has been attributed to higher hysteretic friction in the smooth tire that provides more tire-to-surface contact than the ribbed tire. Friction numbers in the pervious pavements appear to be generally high and within the 65 to 80 percentile range.

#### INTERNATIONAL ROUGHNESS INDEX

International roughness index was measured using the light weight profiler and analyzed with the FHWA PROVAL program. On each test date, three measurements were taken in each of the 4 lanes of the MnROAD facility. The single files were then cropped into test cell (corresponding to the starting and ending stations of each of the test cells) an average of three runs was then recorded and plotted against the day of testing.

Figures 4.233 to 4.251 show the IRI measured in each of the test cell. Evidently, IRI is not merely a texture dependent feature but is indicative of performance of the pavement as a whole. It is also dependent on the season. The test cells are therefore not discussed in terms of texture type but on the design and load history on the cells.

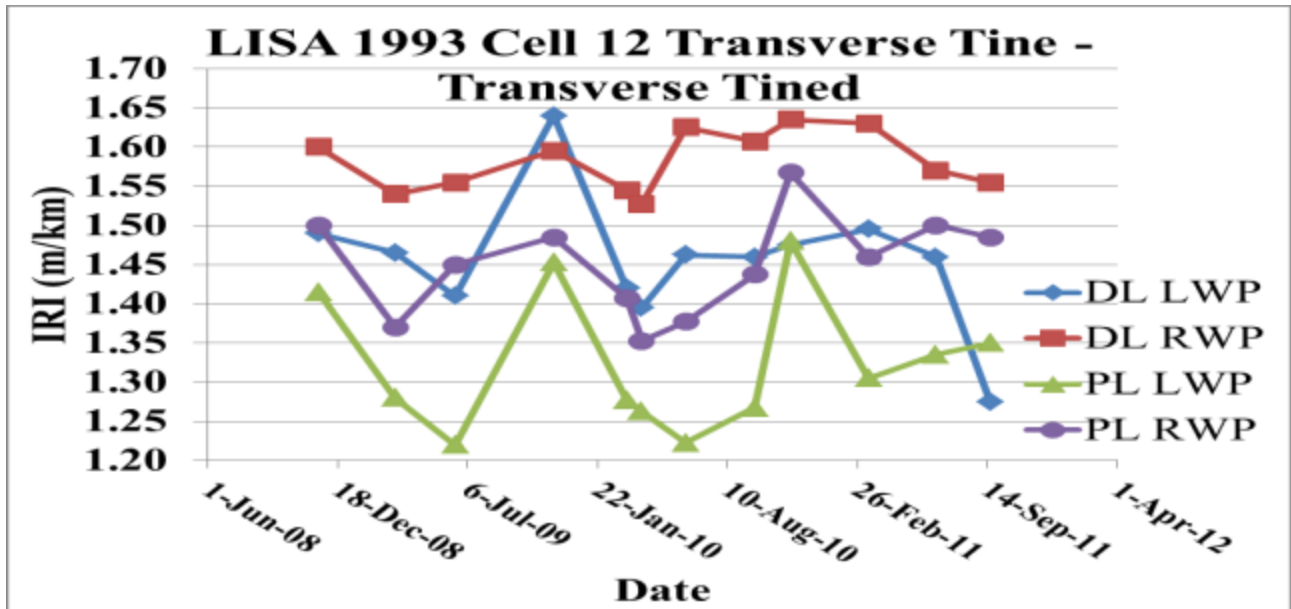


Figure 4.72: IRI of a Transverse Tined Textured Cell (1993 Cell 12 Transverse Tine - Mainline)

1993 Cell 12 Transverse Tine is 18 years old, seasonal IRI is evident as the summer IRI is the lowest. This is because the heave, joint openings and other cold weather related distresses cause higher IRI in colder weather.

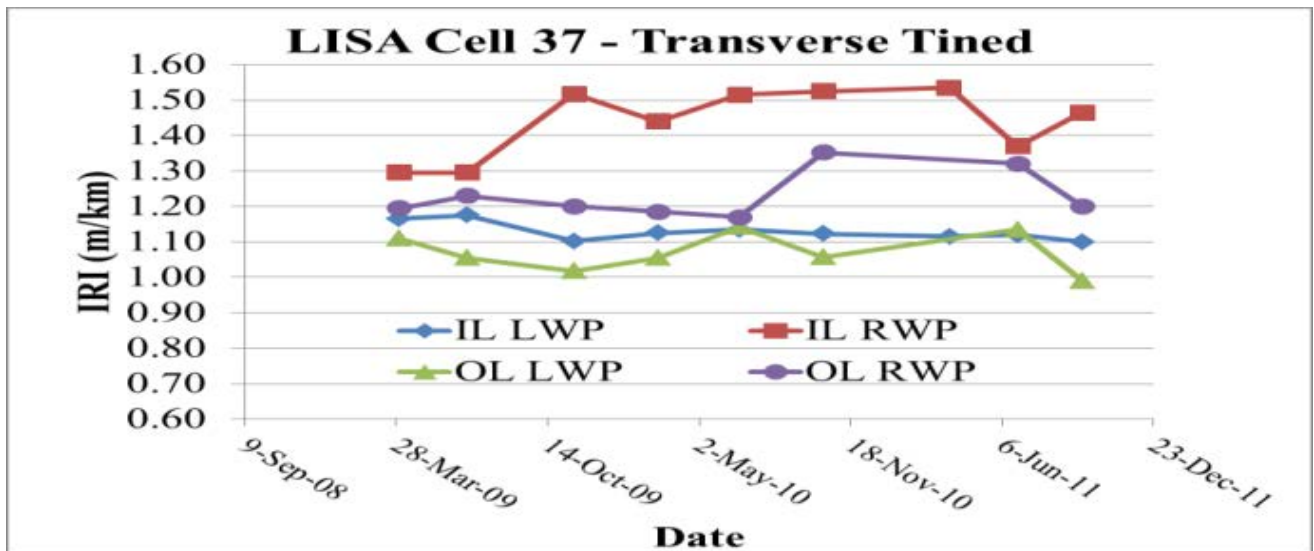


Figure 4.73: IRI of a Transverse tined Textured Cell (Cell 37 - LVR)

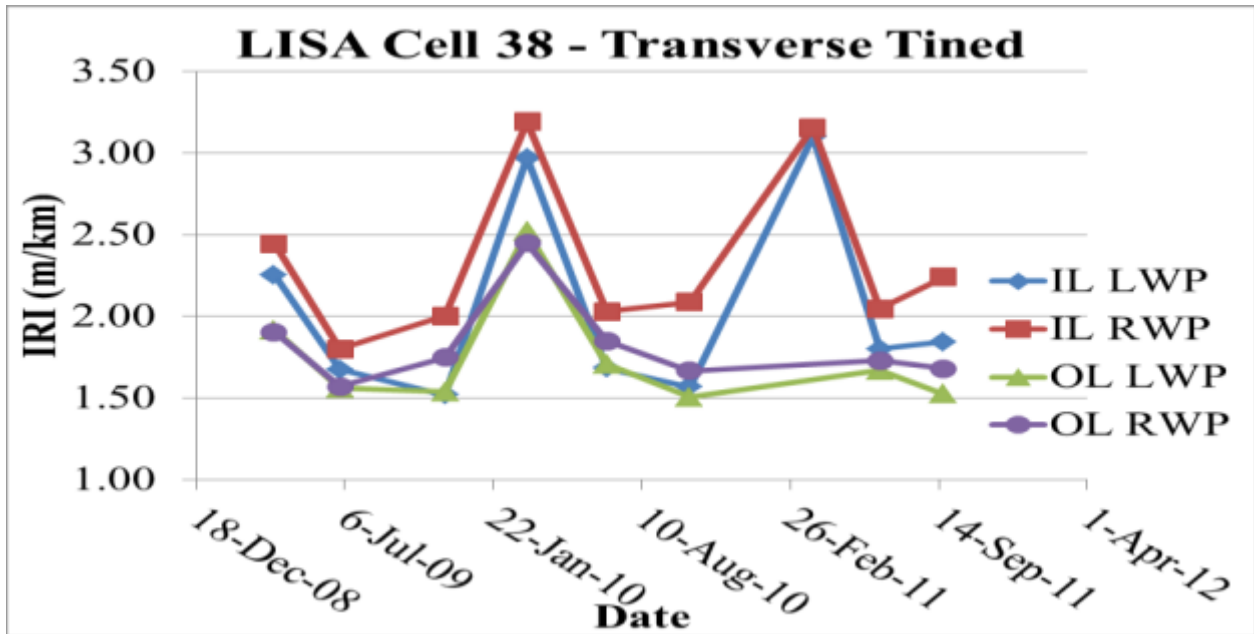


Figure 4.74: IRI of a Transverse tined Textured Cell (Cell 38-LVR)

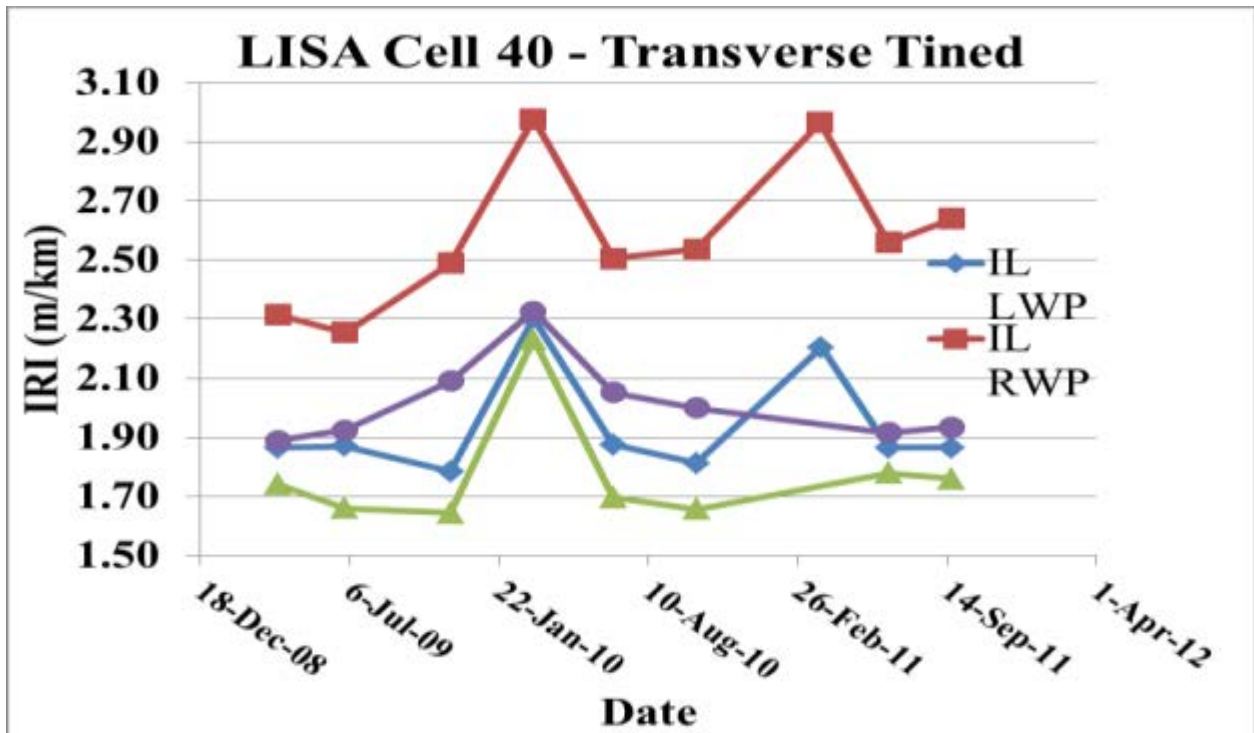


Figure 4.75: IRI of a Transverse Tined Textured Cell (Cell 40 - LVR)

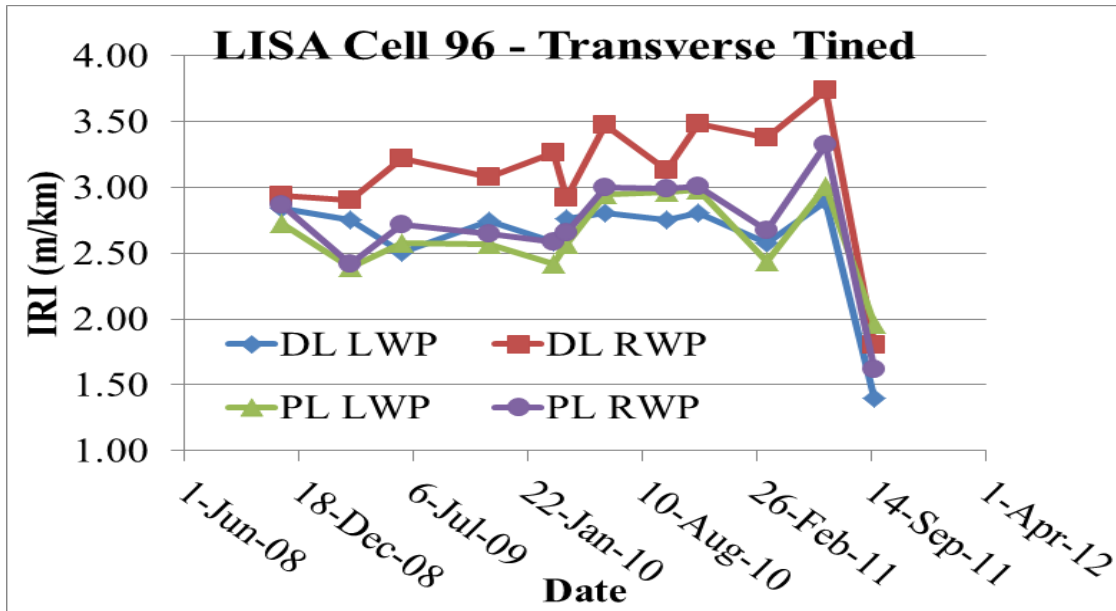


Figure 4.76: IRI of a Transverse Tined Textured Cell (Cell 96 – Mainline)

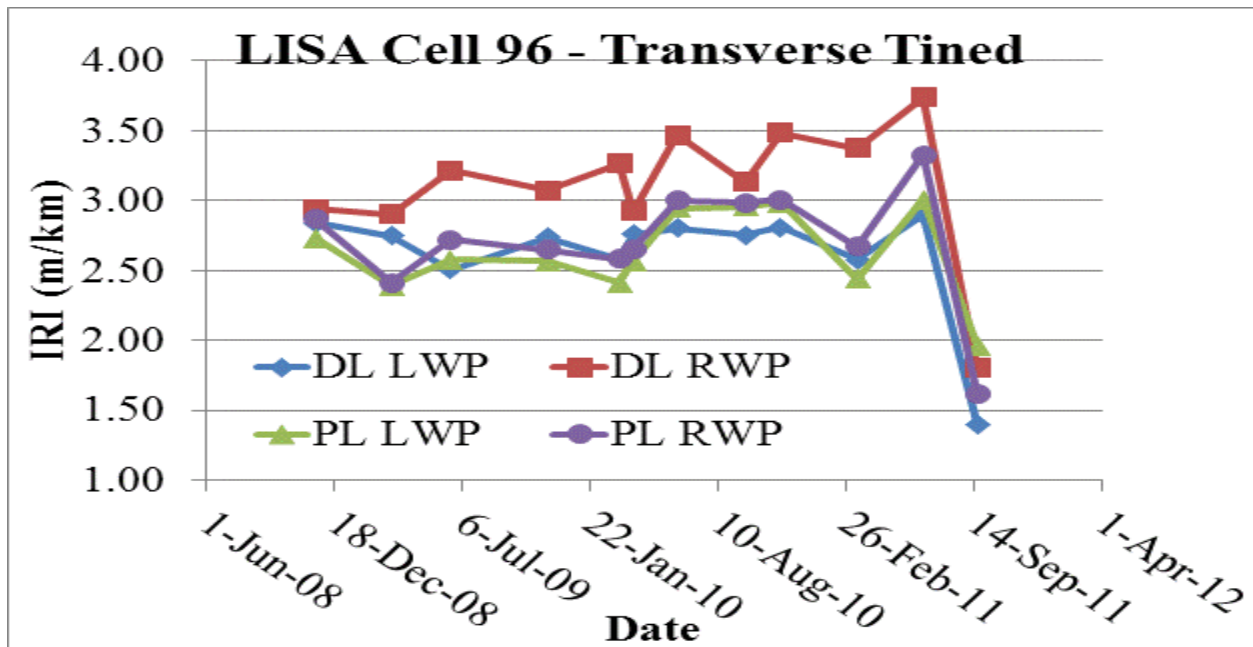


Figure 4.77: IRI of a Transverse Tined Cell that was Diamond Ground (Cell 96 – mainline)

Effect of intervention in inadequate surface property through diamond grinding was exemplified in cell 96. This transversely tined surface was ground to remove bumps dips and faulting that was contributory to the high IRI. After grinding, this was reduced to lower range of 1.4 to 1.8 from the previous range of 2.5 to 3.8 m/km.

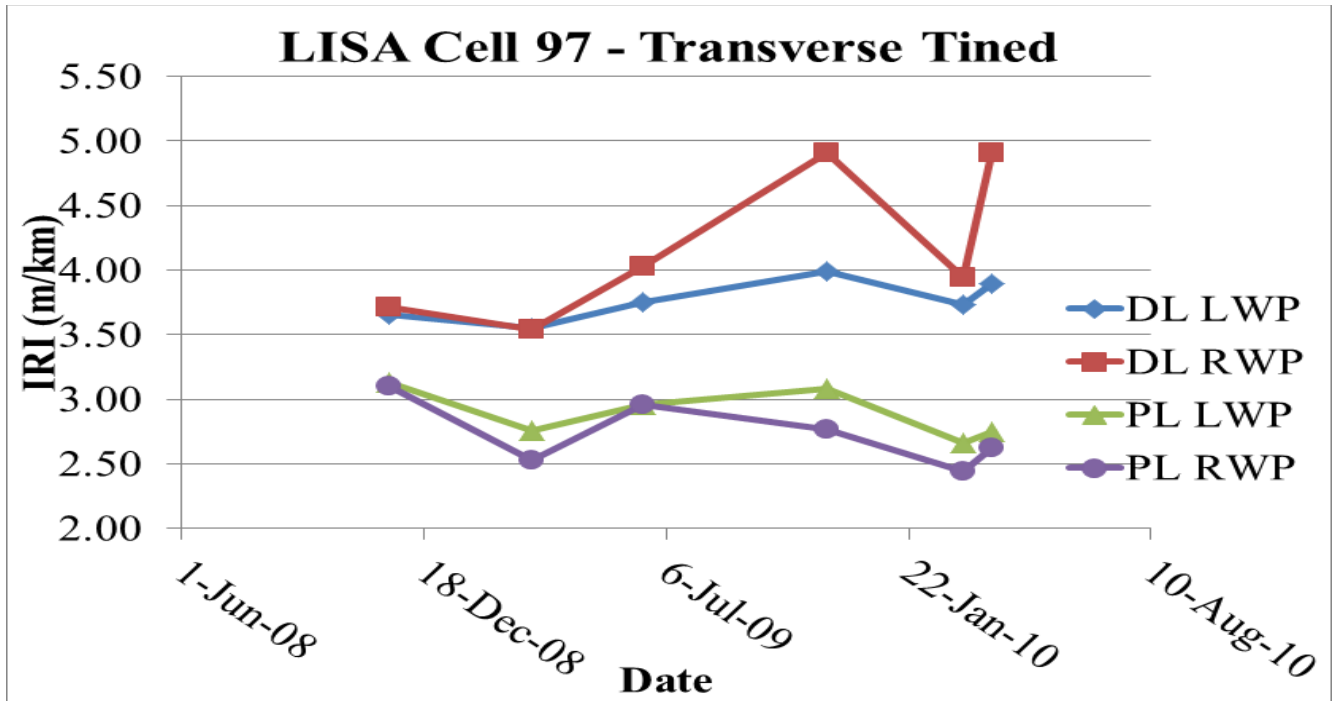


Figure 4.78: IRI of a Transverse Tine Textured Cell (Cell 97 – mainline)

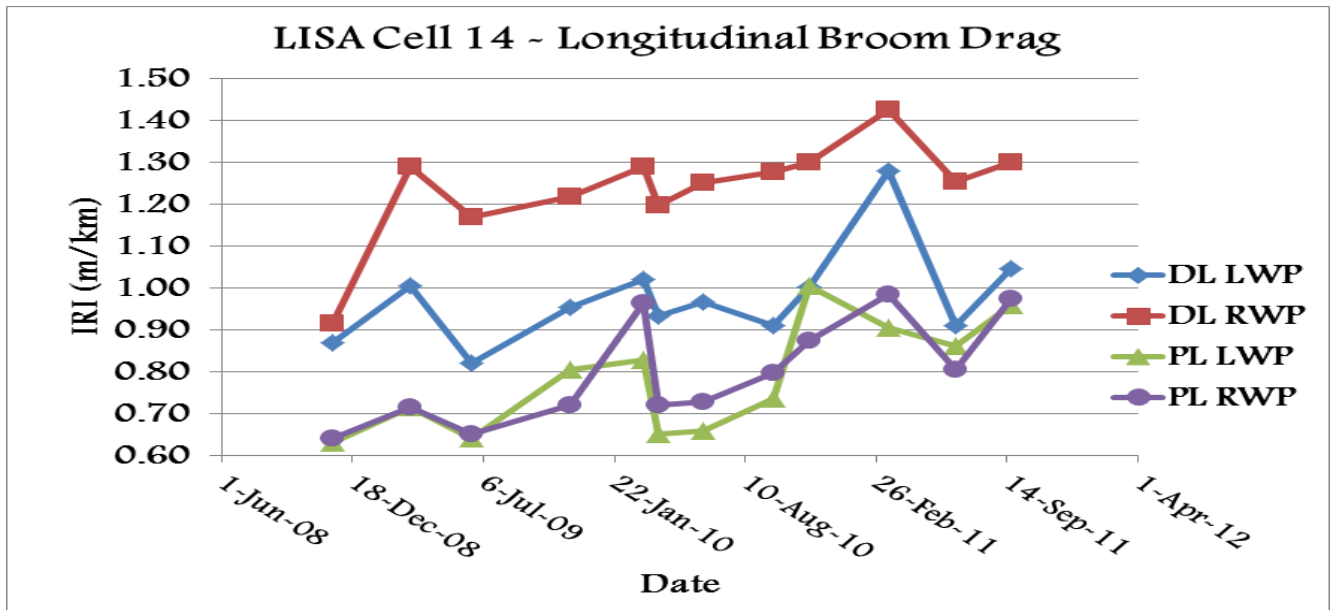


Figure 4.79: Longitudinal drag Test cell (Cell 14 – Mainline).

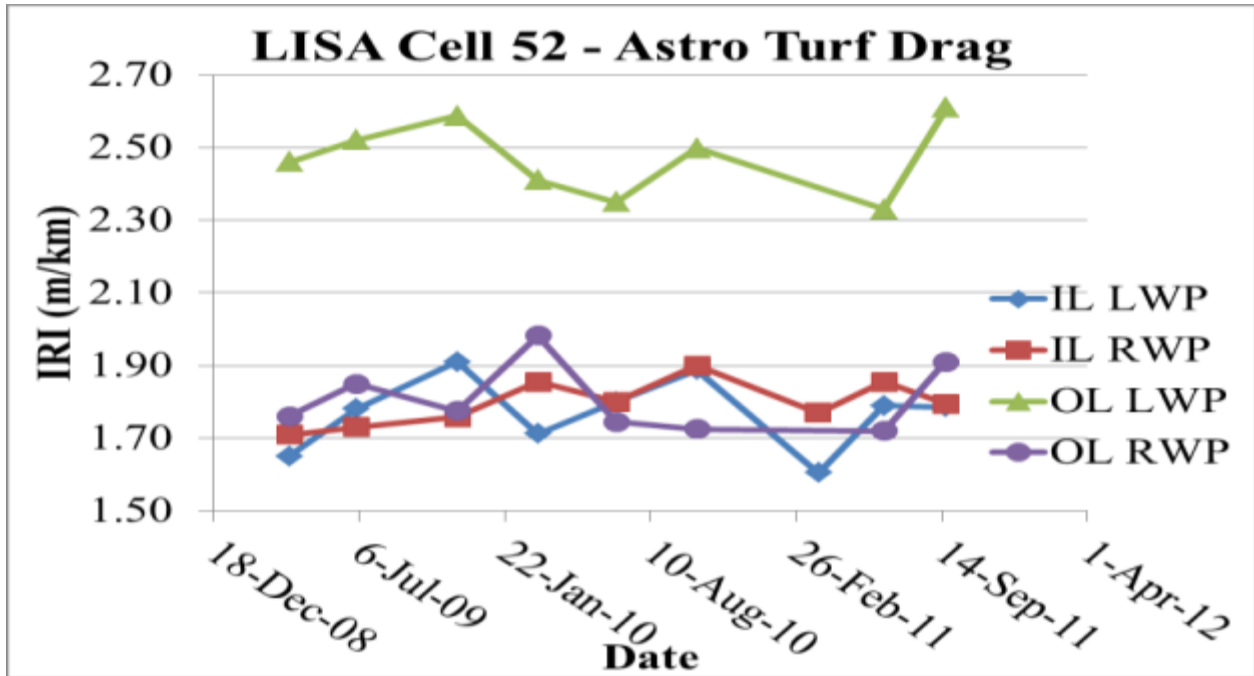


Figure 4.80: IRI of a Drag Textured Cell (Cell 52 – LVR)

While the above cell exhibits somewhat constant IRI if seasonally detrended, there is an anomalous difference in one of the wheel paths. There is no longitudinal crack neither is there a missing line of dowels or a deteriorated set of transverse joints to provide a plausible explanation for the disparity as at the time of this report.

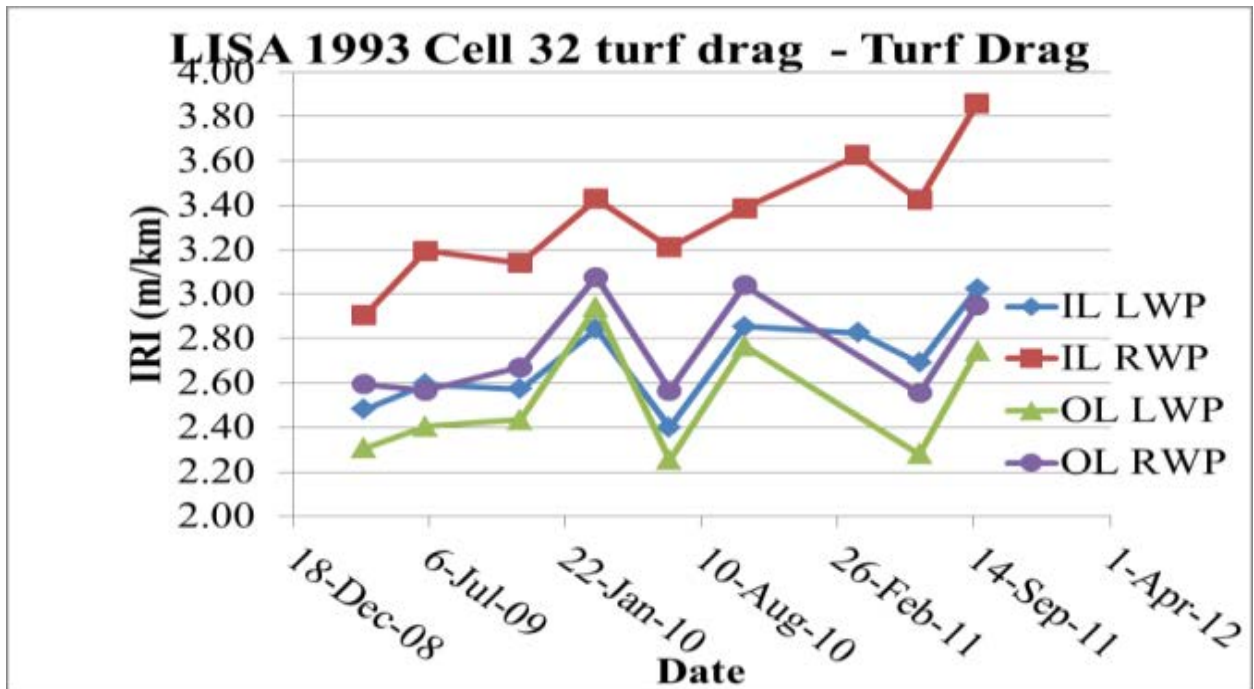


Figure 4.81: IRI of a Drag Textured Cell (1993 Cell 32 Turf Drag – LVR)



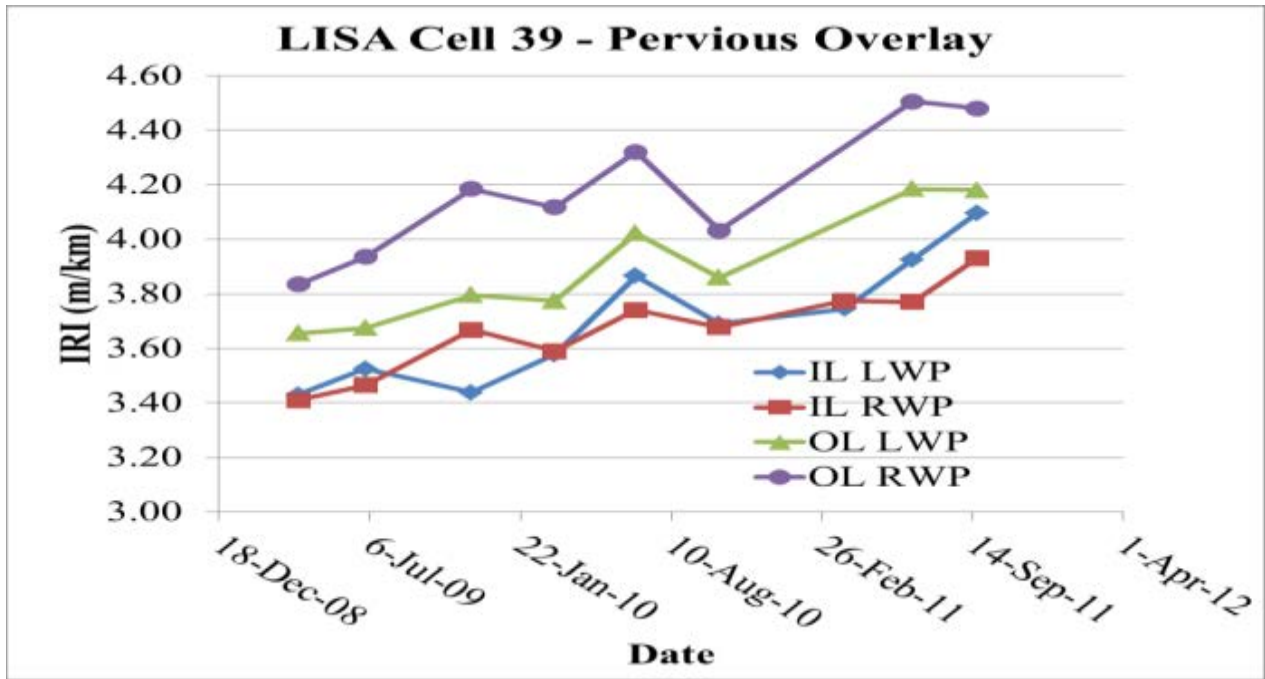


Figure 4.82: IRI of Pervious Concrete Overlay Cell (Cell 39 – LVR)

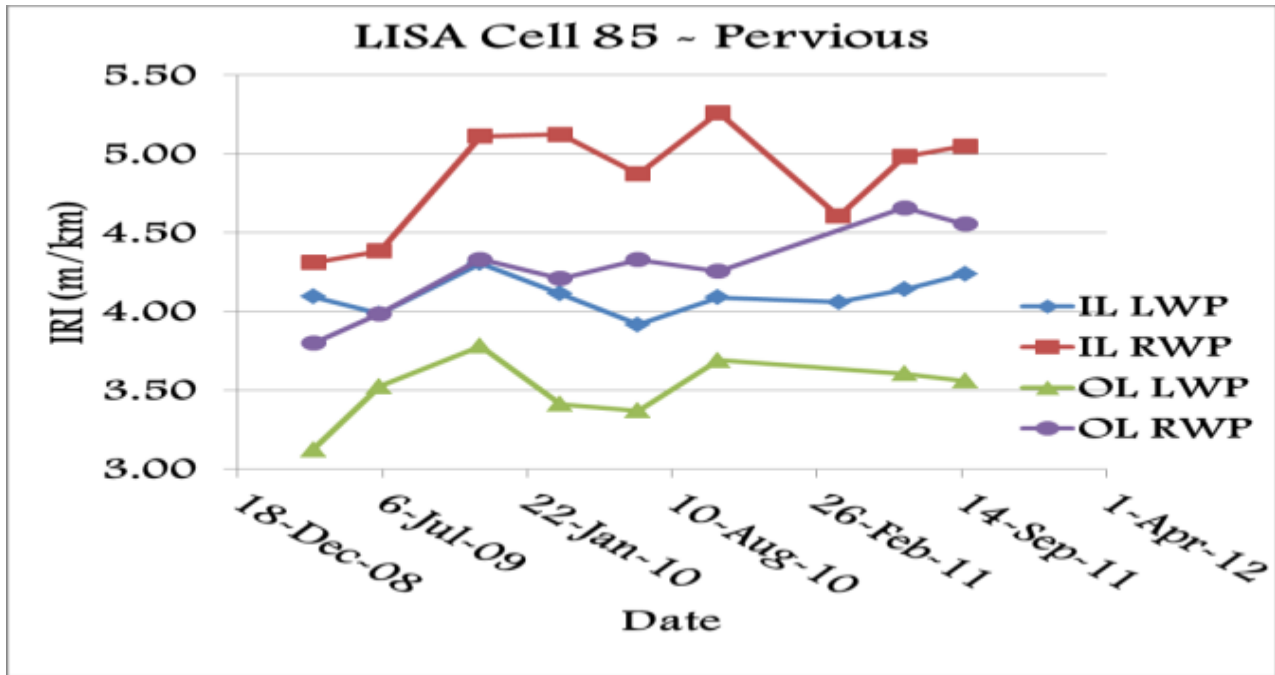


Figure 4.83: IRI of a Pervious Concrete Cell on Sand Subgrade (Cell 85 – LVR)

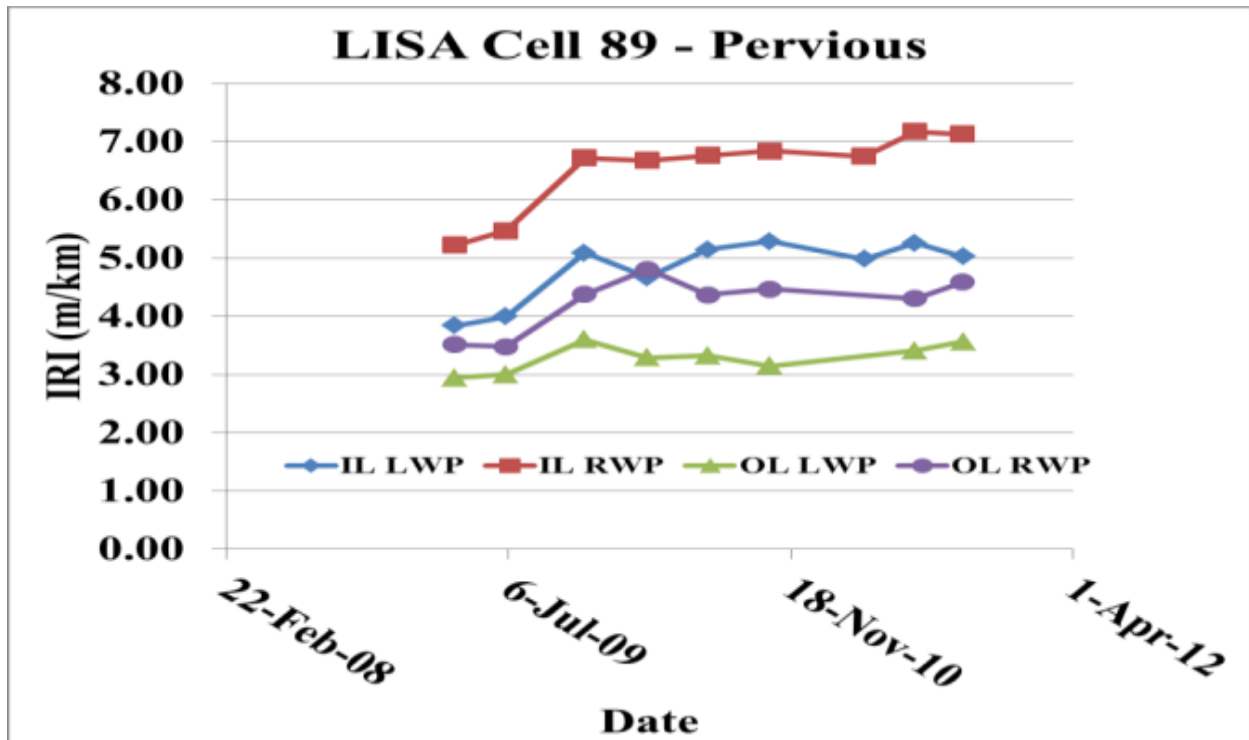


Figure 4.84: IRI of a Pervious Concrete Cell Built on Clay Subgrade (Cell 89 – LVR)

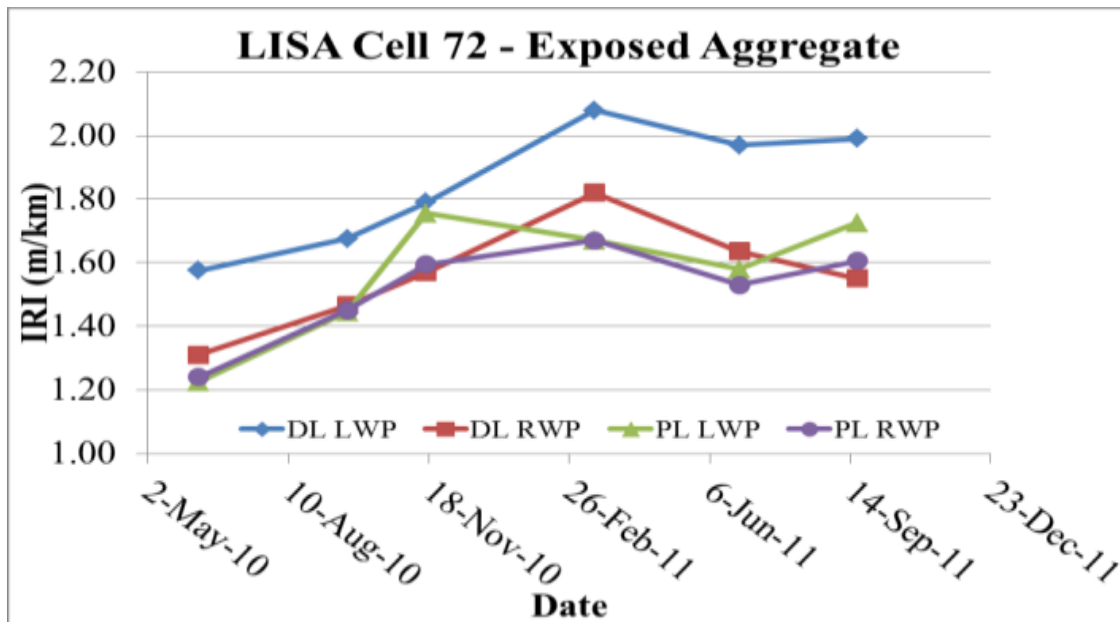


Figure 4.85: IRI of an Exposed Aggregate Textured Two Lift Concrete Cell (Cell 72 – mainline)

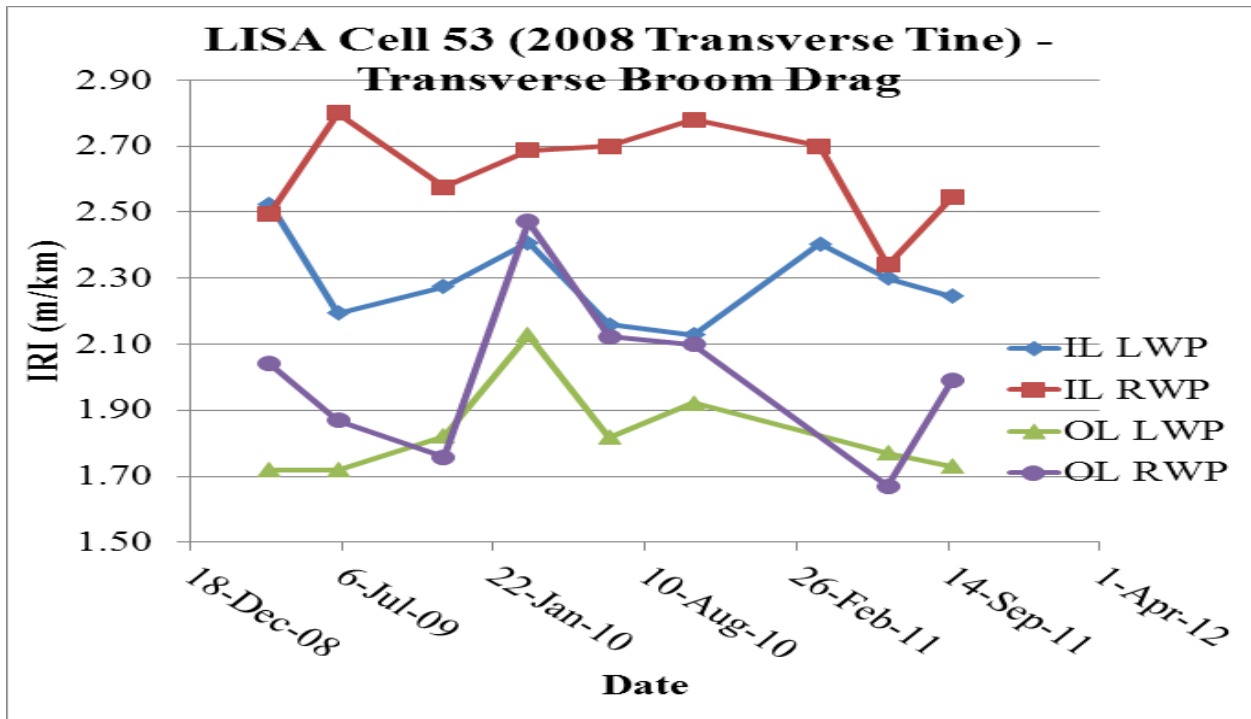


Figure 4.86: IRI of a 60 Year Design – Transverse Broom Drag Cell (Cell 53 (2008 Transverse Tine) – LVR)

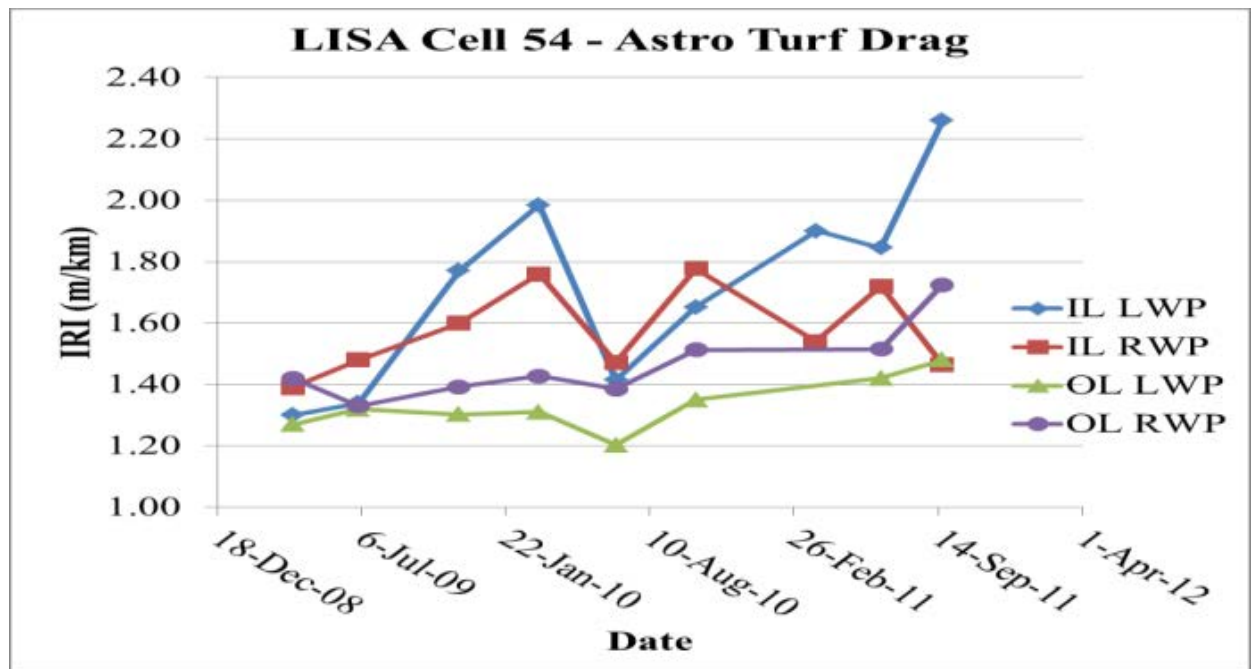


Figure 4.87: IRI of A taconite aggregate Drag Textured Cell (Cell 54 turf drag – LVR)

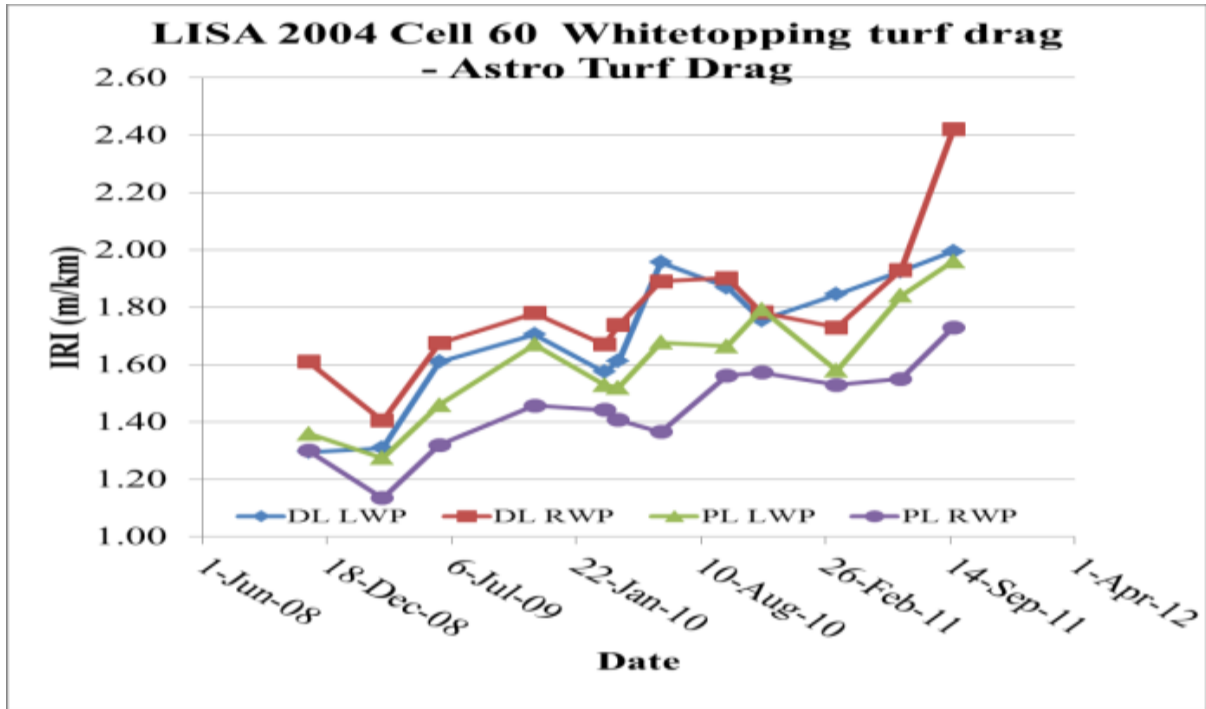


Figure 4.88: IRI of a Turf dragged Whitetopping Cell (2004 Cell 60 Whitetopping turf drag – mainline)

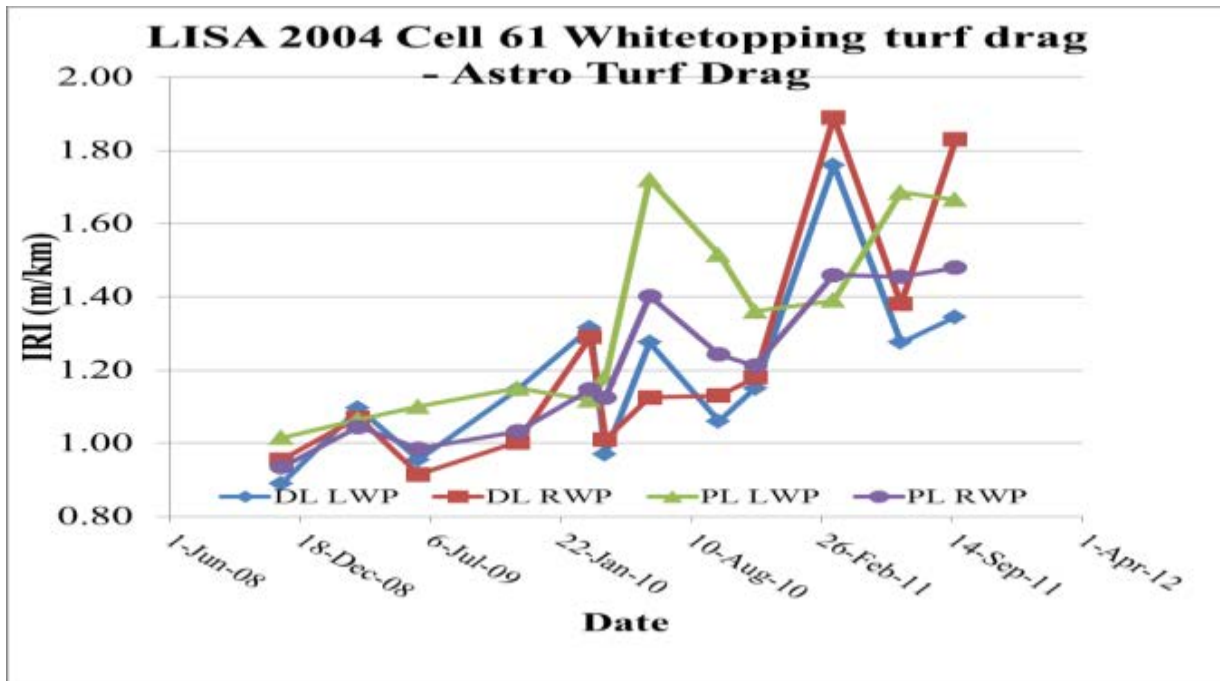
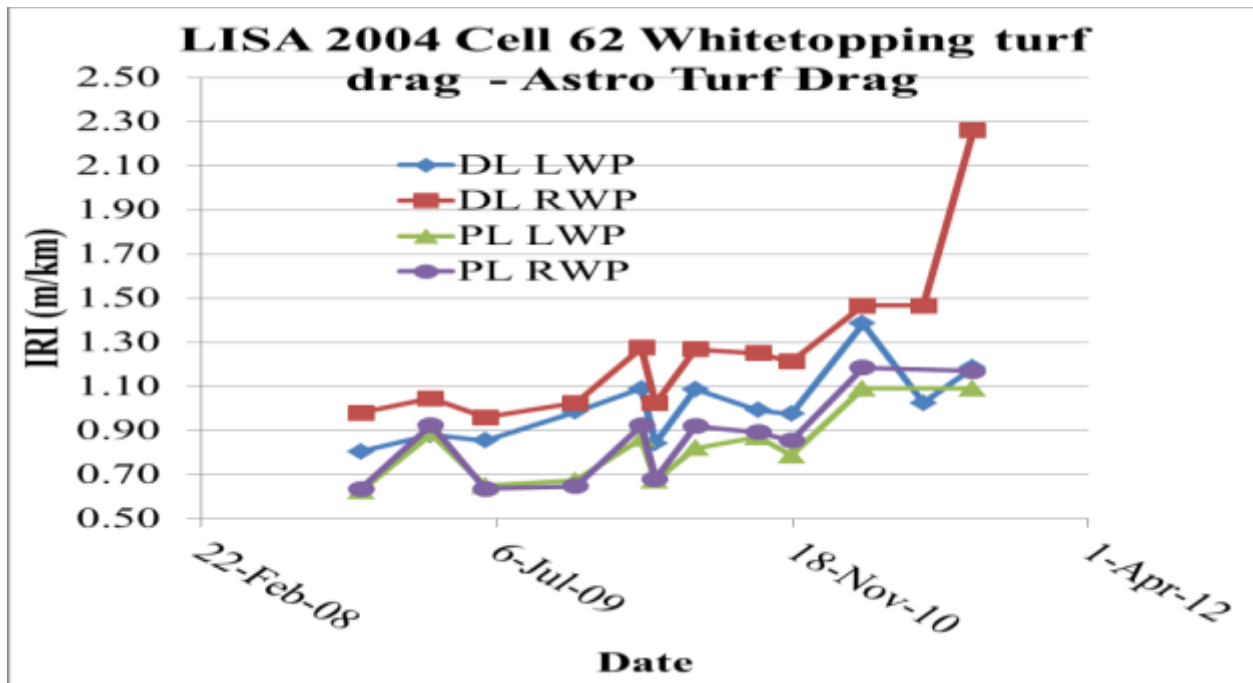


Figure 4.89: IRI of a Turf dragged Whitetopping Cell (2004 Cell 61 Whitetopping Turf Drag – Mainline)



**Figure 4.90: IRI of a Turf dragged Whitetopping Cell (2004 Cell 62 Whitetopping turf drag – mainline)**

### SOUND ABSORPTION

In task 3 the process and equipment for conducting sound absorption testing was developed and calibrated. This method was based on a modification of ASTM E 1050 method of measuring sound absorption coefficient of the pavement surface. For continuity and consistency, test locations were marked on some test cells and in each test day many sound absorption test were conducted and recorded. The data was centered on each of 8 one third octave frequencies starting from 315 Hertz (315, 397, 500, 630, 794, 1000, 1260, 1588 Hz). The sound absorption coefficients across the 8 one-third octave frequencies were recorded in the Database. However, the sound absorption series in this report were those at 1000 Hz for many reasons. According to Sandberg (2005) there is a multi-coincidence of tire pavement noise sources at 1000 Hz frequency. Secondly this is the known frequency at which the tire pavement interaction, experiences tire resonance. Thirdly Izevbekhai (1987) observed peak absorption properties of a Portland cement based material. Lastly, Izevbekhai and Akkari (2012) reported Sound absorption frequencies at 1000 Hz since the most absorbent at all frequencies are also absorbent at 1000 Hz. For convenience OBSI has a defined singular value but SA does not seem to have one, It is not loosely defined in terms of a range of frequencies but these to an unless there is a mathematical algorithm relating the individual SA value, most practitioners will either use SA<sub>(1000)</sub> or provide their own definition.

Non-pervious concrete has low SA values exemplified by Figure 4.252 and 4.253. The variation in SA values across the cell is due to the degree of degradation of the concrete in each location, errors arising from the integrity of seal at the interface of the impedance tube and concrete surface. There appears to be huge variability between the 2 test dates but in any case non-pervious concrete SA seldom exceeds 0.1.

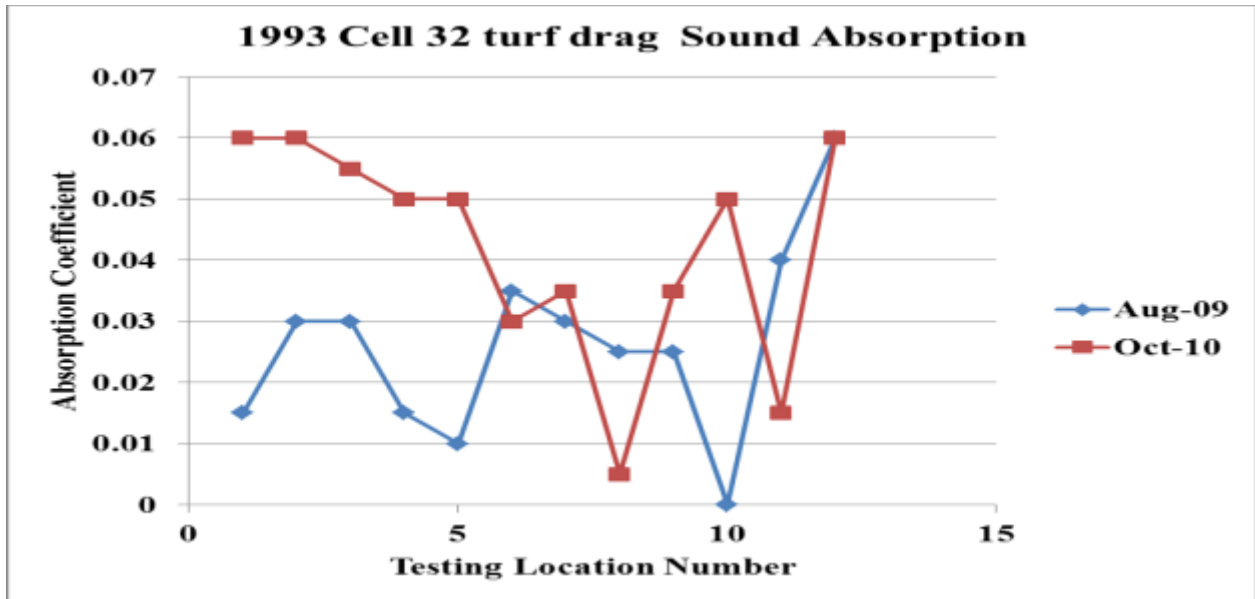


Figure 4.91: Sound Absorption of a Non-Pervious Concrete Cell (1993 Cell 32 turf drag – LVR)

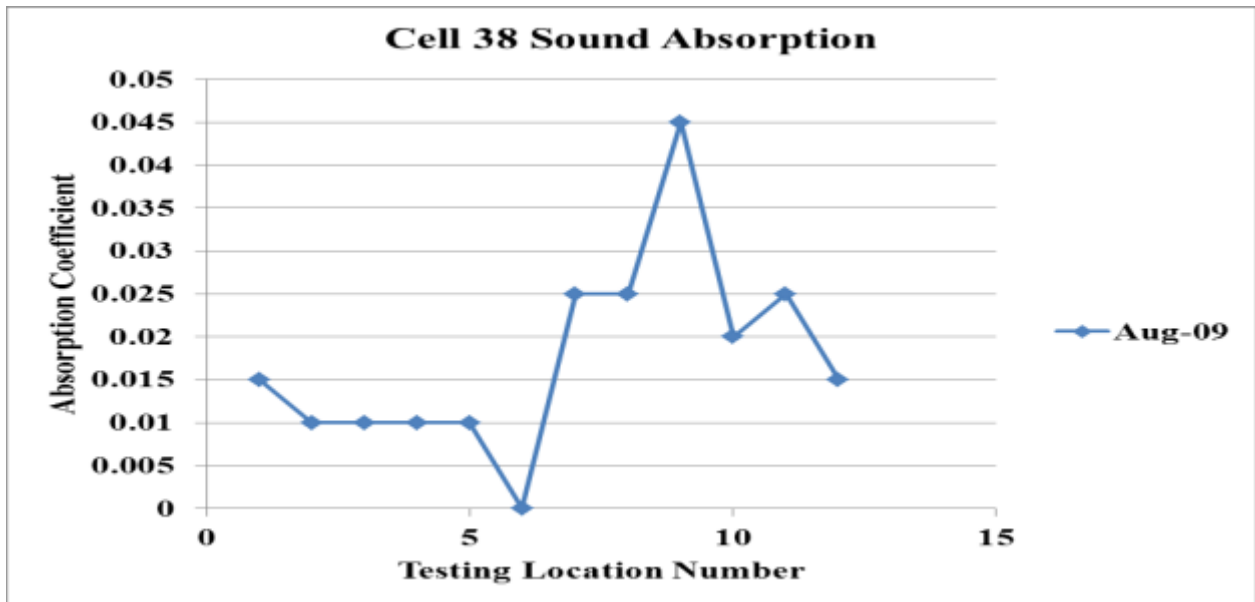


Figure 4.92: Sound Absorption of a Non-Pervious Concrete Cell (Cell 38 – LVR)

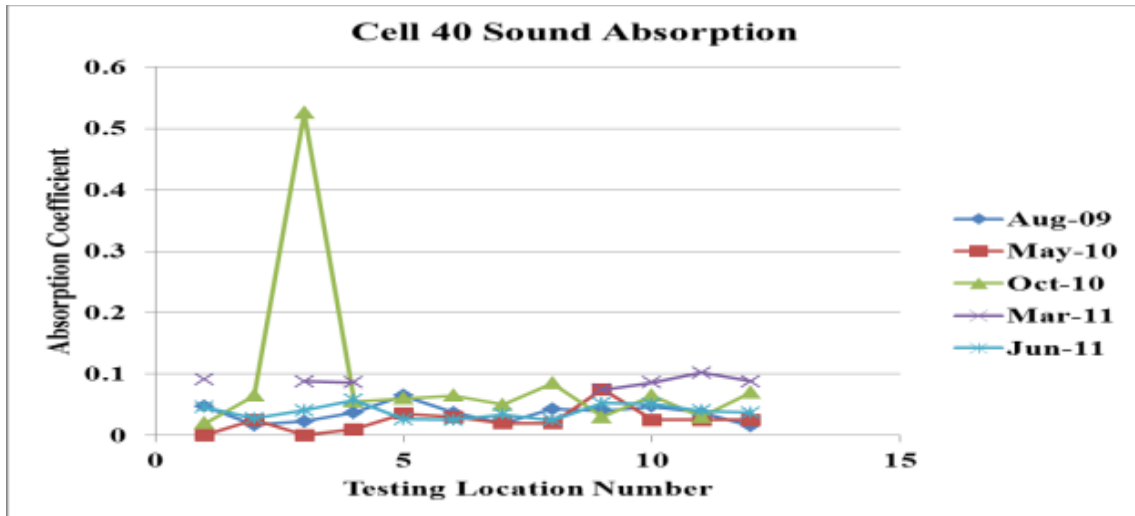


Figure 4.93: Sound Absorption of a Non-Pervious Concrete Cell (Cell 40 – LVR)

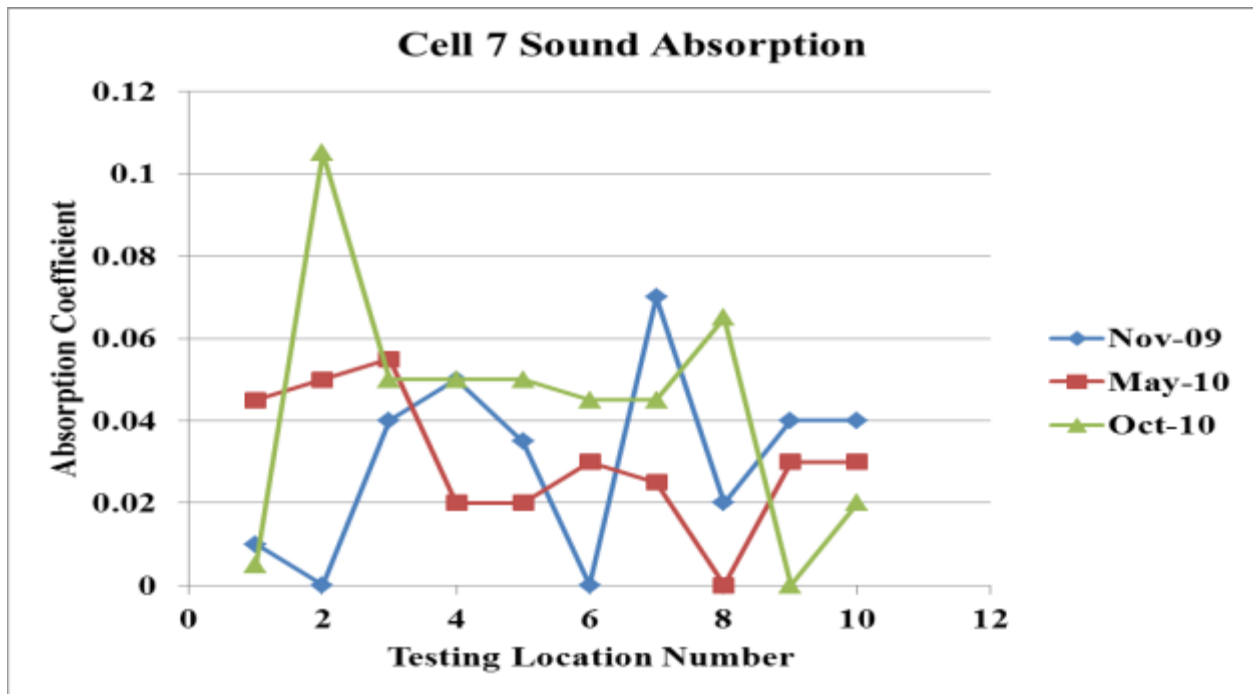


Figure 4.94: Sound Absorption of a Non-Pervious Concrete Cell (Cell 7 – mainline)

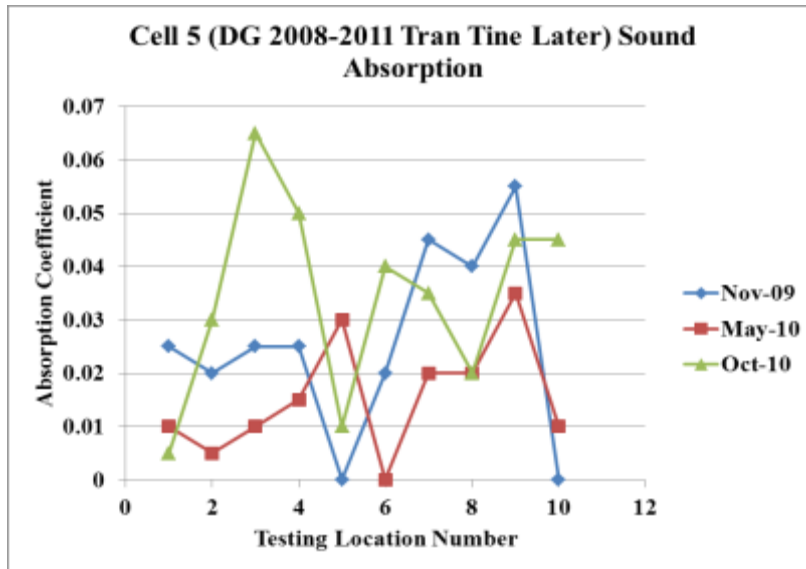


Figure 4.95: Sound Absorption of a Non-Pervious Concrete Cell (Cell 5 (DG 2008-2011 Tran Tine Later – mainline)

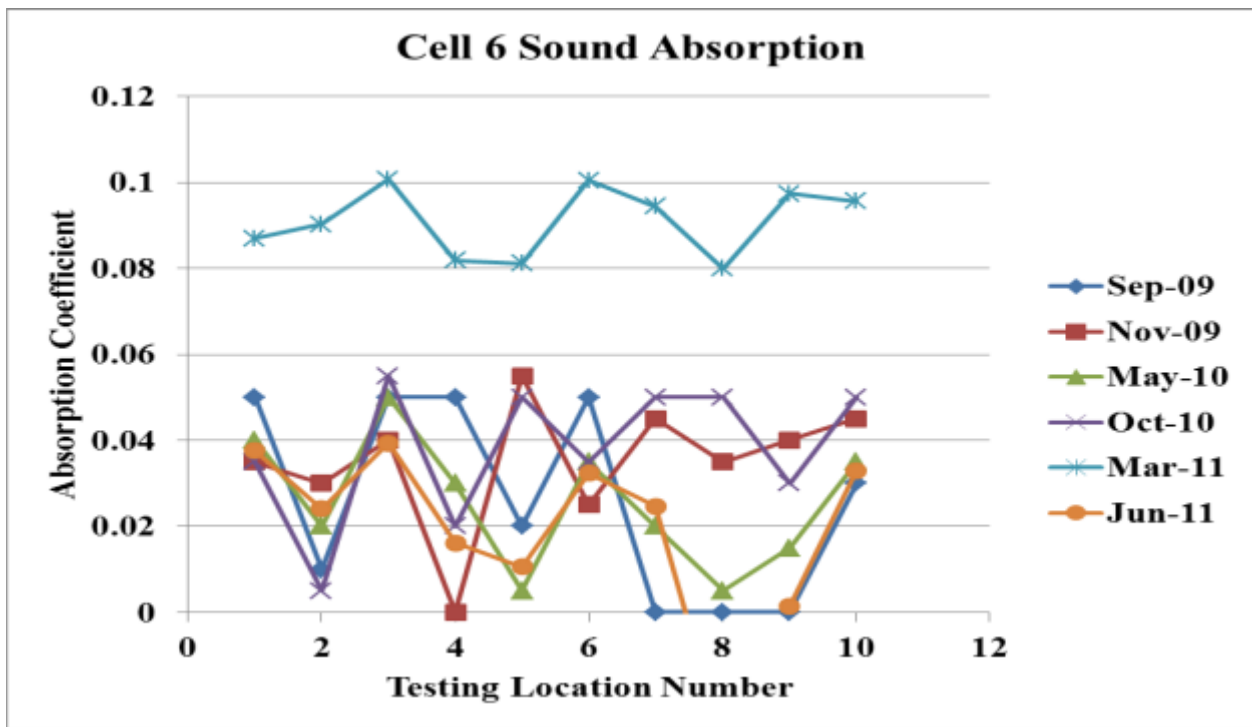


Figure 4.96: Sound Absorption of a Non-Pervious Concrete Cell (Cell 6 – mainline)



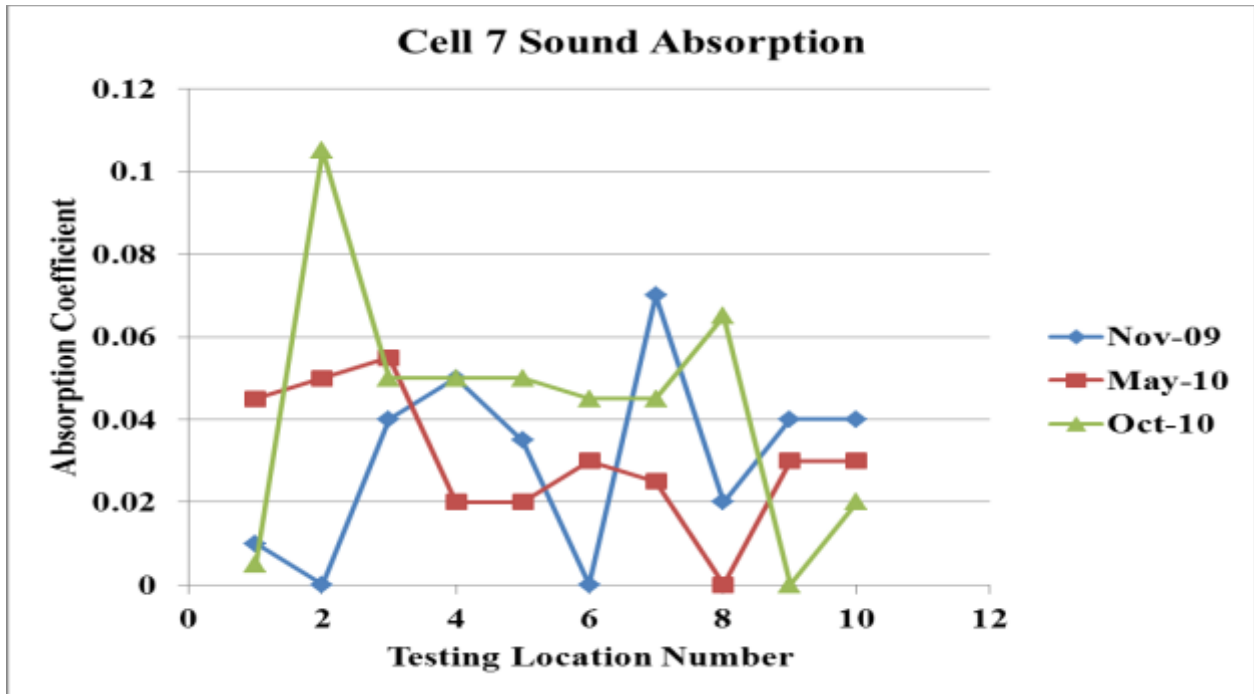


Figure 4.97: Sound Absorption of a Non-Pervious Concrete Cell (Cell 7 – mainline)

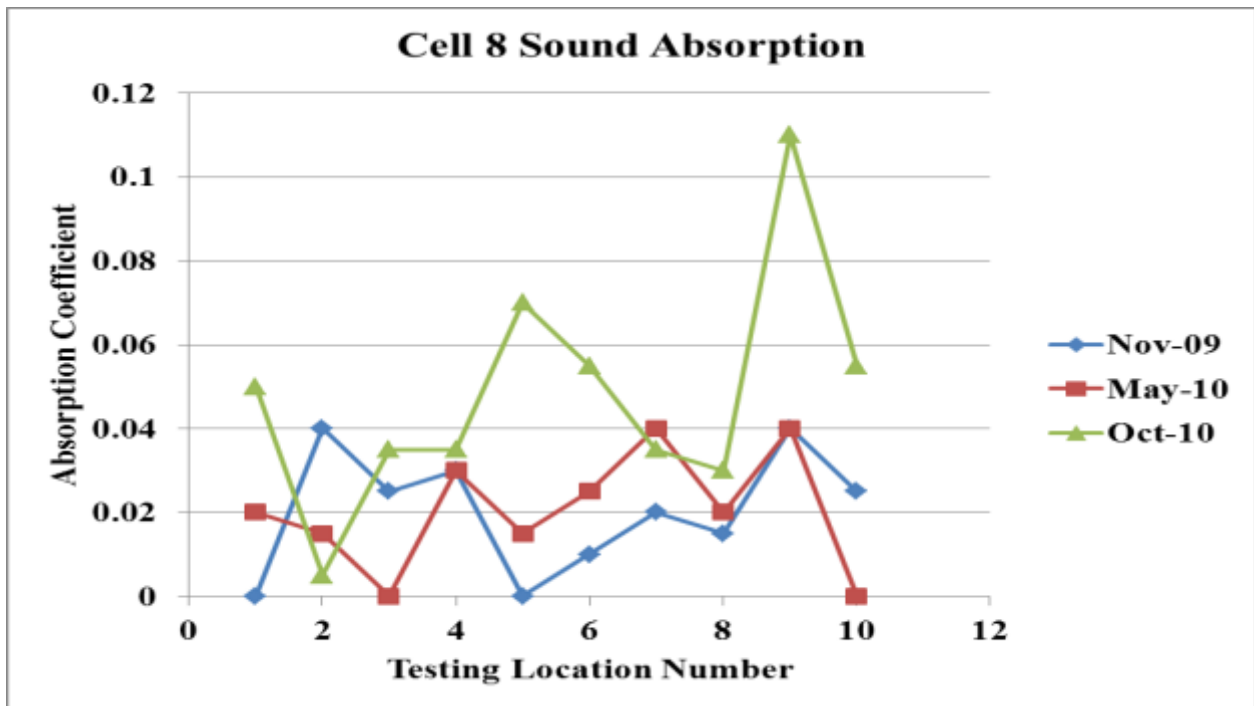


Figure 4.98: Sound Absorption of a Non-Pervious Concrete Cell (Cell 8 – mainline)

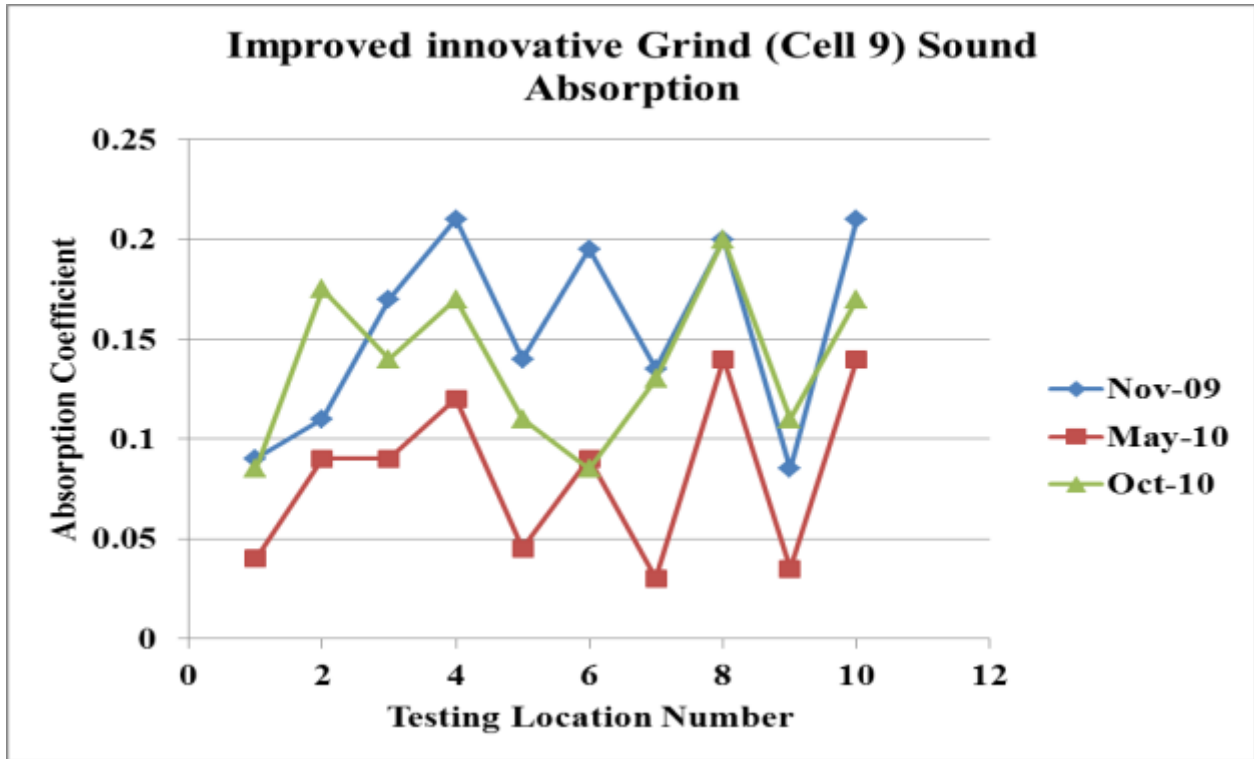


Figure 4.99: Sound Absorption of a Non-Pervious Concrete Cell (Cell 9 – mainline)

There is a likelihood that the seal at the tube, concrete interface was not sure as the grooves in the cell were narrow and deep. The values obtained in this cell are high for a non-pervious cell but not reliable.

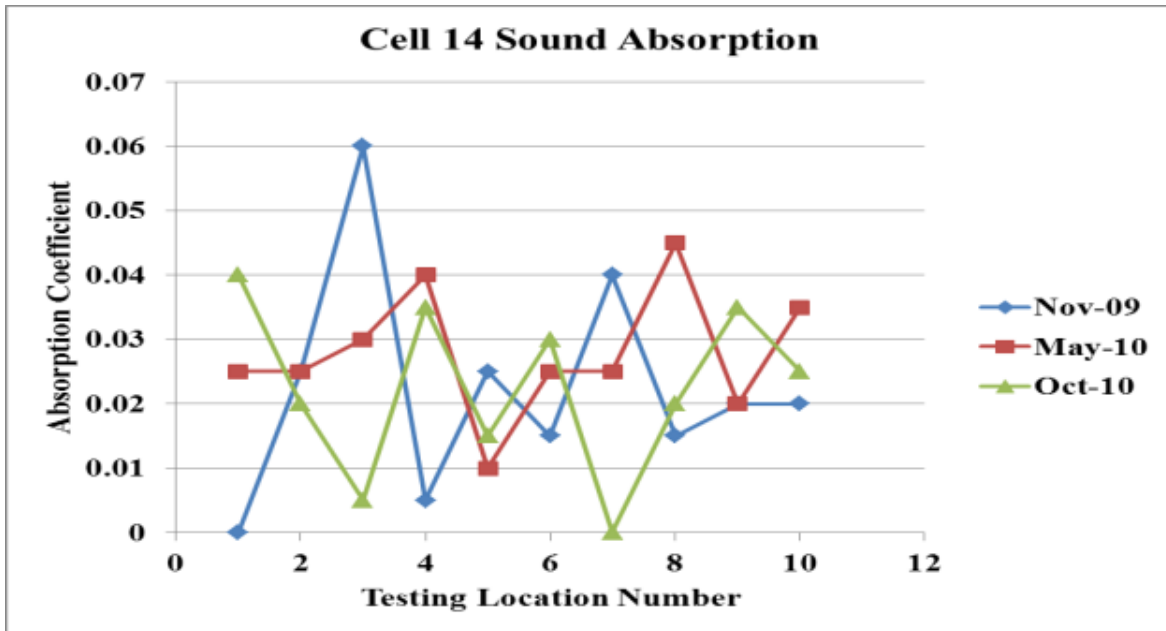
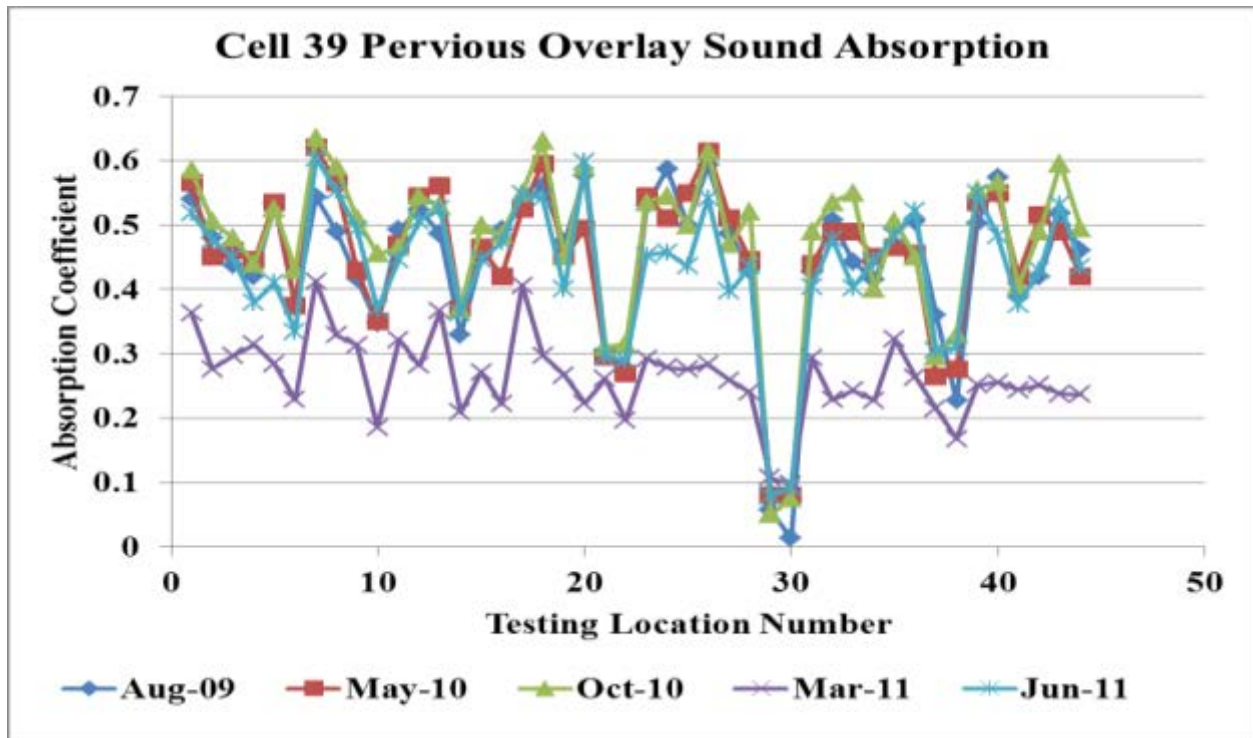


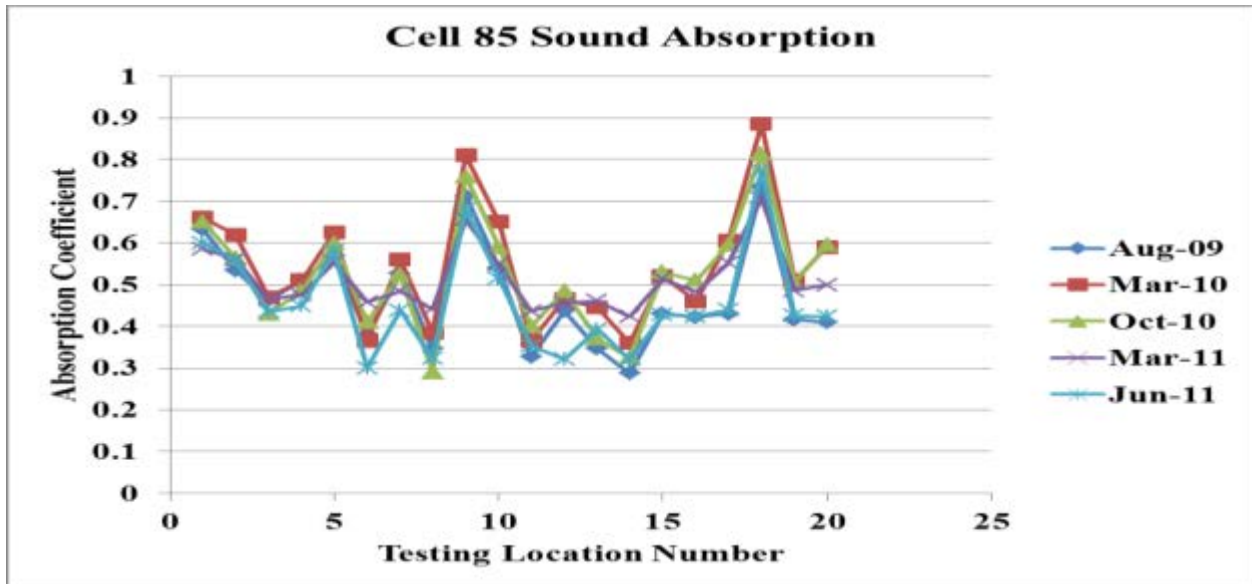
Figure 4.100: Sound Absorption of a Non-Pervious Concrete Cell (Cell 14 – mainline)



**Figure 4.101: Sound Absorption of a Pervious Concrete overlay Cell (Cell 39 – LVR)**

Evidently the sound absorption value in this cell is much higher than those observed in normal concrete. This cell was a 4 inch pervious concrete on a normal concrete substrate. The porosity and durability of this cell was enhanced by the addition of poly olefin mechanical fibers and cellulosic chemical fibers to enhance bond and improve absorption. Ordinarily it was expected to provide improved SA in comparison to the other pervious cells but this would not be possible unless the following conditions are true.

- 1) The thickness of the pervious overlay exceeds the depth at which sound absorption is effective.
- 2) Reflection from a substrate is so small and inconsequential that it plays no significant role in the SA value.
- 3) Fibers improve tortuosity without reducing void content. Tortuosity (which is higher in a fiber based matrix) being improved will increase sound absorption.



**Figure 4.102: Sound Absorption of a Pervious Concrete overlay Cell (Cell 85– LVR)**

It was evident that:

- 1) Full depth pervious concrete (Cell 85 and 89) was designed conceptually to have communicating voids. This design guarantees lesser clogging and more conduction of fines into the lower layers.
- 2) The conduction of fines into lower layers allows potential clogging agents to go through the concrete instead of be lodge within it. It was this concept hat informed the rejection of the idea of as choker layer during the design.
- 3) Unlike cell White topping cell 64 that was remarkable clogged in certain spots, cell 89 had more open structure that enhanced higher sound absorption
- 4) Pervious Cell 85 outperforms pervious cell 89 because the latter has a clay subgrade that may inhibit rapid hydraulic conductivity and in consequence a longer detention period in the concrete base system resulting in more deposit of particles causing more clogging and less sound absorption coefficient.

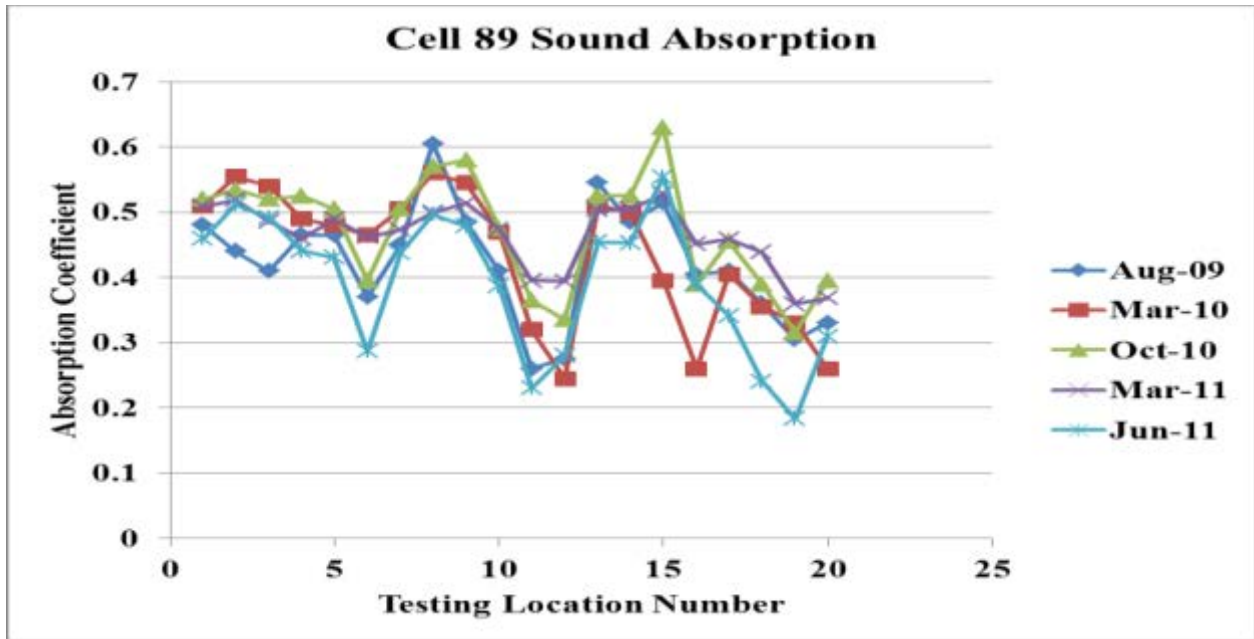


Figure 4.103: Sound Absorption of a Pervious Concrete Overlay Cell (Cell 89 – LVR)

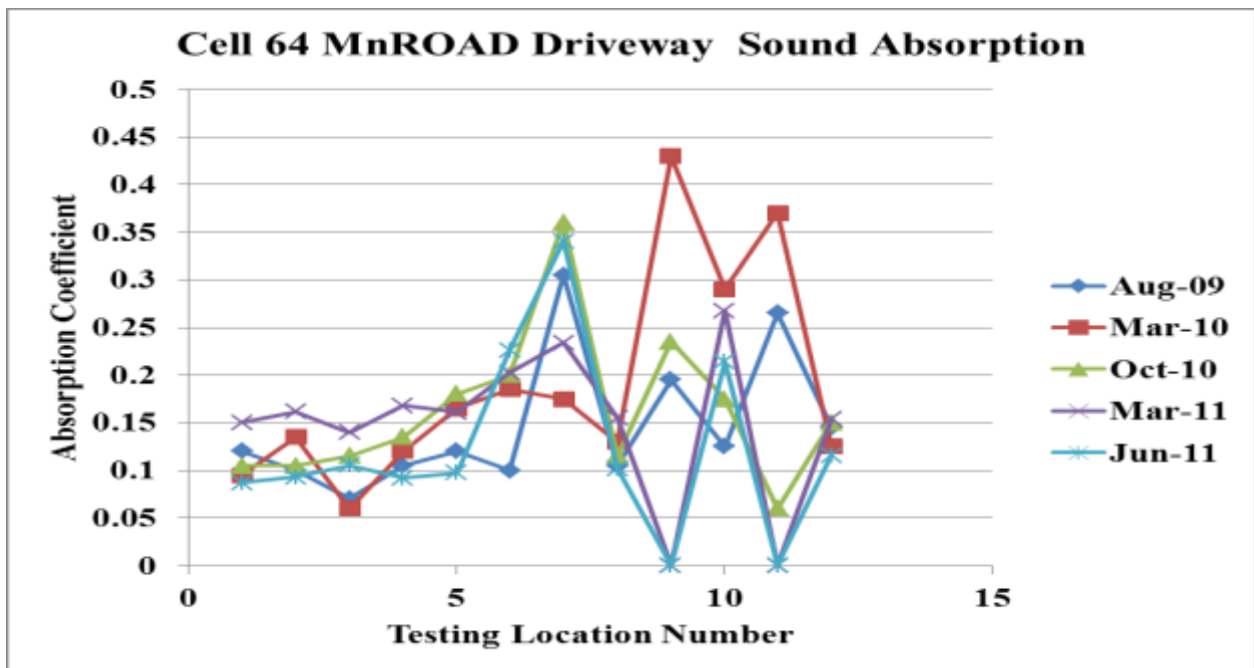


Figure 4.104: Sound Absorption of a Pervious Concrete overlay Cell (Cell 64 – Parking Lot)

**SECTION SUMMARY**

Data for 4 years show the trend of friction, IRI and sound absorption (SA). It appears that monitoring of SA will not be beneficial in non-pervious pavements because there is not much observable or detectable variability with non-pervious pavements. Texture and friction degradation are analyzed in tasks 4 and 5. It is possible to show Time Series and Probability

Density Function of OBSI which has a robust data set and to use Weibull distribution methods for analysis.

### **4.3 Autoregressive Integrated Moving Average Arima and Probability Density Function for MnRoad Surface Characteristics Data**

#### **Background**

This report analyzes the first 4 years of performance of some new surface textures in some test cells at MnROAD and presents some selected variables in time series and probability density function. The report shows data series with respect to time and data series in 5 years and the same data interpreted by way of likelihood of attaining a certain level of surface characteristics. That method is explained as it is a means of circumventing certain environmental and other periodic trending factors to still describe the data referenced to a standard or threshold. It is also a very important tool in setting design goals.

This task discussed the trend of surface characteristic with respect to time. The variables discussed include: Mean profile depth (ASTM E-2157, Friction (ASTM E -274, International Roughness Index IRI (ASTM E-950 and Sound absorption ASTM E-1050 Modified for in-situ testing. OBSI (AASHTO TP 76-09 is discussed under a separate report.

#### **Data Trend with Time and Time Series Analysis**

Results of surface characteristics data obtained in the various cells are plotted with respect to time in each of the cells. Appendix 1 shows the various textured surfaces for the cells. Other supporting data include traffic data, and weather data that are available in the MnROAD Data base.

#### **Introduction**

Models for time series data can have many forms and represent different stochastic processes. When modeling variations in the level of a process, three broad classes of practical importance are the autoregressive (AR) models, moving average (MA) and integrated [4.2] models. These three classes depend linearly on previous data points. Combinations of these ideas produce Auto Regressive Moving Average Integrated (ARIMA) models. An additional set of extensions of these models is available for use where the observed time-series is driven by some "forcing" time-series (which may not have a causal effect on the observed series): the distinction from the multivariate case is that the forcing series may be deterministic or under the experimenter's control.

Non-linear dependence of the level of a series on previous data points has the propensity to create chaotic time series. However, more importantly, empirical investigations of the type in this study of surface properties can indicate the advantage of using predictions derived from non-linear models, over those from linear models but this study will examine only linear models and stationary states.

Among other types of non-linear time series models, there are models to represent the changes of variance over time. This concept is referred to as homoscedasticity accentuates the phenomenon where residuals are truly random. Stationary **process** is described as a stochastic process where

the probability density function (PDF) is reasonably consistent in time whereupon mean and variance would not change with time. This property is referred to as stationarity [4.2] and [4.3]. There are processes in which every sequence or sizable sample is equally representative of the whole (as in regard to a statistical parameter or the probability that any state will re-occur or that there is a zero probability that any state will never re-occur. This concept is called ergodicity. When the time average of a process is equal to the ensemble average, it is said to be **ergodic**. Our simple model process is ergodic by definition. It is obviously very powerful and convenient to be able to substitute one average for the other, but indiscriminate presumption of ergodicity without sound grounds can lead to serious error. If the series is non-stationary then all the typical results of the classical regression analysis are not valid.

#### 4.3.1 Autoregressive Time Series Models

The equation above each graph includes two lags of the measured OBSI data and, consequently, two autoregressive coefficients. To utilize the ARIMA model, it was assumed that the OBSI measurements were taken at equal time intervals, and therefore the dependent variable became the test number, t. The Solver function in excel was used to determine the autoregressive coefficients which minimized the sum of squared error between the measured and predicted values at test number t. Different auto-regressive coefficients were calculated for each lane or each cell to create a model that is specific for that location.

$$Y_t = \mu_t + \phi Y_{t-1} \quad (4.31)$$

$|\phi| < 1$  and  $U_t$  is a Gaussian (white noise) error term.

ARIMA models are characterized by three parameters using the notation ARIMA (p, d and q) for each type. In this notation, p is designated as the number of autoregressive terms in the model, d is the number of non-seasonal differences used, and q is the number of lagged forecast errors included in the model equation. After testing multiple different ARIMA models, it was concluded that the ARIMA (2, 1, and 0) was most able to fit the measured data and produce reasonable forecasted values that followed the expected trend. The equation below was used to generate the forecasted OBSI [4.2] and [4.3].

$$\hat{Y}(t) = \mu + Y_{t-1} + \phi_1 (Y_{t-1} - Y_{t-2}) + \phi_2 (Y_{t-2} - Y_{t-2}) \quad (4.32)$$

where

$\hat{Y}(t)$  = predicted OBSI at test number t

$Y_t$  = measured OBSI at test t

$\mu$  = average difference in measured OBSI

$\phi_1$  and  $\phi_2$  = auto - regressive coefficients 1 and 2

Example of the Process

**Table 4.5: OBSI Time Series of Inner Lane of a 1993 Transverse Tined Cell (Cell 36)**

Test No.	Date	Gap	Y(t): Measured	Moving Average (Yhat?)	Y(t) - Y(t-1)	Y(t-1) - Y(t-2)	Y(t-2)-Y(t-3)	Y(t): Predicted	Error <sup>2</sup>	
1.00	9/27/2007		103.7	103.7						
2.00	4/21/2008		102.4	103.0	-1.3					
3.00	6/13/2008		102.7	102.9	0.3	-1.3				
4.00	3/17/2009		103.9	103.2	1.1	0.3	-1.3	103.6	0.1	
5.00	7/22/2009		103.5	103.2	-0.4	1.1	0.3	103.1	0.1	
6.00	9/15/2009		102.6	103.1	-0.9	-0.4	1.1	102.8	0.0	
7.00	11/19/2009		104.0	103.3	1.4	-0.9	-0.4	103.3	0.5	
8.00	3/8/2010		103.7	103.3	-0.3	1.4	-0.9	104.1	0.1	
9.00	7/30/2010		102.7	103.2	-1.0	-0.3	1.4	103.0	0.1	
10.00	9/17/2010		104.2	103.3	1.5	-1.0	-0.3	103.5	0.5	
11.00	3/15/2011		104.8	103.5	0.6	1.5	-1.0	104.1	0.4	
12.00	6/27/2011		104.3	103.5	-0.5	0.6	1.5	103.5	0.6	
13.00	9/20/2011		104.1	103.6	-0.2	-0.5	0.6	103.3	0.5	
14.00	6/29/2012		104.11	103.6	0.0	-0.2	-0.5	103.9	0.0	
15.00								103.8		
16.00								103.5		
17.00								103.7		
18.00								103.9		
19.00								103.6		
20.00								103.7		
21.00								103.9		
22.00								103.8		
				average lag	0.0				Sum (error <sup>2</sup> )	3.0

Table 4.30 shows the development of the Time series and the in consequence the generation of the time series factors based on the equation

$$Y(t) = \mu + Y_{t-1} + \phi_1 (Y_{t-1} - Y_{t-2}) + \phi_2 (Y_{t-2} - Y_{t-3}) \dots \dots \text{Equation 4.3 3}$$

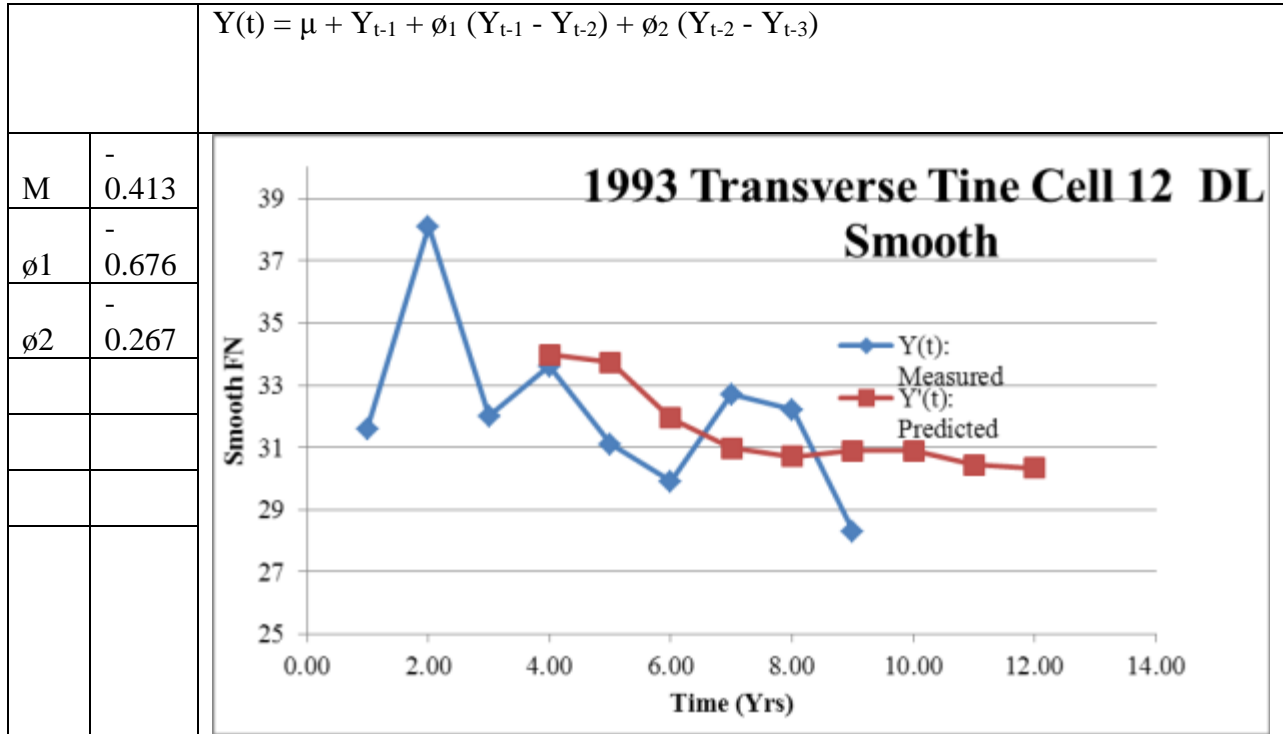
The unique coefficients are thus by least squares substitution found to be

- μ        0.034
- ϕ1      -0.456
- ϕ2      -0.757

Next OBSI predictions for future tests were made from the model using the predetermined coefficients, calculated average difference in the measured OBSI values, and the previous OBSI test values predicted in the optimization step above. For example, for a series of OBSI data that included 7 test measurements, the eighth test measurement would be predicted using the OBSI values for tests 5 and 6 that were generated from the model, and not the actual measurements taken. The following graphs are the auto regressive integrated moving average plots from the various trends in time series. In each case a computation based on going back 3 cycles has been done. Superimposed in the measured data is the ARIMA predicted data also.

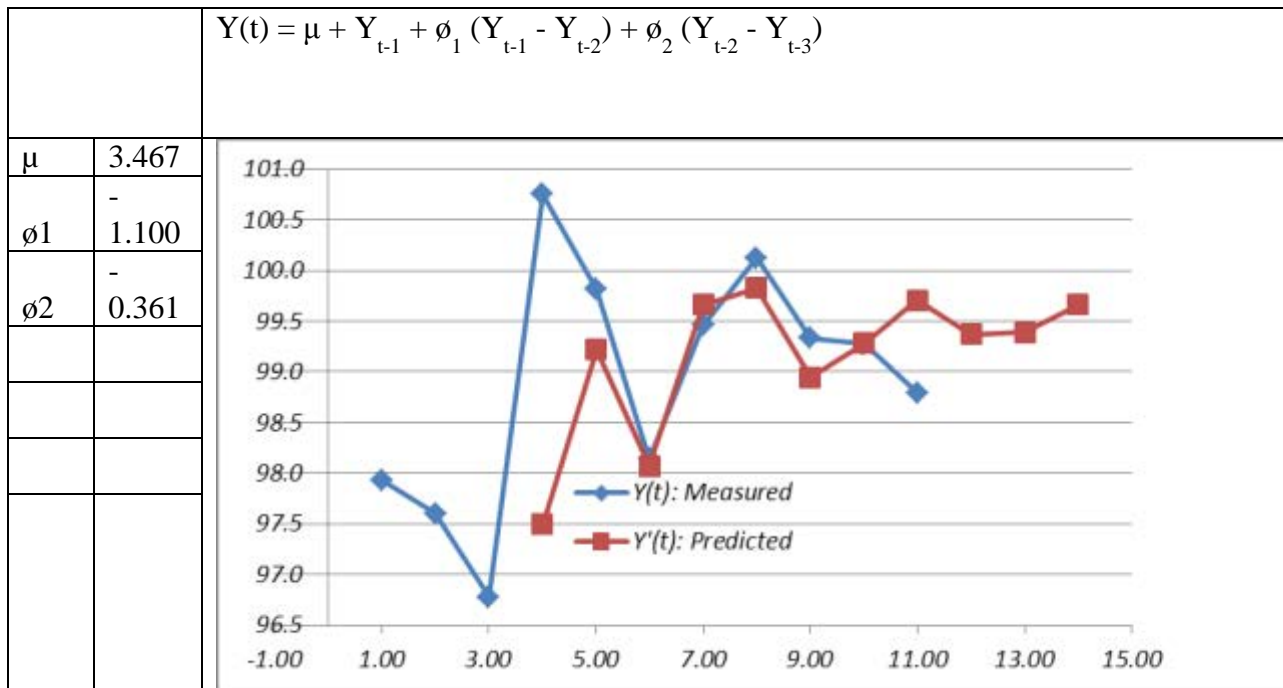
FRICITION



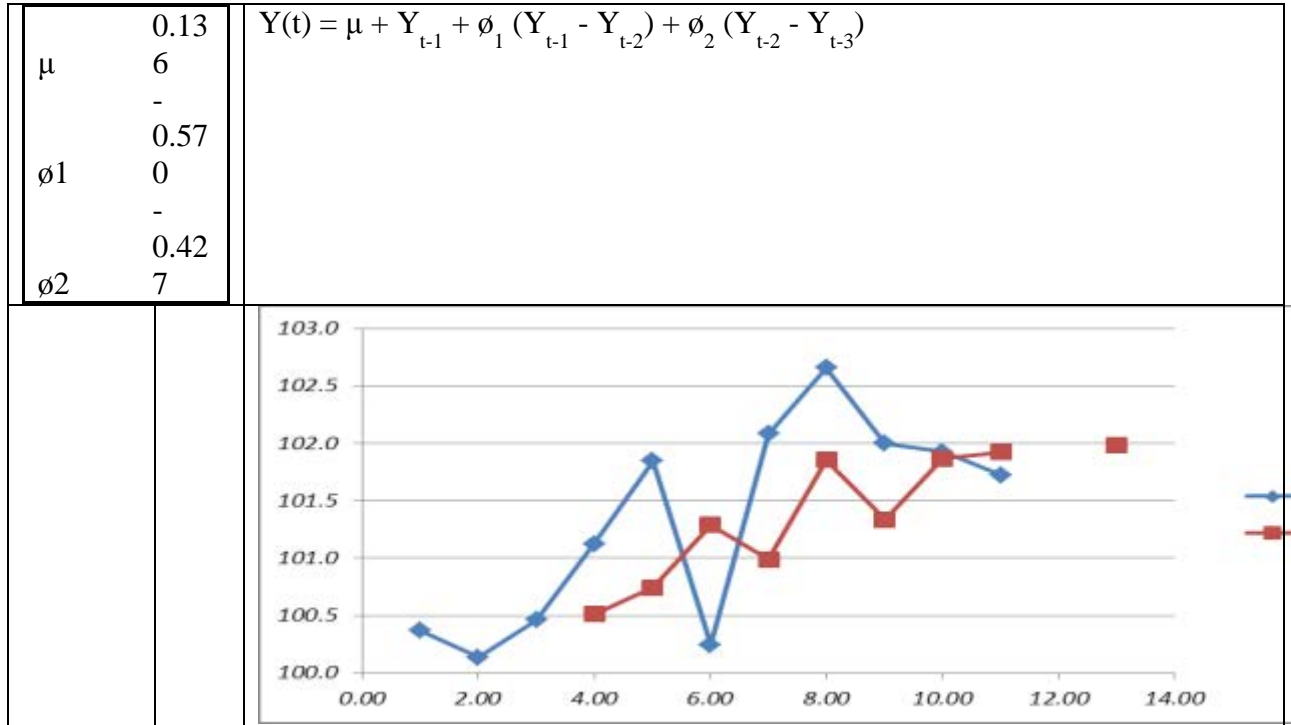


**Figure 4.105: Driving Lane of Cell 12 (1993 Transverse Tine)**

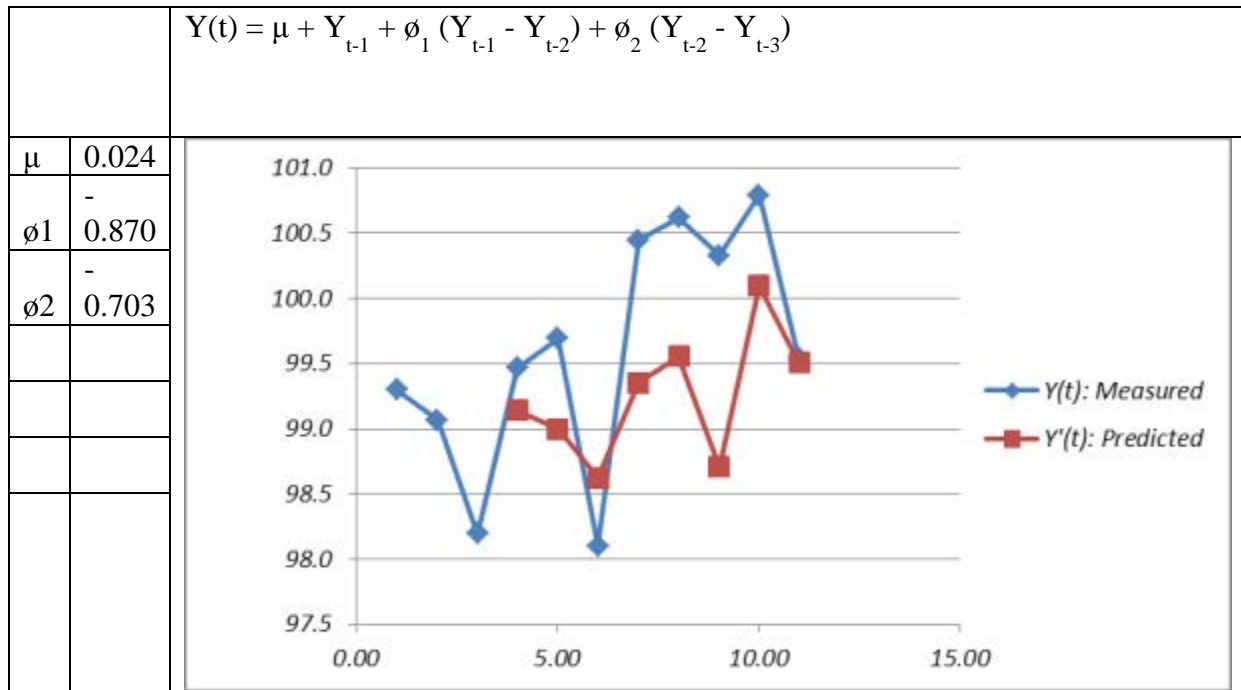
**OBSI TABLES**



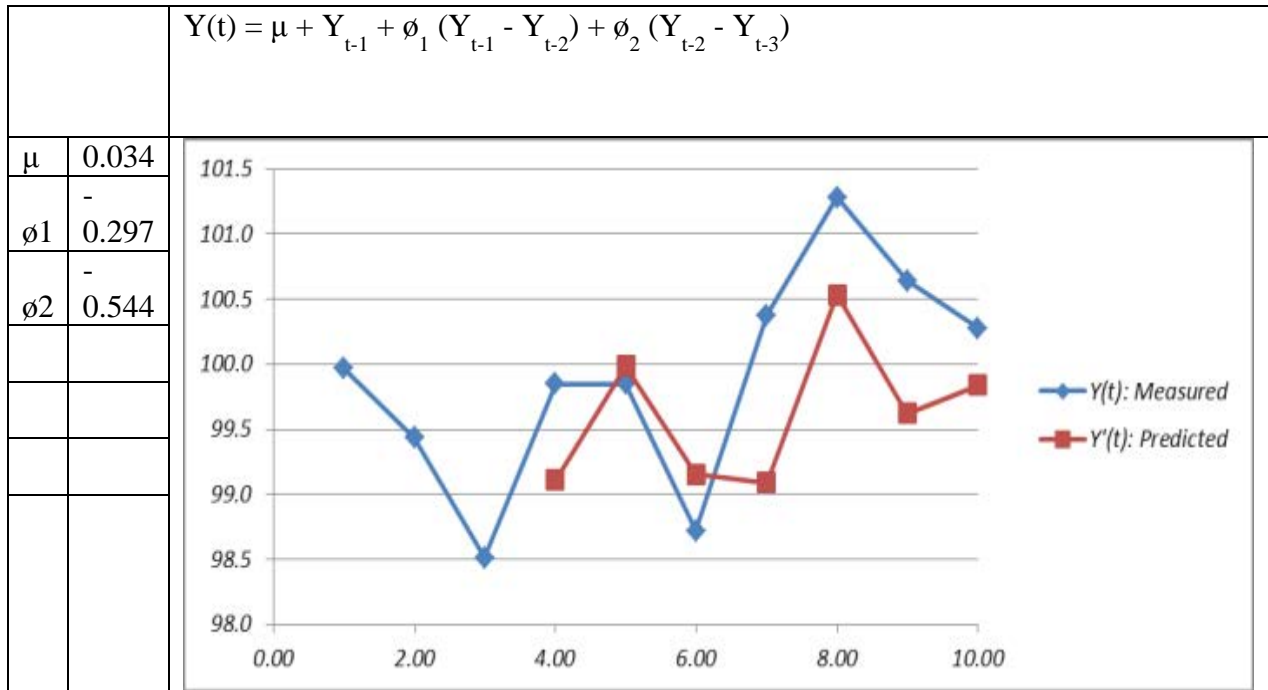
**Figure 4.106: Pervious Concrete Overlay OBSI (Cell 39 Outside Lane – LVR)**



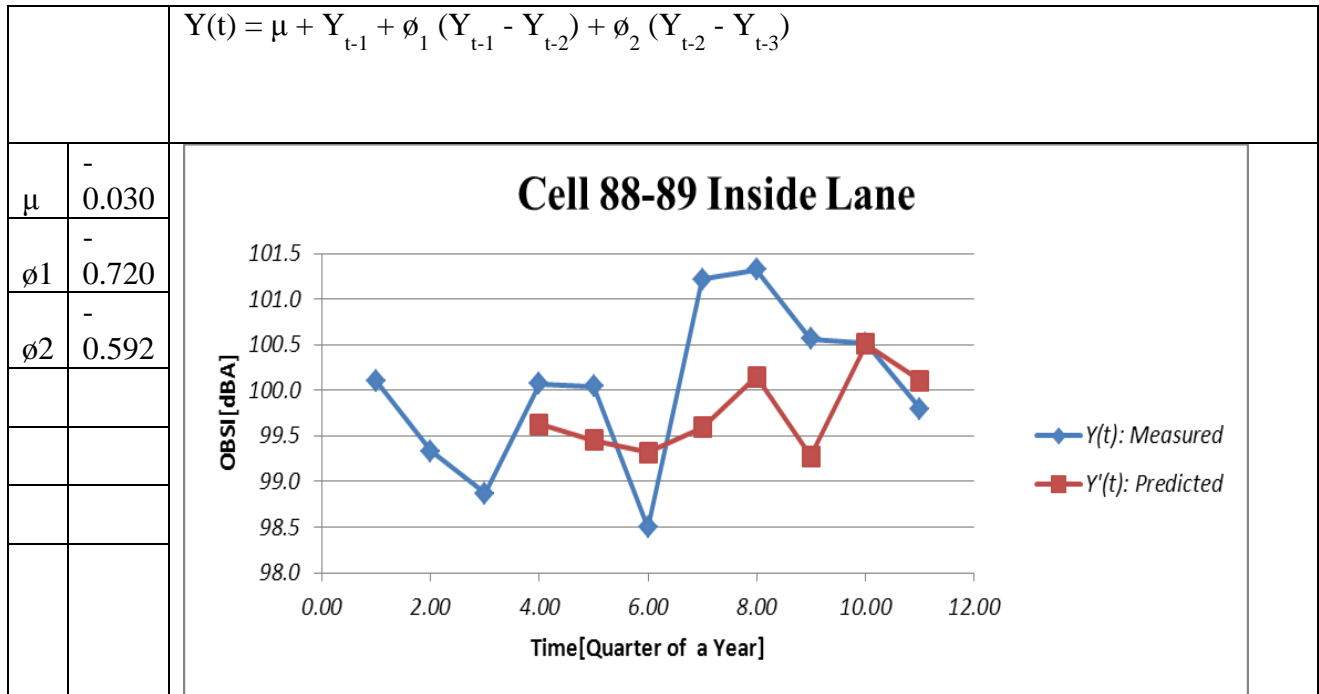
**Figure 4.107: Pervious Cell 39 Inside Lane OBSI**



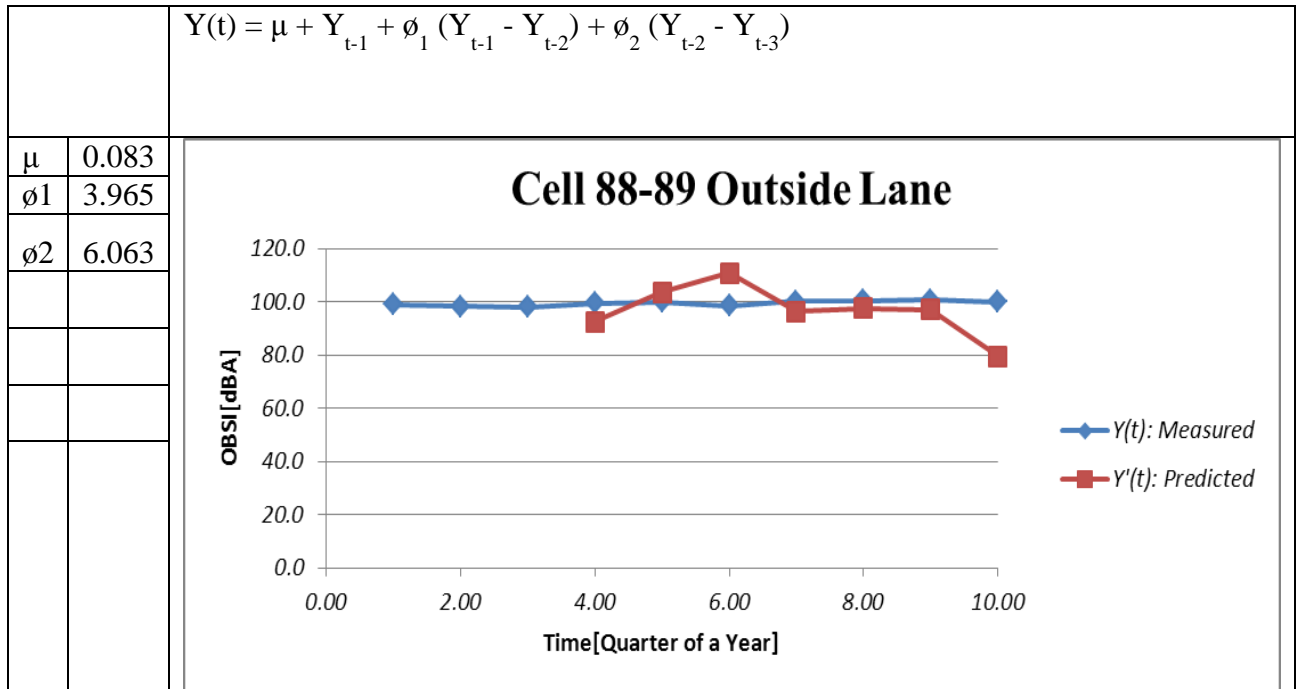
**Figure 4.108: Pervious Cell 85 Inside Lane OBSI**



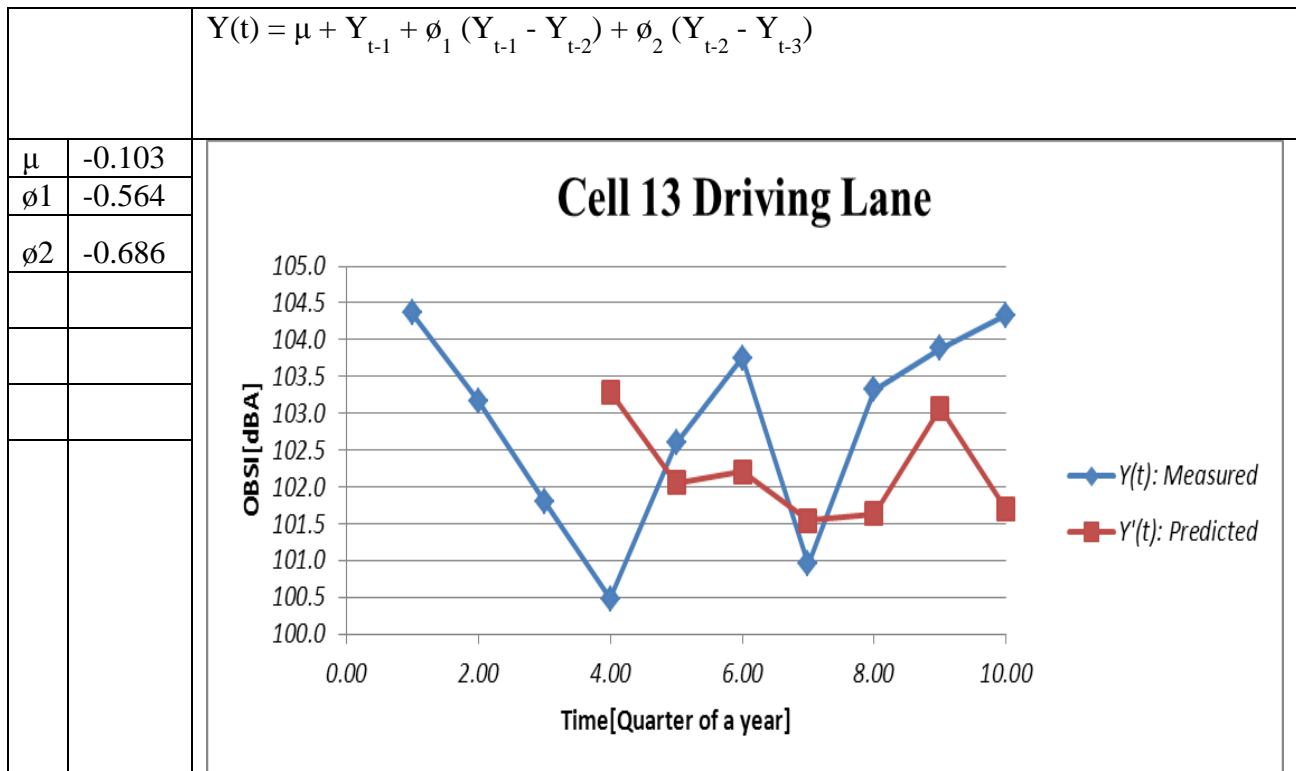
**Figure 4.109: Pervious Cell 85 Outside Lane OBSI**



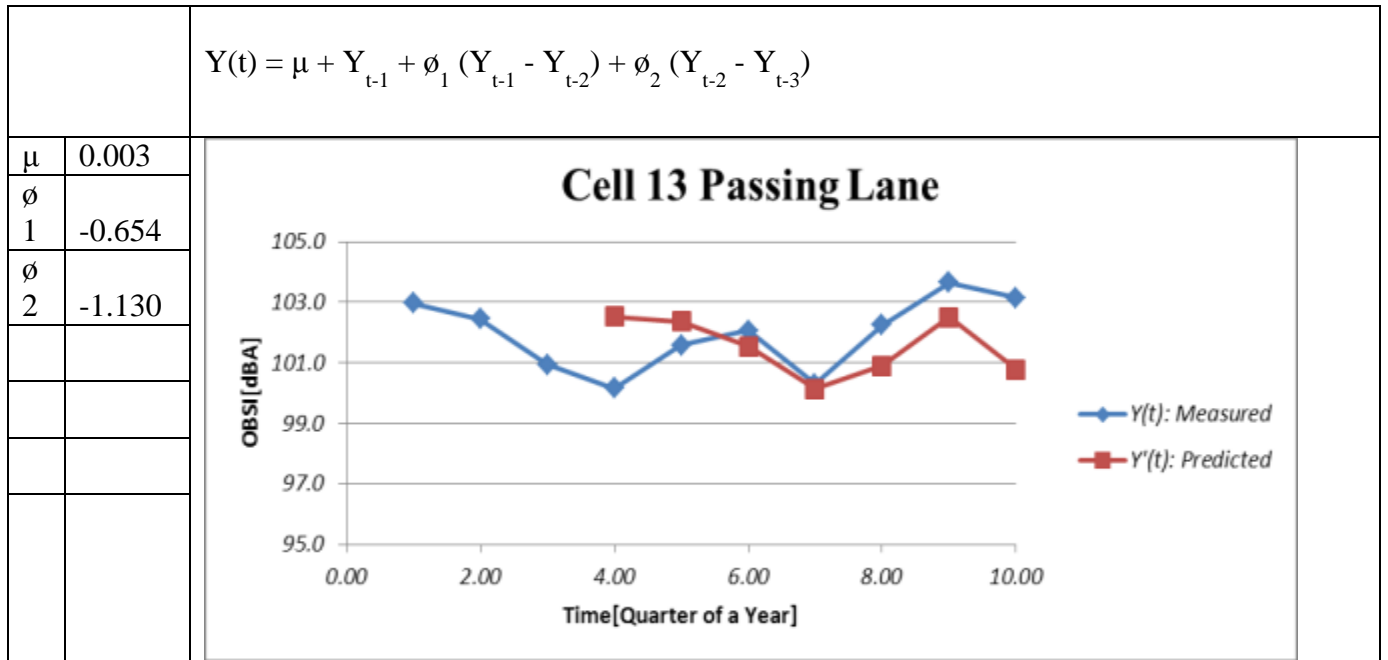
**Figure 4.110: Pervious Cell 89 Inside Lane OBSI**



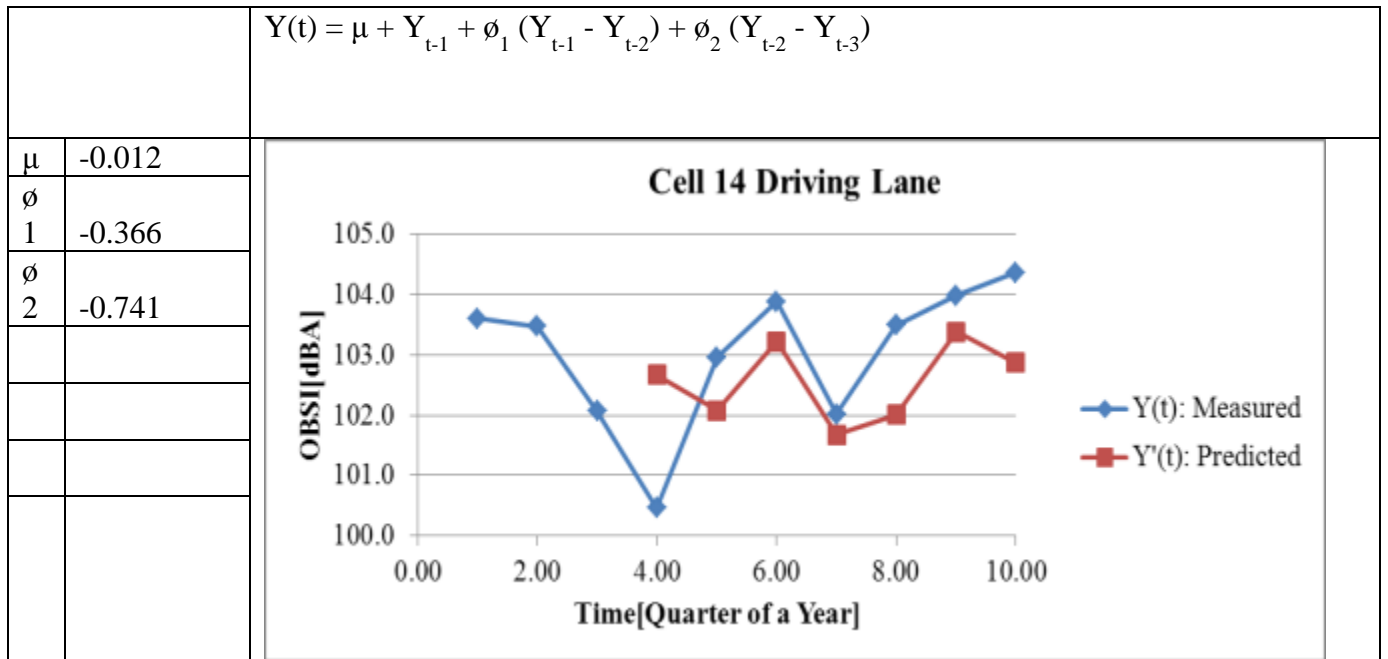
**Figure 4.111: Pervious Cell 89 Outside Lane OBSI**



**Figure 4.112: Cell 13 Driving Lane OBSI**



**Figure 4.113: Cell 13 Passing Lane OBSI**



**Figure 4.114: Cell 14 Driving Lane OBSI**

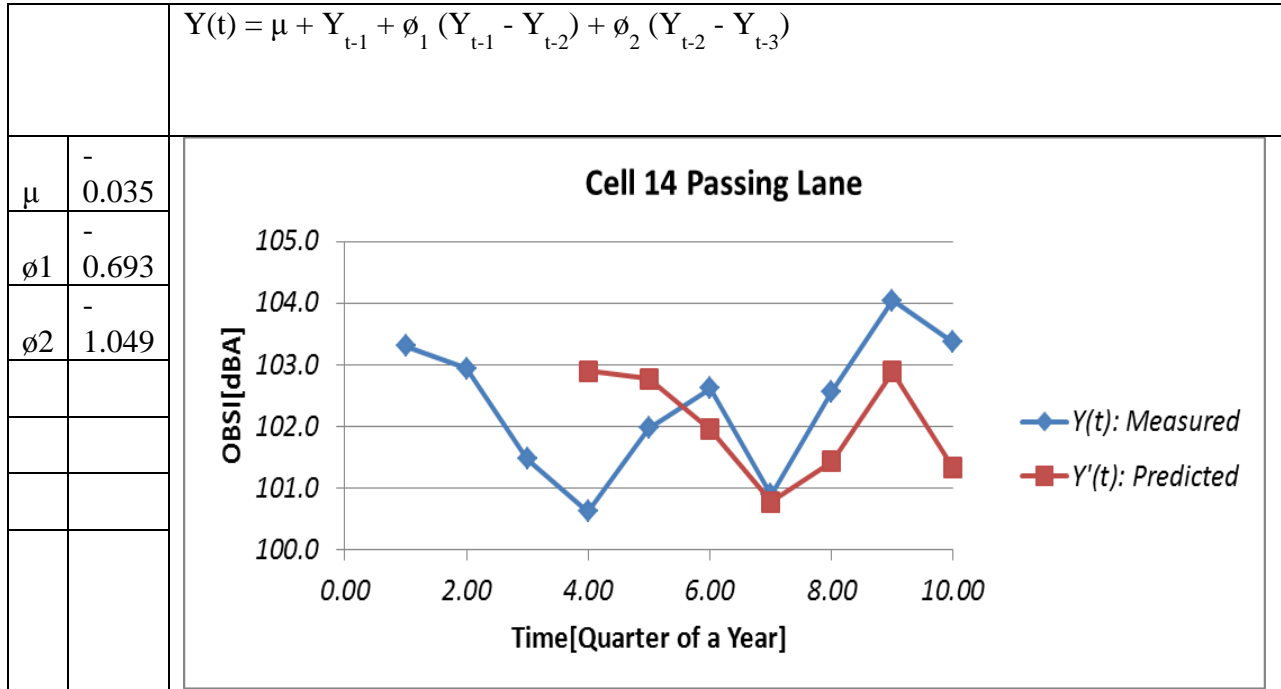


Figure 4.115: Cell 14 Passing Lane OBSI

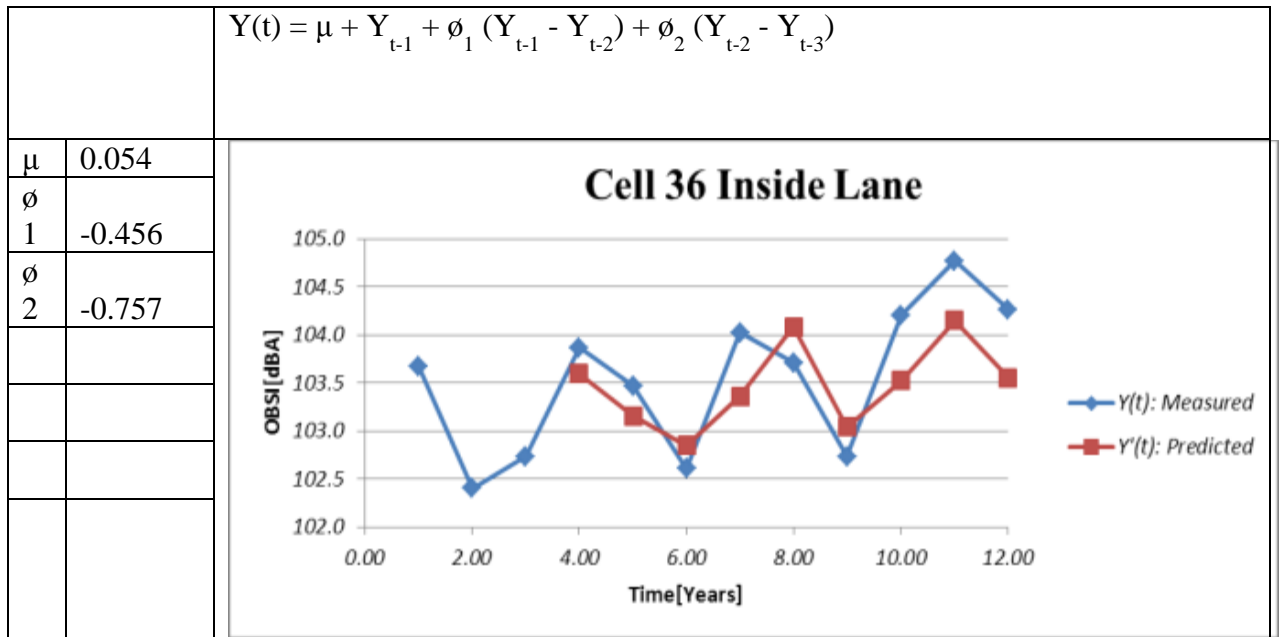
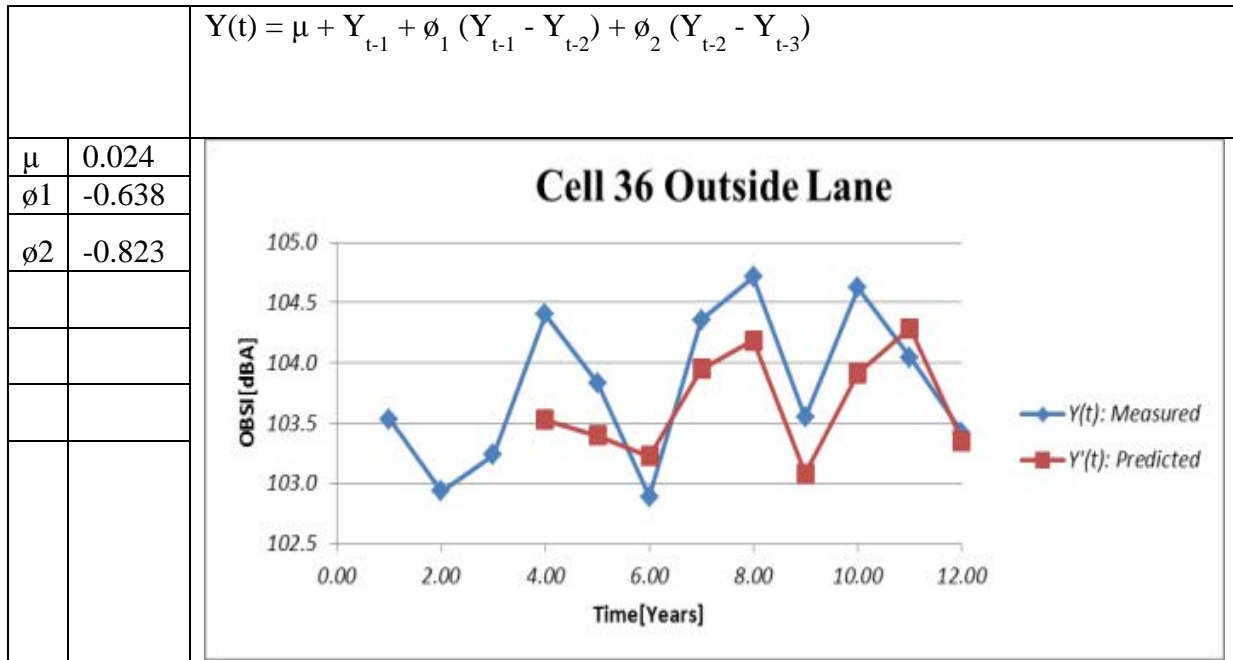
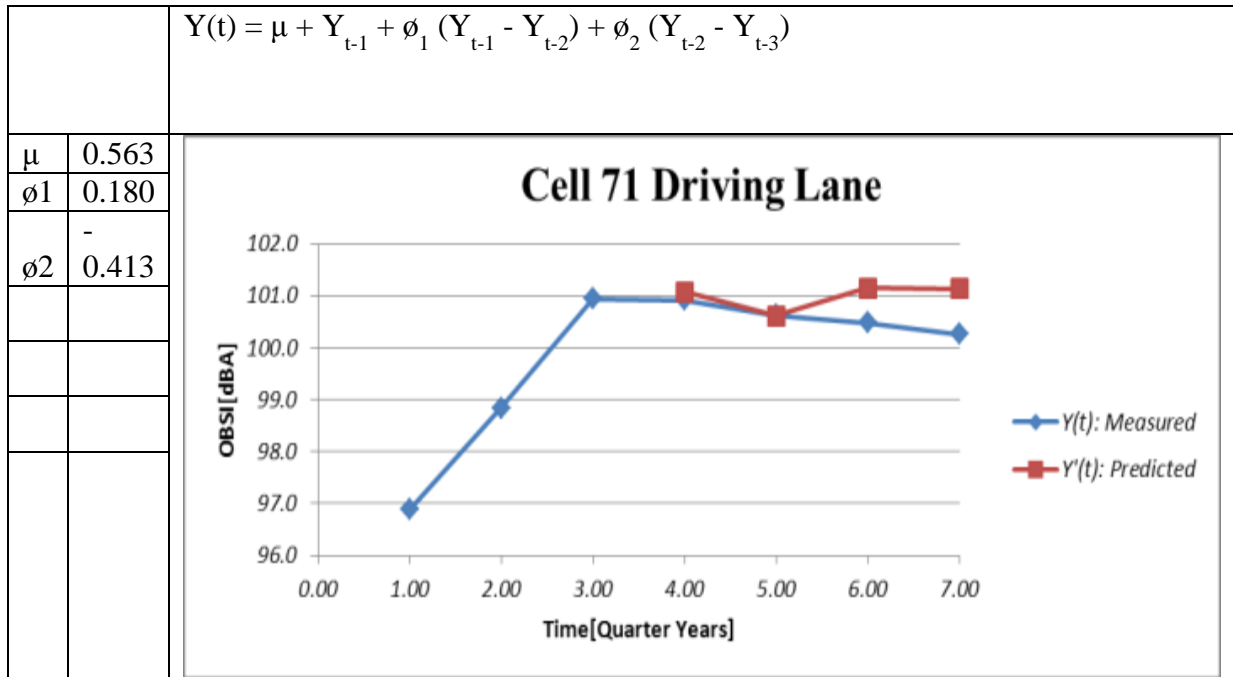


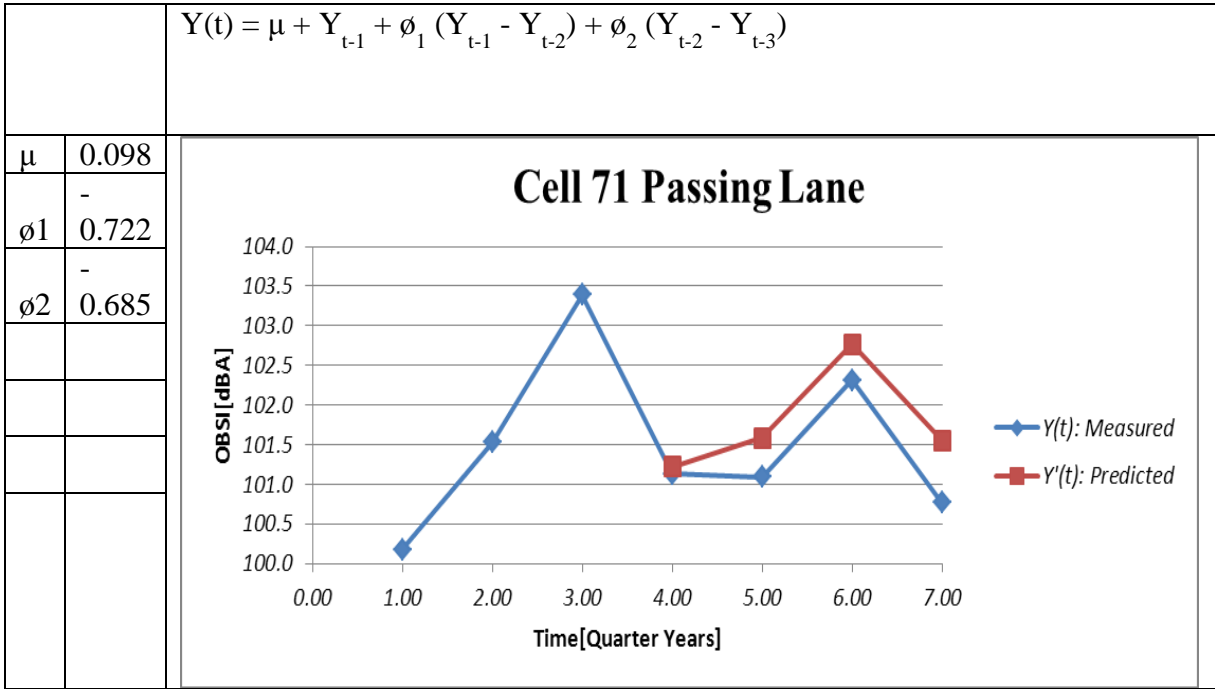
Figure 4.116: Cell 36 Inside Lane OBSI



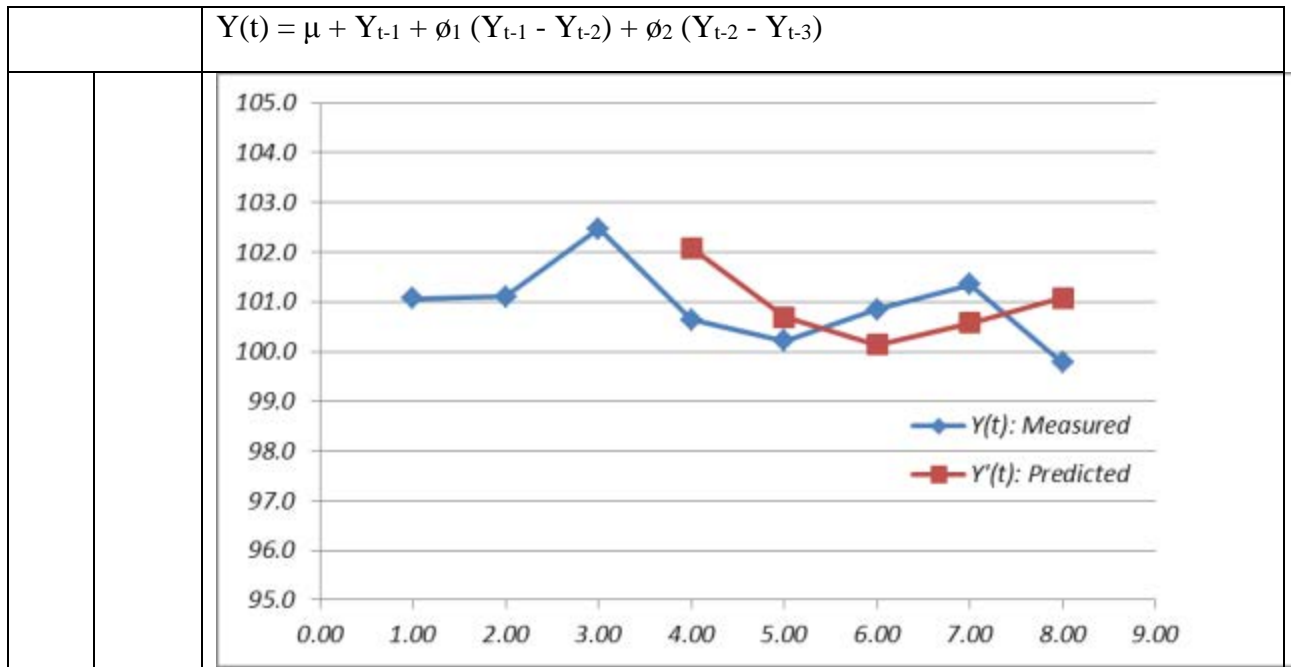
**Figure 4.117: Cell 36 Transverse Tine Outside Lane OBSI**



**Figure 4.118: Cell 71 Driving Lane OBSI**



**Figure 4.119: Cell 71 Passing Lane OBSI**



**Figure 4.120: Cell 32 2000 Thin Concrete Pavement with Turf Dragged Surface OBSI**



FRICION FIGURES

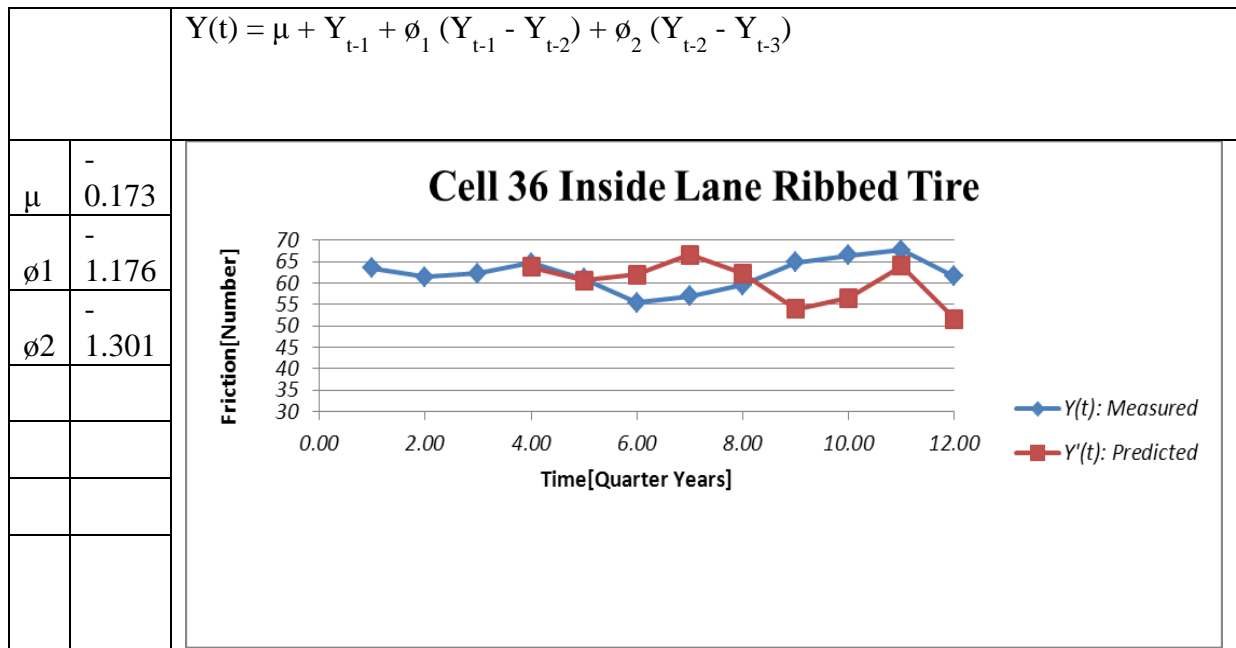


Figure 4.121: Cell 36 Inside Lane Ribbed Friction

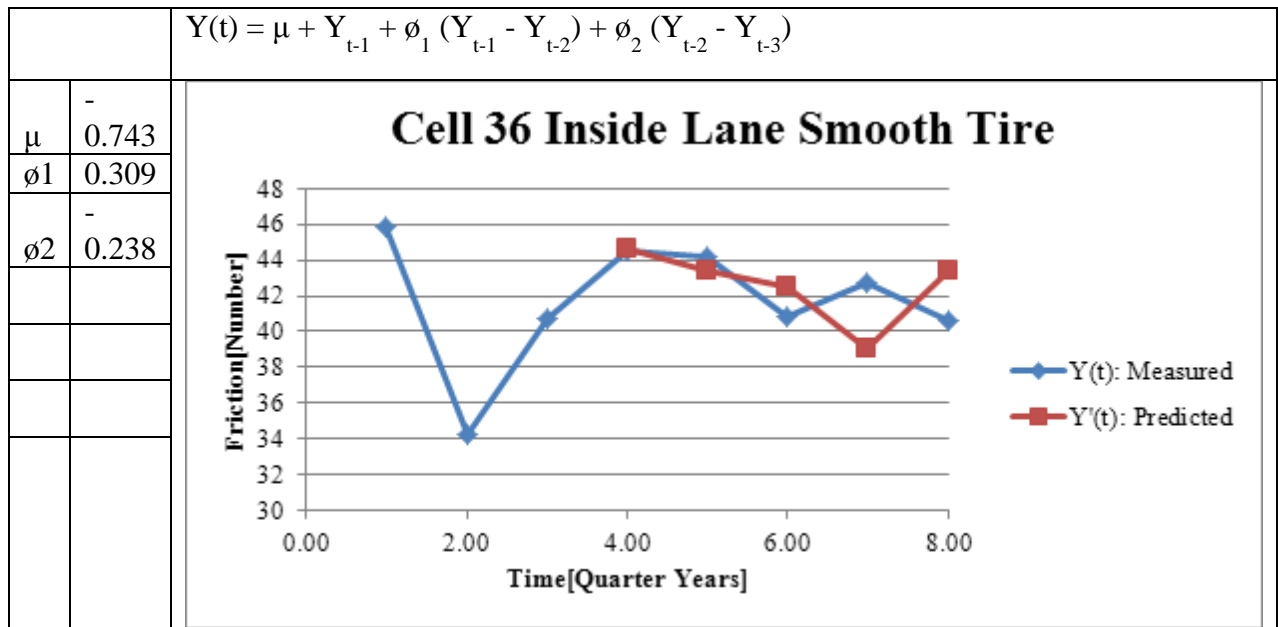
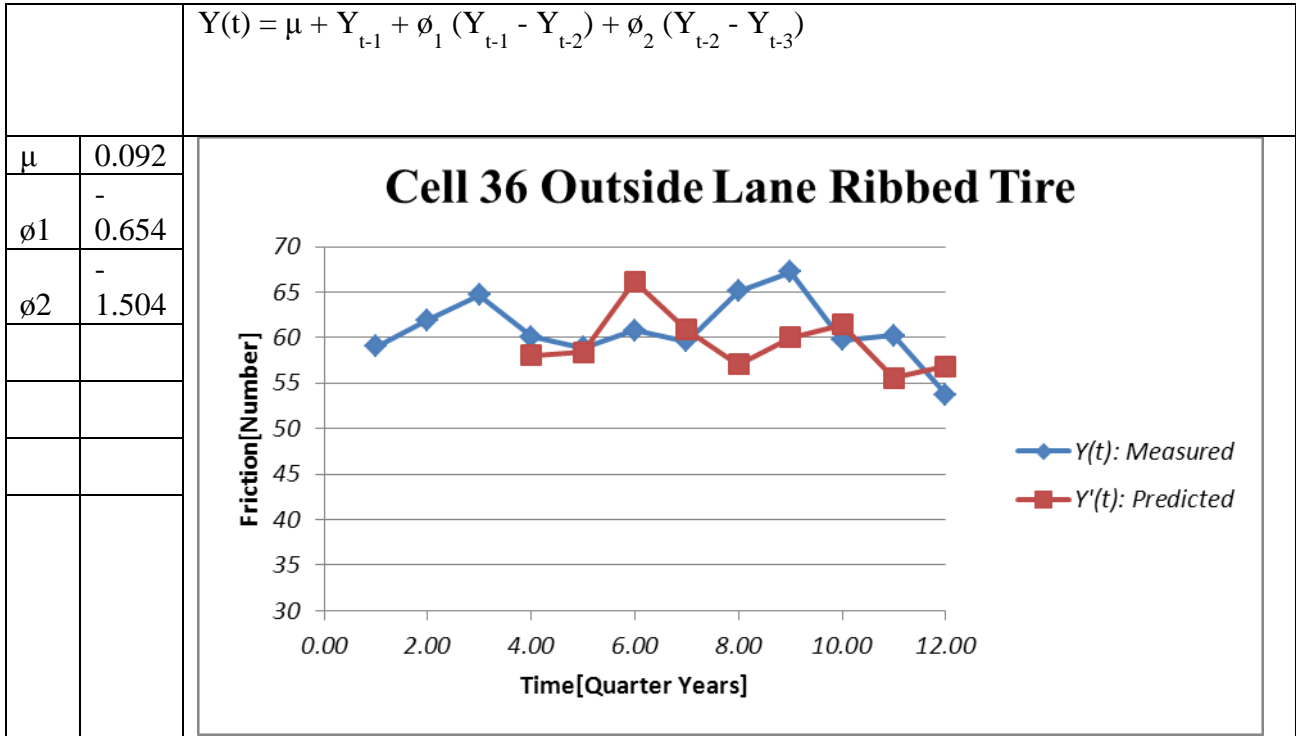
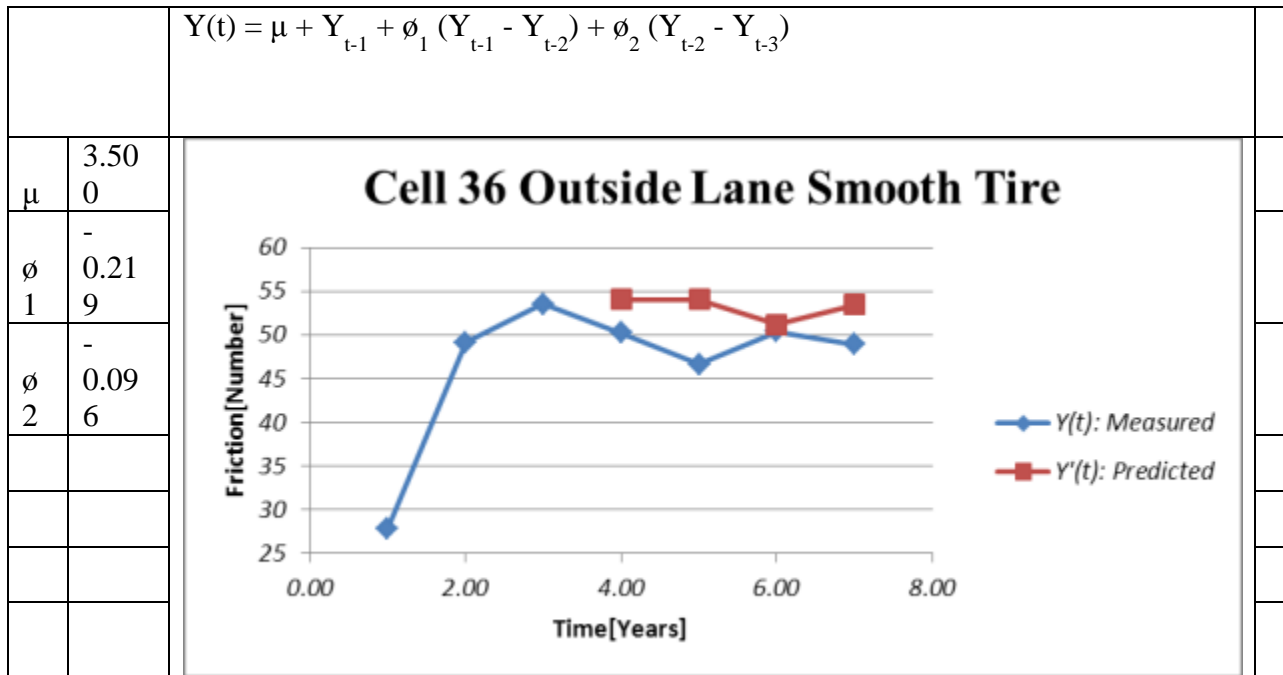


Figure 4.122: Cell 36 Inside Lane Smooth Friction



**Figure 4.123: 1993 Transverse Tine Cell 36 Outside Lane Ribbed Friction**



**Figure 4.124: Cell 36 Outside Lane Smooth Friction**

IRI FIGURES

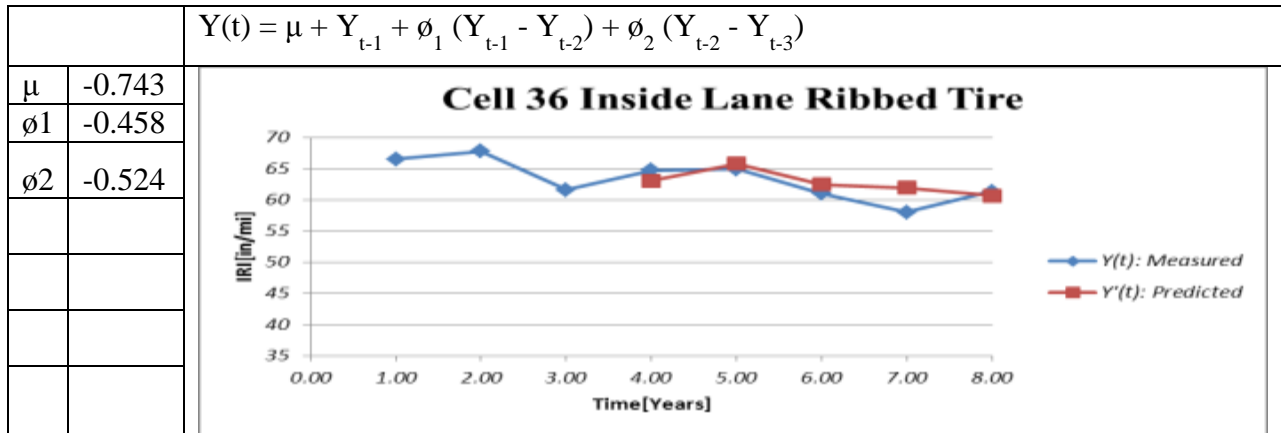


Figure 4.125: Cell 36 Inside Lane Ribbed IRI

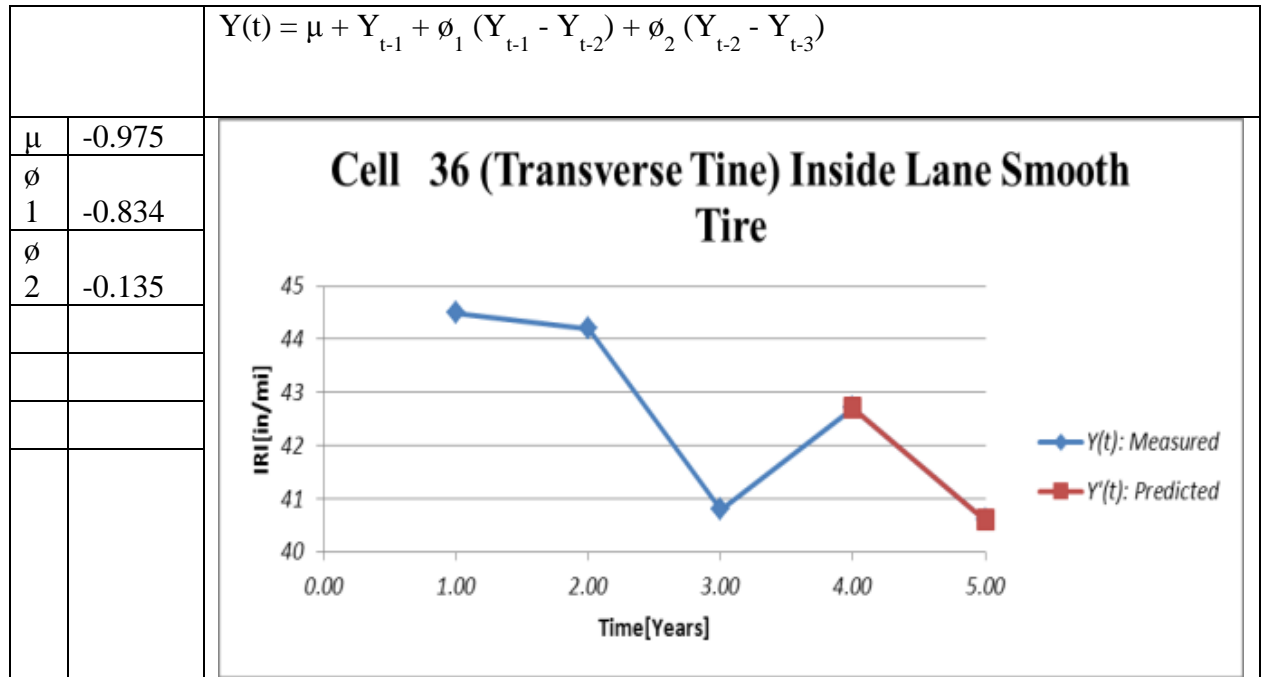
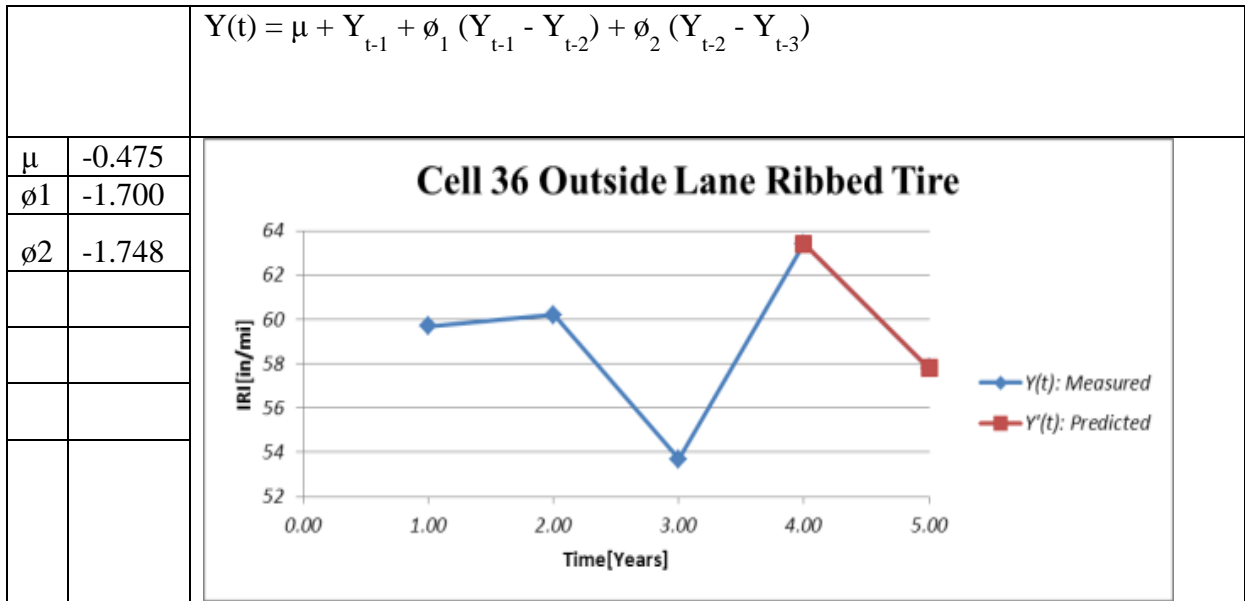
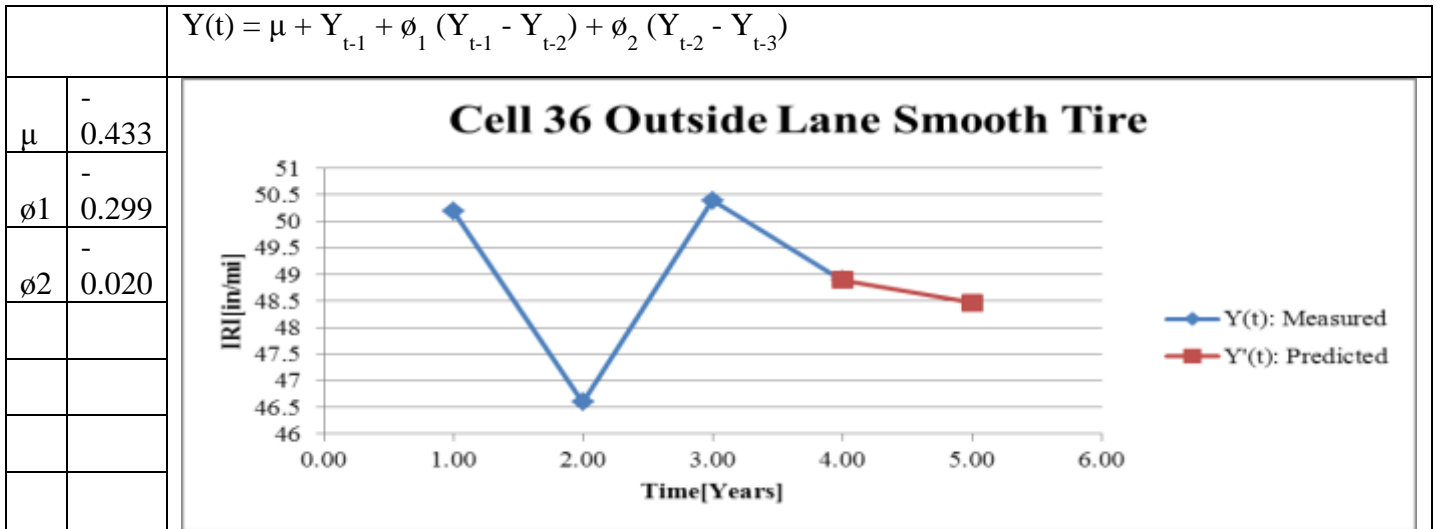


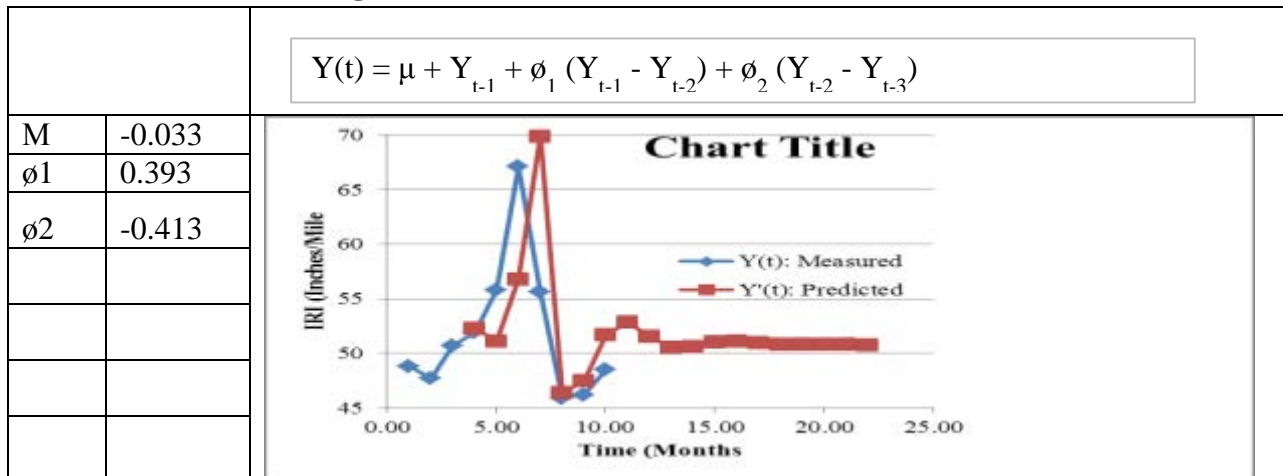
Figure 4.126: Cell 36 Inside Lane Smooth IRI



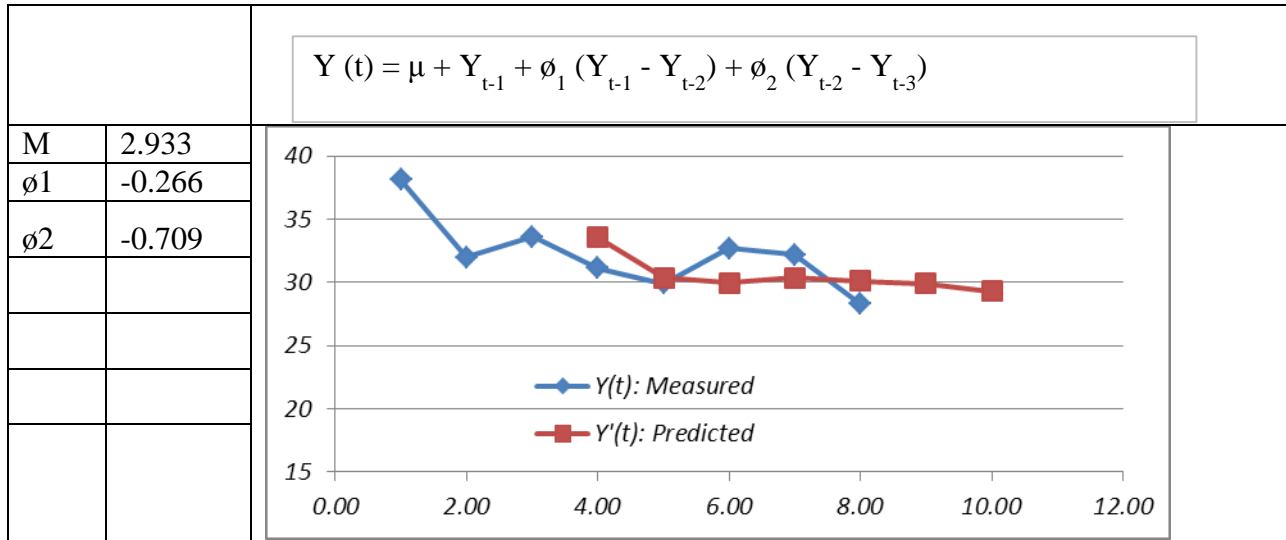
**Figure 4.127: Cell 36 Outside Lane Ribbed IRI**



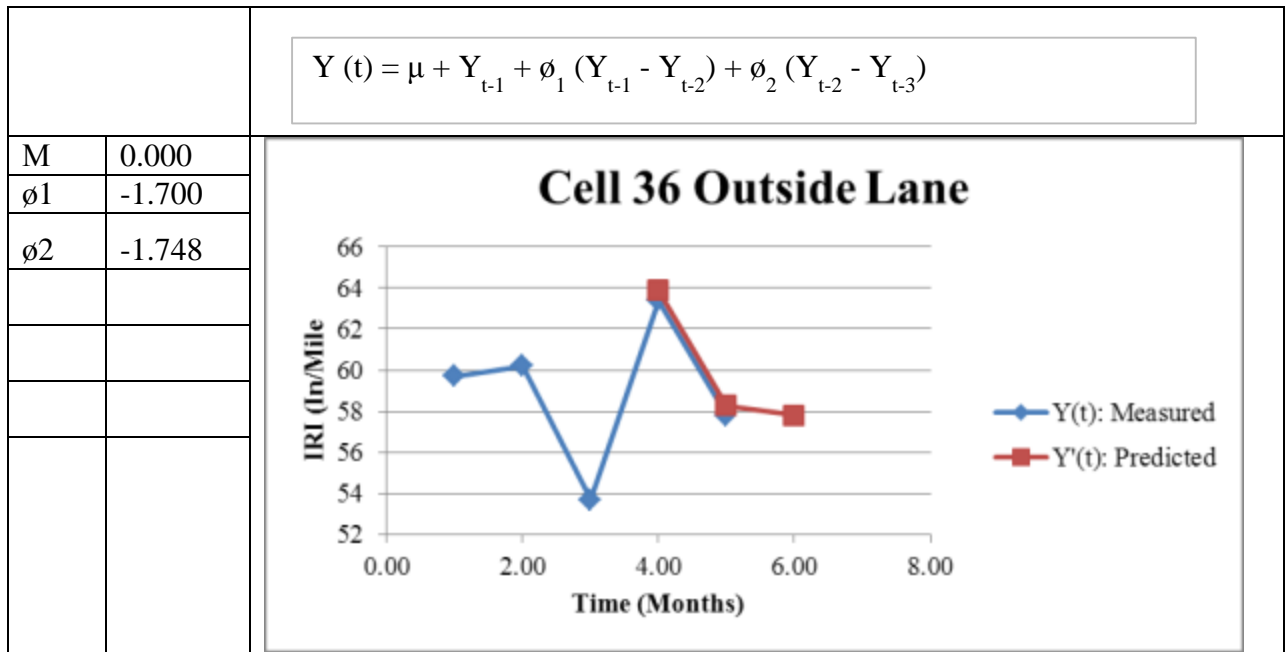
**Figure 4.128: Cell 36 Outside Lane Smooth IRI**



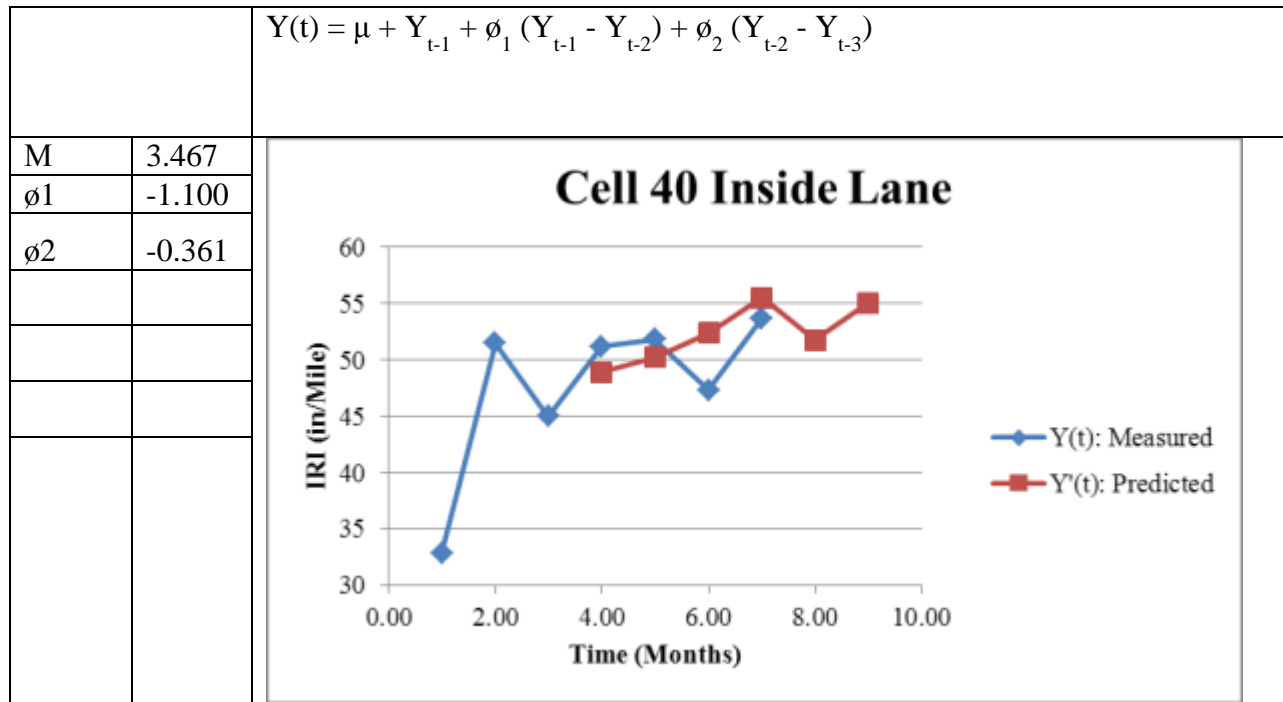
**Figure 4.129: 1993 Transverse Tine Cell 12 DL IRI**



**Figure 4.130: 1993 Transverse tine Cell 12 DL IRI**



**Figure 4.131: Cell 36 Inside Lane IRI**



**Figure 4.132: Cell 40 Inside Lane IRI**

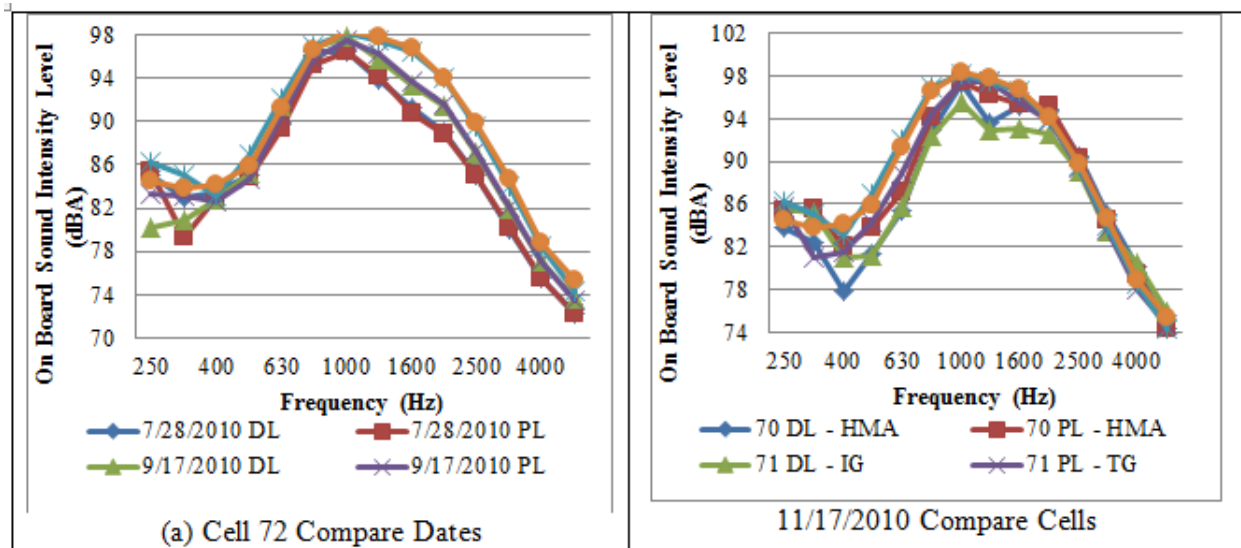
### 4.3.2 Texture Characteristics and Acoustics Over Time

Mean profile depth increased with time in the driving lane where it can be hypothesized that the higher traffic volume resulted in more paste loss which in consequence resulted in deeper inter asperity features. In comparison, there was no corresponding increase in the texture orientation as the skewness increased to a neutral texture from the first test to the second and fell at the third test back to the original negative texture measured on the same spot in three consecutive tests. It changed from -0.24 in summer of 2010 to 0.01 in the fall of 2010, and later to -0.32 in the summer of 2011 in the driving lane was similar to the observation made in the passing lane, although the ESALs in the former were 4 times that of the latter. The passing lane swung from a more negative texture (-0.33) to a more positive texture (0.06) from summer to fall of 2010. It fell to a very negative value of -0.62 in summer of 2011. There was an increase in OBSI through the one-year period but the increase appeared more rapid between the first two readings in both lanes than between the second and third readings.

**Table 4.6: Texture and Noise Performance over Time**

	72x1RR (Driving)			72x1LL (Passing)		
	6/1/2010	10/1/2010	6/1/2011	6/1/2010	10/1/2010	6/1/2011
MPD (mm)	0.36	0.49	0.54	0.45	0.4	0.37
RMS	0.16	0.24	0.26	0.24	0.21	0.18
skewness	-0.24	0.01	-0.32	-0.33	0.06	-0.62
Cumulative ESAL	13301500	13523900	14367100	3369200	3431900	3640900
OBSI	101.3	102.7	103.0	101.7	102.9	103.2

A continuous drop in MPD was observed in the passing lane of lesser traffic contrary to the driving lanes where a continuous increase in MPD was observed. It appears from the observation that the traffic effect at the early stage of the service period does not result in polishing of aggregate but instead in removal of more paste, thus increasing the MPD while increasing the texture spikiness to a point where paste removal is associated with further spike removal and the net effect is negative texture. Never the  $\lim_{n \rightarrow \infty} \left(1 + \frac{1}{n}\right)^n$  less, one year performance shows to some degree some non-descript features that may be more ordered and defined after many years of monitoring. It must be noted however that texture depth changes do not necessarily result in increased noise nor are they necessarily associated with increased MPD in the EAC surface observed. The innovative diamond ground exposed aggregate concrete in cell 71 has the lowest initial OBSI. The traditional diamond grind has similar OBSI to the hot mix asphalt. More significantly, the exposed aggregate finish consistently has the highest OBSI of the four surfaces compared. Pavements are generally considered quiet when they achieve an OBSI less than 100 dBA, in which case the data suggests that the diamond grind in cell 71 is the only composite pavement to be considered quiet. In a survey of exposed aggregate concrete pavements in Europe conducted by the National Concrete Pavement Technology Center, OBSI values were found to range from 101 to 106 dBA, which is similar to the results obtained for cell 72. The 1/3 octave sound intensity spectrums used to calculate the OBSI values are show in Figures 4.134 (a) and (b). All cells show similar shape in their sound intensity spectrums.



**Figure 4.133: 1/3rd Octave Sound Intensity Spectrum (a) Cell 72 Compare Dates and (b) 11/17/2010 Compare Cells**

#### 4.4 Representation of Surface Characteristics by Probability Density Function

Among the many methods used to display surface characteristics data, perhaps the most tenable is one that directly relates to an  $n$  expected or threshold value. This method does not attempt to explain causation but simply shows that probability that in the data collected the surface characteristic will be less than, equal to or less than/equal to or greater than the threshold value. For instance with a mean profile depth of 1mm, one would quickly want to know what the likelihood is that in the data set of pervious overlay textures, the mean profile depth is higher

than 1mm. How does this compare to the Full depth textured surface. The importance of this method is evident in the ease of comparison and its application in relation to a target value. Rob Rasmussen (4.4) used this method extensively in the Iowa State-led surface characteristics studies

#### 4.4.1 A probability density function

**Probability distribution function**) is a function "f" defined on an interval (a, b) and having the following properties.

(a)  $f(x) \geq 0$  for every x Equation 4.33

(b)  $\int_a^b f(x) dx = 1$  Equation 4.34

We allow a, b, or both to be infinite, as in the above example. This would make the integral in (b) an improper one.

A continuous random variable X is specified by a probability density function f. The probability  $P(c \leq X \leq d)$  is specified by

$$P(c \leq X \leq d) = \int_c^d f(x) dx = 1 \quad \text{Equation 4.35}$$

Recent surveys show that textures or function thereof varies continuously at k% per year. We can deduce the probability that a performance criterion will fall below a set value sometime within the next x years. Starting with a sample space of 100 since they are failing continuously at a rate of K % per year, the number left after x years is given by the decay equation

$$\text{Population left} = 100 e^{-kx},$$

number that fell below threshold

$$\begin{aligned} &= \text{total number} - \text{number left} \\ &= 100 - 100 e^{-kx} \\ &= 100(1 - e^{-kx}). \end{aligned}$$

Thus, the percentage that will have fallen at the time x--and hence the probability that we are seek

$$P = 100(1 - e^{-kx})/100 = 1 - e^{-kx}.$$

First, the domain of f is  $[0, +\infty)$ , since x refers to the number of years from now. Checking requirements (a) and (b) for a probability density function, This is a verification of two conditions

Condition (a) The value of f (t) must be  $\geq 0$

(a)  $ke^{-kx} \geq 0,$

Condition (b): Area under PDF as  $x \rightarrow \infty = 1$

(b)  $\int_0^{\infty} ke^{-kx} dx = \lim_{M \rightarrow +\infty} \int_0^M ke^{-kx} dx$



$$\begin{aligned}
&= \lim_{M \rightarrow +\infty} [-e^{-kx}]_0^M \\
&= \lim_{M \rightarrow +\infty} (e^0 - e^{-kM}) \\
&= 1 - 0 = 1.
\end{aligned}$$

Additionally any function of the form

$$f(x) = ae^{-ax}$$

with a positive constant is a probability density function. A density function of this form is referred to as an exponential density function.

### Exponential Density Function

An exponential density function is a function of the form

$$f(x) = ae^{-ax} \text{ ("a" is a positive constant)}$$

with domain  $[0, +\infty)$ . Its graph is shown in the Figure 4.31.

Thus what is the probability that before OBSI will rise above 100 dBA, pavement will last 5 or more years?

These probabilities are given by integrals.

$$\begin{aligned}
P(X \geq 5) &= \int_5^{\infty} ke^{-kx} dx \\
&= \lim_{M \rightarrow +\infty} \int_5^M ke^{-kx} dx \\
&= \lim_{M \rightarrow +\infty} [ke^{-kx} \cdot \frac{1}{-k}]_5^M \\
&= \lim_{M \rightarrow +\infty} (e^{-0.25} - e^{-kM}) \\
&= e^{-0.25} \approx 0.779
\end{aligned}$$

So there a 77.9% chance that it will last 5 or more years. Note that this principle will entail an axis of time in the pdf but for simplicity we stick to the probability and OBSI axis.

Having explained the principle behind the usage of PDF, it is expedient to show how the data Figure 4.331 to 4.337 were obtained and plotted. The 5-years of data was converted using the Excel tool for normal distribution (Norm Dist) into a simulated normal distribution, centered on the mean and standard deviation. This method of probability density function usage is more often referred to as a quasi-normal distribution because it is a data set of the normal distribution that exhibits the same central, and range distribution as the data set. This method therefore allows at a glance to compare the noise level with a standard such as 100 dB for quiet pavement by showing a probability of being quieter than 100 as the area to the left of 100 dB when the total area is equal to unity. This method is simpler than the cumulative normal distribution plot that was used by [4.33] [4.34] and [4.35]. In that method, a line drawn vertically from the axis of noise will intersect the horizontal line of probability of being lesser or equal to that value at the curve.

In order to discuss the loads applied to the various MnROAD lanes in which the noise trends are being discussed it is expedient to understand the load history in the low volume road MnROAD uses a 5-axle semi to provide the loadings to its low volume road (LVR) and provide a known dynamic load to test the dynamic sensor instrumentation. MnROAD LVR is a 2-lane, 2 ½-mile closed loop that contains many different types of pavements. Traffic on the LVR is restricted to a MnROAD operated vehicle, which is an 18-wheel, 5-axle, tractor trailer. MnDOT employed driver operates the MnROAD truck during his normal 8 hour working day averaging around 6 hours of driving or 80 laps a day. Laps are documented by the operator and entered into the MnROAD database. MnROAD does have the ability to track the truck using GPS antennas, which is typically used when collecting dynamic sensor data when location accuracy is required.

The LVR loading vehicle originally started operation on June 16, 1994. MnROAD originally utilized two different loading configurations. Originally from 1994-2008 we operated a "heavy" load configuration results in a gross vehicle weight of 102 kips (102K) configuration in the outside lane 1 day a week and a "legal" load configuration has a gross vehicle weight of 80 kips (80K) configuration, 4 days a week in the inside lane. This results in a similar number of ESALs being delivered to both lanes even though the number of passes differs. Since 2008 MnROAD runs a "legal" 80 kips loading configuration 5 days a week in the inside lane and leaves the outside lane to only receive environmental loadings with no traffic to help meet the research plans for many of the test cells built in 2007-2008. Here is a summary of the traffic loadings and equipment used over the years at MnROAD.

- 80K truck gives 2.35 ESALS/Pass (Flex) and 3.76 ESALS/Pass (Rigid)
- 102K truck gives 7.00 ESALS/Pass (Flex) and 11.50 ESALS/Pass (Rigid)

The ESALs versus time data is shown in Figure 4.136.

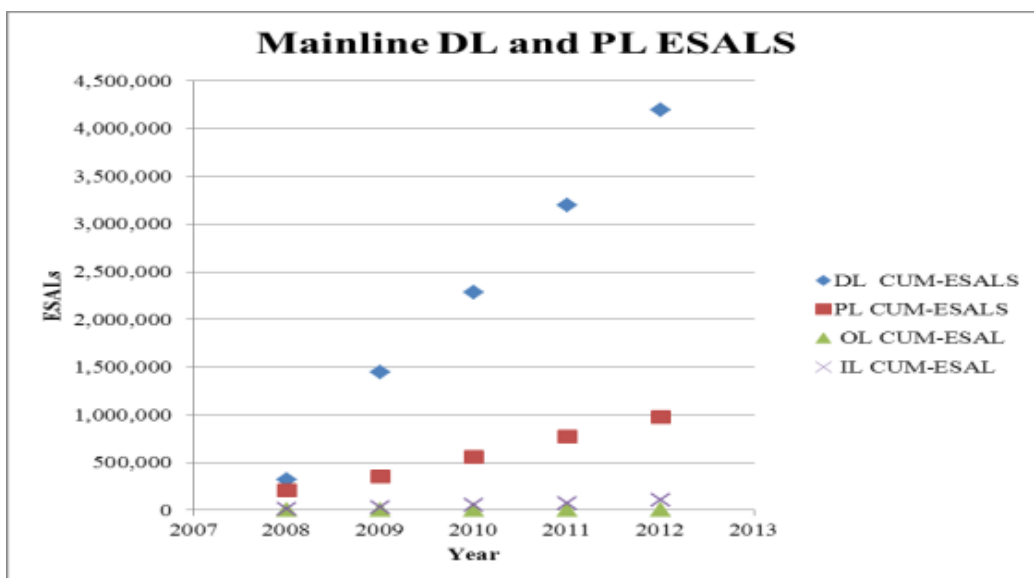
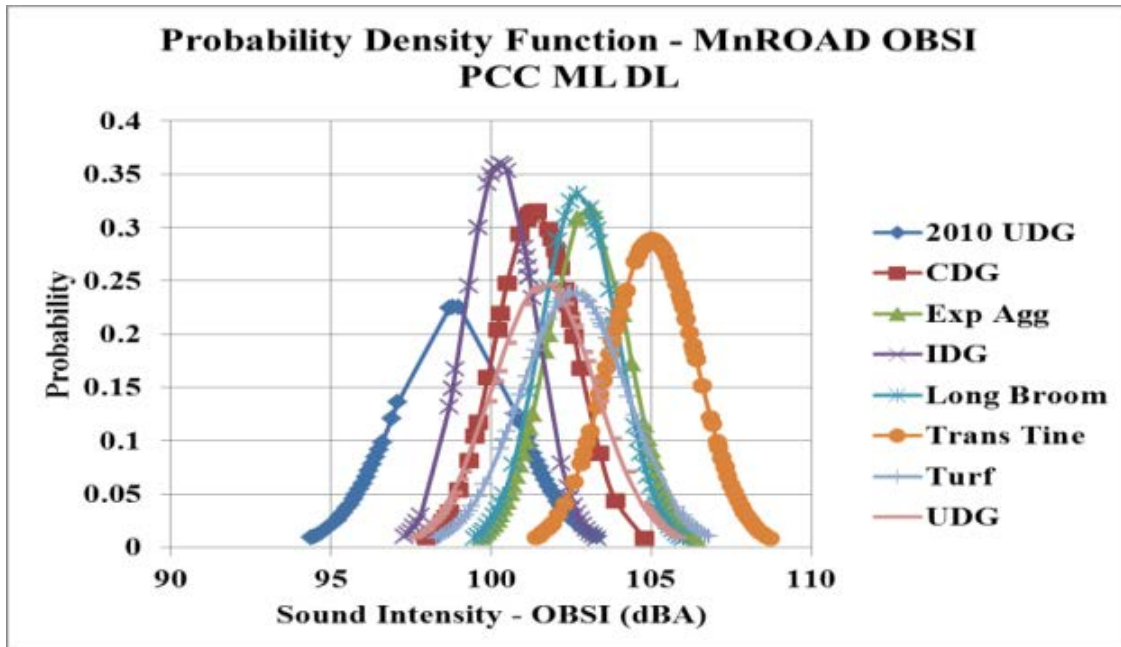


Figure 4.134: Traffic ESALs versus time in the 4 MnROAD Lanes.

Although a formal correlation was not done, it is important to document the traffic levels that resulted in the OBSI data change.



**Figure 4.135: Probability Density Function of Various Test Cells Driving Lane Subject to 5 years of Interstate traffic**

An obvious observation is the relative quietness of the various textures when viewed in terms of probability of attaining a certain level of noisiness or quietness. This is evident from viewing the x-axis where mean of the curves or the noise at peak probability may be compared.

Figures 4.137 to 4.141 show the trend of OBSI in test cells that were subjected to environmental as well as a higher volume of traffic loads than the passing lane. The loading in mainline road was provided by Interstate 94 traffic. Figures 4.137 to 4.141 show that the drag textures maintain peaks at 102 dBA around the mean and the distribution is leptokurtic implying that the data is centrally tended and the effect of traffic is hardly noticeable. In Figures 4.137 and 4.138 it is evident that the peak of the exposed aggregate is similar. The Transverse Tine cells can easily be. Bell is shifted to the right implying higher noise level for the passing lane. It is possible that the effect of traffic was a decrease noise. Additionally the tined cells have been in place since 1993.

It is also evident that the passing lane is noisier than the driving lane when the Transverse Tine bell curves are examined. Random Transverse Tine is negative texture and a reduction of the asperities may have a greater chance of reducing the spikiness unless other obvious degradation patterns occur. Otherwise it may be deduced that in the other textures, there is not enough traffic to cause a clear observation of the traffic effects. An obvious observation is the relative quietness of the various textures when viewed in terms of probability of attaining a certain level of noisiness or quietness. This is evident from viewing the x-axis where mean of the curves may be compared.

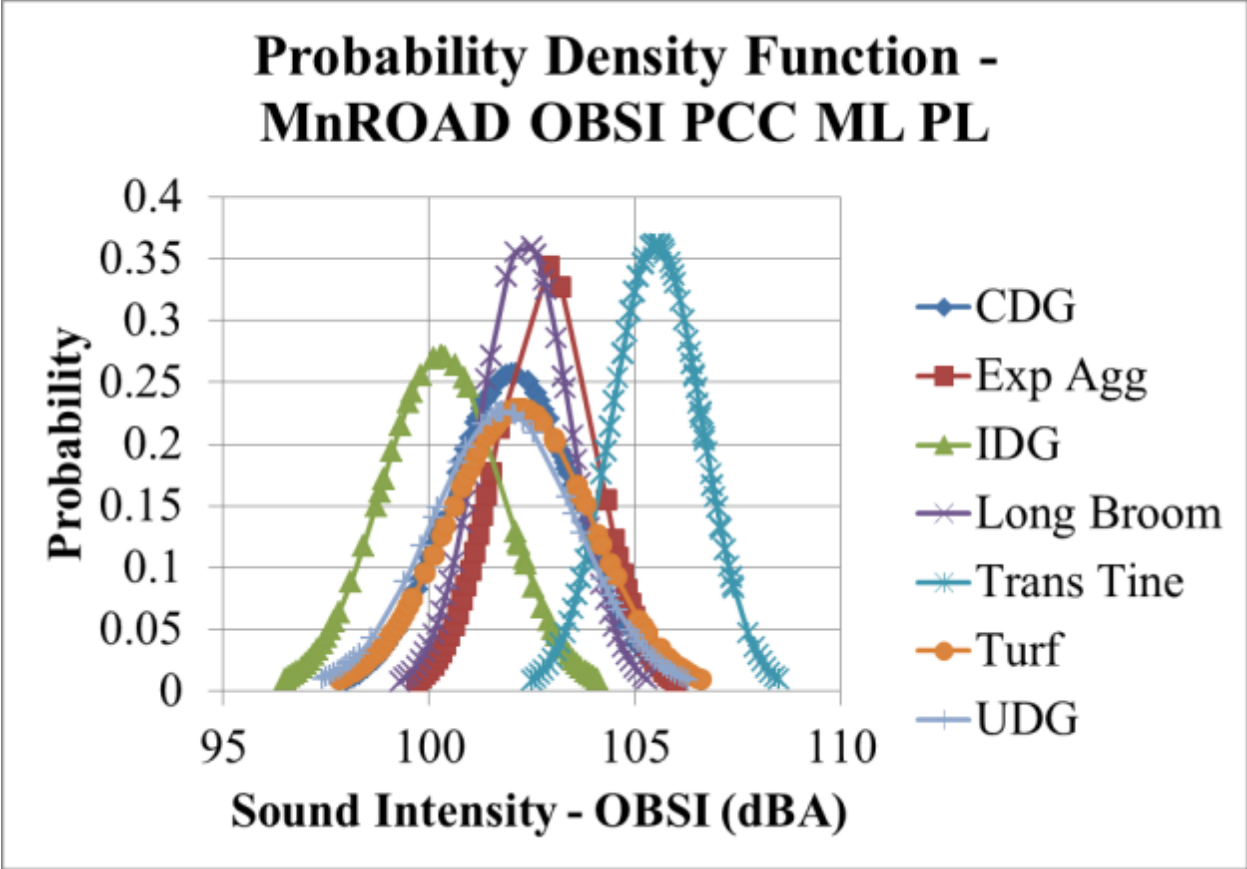


Figure 4.136: Probability Density Function of various Test Cells Subject to 5 years of Passing Lane Interstate traffic

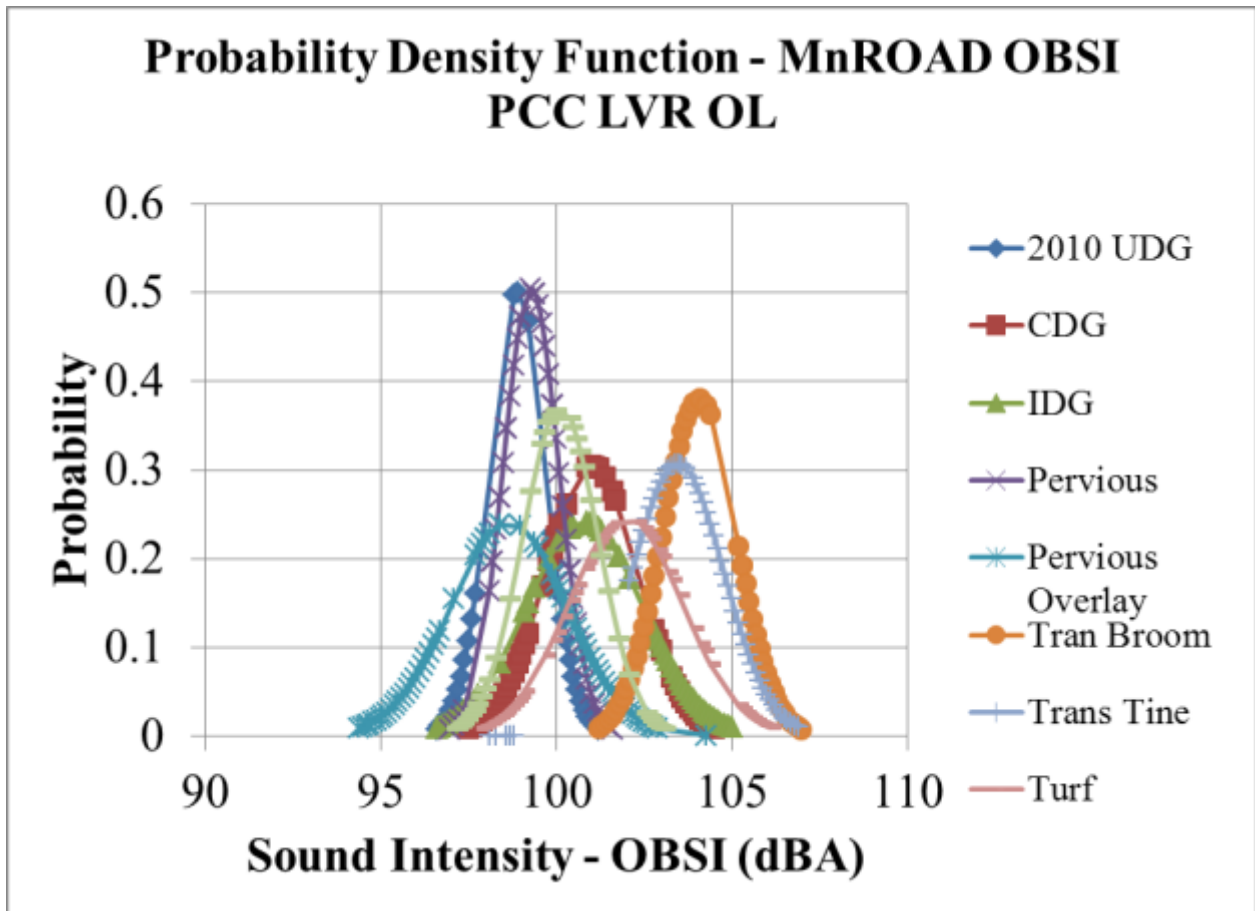


Figure 4.137: Probability Density Function of various Concrete Test Cells Subject to 5 years of Environmental factors (No traffic).

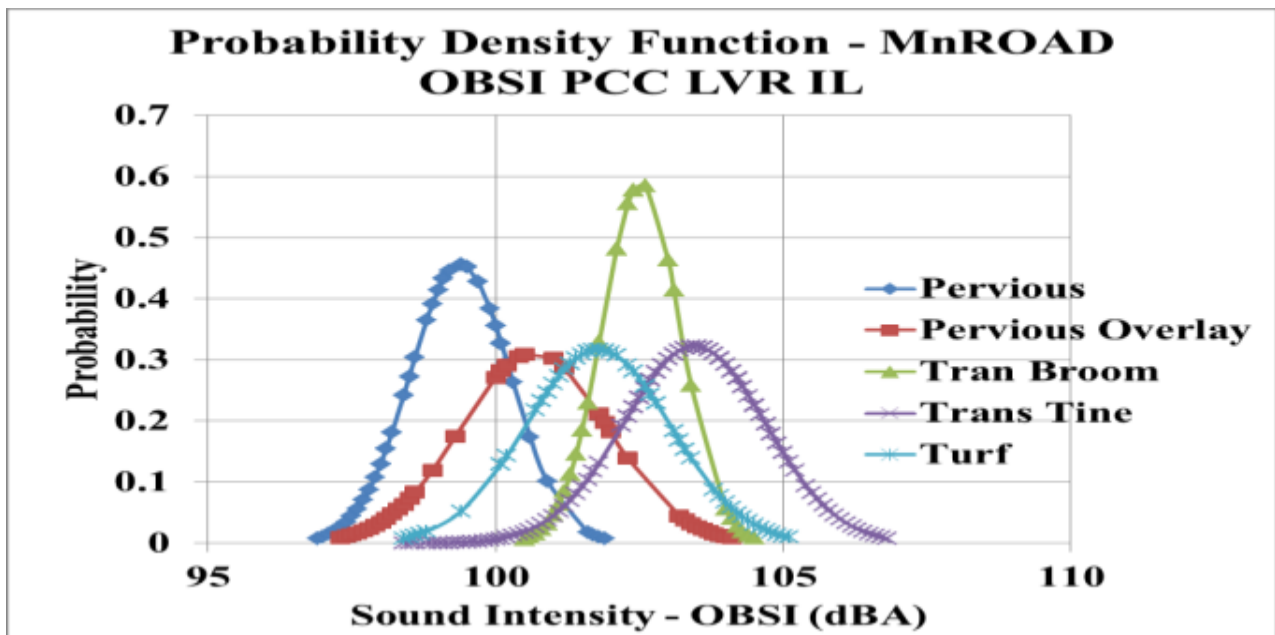


Figure 4.138: Probability Density Function of various Test Cells Traffic Lane Subject to 5 years of Low Volume Traffic.

Figure 4.137 to 4.141 show the trend of OBSI in test cells that were subjected to environmental as well as low volume traffic loads. Examining these figures, the pervious pavements maintain the same peak probability at 99.3 dBA around the mean and the distribution is leptokurtic implying that the data is centrally tended and the effect of traffic is hardly noticeable. Additionally, it is evident that the peak of the pervious overlay is slightly shifted to the left but it is not clear if that is within the margin of error or the disparity will increase with time. The transverse broom cells cannot easily be compared because the external lane was an aggressive texture while the inside lane was a mild Transverse Tine texture. Bell is shifted to the right implying higher noise level for the inside lane. It is possible that the effect of traffic was an increase in the texture spikiness and therefore an increase in noise. However there is no reference point between the adjacent lanes as at the starting texture was different.

It is also evident that the outside lane is noisier than the inside lane when the Transverse Tine bell curves are examined. Random Transverse Tine is negative texture and reductions of the asperities have a greater chance of reducing the spikiness unless other obvious degradation patterns occur.

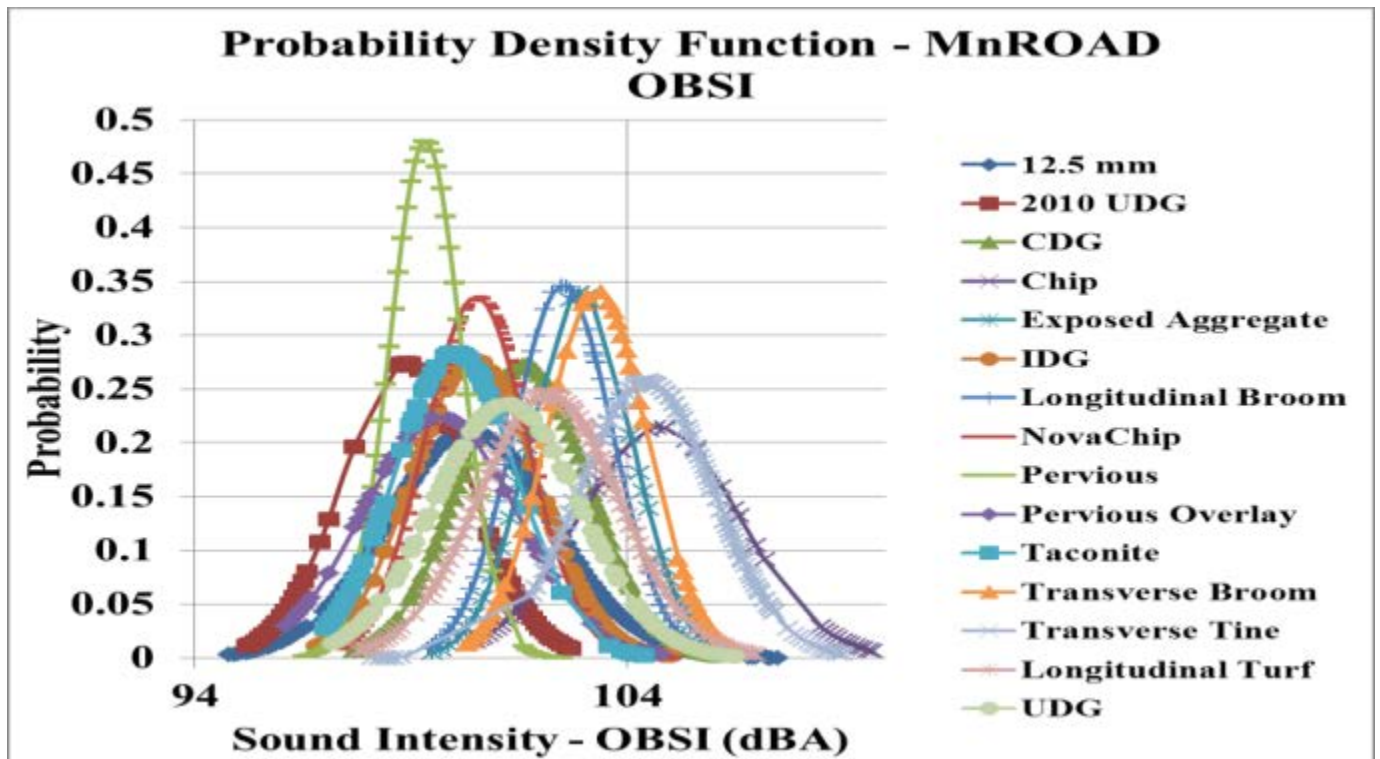


Figure 4.139: Probability Density Function of all MnROAD Concrete Cells Subject to 5 years (or more) of Interstate Traffic

## SUMMARY

For all intents and purposes, probability density function or a quasi-normal distribution representation of data provides the following features

- 1) The extreme data points (maximum and minimum) are easily visible from the plot.
- 2) The mean as well as the data spread is visible from the plot.
- 3) Comparison between texture types is facilitated.
- 4) It is evident that adherence to a standard can easily be rated by the distribution for instance it shows the probability that each texture will be quieter than 100 Hz.

### 4.4.2 Observed IRI OBSI Trends in Various Texture Types after 3 Years

This subsection examines pairs of IRI OBSI correlation in test sections with various textures. Each individual pair consists of the same texture type built at the same time but subjected to different load levels at the MnROAD facility. Within pairs, the effect of loading in increasing the range of IRI is observed thereby. In the MnROAD low volume road consists of the inside lane (IL) and the outside lane (OL) while the mainline consists of a driving lane (DL) and passing lane (PL) and individual test cells are identified by a unique number.

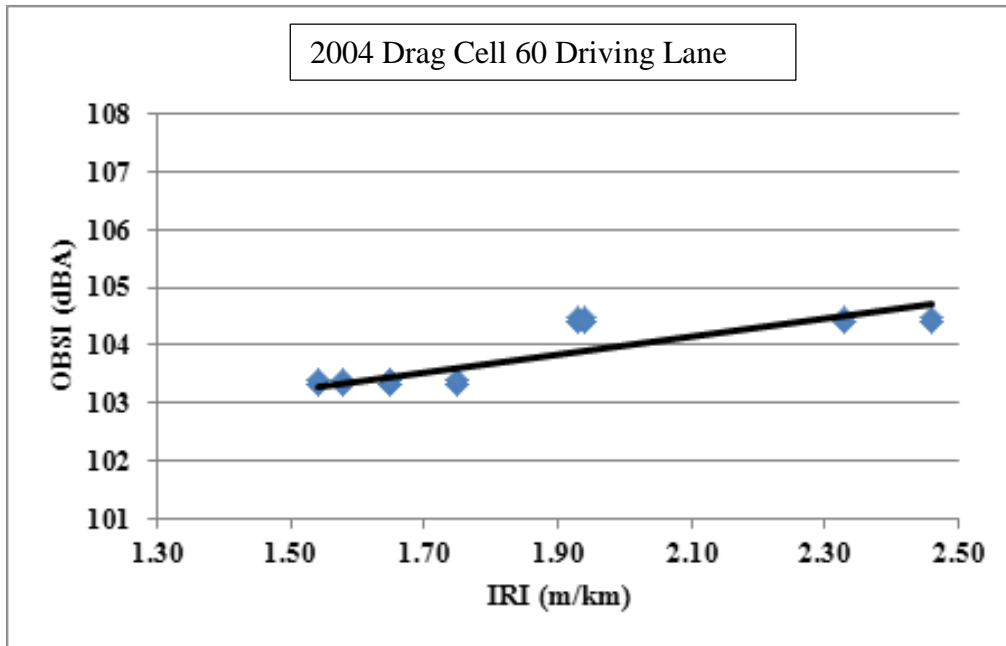
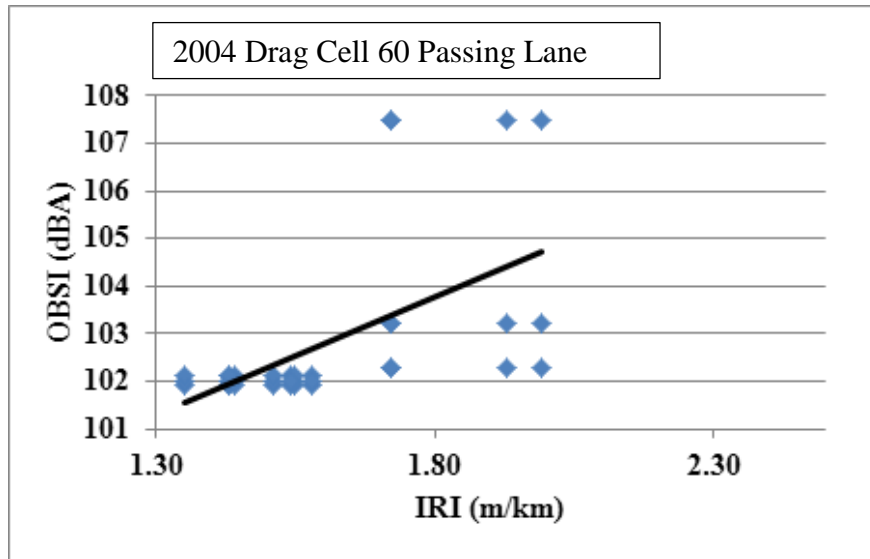


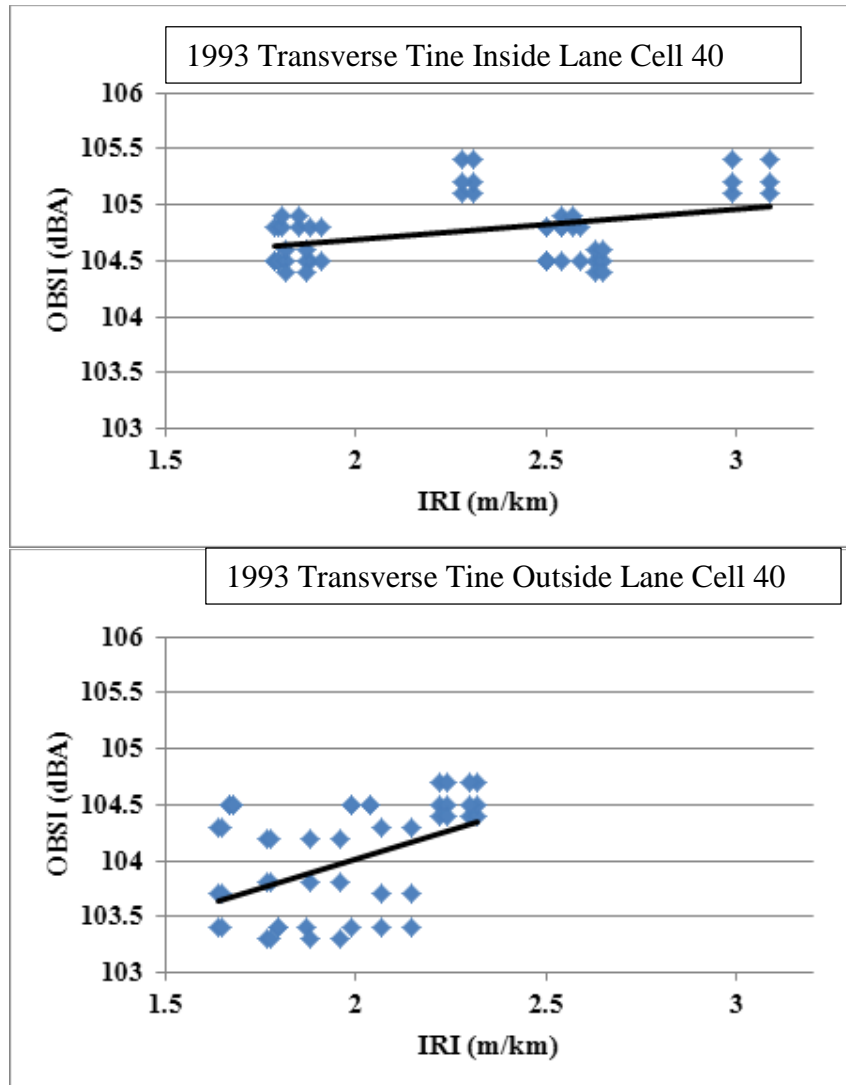
Figure 4.140: OBSI IRI Codependence



**Figure 4.141: IRI OBSI Correlation in a Conventionally Ground Texture on an Unbonded Concrete Overlay**

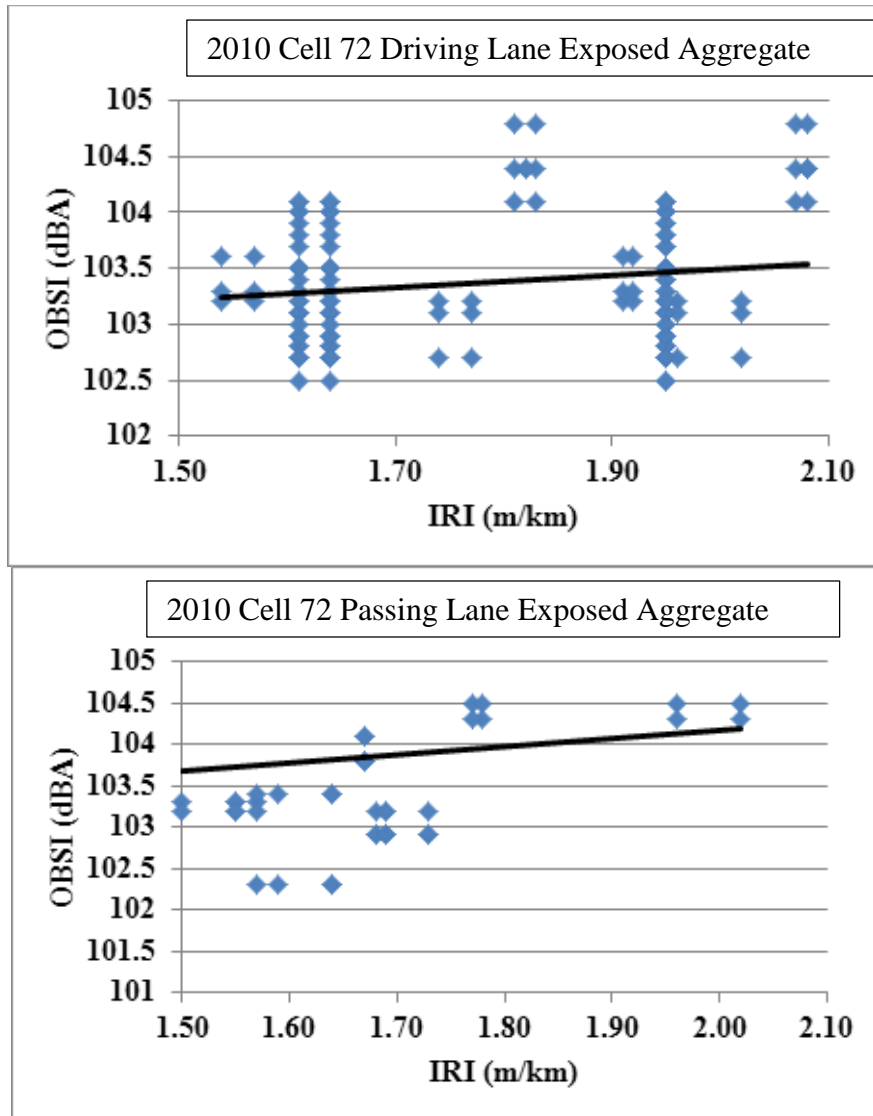
Figure 4.142 shows two lanes of a 500 ft. test cell on Interstate 94 built in 2004 with a whitetopping design and textured with the turf drag configuration. The driving Lane (DL) had undergone a cumulative 10 million ESALs while the passing Lane PL has undergone 3 million ESALs. Although the passing lane has become as noisy as the driving lane in spite of the former experiencing lesser IRI, there was a significant event of panel rotation in the passing lane that began immediately after construction. In both cases there is a steady increase in IRI with increase in OBSI.





**Figure 4.142: IRI versus OBSI in a Transverse Tine Textured Pavement**

Figure 4.143 shows the IRI OBSI correlation for a Transverse Tined concrete. The outside lane (OL) and inside lane (IL) of MnROAD Cell 40 was built in 1993 with an 8 inch concrete surface on a trapezoidal base of thickness varying from 8 inches to 12 inches. From 1993 to 2008, the outside lane was loaded with a 102 Kip 5-axle semi 80 times a day one day a week and was subsequently not loaded. Since 2008, Inside lane has been loaded by an 80 Kip 5-axle semi-trailer 5 days a week but prior to 2008 it was loaded 4 days a week. Although the effect of texture degradation due to accelerated loading on outside lane is a valid point, there is strong evidence of OBSI IRI correlation in this cell. It must be noted that the OBSI values were not temperature adjusted.



**Figure 4.143: IRI OBSI Correlation in an Exposed Aggregate Test Cell**

Cell 72 (Figure 4.144) was constructed in 2010 as a two lift concrete pavement on the Interstate 94 MnROAD Mainline. Consequently the load repetitions are not year large enough to observe a difference in IRI between the Driving lane (2 million ESALs and the Passing lane 0.75 million ESALs however there is evidence of positive correlation between IRI and OBSI in each case. Unlike Cell 72 adjacent cell 71 (Figure 4.145) built with the same design as cell 72 was textured with the innovative diamond grind in the driving lane and with conventional grind in the passing lane. The rate of OBSI Increase in the passing lane is significant possibly due to rapid texture degradation explained by Izevbekhai and Khazanovich [4.5].

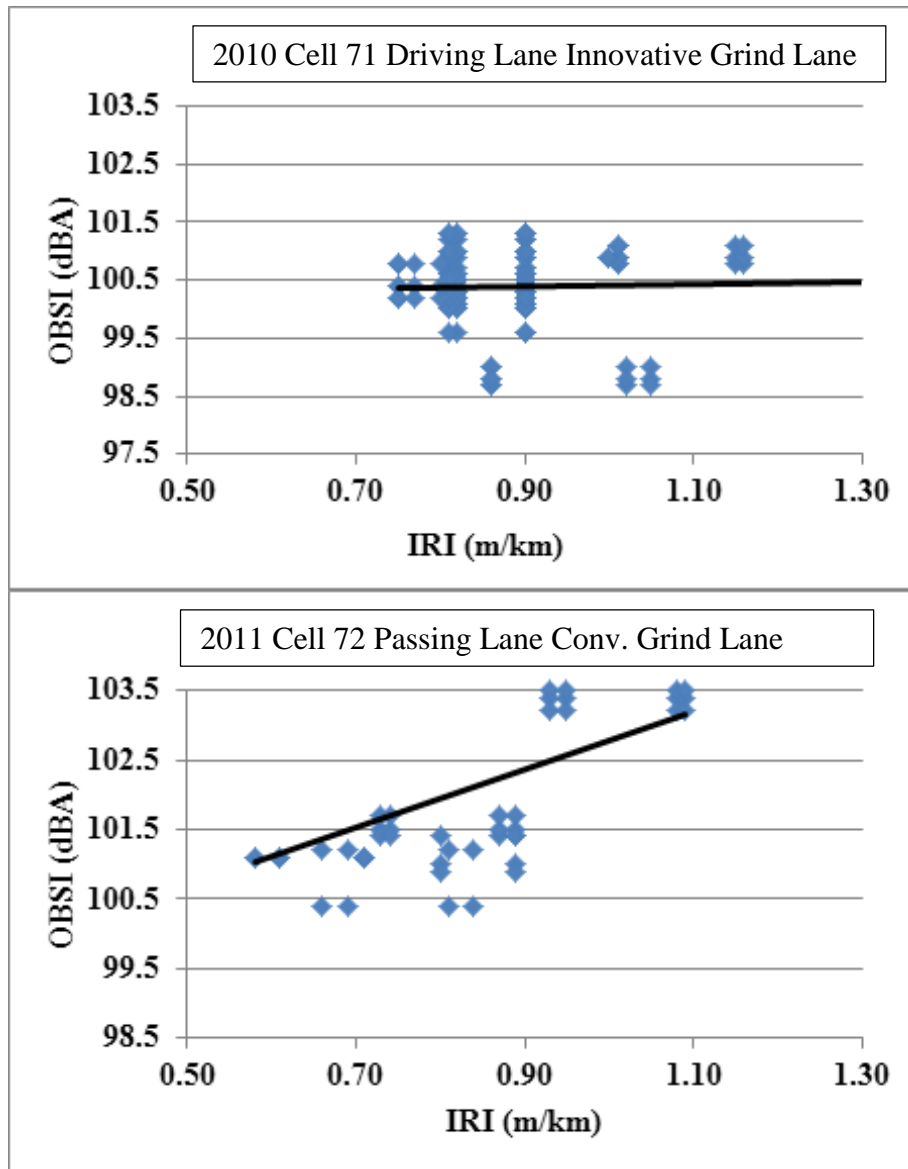
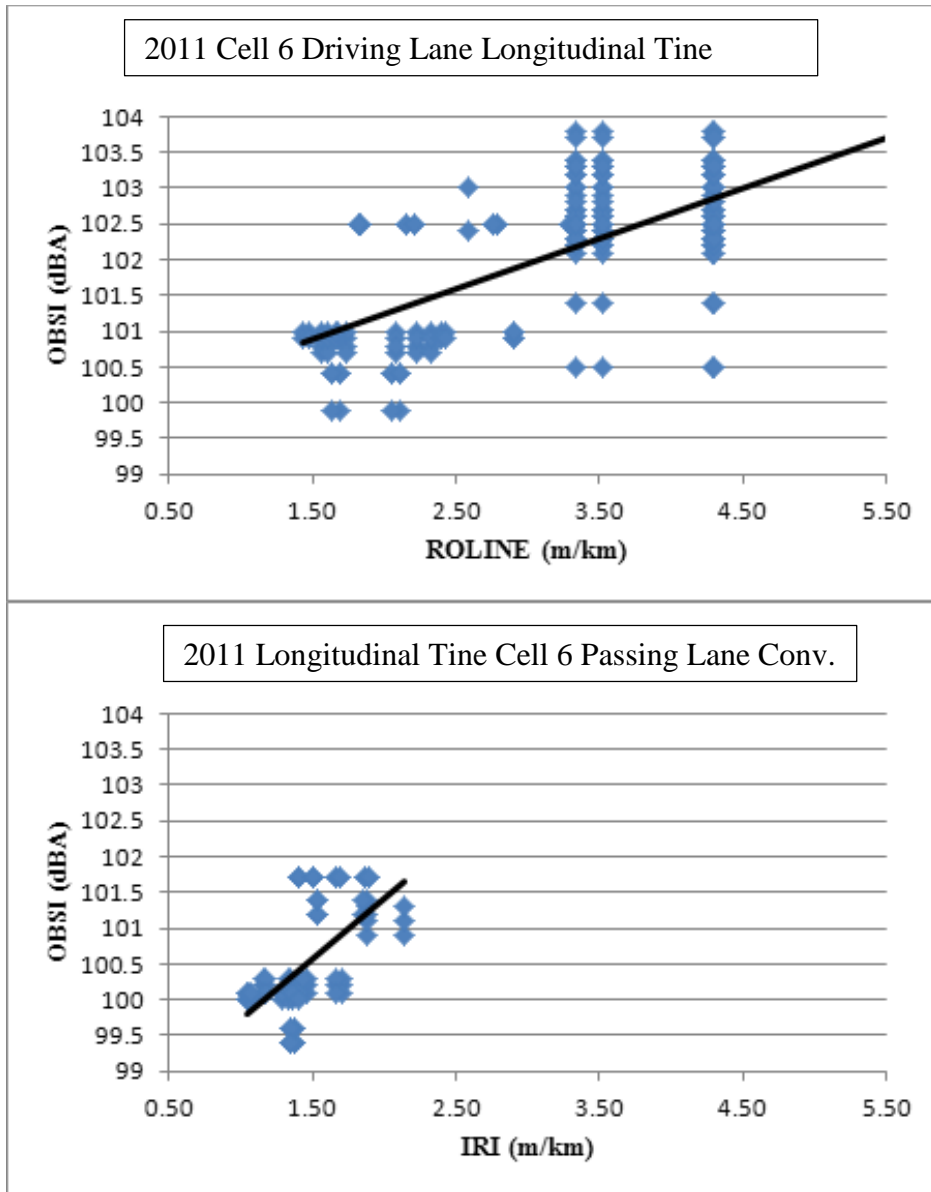
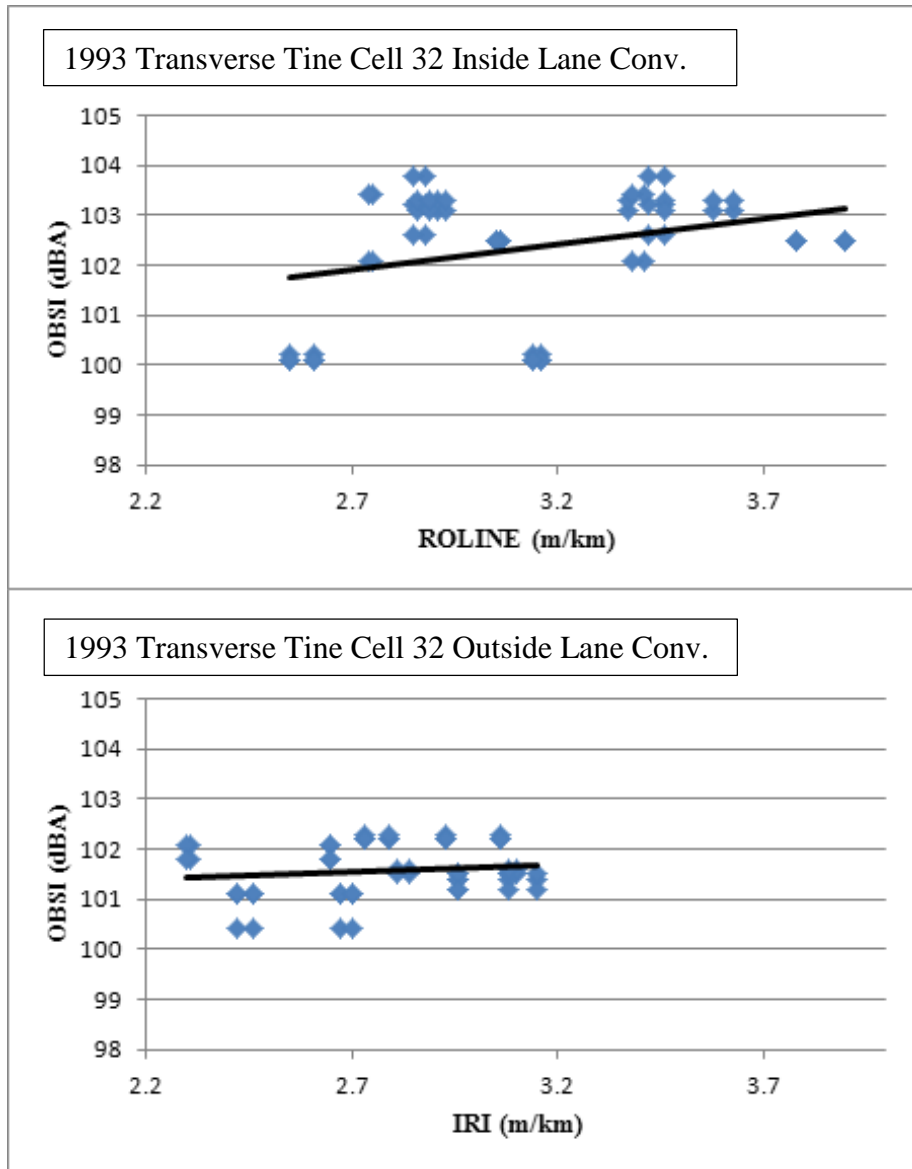


Figure 4.144: Comparative Response of an Innovative Ground texture (Top) and a conventionally ground texture (Bottom)



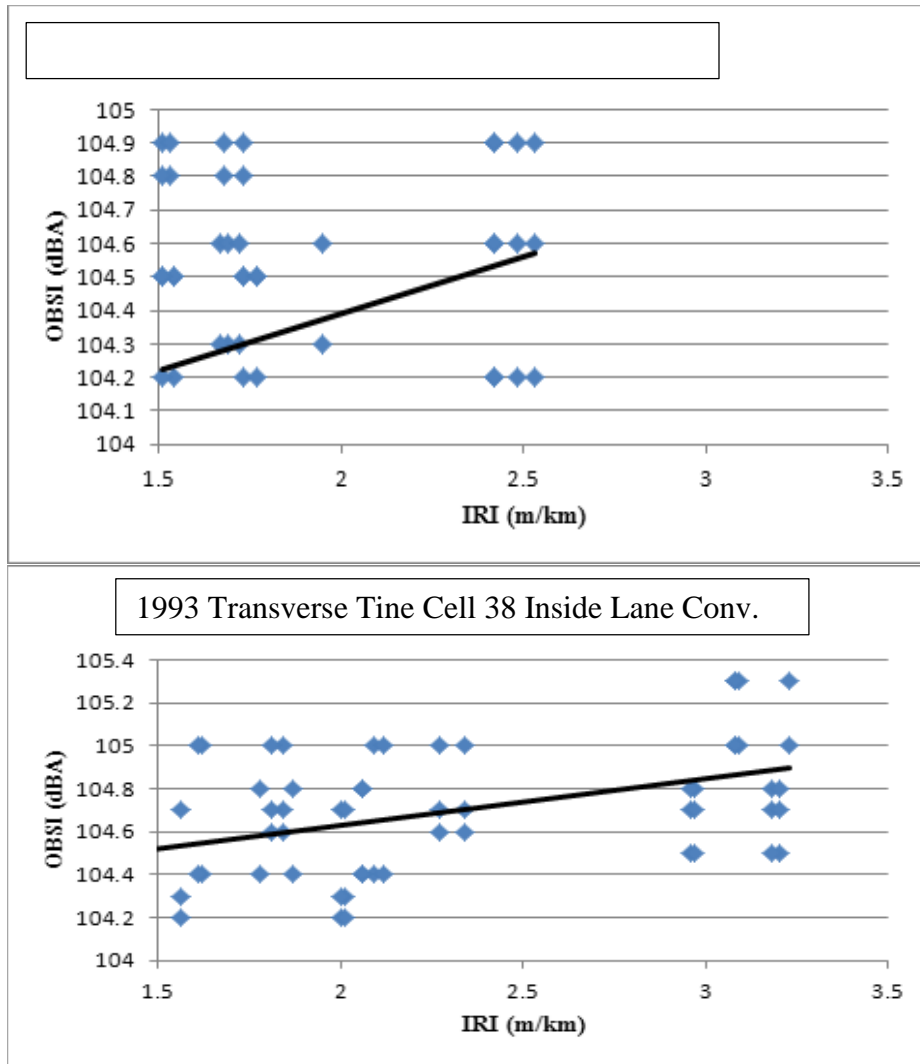
**Figure 4.145: IRI OBSI Relationship in a Conventionally Ground Textured Unbonded Overlay Test Cell**

Cell 6 (Figure 4.341) was constructed in 2011 as a 6 inch thick concrete pavement textured with longitudinal broom on the Interstate 94 MnROAD Mainline. Consequently the load repetitions are not year large enough to observe a difference in IRI between the Driving lane (2 million ESALs and the Passing lane 0.75 million ESALs however there is evidence of positive correlation between IRI and OBSI in each case. This cell shows approximately the same rate of OBSI-IRI correlation and as expected the IRI in the passing lane was less than that of the driving lane.



**Figure 4.146: Comparative response of a Turf Drag texture in the MnROAD Low Volume Road**

Figure 4.147 shows the IRI OBSI correlation in the outside lane (OL) and Inside lane (IL) of MnROAD Cell 32. This cell was built in 2000 with 6 inch concrete surface on a 8 inches base of thickness varying from 8 inches to 12 inches. This cell was finished with a transverse tined texture. From 1993 to 2008, the outside lane was loaded with a 102 Kip 5 –axle semi 80 times a day one day a week and was subsequently not loaded. Since 1993, Inside lane has been loaded by an 80 Kip 5 – axle semi-trailer 5 days a week but prior to 2008 it was loaded 4 days a week. Although the effect of texture degradation due to accelerated loading on outside lane is a valid point, there is strong evidence of OBSI IRI correlation in this cell. It must be noted that the OBSI values were not temperature adjusted.



**Figure 4.147: Comparative Response of a Turf Drag Texture in the MnROAD Low Volume Road**

Figure 4.148 shows the IRI OBSI correlation in The outside lane (OL) and Inside lane (IL) of MnROAD Cell 38 was built in 2000 with 6 inch concrete surface on a 8 inches base of thickness varying from 8 inches to 12 inches. This cell was finished with a transverse tined texture. From 1993 to 2008, the outside lane was loaded with a 102 Kip 5 –axle semi 80 times a day one day a week and was subsequently not loaded. Since 2008, Inside lane has been loaded by an 80 Kip 5 – axle semi-trailer 5 days a week but prior to 2008 it was loaded 4 days a week. There is strong evidence of OBSI IRI correlation in this cell. It must be noted that the OBSI values were not temperature adjusted.

This study examined a plethora of test sections, measuring OBSI and IRI in 32 concrete test cells over a period of 4 years. It is shown analytically that as the deteriorated joint changes the tire pavement acoustics of the pavement thus lending credence to the fact that distress issues that cause joint slap may also be associated with increased IRI. Though a similar analysis was neither made with joint faulting, nor warp and curl phenomena the increase in the intensity and rate of concatenations when tire rides over such features suggests that increased noise may be associated

with more frequent and more severe pavement conditions. In the development of a phenomenological OBSI prediction model, addition of IRI to a set of significant variables increased the adjusted coefficient of determination. Subsequently, a removal of IRI from the set of variables weakened the predictive capability of the model. It was possible to see a correlation between OBSI and IRI in the 32 test cells examined. In confirmation of the effect of loading in each cell, the driving lane in the mainline and the inside lane in the LVR experienced higher IRI within the analysis period than their adjacent lane in each cell. In many cases higher OBSI were associated with the higher IRI. The implications of this finding thus accentuate the existence of a positive correlation between IRI and OBSI though the frequency regimes of the two variables are different. Their correlation may therefore be associative and not necessarily causative. Figures 4.148 to 4.159 show 2012 pictures of the various textured monitored.

#### Pictures of Textures at 3 or more years in Place

---



**Figure 4.148: Drag, Conventional**


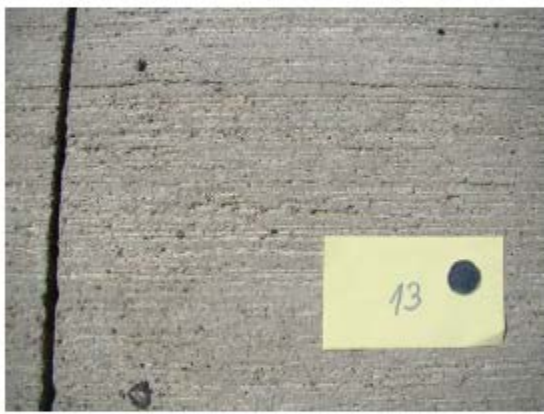



**Figure 4.149: Drag, Conventional Grind Transverse Tine**





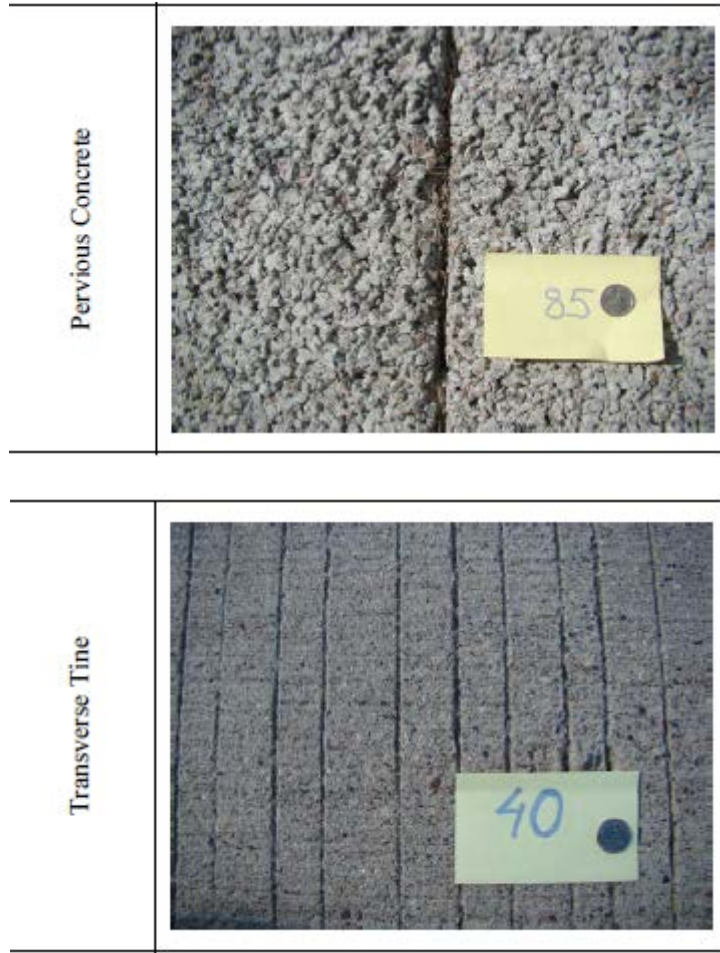
**Figure 4.150: Longitudinal Tine Innovative Grind, Conventional Grind**

Transverse Tine	
Longitudinal Turf Drag	
Longitudinal Broom Drag	

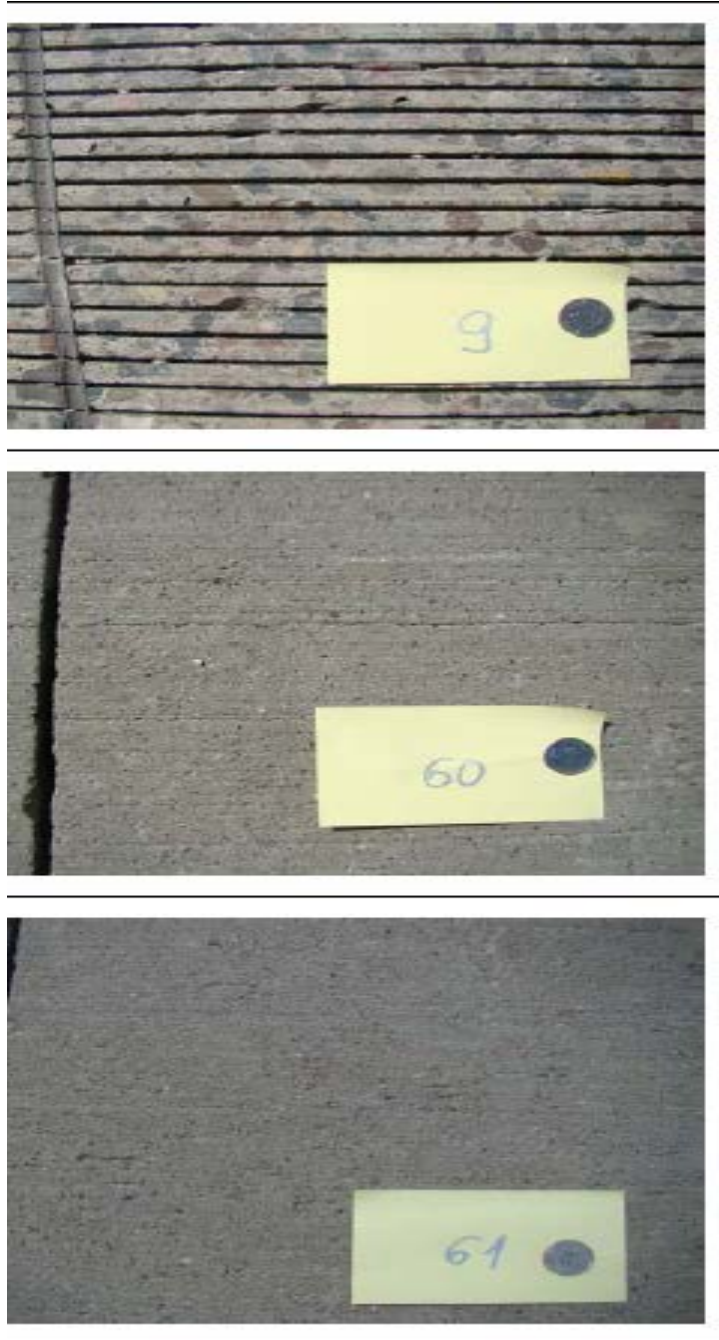
**Figure 4.151: Transverse Tine, Turf Drag, Broom Drag**



**Figure 4.152: Innovative Grind, Transverse Tine, Pervious Concrete**



**Figure 4.153: Pervious Concrete Transverse Tine**



**Figure 4.154: 2008 Innovative Grind, 2004 Drag, and 2004 Drag**



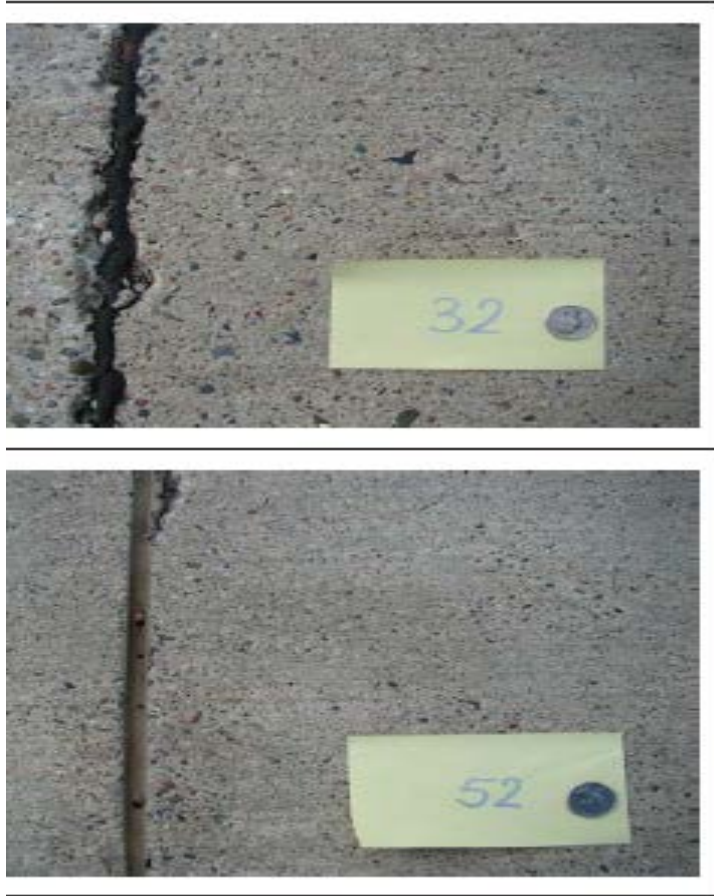
**Figure 4.155: 2004 Drag, 2011 Grind Of Drag Surface, 2011 Grind of Tined Surface**



**Figure 4.156: 2011 Innovative Grind, 2011 Exposed Aggregate**



**Figure 4.157: 2008 Pervious Concrete**



**Figure 4.158: 2000 Drag Surfaces**





**Figure 4.159: 2000 and 2004 Drag Surfaces**

## Chapter 5: Advanced Data Analysis and Model Development

This chapter elucidates five advanced analyses performed on the test results and data discussed already.

**5.1) Effect of Texture Direction and Texture Orientation:** The Mann Whitney Wilcoxon method showed to a 95% confidence level that, there was a clear difference between the OBSI data set for transversely textured pavements and longitudinally textured pavements. This lent credence to the hypothesis that texture direction would affect tire pavement noise. Texture direction did not seem to affect IRI significantly. However, certain longitudinal textures exhibited anomalous IRI with non-continuous (single or triple) lasers.

**5.2) Laser Induced Anomalies in Ride Measurements:** This task compared IRI measured with a triple laser and line laser, shown in figure 4, most of the new textures did not show significant disparity of IRI in the two lasers except the longitudinal one. The problem of laser induced anomalies is also prevalent in the ground textures which are outside the purview of this study.

**5.3) Analysis of Investment in Surface Characteristics:** Benefit cost analysis of investment in quiet pavements was performed. The probability of each surface being quieter than 100dBA (Figure 2) multiplied the ratio to account for likelihood of quietness. It showed that investment in quiet surfaces might be more beneficial than noise walls if an initial 10 dB reduction is unnecessary.

**5.4) Development of Friction Survival Model with MnROAD Concrete Surface Textures:**

This study developed a friction-survival model for ribbed and smooth tire friction of the MnROAD textures. The model retained typical initial Friction Number values as initial values of the model and showed decays that were indicative of the durability of texture types in providing skid resistance. This model was successfully validated in the Minnesota network with their actual traffic volumes. It applies to both the smooth and ribbed tire as shown below where  $F$  is the friction,  $k$  is the growth rate,

**5.5) Analysis of Relationship between Pavement Condition and Pavement Acoustics:** This subsection developed a set of equations that showed that the acoustic signal from a deteriorated joint is different from that of an undeteriorated joint. It also validated this lemma through the analysis of data and showed that there was a correlation between OBSI and IRI. This important observation forms the basis for the development of acoustic monitors for pavement condition.

### 5.1 Statistical Examination of the Effect of Texture Direction and Texture Orientation on Noise & Friction

#### 5.1.1 Effect on Noise

A set of physical equations were derived in the preceding chapters to accentuate what physical correlation may exist between direction and OBSI. The initial approach involved an investigation of a set of textures that are of approximately the same configuration, but are orientated differently into categorical longitudinal and transverse textures. Physical derivations of sound intensity in relation to texture direction had attributed increased sound intensity to transverse textures. In this section, sound intensity of transverse and longitudinal textures of similar configurations is compared. A test with assumed mean difference of zero is assumed, based on a hypothesis that the two are equal. The t test evaluates this hypothesis and compares the probability that the lemma of equality is true to the alpha value of 0.05 based on a 95 percent confidence level.

Two sets of data compare the longitudinal texture to the transverse texture. In the first set, a transverse broom texture is compared to a longitudinal broom texture and in the second set a transverse tire is compared to a longitudinal grind of approximately the same dimensions.

**Data Set 1:**

Cell 53 was built as a 60 year design pavement with a 12 inch thick pavement but innovatively textured in the inside lane with a mild broom drag, and in the outside lane with an aggressive transverse broom. Longitudinal turf and broom drags were respectively placed on cell 13 and 14 at the same time as cell 53.

OBSI data from each set was recorded along with the data of testing. The dimensions of the texture are shown in the Table 5.1 below.

**Table 5.1: Configuration of Textures Data Set 1.**

	Passing lane	Cell 14 (Longitudinal Broom )	Cell 53 inside (Transverse Broom)	Cell 53 outside (Heavy trans Broom)
Groove depth (mm)	0.025	0.026	0.020	0.039
Land width (mm)	0.039	0.039	0.013	0.039
Groove width (mm)	0.029	0.028	0.020	0.039
Model	$A \sin \pi x/L$	$B \sin \pi x/L$	$C \sin \pi y/L$	$D \sin \pi y/L$

L= average asperity spacing

**Data Set 2:**

Cell 12 was built on 1993 with a transverse tire texturing. The average tine width, the kerf and the groove depth are shown in Table 5.1. Cell 7 was a longitudinal grind of approximate texture configuration as cell 12; howbeit in the different direction (Transverse, versus Longitudinal).Corresponding (same day) noise level measurements for each set of measurements were compared.

**Table 5.2: Configuration of Texture Data.**

Dimensions (in)	Cell 12 DL Tran. Tine	Cell 12 PL Tran. Tine	Cell 7 Driving lane IDG	Cell 7 Passing lane IDG
Groove Depth	0.04	0.04	0.0466	0.0466
Land width	0.42	0.42	0.360	0.360
Groove width	0.125	0.125	0.125	0.125

For OBSI measurements conducted between 2008 and 2010, Table 5.1 shows the comparison of the transverse to the longitudinal broom. OBSI change of 3-dB will be detected by the human ear. A difference of 1 may be detected by a little child. OBSI is therefore referenced to 100 BA which is the industry standard for quiet pavement. Table 5.2 shows a comparison of OBSI of

transverse tire to longitudinal grind of approximate surface configuration. The results show the longitudinal texture to be much quieter in all cases. The respective passing lanes and driving lanes of the longitudinal textures were quieter than the respective texture of the transverse configuration.

For a one tailed analysis, if  $P(T \leq t)$  one-tail = 0.00179 and  $t$  Critical one-tail = 1.685, consider that  $t$ -stat = 3.101,  $P(T \leq t)$  is 0.00179 is much less than 0.05 which is the alpha, based on a 95 % confidence level. Thus the probability that the data set of the transverse and the longitudinal textures are similar is 0.00179. This is much less than 0.05. It can thus be established from a 95% confidence level that transverse tire data is not similar to longitudinal tire data but is indeed louder.

Similarly for a two tailed distribution,  $P(T \leq t)$  two-tail = 0.0036 is also much less than 0.05 so that if we compare from a 2 tailed perspective, the probability that the data set is similar is 0.0037. This data can be viewed in Table 5.1. It is evident that the transverse texture is consistently louder than the longitudinal texture. This comparison is limited by the variability between the aggressive texturing of the outside lane and the mild texturing of the inside lane. Modifications of texture dimensions affect sound intensity as well. The lighter transverse brooming was much quieter than the aggressive transverse brooming. Aggressive texturing increases the spikiness of the amplitude distribution function.

For a one-tailed analysis, if  $P(T \leq t) = 1.75E-47$  and  $t$ -Critical is 1.68, consider that  $t$ -stat 55.26  $P(T \leq t)$  is much less than 0.05 which is the alpha based on a 95 % confidence level. Thus the probability that the data set of the transverse and the longitudinal are similar is  $1.75E-47$ . This is much less than 0.05. It can thus be established from a 95% confidence level that transverse tire data is not similar to longitudinal tire data. This lends credence to the importance of texture direction as a variable in the prediction of tire pavement noise. Similarly for a two tailed distribution,  $P(T \leq t)$  two-tail =  $3.5E-47$  is also much less than 0.05. From a 2 tailed perspective, the probability that the data set is similar is only  $3.44 E-47$  which is zero. In TABLE 5.3 it is evident that the transverse texture is consistently louder than the longitudinal texture. This comparison is limited by the absence of a true longitudinal tire or a transverse grind for adequate comparison. Nevertheless the analysis accentuates the importance of texture direction as a significant variable in the prediction of sound intensity

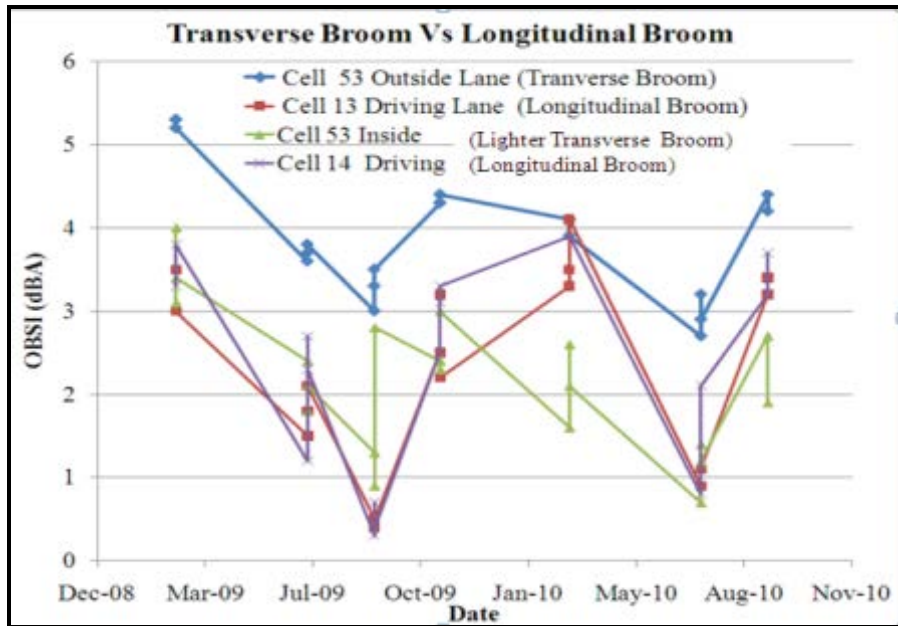


Figure 5.1: Transverse Broom versus Longitudinal Broom

**Table 5.3: Acoustic Response (OBSI-100 dBA) of Transverse Turf & Longitudinal Turf**

	Transverse Vs Longitudinal Broom		Transverse Tine Vs Longitudinal grind	
	Cell 53 Outside Lane (Transverse Broom)	Cell 13 Driving Lane (Longitudinal Broom)	Cell 12 Transverse	Cell 7 Grind
Mean	3.0725	2.3775	5.35576	0.12884
Variance	1.44717	1.47102	0.73937	1.56993
Observations	40	40	52	52
Pearson Correlation	0.311675953		0.8558	
Hypothesized Mean Difference	0		0	
Df	39		51	
t Stat	3.1014		55.2655	
P(T<=t) one-tail	0.001786		1.75E-47	
t Critical one-tail	1.6849		1.6752	
P(T<=t) two-tail	0.003579		3.50E-47	
t Critical two-tail	2.0227		2.00758	

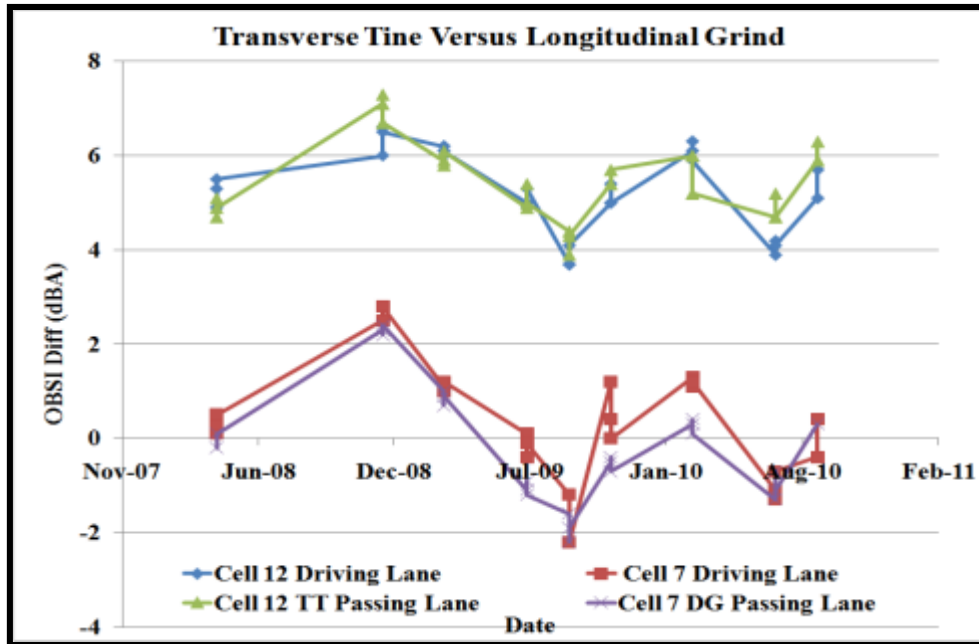


Figure 5.2: Transverse Tine versus Longitudinal Grind Data

### Wilcoxon and T-Tests for Texture Direction

In this section all the textures tested are categorized into transverse and longitudinal. A transverse texture is defined as one in which the main asperity is small in the transverse direction in comparison to the longitudinal direction. According to texturing process, longitudinal textures are developed by advancement of the texturing in the longitudinal direction while transverse textures are imprinted by transverse motion of texturing device. As there are no isotropic textures studied in this research, categorical variables of longitudinal (0) or transverse (1) are defined. The following discusses, the use of Wilcoxon ranked sum test, the T-test and the paired T- test to ascertain if texture direction is of any consequence in OBSI prediction and possibly to ascertain what mean difference exist between them.

The Wilcoxon Rank sum test is a powerful statistical process for ascertaining how germane 2 sets of independent samples are. The method uses one of 2 data types: the categorical and the tabular. The categorical method uses a large dataset in which the entries in a separate column are categorized numerically or descriptively. In the tabular method, the 2 sets of data are entered as the data needing to be evaluated for germaneness.

All the data is converted to ranks and the statistic observes normal approximation for continuity and ties as well as number of tied values. A total of 594 data points were made up of 297 transverse and 297 longitudinal textures. These were arranged such that corresponding rows had test results from the same time of testing so that biases of temperature and other influential variables are minimized. The null hypothesis being tested is that the distribution of the 2 groups is the same. Knowing that data is clustered in the 98 to 106 dBA range, it was expedient to compare the OBSI to 100 dBA which is the industrial pivot for quiet and noisy pavements. Another reason is because, the OBSI difference in a logarithmic scale is related to the ratio of attenuation of pavement noise. Based on a 95 % percent confidence level, P-value of < 0.05 will reject the null hypothesis. A p-value of >0.05 will not reject the null hypothesis. Results showed

a p-value of the order of  $1E-07$  indicating that the null hypothesis is rejected by this test. The Mann Whitney Wilcoxon test is favored for non-parametric as well as parametric data. The Two Sample Test is similar in process to the Wilcoxon test but exploits another statistic. It possesses the capability of analyzing by categorical variable or by table. It is robust enough to accommodate many statistic types such as equal means, equal SD etc but this study proposed hypothesized mean difference of zero as null hypothesis. The process generated a p value of 0.0005 that is  $\ll 0.05$  and indicates that there is remarkable difference between OBSI\*\* (OBSI-97 dBA) of transverse and OBSI \*\* of longitudinal textures. However, the paired t- test is a statistical method of evaluating the likelihood of a plus (+ve) or minus (-ve) when a pair is drawn from the data at random. The statistic examines the hypothesized difference between pairs and computes the mean  $H_0$  difference as 3.0016 with a Standard Error of 0.1050. The upper 95% CI is 3.2082 and the Lower 95% confidence interval is 2.7949. The computed P -value for the OBSI \*\* (OBSI-100) is 0.000001. This shows that the probability that if a pair of transverse and longitudinal textured surfaces is drawn from the data set of (N=297), the transverse is quieter than the longitudinal direction is 0.000001.

#### CHI SQUARE Test for Texture Orientation.

Texture orientation is approached differently from texture direction due to the mathematical possibility of neutral texture orientation. This variable has been defined in Chapter 1 as the SGN skewness of the amplitude distribution function (ADF). Positively skewed means positive texture which describes pointed asperities while negative texture describes indented surfaces. Because, texture orientation can mathematically be neutral as observed in some drag textures, categorical variables assigned were 101 for positive, neutral and negative (OR1) and 110 for positive, neutral and negative.(OR2).

OR1 therefore examines the difference between the effects of non-neutral textures and neutral textures while OR 2 examines the difference between negative and positive textures. In each case the process arranges the data in histograms of 1 dBA interval thus generating 9-sets of data between 98 and 106 dBA. A P value of 0.00003 determined that the effect of texture orientation was significant. It was not possible to determine from the tests which of OR1 or OR2 was more significant as each resulted in P value of zero, indicating that whether it is a comparison of non-neutral to neutral textures or positive to negative, texture orientation is shown by data to be a significant variable.



5.1.2 5.1.2 Effect on Friction

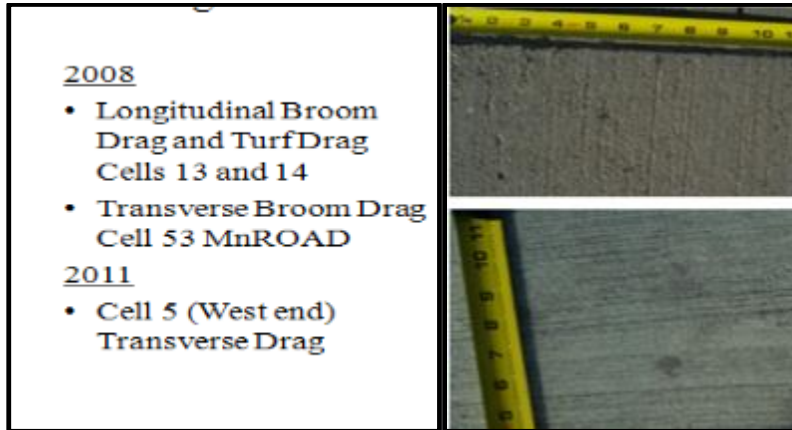


Figure 5.3: Transverse Tine and Longitudinal Tine

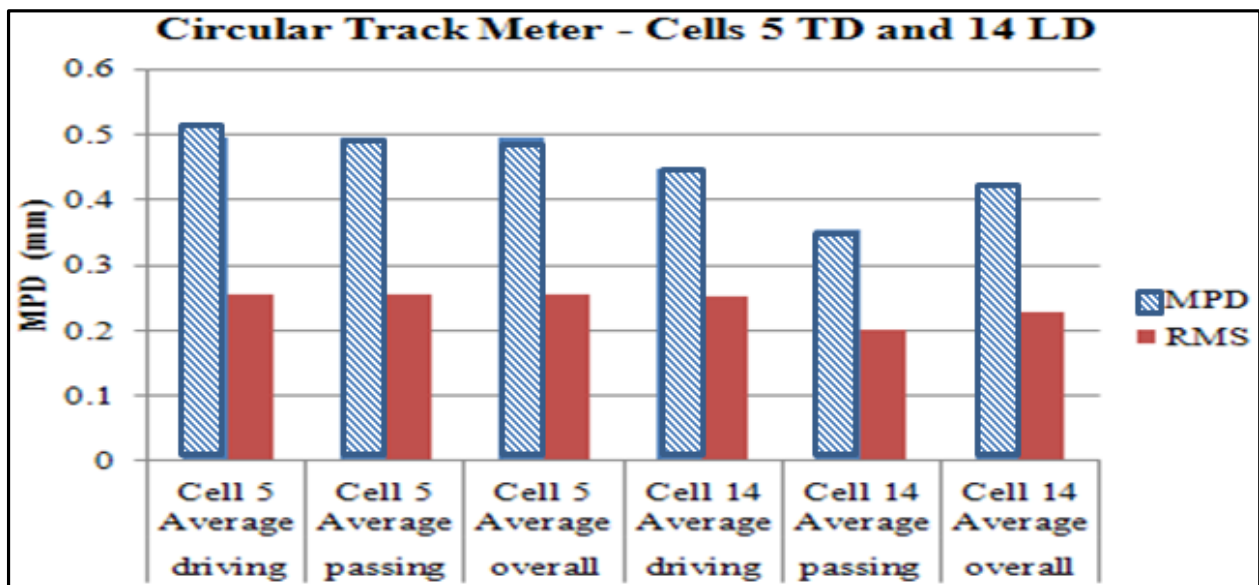


Figure 5.4 Differences in MPD for Longitudinal and Transverse Textures

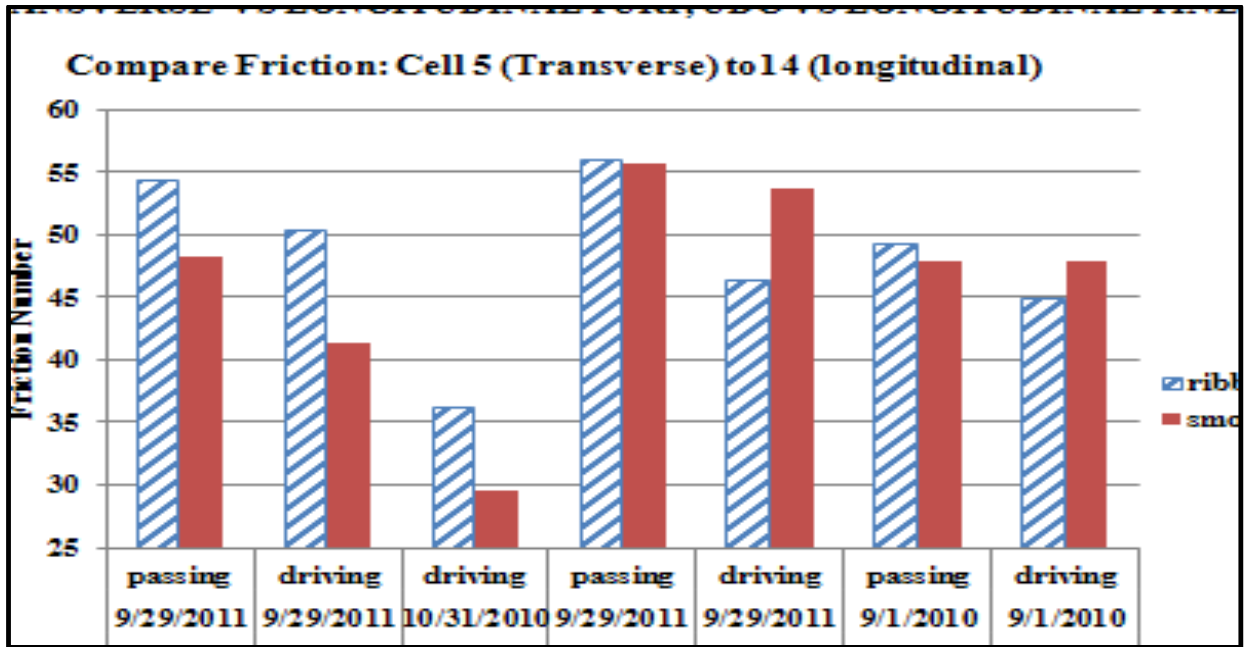


Figure 5.5: Differences in Friction Numbers of Transverse and Longitudinal Grind.

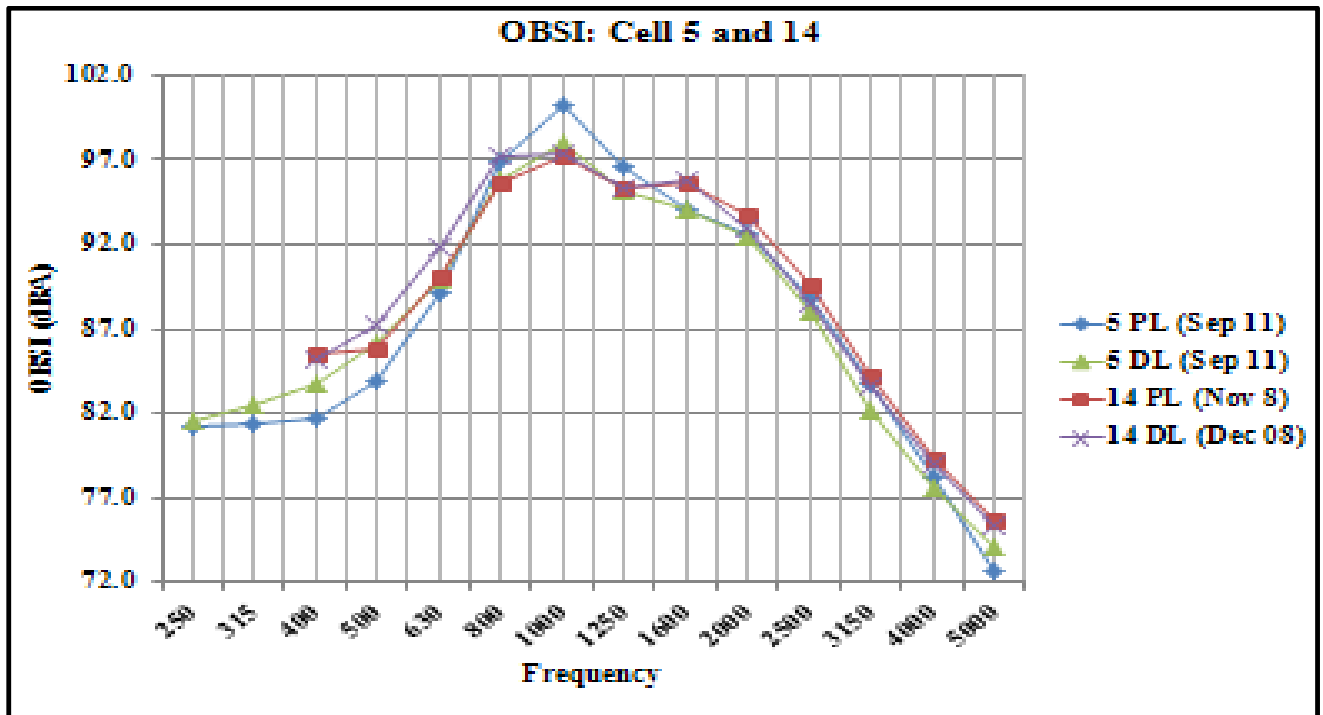


Figure 5.6: Differences in OBSI of Transverse versus Longitudinal Broom.

Figures 5.4 to 5.6 show the differences in texture depth friction number and OBSI for textures of similar configuration but different direction of traffic. It is evident that higher friction numbers appear to be associated with the transverse tine. Izevbekhai et al [4.6] explained how thread block impact and inhibition to hysteresis are more common in transverse textures

### **5.1.3 Section Conclusion**

- It has been shown statistically in the cells examined that transverse textures are generally noisier than longitudinal textures. This rhymes with conceptualization that was discussed in the preceding chapters. Texture direction is definitely a strong variable in the OBSI prediction model.
- It has been shown statistically in the cells examined that texture orientation is significant and positive textures are louder. This rhymes with conceptualization that was discussed in the preceding chapters. Texture orientation is definitely a strong variable in the OBSI prediction model.

This chapter has examined IRI-MPD and texture direction influences on OBSI and concluded that texture direction and IRI may be significant variables for OBSI of non-porous pavements. It is now necessary to examine a typical quiet pavement surface and compare OBSI to other surfaces.

## **5.2 Pavement Texture Induced Roughness Anomalies**

### **5.2.1 Introduction**

Most state agencies including Minnesota Department of Transportation accept constructed pavements based on a smoothness specification [5.1]. MnDOT requires that contractors use an inertial profiler and not a profilograph. There has been a gradual transition from single and triple laser to the line laser. Nevertheless, profilers are required to be certified in a process that calls for acceptable deviation from the institutional standard devices and an acceptable measure of repeatability.

Izevbekhai [5.2] observed a 20 inch per mile IRI difference between longitudinal turf drag surface textured and untextured concrete surfaces using a single laser equipped light weight profiler. The observation in that study and in many other similar studies led to the introduction of a triple laser. The Triple Laser have three point lasers at 1.5 inch interval. It was assumed that at that interval, indiscriminate skipping of the lasers from groove to landing and vice versa would be minimized. Early observations indicated that the problem was not solved with the Triple Laser for the innovative grinding (Boxcar) configurations. The advent of the line /solid laser shed more light on the possible inaccuracies of the previous laser types on certain longitudinal textures. The line laser consists of a continuous laser measuring 3 inches in the transverse direction thus sweeping the tire pavement contact patch. This is referred to as the Roline laser. Generally the IRI numbers generated with the triple laser appeared to be correlated to those generated by the Roline based on commonly accepted levels of confidence in certain texture types. Differences observed between the two laser types over some texture types creates a difficulty of pavement evaluation or acceptance.

A type of distortion occurs when one of the triple laser traverses the configurations at an effectively reduced rate thus receiving the signal as wider configurations at the same speed. This may be the result of a prolonged travel across a configuration in a skewed direction thus enabling the lasers to actually cross the longitudinal configurations. The problem is exacerbated by an intermixing of over-sampling and under-sampling which will expectedly result in a remarkable difference between the Roline response and that of a triple point when their accelerometers are

essentially the same. It will be likely aggravated by aggressive texturing evident in deeper grooves and larger land widths

This section discusses how two laser types (Triple Laser and Roline) respond to texture configuration as well as other longitudinal textures. It examines the relationship of data from one laser type with respect to the other in each of the texture types studied to facilitate adequate construction acceptance specification.

### **5.2.2 Experimental Design**

Most experiments comparing lasers or laser-equipped-profilers involve the different profilers measuring smoothness at approximately the same time. To minimize variability from wander angle and speed or acceleration, this experiment used a single inertial profiler equipped with the Triple Laser and the Roline (Figure 5.1). With this specially equipped profiler it was possible to conduct measurements where the difference between IRI data from the Roline and Triple Laser can be attributed only to the interaction of those lasers on the texture configurations. Two texture configurations observed were the turf drag configuration commonly used by Minnesota Department of Transportation and the (diamond grinding) configuration that is receiving more interest because of its quietness. The experiments which entailed measurement of smoothness on cells in the MnROAD facility were conducted from 2009 to 2011 in each season except winter at the MnROAD research facility in Minnesota. Texturing in the cells include transverse tine, longitudinal turf, transverse turf, longitudinal broom, exposed aggregate and pervious concrete. Some of the grinding configurations include the conventional grind, the innovative grind, and the ultimate innovative grind which was the 2010 culmination of the progressively improved configuration. This is also referred to as Next Generation Concrete Surface by the Industry. Measurements were conducted on cells of various texturing including turf drag, innovative grind, improved innovative grind, ultimate grind and conventional grind. The configurations are shown and described in the chapter 2.

### **Texture Types**

Texture types are described in chapter 2. For the purpose of analysis, the light weight profiler outfitted for this study is shown in Figure 5.7 and some textures are shown in Figure 5.8. The concept of IRI was discussed in chapter 1.



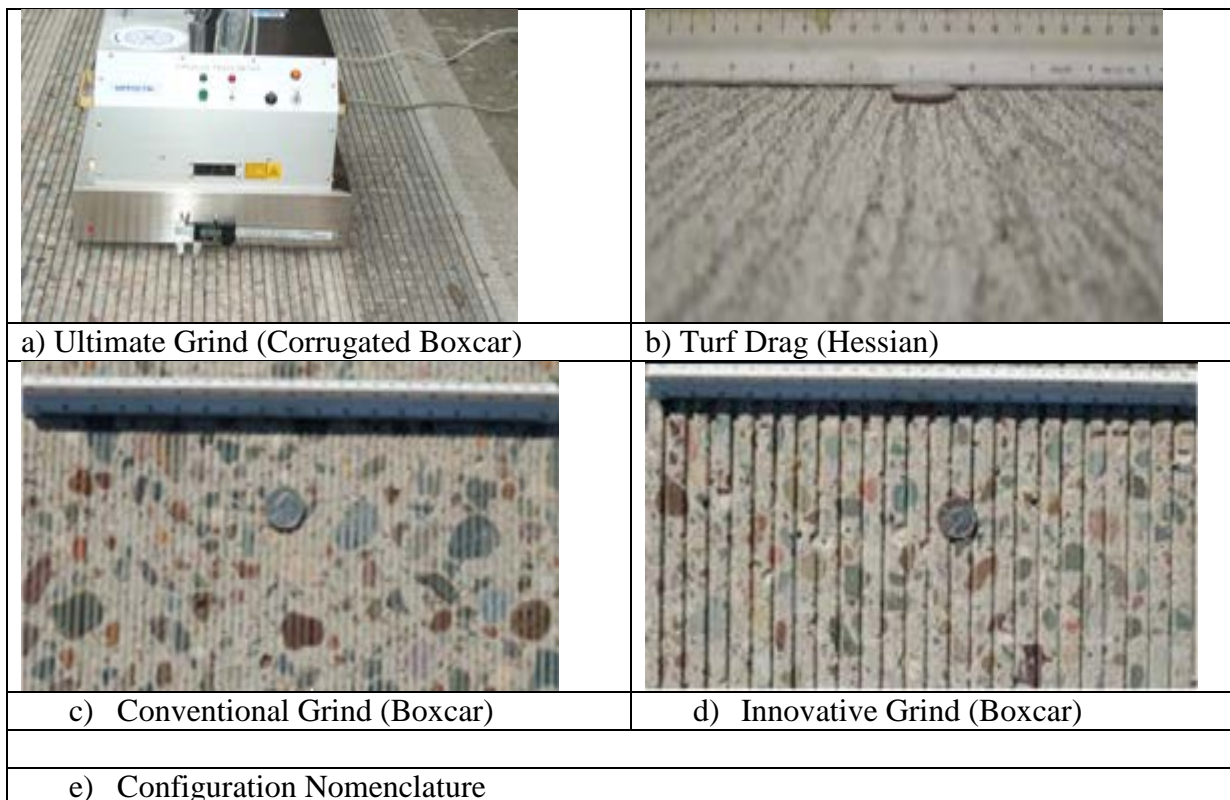
**Figure 5.7: Inertial Profiler Dually Equipped with Roline (Line) Laser and Triple Laser (Triple) laser. Note Line laser beam and triple laser beam on pavement.**

**5.2.3 Spatial Domain Analysis of Lateral Wander in a Light Weight Inertial Device**

This subsection generates an interpretation of a typical Boxcar configuration as traversed by a laser traveling at a skew angle. In an ideal situation where there is no skew angle, there will be no relative effect of the texture configurations and IRI will be based on the pavement roughness alone. However, lateral movement across longitudinal configurations during profiling is inevitable and results in certain misleading pavement smoothness data.

Consider an idealized light weight profiler wandering at 10 degrees angle to the longitudinal direction (Figure 5.23a). Actual texture configuration and the texture configuration projected as traversed by a single point laser (the actual projection of the configuration in the spatial domain) are shown in Figure 5.23b and 5.23c. Traversing velocity =  $V \sin\theta$ . Rate of laterally traversing a wavelength of 1 inch =  $(10 \text{ mph} \times 5280 \times 12 \text{ in/mile}) \sin\theta$  (Equation 5.21).

$\frac{(10 \text{ mph} \times 5280 \times 12 \text{ in/mile}) \sin\theta}{3600\text{s/hr}} = 176 \sin\theta$  cycles per second (Where the angle is small the rate of traverse is  $176\theta$  where  $\theta$  is in radians) Assuming  $\theta$  is  $\frac{\pi}{18}$  Radians the rate of traverse is 30.5 cycles per second. Actual wavelength is 0.63 but the “observed” wavelength of laser is  $0.63/\sin\frac{\pi}{18} = 3.62$  inches per transverse inch of grind. This is the laser observed wavelength of the configuration (Figure 5.23b).



**Figure 5.8: Concrete Surface Configurations Examined**

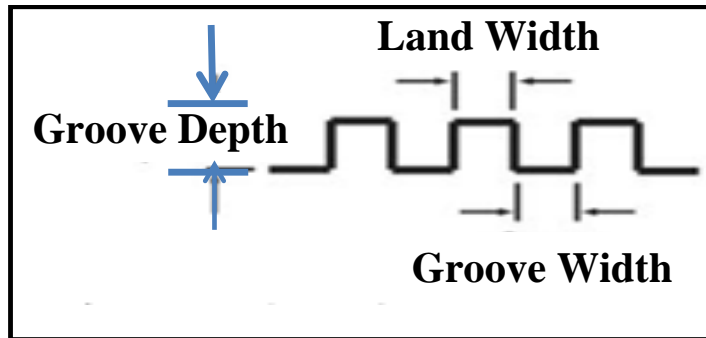


Figure 5.9a: Typical Boxcar Configuration

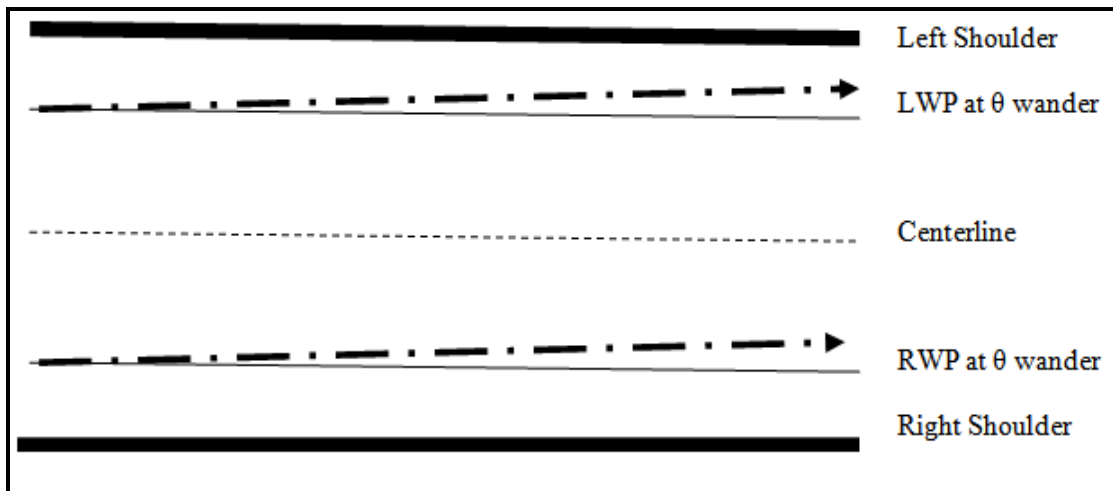


Figure 5.9b: Geometry of Lateral Wander Across an Ultimate Grind Configuration

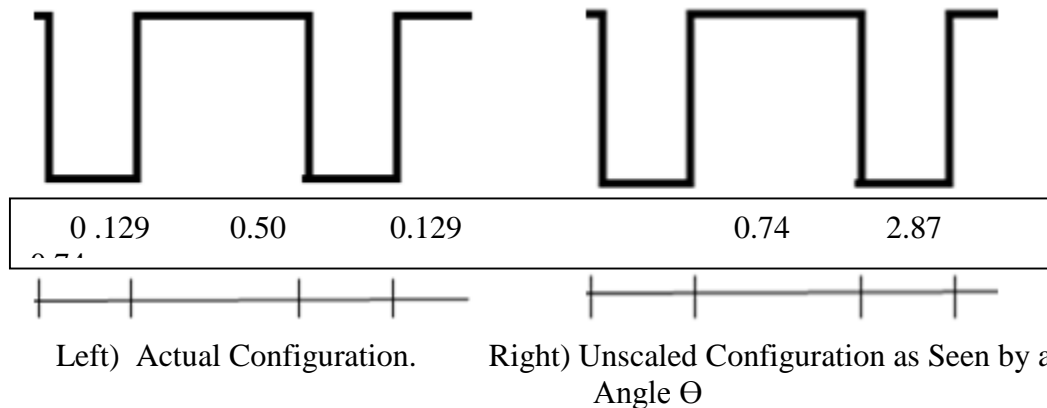
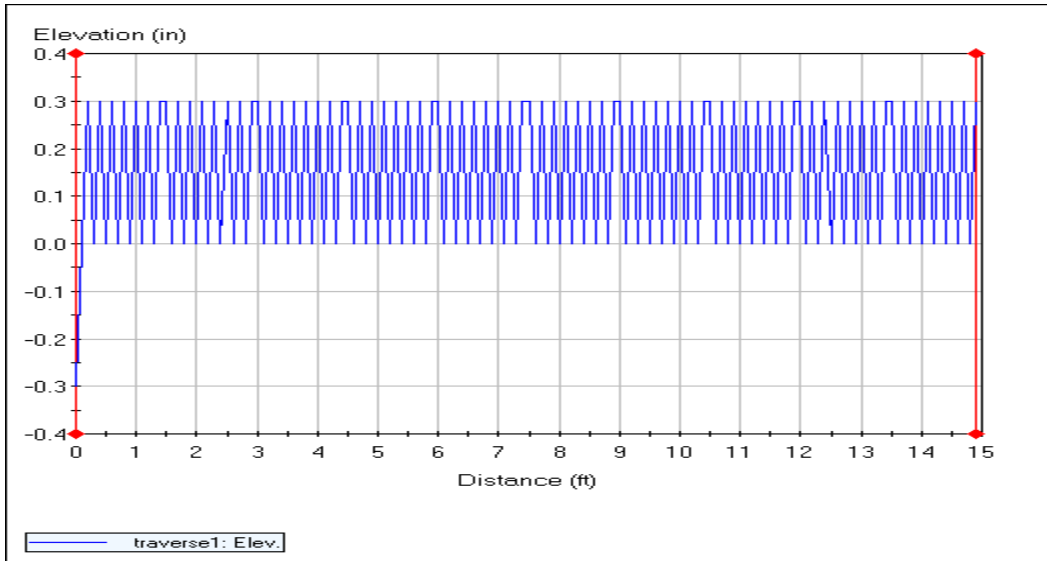
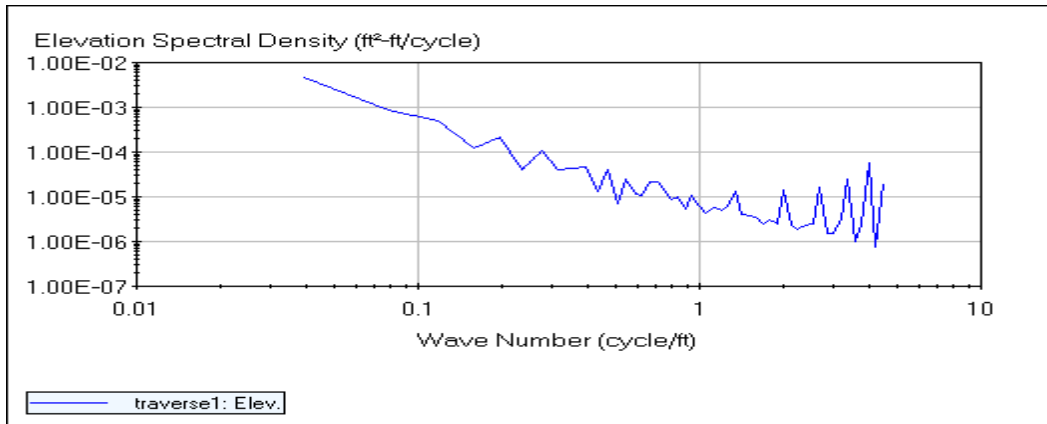


Figure 5.9c: Single Point Laser Interaction with Boxcar Configuration in Lateral Wander

To observe the actual cumulative effect of the Triple Laser, the problem was solved geometrically by constructing a hypothetical lateral movement and averaging the laser (sensed) depth.



**Figure 5.10a: Effective Profilogram of Ultimate Grind Configuration**

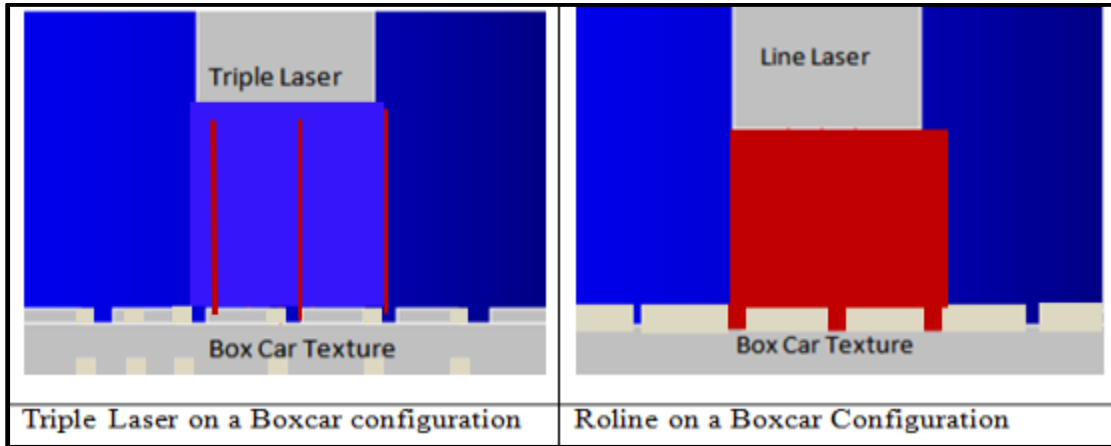


**Figure 5.10b: PSD of Ultimate Grind Configuration**

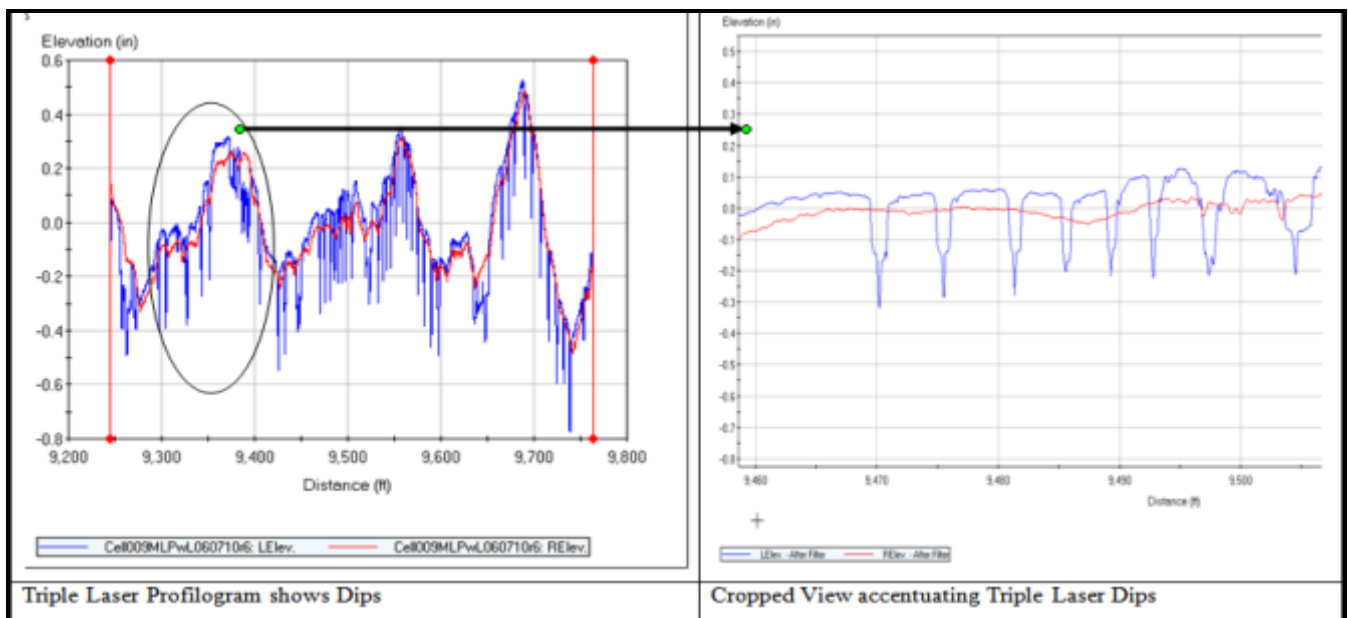
An unfiltered IRI of 446 inches per mile (Figure 5.8) was obtained by running the IRI algorithm through a surface generated by the laser traversing the texture configuration of the ultimate grind at a  $10^\circ$  skew angle. However, when the 25-mm filter was applied IRI of 119-inches per mile is obtained. The PSD shows a dominant frequency of 3.3 cycles per foot which is similar to 3.6 inches per cycle obtained from the laser-visualized configuration. For the average effect of 3 laser points in reality, it will be assumed that for the better part, two lasers are in the landing while one is in the groove. It is also assumed that the single lasers skip in rhythm and that laser thickness is small compared to the width of groove. Figures 5.9a to 5.11a shows a schematic representation of the Roline and Triple Laser with respect to the boxcar configuration. The probability that one laser is in groove is spatially  $1/5$  based on the relative width of groove and landing and the probability of that laser is in landing is  $4/5$ . Probability that 2 lasers are in groove and 1 in landing or vice versa and they skip to opposite locations is:

$$\left(\frac{3!}{2!(3-2)!}\right) (0.20) (.8)^2 + \left(\frac{3!}{1!(3-1)!}\right) (0.20)^2 (0.80) = 0.48 \quad (\text{Equation 5.22})$$

Moreover, lateral wander may not always occur (Figure 5.11a). The probability that all three lasers are in either groove or landing is approximately 52 percent. An actual profilogram of cell 9 (ultimate grind) is characterized by vivid dips (Figure 5.11) in the Triple Laser profilogram (IRI= 266 in/mile). The dips are not present in the Roline profilogram (IRI = 60 in/mile).



**Figure 5.11a: Triple Laser and Roline Laser Interaction with Boxcar Configuration**



**Figure 5.11b: Cell 9 Ultimate Grind Showing Vivid Dips in Triple Laser Profilogram. Second Line without Dips is Roline Profilogram**

### 5.2.4 Results

International roughness index was measured with Roline and Triple Laser lasers. IRI results are compared by texture types for drag, traditional grind and innovative grinds. Table 5B1 shows the various geometries of the innovative grinds at MnROAD.

Figure 5.25 shows the result obtained for the drag textures. The two cells were characterized by a coefficient of determination of greater than 0.97 indicating that there is reasonable correlation



between the Roline laser and Triple Laser. It would appear that the general configurations of the drag textures are not aggressive enough to cause disparities in Roline and Triple Laser. Figure 5.12 and 5.13 show the result obtained for the conventionally ground textures. Comparison of Triple Laser data from the two cells indicated that there is still a reasonable correlation between the Roline Laser and the Triple Laser in the conventional grind configuration though the actual values are different. Statistical similarity evaluation tools are preferred to regression in such situations. It would appear that the general configuration of the conventional grind configurations are not significantly affected by geometrical effects that cause the disparities. Figure 5.15 and 5.16 show the result obtained for the innovative and ultimate ground textures respectively. The two cells were characterized by different coefficient of determination were 0.94 and 0.14 respectively. It must be noted that the two cells are contiguous and the only feature that could explain the difference is the different texture configuration. It would appear that the general configurations of the innovative grind are characterized by some degree of excessive aliasing and overcompensated anti –aliasing. However the problem of a remarkable disparity between the Roline and the Triple Laser is vivid in the ultimate innovative configuration.

**Table 5.4: Summary of Full Width Grind (2007) and Grind Improvement (Cell 9 2009 OBSI, Drag Textures)**

	Cell 7 Innovative		Cell 8 Convention		Cell 9 Trans Tine		Cell 9 Ultimate		Cell 14 Drag	
	mm	Inch	mm	Inch	mm	Inch	mm	Inch	mm	Inch
Mean Land Width	9.5	0.37	3.18	0.13	12.8	0.5	13	0.49	2	0.08
Mean Groove Depth	3.05	0.12	3.18	0.13	7.85	0.31	3.8	0.15	1	0.04
Mean Groove Width	3.13	0.12	3.18	0.13	3.28	0.13	3.8	0.15	1	0.04
Mean Texture E-965	0.9	0.04	1.2	0.05	1.62	0.06	1	0.04	0.7	0.03
Mean Profile Depth ASTM E-2157	0.88	0.04	1.2	0.05	1.45	0.06	0.9	0.04	0.8	0.03

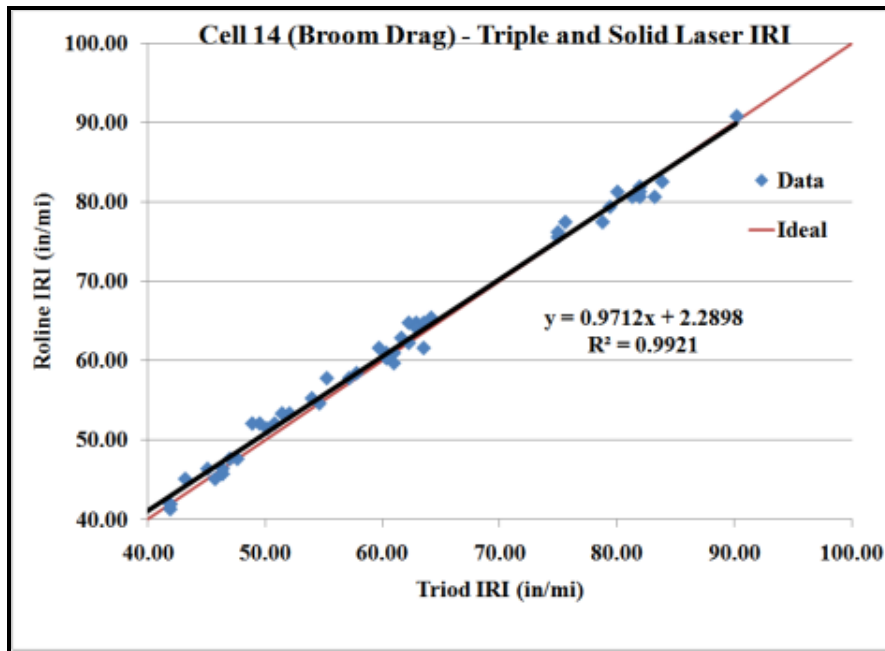


Figure 5.12: Triple Vs Roline on a Broom Drag Texture

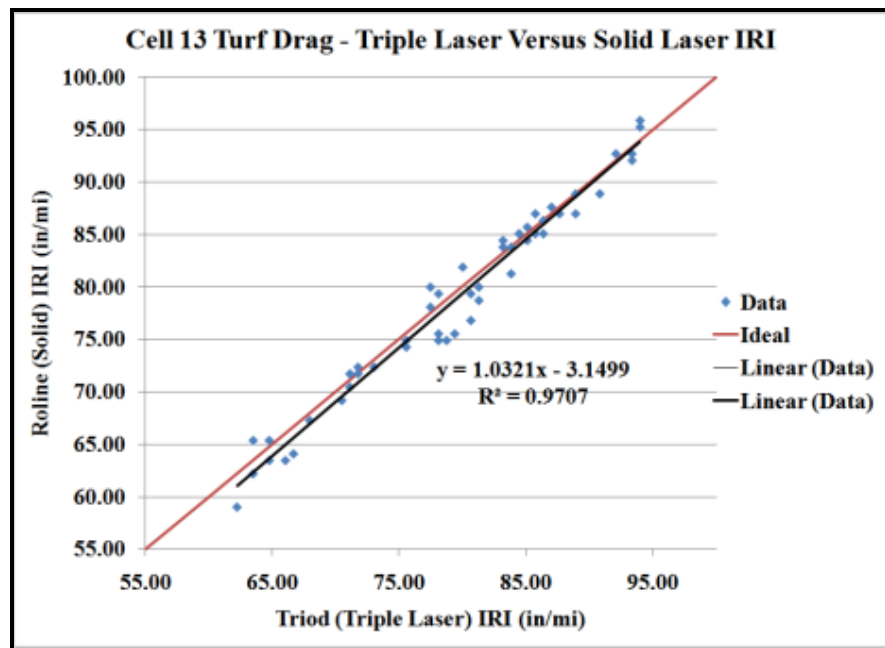


Figure 5.13: IRI of Triple and Roline in Turf Drag Textures

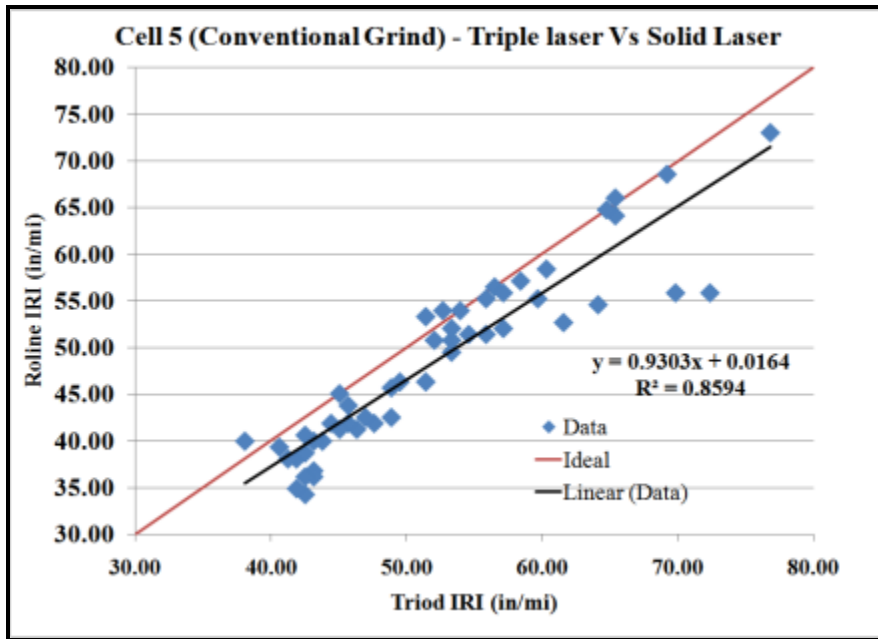


Figure 5.14: Triple Vs Roline in 2 Ultimate Grind Cells

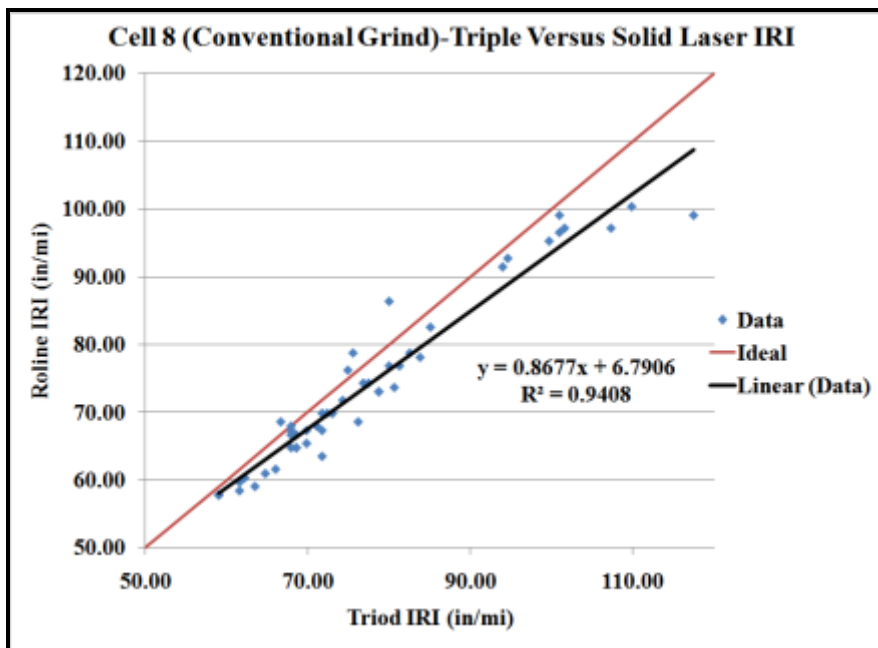


Figure 5.15: Triple Vs Roline in 2 Ultimate Grind Cells

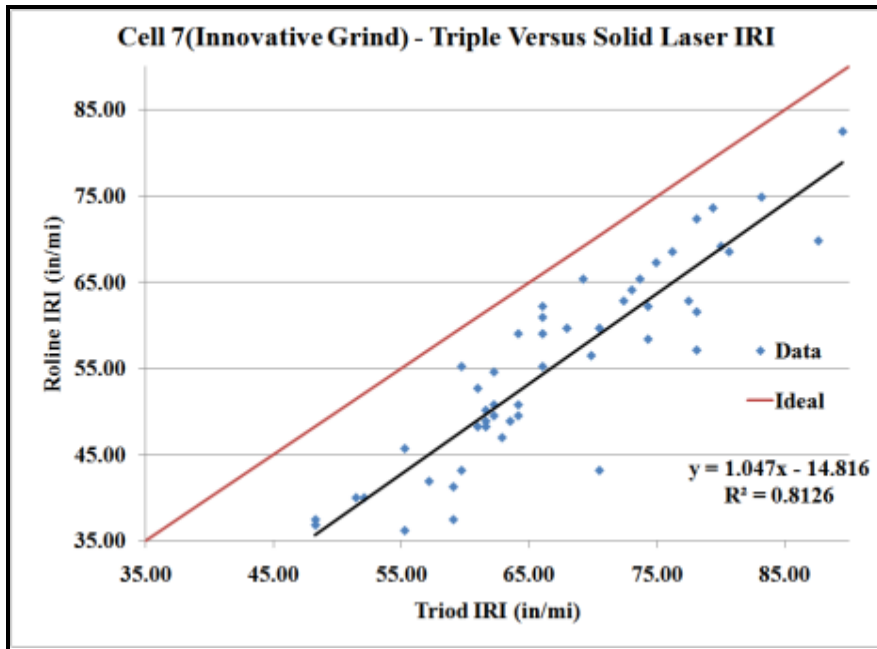


Figure 5.16: Triple versus Roline IRI on an Ultimate Ground Texture

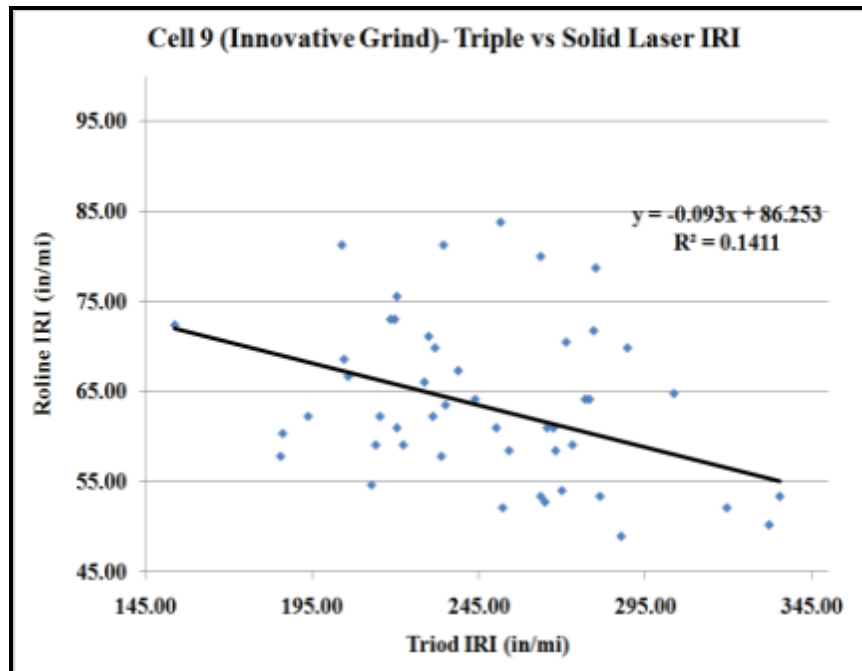
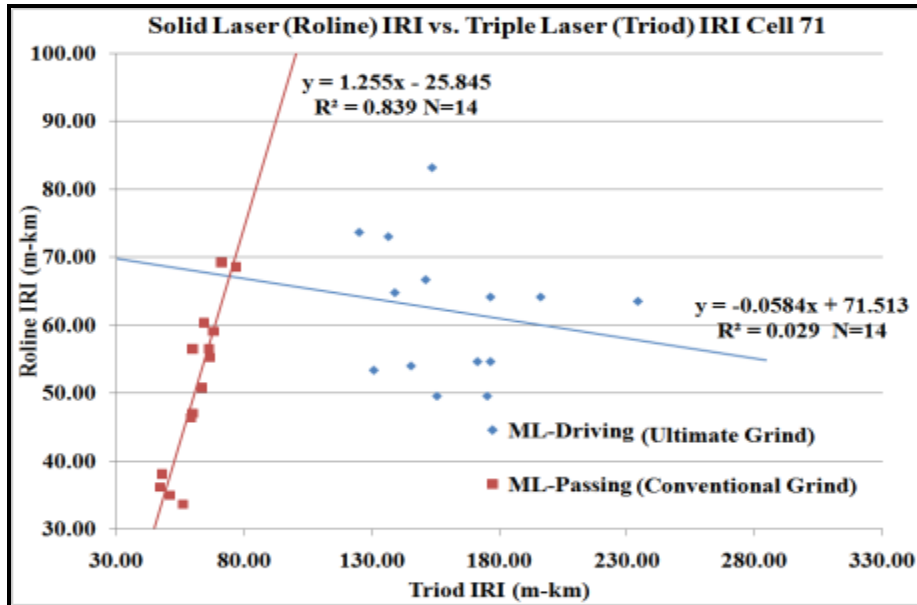


Figure 5.17: Triple versus Roline IRI on an Ultimate Ground Texture

**Table 5.5: Mann Whitney Wilcoxon Test for Data Similarity Roline vs. Triple Laser**

Cell	Lane	Laser	Mean Rank	Two-Tailed P-Value for Normal Approximation	Difference with 95% Confidence?	Difference with 99% Confidence?
Cell 13 Turf Drag (TD)	Driving	Trinle Roline	24.7 24.3	0.926	no	No
	Passing	Trinle Roline	27.4 25.3			
Cell 14 Broom Drag(BD)	Driving	Trinle Roline	24.3 24.7	0.9342	no	No
	Passing	Trinle Roline	25.8 27.2			
Cell 71 UDG Driving, CDG Passing	Driving	Trinle Roline	21.5 7.5	0	yes	Yes
	Passing	Trinle Roline	18 11			
Cell 5 (CDG)	Driving	Trinle Roline	26.7 22.3	0.2833	no	No
	Passing	Trinle Roline	30.6 22.4			
Cell 7 Innovative Grind (IDG)	Driving	Trinle Roline	32.8 16.2	0	yes	Yes
	Passing	Trinle Roline	32.7 20.3			
Cell 8 Conventional Grind (CDG)	Driving	Trinle Roline	28 21	0.0827	no	No
	Passing	Trinle Roline	29 24			



**Figure 5.18: IRI of Triple and Roline in Separate Lanes with Different Configurations**

Regression is not the best method to compare the Roline data to triple line data because good correlation does not guarantee similarity. The Mann Whitney Wilcoxon approach is therefore used.

This disparity is accentuated in cell 71 (Figure 5.18) finished with the ultimate innovative grind in the outer (driving lane) and with the conventional grind in the inside (passing) lane. The respective coefficients of determination of 0.029 and 0.839 for the innovative grind configuration and conventional grind configuration are indicative of an anomaly in the way Triple Laser reads and processes ultimate grind's spatial geometry. The above observation was also examined from a statistical level of confidence to ascertain how data from both laser types relate to each texture configuration using the Mann Whitney Wilcoxon test for similarity of data sets [5.7] [5.8]. Table 5.5 summarizes this evaluation. The method uses one of 2 data types: the categorical and the tabular. The categorical method uses a large dataset in which the entries in a separate column are categorized numerically or descriptively. In the tabular method, the 2 sets of data are entered as the data needing to be evaluated for similarity. All the data is converted to ranks and the statistic observes normal approximation for continuity and ties as well as number of tied values. A total of 25 data points were observed for each texture type and less for cell 71 which had different configurations on each lane. Extraneous biases were minimized by the observation of at least 2 cells with each configuration type. It is also minimized by pairing tests in each case for the 2 laser types. The null hypothesis is that the distribution of the 2 groups is dissimilar. Results (Table 5.5) showed various p values for the surface types. Based on a 95 % percent confidence level, p-value of  $< 0.025$  will accept the null hypothesis. A p-value of  $> 0.025$  will not reject the null hypothesis. There is evidently no correlation between the ROLINE readings and the Triple Laser readings in the innovative grind (Table 5.5) shows a statistical comparison of the Roline and Triple Laser for different surface types. A statistical test for similarity is performed based on a 99 percent and 95 percent confidence level. The statistical test actually shows that in addition to the ultimate grind texture, the innovative grind texture does not appear to receive the same response from the two laser types. The results thus exhibit the seriousness of the Roline-Triple Laser disparity in all longitudinal boxcar cells tested except the conventional grind.

### **5.2.5 Section Summary**

This study evaluated the influence of different laser configurations on various texture configurations particularly focusing on the new Boxcar configurations. The configurations examined are the broom and turf drag, the conventional grind, the innovative grind and the ultimate grind. International Roughness indices measured in drag textured surfaces with the Triple Laser were similar to those measured with the Roline. In practice, the effect of laser wander is minimized in drag textures due to their shallow texturing. International roughness indices measured in conventional ground surfaces with the Triple Laser were not significantly different from those measured with the Roline. In practice, the effect of laser skipping exists but is not significant enough in conventional grind configurations to warrant quality assurance specification changes.

It is evident that there is very significant difference between international roughness indices measured in innovative or ultimate grind surfaces with the Triple Laser and those measured with the Roline. This disparity shows such a radical difference that cannot be attributed to minor equipment error but to laser-surface configuration interaction. In practice, the effect of laser

wander is obviously significant and thus cannot be ignored in the new innovative and ultimate innovative diamond grinding configurations that are sought after because of the acoustic benefits they provide.

The innovative grind configurations are used because of excellent acoustic properties. Due to possible disparities in different laser devices it may be necessary to require Roline profilers with the innovative texture configuration. In exceptional cases where a good regression has been established between the Triple Laser and the Roline, then both may be used interchangeably but not without some caution. It is recommended that any longitudinal grinding with the innovative or ultimate grinding configuration should be evaluated with a Roline laser and not the triple or single point laser for construction acceptance. This is particularly important in quality assurance where the contractor may likely use a Roline. The Agency will need to run quality assurance with the Roline and not the Triple laser.

### **5.3 Return on Investment in Quiet Pavements in Comparison to Standard Sound Abatement Walls**

#### **5.3.1 Background**

Transportation infrastructure represents a large investment for the public. While such investments are quantifiable, the benefits are not usually easily monetized though occasionally they can be itemized. Noise abatement decisions are made based upon their ability to achieve a minimum of 7 dBA noise reduction at a maximum cost of \$43,500 per benefited receptor. To determine quiet pavement effects, a mathematical transcription of near field noise to far field effects was derived. Tire Pavement Interaction Noise (TPIN) was measured by the On Board Sound Intensity (OBSI) procedure. For each texture type, the cost and benefits accruing from initial construction activities followed by maintenance through the service period were analysed using transverse tine texture as a reference surface. A 20-year life cycle cost analysis for the various pavement types were compared to that of a noise wall.

#### **5.3.2 Introduction**

To be cost-effective, acoustic benefits of quiet pavements should result in significant noise reduction. Hanson et al [5.7] identified traffic noise sources as stack noise, aerodynamic noise, power train and tire-pavement interaction. They showed that below 30 miles per hour for trucks and below 25 miles per hour for cars, the power train and stack are dominant but above these speeds, the tire pavement noise is dominant, particularly at cruising speeds. An acoustic benefit in tire pavement noise should therefore translate into a benefit in the overall noise. The study conducted by Kummel et al [5.8] showed drag-textures to be quiet in comparison to various concrete finish textures. At that time there were not many innovative quiet concrete textures. Hanson et al [5.4] discussed four types of texture for Portland cement concrete pavements that National Center for Asphalt Technology (NCAT) tested in Minnesota in 2004. They were: random transversely tined, turf / broom drag, diamond ground and bituminous surfaces. They [5.7] [5.8] [5.9] showed the frequency spectra for these surface types. The tined surface had three peak noise levels (700 Hz, 1000 Hz, and 1400 Hz) and was reportedly characterized by a low rumbling noise at 700 Hz and a whining sound at 1400 Hz. The other surfaces had a moderate noise level at all frequencies. Izevbekhai and Khazanovich [1.8], observed the noisiest test cell in MnROAD was also the worst riding cell thus suggesting a correlation between noise and

pavement condition. Rymers and Donavan [5.11] as well as Donavan and Lodico [5.12] performed actual near field and far field testing to quantify the far field implication of near field measurements. Dick, Izevbekhai and Casey [5.13] performed a statistical Passby evaluation of quiet textures and observed that the relative quietness of the various configurations reflected by the OBSI measurements was also reflected in the Statistical Pass By.

### 5.3.3 Implication of OBSI Difference

If the sound intensity level with an original texture transverse tined surface was  $SI_1$  and after grinding (or other surface intervention) it becomes  $SI_2$ ; the difference between the sound intensity levels (dBA) is X. If the sound intensity at the threshold of human hearing is  $SI_0$  it can be shown that

$$\begin{aligned} x &= 10\text{LOG}_{10} \left( \frac{SI_1}{SI_0} \right) - 10\text{LOG}_{10} \left( \frac{SI_2}{SI_0} \right) = 10\text{LOG}_{10} \left( \frac{\left( \frac{SI_1}{SI_0} \right)}{\left( \frac{SI_2}{SI_0} \right)} \right) \\ &= 10\text{LOG}_{10} \left( \frac{SI_1}{SI_2} \right) \end{aligned} \quad \text{(Equation 5.35)}$$

$$\text{Then \% change in sound intensity} = 100 \left( 1 - 10^{-\left( \frac{x}{10} \right)} \right) \quad \text{(Equation 5.36)}$$

Where

x is OBSI difference

$SI_0$  is sound intensity at threshold of human hearing

$SI_1$  is sound intensity prior to a quiet pavement intervention

$SI_2$  is sound intensity after a quiet pavement intervention



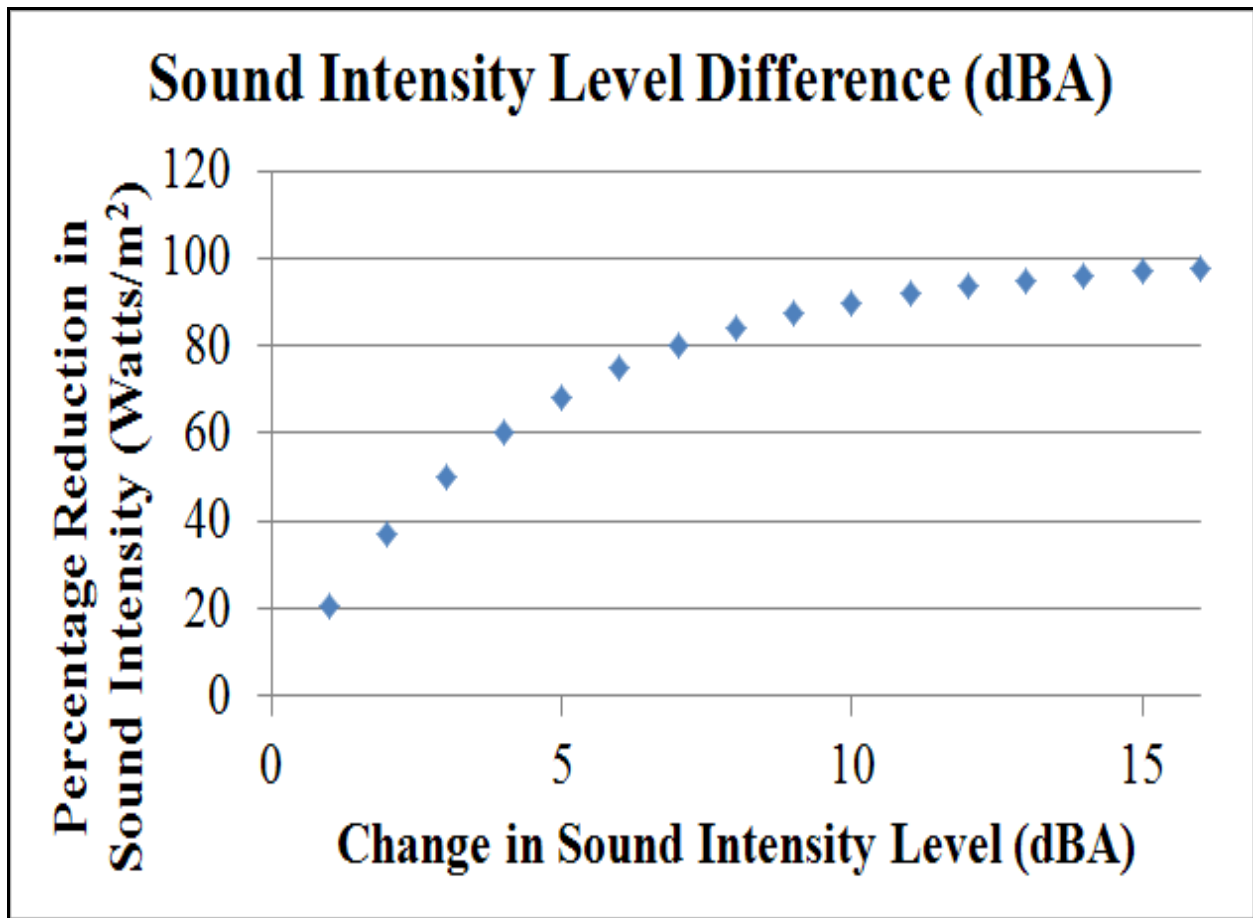


Figure 5.19: Implication of sound Intensity reduction in the “A” weighted scale.

Equation 5.3 6 is schematically plotted in Figure 5.34. Gains in quiet pavements are manifestly reported in dBA viewed in terms of a change in OBSI. It is evident that an OBSI change of 3-dBA is tantamount to reducing a uniform source by 50%. The definition of sound intensity in the decibel scale is responsible for this scenario as explained in the preceding section. A quick and easy correlation in Figure 5.34 elucidates actual quietness gains with respect to changes in OBSI. It shows that a sound intensity level change of 10 dBA is equivalent to elimination of 95% of the noise from a uniform source. An average of 4 dB difference implies that transitioning from a conventional grind to an innovative grind would cause a noise reduction that is perceived as reducing the traffic by 60 %. The mitigation inherent in replacing the conventional grind by the innovative grind (4 dB) is significant as a change of 3dB is the smallest noticeable difference by the human ear.

#### 5.3.4 Near Field – Far Field Compatibility

Using AASHTO set up for OBSI test vehicle, microphones, rig and cables for the OBSI measurement using this near field method described in Chapter 1, numerous measurements taken between 2007 and 2011 on 32 concrete cells were shown in a cumulative frequency distribution (Figure 5.32). Quiet pavement is usually measured by near field procedure such as OBSI whereas the public likes to know the actual far field effect. A near field to far-field transformation is thus performed. Additionally, a life-cycle cost and a benefit/cost analysis is performed to compare the relative benefit of noise reduction through pavement texturing to

sound attenuation through noise abatement walls. The process utilizes a comparative scenario where the number of benefitting receptors based on the MnDOT FHWA cost effectiveness criterion brings the benefit/ cost to unity.

An explanation of tire-pavement noise metrics facilitates evaluation of a quiet-pavement initiative. Sound waves are generated by the interaction of the pavement and tire. These waves are associated with air compression and rarefaction in the tire-pavement interaction contact. The interaction is also associated with tire-deformation and restoration as well as vibrations in the tire wall. Sound waves are also transmitted by tire resonance transmitting energy to the air medium. The amount of energy transmitted is dependent upon the amplitude of vibration. The intensity of tire pavement noise depends on speed, tire type, and surface distress. However, for near field to far field transformation, the surface may absorb some of the sound thus reducing the effective far field effect. Noise is understood as “undesirable sound” according to differing perception and interest of the recipient [5.10] [5.11] [5.12] [5.13] & [5.14]. Sound is made up of pressure waves generated by a vibrating source and then transmitted through a solid, liquid, or gas. A given sound wave is characterized by frequency and amplitude. At a point away from the source, the sound intensity (defined as the power per unit area) of a given sound wave at a given frequency can be expressed as:

$$SI=p*v \quad \text{(Equation 5.32)}$$

where

p, referred to a sound pressure, is the root mean of the pressure variations at the point in question, and v is the velocity of the sound wave. From this definition the sound intensity level measured as decibels dB, can be defined in terms of a background level.

$$SIL = 10 \log \left( \frac{SI}{SI_0} \right) \quad \text{(Equation 5.33)}$$

where

background reference sound intensity is set as  $SI_0 = 10^{-12}$  Watts/m<sup>2</sup>: the quietest sound a young human with undamaged hearing can detect at 1,000 Hz. [5.15] [5.16] & [5.17]

Typically the value of SI falls off as the inverse square of the distance from the source. In the vicinity of the source typical values span from 190 dB at a distance of 1000 feet for a jet engine to the quiet whisper of 30 dB in a library.

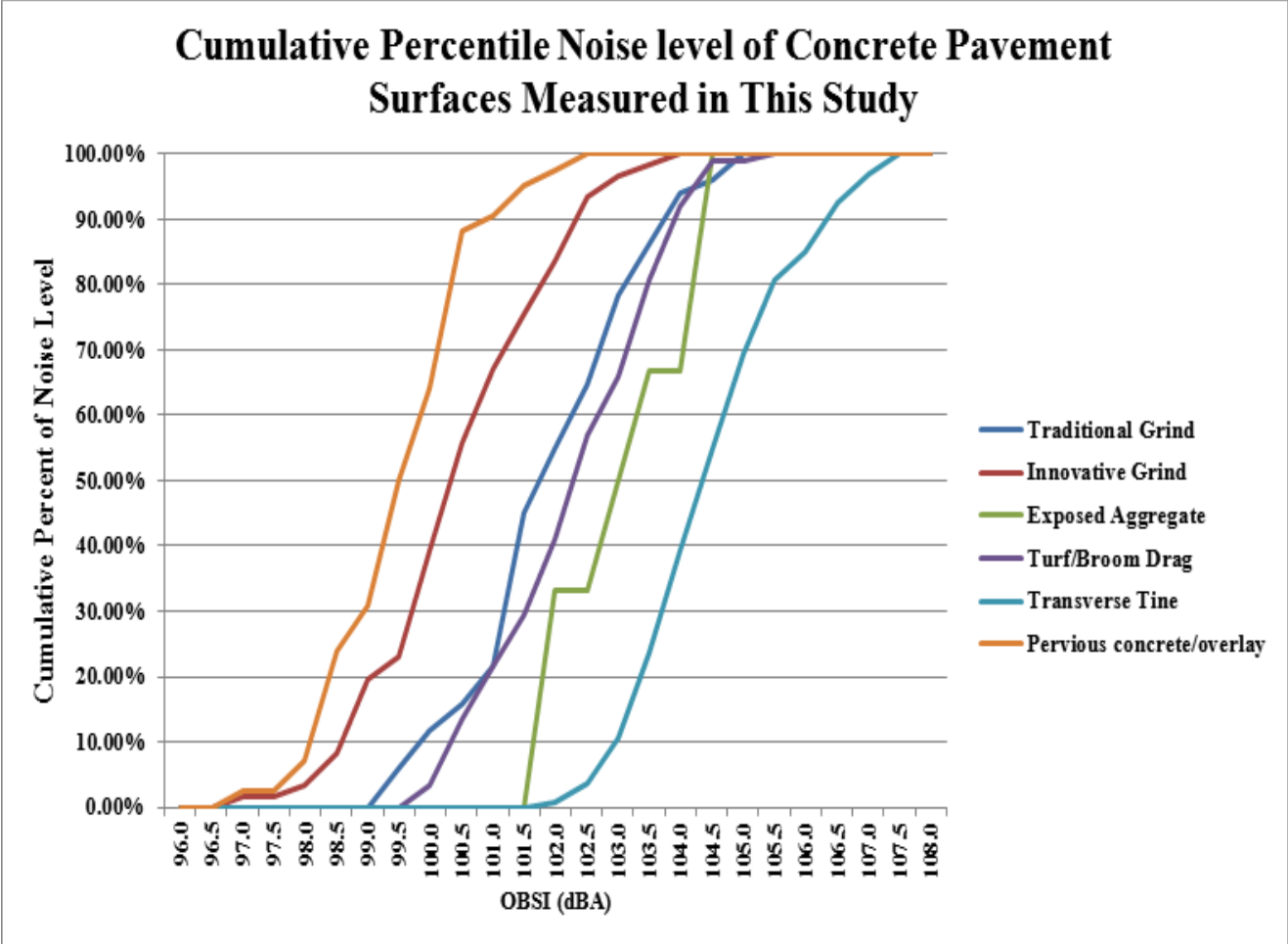
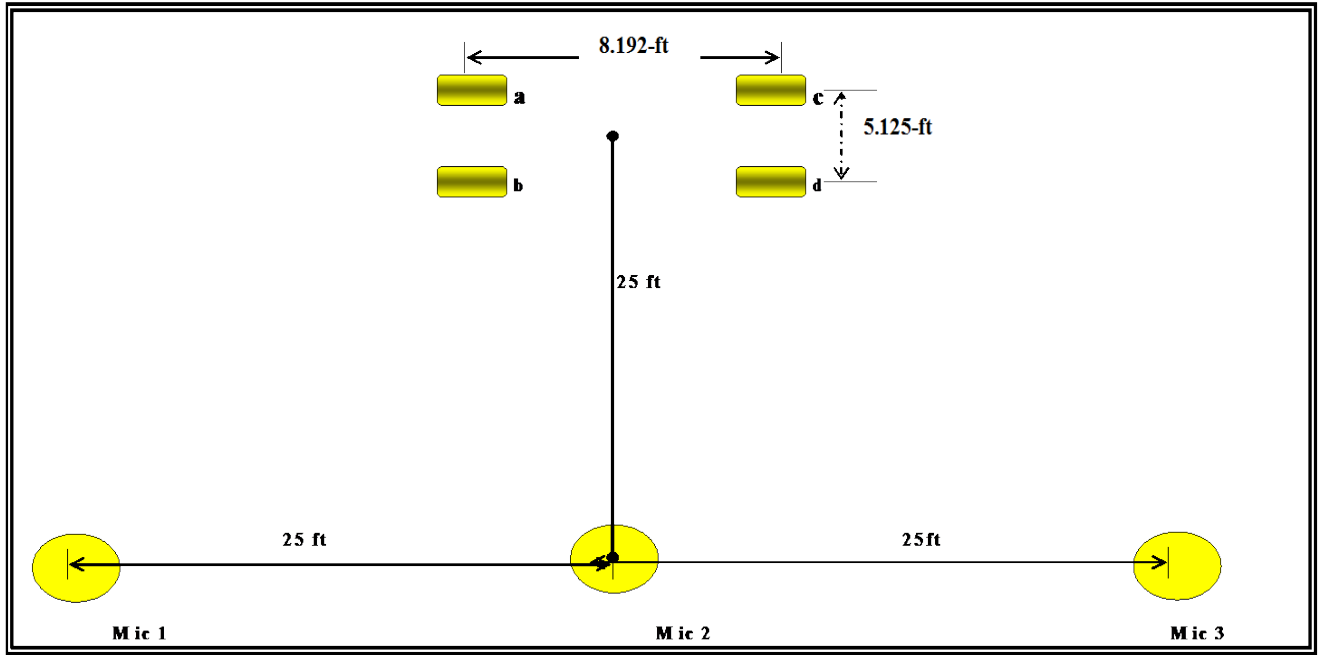


Figure 5.20: Cumulative Percentage OBSI Data (Izevbekhai [1.52])

Figure 5.21 shows a schematic arrangement of the noise effect of 4 standard tires as perceived from OBSI and the noise implication (based on inverse square law) at 25-ft offset from the vehicle center and 25-ft transverse and longitudinal offset from leading as well as trailing from vehicle center. Table 5.31 shows the corresponding far field measurement in the last column for each of the microphones where D is the offset of OBSI [5.310] microphone from tire. K represents the actual distance from tire to wayside microphone, the suffix a, b, c & d refer to the tires while the microphones are L<sub>1</sub>, L<sub>2</sub> and L<sub>3</sub>. For instance, “L<sub>3</sub>a” shows the effect of tire “a” on microphone 3. The Table shows that for a measured OBSI of 98.7 dB, we would expect a microphone located at 1, 2 and 3 to receive 63.02, 65.78 and 63.02 dBA respectively and cumulatively from all 4 similar tires of the test vehicles. Corrections are not made for Doppler Effect in the respective locations as they are not considered significant in the relative OBSI levels. This facilitates prediction of the far field results from near field (such as OBSI) test results. An analytic process to translate OBSI to far field response of microphones located 25 ft. offset from vehicle (as shown in Figure 5.3 3) were then developed. From the above EQUATION 5.33 as well as Figure 5.21 it is evident that a 3-dBA reduction in pavement noise is approximately 50 % reduction in pavement noise (watt/m<sup>2</sup>) and a 9-dBA savings is tantamount to almost 90 % reduction in the Noise Sound Intensity (watts/m<sup>2</sup>). The set up (Figure 5.3 3) identifies four standard tires a, b, c, d and three microphones L<sub>1</sub>, L<sub>2</sub> and L<sub>3</sub>.



**Figure 5.21: Near field far field (25-ft Offset) Geometry from source.**

By the inverse square law, the near field noise translates to the far field noise. According to the ratio

$$Y = \frac{K^2}{D^2} \quad (4)$$

Where

- D is actual distance from car to wayside microphone.
- K is distance from contact patch to near field microphone
- n is # of tires allows cumulative effect of the 4 tires

Research [5.111] & [5.13] comparing far field noise levels to near field levels have been published. The studies have generated correlative algorithms between OBSI and Controlled Pass-By (CPB) for light vehicles and for heavy vehicles at 25-ft and at 50-ft offset. Donovan and Rymers [5.11] Donovan and Lodico [5.12] from the NCHRP 1-44 project developed and validated this relationship with a coefficient of determination of 0.96.

Figure 5.21 and Table 5.6 show through a mathematical process that an “n-dB” reduction in the near field measurement will correspond to an “n-dB” reduction in a far field measurement based on the assumption that the field is free and void of acoustic attenuating factors, and that there is no significant difference in acoustic attenuation between frequencies within the medium of transmission. It is also assumed that there are no significant acoustic absorption in the intervening space between the tire contact and the Passby microphone. It is noteworthy that this analysis is therefore idealized and actual measurements may indicate slight variability. However, the study conducted by MnDOT [5.13] showed that near field differences obtained by using OBSI can be captured also by farfield (statistical Passby). This forms a basis for using OBSI measurements and results for the benefit cost analysis

**Table 5.6: Interactive Prediction of Far Field Response from Near Field Response.**

98.5 dB Source	X (m)	Y(m)	D (m)	$k^2/D^2$	Int SPB		Sum (SI Li ai)
L1a	20.906	23.448	31.414	9.112E-05	1.81E-06	62.600	
L1b	29.094	23.448	37.367	6.446E-05	1.28E-06	61.000	
L1c	29.094	28.552	40.764	5.416E-05	1.08E-06	60.337	
L1d	20.096	28.552	34.915	7.383E-05	1.47E-06	61.682	
				Total (4 Tires)		5.6594E-06	67.528
L2a	4.094	23.448	23.803	0.000156	3.16E-06	65.010	
L2b	4.094	23.448	23.803	0.000159	3.16E-06	65.010	
L2c	4.094	28.552	28.844	0.000108	2.15E-06	63.341	
L2d	4.094	28.552	28.844	0.000108	2.15E-06	63.341	
				Total (4 Tires)		1.065E-05	70.276
L3a	29.094	23.448	37.367	6.446E-05	1.28E-06	61.093	
L3b	20.906	23.448	31.414	9.112E-05	1.81E-06	62.600	
L3c	20.906	28.552	34.915	7.383E-05	1.47E-06	61.682	
L3d	20.906	23.448	40.764	5.416E-05	1.08E-06	60.337	
				Total (4 Tires)		5.659E-06	67.528

**Table 5.7: Effect of Near field Detected Difference on Projected Far Field Difference**

OBSI		Receiver 1		Receiver 2		Receiver 3	
OBSI	OBSI Difference	SPB	SPB Difference	SPB	SPB Difference	SPB	SPB Difference
98.5	0	63.028	0	65.776	0	63.028	0
99	0.5	63.528	0.5	66.276	0.5	63.528	0.5
99.5	1.0	64.028	1.0	66.776	1.0	64.028	1.0
100	1.5	64.528	1.5	67.276	1.5	64.528	1.5
100.5	2.0	65.028	2.0	67.776	2.0	65.028	2.0
101	2.5	65.528	2.5	68.276	2.5	65.528	2.5
101.5	3.0	66.028	3.0	68.776	3.0	66.028	3.0
102	3.5	66.528	3.5	69.276	3.5	66.528	3.5
102.5	4.0	67.028	4.0	69.776	4.0	67.028	4.0
103	4.5	67.528	4.5	70.276	4.5	67.528	4.5

### 5.3.5 Benefit Cost Analysis of Pavement Surfacing / Overlay

This section analyses the true benefit of surface treatments by comparing them with alternate activities such as noise wall construction or berm construction. As a zero reference, the transverse tine is the assumed surface texture before a quiet pavement or acoustic noise barrier intervention. The quiet pavement alternatives include conventional grinding, innovative grinding, and pervious concrete and pervious asphalt. Unit costs are used along with a discount rate of 4%. A discount rate is the factor used to identify a present value of goods or services when dealing

with a future cost expressed in constant dollars. Discount rate selection is a critical process in life cycle cost analysis (LCCA) and directly impacts choice or implication a-priori of fix. Most states use a set value of 4.0% for their discount rate [5.18]. From a survey conducted on a number of states, the average for the states that participated is 3.8% A high discount rate favors projects with low initial construction costs and higher maintenance costs dispersed throughout the remaining life of the project. The higher maintenance costs are discounted at a greater value making it more beneficial to defer those costs. A low discount rate favors the projects with high initial costs. The analysis period of 20-year was chosen because it affords sufficient cycles of maintenance and repairs over time to establish maintenance costs within the reasonableness of the discount rate. In this analysis, a benefit of \$43500 per inhabitant [5.19] forms the basis for computation of benefits. This value was agreed upon between the FHWA and MnDOT. Some other concomitant terminologies are defined:

**Discount Rate (r):** This is the difference between the interest rate and the inflation rate, which gives a value to money if saved rather than spent.

**Net present value (NPV):** Benefits and costs over an alternative's life cycle are discounted to the present (5.312), and the costs are subtracted from the benefits to yield a NPV. If benefits exceed costs, the NPV is positive, implying project viability. Where two or more alternatives for a project exist, the one with the highest NPV over an equivalent analysis period should be a worthy investment. Policy issues, perceived risk, and funding availability or corridor-wide uniformity, however, may lead to the selection of an alternative with a lower, positive NPV [5.19]. In this analysis, NPV was the value obtained from cost alone as benefit was treated separately to realize a tenable benefit/cost ratio.

$$PV = \frac{1}{(1+r)^t} A_{(t)} \quad \text{(Equation 5.37)}$$

$$\text{Moreover, NPV} = \sum_{i=1}^T \left( \frac{1}{(1+r)^t} A_{(t)} \right) \quad \text{(Equation 5.38)}$$

where

PV = Present value at time zero (the base year);

$r$  = Discount rate;

$t$  = Time (year); and

$A$  = Amount of benefit or cost in year  $t$ .

NPV = Net present value

$T$  = Analysis period (years)

**Benefit / Cost (B/C) ratio (BCR)** [5.18] [5.20] is frequently used to select among projects when funding restrictions apply. In this measure, the present value of benefits is placed in the numerator of the ratio as a ratio to the investment in construction and maintenance. FHWA [5.21] recommends the use of either the NPV or BCR measures for most economic evaluations. Other B/C analysis measures are available and may be used. Technical Advisories on texture intrinsically necessitate economic evaluations for adequate decision making.

### **Noise Abatement Wall and Berm**

This analysis assumes that when a noise wall is built, it will result in a change of 8-dBA in the perception of an inhabitant or as would be captured from a microphone placed at 25 feet from the

vehicle and that the wall will last maintenance-free for 20 years. Every cost of noise wall is additional to the pavement or bridge structure. The unit cost—per-square-foot of the standard abatement wall is therefore used. In Minnesota Department of Transportation, a standard noise abatement wall consists of wooden panels held by rectangular concrete posts at 12 to 20 ft. intervals. The posts are supported by cylindrical isolated concrete footings or by granular soil. Lean mix backfill occasionally replaces granular material as backfill. For a benefit/ cost analysis, the noise wall costs \$3,000,000 per mile for a 20 ft. high continuous wall. A sound abatement berm (20 feet high) costs \$2,000,000- 2,500,000 per mile to construct and holds an assumed 10-dBA savings. The limitations of noise walls include thermal inversions at various temperature regimes that cause the walls to actually amplify traffic sounds. This shortcoming is not accounted for in the analysis, since the frequency of occurrence is unknown.

### **The B/C Evaluation Process**

Unit costs, maintenance types and representative maintenance cycles for each pavement fix is required for a tenable benefit. / cost. Most of the lane mile costs were obtained from MnDOT Office of Estimating or from our experience at the MnROAD facility adjusted by economy of scale. Costs may not reflect perspectives of other agencies but relative B/C comparison between strategies will not differ largely from results obtained in this study except other assumptions are made. Unit costs and maintenance cycle for each fix is shown in Table 5.37. The NPV was computed for each fix using the 4% discount rate and incorporating the maintenance fixes. For each fix, the initial noise reduction from a Transverse tined pavement was recorded as the noise benefit. This quantity multiplied the standard benefit per decibel per family unit (\$42500 / dB) [5.313] by the dB savings to obtain the monetized benefit for that fix. To obtain the B/C for each fix the monetized dB was divided by the corresponding NPV. Based on a rational approach using 100-dBA as the industry pivot for quiet pavement, a likelihood function “P” of the OBSI, measured on each fix, being less than 100-dBA from all the tests conducted at MnROAD (Figure 5.31) was multiplied by the B/C to obtain the adjusted B/C. The statistical value P is the probability of the pavement / texture option being quieter than 100-dBA based on test data at MnROAD. **In case 1, (Table 5.33) improvements over a transverse tined pavement are evaluated and in case 2 improvements over a drag pavement texture is evaluated.** Using 4% as the discount rate over a 20 year period, a cost benefit analysis of noise abatement was computed from OBSI MnROAD surface data and theoretical noise walls and berms. The most cost effective noise reduction method was shown to be ultimate diamond grinding; the least, exposed aggregate finish (using retardant). The calculations were done per-lane-mile and a Standard Benefit per decibel per benefitting recipient of \$43500 [5.8] was used for the entire analysis.

For an improvement or rehab work on a drag texture, only the Ultimate grind and the pervious concrete will be acoustically cost effective. Although a texture durability factor has not been applied that will be the basis for modification of these results in future.

**Table 5.8: Cost Benefit Analysis Results; Case 1 Rehab of Drag Texture**

	Unit Cost/ 2 lanes	NPV Cost	Savings S (dBA) Based on Rehab on TT	Benefit= S*43500*4	B/C	P(OBSI<100dBA)	Adjusted B/C (B/C)*P
Sound Abatement Berm + Row 20 ft. high	\$2,100,000	\$350000	10	\$870,000	1.00	0.95	0.95
Noise Wall 20 ft. High including Foundation	\$1500000	\$1600000	8	\$696,000	1.00	0.95	0.95
Astro Turf Drag	\$80,000	\$14,000	2	\$174,000	7.14	0.03	0.21
Conventional/Traditional Diamond Grind	\$100,000	\$21,000	3	\$261,000	7.14	0.12	0.86
Innovative Diamond Grind	\$129,000	\$15,461	5	\$435,000	16.17	0.39	6.31
Ultimate Diamond Grind	\$120,000	\$15,461	6	\$522,000	19.40	0.57	11.06
Pervious Concrete Overlay (100 mm)	\$560,000	\$58,500	6	\$522,000	5.13	0.64	3.28
Pervious Concrete Full Depth and Pervious Base	\$800,000	\$64,500	6	\$522,000	4.65	0.64	2.98
Pervious Asphalt (130 mm) & Pervious Base	\$400,000	\$82,800	6	\$522,000	3.62	0.64	2.32
Bituminous Superpave	\$400,000	\$96,000	5	\$435,000	2.60	0.51	1.33
NovaChip	\$180,000	\$43,200	2	\$174,000	2.31	0.27	0.63
Bituminous Insulation 75 mm Aggregate (3 inches)	\$420,000	\$100,800	5	\$435,000	2.48	0.50	1.24
Exposed aggregate Finish (Using Retardant)	\$100,000	\$26,400	3	\$261,000	5.68	0.01	0.06



**Table 5.9: Cost Benefit Analysis Results; Case 1 Rehab of a Transverse Tined Pavement Texture**

	Unit Cost	NPV Cost	Savings S (dBA)	Benefit= S*43500*4	B/C	P(OBSI) <100dBA)	Adjusted B/C (B/C)*P
			Based on Rehab on ATD				
Sound Abatement Berm 20 ft. high	\$2,100.00	\$1,001,000	10	\$870,000	0.50	0.95	0.47
Noise Wall 20 ft. High including Foundation	\$6,000,000	\$1,200,100	8	\$696,000	0.33	0.95	0.32
Astro Turf Drag	\$80,000	\$14,000	0	\$0	0.00	0.03	0.00
Conventional Diamond Grind	\$100,000	\$21,000	1	\$43,750	2.08	0.12	0.25
Innovative Diamond Grind	\$129,000	\$31,000	3	\$131,250	4.23	0.39	1.65
Ultimate Diamond Grind	\$120,000	\$31,000	4	\$175,000	5.65	0.57	3.22
Pervious Concrete Overlay (100 mm)	\$560,000	\$117,000	4	\$175,000	1.50	0.64	0.96
Pervious Concrete Full Depth and Pervious Base	\$800,000	\$129,000	4	\$175,000	1.36	0.64	0.87
Pervious Asphalt (130 mm) & Pervious Base	\$400,000	\$82,800	4	\$175,000	2.11	0.64	1.35
Bituminous Superpave	\$400,000	\$96,000	3	\$131,250	1.37	0.51	0.70
NovaChip	\$180,000	\$43,200	0	\$0	0.00	0.27	0.00
Bituminous Insulation 3 inch	\$420,000	\$100,800	3	\$131,250	1.30	0.50	0.65
Exposed aggregate Finish (Using Retardant)	\$100,000	\$26,400	1	\$43,750	1.66	0.01	0.02

### **5.3.6 Sensitivity & Limitation**

The quietness benefit used was based on difference between initial noise level and that of transverse tined surface. Subsequent measurements made on these surfaces reflected a likelihood (P) of being quieter than 100-dBA. The B/C analysis was conducted on the basis of the project unit costs in Table 5.9 and 5.10 above. Apart from the application of P to adjust B/C, the computed benefits of \$43500/ dBA were not subjected to an acoustic performance function over time. The B/C analysis is sensitive to discount rate, initial investment and unit rates that vary with project size. Additionally, surfaces between the noise abatement structure or pavement and the recipient may absorb noise to various degrees depending on their sound absorption coefficient. ( $\alpha$ ). If  $\alpha$  is the sound absorption coefficient, the degree of attenuation is corrected by

$$L_c = \text{Log}_{10} \left( \frac{SI_1}{SI_0} \right)^{(1-\alpha)} \quad (\text{Equation 5.39})$$

Where

$L_c$  = corrected Sound intensity (in dBA)

$SI_1$  = Sound intensity response in Watts/ m<sup>2</sup>

$SI_0$  = Threshold of hearing (10<sup>-12</sup> Watts/ m<sup>2</sup>)

That correction will account for the difference caused by the pavement or shoulder type as well as flora between the source and receiver. Benefit/cost ratio life cycle cost analysis does not necessarily invalidate results from other commonly used assessment strategies such as “Cost Effectiveness” and “Estimated Annual Equivalent Costs”. This study did not evaluate the alternative metrics. However, Benefit/Cost ratio is a preferred assessment tools for investment decisions in pavement infrastructure [5.19].

### **5.3.7 Section Conclusion**

There is a correlation between near field and farfield noise reduction. This has been applied in the use of OBSI to evaluate the economic benefit of pavements. From the methods used and the surfaces evaluated, the Ultimate grind and pervious concrete appear to be the 2 surface that are cost effective when either drag surfaces or transverse tined surfaces are rehabilitated. When transverse tined surfaces are rehabilitated, then the innovative grind, the asphalt 4.75 mm aggregate surface, as well as new SuperPave asphalt surface appear to be relatively cost-effective.

## **5.4 Development of Friction Degradation Models**

### **5.4.1 Background**

Research on the skid resistance of ribbed tire and smooth tire pavement sections was in response to the Federal Highway Administration’s (FHWA) Texture advisory TP 5040 of June 2005 (5.41). The advisory requires monitoring of unconventional pavement textures. Unconventional textures include the inverted turf drag and the longitudinal broom drag both used in Minnesota. Study monitored periodic friction measurements on some MnROAD test sections and created a degradation model characteristic of each pavement type. Designated study sections in the network were also monitored for many years in order to establish degradation characteristic.

Researchers found a higher rate of friction decay in test sections where the initial turf texture was less than 1mm and a more gradual rate of degradation in the tined pavements. Turf drag textures in MnROAD preceded the current texture depth requirements. Due to widespread response to the advisory many standards and research reports have been generated [5.21] [5.22] [5.23] [5.24].

#### **5.4.2 Introduction**

Friction at the tire pavement interface is an important safety issue in Transportation. The absence of friction at the interface results in hydroplaning, skidding and collisions due to longer stopping distances.

##### **Hysteresis effects in Tire Pavement Interaction**

Hysteresis is that component of tire-pavement friction that does not significantly depend on aggregate asperities, micro-texture or macro-texture but on the suction forces between the surfaces in contact. This condition is formed when energy is dissipated in the instantaneous deformation of the tire over a contact patch and the rarefaction of the deformed part over the same patch. The effective contact area is reduced when texture degradation occurs.

Ten field sites representing a variety of asphalt pavements in the State of Ohio were selected for the study. Five laboratory briquettes made from the same materials used in the construction of the pavements were prepared for each of the sites. Skid resistance measurements were performed on the briquettes using a portable British pendulum tester. The friction force was considered to consist of two parts, namely, the wet adhesion and the hysteresis components. The adhesion and hysteresis components were measured separately using water and liquid hand soap as lubricants. To simulate the changes due to wear and aging of pavements, several cycles of mechanical polishing were conducted and the available contact area after polishing was determined using a digital image processing technique. Tests were conducted at five different temperatures. The hysteresis component of friction decreased with increasing temperature regardless of surface texture state. The adhesion component was more sensitive to surface texture effects. Hysteresis was found to account for the larger part of the total friction force. Combined friction decreased with increasing temperature on a polished surface; hence it is recommended that skid numbers obtained at any arbitrary temperature be normalized with respect to a value at a reference temperature, for example, 293 K (68°F).

#### **5.4.3 Data Analysis**

This section analyzes texture and friction degradation characteristics of rigid pavements in monitored test sections.

Tire pavement interaction in the development of limiting frictional force was analyzed in all the test sections in MnROAD and in selected sections in the network. Further analysis of the TPIN forces included an idealization of the asperities of the contact patch and a deployment of energy conservation equations to analyze adhesion and hysteresis. Texture degradation models are developed with the Levenberg-Marquardt nonlinear least squares method. The resulting models are compared to those obtained from test sections in the network that MnDOT has monitored for many years. The degradation models obtained in MnROAD Cells are shown in Table 5.43 monitoring. That earlier study evaluates these test sections with crash rates and wet weather accidents. This study evaluates the same test sections using friction survival as the sole criterion and hysteresis analysis for some intrinsic characteristics. Additionally friction data from all MnROAD cells since 1997 was analyzed. The friction degradation pattern of some MnROAD textures was studied were hypothesized to follow the function:

$$FN_{\text{Survival}} = C_2 + C_1 e^{-(C_3 T)} \dots\dots\dots \text{(Equation 5.41)}$$

where

$C_1$  is a multiplier constant that is characteristics of Environmental effects and texture

$C_2$  is a constant that is similar to the original friction of that section

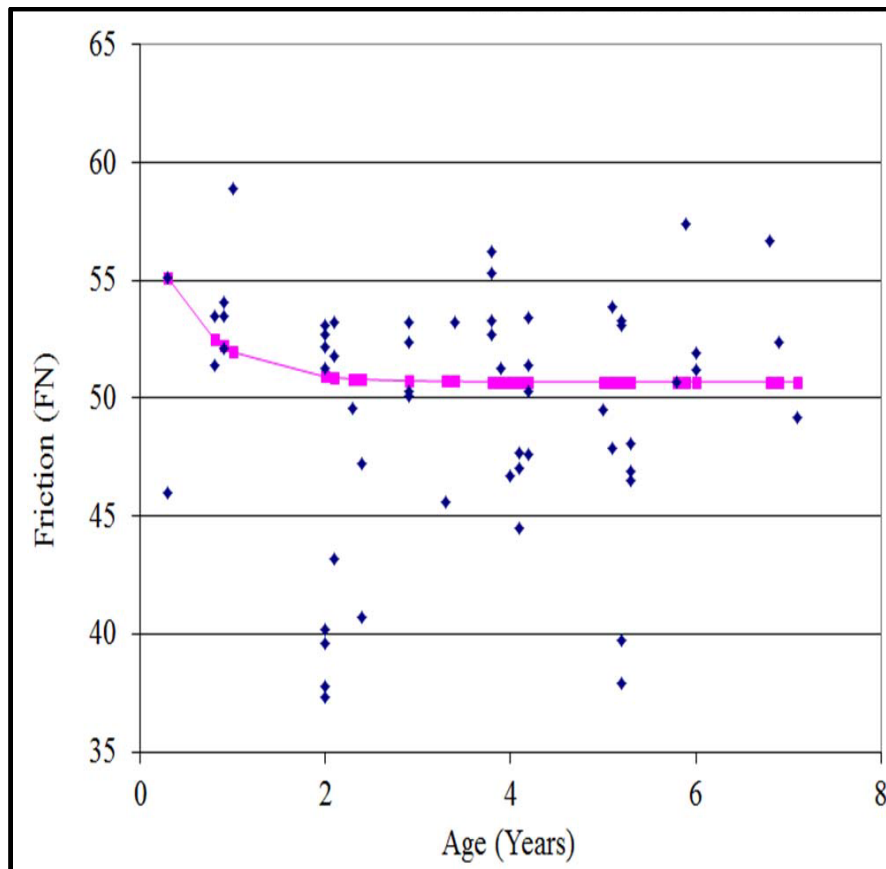
$C_3$  is an exponential correction for the rate of degradation

T is age of pavement in years. Note is made of age of texture when pavement and texture ages are different

FN is the remaining Friction number after T years

PCC Friction Survival in the Minnesota Network

Causative and associative parameters of texture degradation are discussed. Non-uniformity of texture friction trend is associated with hysteresis effects. This research did not separate FN into its components: adhesion, hysteresis and wear but discusses some observed friction gradient extrapolations that facilitated a postulation of the durability of asperities of the Turf drag. Raw data of friction measurements performed in the designated cells are shown in Table 5 .1.



**Figure 5.22: Network Ribbed Tire Friction for Concrete. (Concrete textures are Turf & Broom Drag)**

The derived models are based on measurements taken in the test sections since 1997 using the MnDOT lock wheel skid trailer for the network test cells at the MnROAD test sections. Tables 5.10 and 5.11 show the friction survival models obtained in Minnesota Turf Drag surfaces in the network.

**Table 5.10: Summary Network Ribbed-Data for MnDOT Current Texturing**

Date	Section	Lane/D	Start	End	Tire	Avg	Ave
25-Oct-	TH 21 Jordan	NB RT	33.5	35.5	SMOOT	25.3	40.3
6-Jun-00	TH 21 Jordan	NB RT	32.511	34.51	SMOOT	25.7	40.2
24-Jul-01	TH 21 Jordan	NB RT	32.5	34.5	SMOOT	27.8	40.3
13-Nov-	TH 21 Jordan	NB RT	32.5	34.5	SMOOT	33	40.3
4-Jun-03	TH 21 Jordan	NB	32.5	34.5	SMOOT	29.4	40.1
9-Sept-04	TH 21 Jordan	NB RT	32.5	36	SMOOT	20.8	40.3
15-Jul-99	Estimated Constructed						
12-Oct-	I 35, RP 68 to 79	SB RT	77	70	SMOOT	33.9	40
26-Oct-	I 35, RP 68 to 79	SB RT	77	70	SMOOT	29.6	38
12-Jul-06	I 35, RP 68 to 79	SB RT	77	70	SMOOT	24.8	40
27-Jun-	I 35 RP 68 to 79	SB RT	77	70	SMOOT	26.8	40.7
15-Jul-04	Estimated Constructed						
15-May-	35W, RP 9 to 11	NB RT	9.114	10.11	SMOOT	22.9	40.7
14-May-	Estimated Constructed						
26-Jul-01	I-94, RP 115 to 128	WB RT	127	115.5	SMOOT	36.6	40.2
1-May-03	I-94, RP 115 to 128	WB RT	127	116	SMOOT	34.9	40
23-Sept-	I-94, RP 115 to 128	WB RT	127	116	SMOOT	27.9	40.1
14-Jun-	I-94, RP 115 to 128	WB RT	127	116	SMOOT	31.9	40
2-Aug-06	I-94, RP 115 to 128	WB RT	127	116	SMOOT	27.5	40.5
3-Aug-06	I-94, RP 115 to 128	WB RT	127	116	SMOOT	51	40.1
15-Jul-99	Estimated Constructed						
26-Jul-01	TH 94, RP 115 to 128	EB RT	116	127	SMOOT	41.6	40.1
1-May-03	TH 94, RP 115 to 128	EB RT	116	126.5	SMOOT	40.6	40
23-Sep-	TH 94, RP 115 to 128	EB RT	116	127	SMOOT	32.2	40.1
14-Jun-	TH 94, RP 115 to 128	EB RT	116	127	SMOOT	40.9	39.9
3-Aug-06	TH 94, RP 115 to 128	EB RT	116	127	SMOOT	32	40.6
15-Jul-99	Estimated Constructed						
16-May-	TH 94, RP 21 to 27	WB RT	22.378	21.53	SMOOT	32.3	40.8
15-Jul-00	Estimated Constructed						
9-Sep-04	TH 169, RP 88 to 90	NB RT	89	90.1	SMOOT	21.6	40.1
27-Oct-	TH 169, RP 88 to 90	NB RT	89	90	SMOOT	26.9	40.3

**Table 5.11: Summary Network Ribbed – Data for MnDOT Current Texturing**

Date	Age (2010)	Section	Lane/Direction	Tire	Avg	Ave
15-Jul-00	10.46					
27-Oct-99	11.18	I-90, RP 222 to	EB RT LN	SMOOTH	46.1	40.3
21-Jun-00	10.53	I-90, RP 222 to	EB RT LN	BLANK	41.7	40.2
11-Jul-01	9.47	I-90, RP 222 to	EB RT LN	SMOOTH	36.2	40.3
7-Nov-02	8.15	I-90, RP 222 to	EB RT LN	SMOOTH	37.7	40.1
13-May-	7.64	I-90, RP 222 to	EB RT LN	SMOOTH	35.9	40.3
2-Jun-05	5.58	I-90, RP 222 to	EB RT LN	SMOOTH	32.3	40.5
11-Apr-06	4.72	I-90, RP 222 to	EB RT LN	SMOOTH	37.2	40.8
15-Jul-99	11.46					
13-Nov-	9.13	I-35W, RP 35 to 41	NB RT LN	SMOOTH	29.2	40.2
13-Nov-	9.13	I-35W, RP 35 to 41	NB RT LN	SMOOTH	19.2	55.1
13-Nov-	9.13	I-35W, RP 35 to 41	SB RT LN	SMOOTH	27.9	40.3
13-Nov-	9.13	I-35W, RP 35 to 41	SB RT LN	SMOOTH	18.9	55.2
15-Jul-00	10.46					
15-Nov-	9.13	I-90, RP 222 to	EB RT LN	SMOOTH	31.7	40.6
15-Nov-	9.13	I-90, RP 222 to	EB RT LN	SMOOTH	23.3	55.3
15-Jul-99	11.46					
13-Nov-	9.13	I-94, RP 115 to	EB RT LN	SMOOTH	38.7	40.3
13-Nov-	9.13	I-94, RP 115 to	EB RT LN	SMOOTH	30	55.2
13-Nov-	9.13	I-94, RP 115 to	WB RT LN	SMOOTH	35.8	40.4
15-Jul-99	11.46					
14-Nov-	9.13	US 169, RP 96 to	NB RT LN	SMOOTH	32.3	40.1
14-Nov-	9.13	US 169, RP 96 to	NB RT LN	SMOOTH	22.9	55.2
14-Nov-	9.13	US 169, RP 96 to	SB RT LN	SMOOTH	30.9	40.2
14-Nov-	9.13	US 169, RP 96 to	SB RT LN	SMOOTH	20	54.9
15-Jul-00	10.46					
4-May-01	9.66	TH 35W, RP 35 to	NB RT LN	SMOOTH	30.2	40
4-May-01	9.66	TH 35W, RP 35 to	SB RT LN	SMOOTH	27.6	40
3-Jun-03	7.58	TH 35W, 35 to 41	NB RT LN	SMOOTH	30.8	40.1
3-Jun-03	7.58	TH 35W, RP 35 to	SB RT LN	SMOOTH	26	40.2
21-Sep-04	6.28	TH 35W, RP 35 to	NB RT LN	SMOOTH	20.9	40.3
21-Sep-04	6.28	TH 35W, RP 35 to	SB RT LN	SMOOTH	20.5	40.5

A classic example of a Turf Drag surface is TH 94 in Sauk Rapids. This section has been monitored since inception in 1999 (Figure 5.42). Minimum measured ribbed tire friction number and smooth tire friction numbers were 53.2 and 34.9 respectively in the second year and 51.2 and 31.9 respectively in the 6<sup>th</sup> year. Similar values in the TH 21 segment in Jordan were 43 and 27 in the second year and 40 and 20 in the 5<sup>th</sup> year. TH 94 section starts out higher than the 21 section. A similar pattern was observed in TH 21 in Jordan but this was at the lower end of friction performance. Ribbed and Smooth tire friction numbers are similar to the lower bound of network typical friction numbers as the state does not set a threshold for FN ribbed or FN smooth.

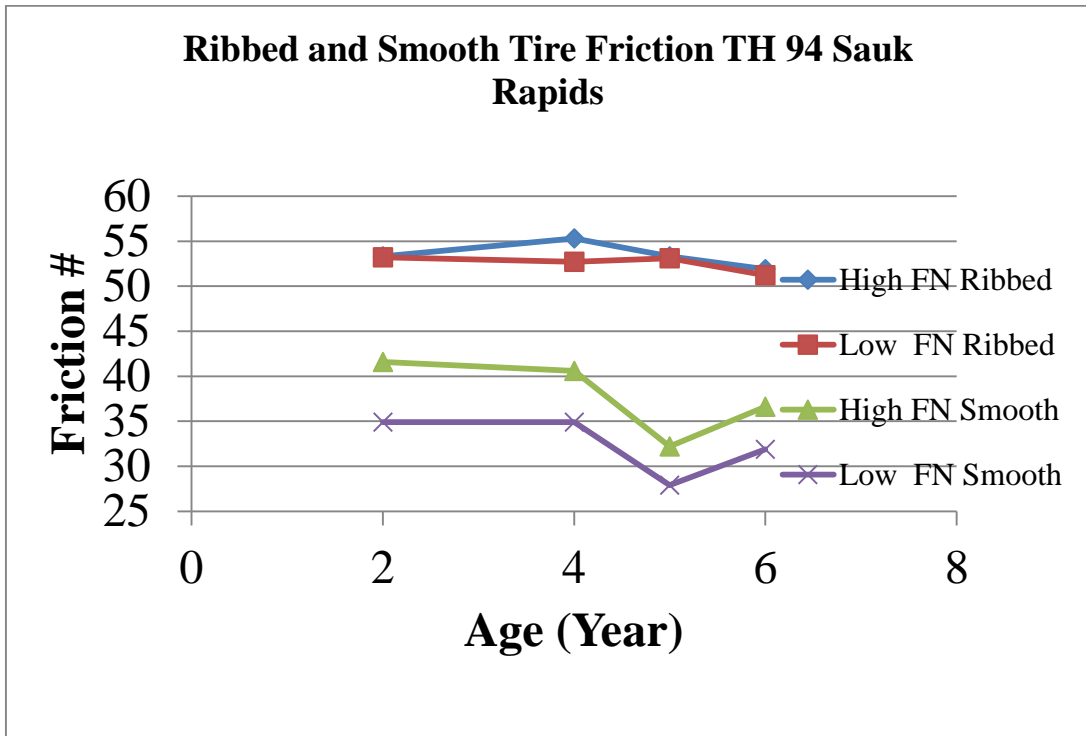


Figure 5.23: Friction Survival in I-94 Turf Drag Test Section in Sauk Rapids MN

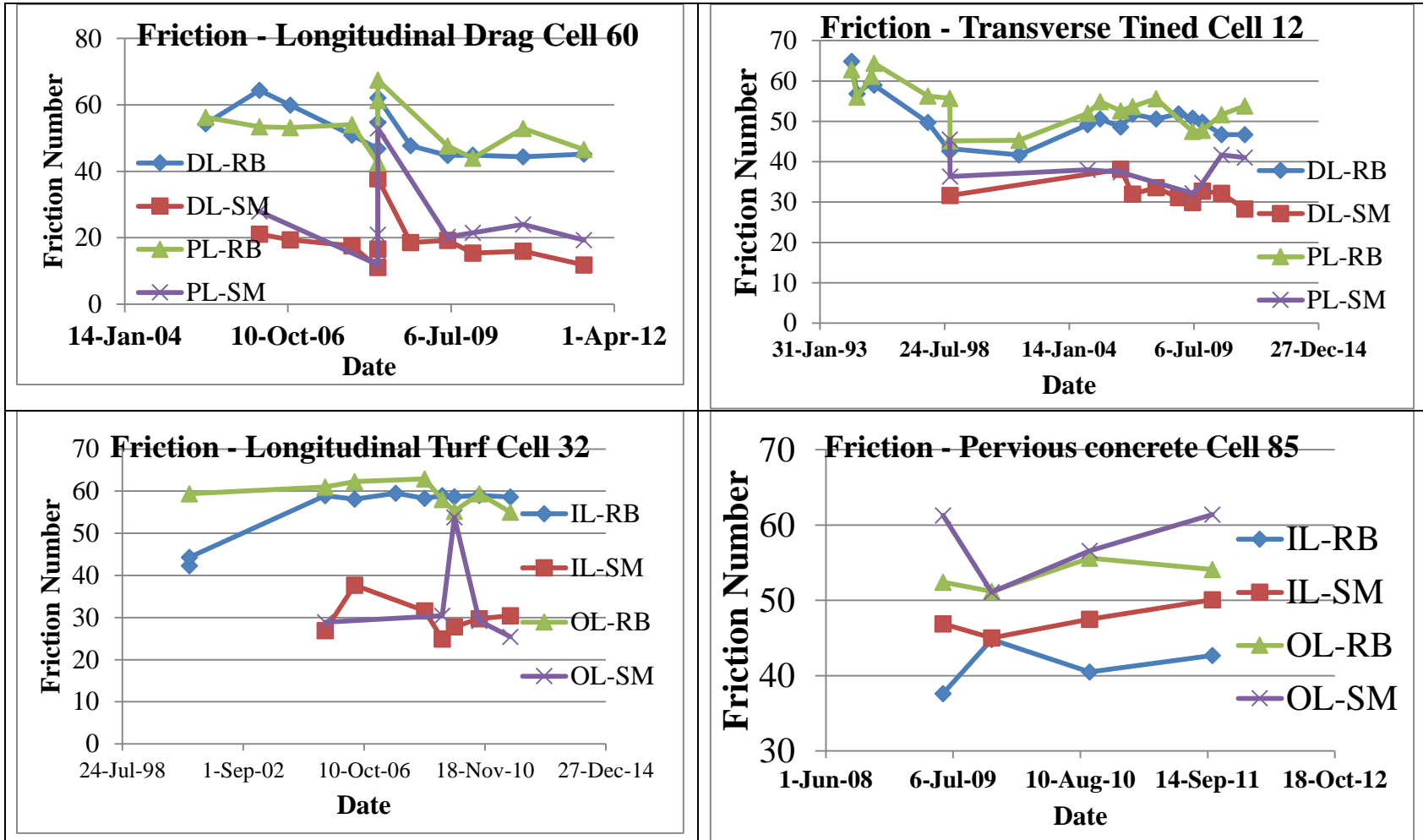
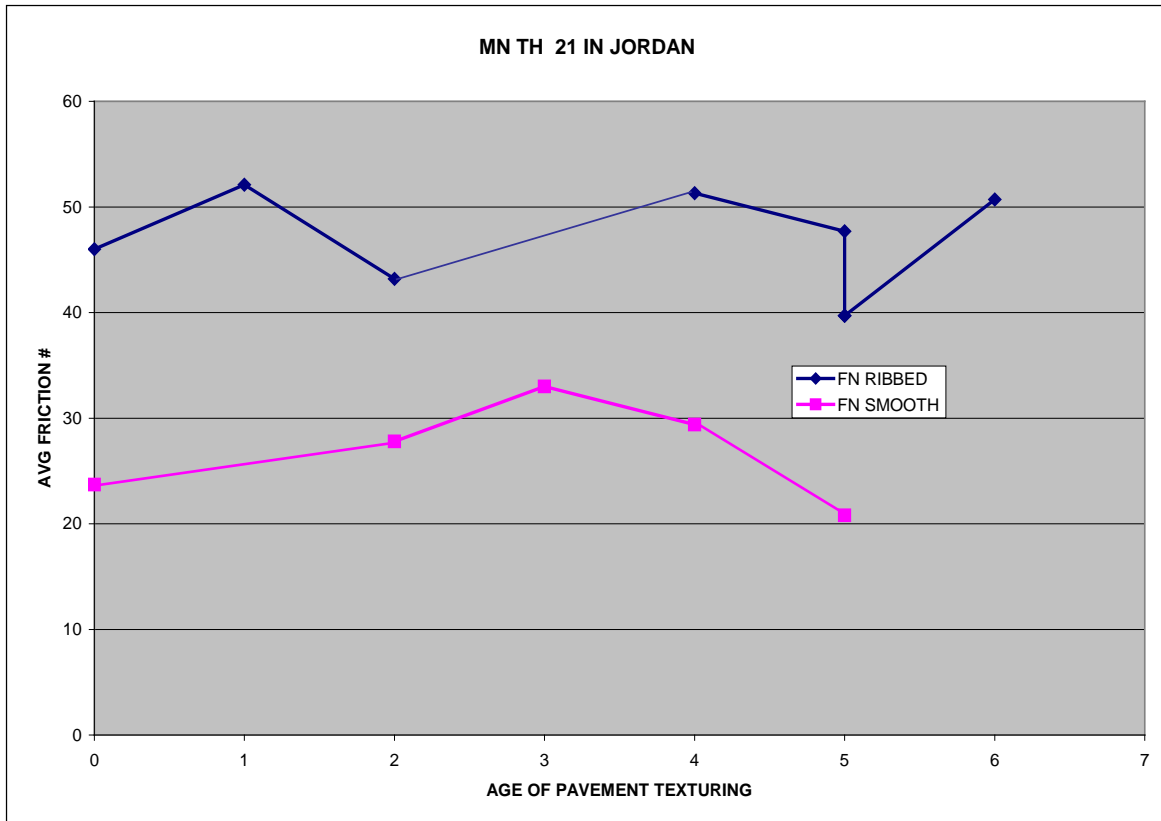


Figure 5.24: MnROAD Texture Versus Time Patterns





**Figure 5.25: Friction Survival in MN-21 Turf Drag Section in Jordan MN**

The MnDOT texture requirement behind the paver was increased to 1 mm in 1999. In some instances friction measurements were conducted only when certain incidents occurred on a section of roadway or when there were complaints about traction. There was therefore no network wide friction Vs texture measurements as these were available where friction measurements had been made in response to public complaints led to friction measurements and subsequent monitoring of pavement sections. None of the sections under investigation was so created but the turf sections were deliberately set up for monitoring in order to ascertain survival trends and to validate the other test sections.

There were variations in the Residual FN values and patterns across test sections. The test sections are subject to various traffic loads and percent truck distribution. The configurations of the turf drag across test sections are similar. In the sections chosen, the average mean texture depths measured immediately after paving was similar to the post paving MTD although the standard changed from 0.8 mm to 1.0 mm in 2001.

One important parameter in the model is the C2 Model constant. This was the most descriptive component of the model parameters and it relates closely to the original values at inception. The C1 and C3 values are multiplier and exponential constants. Evidently, when C3 is small C1 governs the degradation. However when C3 is closest to zero, the function approximates to a linear decay model. It is consequently implicit from Table 5.44 that the degradation model for the ribbed tire is an exponential decay model whereas the smooth tire model is almost linear. The network model does show initial ribbed tire and smooth tire (C<sub>2</sub>) values at 58 and 28

respectively. This is very true for the ribbed tire data while the smooth tire data is somewhat diminished. This was attributed to a statistical factor in which there were more consistent ribbed tire monitoring than smooth tire monitoring due to prevailing institutional requirements and directives at that time.

Network Model parameters derived for Turf Drag survival based on a generic model

$$\text{Generic Model} = C_2 + C_1 * (1 - e^{-(C_3 * t)}) \quad e = 2.718282 \quad (\text{Equation 5.41})$$

Ribbed tire FN Model

$$C_1 = -7.4884 \quad C_2 = 58.1882 \quad C_3 = -1.7723 \quad t = \text{years from original paving}$$

Smooth Tire FN Models

$$C_2 + C_1 * (1 - e^{-(C_3 * t)}) \quad (\text{Equation 5.42})$$

$$C_1 = \text{Alpha } 8.5423 \quad C_2 = 28.29 \quad C_3 = -0.08 \quad t = \text{years from original paving}$$

Similar friction survival was observed on TH 21 in Jordan (drag texture) but this was at the lower end of friction performance. Ribbed and Smooth tire friction numbers are similar to the lower bound of network typical friction numbers as MnDOT does not set a threshold for FN ribbed or FN smooth. Low friction numbers characterized the original textures of TH 21 because the standard at that time was 0.8 mm behind the paver. Subsequently, that standard was upgraded to 1mm behind the paver by MnDOT to accommodate early degradation caused by snowplows. Evident in Table 5.41a and b is that all other segments performed well and did not exhibit friction levels lower than characteristic network values. Disturbing trends are tied to wet weather accident calls that lead to friction measurements and subsequent monitoring of pavement sections. None of the sections under investigation was so created but the turf sections were deliberately set up for monitoring in order to ascertain survival trends validate the other test sections and respond to stipulations of the FHWA Texture Advisory.

### **MnROAD Friction Survival Models**

All test sections in MnROAD that were monitored since 1987 were arranged in groups of defined texture types. The friction data is shown in Table 5.10 and 5.11 group models are presented in Tables 5.13 and 5.13. This aspect of the MnROAD model is comparable to the network model. In Figure 5.42, the similarities are accentuated as it shows the similar decay models for ribbed and smooth tire friction. MnROAD model was indirectly validated by comparing with the network model. The MnROAD Low Volume Road ATD model did not correspond the test section performance curve because the former did not have sufficient data. The latter was subjected to less traffic that would cause appreciable degradation within the first decade of service. Annual ESALS recorded for the MnROAD Low Volume Road. This is based on the 5-axle semi loaded to 102 kilo pounds making 80 runs per day one day a week on the Outside lane and 80 k load 80 times a day 4 days a week in the inside lane. The cumulative ESALS in the LVR in 1994 were 7,412 and 6,760 and 188,676 and 184,749 in 2005 respectively.

In the mainline, 14 year ESALs based on the WIM is 9 million ESALs in the driving lane and 2.5 million ESALs in the passing lane. The driving lane degradation is therefore closer to the network where ESALs range from 7 million to 13 million in the new turf cells. Original MnROAD design expected the damage to be similar. The load levels are not significant enough and the test sections are not sufficient to compare the texture degradation in the inside and outside lanes (5.43) showed that the tire pavement interaction noise changes in the outside and inside lane were similar. Final texture friction degradation models are shown in tables 5.12 and 5.13.

**Table 5.12: MnROAD Friction Survival Model.**

$FN = C_2 + C_1 \mathbf{1} - e^{C_3 t}$		Ribbed					Smooth					Sample
Code /Cell Type	Cells	C <sub>1</sub>	C <sub>2</sub>	C <sub>3</sub>	SSE	AB S	C <sub>1</sub>	C <sub>2</sub>	C <sub>3</sub>	SSE	AB S	Size
PCC- ML-WT-TT	92-97	-750	63.4	-0.001	556	781	-416	70.2	-0.0078	4097	132.8	27
PCC- ML-WT-ATD	60-63	-1241	56.1	-0.001	343	84.5	-75.4	93.21	-1.605	203	46.8	32
PCC- ML-TT	5-13	-29	79.6	-0.676	7210	994	-65.3	37.67	-0.009	4539	482	224
PCC- LVR-TT	36-40	-347	60.8	0.001	1401	279	-8.9	50	-5.601	2665	249	107
PCC- LVR-ATD	32, 52-54	524	51.9	-0.0002	333	54	-207	38.4	-0.002	443	39.4	20

**Table 5.13: Legend of Texture Descriptors**

Code	Legend
PCC- ML-WT-TT	Portland Cement Concrete- Mainline- Whitetopping –Transverse tined
PCC- ML-WT-	Portland Cement Concrete- Mainline- Whitetopping –Turf Drag
PCC- ML-TT	Portland Cement Concrete- Mainline- Concrete on Aggregate Base–Transverse
PCC- LVR-TT	Portland Cement Concrete- Low Volume Road- Whitetopping –Transverse
PCC- LVR-ATD	Portland Cement Concrete- Low Volume Road- Concrete on Aggregate Base –

#### 5.4.4 Model Improvement and Validation

As part of this research project, the friction degradation models developed for the MnROAD cells were applied to the network sections with historical friction measurements. It became necessary to introduce a traffic parameter ESALs to the factorial as this variable was not necessarily dependent on time to the same degree in each test section. The model was improved therefore and subsequently validated through a set of statistical hypothesis validation tools. A total of three equations were used to model the pavement friction values: two for the Mainliner’s model (equations 5.43 and 5.44) and one for the LVR (equations 5.45). The LVR’s ribbed equation was not employed on the test sections because upon comparison of the number of annual ESALs and the friction data between the Mainline, LVR and the test sections showed that the ribbed equation couldn’t be made with any accuracy and that the Mainline’s equation would have better success. The LVR’s smooth tire equation was still used because the texture of the concrete might have had a better representation when the ESALs are fairly close. In the equations 5.43 to 5.45,  $F$  is the friction value,  $k$  is the growth rate,  $t$  is the age of the concrete in

years,  $FE$  is the number of ESALs for the forecasted year (20 years after the design year) and  $DE$  is the number of ESALs for the design year.

- Mainline Ribbed

$$F = 22.01 \sin(kt) + 29.21 \cos(kt)[1 + e^{-0.1t}] \quad (\text{Equation 5.43})$$

- Mainline Smooth =  $\left[ \left( \frac{801000}{DE} \right) \left( \frac{FE}{DE} \right) \right] [\sin(kt) + 18.36 \cos(kt) [1 + e^{-0.8t}]]$   
(Equation. 5.44)

- LVR Smooth

$$F = -4.56 \sin(kt) + 15.56 \cos(kt) [1 + e^{0.031t}] \quad (\text{Equation 5.45})$$

In equations 5.43 to 5.45,  $F$  is the friction value,  $k$  is the growth rate,  $t$  is the age of the concrete in years,  $FE$  is the number of ESALs for the forecasted year (20 years after the design year) and  $DE$  is the number of ESALs for the design year.

After the equations were correctly entered for the data points, the modeled pavement friction values ( $F$ ) was computed. The process of data selection analysis and the description of methods used in this process are published in a separate report

#### 5.4.5 Section Summary

This study examined the various texture types for friction survival and generated model coefficients for the friction degradation model. Prominent texture types as at the time of analysis included transverse tined, and broom dragged textures. In the models developed, the constant independent of time appears to be the same as the original friction measured immediately after testing. Though that value was not so imposed

- Pattern of friction survival in current texturing Minnesota textures subjected to 500,000 ESALs or more have been examined. A network model developed exhibited a decay that compares favorably with typical network texture performance.
- Friction survival models of current turf and broom drag segments in the network as well as all the test cells in MnROAD have been developed. The MnROAD Model for Turf Drag in the Mainline is similar to the Network. The Low volume road model is different because the rate of loading is not sufficient to cause sufficient degradation for a model to be tenable.
- Hysteresis extrapolations suggest that macrotexture preponderance in friction potential of current texturing experiences a crossover at the 10<sup>th</sup> year. Aggregate exposure and hysteresis then governs the friction potential in the second decade.
- Ribbed tire friction is an effective pavement performance tool. Evident in MnROAD Model groups 5-10 is the characteristic decay of friction number versus this task report fulfills the requirement of FHWA texture advisory that requires monitoring of innovative textures.

#### 5.5 **Effects of Pavement Condition on Concrete Pavement Smoothness and Acoustics**

Tire pavement interaction noise mechanisms include HelmHoltz and pipe resonance. Acoustic properties of pavements are dependent on the pavement conditions. For instance, when concrete pavements are in incipient stages of degradation, changes in acoustic impedance may not be very

obvious but as the joints deteriorate by spalling and scouring, it has been shown analytically that the acoustic resistance of the pavement reduces.

By basic fluid mechanics and acoustic analysis of idealized conditions of pavement distress, sound pressure level changes can be predicted. In more direct conditions, faulted pavements cause impulsive loading at the joints. These can be viewed in the time domain as periodic sound pressure waves of low frequency. Onboard sound intensity being a summation of twelve third octave frequencies starting with 400-Hertz is not a good validation tool for condition induced acoustics of pavements. Statistical Pass by Measurements detected very high emission levels in Cell 92 MnROAD where the joints are badly faulted and deteriorated.

Since acoustic properties are predictable from pavement condition, pavement evaluation using acoustic impedance may be more feasible evaluation tool process.

### **5.5.1 Introduction**

Noise is generated through various active processes in the tire pavement interaction. These processes have been better understood through various research conducted by Izevbekhai [5.22]. Rohne & Burnham [5.26] elucidated that mechanical deterioration processes characterize certain concrete pavements when they are not adequately drained.

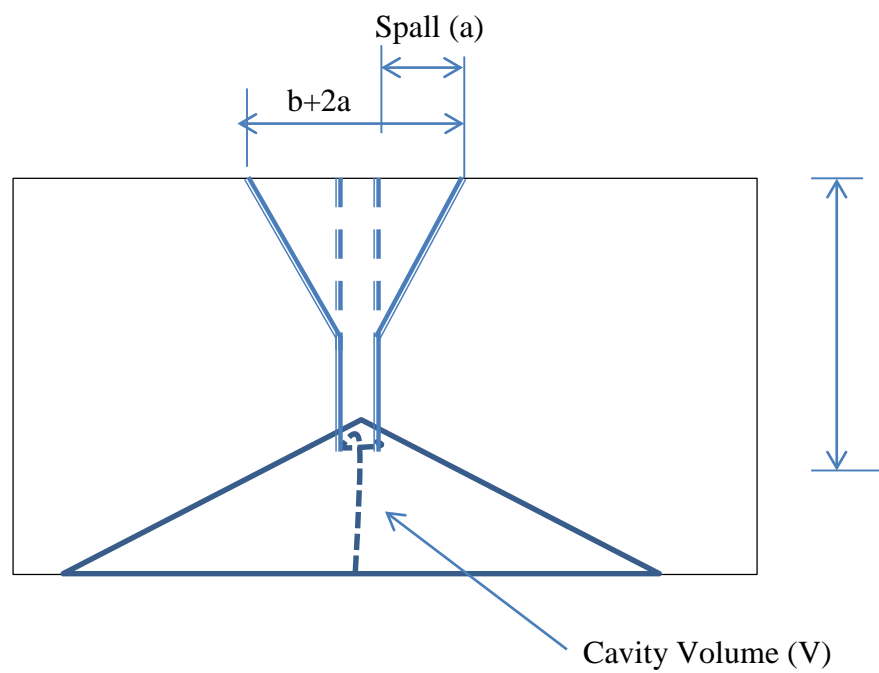
#### **The stick snap phenomenon (Plunger Simulation)**

This “stick-snap” phenomenon also causes vibration in the tire tread and carcass and produces sound energy. This is similar to the sound produced when a suction cup is pulled off a surface. Inside the contact patch, the tread blocks stick momentarily and then slip against the roadway surface in a tangential direction [1.32] and the implication in resonance or acoustic impedance [1.33] to [1.35]. There were listed as the stick slip phenomenon, the clap phenomenon and the horn (amplification) effect. Others include the pipe (organ pipe effect) and the cavity resonance (balloon simulation). The enclosed space inside the tire has a cavity resonance that is perceptible internal and external to the vehicle. Vibration of the air within the tire carcass produces a sound like thumping a balloon or kicking a tire. This is important to the effect of distress phenomena on certain surface characteristics.

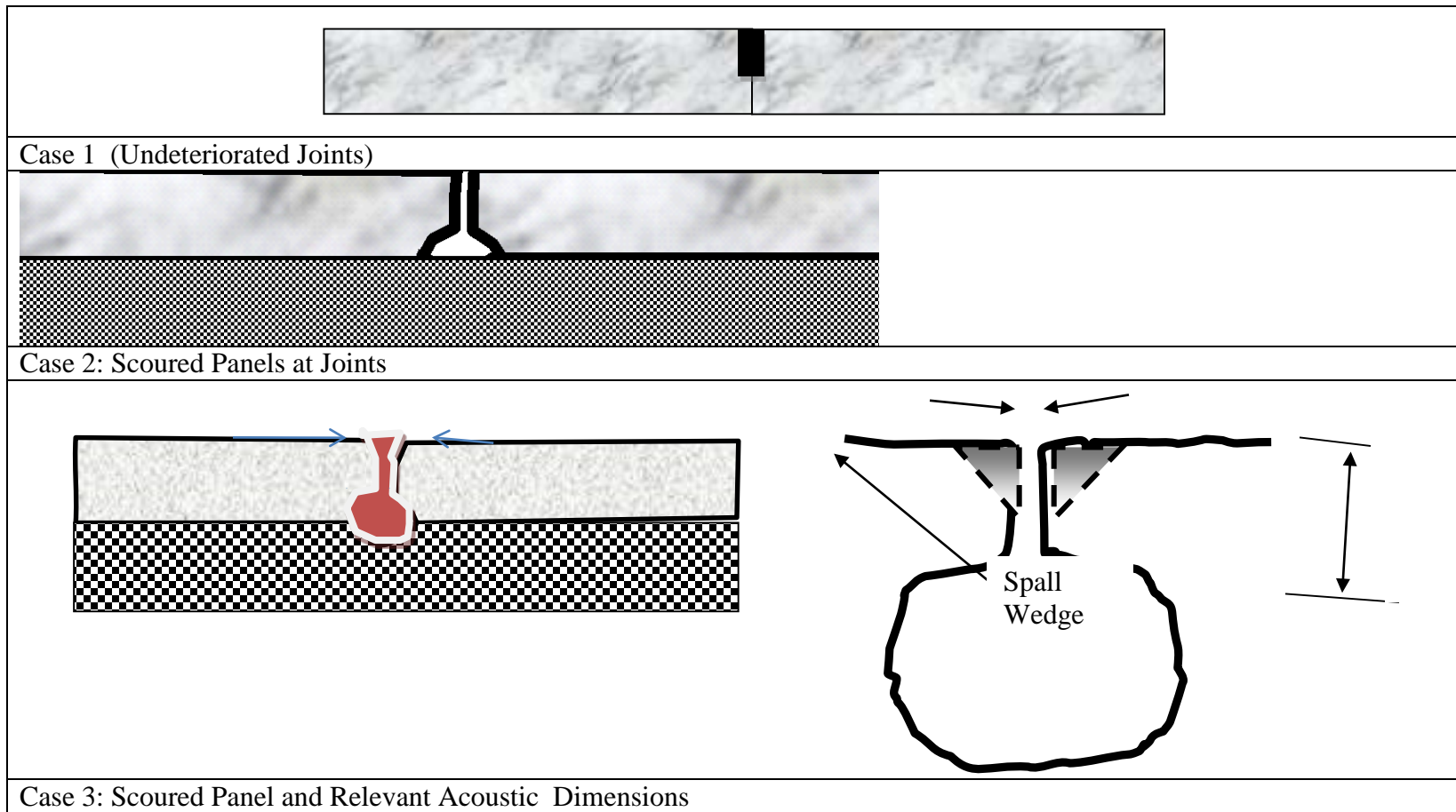
In a more mechanistic approach, Hamet et al showed that the envelopment of texture by tire at the contact patch influences Tire pavement acoustics more than the actual texture. Hamet and Klein [1.40] showed that the envelopment process was analytically ramified in the dynamic and static envelopment process. Clapp and Eberhardt [1.23] showed mechanistically a prediction model for the interaction noise based on the distribution of pressures in the contact patch.

### **5.5.2 Pipe Resonance and Helmholtz Resonance in Deteriorated Concrete Joints**

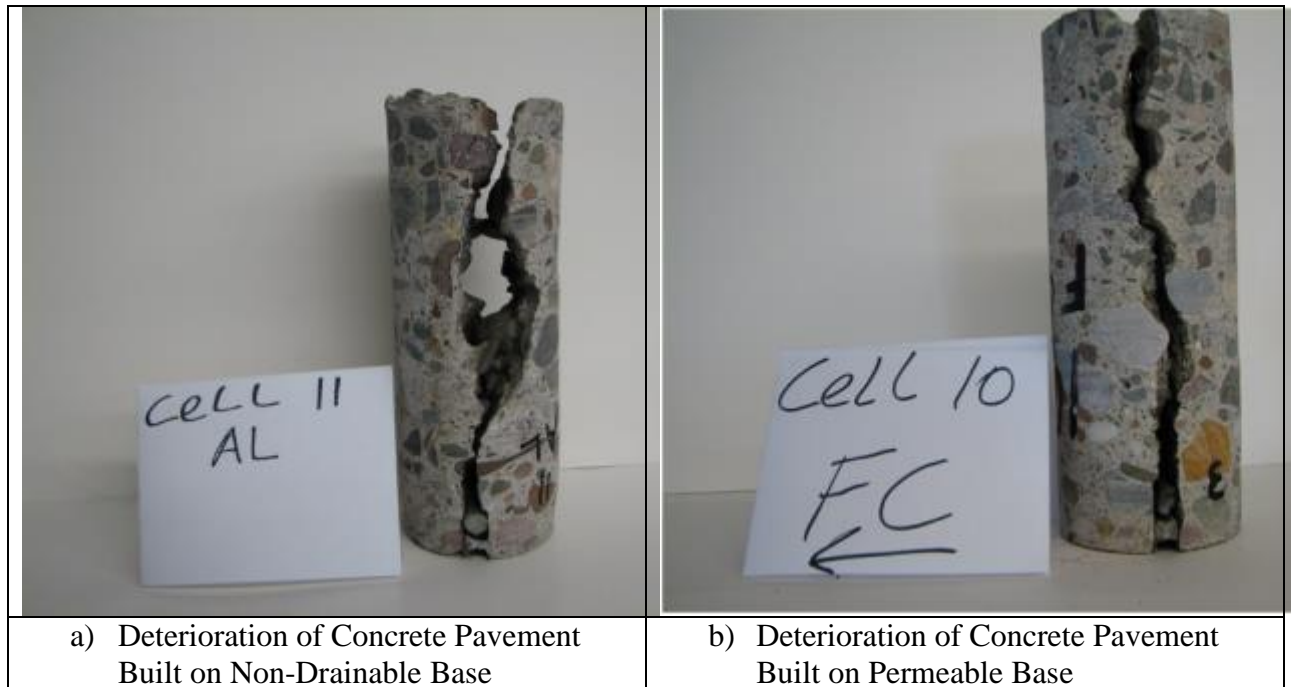
This section discusses the progression and mechanism of concrete joint deterioration and relates the degradation to acoustic properties. Pipe resonance and Helmholtz resonance in concrete pavement joints are subsequently separately discussed. The Helmholtz resonance and pipe resonance phenomena have been introduced in chapter 1.



**Figure 5.26: Details of Dimensions of Spalled and Deteriorated Joints**



**Figure 5.27: Progression of Joint Deterioration Showing Dimensions of Acoustic Relevance**



**Figure 5.28: Evidence of Concrete Joint Deterioration in MnROAD Cells after 13 Years**

Progressing from the new joint shown in Figure 5.27, the main observation of exposed concrete panel joints prior to rehabilitation is scouring below the neutral axis. This scour shown in Figure 5.28 results in the loss of aggregate interlock that results in the loss of stress load transfer and deflection load transfer between consecutive panels. Associated with this scour is the creation of a resonant cavity that increases the joint-induced noise in the tire pavement interaction. The cavity increase results in a source strength that is far greater than the undeteriorated joint even if the latter was undowelled. It will be shown that a combination of both the sliver-spalling on the surface around the joints and the scouring at the bottom of the panels around the joint, does collectively contribute to increase tire pavement acoustics.

### Pipe Resonance Phenomenon

Pipe resonance will occur if there is a defect in the joint sealer from which air gets in and gets trapped. Tire pavement action at the joint forces air through the horizontal column of air beneath the joint as if the column were a pipe. The acoustic phenomenon resembles an organ pipe for which the name derives. Consider an idealized joint in the pavement joint in the similitude of a rectangular box. Assume that the action of tire though transient exerts pressure into the cavity as would a piston to a cylinder. In this case there is pressure relief at the end of the pipe. According to Kinsler et al [5.30] the acoustic pressure is of the general form

$$P (lmn) = A_{(x)} \cos K_{xl} X \cos K_{ym} Y \cos K_{zn} Z e^{j\omega t} \dots \dots \dots \text{(Equation 5.51)}$$

Where A is amplitude, K is the wave number and  $\omega$  is angular speed and P is sound pressure and X, Y & Z are three axes. As a general principle resonance occurs when the reactance is minimal and the resistance is non-zero.



For a rectangular pipe of dimensions  $L_x$   $L_y$  and  $L_z$  it can be shown that the pipe resonant frequencies [5.52] are expressed as

$$w = c \sqrt{\left(\frac{l\pi}{L_{jx}}\right)^2 + \left(\frac{m\pi}{L_{jy}}\right)^2 + \left(\frac{n\pi}{L_{jz}}\right)^2} \dots\dots\dots \quad (\text{Equation 5.52})$$

Where  $c$  is the acoustic speed  
 $l$ ,  $m$  and  $n$  are non-zero non-negative whole numbers.  
 $L_x$   $L_y$   $L_z$  and the geometric dimensions of the pipe or joint in this special case.  
 From the above Equation 5.52, it can be deduced that there are many combinations of different geometric dimensions that will bring about resonance.

This is valid for a continuous rectangular pipe system with uniform cross section and minimal deterioration. Also it can be shown that the condition of the joint is an important factor in the acoustics of pavements.

**Helmholtz Resonance in Concrete Joints: Radiation Resistance of Spalled and Unspalled Joints**

The progression of surface configurations resulting in joint deterioration does not necessarily follow predictable geometric patterns. However the joint deterioration in this problem is idealized to be a continuum of “sliver” spalling at the panel joint surface as well as beveling or scouring of the materials close to the joint below the neutral axis and into the base. A continuous joint is idealized as a continuum of pockets of discontinuous finite Helmholtz resonators. The region beneath the tire contact is regarded as a single Helmholtz resonator of the dimensions shown in Figure 5.51.

Typically, concrete joints deteriorate on the surface by regular spalling and “sliver” spalling. Regular spalling occurs when the joints deteriorate by loss of wedges at the top corners of the leave and approach slab. This occurrence is due to traffic and weather as well as mix design. Sliver spalls are also characterized by loss of material at the top corners of the slab at the joints. Contrary to regular spalls these are caused by inadequate and incorrect timing for sawing of joints. They are visible immediately after joint establishment.

The dimensions and geometry of a delaminated joint affects its acoustics through the phenomena of Helmholtz resonance. This is illustrated by a solution to a problem discussed in the following.

Consider a joint with different progressive steps of deterioration. This cavity is idealized as a device of a rigid-walled cavity of volume  $V$  with a neck of area  $S$  and length  $L$ . If wavelength  $\lambda \gg V^{1/3}$ , the acoustic pressure within the cavity provides the stiffness element. If wavelength  $\lambda \gg S^{1/2}$ , the opening radiates sound as a simple source does, thus providing the resistance element. In their initial state most concrete pavement joints are as shown in Figure 5.27. Due to time, traffic and moisture, gradual spalling and scouring occur in the joint. Deterioration patterns observed are associated with increase in the overall joint cavity ( $V$ ). The increase is due to spalling is shown in Figure 5.27 and scouring 5.28. Typical deterioration pattern was observed in the concrete with non-permeable base as discussed by Rohne & Burnham discussed this pattern

of deterioration noting their absence from pavements with permeable bases in the MnROAD test section as well as the test sections chosen from the Minnesota concrete pavement network for study.

Figure 5.28 shows evidence of concrete joint deterioration after 13 years in some MnROAD test cells. This cell consists of 10 inch concrete pavement on virgin non-permeable aggregate base. Motion of the slab aggravated by freeze thaw effect possibly results in the creation of high positive and low negative pressures resulting in erosion of the concrete materials in a phenomenon similar to cavitation in dam spillways. Conclusively, effective volume of the joint is increased when pavements deteriorate.

It was shown by Pierce A.D. [5.29] that the effective length of the orifice depends on the taper about a centroidal axis. The phenomenon of tapering of joints occurs in practice as sliver spalling at the angular face of the leave and approach slabs. Several authors including Pierce AD and Kinsler et al [5.30], showed that

$$(outer\ end\ spalled)L' = L + 2(0.85a) = L + 1.7a \quad \dots\dots\dots (Equation\ 5.53)$$

$$(outer\ end\ unspalled)\ L' = L + (0.85 + 0.6)a = L + 1.5a \quad \dots\dots\dots (.Equation\ 5.54)$$

Where L is the effect length of the neck of a resonator and L' is the effective length if the neck of cavity is tapered or if the pavement joint undergoes sliver spalling. L' is the effective length of the orifice.

When a fluid enters the cavity through the neck, the fluid in the neck has a total effective mass  $m = \rho_0SL'$ ..... (Equation 5.55)

Where m is mass of air S is surface area of orifice and L' is effective orifice length

$$p = \frac{\rho_0 c^2 S}{V} \xi \dots\dots\dots (Equation\ 5.56)$$

Where p is pressure,  $\rho_0$  is the initial air density, c is the speed of sound,  $\left(\frac{\Delta\rho}{\rho}\right)$  is the ratio of the density change to the initial density of the fluid

$\xi$  is the displacement in the cavity.

S is the orifice area of the joint.

$$p = \rho_0 c^2 \left(\frac{\Delta\rho}{\rho}\right) \dots\dots\dots . (Equation\ 5.57)$$

It can be proven that if  $\xi$  is the displacement in the cavity.

$$p = \frac{\rho_0 c^2 S}{V} \xi \dots\dots\dots \text{(Equation 5.58)}$$

The force  $f = pS$  required to maintain the displacement is  $(\rho_0 c^2 S^2 / V) \xi$  and the effective stiffness  $s$  is given by

$$s = \rho_0 c^2 \frac{S^2}{V} \dots\dots\dots \text{(Equation 5.59)}$$

For very small  $\lambda \gg a$  the radiation resistance in the cavity [5.29] [5.30] is given by

$$R_r = \rho_0 c \frac{k^2 S^2}{2\pi} \quad (\text{spalled joint}) \quad \text{(Equation 5.510)}$$

$$R_r = \rho_0 c \frac{k^2 S^2}{4\pi} \quad (\text{unspalled joint}) \quad \text{(Equation 5.5 11)}$$

*Thus the radiation resistance is higher for unspalled joint than for a spalled joint.*

The instantaneous complex driving force produced by a sound wave of amplitude  $P$  impinging on the resonator [5.51] opening is

$$f = SP e^{j\omega t} \dots\dots\dots \text{(Equation 5.5 12)}$$

This is the solution to a differential equation of the form:

$$m \frac{d^2 \xi}{dt^2} + R_r \frac{d\xi}{dt} + s\xi = SP e^{i\omega t} \quad \text{(Equation 5.5 13)}$$

This is the resulting differential (Equation 5.514)  
for the inward displacement  $\zeta$  of the fluid in the neck is

Since this equation is analogous to that of a driven oscillator, its solution may be obtained by analogy [5.51], [5.53]. In particular, the mechanical impedance of a Helmholtz resonator is of the form

$$Z_m = R_r + j \left( \omega m - \frac{s}{\omega} \right) \dots\dots\dots \text{(Equation 5.5 15)}$$

Substituting for  $r$  in equations -----, at resonant frequency, the inductance-capacitance go to zero and

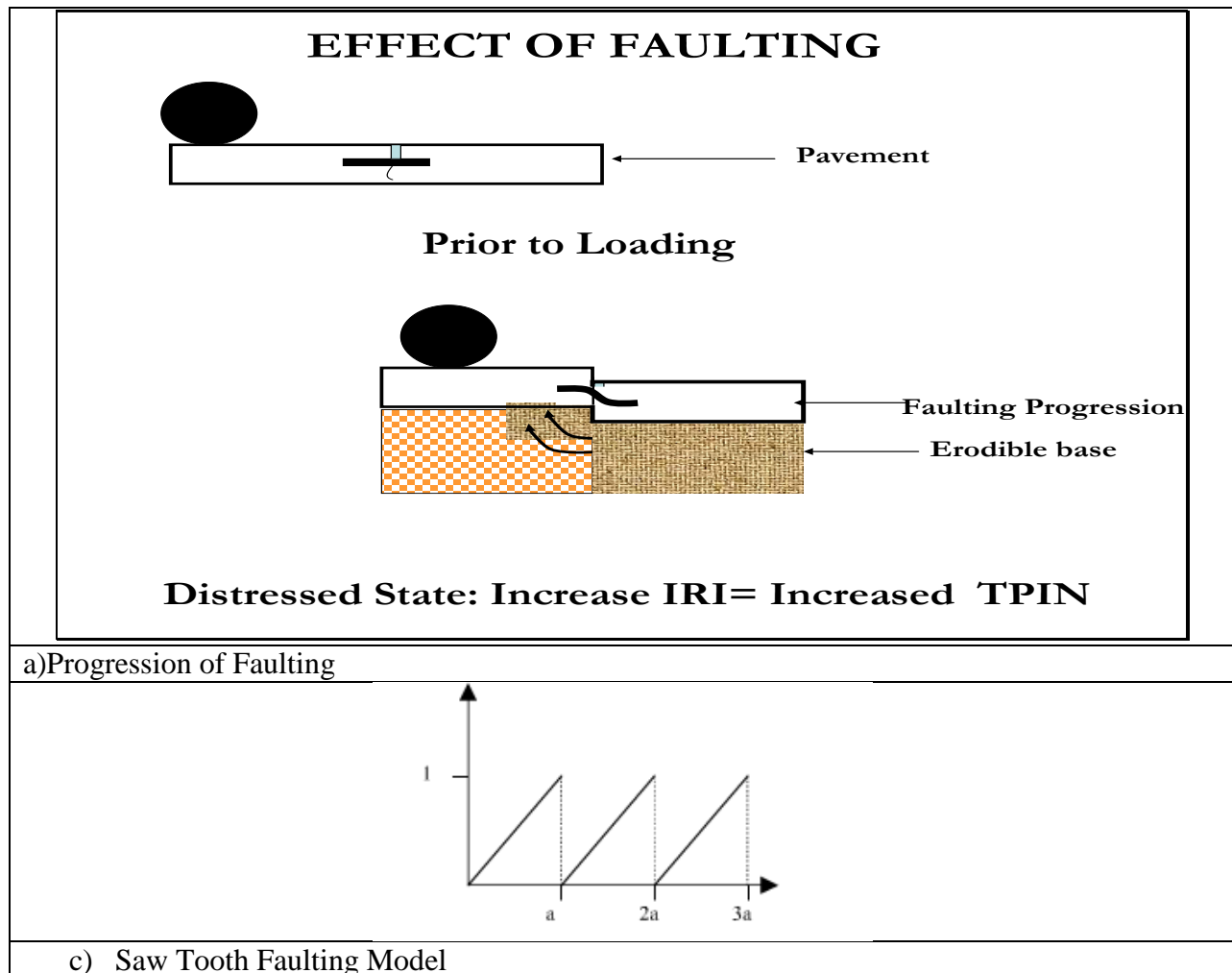
$$\omega_0 = c \sqrt{\frac{s}{L'V}} \dots\dots\dots \text{(Equation 5.5 16)}$$

From the above equation, the resonant frequency of the joint system depends on the effective volume of the joint cavity. If the seal and backer rod are in place the volume is reduced and the source strength of the joint is correspondingly reduced and the natural frequency is increased.

Moreover, a badly deteriorated joint over an impervious base provides a large confined volume  $V$ . In consequence the natural frequency is reduced and is easily encountered by the tire pavement interaction.

### 5.5.3 Effect of Faulting Induced International Roughness Index on Board Sound Intensity Levels

Joint slap occurs when a vehicle travels over a faulted pavement. The transient event happens over a period of approximately 0.01 seconds at 60 mph (96 km per hour). The mechanism of faulting is shown in Figure 5.53. In the following analysis, the noise source is assumed to be coming from the faulting alone. Consequently, the translational effect of an impulsive noise in spatial domain to a sinc function in the time domain is assumed



**Figure 5.29: Effect of Faulting on IRI, Which Affects OBSI.**

Faulting is an interesting pavement distress phenomenon that progresses through sacrificial loss of erodible base material under the leave slab to the approach slab as vehicles ride on the pavement. Faulting is visible through a rearview mirror and it presents as a saw-tooth profile that causes body acceleration at the joints. This is associated with increased pavement roughness.

**Analysis of Joint Induced Roughness**

It has been shown by Izevbekhai [5.25] that the cumulative effects of amplitudes and discrete phenomena in ride quality are linear. For example it can be shown analytically that a 1-inch mid slab sag in a concrete panel results in an IRI of 774 inches per mile if all the panels have the one inch sag. For 5% of the panel, with the one inch sag an IRI of 38.7 in/ mile is expected. If half of the panels have 2-inch sag, the IRI is 774 provided the remaining slabs have no measurable sag. It has been shown below that one inch faulting in all panels resulted in approximately 629 inches per mile. The Sawtooth model was developed with the equation

$$Y = \text{FRAC} \frac{X}{SP} \text{ inches} \dots\dots\dots \text{(Equation 5.516)}$$

Where Y is the vertical profile of the slab  
 X is the position in slab in the direction of travel, measured from the joint (ft.) and SP is the Slab span length (ft.).

For the first panel and repeated for each panel. A continuum of panels with the same equation was then plotted. The process entailed generation of a 1 inch faulted pavement and forcing the profile through the quarter car algorithm. It generated an IRI value as well as a dominant frequency plot from a PSD analysis.

It can also be shown in time domain as  $Y(t) = (1/a) t$  is a generic equation  
 An interesting feature of the saw tooth wave is that the time independent term  $a_0$  in Fourier transform as well as the cosine terms are zero. The sine terms are as follows

$$\begin{aligned} f(t) &= \sum_{n=1}^{\infty} \frac{2(-1)^{n+1}}{n} \sin(nt) \\ &= 2 \sin(t) - \sin(2t) + \frac{2}{3} \sin(3t) - \frac{1}{2} \sin(4t) + \frac{2}{5} \sin(5t) \dots \end{aligned} \text{(Equation 5.517)}$$

In the spectral domain, the saw tooth is made up of an additive set of  $\sin nt$  waveforms but it is easily analyzable because it is governed by a fundamental frequency.

In the time domain the acoustic function resulting from a pattern of joint defects is shown in Figure 5.54. It portrays as a sinc function as each of the impacts if an impulsive function with initially high acoustic energy that diminishes asymptotically before the next impulse, where it rises again and repeats the sequence. The Unfiltered IRI from FHWA Proval version 2.73 is 629.6 inches/ mile and the RN is 0.07.

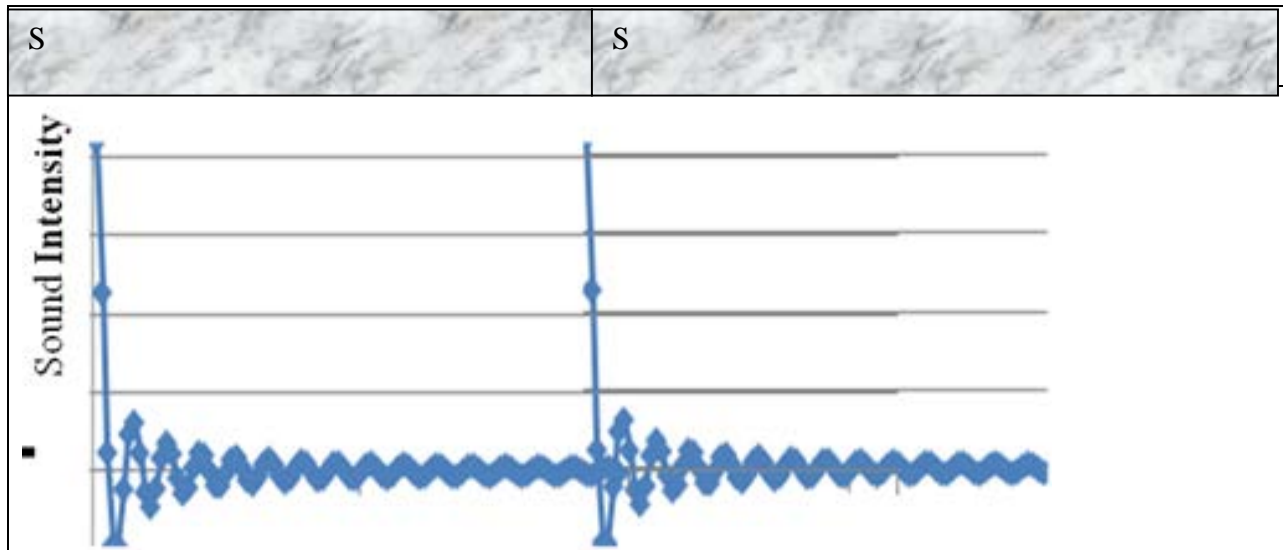
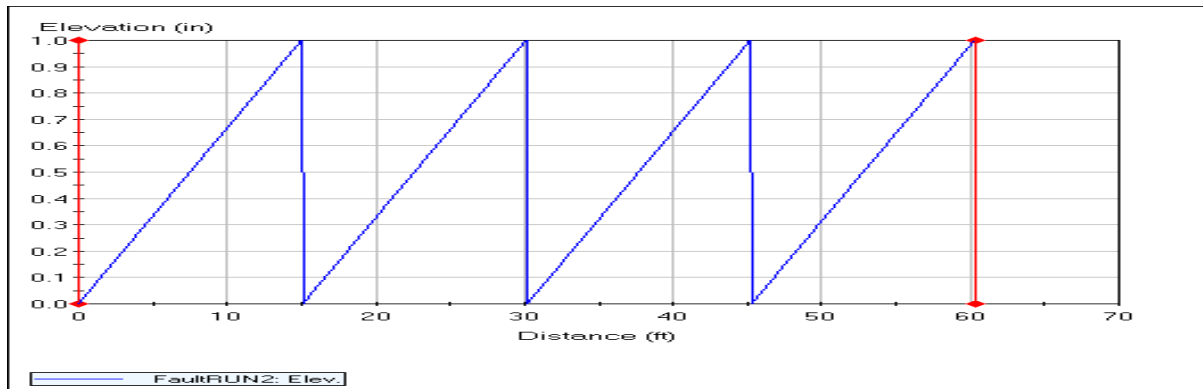
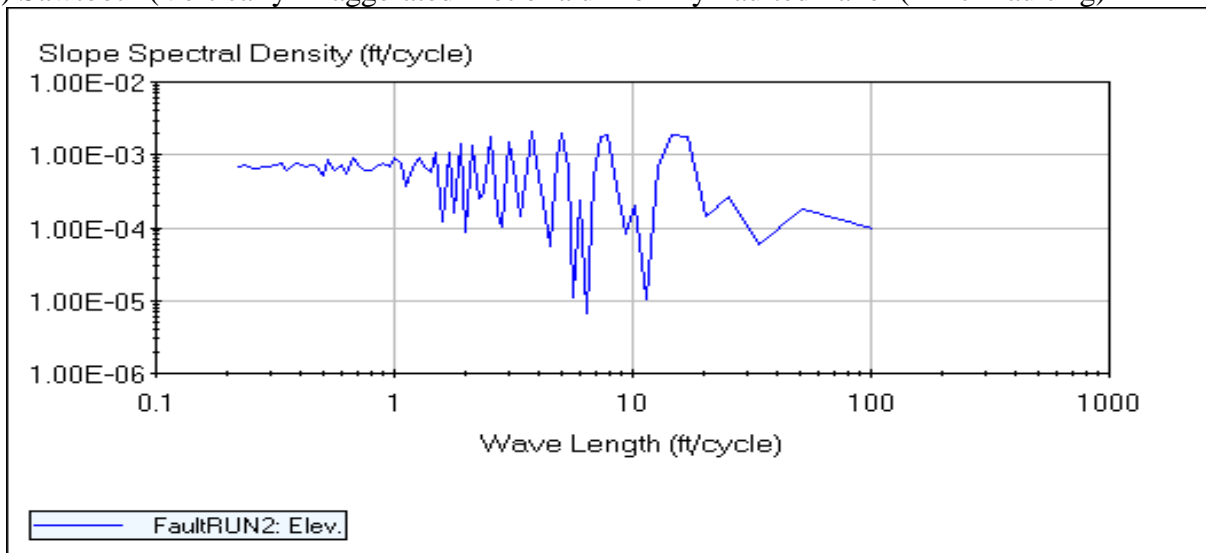


Figure 5.30: Sinc Wave of Sound Intensity Function in the Spatial/ Time Domain



a) Sawtooth (Vertically Exaggerated Plot of a uniformly Faulted Panel (1 inch faulting))



1b) PSD of a Uniformly Faulted Panel 15-foot Panel

Figure 5.31: Proval IRI Analysis - Power Spectral Density

From the above analysis, the influence of faulting is severe and cannot be ignored particularly as it causes severe dynamic loads that are felt by riders. The immediate effect of IRI on sound can be considered from the above as a progression of the increase in dynamic loads due to the bump dip or in this particular case faulting.

Consider the dynamic loads and energy dissipated when a faulted panel is traversed by the additional standard axle load to be converted into sound energy.  
It can be shown that

$$\text{IRI (Faulting Induced)} = \text{IRI(Max)} * \sum_{i=1}^N \frac{F_i}{F_{max}} \frac{n_i}{N} \quad (\text{Equation 5.518})$$

N is number of panels, n represents the number of warped panels in the range F is the warp in mm and Fmax is the maximum warp mm.

Where  $\frac{F_i}{F_{max}}$  = ratio of the fault to 1 inch and  $\frac{n_i}{N}$  is the number of panels in the faulting range.

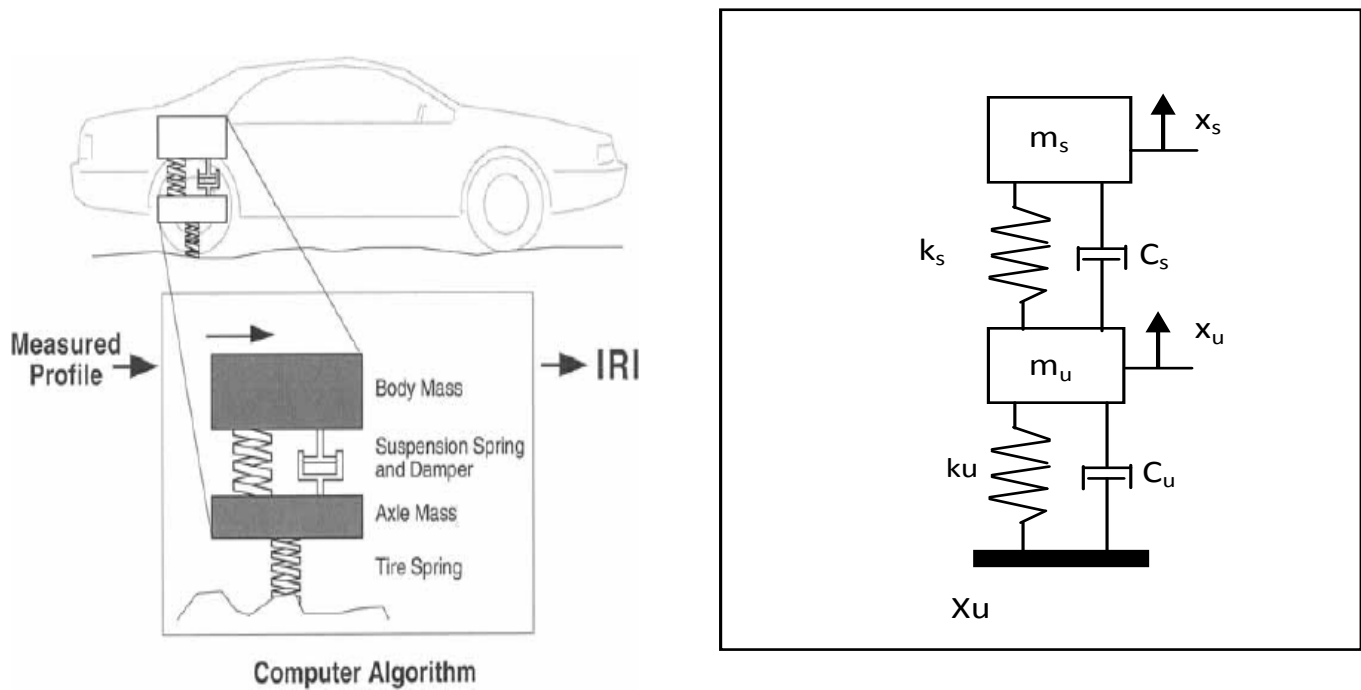
This is applicable to a situation where various degrees of faulting occurs throughout the test sections and a reasonable bar chart represents ranges of faulting whose mean is represented by  $F_i$ . IRI (Max) is the IRI obtained when all the 15 ft. panels are warped to 1 inch. IRI (Faulting Induced) is the dependent variable. IRI Max may be obtained for other panel lengths if they are not 15-ft. It can be seen from equation that the slab length introduces a frequency component to the equation if testing is done at uniform speed.

IRI total = 629 inches per mile as determined from FHWA PROVAL [5.57]. For longer panels IRI total is less than 629 inches per mile because the frequency is less. However, that is not always true for all frequencies because IRI algorithm has peak gain multipliers for certain frequencies such as 32 ft.

The second order Dynamic equation for the quarter car model [5.5.5] is given by

$$m_s \ddot{x}_s + b_s \dot{x}_s + k_s x_s = b_s \dot{x}_u + k_s x_u$$

$$m_u \ddot{x}_u + (C_s + C_u) \dot{x}_u + (k_s + k_u) x_u = C_s \dot{x}_s + k_s x_s + C_u \dot{X}_u + k_u X_u \quad (\text{Equation 5.519})$$



**Figure 5.32: Quarter Car Vibration Variables**

Where  $X$  is the displacement and the derivatives and second derivatives are respectively accented.  $C$  is the dash pot constant and  $K$  is the spring constant. Subscripts  $u$  and  $s$  represent sprung and unsprung mass respectively.

For the impulsive sound generated per panel it is evident that

The Impulsive events  $\sim$  number of faulted slabs

Although the acoustic source power has not been properly analyzed and quantitatively determined, it can be deduced that:

IRI  $\sim$  number of impulsive events ( $n$ ).

IRI  $\sim$  Severity of Impulse  $\sim$  faulting ( $F$ )

OBSI  $\sim$  number of impulsive events

OBSI  $\sim$  Severity of Impulse  $\sim$  faulting

IRI  $\sim$  OBSI

Higher IRI will cause higher OBSI

Similarly IRI  $\sim$  number of faulted slabs

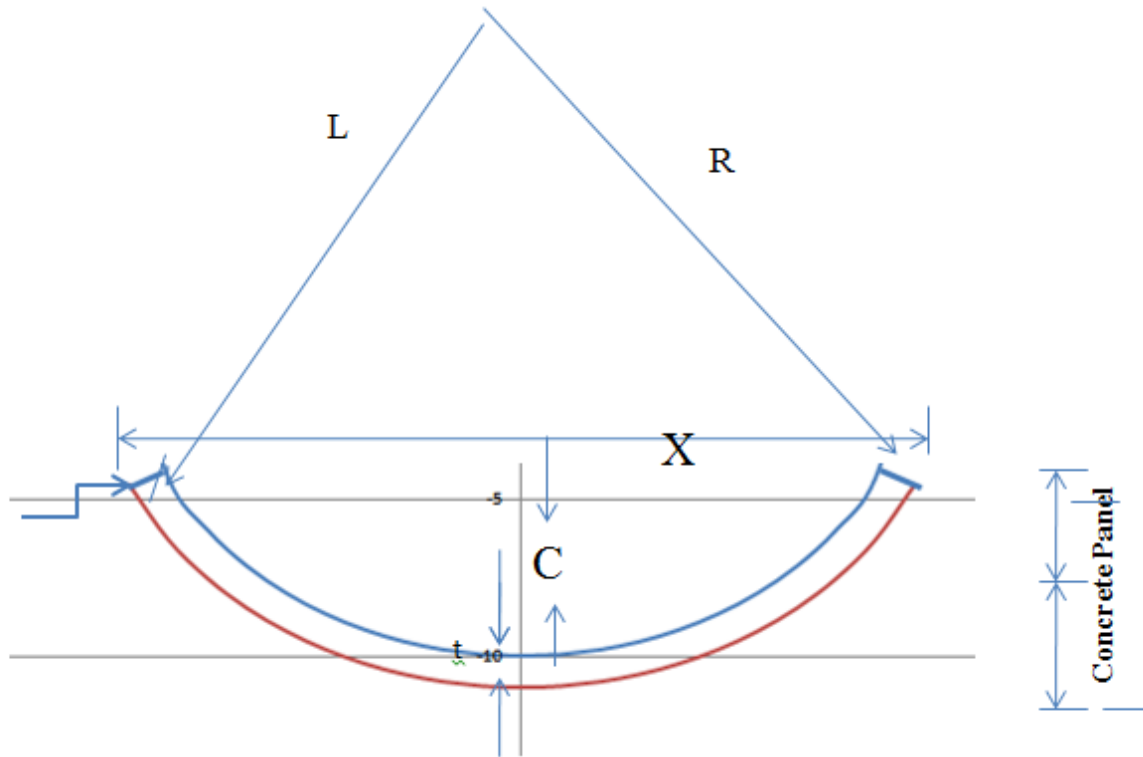
#### **5.5.4 Effect of Built In Warp or Curl**

It will be shown that built in warp also indirectly influences tire road noise through its effect on warp and cur of rigid pavements. This results in secondary effects implicit in changes in IRI, faulting and consequent vertical acceleration that primarily affects international roughness index. These are discussed in a latter section.

It can be shown that for an unrestrained slab on a base, with a temperature difference  $\Delta T$  through the thickness  $t$ .

If it is assumed that the pavement system is homogenous unrestrained by mechanical devices and isotropic, It can be shown [5.31] from geometry that  $R = t / \alpha \Delta T$  ----- (Equation 5.520)





**Figure 5.33: An Exaggerated Warped Slab**

From properties of circles  $(X/2)^2 = (2R-C) C$  ----- (Equation 5.521)

Neglecting small terms  $X^2 = 2RC$  whence  $C = X^2/8R$  ----- (Equation 5.5 22)

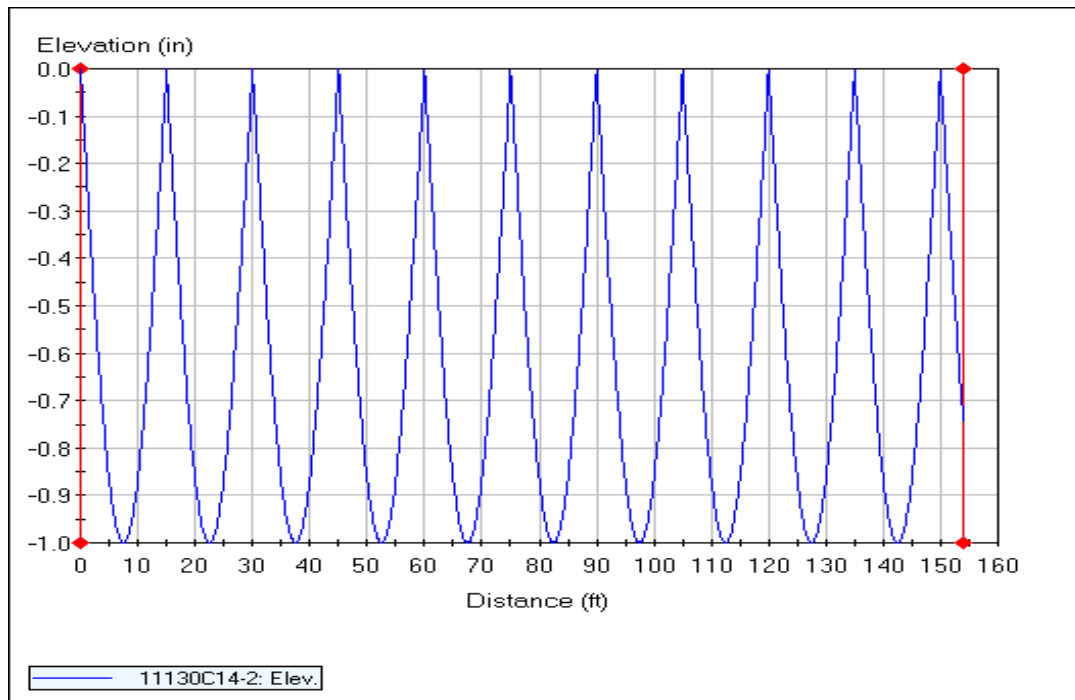
Combining Equation 5.5 21 and Equation 5.5 22),  $C = \frac{\alpha \Delta T X^2}{8t}$  (Equation 5.5 23)

In concrete pavements, there is an effective C which is calculated as the difference between C and w where w is the drop induced in C due to subgrade drag when the base is in continuous contact with the pavement [5.31] . The value of C-eff is approximately the mid slab curl. It is responsible for severe body mass acceleration and subsequent increase in international roughness index. Nevertheless the severity of small values of C-eff in the increase of IRI is tremendous. It has been shown that IRI will increase with the rate of curl or warp as well as the degree of curvature. It has also been shown that OBSI will increase with the percentage of curled slabs in a test section events and degree of warpage. The curling events cause body mass acceleration in each affected panel. The events as earlier explained manifest in the time domain as sinc functions of acoustic values that diminish It is conclusive therefore that faulting Induced IRI will affect OBSI.

A warp profile was idealized for a continuum of panels each with 1-inch C effective. Using the equation

$$Y = - (ABS \sin \text{PI } X/15) \text{ inches.} \quad \text{(Equation 5.524)}$$

The surface generated was of the profile shown below. Based on the process developed and copiously described the effect of running the quarter car on this profile was simulated. This provided an ERD file that was analyzed. Results showed an IRI of 779 inches per mile.



**Figure 5.34: Idealized Profile of Warped Slab**

It is noted also that there is an arithmetic addition deduced from multiple analysis of various curl values ranging from 0.1 inch to 1 inch. There is a proportional increase in the IRI per unit curl. Also when x percent of the slabs showed that warp, there was x-percent of the IRI. This led to the equation

$$\text{IRI Warp (15 ft. panels)} = \text{IRI (Total)} * Q * R \quad 5.525$$

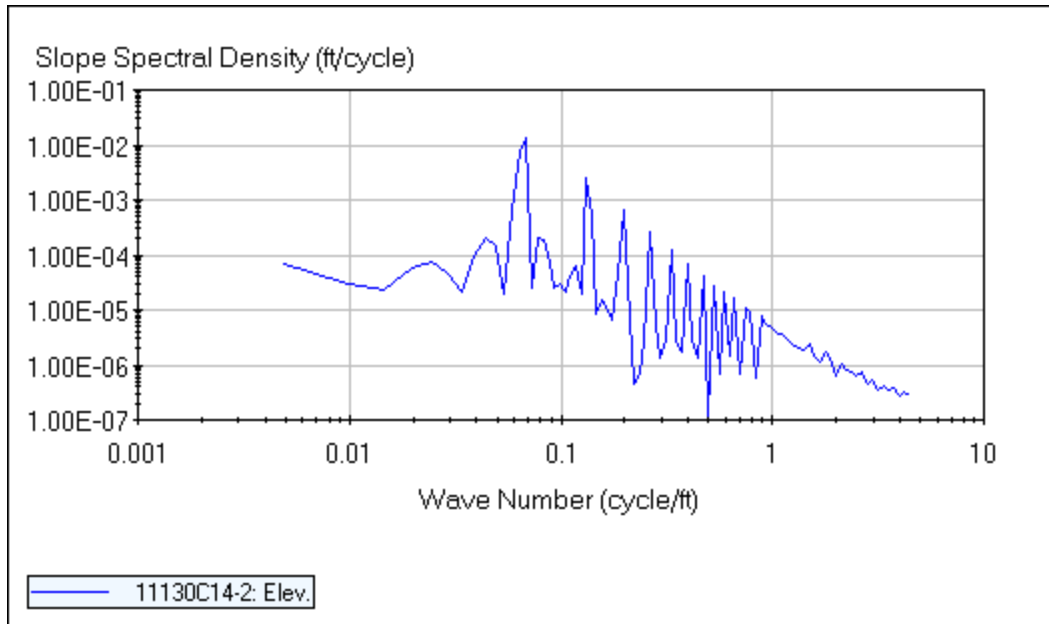
where Q is the percentage of panels with 1 inch curl and R is the ratio of the fault to 1 inch. This is applicable to a situation where the same value of faulting occurs throughout the test sections. For various degrees of faulting, a reasonable bar chart with ranges may be created. This was improved further to

$$\text{IRI} = \sum_{i=1}^{m,n} G \frac{m_i}{N}, K \frac{n_i}{N} \quad 5.526$$

IRI (15 ft. panels Warp) is the IRI obtained when all the 15 ft. panels are warped to 1 inch. G and N are the respective 15 ft. warp,  $n_i$  is a product of the mean range of faults and the population while  $m_i$  is the product of a mean range of warp and the population in that range. N is the total number of slabs of faults, K is the IRI with 15 ft. slab all with 1 inch fault and G is the IRI with 15 ft. slab all with 1 inch warp.

Where IRI total = 779 inches per mile

N is number of panels, n represents the number of warped panels in the range N is total number of panels, m is the warp in mm and G is the maximum warp mm. Figure 5.59 shows the PSD for a uniformly warped panel



**Figure 5.35: Analysis - Power Spectral Density for Uniformly Warped Panel**

### 5.5.5 Association of faulting with international roughness index

Figure 5.51A shows that IRI is correlated to faulting with a coefficient of determination of 0.44. Figure 5.510 shows that OBSI is only slightly correlated to faulting. This was attributed to the low levels of faulting measured in the MnROAD Cells. Figure 10 c shows a correlation of OBSI to IRI in the Transverse tined pavements which are the oldest cells at MnROAD. A coefficient of determination of 0.31 was obtained. It is noteworthy that OBSI is a log summation of 12 3<sup>rd</sup> octave frequencies from 400 Hz to 5000 Hz. The lower frequencies are omitted from OBSI. This explains why a good correlation is not obtained. However a set of IRI and Faulting trend pairs have been placed below to accentuate the effect faulting has on IRI

### Faulting and IRI

IRI is a proxy for pavement surface variables with wavelengths between 2 ft. and 160 ft. (wavelength  $\lambda$ : 50 mm <  $\lambda$  < 50 m). According to Khazanovich et al, IRI is correlated to joints by the formula:

$$IRI = 0.2933 (\text{Faulting}) + 1.4521$$

Where IRI is in M/Km and Faulting is in mm. Khazanovich et al also showed age relation and Faulting to follow the pattern

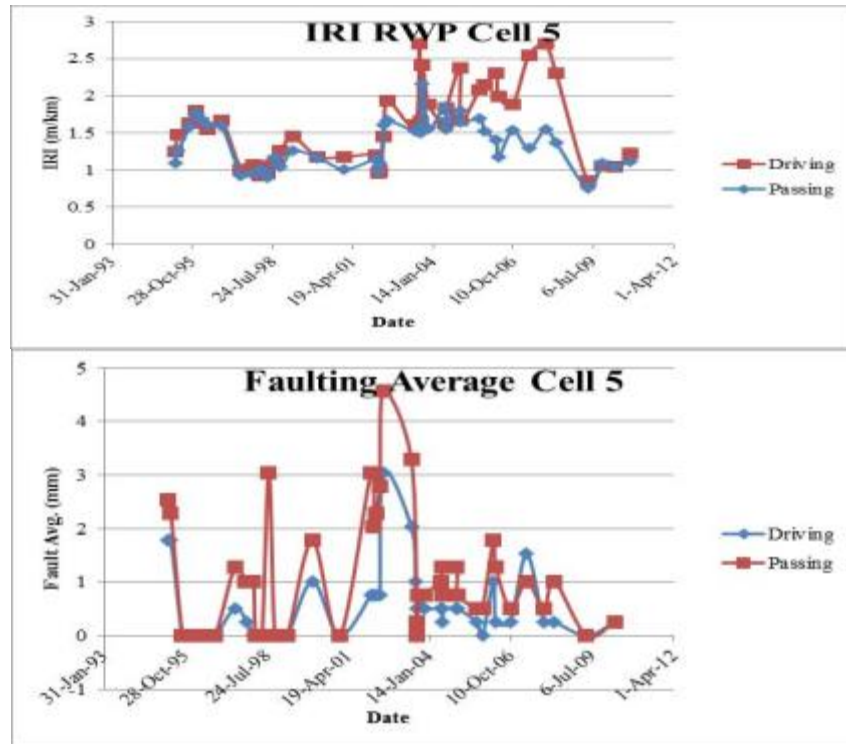
$$\text{For Faulting to be } K (\text{Age}/20)^{0.25}$$

Where Age is in years and Faulting is in mm.

Pavements perform well if  $K < 2$  and normally if  $2 \leq K < 4$ . They perform poorly if  $K \geq 4$

Age may be related to IRI in each test section if there is a constant or constantly changing rate of traffic.

Khazanovich et al [1.16] thus show that Faulting will lead to some IRI effects. The following figures show a plot of IRI and corresponding plots of Faulting. A cursory inspection shows that when Faulting is measureable and significant it appears to be better correlated to IRI. It follows that when the dominant IRI source is Faulting in the joints, Faulting can be correlated to IRI and then to OBSI. This forms the basis for the development of acoustic monitoring devices for deteriorated joints in pavements and possible delamination in pavements and bridges.



**Figure 5.36: Faulting Vs IRI in Cell with 2008, 2011 Intervention after 1993 Construction**

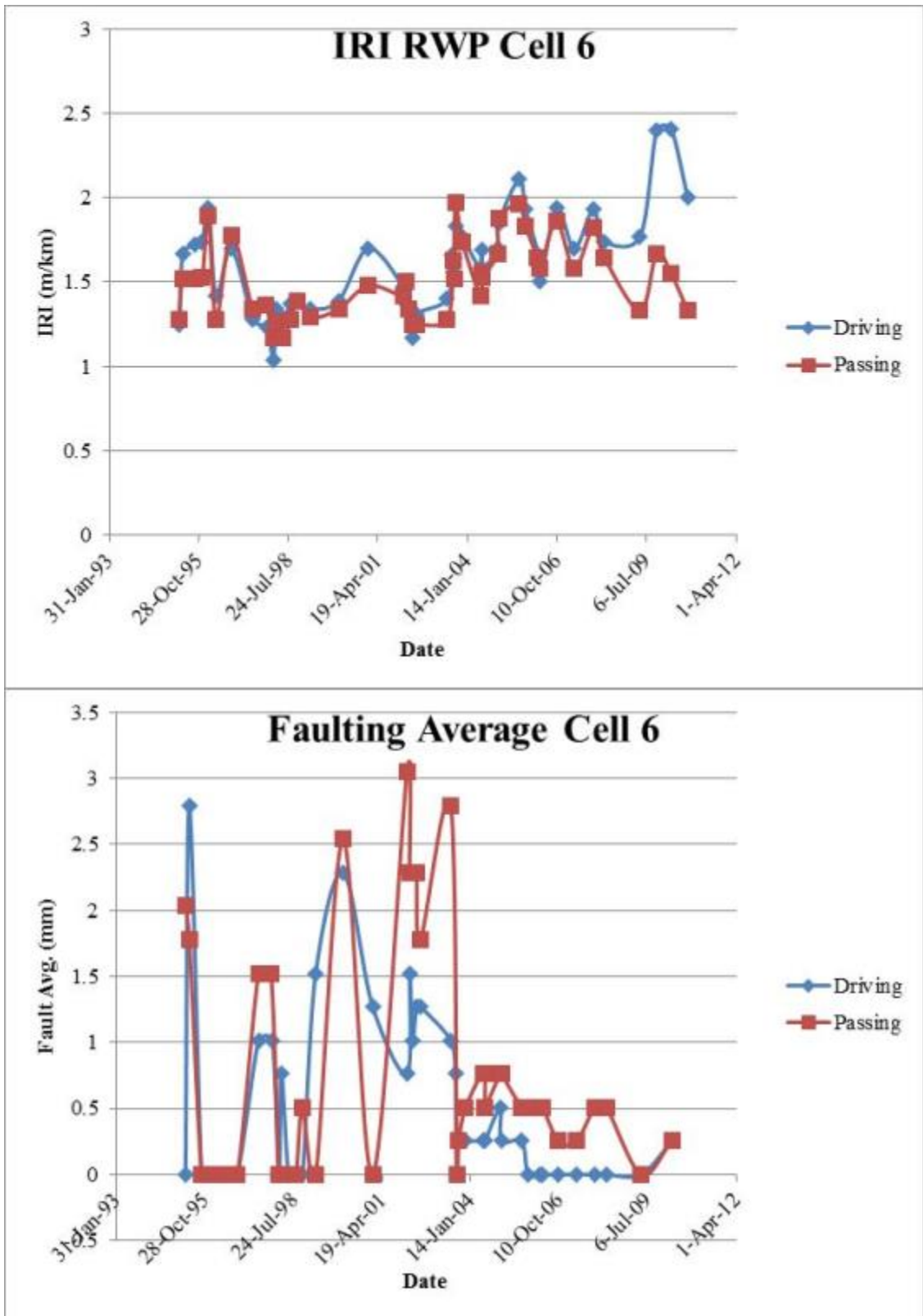


Figure 5.37: Faulting Vs IRI in Cell with 2008, 2011 Intervention after 1993 Construction

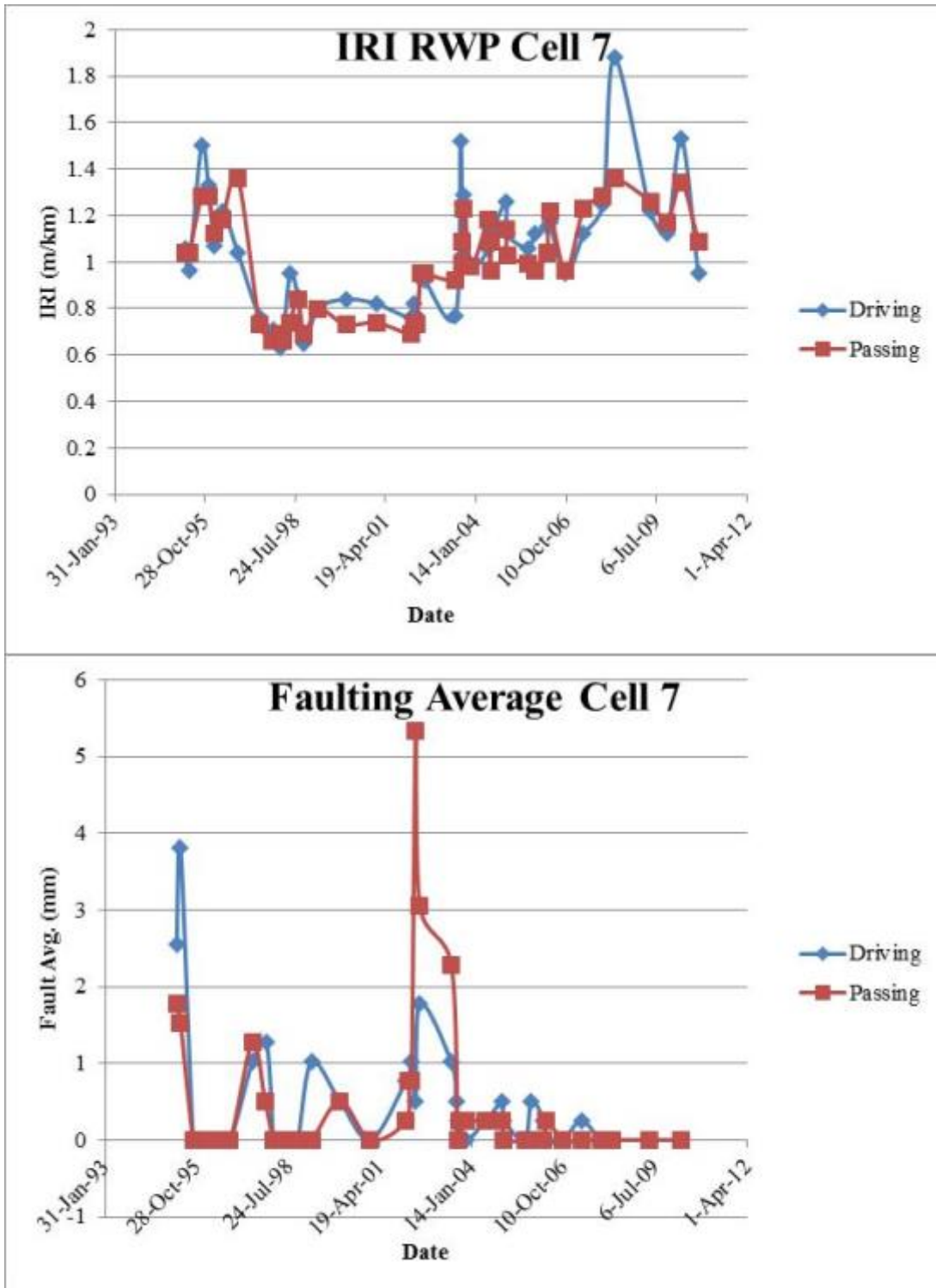


Figure 5.38: Faulting Vs IRI in Cell Ground in 2007 after 1993 Construction

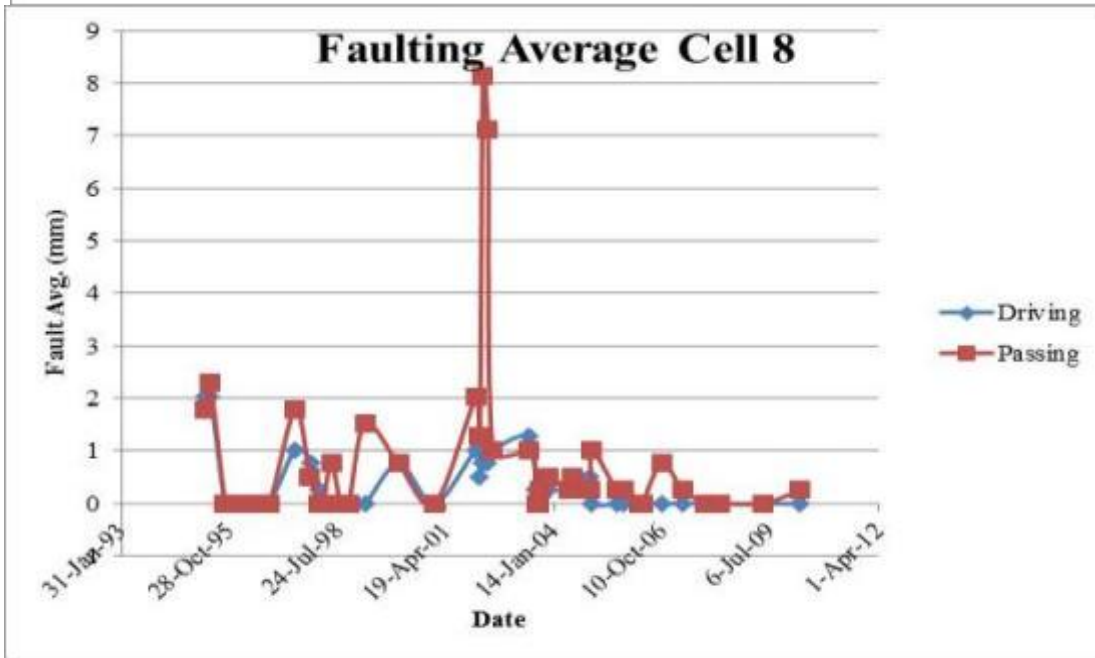
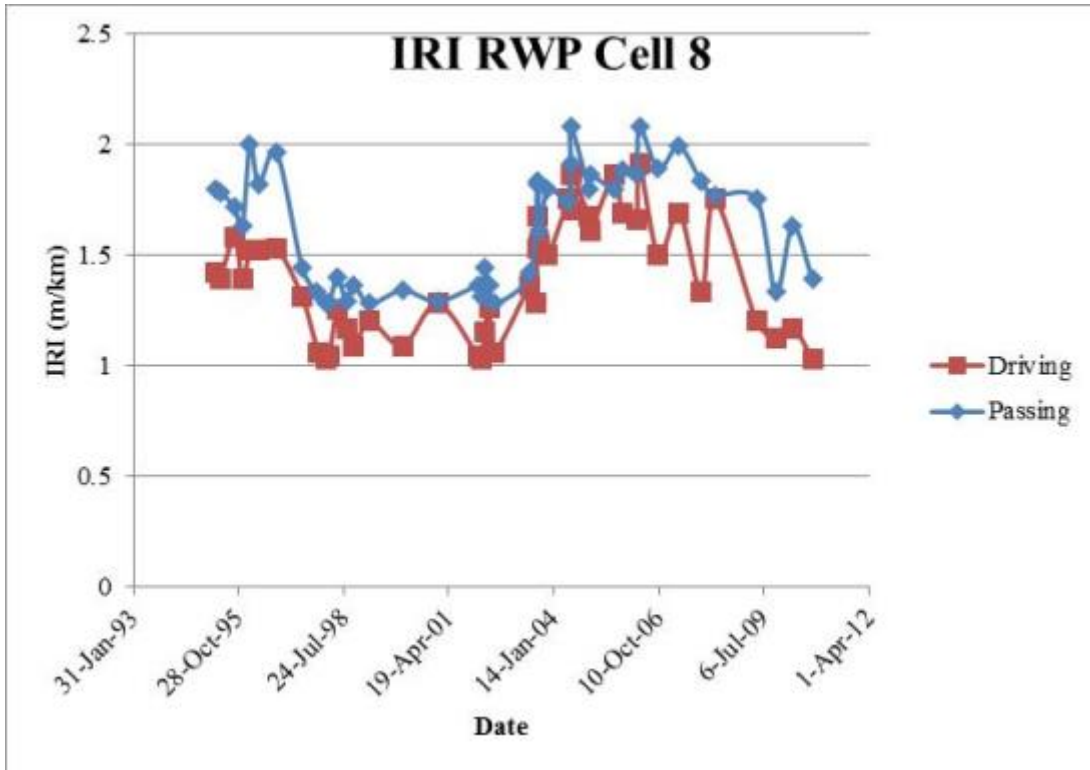


Figure 5.39: Faulting Vs IRI in Cell Ground in 2007 after 1993 Construction

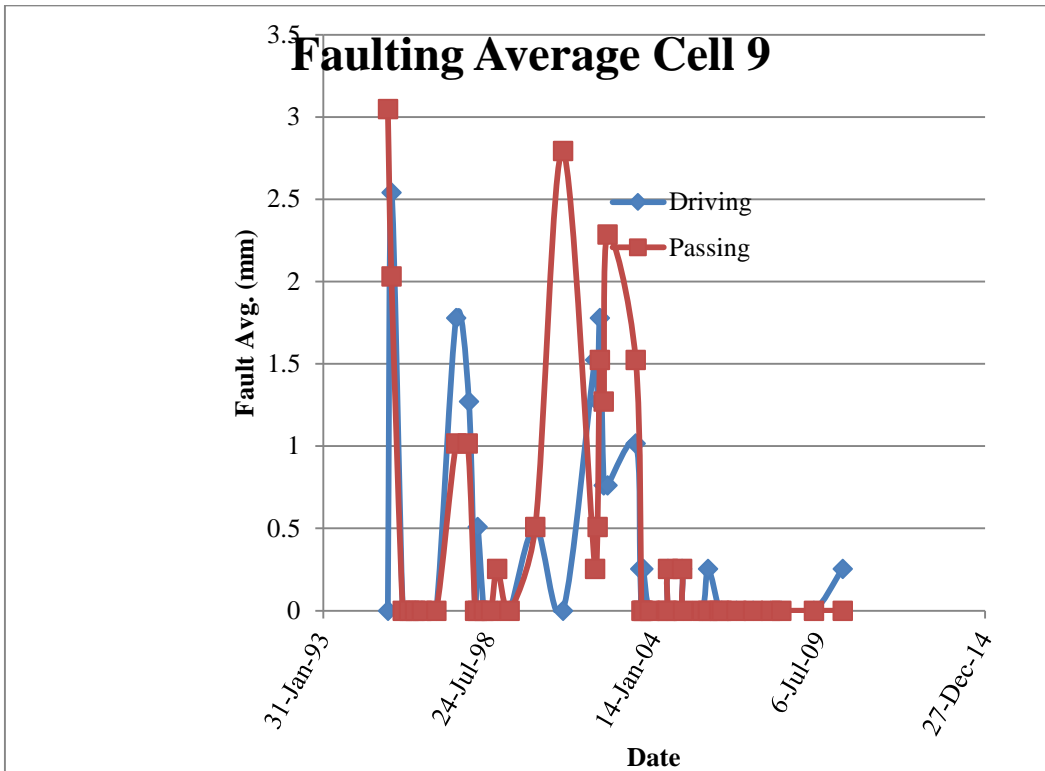
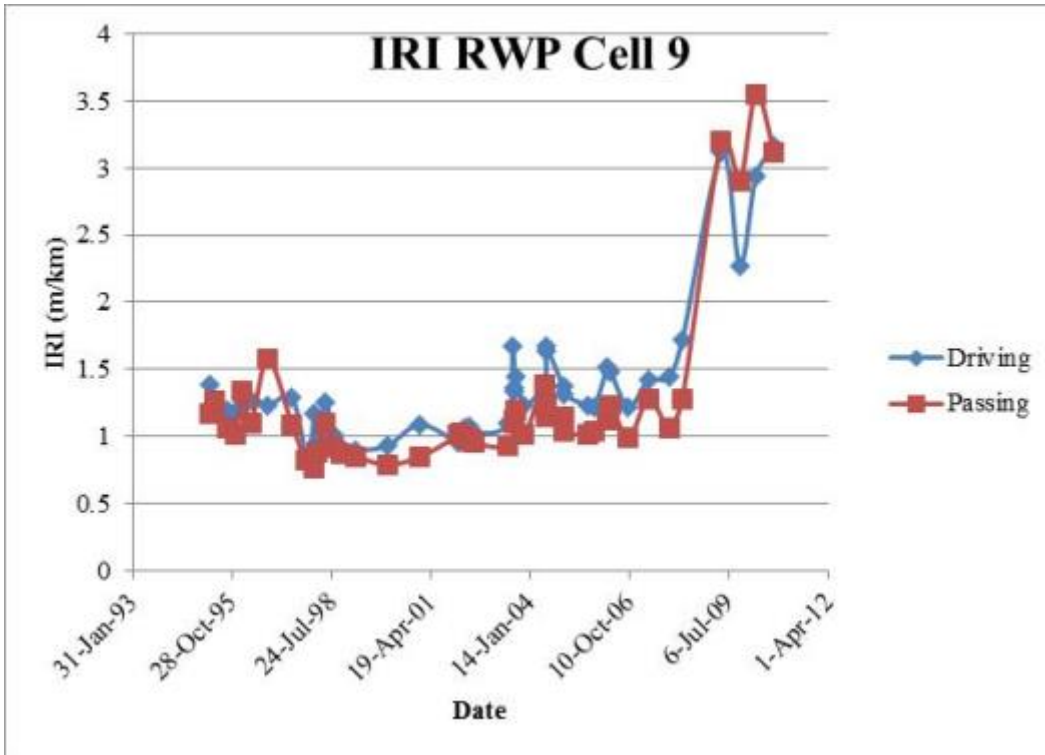
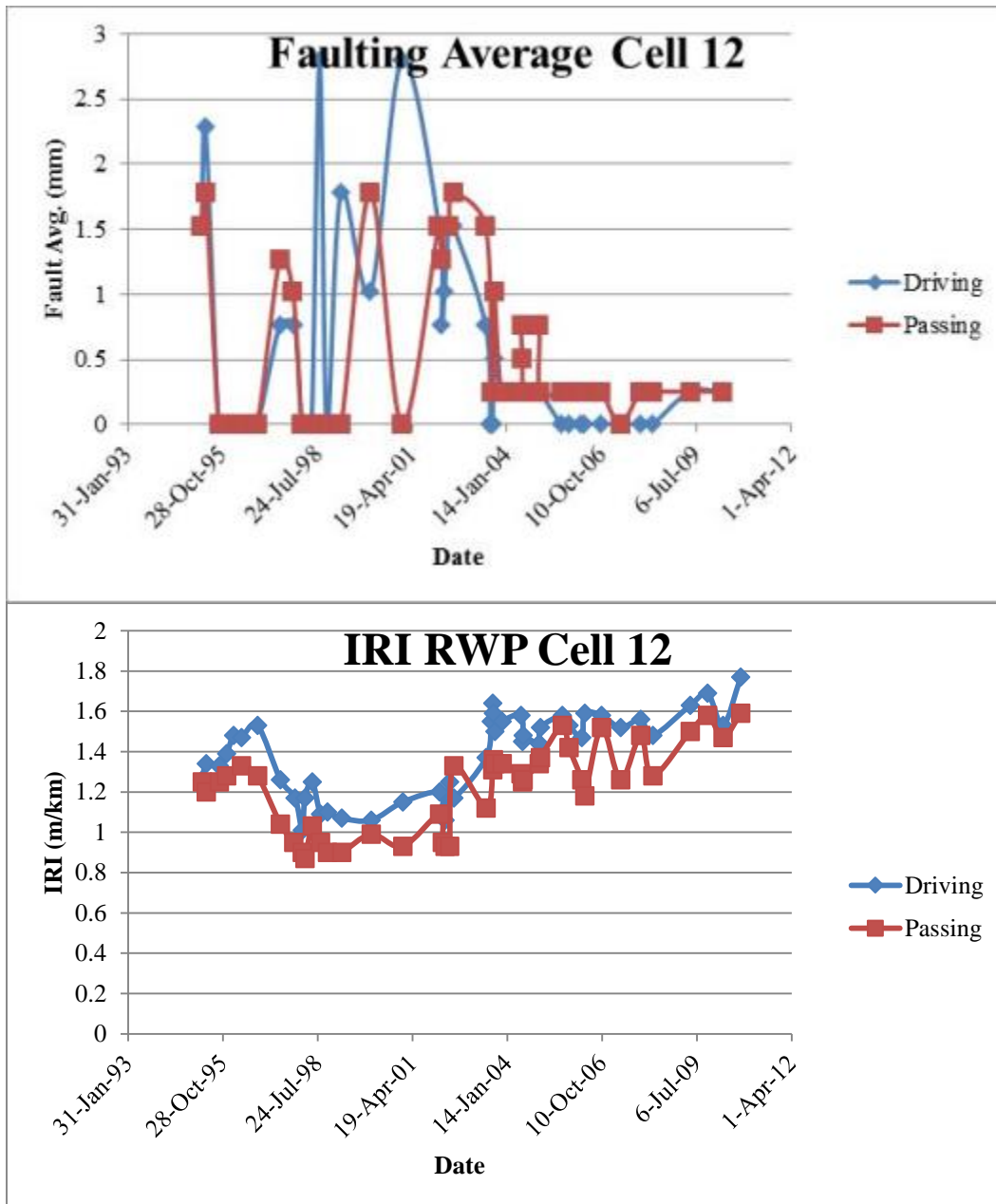
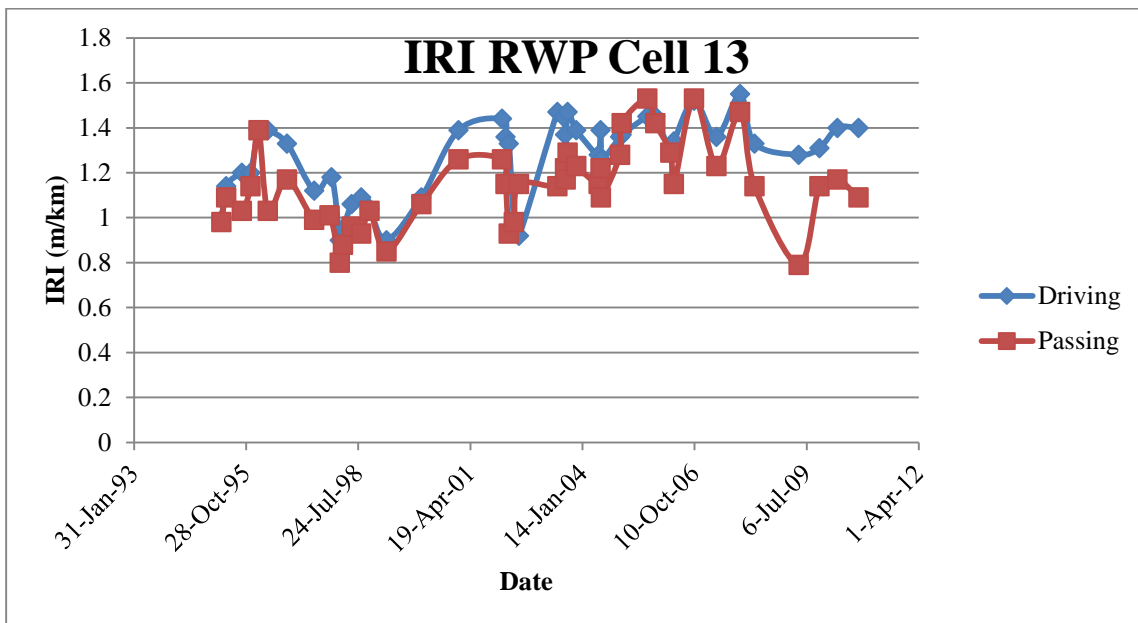
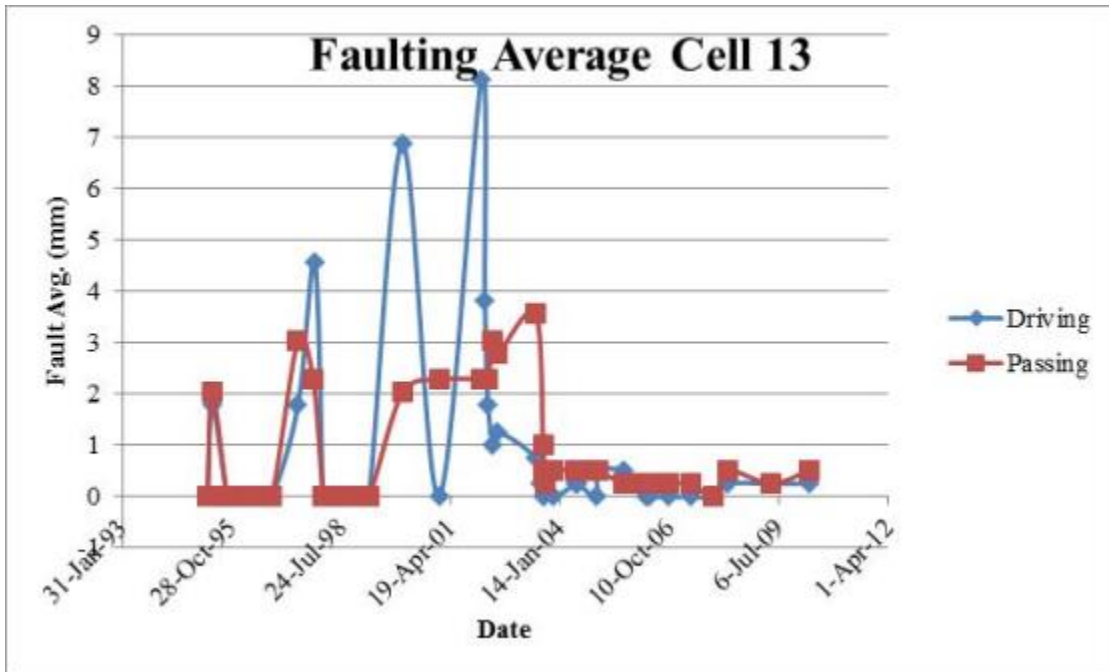


Figure 5.40: Faulting Vs IRI in Cell with 2008 Grinding after 1993 Construction





**Figure 5.41: Faulting Vs IRI in Cell without Intervention Since 1993 Construction**



**Figure 5.42: Faulting Vs IRI in Cell with 2008 Intervention after 1993 Construction**

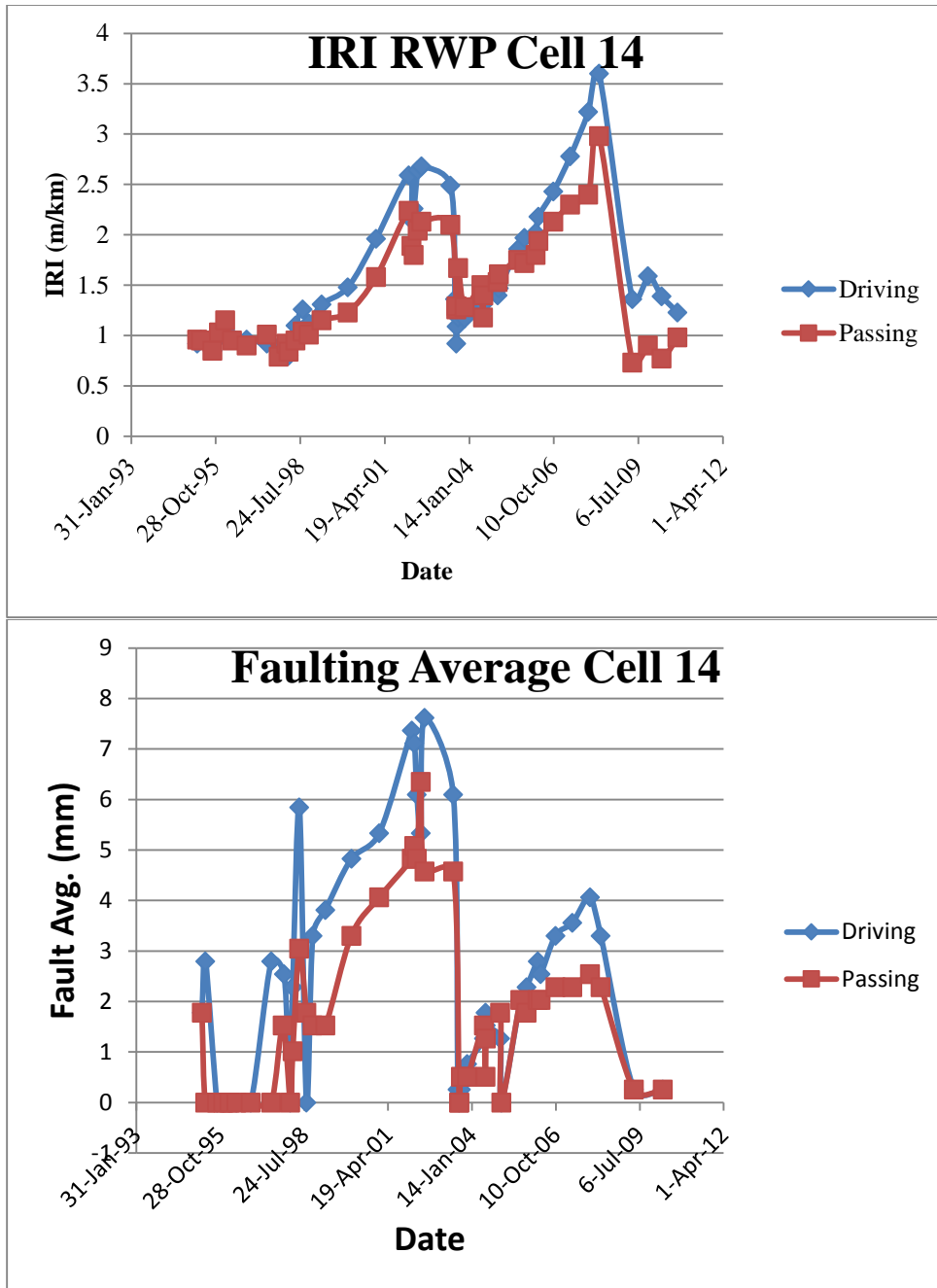
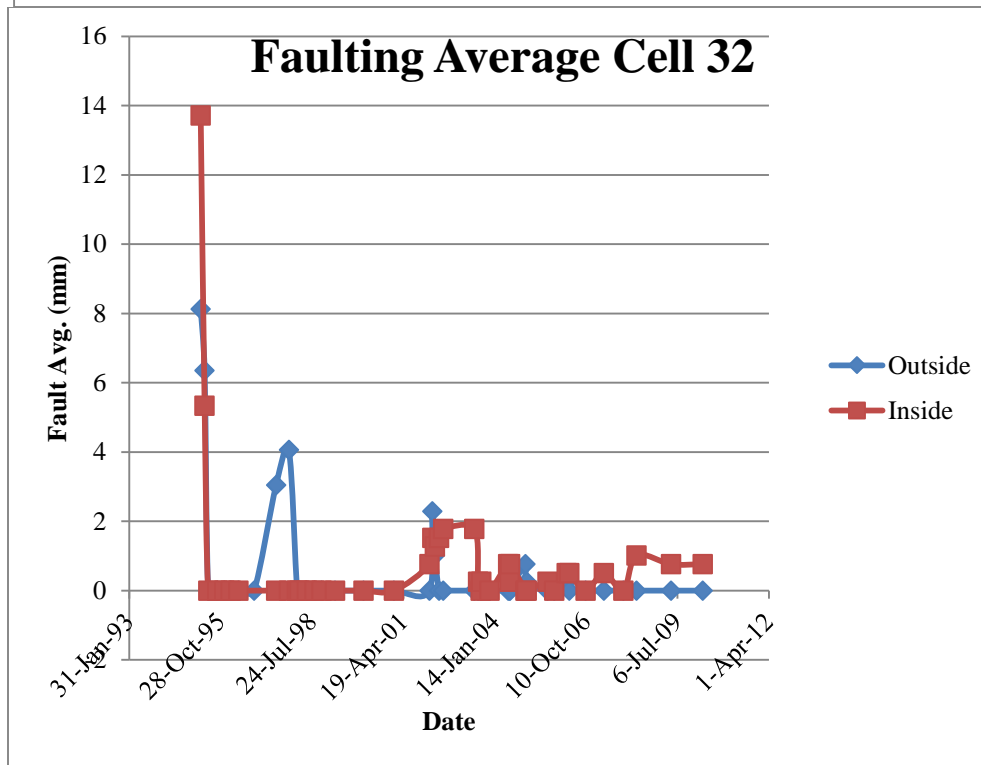
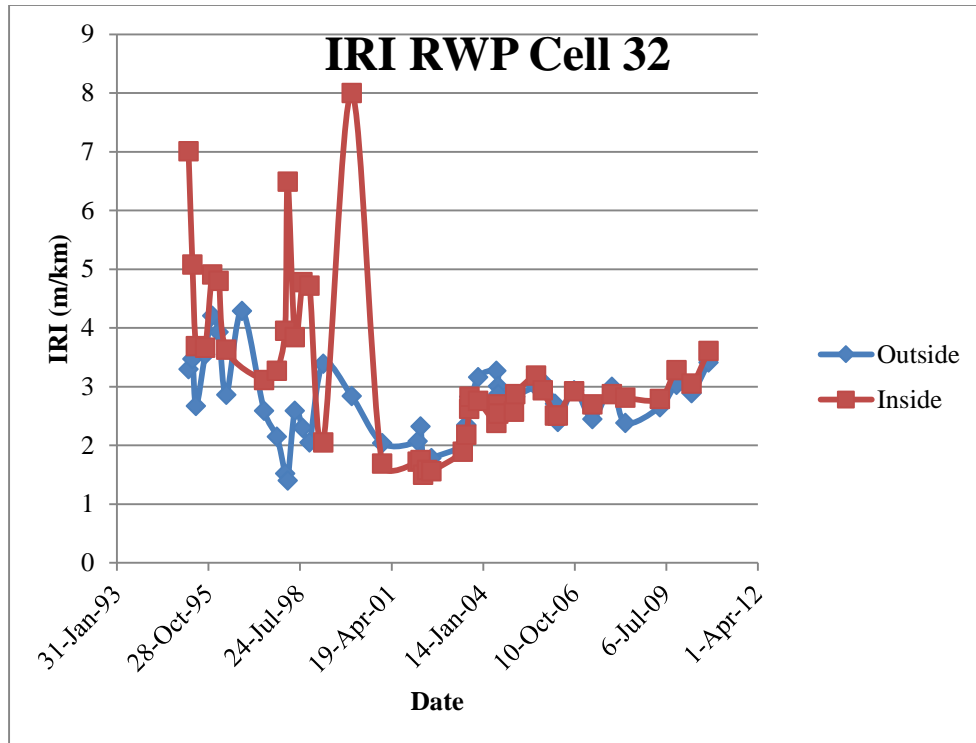
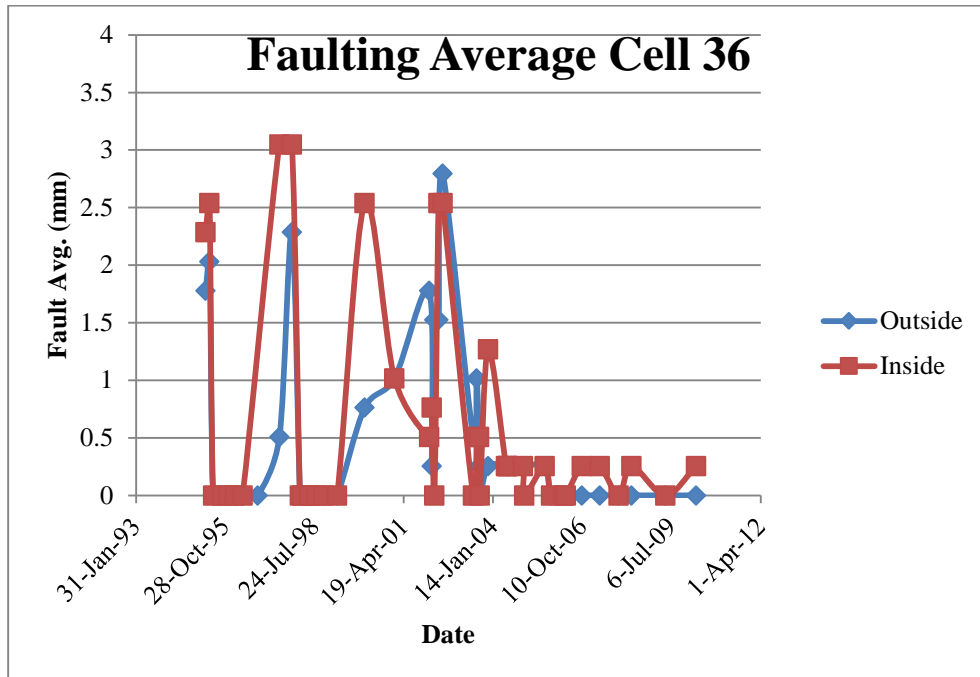
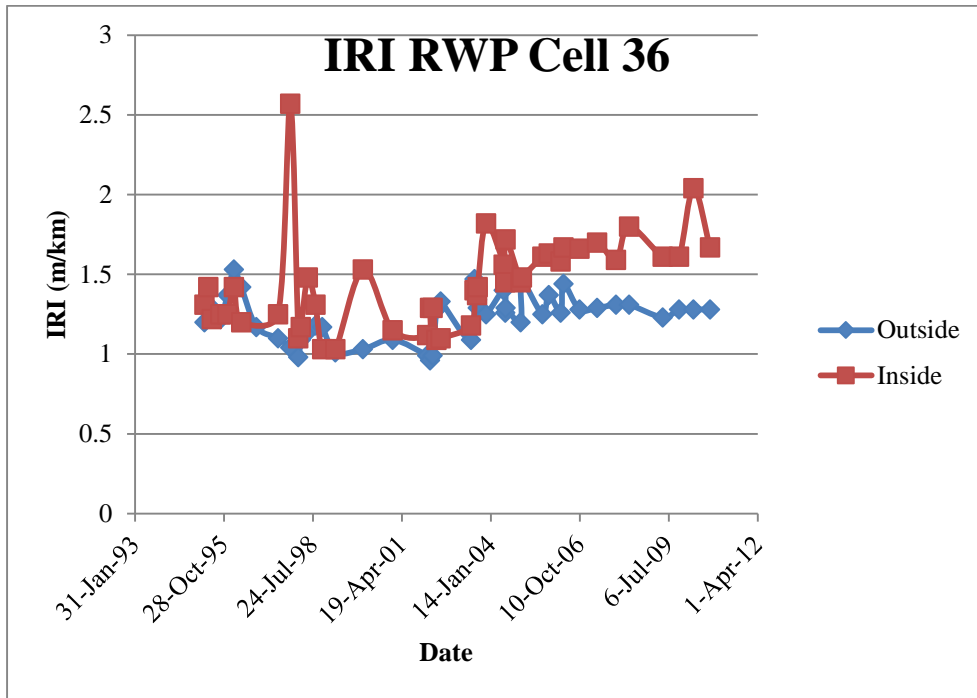


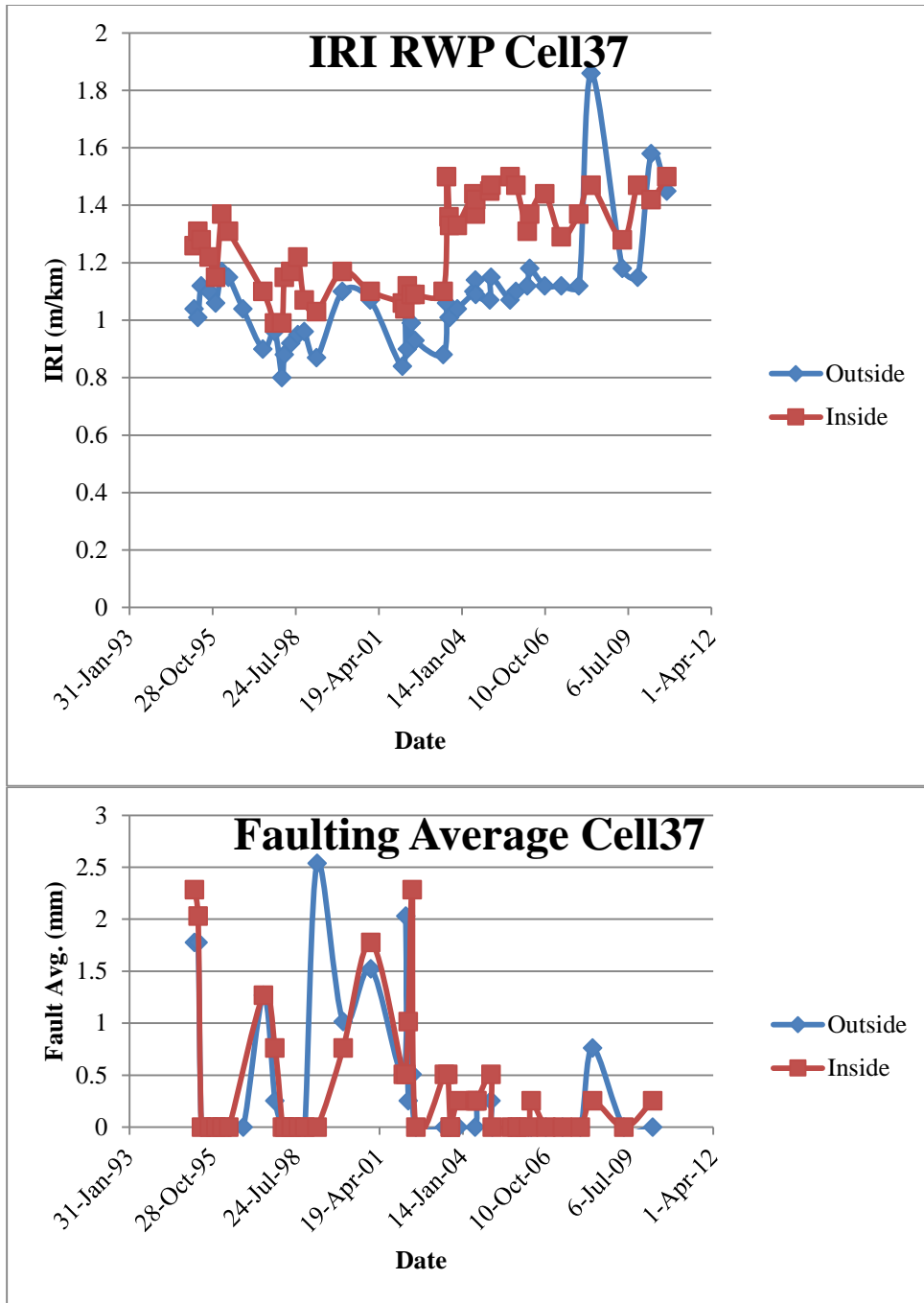
Figure 5.43: Faulting Vs IRI in Cell with 2008 Intervention after 1993 Construction



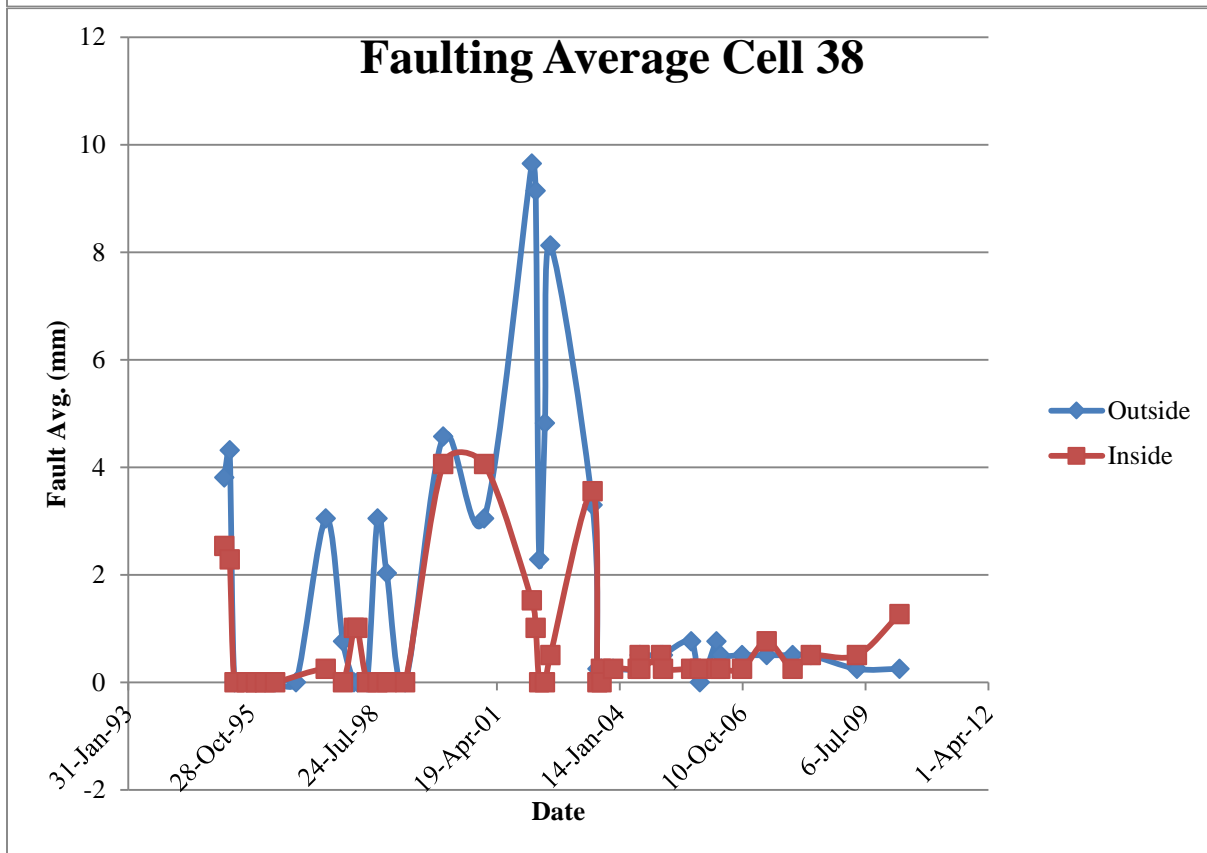
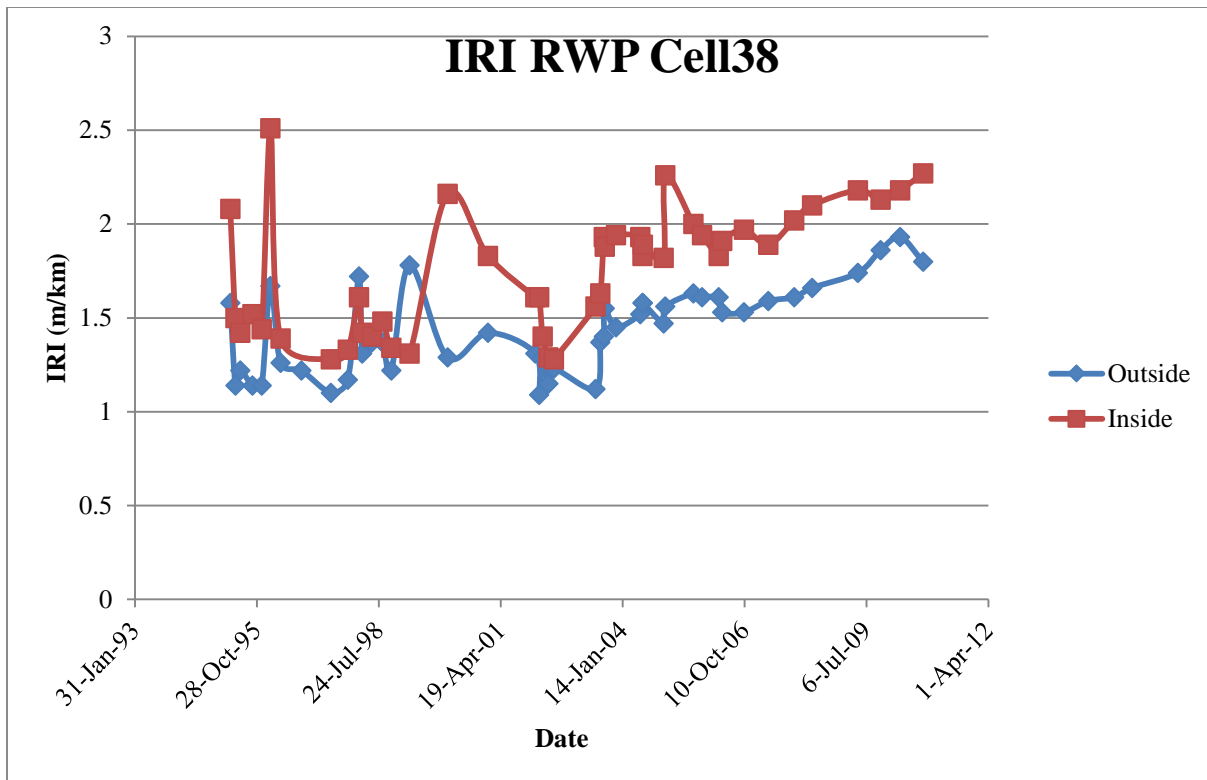
**Figure 5.44: Faulting Vs IRI in Cell with 2000 Intervention and 2013 Rehabilitation Including Grinding after 1993 Construction**



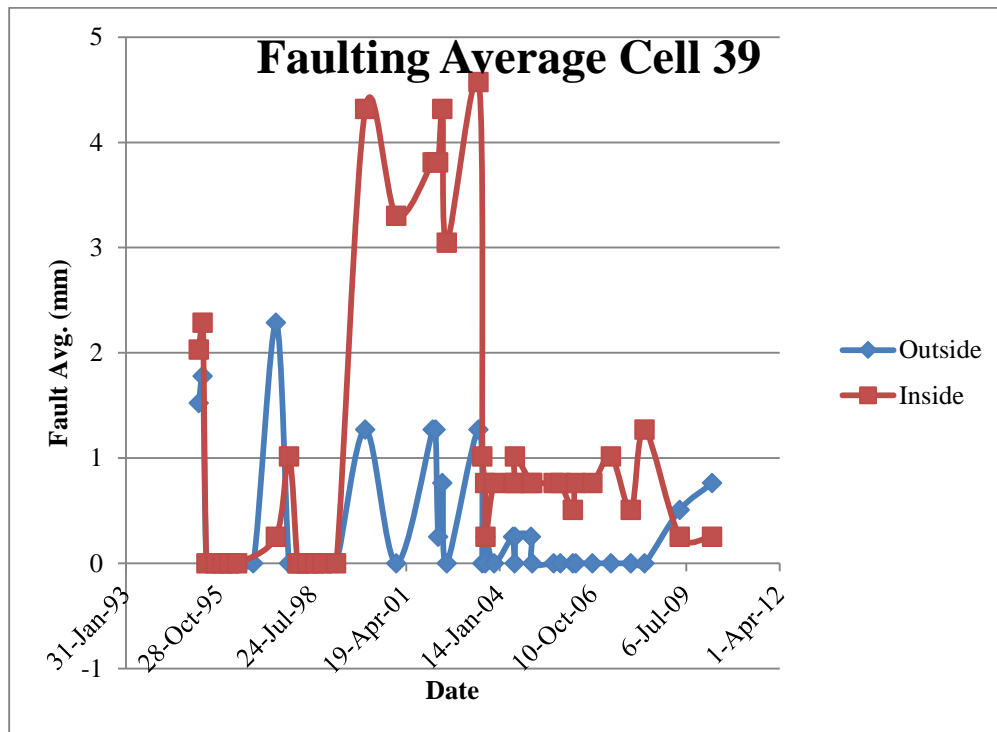
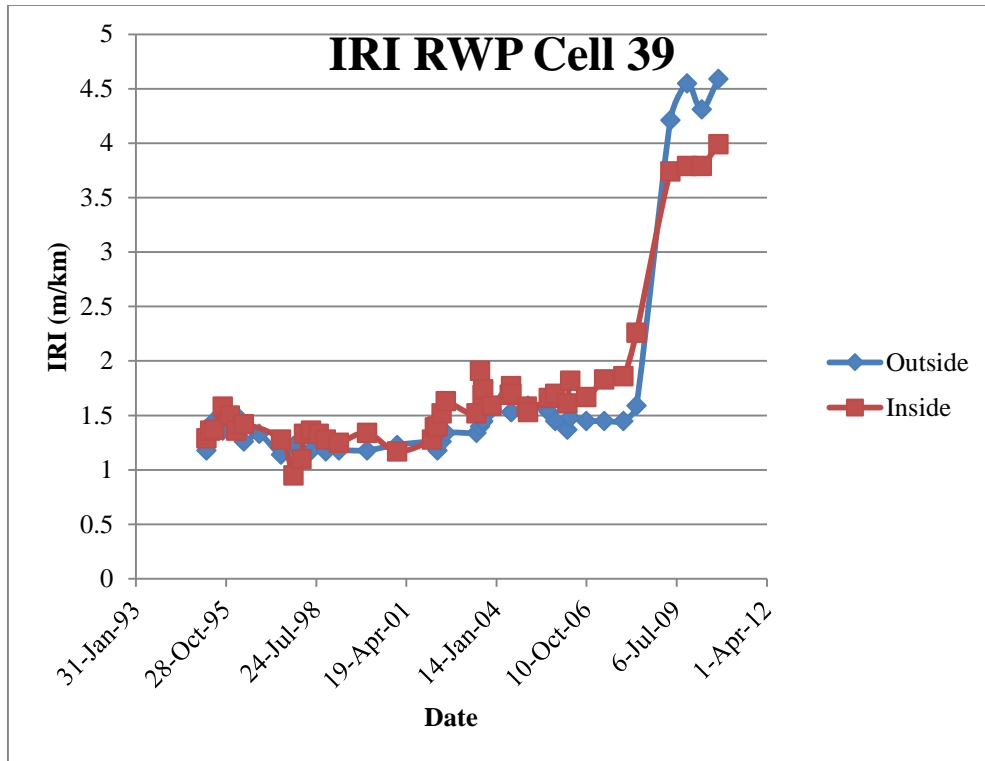
**Figure 5.45: Faulting Vs IRI in Cell without Intervention after 1993 Construction**



**Figure 5.46: Faulting Vs IRI in Cell with 2007 Grinding Strips on the outside Lane after 1993 Construction**

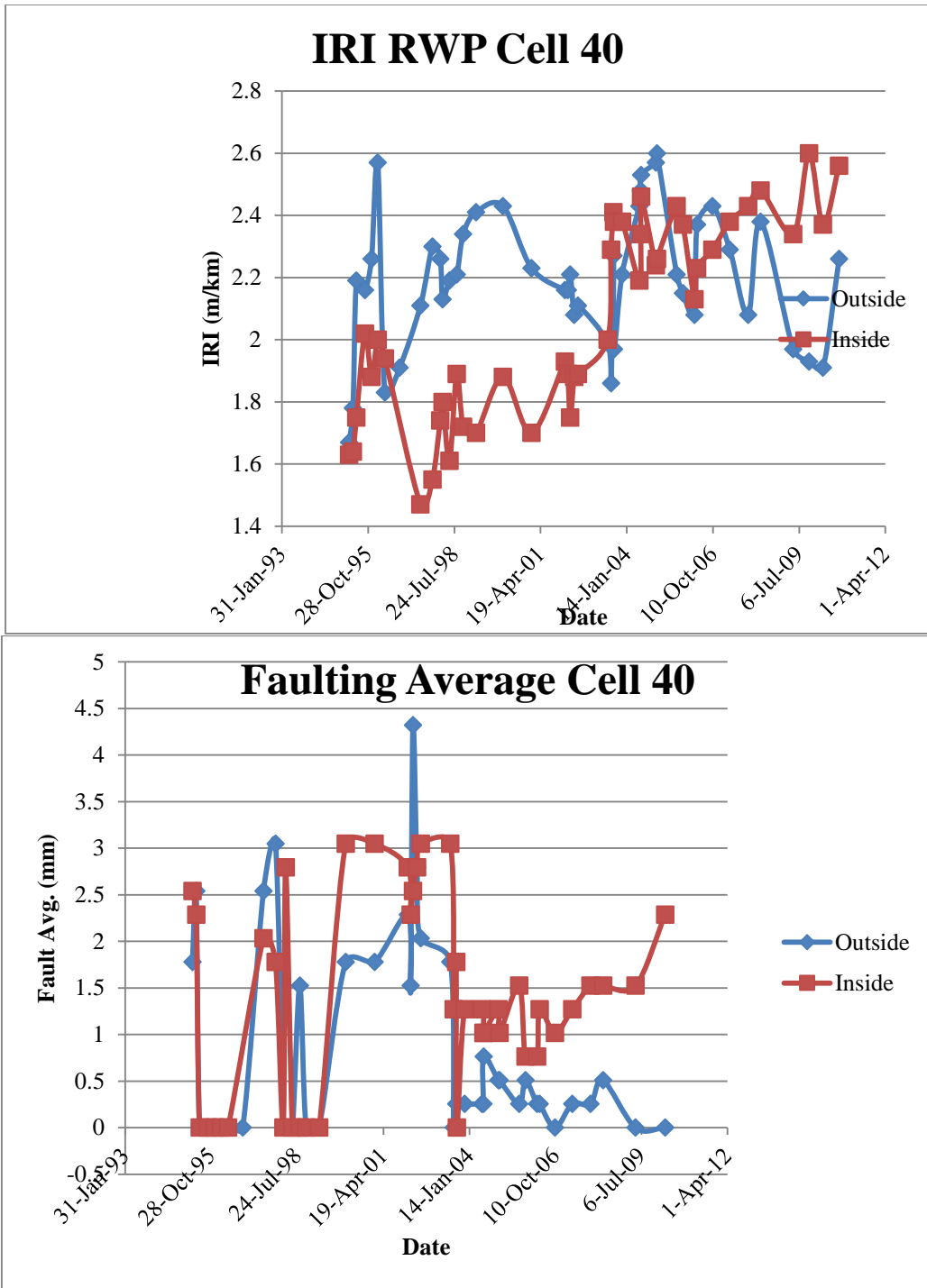


**Figure 5.47: Faulting Vs IRI in Cell without Intervention after 1993 Construction**

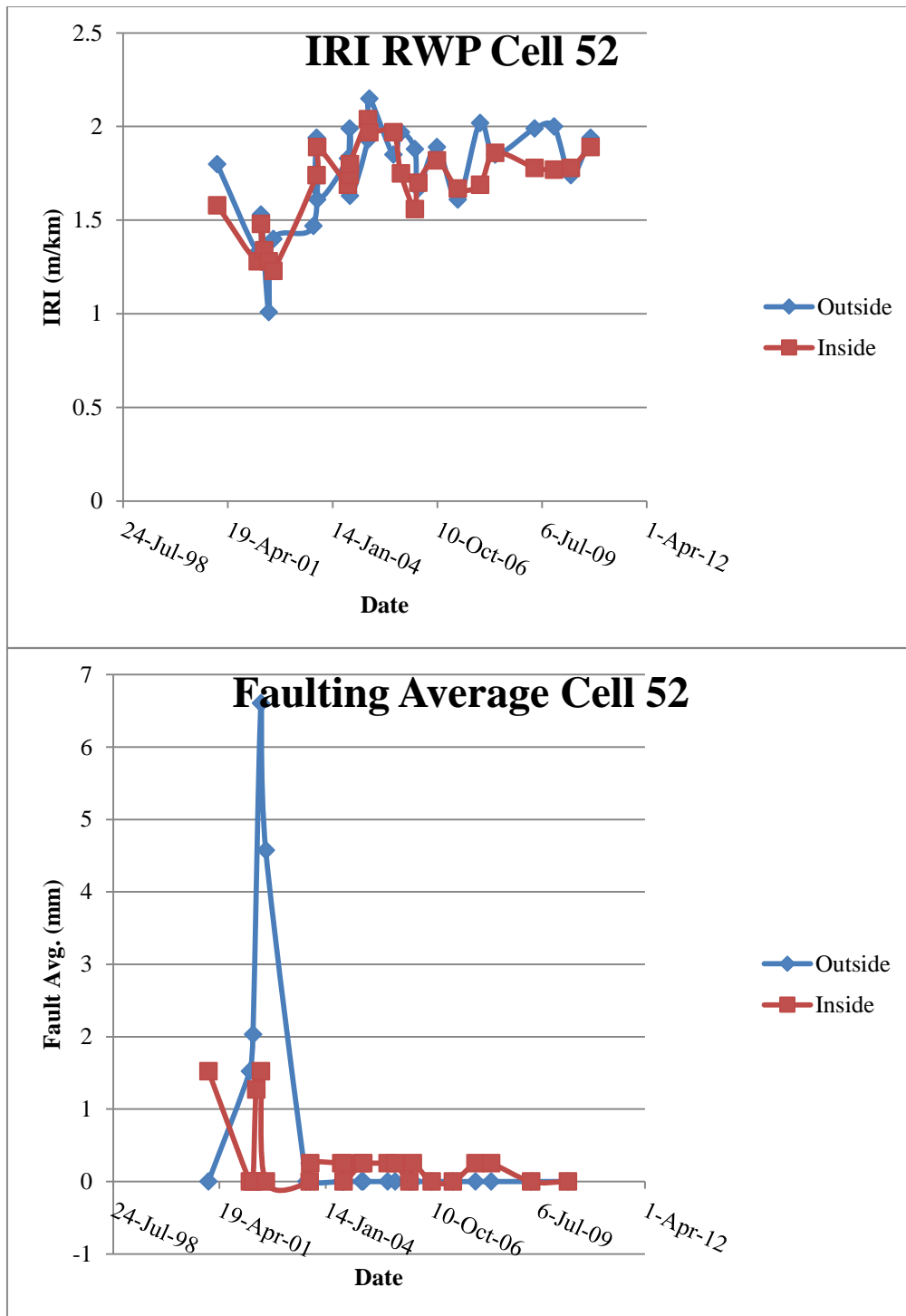


**Figure 5.48: Faulting Vs IRI in Cell with Pervious Overlay 2008, Grinding 2013 after 1993 Construction**

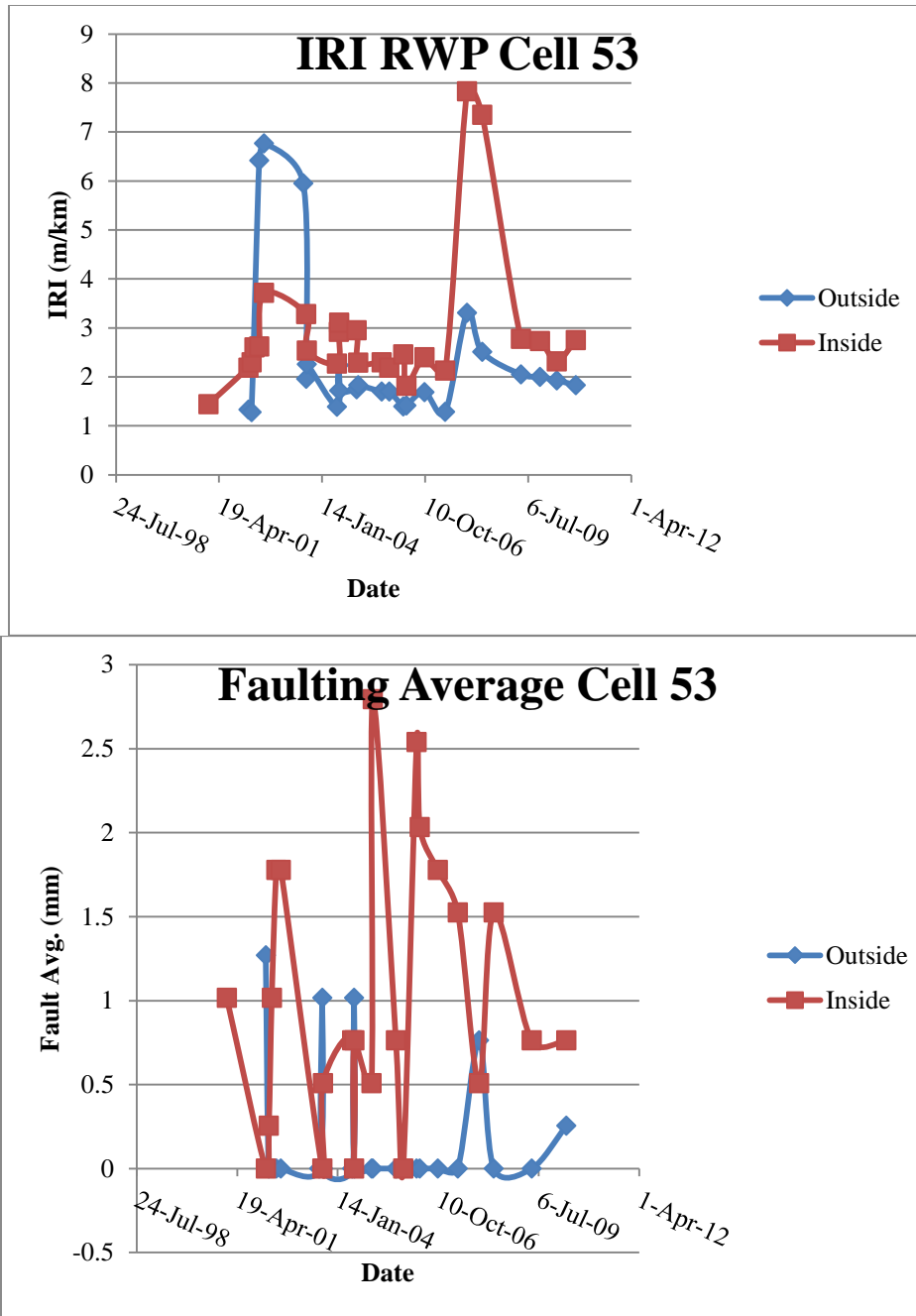




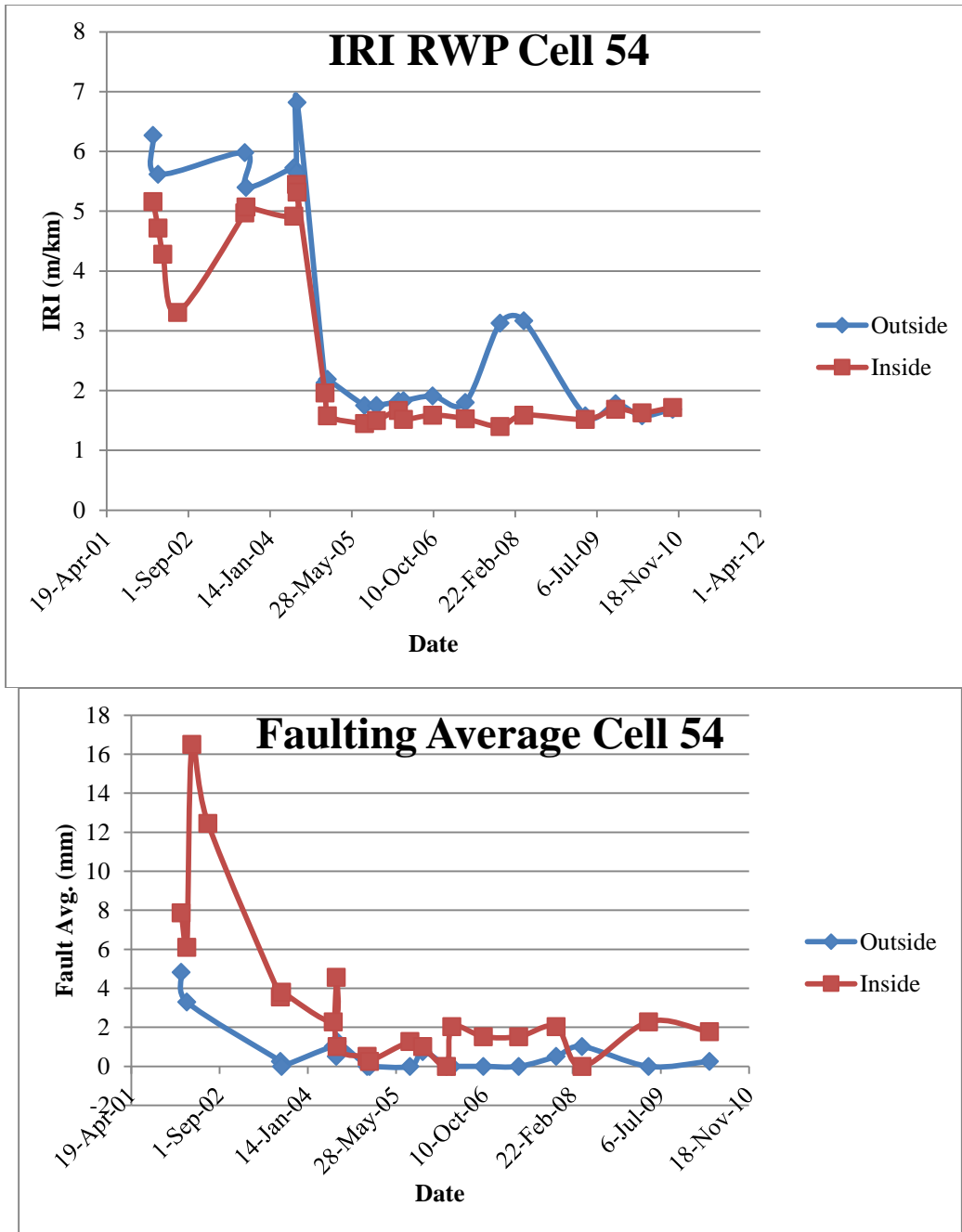
**Figure 5.49: Faulting Vs IRI in Cell with 2013 Intervention after 1993 Construction**



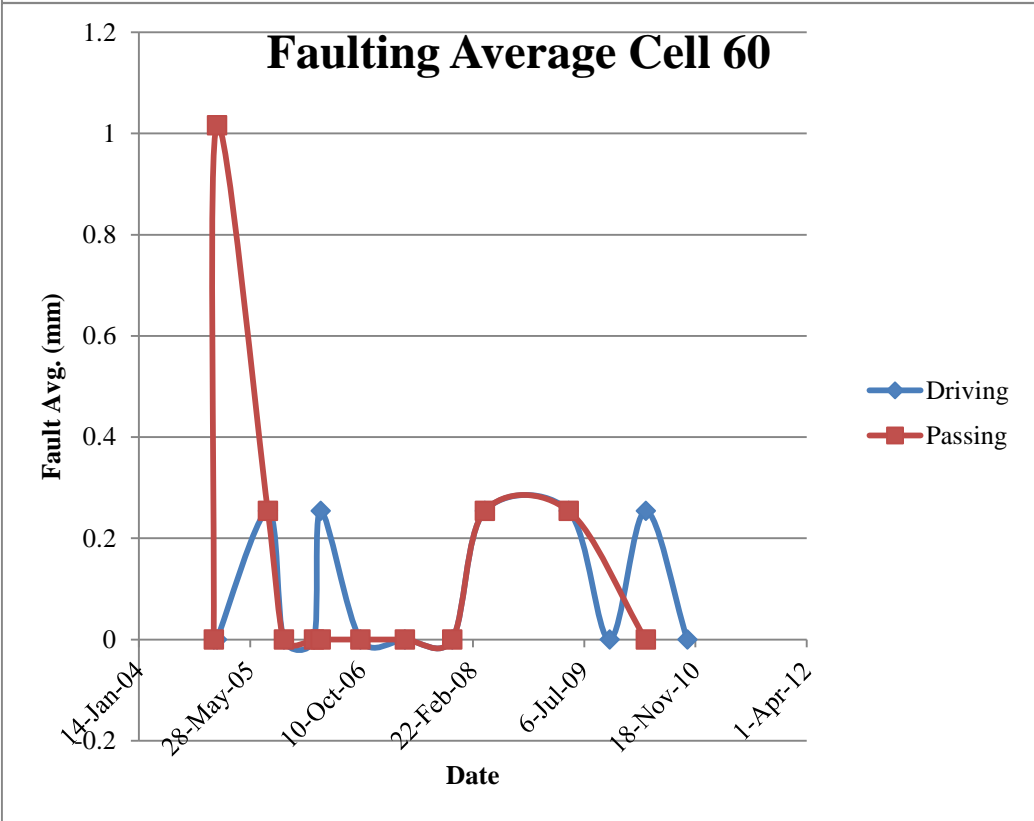
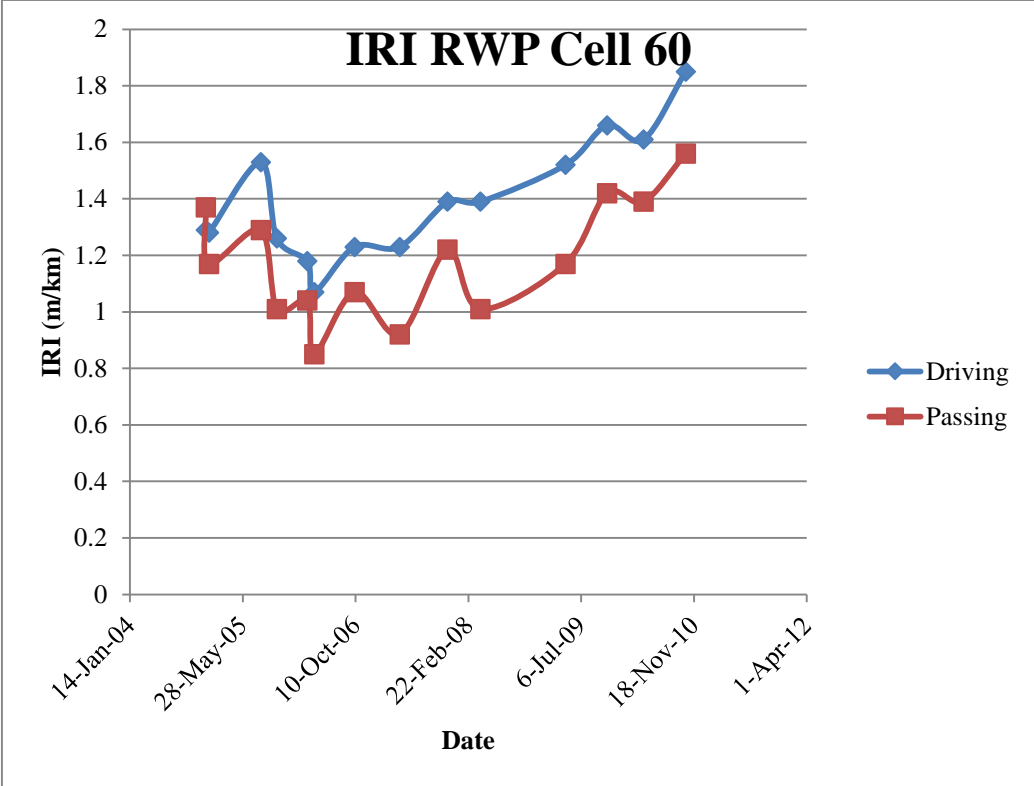
**Figure 5.50: Faulting Vs IRI in Cell with 2000 Intervention after 1993 Construction**



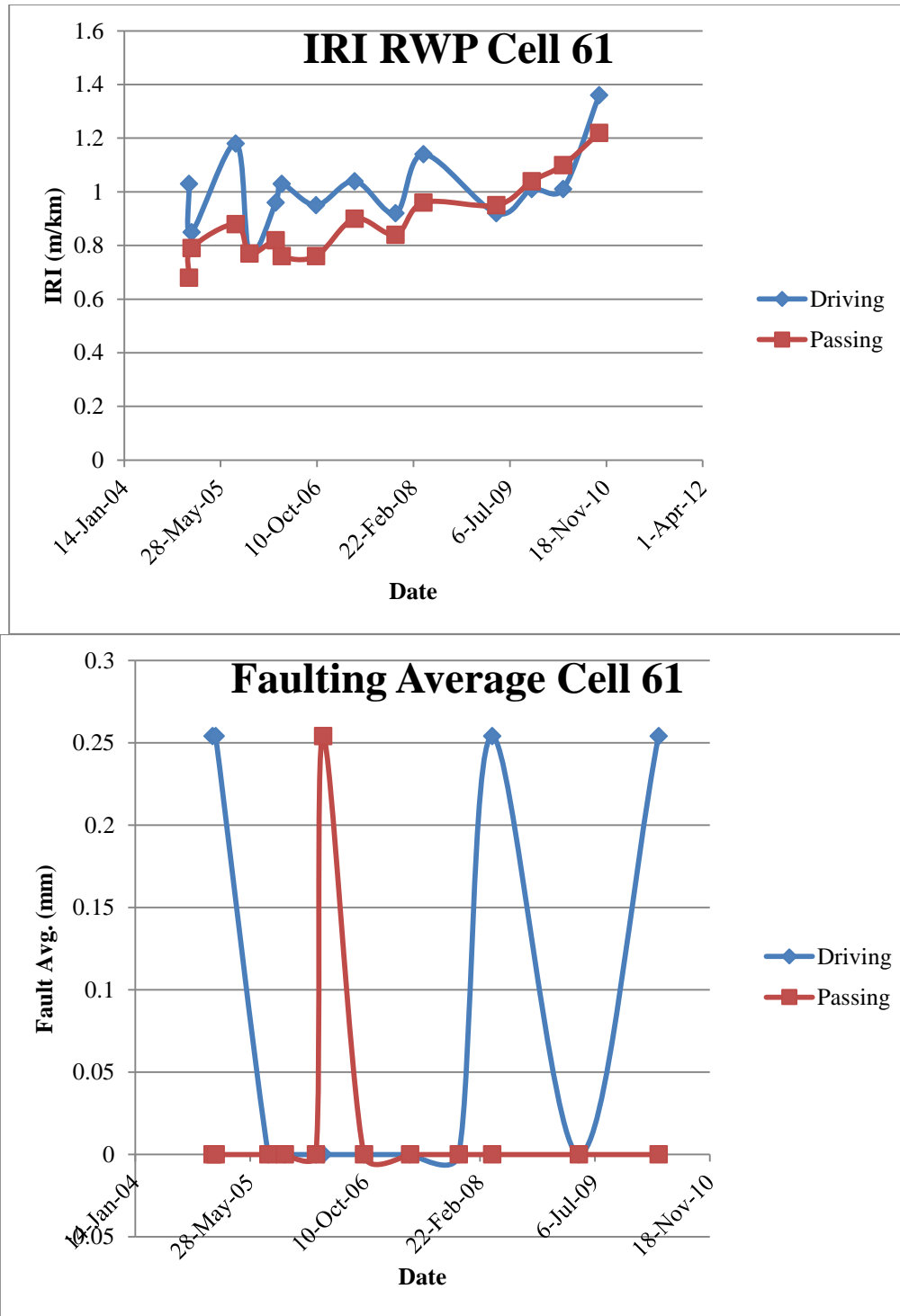
**Figure 5.51: Faulting Vs IRI in Cell with 2008 Intervention Following Culvert Study after 1993 Construction**



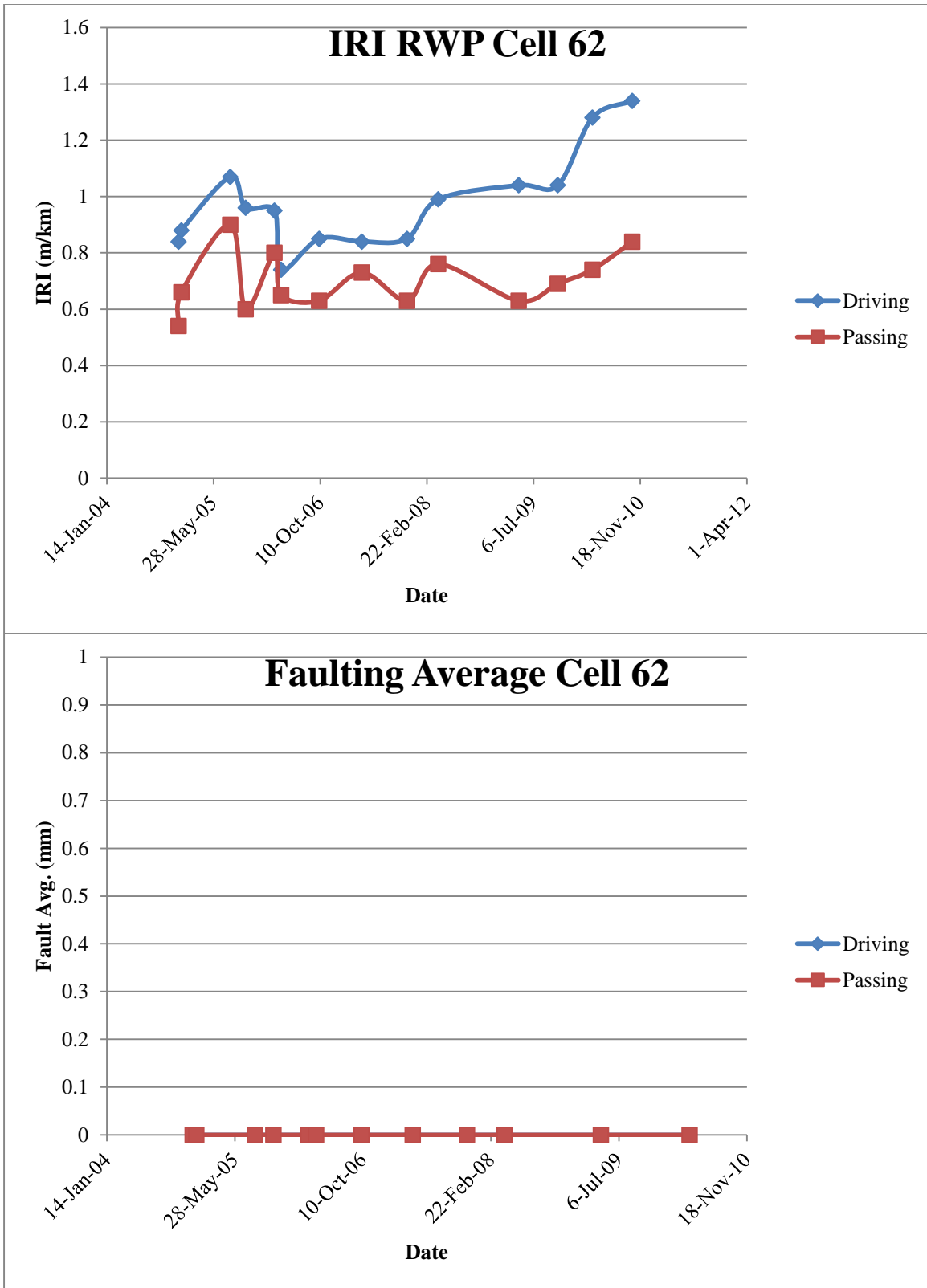
**Figure 5.52: Faulting Vs IRI in Cell with 2004 Intervention after 1993 Construction**



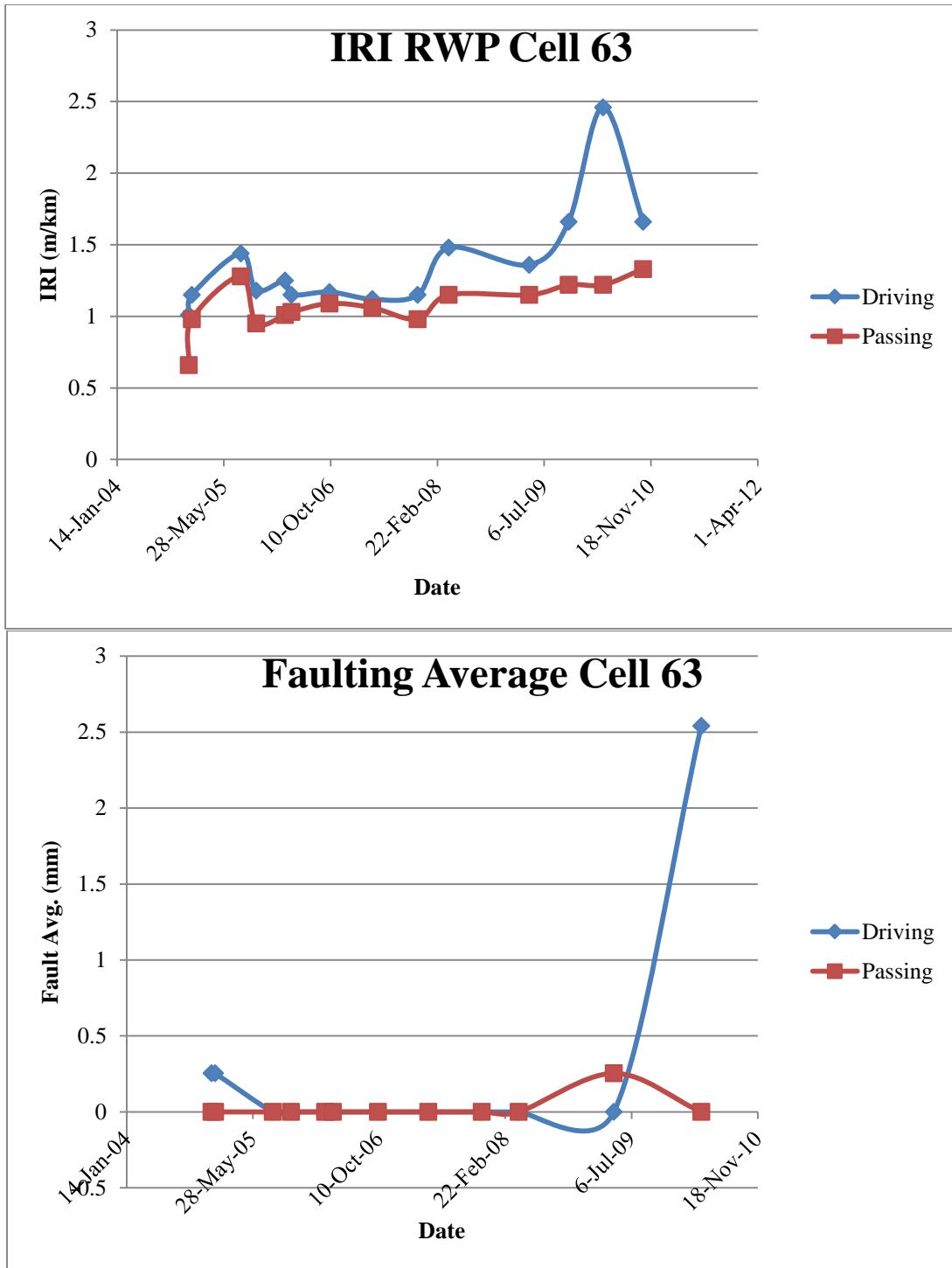
**Figure 5.53: Faulting Vs IRI in Cell with 2004 and 2013 Intervention after 1993 Construction**



**Figure 5.54: Faulting Vs IRI in Cell with 2004 and 2013 Intervention after 1993 Construction**

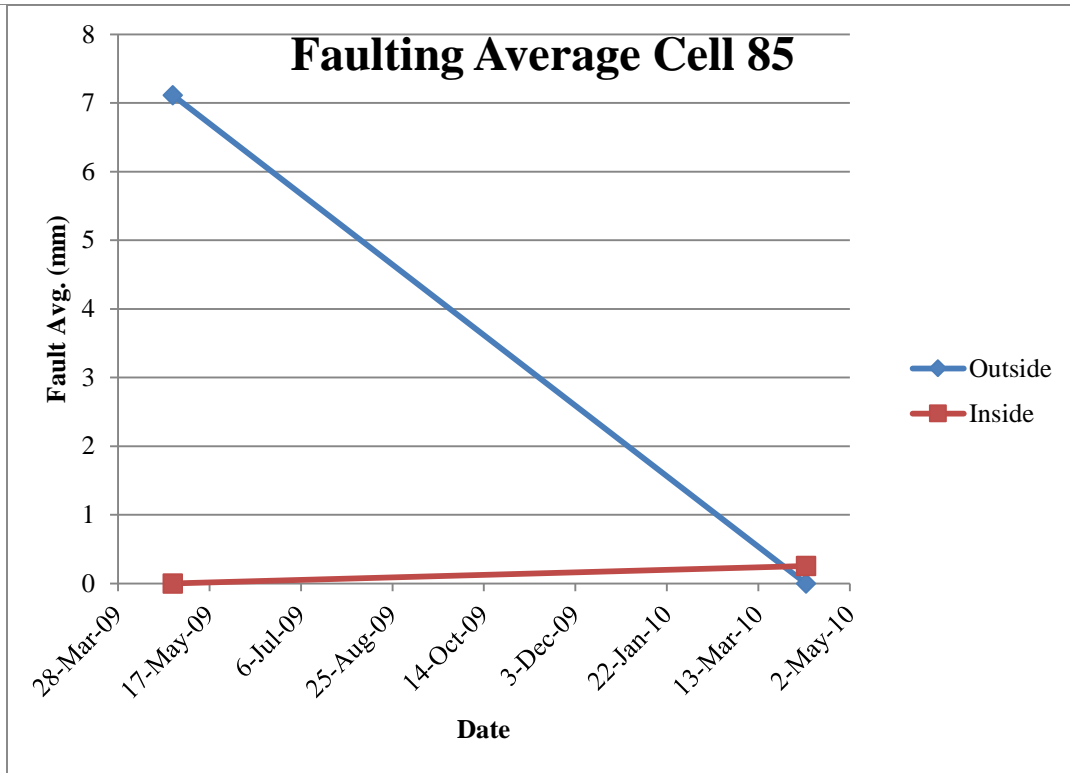
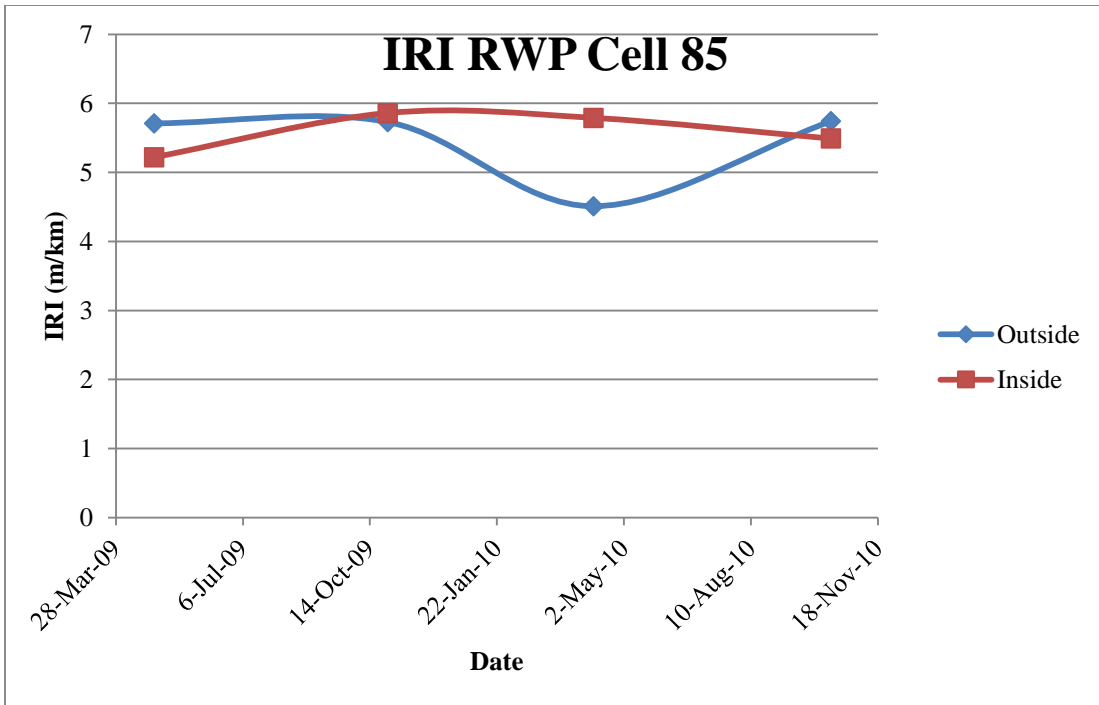


**Figure 5.55: Faulting Vs IRI in Cell with 2004 and 2013 Intervention after 1993 Construction**

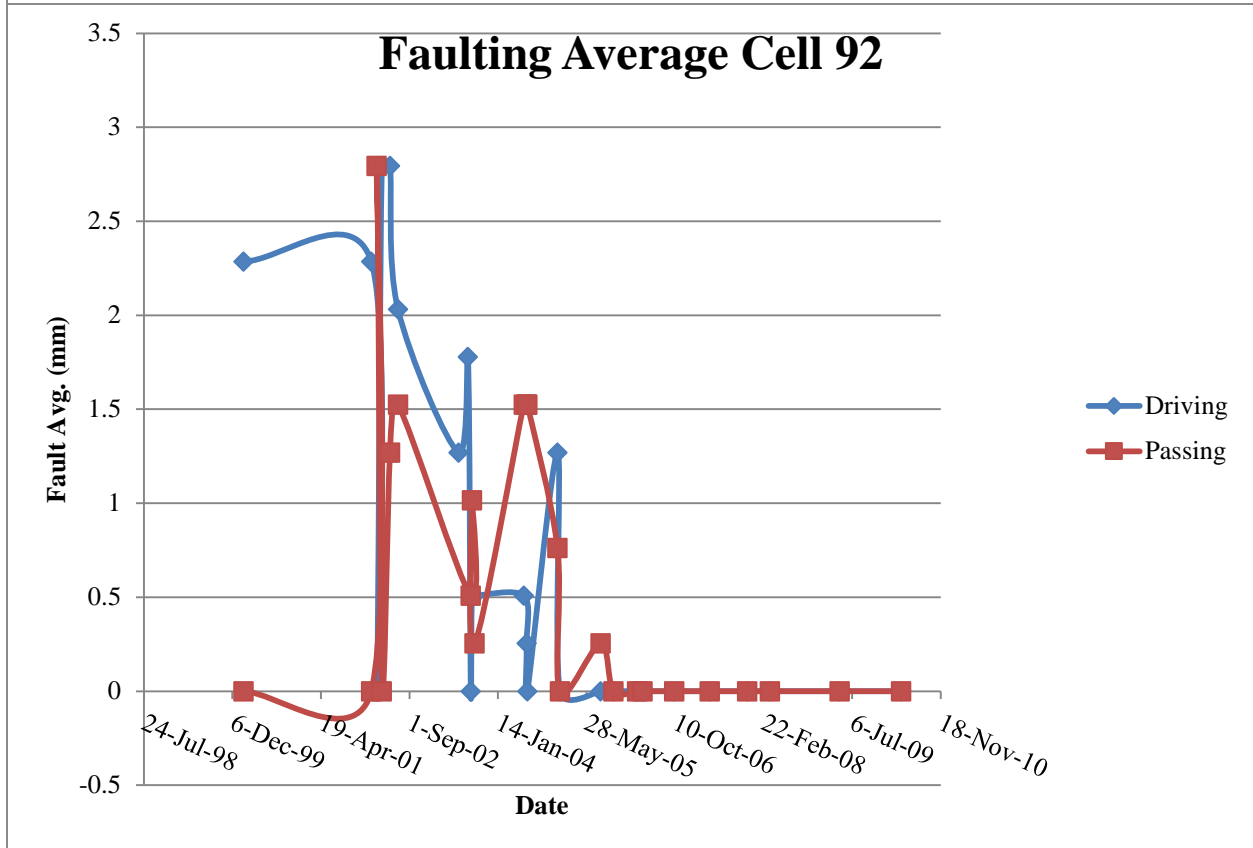
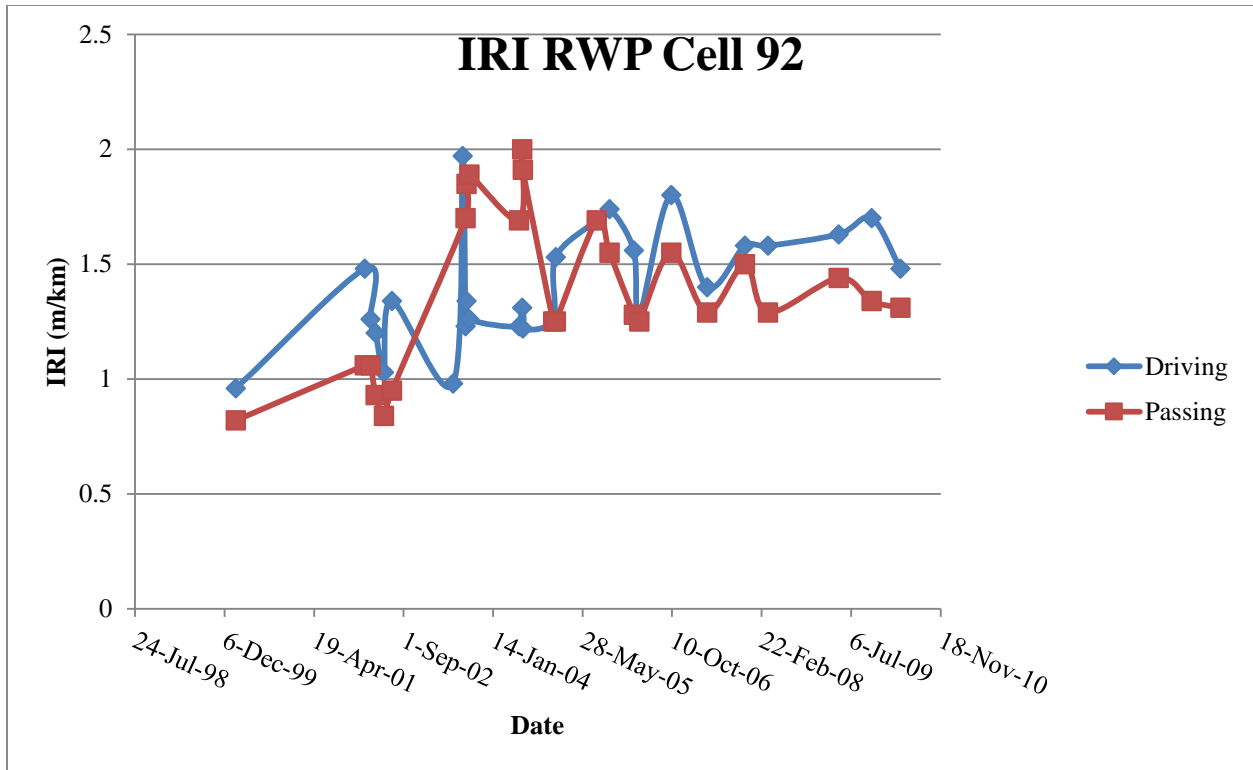


**Figure 5.56: Faulting Vs IRI in Cell with 2004 and 2013 Intervention after 1993 Construction**

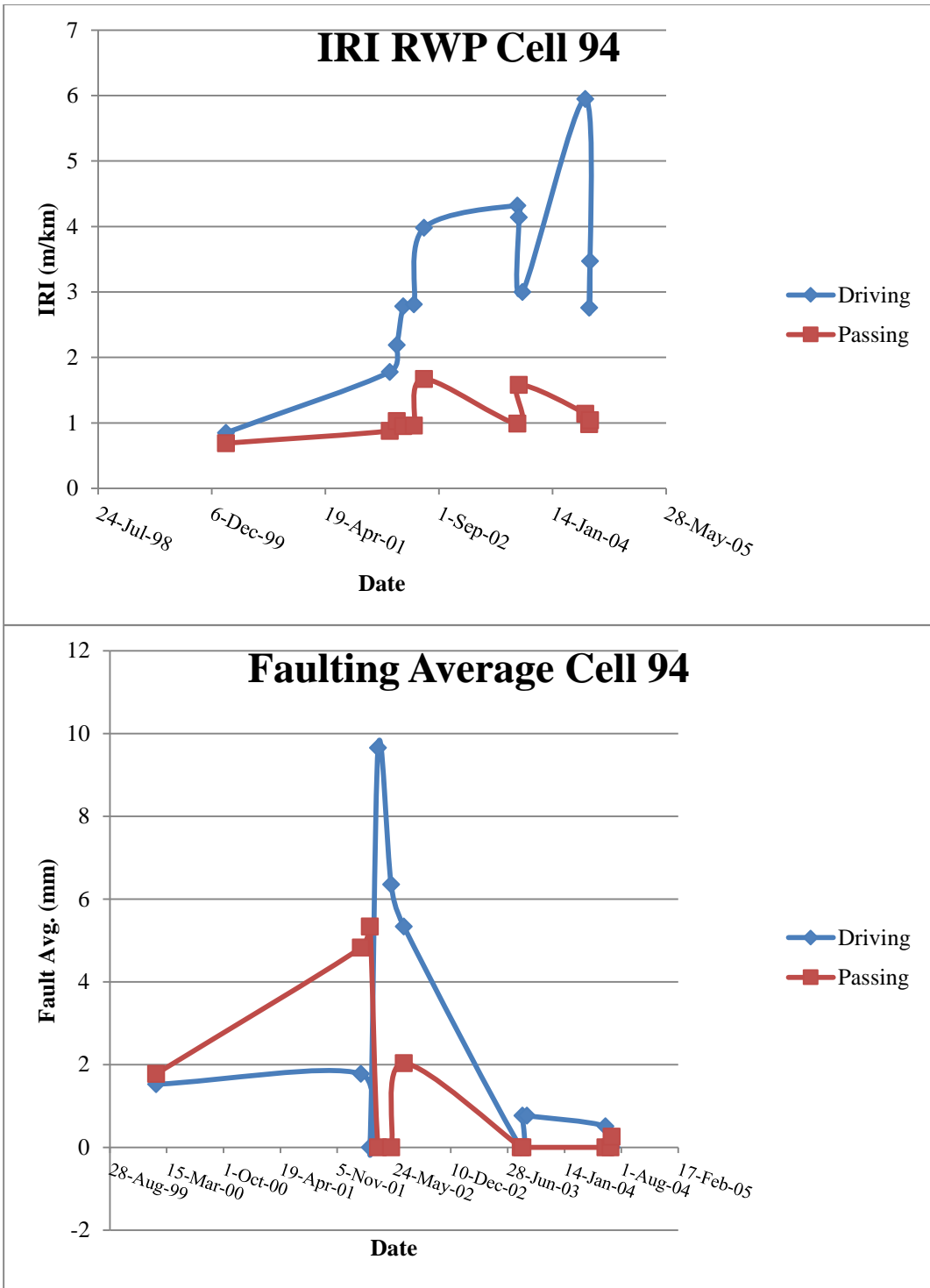




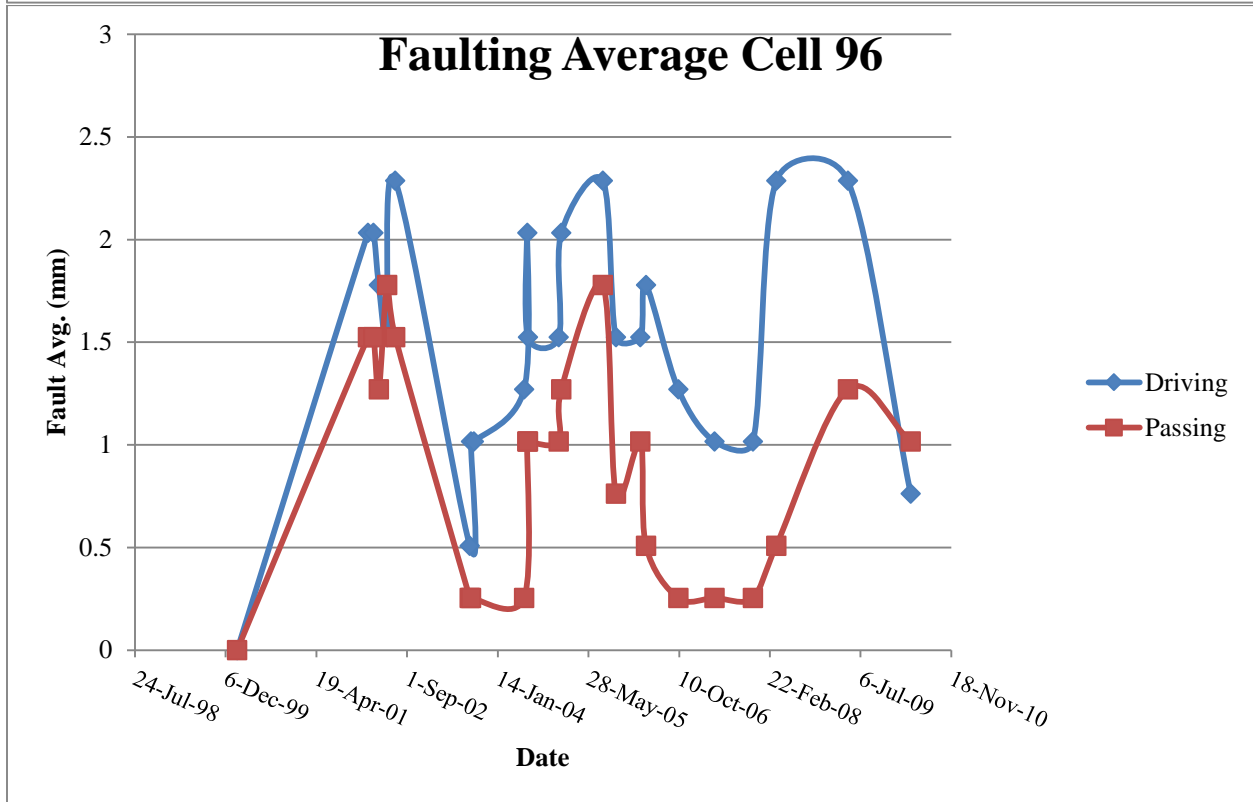
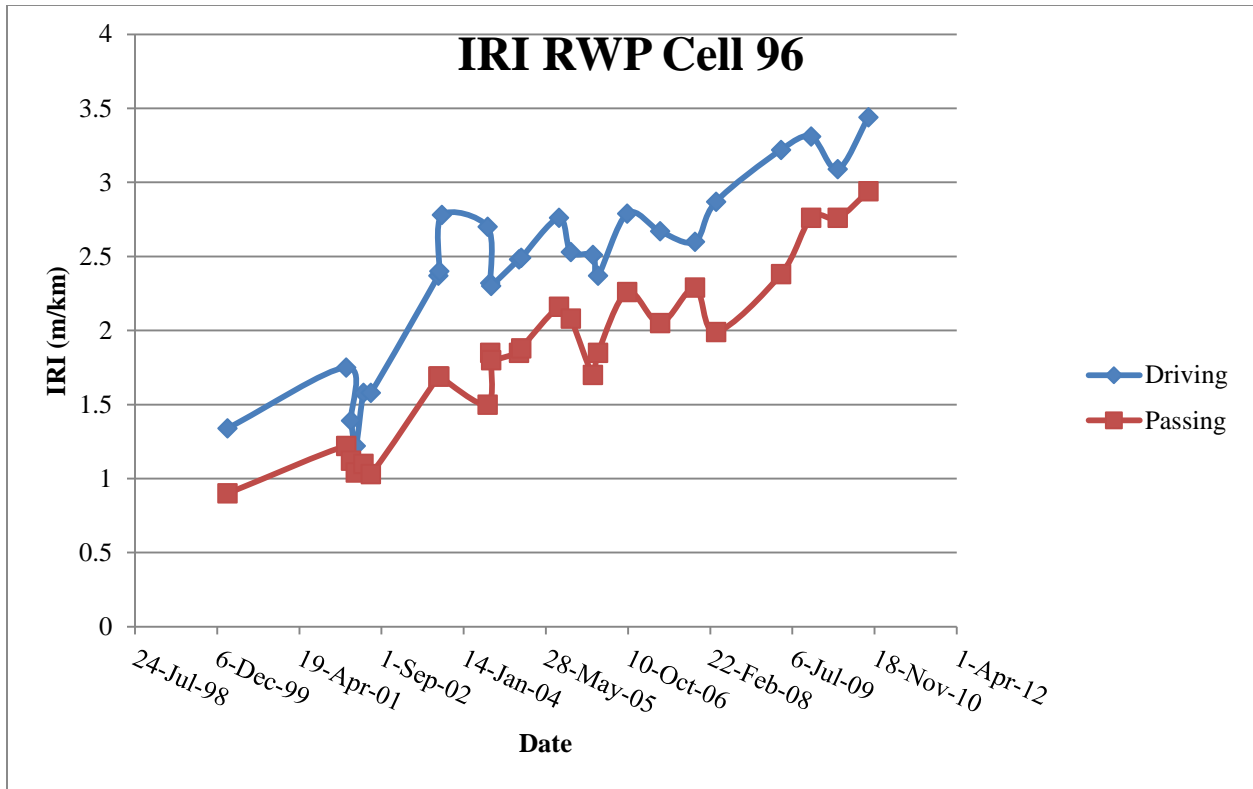
**Figure 5.57: Faulting Vs IRI in Cell with 2008 Pervious Intervention after 1993 Construction**



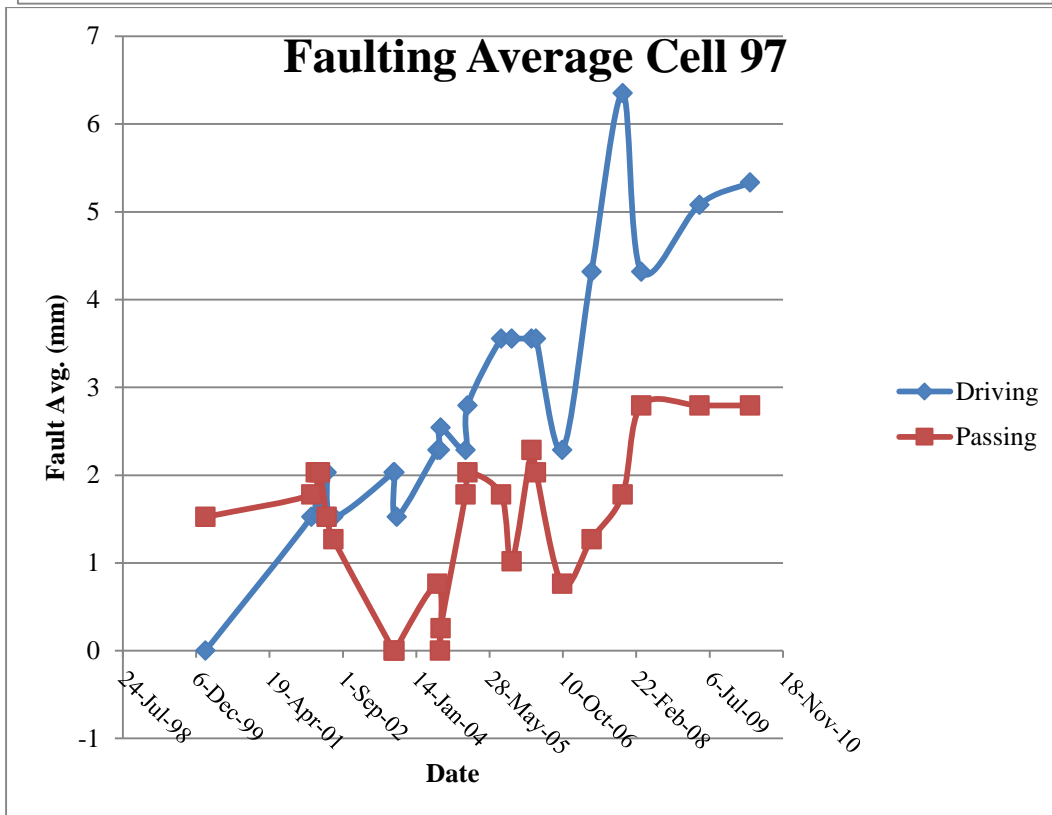
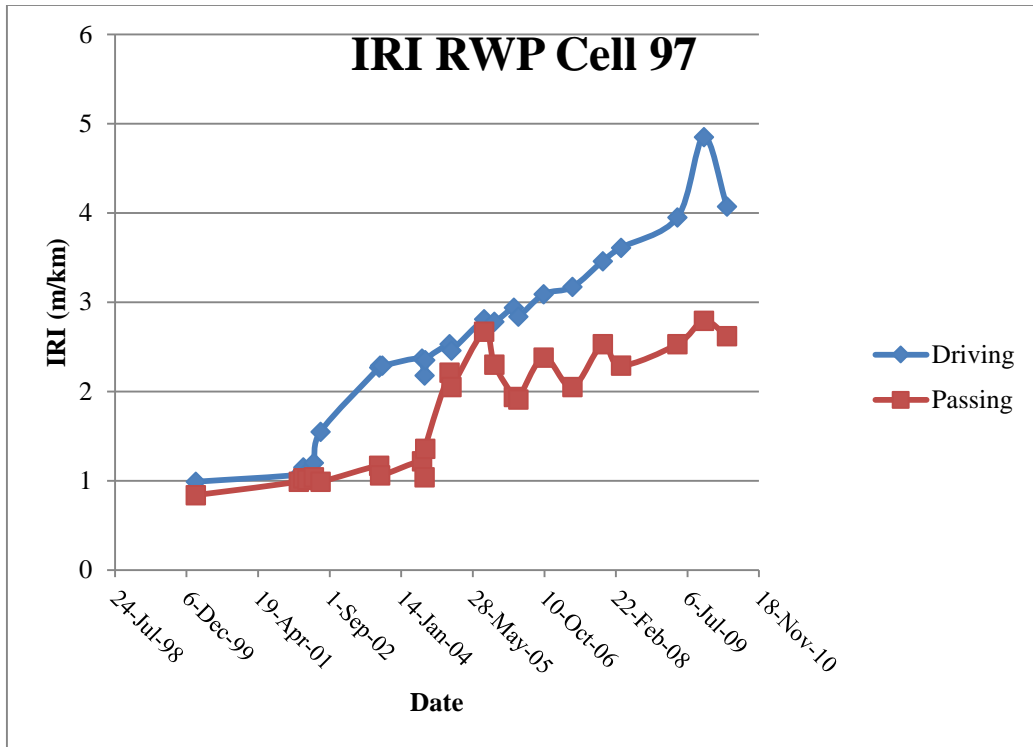
**Figure 5.58: Faulting Vs IRI in Cell with 2010 Composite Pavement Intervention after 1993 Construction**



**Figure 5.59: Faulting Vs IRI in Cell Original form Before Interventions**



**Figure 5.60: Faulting Vs IRI in Cell with Original Whitetopping cells Before 2011 Grinding**



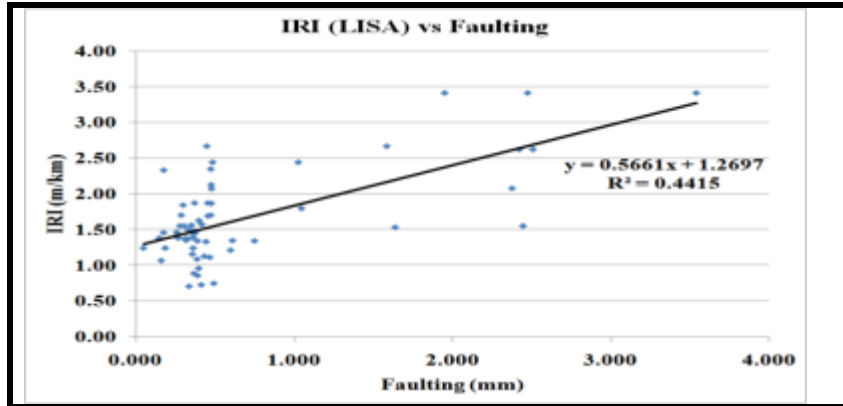
**Figure 5.61: Faulting Vs IRI in Cell with 2008 Pervious Intervention after 1993 Construction**

### **5.5.7 Section Conclusion**

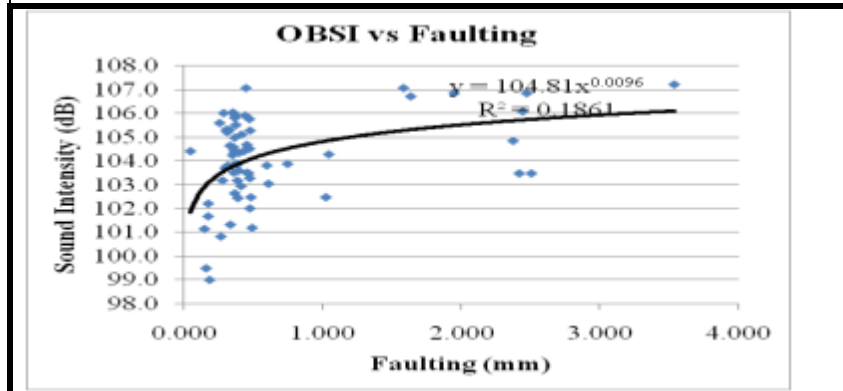
A set of physical equations have logically illustrated the effect of concrete pavement condition on OBSI. It has been shown that increased joint deterioration, faulting and warp or curl increase pavement roughness and correspondingly increase tire pavement noise.

However, OBSI is defined for 12 one-third octave frequencies of which the lowest is of 400-hertz and would not necessarily capture steady state impulses on the pavement joints which are generally low frequency. It is evident that for every tire event on a joint, there is an impulsive sound. This sound is produced by at least one of the pipe resonance and Helmholtz resonance phenomena.

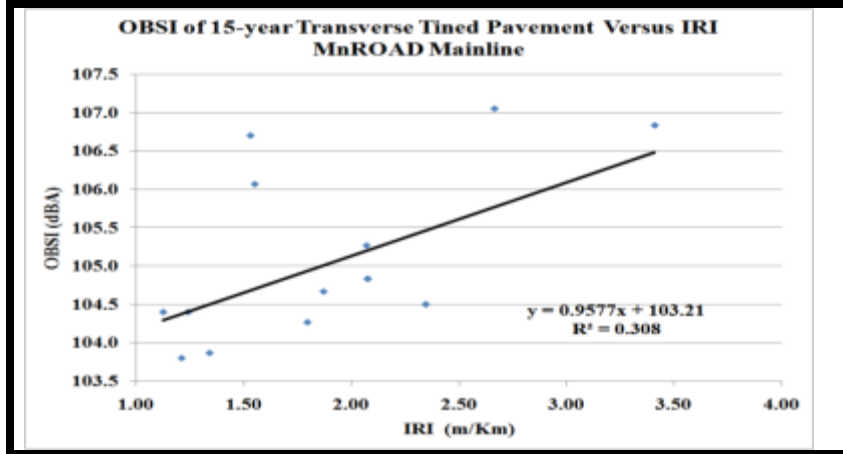
Field validation of the correlation between pavement condition and sound intensity was limited by the already defined limits of OBSI. However there was a slight correlation between OBSI and faulting and a reasonable correlation between OBSI and IRI. As IRI is induced partially by joint condition, it is evident that pavement degradation may be correlated to OBSI if the latter is measured and recorded as continuous data that can be cropped over the joints to isolate their contribution to sound intensity. Validation may be enhanced by using a sound intensity metric that has accommodations for low frequency noise. Carrying this into implementation, acoustic devices may be designed to detect potential delamination or distress forms even when such distress forms are beneath the surface. Features such as joints warp and curl that are causative to IRI are also causative to tire pavement noise though the two parameters are not in the same order of magnitude of frequency.



a) IRI versus Faulting



b) OBSI versus Faulting



c) OBSI in Transverse Tined Pavements Versus IRI

**Figure 5.62: Validation of effect of Faulting on IRI**

## Chapter 6: Conclusions and Recommendation

### SUMMARY FINDINGS

This study investigated measurements, characteristics, correlation and application of surface parameters. Earlier subtasks investigated time series analysis and representation of data in a quasi-probability density function as a method to represent large volumes of surface data in perspective. This form of data is applicable to reliability analysis and durability analysis. It showed the surface that maintained a statistically significant acoustic benefit over time. It was used in a benefit cost evaluation of quiet pavements as the statistics showed a likelihood of providing an acoustic value below 100 dB as an adjustment multiplier on the benefit/cost to obtain the true benefit/cost.

Similarly the time series analysis provided a prediction of performance over time based on the performance with the seasonal features un-detrended. This provided another method of modeling the friction noise and ride quality data obtained and predicting within seasonal trends.

Texture direction and texture orientation were found to be influential to surface characteristics. Higher noise and friction were observed in transverse tines thus validating the effect of texture direction on friction and OBSI. It is evident that higher friction numbers appear to be associated with the transverse tine. Izevbekhai (1.67) explained how thread block impact and inhibition to hysteresis are more common in transverse textures.

At MnROAD, Drag cells 32, 52 to 54 and 60 to 63 were used for the evaluation because they were the only current cells that had the concrete finished using the Astro turf drag standard. The friction numbers were measured following the American Society for Testing and Materials standard (ASTM E 274) which comprises of testing friction with both a smooth and ribbed tire. The model was computed using the measured friction values and equivalent single-axle loading (ESAL) data for the corresponding cells. It was created for both the smooth and ribbed tire and shown below where  $F$  is the friction,  $k$  is the growth rate,  $t$  is the age of the concrete in years,  $DE$  is the number of ESALs calculated for when the pavement was designed and  $FE$  represents the number of ESALs forecasted for twenty years after the design year:

- Ribbed

$$F = 22.01 \sin(kt) + 29.21 \cos(kt)[1 + e^{-0.1t}]$$

- Mainline Smooth

$$F = \left[ \left( \frac{801000}{DE} \right) \left( \frac{FE}{DE} \right) \right] [\sin(kt) + 18.36 \cos(kt) [1 + e^{-0.8t}]]$$

- Low Volume Smooth

$$F = -4.56 \sin(kt) + 15.56 \cos(kt) [1 + e^{0.031t}]$$

The smooth model was still used for the Low Volume Road because the data appeared to follow the general trend in the two test sections that could be considered to be of low volume. The ribbed equation appeared to be a straight declining model, the mainline's smooth model declined at first and then leveled off and the low volume smooth model increased slowly and appeared as a straight line. These three model equations were then used to calculate the model friction values for the twelve test sections that were used. Four analysis tests were conducted to find out if the



models from the MnROAD facility and the twelve test sections were similar or not. Each was chosen because of a unique quality that they possessed, which allowed for better conclusions to be made about the model. The four analysis tests that were used include:

Visual Analysis, Descriptive Statistics, Chi-Squared Analysis and the Mann Whitney Z test validated the hypothesis on which the model was based. After examining the various results of the four analysis tests, it was concluded that the MnROAD friction degradation model for the Astro turf texture was valid in the network. The data within each of the test sections were well modeled using those equations and could be used in design, rehabilitation considerations and the timing of various maintenance activities.

- The ribbed tire for the LVR was the only model not to be validated because of conflicting data issues and the insufficient number of low volume roads available to test the model.
- The ribbed tire model for the interstate system was accurate for most of the twelve test sections that it was tested for. This model appeared to be a straight declining line.
- In the smooth interstate model, it appeared to start by declining and then easily leveling off as the age of the pavement increased. This model was also consistently providing acceptable results for the test sections used.
- For the LVR's smooth tire model, it was validated from the two test sections that were available because of the low number of ESALs on those highways but it was continuously increasing as the age progressed.
- The three models can depict the friction numbers on various pavements where it can be used to determine how much relative friction an Astro turf dragged concrete pavement slab has at a given time.
- The models can be applied together with wet-weather accident counts to determine if certain pavements keep motorists safe enough or if maintenance is needed to give it more friction.
- Pattern of friction survival in current texturing Minnesota textures subjected to 500,000 ESALs or more have been examined. A network model developed exhibited a decay that compares favorably with typical network texture performance.
- Friction survival models of current turf and broom drag segments in the network as well as all the test cells in MnROAD have been developed. The MnROAD Model for Astro turf drag in the Mainline is similar to the Network. The Low volume road model is different because the rate of loading is not sufficient to cause sufficient degradation for a model to be tenable.
- Hysteresis extrapolations suggest that macrotexture preponderance in friction potential of current texturing experiences a crossover at the 10<sup>th</sup> year. Aggregate exposure and hysteresis will then governs the friction potential in the second decade.

- Ribbed tire friction is an effective pavement performance tool. Evident in MnROAD Model groups 5-10 is the characteristic decay of friction number versus time and the saw-tooth function is discontinuous and jumps characteristics steps dependent on the surface rehab type.
- This task report fulfills the requirement of FHWA texture advisory that requires monitoring of innovative textures.

## **NOISE**

Results suggest that the exposed aggregate concrete surface does not provide significant noise reduction. Innovative diamond grinding of composite pavements may be beneficial for noise reduction. Exposed aggregate surfacing can provide more than adequate friction for driver safety, but does not show any improvement from typical HMA or diamond ground surfaces. Exposed aggregate surfaces have a similar texture (or mean profile depth) to traditional diamond ground surfaces, but may be detrimental to ride quality. Continued monitoring of these test cells will help develop the wide understanding of exposed aggregate surfaces and composite pavements needed for more effective design and accurate service life models. New pavement textures were quiet and became noisy when the pavement roughness increased. The factor enhancing pavement noise did not seem to be significantly governed by MPD. In pervious pavements there was no significant correlation between sound absorption and OBSI in the spatial domain however in the spectral domain, a detectable association was observed. In general when other factors extrinsic to texture are not influential, tire pavement noise of concrete pavement does not vary significantly with time in a pavement. Tire pavement noise appears to decrease with increase in temperature.

The observation thus accentuate findings from other research work (1.26) and that tread block impact and air compression relief are probably the most important mechanisms by which tire pavement noise is reduced. Comparison of transverse tined and longitudinal tined surfaces and transverse broom to longitudinal broom surfaces resulted in a clear conclusion that longitudinal textures are quieter than transverse textures all things equal. An examination of alternative cost and benefit metrics is a subject for continuing research on this subject.

Authors believe that quiet pavements can be used for noise mitigation and encourage at least for a start a gradual deployment of quiet pavements. This can be achieved by reducing the height of noise walls where quiet pavements. Another common observation was the wide range of OBSI values in each pavement type. This range creates room for a statistical representation which can be used in reliability analysis.

There is a correlation between near field and farfield noise reduction. This has been applied in the use of OBSI to evaluate the economic benefit of pavements. From the methods used and the surfaces evaluated, the Ultimate grind and pervious concrete appear to be the 2 surface that are cost effective when either drag surfaces or transverse tined surfaces are rehabilitated. When transverse tined surfaces are rehabilitated, then the innovative grind, the asphalt 4.75 mm aggregate surface, as well as new SuperPave asphalt surface appear to be relatively cost-effective.

## **RIDE QUALITY AND SMOOTHNESS**

It was possible to compare the line laser IRI values to the triple point laser values. Interestingly significant disparities were not observed in the exposed aggregate, drag and tined textures. It must be noted that significant disparities were observed in the grind configurations though those were not part of this study.

Occasional spike in OBSI were found to be associated with rocking panels as in cells 60 to 63 the 2004 whitetopping cells where a recent diamond grinding resulted for an IRI improvement of 20 -50 inches per mile. The Sawtooth model associated with surface improvements were found to be valid in concrete surface textures tested.

Sequencing of the test sections impacted the rating values that the test section received. Transitioning from a fast-paced, louder, concrete section (test section 5) to a slower bituminous surface (test section 6) may have created the false impression that the quieter pavement had a better smoothness rating. The previous section thus biased the rating of the next section.

This is the first pavement rating that was followed immediately by a noise evaluation. The effect of age of pavements and the noise spectral changes are not known. Subsequent pavement rating should include corresponding noise evaluation in order to increase the sample space. The matter of sequencing is in the purview of psychoacoustics, an area that is actively involved in the way noise is perceived irrespective of how it is received. It is very probable that subjects are biased by or conditioned to a previous rating and may apply that bias to subsequent sections. Such phenomena are active periodic pavement evaluation and to eradicate a sequence of testing is to abrogate pavement evaluation altogether. A suggested method of minimizing acoustic perception effects is by performing multiple tests in different sequences thereby deploying the central limit theorem.

## **GENERAL SURFACE VARIABLES**

After studying the new textures for 5 years and the existing transverse tined and drag textures for over 5 years it the following key conclusions have been made:

Most new concrete textures exhibit texture degradation pattern that are very rapid within the first few years. The residual texture thereafter is based not only on the mix design but on the texture configuration. The degradation of exposed aggregate is so rapid that even texture orientation changes between positive and negative in consecutive years. A successful improvising of an impedance tube for in-situ sound absorption measurements in this study showed that both pervious and non-pervious pavements mainly reduce noise by tread block impact relief and air compression relief instead of absorption. Most non-pervious absorptions are within 0.02 to 0.04 while pervious absorptions range from 0.15 to 0.8 yet some non-pervious textures are 50% of the time quieter than pervious concrete.

Most new concrete surface characteristics are in somewhat non-stationary timer series. This is largely so because of weather influences on OBSI, friction, ride quality and mean profile depth. The time series are not necessarily ergodic.

## **IMPLEMENTATION PATH AND RECOMMENDATIONS**

A set of physical equations have logically illustrated the effect of Concrete pavement condition on OBSI. It has been shown that increased joint deterioration, faulting and warp or curl increase pavement roughness and correspondingly increase tire pavement noise.

However, OBSI is defined for 12 one-third octave frequencies of which the lowest is of 400-hertz and would not necessarily capture steady state impulses on the pavement joints which are generally low frequency. It is evident that for every tire event on a joint, there is an impulsive sound. This sound is produced by at least one of the pipe resonance and Helmholtz resonance phenomena.

Field validation of the correlation between pavement condition and sound intensity was limited by the already defined limits of OBSI. However there was a slight correlation between OBSI and faulting and a reasonable correlation between OBSI and IRI. As IRI is induced partially by joint condition, it is evident that pavement degradation may be correlated to OBSI if the latter is measured and recorded as continuous data that can be cropped over the joints to isolate their contribution to sound intensity. Validation may be enhanced by using a sound intensity metric that has accommodations for low frequency noise. Carrying this into implementation, acoustic devices may be designed to detect potential delamination or distress forms even when such distress forms are beneath the surface.

Most quiet pavements are proven to be cost effective when their decibel savings are prorated and a 7 dB reduction is not necessarily required. Above all this study provided useful information on pavement functional requirements: ride, friction, texture, tire pavement noise, sound absorption, isotropy or direction and mathematical variables such as texture orientation. These useful tools facilitate pavement infrastructure planning particularly because most rehabilitation projects will likely occur not for want of structural sufficiency but for want of functional reliability.

This study has lent itself to spontaneous implementation. Apart from providing strategies for a logical process of choosing texture types it describes the benefits derivable from them. Along with the use of the longitudinal turf drag, there may be occasional benefit in using the drag as pre-texture and longitudinal tine as texturing. This is particularly important when fibers are used. There is no vivid frictional advantage of using the transverse drag which is noisier and drains quicker. It may be beneficial to perform diamond grinding as a preventative maintenance in the 10<sup>th</sup> year of the 60 year design and shift the first rehab from the 17<sup>th</sup> year to the 25<sup>th</sup> year. This will maximize the acoustic benefits, reduce IRI and increase reliability.

A 4 inch pervious overlay may be used as a sacrificial noise reducing wear course since it provides good friction and can be diamond ground later for further noise reduction. A webinar on the findings of this research is recommended after publication.

## REFERENCES

- 1.1) Swanlund M. (2000) "Enhancing Pavement Smoothness" FHWA Public Roads September / October 2000 Vol 64 federal Highway Administration, Washington DC.
- 1.2) Izevbekhai B.I. (2004) Optimization of Pavement Smoothness and Surface Texturing in Pavement Infrastructure. Center for the Development of Technological Leadership (CDTL) University of Minnesota Minneapolis MN, USA.
- 1.3) Izevbekhai, B.I. Watson M. G. (2009) Evaluation of Concrete pavement textures using Wet weather accident Evaluation Criteria Minnesota Department of transportation Research Publication # 2008-46ASTM
- 1.4) ASTM E965-15, Standard Test Method for Measuring Pavement Macrotexture Depth Using a Volumetric Technique, ASTM International, West Conshohocken, PA, 2015, [www.astm.org](http://www.astm.org)
- 1.5) ASTM E2157-15,(2015) Standard Test Method for Measuring Pavement Macrotexture Properties Using the Circular Track Meter, ASTM International, West Conshohocken, PA, 2015, [www.astm.org](http://www.astm.org)
- 1.6) Rasmussen, R.O., Bernhard, R.J., Sandberg, U., Mun E.P. (2007).The little book of Noise. U.S. Department of Transportation Federal Highway Administration FHWA-IF-08-004 July 2007
- 1.7) Wayson R. (2002) Relationship between Surface texture and Highway Traffic Noise. National Academy Press ISBN 0309068215
- 1.8) Izevbekhai, B.I. Khazanovich L., Voller, V. (2012) A phenomenological Model for Tire Pavement Interaction Noise. Transportation Research Board Compendium of January 2012 Transportation Research Board Conference. Washington DC.
- 1.9) Gillespie, T. D. (1992) Everything You Always Wanted to Know about the IRI, But Were Afraid to Ask. The University of Michigan Transportation Research Institute Road Profile Users Group Meeting September, Lincoln, Nebraska.
- 1.10) Sayers, M.W., and Karamihas, S.M. (1998). Little Book of Profiling.. URL <http://www.umtri.umich.edu/content/LittleBook98R.pdf>. Accessed 2010-03-07. University of Michigan Transportation Research Institute Ann Arbor MI USA
- 1.11) Sayers, M.W., Gillespie, T. D., and Paterson, W.D.(1986) Guidelines for the Conduct and Calibration of Road Roughness Measurements, World Bank Technical Paper No.46, The World Bank, Washington DC,.
- 1.12) ASTM E950 / E950M – 09 (2009) Standard Test Method for Measuring the Longitudinal Profile of Traveled Surfaces with an Accelerometer Established Inertial Profiling Reference. ASTM International, West Conshohocken, PA, 2015,
- 1.13) Chang P, Orthmeyer R FHWA PROVAL Version 3.4 (2012). The Transtec Group, Inc., 6111 Balcones Drive, Austin, TX, 78731 and the Federal Highway Administration <http://www.roadprofile.com/?q=node/23> assessed 10/03/2012.
- 1.14) Newland D.E (1998) Random Vibration, Handbook of Noise and Vibration Control, Ch.13, 205- 211, Wiley New YorkNewYork:.
- 1.15) Donavan P. (2010).Acoustic Radiation from Pavement Joint Grooves Between Concrete Slabs. Journal Transportation Research Record: Journal ISSN 0361-1981 Issue Volume 2158 / 2010 Pages 129-137 DOI 10.3141/2158-16.

- 1.16) Khazanovich, L., Darter, M., Bartlett, R., McPeak, T. (1998) Common Characteristics of Good and Poorly Performing PCC Pavements. Federal Highway Administration <http://ntl.bts.gov/lib/6000/6300/6348/131.pdf> Database: TRIS Online AN: 00760483.
- 1.17) Wilde, W.J., Izevbekhai, B.I, and Krause M H (2007). Comparison of Profile Index and International Roughness index for Incentive Specification. Transportation Research Board Conference Jan 21-25 2007. Washington DC.
- 1.18) Whitehouse D.J (2009) A Handbook of Surface Nanometry Geometrical Product Specifications (GPS) -- Surface texture: Profile -- Terms, definitions and surface texture parameters. International Standards Organization. Second Edition Taylor and Francis Abingdon OX14 4RN, United Kingdom
- 1.19) Stoimenov, B; Maruyama, S; Adachi, K; Kato, K. (2007) The Roughness Effect on the Frequency of Frictional Sound. 2007 04; Vol.No.4 V.40; pp.659-664; Tribology international Guildford, Surrey UK : IPC Science and Technology Press, -.
- 1.20) Takahashi K. (1973) The friction noise under heavy load Bulletin of Faculty of Science & Engineering Chuo Univ Japan.; #16:53–69.
- 1.21) Wu C, Nagi, M.A. (1995) “Optimizing Surface Texture of Concrete Pavement” Portland Cement Association Research and Development Bulletin RD111T 1995. Skokie IL USA.
- 1.22) Clapp T.G., Eberhardt, A.C., Kelley, C.T. (2005) Development and Validation of a Method for Approximating Road Surface Texture Induced contact Pressure in Tire Pavement Interaction. Tire science and technology TSTCA Jan- Mar 1988 # 16(1) 2-17
- 1.23) Subhi M. B., Farhad R, (2005). Changes in Asphalt Pavement Friction Components and Adjustment of Skid Number for Temperature 2005.131:470-476. Copyright (c) 2012. American Society of Civil Engineers Reston VA USA.
- 1.24) Peter Cairney and Anthony Germanchev (2006) A Pilot Study of the Effects of Macrotecture on Stopping Australian Government. Australian Transportation Safety Bureau Sydney Australia.
- 1.25) Izevbekhai, B.I., Watson, M. G. Evaluation of Concrete Pavement Textures using Wet Weather Accident Evaluation Criteria. Minnesota Department of Transportation. Research Publication 2008-46.2009 St. Paul MN.
- 1.26) Hanson D. I. & Brian D. Prowell (2004) Evaluation Of Circular Texture Meter For Measuring Surface Texture National Center for Asphalt Technology NCAT Report 04-05 Pavements Technology Parkway Auburn, AL 36830. September 2004.
- 1.27) Sandberg U., Ejsmont J, (2012) Tire Road Noise Reference Manual Informex Ejsmont & Sandberg Handelsbolag Harg SE 59040 Kisa Sweden 2002 4.3.
- 1.28) AASHTO TP76-08. (2008) Interim Standards for conducting on board sound intensity (OBSI) AASHTO 2009 Washington DC USA.
- 1.29) Rasmussen, R.O., et al. (2008) “Identifying Quieter Concrete Pavements using On-board Sound Intensity.” Transportation Research Board Annual Meeting, Washington, Compendium of Transportation Research Board Conference Papers January 13 to 17 2008 Washington DC USA.
- 1.30) Robert O. Rasmussen, et al., “How to Reduce Tire-Pavement Noise: Better Practices for Constructing and Texturing Concrete Pavement Surface”, National Concrete Pavement Technology Center, 2011.
- 1.31) Fahy F.J. Sound Intensity Second Edition 1995. Taylor & Francis ISBN-10: 0419198105 Abingdon OX14 4RN, United Kingdom

- 1.32) Bernhard, R.J. and Rebecca McDaniel (2005) Noise Generation for Pavement Engineers. Journal Transportation Research Record: Journal of the Transportation Research Board Transportation Research Board of the National Academies ISSN 0361-1981 Issue Volume 1941 / 2005 Washington DC USA.
- 1.33) Bérengier M.; Garai, M. Guidorze, P., L’Hermite, P. (1998) Procedure for Measuring Sound Absorption of Road Surfaces In-Situ. EuroNoise 1998 Conference *Munich* Germany 4-8 October 4 - 8, 1998.
- 1.34) ASTM E1050 – 08 (2008) Standard Test Method for Impedance and Absorption of Acoustical Materials Using A Tube, Two Microphones and A Digital Frequency Analysis System. ASTM International, 100 Barr Harbor Drive, PO Box C700, West Conshohocken, PA, 19428-2959 USA
- 1.35) Horoshenkov, K.V, Hothersall, D.C., Attenborough, K. (1996) Pervious Materials for Scale Model Experiments in Outdoor Sound Propagation. Journal of Sound and Vibration (1996) 194 (5) 685-708
- 1.36) Allard J.F., Dazel O, Gautier G, Groby JP, Lauriks W.J Prediction of sound reflection by corrugated porous surfaces. Acoustic Society of America 2011 Apr; 129(4):1696-706. doi: 10.1121/1.3552870. Source Laboratory of University of Maine. CNRS, Olivier Messiaen, 72085 Le Mans, France.
- 1.37) Sandberg, U. (2003) The Multi-Coincidence Peak around 1000 Hz in Tire/Road Noise Spectra. Proceeding of Euronoise Conference Staples Italy 2003 Paper Id498.
- 1.38) Hamet J; Texture Envelopment INRETS. European Noise Conference, Spain 2003
- 1.39) Hamet J.-F and P. Klein. Road Texture and tire Noise INRETS, 25 av. F. Mitterrand, F69675, Bron, France URL: [http://www.inrets.fr/ur/te/publications/publications-pdf/web-hamet/in00\\_674.pdf](http://www.inrets.fr/ur/te/publications/publications-pdf/web-hamet/in00_674.pdf). Assessed: 4/20/2010.
- 1.40) Flintsch, G. W., De Leon, E., McGhee, K. K., Al-Qadi, I. L., (2003) “Pavement Surface Macrotecture Measurement and Applications.” Transportation Research Record: Journal of the Transportation Research Board, No.1860, TRB, National Research Council, Washington, D.C., 2003, pp 168-177.
- 1.41) Bendtsen, H. and Andersen, B. (2005): Noise Reducing Pavements – State of the Art in Denmark. Road Directorate, Danish Road Institute Report 141 Copenhagen Denmark.
- 1.42) Fujikawa, T, Hiroshi Koike, Yasuo Oshino and Hideki Tachibani (2005) Definition of Road Roughness parameters for tire Vibration Noise Control. Journal of Applied Acoustics. Volume 66.2005. pages 501 to 515.
- 1.43) Byrum C.R., Raymond, C, Swanlund, M., and Thomas Kazmierowski (2009). Experimental Short-Wavelength Surface Textures in Portland Cement Concrete Pavements. Journal of Transportation Research Board of the National Academies ISSN 0361-1981 Issue Volume 2155 / 2010, 170-178°
- 1.44) Aström K. J. and C. Canudas-de-Wit (2008 )Revisiting the LuGre Model Stick-slip motion and rate dependence Author manuscript, published in "IEEE Control Systems Magazine 28, 6 (2008) 101-114".44
- 1.45) Konishi S., Fujino T., Tomita N., Ozaki T. (1997); Temperature Dependency of Pass-By Tire Road Noise, Society of Automotive Engineers, Warrendale, PA, USA. URL <http://eurlex.europa.eu/LexUriServ/LexUriServ.do?uri=CELEX:32001L0043:EN:HTML>. Assessed 10/10/2009

- 1.46) Langberger, B.J., Demoss, J; McNermy (2001) Effect of Air and Surface Temperature on Tire Pavement Noise on an ISO10844 Surface. SAE Paper 2001-01-1598 Society of Automotive Engineers Warrendale PA, USA.
- 1.47) Sound Intensity URL <http://physicsx.pr.erau.edu/Courses/CoursesS2010> . Accessed 5/12/2010.
- 1.48) Sengpiel E. Form Zur Mikrofonaufnahmetechnik und Tonstudioteknik URL: <http://www.sengpielaudio.com> Assessed 5/24/10.
- 1.49) USEPA: United states Environmental Protection Agency. Module 2: Characteristics of Gases - Flow Characteristics URL: <http://www.epa.gov/apti/bces/module2/character/character.htm> Assessed 5/12/10.
- 1.50) Ulf Sandberg (2001) U I-INCE Working Party on Noise Emissions of Road Vehicles (WP-NERV) Swedish National Road and Transport Research Institute SE-581 95 Linköping, Sweden. Gade S. Technical Review 3-1982 Sound Intensity Theory. Bruel & Kjaer DK-2850 Denmark.
- 1.51) Nelson T. (2011) Evaluation of Skid Resistance of Turf Dragged Textured Concrete. URL <http://www.dot.state.mn.us/research/TS/2011/201112.pdf> . MnDOT Report #2011-11 St. Paul Minnesota USA.
- 1.52) Bruel & Kjaer Sound Intensity Primer. Bruel & Kjaer DK-2850 Denmark.
- 1.53) ASTM F2493 - 08 Standard Specification for P225/60R16 97S Radial Standard Reference Test Tire.
- 1.54) Engineering Toolbox. The Engineering Toolbox Resources, Tools and Basic Information for Engineering and Design of Technical Applications URL <http://www.engineeringtoolbox.com> Assessed 12/1/2009
- 1.55) Bohn, A.D., Environmental Effects on the Speed of Sound.83rd Convention of the audio Engineering Society NewYork 1987. J. Audio Eng. Soc., Vol.36, No.4, April1988
- 1.56) USEPA: United states Environmental Protection Agency. Module 2: Characteristics of Gases - Flow Characteristics URL: <http://www.epa.gov/apti/bces/module2/character/character.htm>
- 1.57) Pierce, A.D. Acoustics: an Introduction to its Physical Principles and Applications.1989. Acoustical Society of America. New York.4.3
- 1.58) Kinsler, L. E., Frey, A., Coppens, A.B., Sanders, J.V. Fundamentals of Acoustics. Third Edition.1980. John Wiley & Sons. New York.
- 1.59) McLennen J. Helmholtz resonance (2003) URL (<http://www.phys.unsw.edu.au/jw/Helmholtz.html>) Assessed 10/20/0
- 2.1) Akkari, A,K., Izevbekhai, B.I, Siekmeier J.A. 2011 MnROAD Mainline Concrete Construction Cells 5, 6, and 63, URL: <http://www.lrrb.org/media/reports/201229.pdf>. Assessed 10/20/2012
- 2.2) Akkari, A, K., Izevbekhai, B.I, Siekmeier J.A. 2011 MnROAD Mainline Concrete Construction Cells 5, 6 and 63. URL: <http://www.lrrb.org/media/reports/201229.pdf>. Assessed 10/20/2012
- 3.1) ISO 10534-2, "Acoustics – Determination of Sound Absorption Coefficient and Impedance in Impedance Tubes – Part 2: Transfer-Function Method."



- 3.2) ASTM E-1050, "Standard Test Method for Impedance and Absorption of Acoustical Materials using a Tube, Two Microphones and a Digital Frequency Analysis System."
  - 3.3) Berengier, M., et al. Procedure for Measuring the Sound Absorption of Road Surface In-Situ. Euro Noise '98 Conference. Munchen, Germany, 4-7 October 1998
  - 3.4) Izevbekhai, B.I. Acoustic Properties of Clogged and Unclogged Pervious Concrete Pavements URL: <http://www.mrr.dot.state.mn.us/research/pdf/2011MRRDOC009.pdf>. Accessed 1/12/15
  - 3.5) Hodgson, M. (1993). "Experimental evaluation of the accuracy of the Sabine and Eyring theories in the case of non-low surface absorption," Journal of acoustics and vibration.
  - 3.6) Eyring, C. F. (1930) Acoust. Soc. Am. 94, 835–840. "Reverberation time in 'dead' rooms," J. Acoust. Soc. Am. 1, 168. 5)
  - 3.7) Izevbekhai, B.I. (1987) Properties of Sawdust as Aggregate for Concrete Master of Engineering. (MEng) Thesis - University of Benin, Nigeria
- 4.1) Donavan, P, Lodico, D. M (2009) Evaluation of Test Variables for Onboard Sound Intensity (OBSI) Measurements Transportation Research Board Paper # 09-3261 January 2009
  - 4.2) Box, G. E. P., Jenkins, G. M A (1994) First Course on Time Series Analysis - an open source book on time series analysis with SAS (Chapter 7) Prentice Hall, Englewood Clifs, NJ USA
  - 4.3) Box, G. E. P., Jenkins, G. M., and Reinsel, G. C. (1994). Time Series Analysis, Forecasting and Control, 3rd ed. Prentice Hall, Englewood Clifs, NJ USA
  - 4.4) Rasmussen R.O. Sohaney, R.C., Gary J. Fick, G and E. T. Cackler, (2007) How to Design and Construct Quiet Pavements. 10th International Conference on Concrete Pavements URL [http://www.thetranstecgroup.com/wordpress/wp-content/uploads/2013/07/How\\_to\\_Design\\_and\\_Construct\\_Quieter\\_Concrete\\_Pavements.pdf](http://www.thetranstecgroup.com/wordpress/wp-content/uploads/2013/07/How_to_Design_and_Construct_Quieter_Concrete_Pavements.pdf) July 8-12 Quebec Canada.
  - 4.5) Izevbekhai, B.I. & Khazanovich, L. (2012) Acoustic Enhancement of Concrete pavement Surface through Diamond. International Journal of Pavement Engineering Taylor and Francis. DOI:10.1080/10298436.2012.690517 May 2012 Taylor and Francis Ltd Abingdon OX14 4RN, United Kingdom
  - 4.6) Izevbekhai, Bernard Igbafen; Voller, Vaughan R. (2012)Development and validation of a tenable process for quantifying texture spikiness for pavement noise prediction International Journal of Pavement Engineering, Volume 14, Number 2, 1 February 2013, pp.190-205 16 Taylor and Francis Ltd Abingdon OX14 4RN, United Kingdom
  - 5.1) Izevbekhai, B.I (2006) a field investigation of the influence of pavement texture on Pavement Smoothness measurements. MnDOT MnROAD Reports. URL: <http://www.mrr.dot.state.mn.us/research/pdf/2007mrrdoc009.pdf> Assessed 7/3/2009
  - 5.2) Izevbekhai, B.I. (2004) Optimization of Texture and Ride Quality in Pavement Infrastructure. Dissertation for Master of Science in Infrastructure Systems Engineering. Technological Leadership Institute, College of Science and Engineering, University of Minnesota.
  - 5.3) Smith, S.W. (2002)- Digital Signal Processing - A Practical Guide for Engineers and Scientists, Newnes, ISBN 0-7506-7444-X
  - 5.4) Hanson D I. Waller B. (2005) Evaluation of Noise Characteristics of Minnesota Pavements

<http://www.mrr.dot.state.mn.us/pavement/PvmtDesign/noise/MNCPXnoiseresultsfinalreport.pdf>. Assessed 2/29/08 July 2005. Minnesota Department of Transportation, St. Paul MN USA

- 5.5) Izevbekhai, B.I. (2004) Optimization of Texture and Ride Quality in Pavement Infrastructure. Dissertation for Master of Science in Infrastructure Systems Engineering. Technological Leadership Institute, College of Science and Engineering, University of Minnesota. Minneapolis MN USA.
- 5.6) Smith, S.W. (2002) Digital Signal Processing - A Practical Guide for Engineers and Scientists, ISBN 0-7506-7444-X Newnes, USA
- 5.7) Hanson D I. and James R. S. (2004) Noise Evaluation of Colorado Pavements Report No. CDOT- DTD-R-2004-5 Colorado Department of Transportation 4201 E. Arkansas Ave. Denver, Colorado 80222 USA
- 5.8) Kuemmel A. A Sonntag R.C. Jackel, J.R. Satanovsky A. (1989) Noise and Texture on PCC Pavements Report of a Multi-State Pooled Fund Study. Wisconsin Department of Transportation Report # WI/ SPR 08 –09 Madison WI USA.
- 5.9) Izevbekhai B.I. Wilde W.J. (2010) Innovative Diamond Grinding on MnROAD Cells 7, 8, 9 and 3. 2010. URL: <http://www.lrrb.org/pdf/201105.pdf> assessed 4/30/11. Report Number 2011-05. Minnesota Dept of Transportation. St Paul MN.
- 5.10) Izevbekhai, B.I., Khazanovich L. (2008), Implications of Texture Degradation on Board Sound Intensity Measurements at MnROAD Test Cells. Proceedings of the International Noise Conference. DearBorn Michigan USA. July 2008.
- 5.11) Rymers, B; Donavan, P. California Applications and Experiences Using the OBSI Method Transportation Research Board Paper # 09-3579 January 2009.
- 5.12) Donavan, P, Lodico, D. M. (2009) Evaluation of Test Variables for On Board Sound Intensity (OBSI)Measurements Transportation Research Board Paper # 09-3261 January 2009
- 5.13) Dick E.B., Izevbekhai, B.I., Casy T. (2010) Influence of Pavement on Traffic Noise -- Statistical Pass-By Measurements of Traffic on Several Interstate Pavements. URL <http://www.lrrb.org/media/reports/201040.pdf>. Accessed 1/29/2012 MnDOT Research Report MN 2010-40 St Paul MN USA
- 5.14) Izevbekhai, B.I. (2012). Tire Pavement Interaction Noise of Concrete Pavements. Thesis for Doctor of Philosophy in Civil Engineering. Department of Civil Engineering University of Minnesota Minneapolis MN USA. May 2012.
- 5.15) AASHTO TP 76-08. (2008) Standard Method of Test for Measurement of Tire/Pavement Noise Using the On-Board Sound Intensity (OBSI) Method.
- 5.16) Rasmussen, R O., Whirledge, R. P., Light, D. et al.(2008) Identifying Quieter Concrete Pavements using On-Board Sound Intensity Transportation Research Board Annual Meeting 2008 Paper #08-2335 .
- 5.17) Sandberg U., Ejsmont J Tire Road Noise Reference Manual Informex Ejsmont & Sandberg Handelsbolag Harg SE 59040 Kisa Sweden 2002.
- 5.18) Federal highway Administration (1999) US Department of Transportation URL Economic Analysis Primer. URL <http://www.fhwa.dot.gov/infrastructure/asstmgmt/primer.pdf> Assessed 6/15/2009US Department of Transportation Federal Highway Administration (2012).
- 5.19) Noise Policy For Type I Federal-Aid Projects as per 23 CFR 772 MnDOT Office of Environmental Stewardship on Evaluation of Cost Effectiveness for Establishing

Rational for Noise Walls URL:

<http://www.dot.state.mn.us/environment/noise/pdf/2011mndotnoisepolicy.pdf> assessed 3/12/2012

- 5.20) Office of Asset Management McLean, VA 22101 USA. Harris, S. Colorado Department of Transportation's Current Procedure For Life Cycle Cost Analysis and Discount Rate Calculations Report No. CDOT-2009-2. Colorado Department of Transportation in Cooperation with the U.S. Department of Transportation McLean VA USA
- 5.21) Federal Highway Administration. (2005) Technical Advisory, Surface Texture for Asphalt and Concrete Pavements, T 5040.36, June 17, 2005. Federal Highway Administration McLean VA USA 5.42)
- 5.22) Izevbekhai B. I. (2004) Effect of Texture On Ride Quality. Thesis Master of Science Infrastructure Systems Engineering Center for the Development of Technological Leadership University of Minnesota Minneapolis MN USA. December 2004.43)
- 5.23) Izevbekhai, B.I. Innovative Diamond Grinding Research Summary. Minnesota Department of Transportation Internal Document 1400 Gervais Avenue Maplewood MN 55109 February 2008. <http://www.mrr.dot.state.mn.us/research/4> pagers. Assessed 3/13/08
- 5.24) Izevbekhai, B.I., Eller A.J. Evaluation of Current Texturing Practices in Minnesota. transportation research Board 2008 Annual Conference paper 08-1164, 2008
- 5.25) Izevbekhai, B.I. A review paper on the "The Effects of Stringlines on Concrete Pavement Construction". University of Minnesota Minneapolis MN USA. (Original Paper: Robert Otto Rasmussen, Steven M. Karamihas, William R. Cape, George K. Chang, and Ronald M. Guntert, Jr Stringline Effects on Concrete Pavement Construction. Transportation Research Board of the National Academies ISSN 0361-1981 Issue Volume 1900 / 2004 .DOI 10.3141/1900-01 Pages 3-11 January 29, 2007.]
- 5.26) Ryan Rohne, Thomas Burnham (2010) Investigation of Joint Deterioration in MnROAD Phase 1 Jointed Concrete Pavement Test Sections. Report Number: 2010-18 Report/Product: <http://www.lrrb.org/pdf/201018.pdf> (2MB)
- 5.27) Gillespe, T, D., S.M. Karamihas, M.W. Sayers, M.A. Nasim, W. Hansen, N. Ehsan and D. Cebon.(1993) Effect of Heavy vehicle Characteristics on Pavement Response and Performance. NCHRP 353 National Cooperative Highway Research Program. Transportation Research Board National Research Council. National Academy press. Washington DC 1993.
- 5.28) Chang G., Orthmeyer, R. (2002) FHWA PROval .FHWA DTH.... Washington DC 2002Ralph Haas, W. Ronald Hudson, John Zaniewski (1994). Modern pavement management Krieger Pub. Co. (Malabar, Fl USA) 1994.
- 5.29) Pierce A.D. (1984): Acoustics. An Introduction To its Physical Principles and Applications. 3rd edition, American Institute of Physics, College Park Maryland USA 1984.
- 5.30) Kinsler Lawrence E. Kinsler Austin R. Frey Alan B. Coppens, James V. Sanders (1999) Fundamentals of Acoustics 4th edition John Wiley & Sons New York USA 1999.
- 5.31) Huang, Yang H. Pavement Analysis and Design (2nd Edition) (Hardcover - Aug 18, 2003) Pearson Prentice Hall Upper Saddle River New Jersey USA